Scuola di Dottorato in Fisica, Astrofisica e Fisica Applicata
Dipartimento di Fisica

Corso di Dottorato in Fisica, Astrofisica e Fisica Applicata
Ciclo XXVIII

Dynamical properties of many-body systems from Quantum Monte Carlo simulations

Settore Scientifico Disciplinare FIS/03

Supervisore: Dr. Davide Emilio GALLI

Co-supervisore: Prof. Luca Guido Arthur MOLINARI

Tesi di Dottorato di:
Mario MOTTA

Anno Accademico 2014-2015

Commission of the final examination:

External Referee:
Dr. Markus Holzmann (Université Joseph Fourier, 38042 Grenoble Cedex, France)

External Member:
Prof. Alberto Parola (Università dell'Insubria, 22100 Como, Italy)

Internal Member:
Dr. Davide E. Galli (Università degli Studi di Milano, 20133 Milano, Italy)

Final examination:

Date: November 27, 2015

Università degli Studi di Milano, Dipartimento di Fisica, Milano, Italy

Cover illustration:
artist's view of the scattering
of electromagnetic radiation on a many-body system
(design: Alessandro Colombo)

MIUR subjects:

FIS/03

PACS:

03.65.Nk; 02.70.Ss, 05.40.-a; 71.10.Pm, 67.25.-k; 05.30.Fk, 71.27.+a; 71.45.Lr; 71.18.+y

To my mother Rosella Cologni,
to my brothers Giacomo and Jona Motta
and to the memory of my father Alvino Motta

Contents

Introduction **vi**
Motivation vii
Thesis overview vii

1 Measurable properties of many-body systems **1**
1.1 Dynamic properties 1
1.2 Static properties 6

2 The Variational Monte Carlo method **11**
2.1 Introduction 11
2.2 Monte Carlo Integration 12
2.3 Variational Monte Carlo Method 16
2.4 Optimization of Jastrow-Feenberg and Backflow correlations 27

3 Projective configurational quantum Monte Carlo methods **45**
3.1 Introduction 45
3.2 Path Integral Ground State 47
3.3 Diffusion Monte Carlo 56
3.4 Reptation Monte Carlo 67

4 One-dimensional ^{4}He: Luttinger liquid theory and beyond. **71**
4.1 Introduction 71
4.2 The Tomonaga-Luttinger liquid theory 72
4.3 Nonlinear Tomonaga-Luttinger liquid theory 79
4.4 Exactly solvable models 81
4.5 Dynamic structure factor of a system of hard rods. 96
4.6 ^{4}He: equation of state and Luttinger parameter 102
4.7 ^{4}He: dynamical structure factor 107
4.8 ^{4}He: drag force exerted on a soft impurity 109

5 The phaseless Auxiliary Field Quantum Monte Carlo **115**
5.1 Imaginary-time correlations and the fixed-node approximation 115
5.2 Properties of Slater determinants 117
5.3 The Hubbard-Stratonovich transformation 123
5.4 The phaseless auxiliary fields quantum Monte Carlo method 126

6 Imaginary-time correlations and the phaseless AFQMC **137**
6.1 Phaseless AFQMC estimator of imaginary-time correlations 137
6.2 Computational Cost 140
6.3 Assessment of accuracy 141
6.4 Numeric Stabilization 145

7 Imaginary-time correlations of high-density two-dimensional electron gases **151**
7.1 Introduction 151
7.2 The two-dimensional homogeneous electron gas 152
7.3 Hubbard-Stratonovich Transformation in the plane-wave basis set 153
7.4 Evaluation of the local energy 155
7.5 Evaluation of the density-fluctuation ITCF 156
7.6 Results 157
7.7 Conclusions 162

8 Effective mass of high-density two-dimensional electron gases from AFQMC **169**
8.1 Introduction 169
8.2 Landau's Fermi liquid theory 172
8.3 AFQMC evaluation of the greater Green's function 174
8.4 Results 176

Appendices **187**

9 Some results about time-dependent random phenomena **189**
9.1 Markov chains 189
9.2 Stochastic processes 191

10 Details of configurational QMC calculations for electronic systems **199**
10.1 Wavefunctions for homogeneous electronic systems 199
10.2 Efficient Optimization of Backflow Correlations 205
10.3 DMC calculation of the static density susceptibility 208

11 Some results about one-dimensional systems **213**
11.1 Details of the Bosonization procedure 213
11.2 Mobile impurity Hamiltonian 217
11.3 Diagonalization of the nonlinear Luttinger liquid Hamiltonian 218

12 The GIFT method **223**

13 Details of AFQMC calculations for electronic systems **235**
13.1 Ewald summation 235
13.2 Statistical data analysis 244
13.3 Systematic Errors 246
13.4 Numeric stabilization of AFQMC calculations 246
13.5 RPA for Finite Homogeneous Systems 249

Acknowledgments **265**

Introduction

Motivation

The numerical simulation of quantum many-body systems is an essential instrument in the research on condensed matter Physics. However, the very mathematical foundations of quantum mechanics severely restrict the current possibility to treat many relevant problems exactly. Indeed, shortly after the formulation of quantum mechanics, P. Dirac recognized the need of finding practical methods for solving the many-body Schrödinger equation in a tolerable amount of time, and yet without sacrificing its physical content:

The underlying physical laws necessary for the mathematical theory of a large part of Physics [...] are thus completely known, and the difficulty is only that the exact application of these laws leads to equations much too complicated to be soluble. It therefore becomes desirable that approximate practical methods of applying quantum mechanics should be developed, which can lead to an explanation of the main features of complex atomic systems without too much computation. [1]

The application of quantum Monte Carlo (QMC) methods to non-relativistic Bose systems is a well consolidated achievement of modern computational Physics [2, 3]. Moreover, remarkable progress has been made in studying dynamical properties of such systems, which are of great relevance for the interpretation of experimental data and the understanding of excitations in many-body quantum systems.
On the other hand, exact ground-state and dynamical properties of non-relativistic Fermi systems are currently inaccessible to existing QMC methods. The study of such systems often requires uncontrolled approximations, that can cause systematic errors.
Advances in the numerical study of Fermi systems is a still open problem of great relevance, as fermions constitute a substantial part of ordinary matter and methods for the accurate calculation of their ground-state and dynamical properties would be useful instruments in condensed matter Physics.

Thesis overview

A large part of this thesis has been dedicated to the introduction, implementation, extension and application of some of the existing approximate schemes for studying ground-state and dynamical properties of quantum many-body systems.

- in Chapter 1, the properties investigated in the thesis are briefly reviewed.

- in Chapter 2, the Variational Monte Carlo method is reviewed and the optimization of Jastrow-Feenberg and backflow correlations is discussed.
- in Chapter 3, the projective QMC methods used to investigate dynamical properties of Bose and Fermi systems (Diffusion Monte Carlo, Path Integral Ground State, Reptation Monte Carlo) are reviewed.
- in Chapter 4, the fascinating Physics of one-dimensional systems is reviewed, and the Path Integral Ground State method is applied to the study of density fluctuations in ^{4}He and hard-rods systems.
- in Chapter 5, the phaseless auxiliary field QMC (AFQMC) method is reviewed.
- in Chapter 6, the phaseless AFQMC is extended to the calculation of dynamical properties, and applied to exactly solvable few-fermion systems. It is proved that the methodology provides accurate estimates of ground-state and dynamical properties.
- in Chapter 7, the phaseless AFQMC is used to investigate density fluctuations in medium-sized high-density homogeneous electronic gases. Performance and limitations of the methodology are discussed.
- in Chapter 8, the phaseless AFQMC is used to investigate the electronic band and effective mass of the two-dimensional high-density homogeneous electron gas.

All the methodologies studied in the present thesis (except the Path Integral Ground State and GIFT methods) the have been implemented and constitute two MPI-parallelized Fortran 90 libraries. The thesis is supplemented by Appendices providing details of the theoretical background and calculations, in such a way as to enhance the clarity and reproducibility of the results presented in Chapters 1–8.

CHAPTER 1

Measurable properties of many-body systems

The present chapter provides a brief review of the quantities computed in the remainder of the thesis. Rather than aiming at providing a comprehensive introduction to the properties of many-body systems, it provides the definitions and the notations used in the following chapters. The interested reader is deferred to the rich body of literature on this topic, e.g. [4, 5, 6] for more detailed descriptions.

1.1 Dynamic properties

1.1.1 Static response functions

In order to experimentally study the physical properties of a many-body system, it is necessary to act on it with some external probe. This amounts to add to the original Hamiltonian $\hat{H}$ of the system a perturbation $\hat{H}'(t)$, possibly time-dependent, that models the action of the external probe. In a typical and simple situation, $\hat{H}'(t)$ results from the coupling of a set of external time-independent classical fields F_i with some observables $\mathcal{O}_i$ of the system, described by the hermitian operators $\hat{O}_i$:

$$\hat{H}' = \sum_i F_i \hat{O}_i \tag{1.1}$$

Due to the presence of the external perturbation, the expectation values of all observables, including $\mathcal{O}_i$, change accordingly. For a canonical system of N particles at zero temperature, the response to the external fields is measured by the static susceptibilities:

$$\chi_{ij} = \frac{1}{N} \lim_{F \to 0} \frac{\partial \mathcal{O}_i(F)}{\partial F_j} \tag{1.2}$$

where $\mathcal{O}_i(F)$ denotes the ground-state average of $\hat{O}_i$ at the field configuration F:

$$\mathcal{O}_i(F) = \langle \Phi_0(F) | \hat{O}_i | \Phi_0(F) \rangle \tag{1.3}$$

$\Phi_0(F)$ standing for the ground state at the field configuration F. By the Hellmann-Feynman theorem [7, 8]:

$$\mathcal{O}_i(F) = \langle \Phi_0(F) | \partial_{F_i} \hat{H} | \Phi_0(F) \rangle = \frac{\partial}{\partial_{F_i}} \langle \Phi_0(F) | \hat{H} | \Phi_0(F) \rangle = N \frac{\partial \mathcal{E}_N(F)}{\partial_{F_i}} \tag{1.4}$$

where $\mathcal{E}_N(F)$ is the ground-state energy per particle at the field configuration F. Therefore, the static susceptibility χ_{ij} can also be obtained from the ground-state energy per

particle as:

$$\chi_{ij} = \lim_{F\to 0} \frac{\partial^2 \mathcal{E}_N(F)}{\partial F_j \partial F_i} \tag{1.5}$$

1.1.2 Dynamic response functions

The static susceptibilities χ_{ij} provide precious information about the time-independent response of the system to an external field. However, when the perturbation $\hat{H}'(t)$ is time-dependent, it can induce spectral transitions providing further information about the excited states. In principle, the study of such transitions requires the solution of the real-time Schrödinger equation in presence of a the time-dependent Hamiltonian $\hat{H}(t) = \hat{H} + \hat{H}'(t)$. The calculation of dynamical properties requires, in principle, methodologies having access to to the real-time evolution of a many-body system [9, 10, 11]. However, if the interaction with the probe is sufficiently weak, the response of the system is completely determined by the eigenvalues and eigenvectors of $\hat{H}$ alone. This is the main result of the linear response theory, briefly reviewed in the forthcoming Subsection. In the present thesis, dynamical properties of Bose and Fermi systems have been computed within the linear response theory.

1.1.3 Linear response theory

Consider a many-body system at equilibrium at $T = 0$ under the action of the Hamiltonian $\hat{H}$ and suppose that, at time $t = 0$, a perturbation of the form:

$$\hat{H}'(t) = \sum_i F_i(t)\hat{O}_i^\dagger \tag{1.6}$$

is turned on, where $F_i(t)$ are now time-dependent input fields and the operators $\hat{O}_i$ are possibly non-hermitian. For $t > 0$ the state of the system is:

$$\hat{\rho}(t) = \hat{U}(t)|\Phi_0\rangle\langle\Phi_0|\hat{U}^\dagger(t) \tag{1.7}$$

where the evolution operator, written in the interaction picture, is:

$$\hat{U}(t) = \sum_{n=0}^{\infty} \left(-\frac{i}{\hbar}\right)^n \int_0^t dt_1 \ldots \int_0^{t_{n-1}} dt_n \, \hat{H}'(t_1)\ldots\hat{H}'(t_n) \tag{1.8}$$

The average of $\mathcal{O}_i$ over the perturbed state (1.7) is:

$$\mathcal{O}_i(t) = \mathrm{Tr}\left[\hat{\rho}(t)\hat{O}_i(t)\right] = \langle\Phi_0|\hat{U}^\dagger(t)\hat{O}_i(t)\hat{U}(t)|\Phi_0\rangle \tag{1.9}$$

The linear response approximation amounts to truncating the evolution operator (1.8) and the average (1.9) to first order in the interaction Hamiltonian (1.6):

$$\mathcal{O}_i(t) \simeq \mathcal{O}_i(0) + \frac{1}{\hbar}\int_{-\infty}^{\infty} dt' \sum_j F_j(t')\,\chi_{ij}(t-t') \tag{1.10}$$

where:

$$\chi_{ij}(t) = -i\,\Theta(t)\,\langle\Phi_0|\left[\hat{O}_i(t), \hat{O}_j^\dagger\right]|\Phi_0\rangle \qquad \hat{O}_i(t) = e^{\frac{it}{\hbar}\hat{H}}\hat{O}_i e^{-\frac{it}{\hbar}\hat{H}} \tag{1.11}$$

is called time-dependent susceptivity or real-time correlation function of $\hat{O}_i$ and $\hat{O}_j$. Real-time correlation functions are archetypal examples of dynamic properties, that the system exhibits when driven out of equilibrium by the action of a time-dependent external probe.

It proves very useful to express (1.11) in the Källén-Lehmann representation [12, 13]:

$$\chi_{ij}(t) = -i\,\Theta(t)\,\sum_n e^{-i\omega_n t} O_{i,0n} O^*_{j,0n} - e^{i\omega_n t} O_{i,n0} O^*_{j,n0} \tag{1.12}$$

where $\{\epsilon_n, \Phi_n\}_{n\geq 0}$ are the eigenvalues and eigenvectors of the unperturbed Hamiltonian $\hat{H}$, $O_{i,mn} = \langle \Phi_m | \hat{O}_i | \Phi_n \rangle$ and $\hbar\omega_n = \epsilon_n - \epsilon_0$. Using the Källén-Lehmann representation (1.12) and recalling that the Fourier transform of the Heaviside theta function $\Theta(t)$ is:

$$\tilde{\Theta}(\omega) = \lim_{\eta\to 0^+} \int dt\, e^{i\omega t} e^{-\eta t} \Theta(t) = \lim_{\eta\to 0^+} \frac{1}{\eta - i\omega} = \pi\delta + i\pi\mathcal{P}\left(\frac{1}{\omega}\right) \tag{1.13}$$

by the Sokhotski–Plemelj theorem [14, 15], $\mathcal{P}$ denoting the Cauchy principal value, we find that the Fourier transform of (1.11) is:

$$\begin{aligned} \tilde{\chi}_{ij}(\omega) = &\sum_n O_{i,0n} O^*_{j,0n} \left(\mathcal{P}\left(\frac{1}{\omega - \omega_n}\right) - i\pi\delta(\omega - \omega_n)\right) - \\ &\sum_n O_{i,n0} O^*_{j,n0} \left(\mathcal{P}\left(\frac{1}{\omega + \omega_n}\right) - i\pi\delta(\omega + \omega_n)\right) \end{aligned} \tag{1.14}$$

The time-dependent susceptivity (1.11) is a causal function, i.e. $\chi_{ij}(t) \equiv 0$ for all $t < 0$, or equivalently $\chi_{ij}(t) = \Theta(t)\,\chi_{ij}(t)$. Its Fourier transform (1.14) therefore satisfies [16] the convolution relation:

$$2\pi\tilde{\chi}_{ij}(\omega) = \int d\omega' \tilde{\Theta}(\omega - \omega')\,\tilde{\chi}_{ij}(\omega') \tag{1.15}$$

whence the Kramers-Krönig relations [17, 18]:

$$\mathrm{Re}\tilde{\chi}_{ij}(\omega) = -\frac{1}{\pi}\mathcal{P}\int d\omega' \frac{\mathrm{Im}\tilde{\chi}_{ij}(\omega')}{\omega - \omega'} \quad , \qquad \mathrm{Im}\tilde{\chi}_{ij}(\omega) = \frac{1}{\pi}\mathcal{P}\int d\omega' \frac{\mathrm{Re}\tilde{\chi}_{ij}(\omega')}{\omega - \omega'} \tag{1.16}$$

immediately follow. Equation (1.16) shows that the real and imaginary parts of $\tilde{\chi}_{ij}(\omega)$ can be computed from each other. As a relevant example, consider a system perturbed with an external potential $V(\mathbf{r}, t)$ coupling to the density $\hat{\rho}(\mathbf{r})$:

$$\hat{H}'(t) = \int d\mathbf{r}\, V(\mathbf{r}, t)\,\hat{\rho}(\mathbf{r}) = \frac{1}{\Omega}\sum_{\mathbf{q}} V_{\mathbf{q}}(t)\,\hat{\rho}_{-\mathbf{q}} \tag{1.17}$$

where Ω is the volume of the system and, in the last passage, we have moved to the Fourier space and introduced the density fluctuation operator:

$$\hat{\rho}_{\mathbf{q}} = \sum_{i=1}^{N} e^{i\mathbf{q}\cdot\hat{\mathbf{r}}_i} \tag{1.18}$$

The mean value of the density at time t can then be computed using the density-density

response function:

$$\chi(\mathbf{q},t) = \frac{1}{\hbar\Omega}\,\chi_{\rho_{\mathbf{q}},\rho_{-\mathbf{q}}}(\mathbf{q},t) = -\frac{i}{\hbar\Omega}\,\Theta(t)\,\langle\Phi_0|\,[\hat{\rho}_{\mathbf{q}}(t),\hat{\rho}_{-\mathbf{q}}]\,|\Phi_0\rangle \tag{1.19}$$

1.1.4 Dynamic structure factors.

A typical situation in which dynamical properties are measured is represented by scattering experiments, schematized in Figure 1.1. The system, at equilibrium at $T = 0$, is impinged with a beam of particles (typically photons or neutrons) having initial momentum $\hbar\mathbf{k}_i$ and energy $\hbar\omega_i$. Due to the interaction with the system, the impinging particles are scattered to a final momentum $\hbar\mathbf{k}_f$ and energy $\hbar\omega_f$, possibly different from the initial ones.

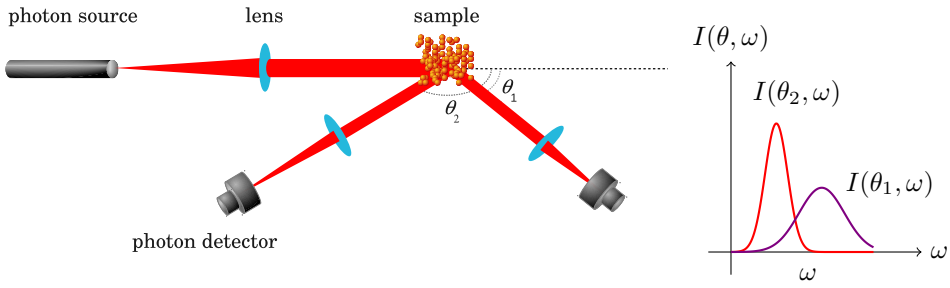

(a) (b)

Figure 1.1: (a) Pictorial representation of the scattering of electromagnetic radiation on a charged system. The incident photons radiation is prepared with momentum $\hbar\mathbf{k}_i$ and energy $\hbar\omega_i$. The interaction with the system provoques density fluctuations with momentum $\hbar\mathbf{q}$ and energy $\hbar\omega$, which scatter the incident photons to $\mathbf{k}_f = \mathbf{k}_i - \mathbf{q}$ and energy $\omega_f = \omega_i - \omega$. (b) The observed intensity $I(\theta,\omega)$ is related to the dynamical structure factor $S(\mathbf{q},\omega)$ of the system.

Fermi's golden rule [19] yields the following estimate:

$$p_{|\mu_i,\Phi_0\rangle\to|\mu_f,\Phi_n\rangle} = \frac{2\pi}{\hbar}\,|\,\langle\mu_i;\Phi_0|\hat{H}'|\mu_f,\Phi_n\rangle\,|^2\,\delta(\epsilon_n + \hbar\omega_f - \epsilon_0 - \hbar\omega_i) \tag{1.20}$$

for the transition probability from an initial state $|\mu_i,\Phi_0\rangle$, where $\mu_i = (\mathbf{k}_i,\sigma_i)$ and σ_i takes into account the internal degrees of freedom (spin, polarization) of the probe particles, to a final state $|\mu_f,\Phi_n\rangle$. Notice that the state $|\mu_i\rangle$ can be written as:

$$\langle\mathbf{r},\omega|\mu_i\rangle = \chi_{\sigma_i}(\omega)\,\frac{e^{i\mathbf{k}_i\cdot\mathbf{r}}}{\sqrt{\Omega}} \tag{1.21}$$

where $\chi_{\sigma_i}(\omega)$ is some internal wavefunction. If the interaction Hamiltonian has the form

$\hat{H}' = \sum_i \hat{F}_i \otimes \hat{O}_i^\dagger$, then:

$$p_{\mu_i \to \mu_f} = 2\pi \sum_{ij} \langle \mu_i | \hat{F}_i^\dagger | \mu_f \rangle \langle \mu_f | \hat{F}_j | \mu_i \rangle \; S_{ij}(\omega) \tag{1.22}$$

where $\omega = \omega_i - \omega_f$, and:

$$S_{ij}(\omega) = \sum_n O_{i,0n} O^*_{j,0n} \delta(\omega - \omega_n) = \int_{-\infty}^{\infty} \frac{e^{i\omega t}}{2\pi} \langle \Phi_0 | \hat{O}_i(t) \hat{O}_j^\dagger | \Phi_0 \rangle \tag{1.23}$$

is the dynamical structure factor (DSF) of the operators $\hat{O}_i, \hat{O}_j$. The differential cross section of the scattering process is readily found given (1.22) [20, 21]. As a relevant example, consider the scattering of thermal neutrons on liquid Helium, described by the interaction Hamiltonian:

$$\hat{H}' = \sum_{i=1}^{N} V(\mathbf{r} - \mathbf{r}_i) = \sum_{i=1}^{N} \sum_{\mathbf{q}} V_{\mathbf{q}} \frac{e^{i\mathbf{q}\cdot(\mathbf{r} - \hat{\mathbf{r}}_i)}}{\Omega} = \sum_{\mathbf{q}} \frac{V_{\mathbf{q}}}{\Omega} e^{i\mathbf{q}\cdot\mathbf{r}} \hat{\rho}_{-\mathbf{q}} \qquad V_{\mathbf{q}} = \int e^{-i\mathbf{q}\cdot\mathbf{r}} \, V(\mathbf{r}) \tag{1.24}$$

The transition probability takes the form:

$$p_{\mu_i \to \mu_f} = 2\pi \frac{2|V_{\mathbf{q}}|^2}{\Omega^2} N S(\mathbf{q}, \omega) \tag{1.25}$$

where $\mathbf{q} = \mathbf{k}_i - \mathbf{k}_f$ and $\omega = \omega_i - \omega_f$ are the wavevector and frequency transferred to the system, the factor 2 takes into account the neutron spin, and:

$$S(\mathbf{q}, \omega) = \frac{1}{N} \int_{-\infty}^{\infty} \frac{e^{i\omega t}}{2\pi} \langle \Phi_0 | \hat{\rho}_{\mathbf{q}}(t) \hat{\rho}_{-\mathbf{q}} | \Phi_0 \rangle \quad , \qquad \mathbf{q} \neq \mathbf{0} \tag{1.26}$$

The differential cross section is proportional to the dynamical structure factor, the proportionality constant being a funcion $F(\mathbf{k}_i, \mathbf{q})$ that takes into account the initial wavevector $\mathbf{k}_i$, the transferred wavevector $\mathbf{q}$, the strength g of the interaction and the density of final states.

As an interesting observation, we remark that dynamical structure factors are related to real-time correlation functions by the fluctuation-dissipation theorem [22, 23, 24], which at zero temperature takes the form:

$$-\pi \, S_{ij}(\omega) = \Theta(\omega) \, \mathrm{Im} \left(\tilde{\chi}_{ij}(\omega) \right) \tag{1.27}$$

readily obtained comparing the Källén-Lehmann representations (1.14) and (1.23).

1.1.5 Imaginary-time correlation functions

The calculation of dynamical properties requires, in principle, methodologies having access to to the real-time evolution of a many-body system. Recent times have witnessed the elaboration of dedicated QMC methods giving such possibility [9, 10, 11] but, as thoroughly discussed in Chapter 3, many well-estabilshed QMC methods do not have access to the real-time evolution.

Within such methods, however, it is possible to compute dynamical structure factors and time-dependent susceptivities exploiting the strong relationship between those quanti-

ties and imaginary-time correlation functions (ITCFs):

$$F_{ij}(\tau) = \langle \Phi_0 | \hat{O}_i(\tau) \hat{O}_j | \Phi_0 \rangle \qquad \tau \geq 0 \quad , \quad \hat{O}_i(\tau) = e^{\frac{\tau}{\hbar}\hat{H}} \hat{O}_i e^{-\frac{\tau}{\hbar}\hat{H}} \tag{1.28}$$

These objects are constructed with the imaginary-time evolution operator, which lies at the basis of many QMC methods. Moreover, as the Källén-Lehmann representation:

$$F_{ij}(\tau) = \sum_n O_{i,0n} O^*_{j,0n} \, e^{-\tau \omega_n} \tag{1.29}$$

makes evident, the energy-resolved structure factor $S_{ij}(\omega)$ is the Laplace transform of the ITCF $F_{ij}(\tau)$:

$$F_{ij}(\tau) = \int_0^\infty e^{-\tau\omega} \, S_{ij}(\omega) \tag{1.30}$$

For instance, the DSF (1.26) is the Laplace transform of the imaginary-time density-density correlation function:

$$F(\mathbf{q}, \omega) = \frac{1}{N} \int_0^\infty \langle \Phi_0 | \hat{\rho}_{\mathbf{q}}(\tau) \hat{\rho}_{-\mathbf{q}} | \Phi_0 \rangle \tag{1.31}$$

1.2 Static properties

In the present thesis, the calculation of dynamic properties has been accompanied and benchmarked to the calculation of static properties, i.e. those shown by the system at equilibrium. For a canonical system of N particles at zero temperature, if the Hamiltonian $\hat{H}$ has a non-degenerate ground state Φ_0, a static property $\mathcal{O}$ is computed as the average:

$$\mathcal{O} = \frac{\langle \Phi_0 | \hat{O} | \Phi_0 \rangle}{\langle \Phi_0 | \Phi_0 \rangle} \tag{1.32}$$

of a suitable hermitian operator $\hat{O}$ over the ground-state wavefunction Φ_0. The static properties computed in the present thesis are briefly presented below, highlighting their connection to dynamic properties.

1.2.1 Ground-state energy per particle.

A static property of fundamental importance, under both the theoretical and the experimental point of view, is the ground-state energy per particle:

$$\mathcal{E}_N = \frac{1}{N} \frac{\langle \Phi_0 | \hat{H} | \Phi_0 \rangle}{\langle \Phi_0 | \Phi_0 \rangle} \tag{1.33}$$

The calculation of the ground-state energy per particle gives access to the equation of state of the system, i.e. the functional relationship between $\mathcal{E}_N$ and state variables like density and spin polarization. Knowledge of the ground-state energy per particle permits to compute quantities of great interest in thermodynamics, like the compressibility:

$$\kappa^{-1} = \rho \frac{\partial}{\partial \rho} \left(\rho^2 \mathcal{E}_N(\rho) \right) \tag{1.34}$$

and the chemical potential:

$$\mu = \mathcal{E}_{N+1} - \mathcal{E}_N \tag{1.35}$$

Equation (1.33) is well-defined and numerically computable for a system of finite and fixed number of particles N and volume Ω. In order to be independent of the specific N, Ω used in calculating static properties, it is understood that the thermodynamic limit of very large system size, i.e. $N, \Omega \to \infty$ with $\rho = \frac{N}{\Omega}$ kept fixed, of (1.33) should be taken. Equation (1.5) shows that the calculation of (1.33) in presence of a time-independent perturbation leads to the static susceptibility χ_{ij}.

1.2.2 One-body density matrix and momentum distribution.

The ground-state wavefunction Φ_0 contains all information about a many-body system at equilibrium at $T = 0$. An equivalent description is obviously provided by the N-body density matrix:

$$\rho_N(\mathbf{x}_1 \dots \mathbf{x}_N; \mathbf{x}'_1 \dots \mathbf{x}'_N) = \Phi_0(\mathbf{x}_1 \dots \mathbf{x}_N)\Phi_0^*(\mathbf{x}'_1 \dots \mathbf{x}'_N) \tag{1.36}$$

where $\mathbf{x}$ is understood as a combined space-spin coordinate $\mathbf{x} = (\mathbf{r}, \sigma)$ and:

$$\int d\mathbf{x}\, f(\mathbf{x}) = \sum_\sigma \int d\mathbf{r}\, f(\mathbf{r}, \sigma) \tag{1.37}$$

The N-body density matrix is the ground-state average of the operator:

$$\hat{\rho}_N(\mathbf{x}_1 \dots \mathbf{x}_N; \mathbf{x}'_1 \dots \mathbf{x}'_N) = \frac{1}{N!}\, \hat{\psi}^\dagger(\mathbf{x}'_N) \dots \hat{\psi}^\dagger(\mathbf{x}'_1)\hat{\psi}(\mathbf{x}_1) \dots \hat{\psi}(\mathbf{x}_N) \tag{1.38}$$

where the field operator $\hat{\psi}(\mathbf{x}) = \hat{\psi}_\sigma(\mathbf{r})$ destroys a particle with spin σ at the position $\mathbf{r}$. From the N-body density matrix, one can construct the p-body density matrix:

$$\rho_p(\mathbf{x}_1 \dots \mathbf{x}_p; \mathbf{x}'_1 \dots \mathbf{x}'_p) = \binom{N}{p} \int d\mathbf{x}_{p+1} \dots d\mathbf{x}_N \Phi_0(\mathbf{x}_1 \dots \mathbf{x}_N)\Phi_0^*(\mathbf{x}'_1 \dots \mathbf{x}'_p \mathbf{x}_{p+1} \dots \mathbf{x}_N) \tag{1.39}$$

which is the ground-state average of the operator:

$$\hat{\rho}_p(\mathbf{x}_1 \dots \mathbf{x}_p; \mathbf{x}'_1 \dots \mathbf{x}'_p) = \frac{1}{p!}\, \hat{\psi}^\dagger(\mathbf{x}'_p) \dots \hat{\psi}^\dagger(\mathbf{x}'_1)\hat{\psi}(\mathbf{x}_1) \dots \hat{\psi}(\mathbf{x}_p) \tag{1.40}$$

Reduced density matrices are relevant quantities for the description of a many-body system, because the most interesting static properties (e.g. total, kinetic and potential energy) are described by one-body and two-body hermitian operators:

$$\begin{aligned} \hat{O}_1 &= \int d\mathbf{x} d\mathbf{x}'\, O(\mathbf{x}', \mathbf{x})\, \hat{\psi}^\dagger(\mathbf{x}')\hat{\psi}(\mathbf{x}) \\ \hat{O}_2 &= \frac{1}{2} \int d\mathbf{x}_1 d\mathbf{x}_2 d\mathbf{x}'_1 d\mathbf{x}'_2\, O(\mathbf{x}'_1, \mathbf{x}'_2; \mathbf{x}_1, \mathbf{x}_2)\, \hat{\psi}^\dagger(\mathbf{x}'_2)\hat{\psi}^\dagger(\mathbf{x}'_1)\hat{\psi}(\mathbf{x}_1)\hat{\psi}(\mathbf{x}_2) \end{aligned} \tag{1.41}$$

The ground-state averages of (1.41) are completely determined by the one-body and two-body density matrices (OBDM,TBDM). In fact:

$$\begin{aligned}\mathcal{O}_1 &= \int d\mathbf{x}d\mathbf{x}'\, O(\mathbf{x}',\mathbf{x})\,\rho_1(\mathbf{x},\mathbf{x}') \\ \mathcal{O}_2 &= \int d\mathbf{x}_1 d\mathbf{x}_2 d\mathbf{x}_1' d\mathbf{x}_2'\, O(\mathbf{x}_1',\mathbf{x}_2';\mathbf{x}_1,\mathbf{x}_2)\,\rho_2(\mathbf{x}_1,\mathbf{x}_2;\mathbf{x}_1',\mathbf{x}_2')\end{aligned} \tag{1.42}$$

Any other information present in the ground-state wavefunction is thus irrelevant for the study of observables described by one-body and two-body operators [25].

Diagonalizing the OBDM yields:

$$\rho_1(\mathbf{x},\mathbf{x}') = \sum_i n_i\,\varphi_i(\mathbf{x})\varphi_i^*(\mathbf{x}') \tag{1.43}$$

where the basis $\{\varphi_i(\mathbf{x})\}_i$ for the single-particle Hilbert space is constituted by the eigenfunctions of the OBDM, called natural orbitals. Defining the creation and destruction operators relative to the natural orbitals as:

$$\hat{a}_i^\dagger = \int d\mathbf{x}\,\varphi_i(\mathbf{x})\,\hat{\psi}^\dagger(\mathbf{x}) \tag{1.44}$$

we readily find that n_i is the occupation number of the natural orbital $\varphi_i(\mathbf{x})$:

$$n_i = \langle\Phi_0|\hat{a}_i^\dagger\hat{a}_i|\Phi_0\rangle \tag{1.45}$$

Equation (1.45) implies that $n_i \geq 0$, $\sum_i n_i = N$. The OBDM and TBDM not only permit to compute the ground-state averages of one-body and two-body operators, but have proved objects of fundamental importance for characterizing the properties of interacting many-body systems. For instance, the existence of one or more macroscopic occupation numbers has been proposed by O. Penrose and L. Onsager [26] as a criterion for Bose-Einstein condensation. For a fermion system (where the OBDM cannot exhibit macroscopic eigenvalues due to the Pauli exclusion principle) a criterion for Cooper pairing is the existence of macroscopic eigenvalues in the reduced two-body density matrix [27]. Moreover, in recent years the Rényi entropies [28]:

$$S_\alpha(\rho_p) = \frac{1}{1-\alpha}\mathrm{Tr}\left[\rho_p^\alpha\right]\ \alpha \geq 0\,,\ \alpha \neq 1 \tag{1.46}$$

of the reduced p-body density matrices have been proposed [29, 30, 31] as measures of the entanglement between the particles constituting the system.

As a useful remark, we notice that in homogeneous systems, under the periodic boundary conditions discussed in Appendix 13.1, the natural orbitals are spin-definite plane waves:

$$i = (\mathbf{k},\sigma) \qquad \varphi_{\mathbf{k},\sigma}(\mathbf{r},\omega) = \chi_\sigma(\omega)\,\frac{e^{i\mathbf{k}\cdot\mathbf{r}}}{\sqrt{\Omega}} \tag{1.47}$$

and the occupation numbers $n_{\mathbf{k},\sigma}$ constitute the spin-resolved momentum distribution. $n_{\mathbf{k},\sigma}$ completely determines the ground-state average of observables $\mathcal{O}$ which are diagonal in the momentum space like the kinetic energy, whose ground-state average reads:

$$\mathcal{T} = \sum_{\sigma} \sum_{k} \frac{\hbar^2 |\mathbf{k}|^2}{2m} n_{\mathbf{k},\sigma} \tag{1.48}$$

1.2.3 Pair distribution function and static structure factor.

Detailed information on the structure of a many-body system can be obtained from several static distribution functions, including the very important pair distribution function:

$$g(\mathbf{r}_1, \mathbf{r}_2) = \frac{p_2(\mathbf{r}_1, \mathbf{r}_2)}{p_1(\mathbf{r}_1) p_1(\mathbf{r}_2)} \tag{1.49}$$

which is equal to the probability of finding a particle at $\mathbf{r}_1$ provided there is another particle at $\mathbf{r}_2$. In fact, in (1.49):

$$p_1(\mathbf{r}_1) = \sum_{\sigma_1} \rho_1(\mathbf{r}_1 \sigma_1; \mathbf{r}_1 \sigma_1) \tag{1.50}$$

denotes the probability distribution for the localization of a particle at $\mathbf{r}_1$, and:

$$p_2(\mathbf{r}_1; \mathbf{r}_2) = \sum_{\sigma_1 \sigma_2} \rho_1(\mathbf{r}_1 \sigma_1 \mathbf{r}_2 \sigma_2; \mathbf{r}_1 \sigma_1 \mathbf{r}_2 \sigma_2) \tag{1.51}$$

is the probability distribution for the localization of two particles at $\mathbf{r}_1, \mathbf{r}_2$.
For a homogeneous and isotropic system, $\rho_1(\mathbf{r}_1) \equiv \rho$ and $g(\mathbf{r}_1, \mathbf{r}_2)$ depends on the positions $\mathbf{r}_1, \mathbf{r}_2$ only through the distance $r_{12} = |\mathbf{r}_1 - \mathbf{r}_2|$. In such case, $g(\mathbf{r}_1, \mathbf{r}_2)$ is denoted $g(r)$ and usually called the radial distribution function. From the knowledge of $g(r)$, it is possible to analyze the local microstructure of the system and also calculate macroscopic thermodynamic properties [32, 33].
As an useful observation, we note that $\rho\, g(r)$ is equal to the average density of particles at distance r from a given one. In fact, the integral of the radial distribution over the system volume is:

$$\rho \int d\mathbf{r} g(r) = (N - 1) \tag{1.52}$$

The radial distribution function is related to the static structure factor:

$$S(\mathbf{q}) = \frac{1}{N} \left(\langle \Phi_0 | \hat{\rho}_{\mathbf{q}} \hat{\rho}_{-\mathbf{q}} | \Phi_0 \rangle - |\langle \Phi_0 | \hat{\rho}_{\mathbf{q}} | \Phi_0 \rangle|^2 \right) \tag{1.53}$$

of the system by the following equation:

$$\begin{aligned} S(\mathbf{q}) &= \frac{1}{N} \sum_{ij} \langle \Phi_0 | e^{i\mathbf{q}\cdot(\hat{\mathbf{r}}_i - \hat{\mathbf{r}}_j)} | \Phi_0 \rangle - N\, \delta_{\mathbf{q},\mathbf{0}} = \\ &= 1 + (N-1) \int d\mathbf{r}\, d\mathbf{r}'\, e^{i\mathbf{q}\cdot(\mathbf{r}-\mathbf{r}')} p_2(\mathbf{r}, \mathbf{r}') - N\, \delta_{\mathbf{q},\mathbf{0}} \end{aligned} \tag{1.54}$$

having recalled that $\langle \Phi_0 | \hat{\rho}_{\mathbf{q}} | \Phi_0 \rangle = N\, \delta_{\mathbf{q},\mathbf{0}}$. Indeed if the ground state is an eigenvector of the momentum operator $\hat{\mathbf{P}} = -i\hbar \sum_{i=1}^{N} \partial_{\mathbf{r}_i}$ with eigenvalue $\mathbf{0}$ (as for instance in translationally invariant systems), thanks to the equality $[\hat{\mathbf{P}}, \hat{\rho}_{\mathbf{q}}] = \mathbf{q}\, \hat{\rho}_{\mathbf{q}}$ the state $\hat{\rho}_{\mathbf{q}} \Phi_0$ is an eigenvector of the momentum operator with eigenvalue $\hbar\mathbf{q}$. The two states are orthogonal unless $\mathbf{q} = \mathbf{0}$ and, in such case, they coincide. For a homogeneous system, (1.54)

takes the form:

$$S(\mathbf{q}) = 1 + \rho \int d\mathbf{r}\, e^{i\mathbf{q}\cdot\mathbf{r}}\ (g(r) - 1) \tag{1.55}$$

having recalled that $\int d\mathbf{r}\, e^{i\mathbf{q}\cdot\mathbf{r}} = \Omega\, \delta_{\mathbf{q},\mathbf{0}}$. $S(\mathbf{q})$ is a quantity directly measurable in the scattering experiments illustrated in Subsection 1.1. Indeed, for $\mathbf{q} \neq \mathbf{0}$ the static structure factor is the integral of the DSF $S(\mathbf{q}, \omega)$ over the frequency ω:

$$\int d\omega S(\mathbf{q},\omega) = \int d\omega \int dt \frac{e^{i\omega t}}{2\pi} \langle \Phi_0 | \hat{\rho}_{\mathbf{q}}(t) \hat{\rho}_{-\mathbf{q}} | \Phi_0 \rangle = \int dt \delta(t) \langle \Phi_0 | \hat{\rho}_{\mathbf{q}}(t) \hat{\rho}_{-\mathbf{q}} | \Phi_0 \rangle = S(\mathbf{q}) \tag{1.56}$$

Like the ground-state energy, (1.39), (1.49) and (1.55) are defined for a system of N particles inside a region of volume Ω. In order to be independent of the specific N, Ω used in the calculation, the thermodynamic limit should be taken.

CHAPTER 2

The Variational Monte Carlo method

In the present Chapter, the Variational Monte Carlo method (VMC) is introduced. It is used to compute expectation values of quantum mechanical operators on a given trial wavefunction. The VMC method is commonly used in conjunction with optimization methods, used to find the the best approximation to the actual ground state of the system under study within a given family. The recent work [34] about the optimization of Jastrow-Feenberg and backflow correlations within the Linear Method by J. Toulouse and C. J. Umrigar [35] is presented in Section 2.4.

2.1 Introduction

Monte Carlo methods are a vast class of computational algorithms [36] that represent the solution x of a deterministic problem as the expectation of a random variable X with finite variance $\sigma_X^2 < \infty$. Monte Carlo methods provide an estimate for x by sampling a large number n of independent random variables $(X_1 \dots X_n)$, identically distributed as X, and computing the sample mean:

$$M_n = \frac{1}{n}\sum_{i=1}^{n} X_i \tag{2.1}$$

The effectiveness of Monte Carlo methods relies on the Central Limit theorem [37], ensuring that the sample mean (2.1) is asymptotically normal:

$$\sqrt{n}\,(M_n - x) \xrightarrow{d} \mathcal{N}(0, \sigma_X^2) \tag{2.2}$$

independent of the distribution of X. This circumstance implies that x lies within the confidence interval:

$$\left[M_n - \phi_\epsilon \frac{S_n}{\sqrt{n}}, M_n + \phi_\epsilon \frac{S_n}{\sqrt{n}}\right] \tag{2.3}$$

with probability $1 - \epsilon$, S_n being the sample variance:

$$S_n = \frac{1}{n-1}\sum_{i=1}^{n} (X_i - M)^2 \tag{2.4}$$

and ϕ_ϵ the $(1-\epsilon)$-quantile of the standard normal distribution. Since, by the strong law of large numbers, $S_n \xrightarrow{a.s.} \sigma_X^2 < \infty$, the confidence interval (2.3) gets more and more narrow as the number of samples increases, thus ensuring a more and more precise determination of x. For Monte Carlo methods to represent an adequate approach to the

determination of x it is evident, from these considerations, that the following requirements should be fulfilled:

1. the random variable X should have expectation $E[X] = x$.
2. the sampling of the random variables X_i should be performed efficiently.
3. the random variable X should have small variance.

The misfulfilment of condition (1) biases the the Monte Carlo method towards an incorrect result, and that of conditions (2) and (3) determines unacceptably long calculation times.

2.2 Monte Carlo Integration

The first precise and persuasive motivation for employing Monte Carlo methods was provided by the problem of evaluating a definite multiple integral:

$$I = \int_{\Omega \subset \mathbb{R}^n} d^n x \, f(\mathbf{x}) \tag{2.5}$$

Integrals of the form (2.5) systematically appear in Physics-related problems involving a large number of coupled degrees of freedom (e.g. classical and quantum systems of many interacting particles). The problem of evaluating them is often not amenable of a closed-form solution, and cannot be addressed with a numerical integration algorithm since this would require a number of operations growing exponentially with n. Without loss of generality, (2.5) can be expressed as:

$$I = \int_{\Omega} d^n x \, p(\mathbf{x}) \, g(\mathbf{x}) \tag{2.6}$$

for some non-negative function $p(\mathbf{x}) \geq 0$ such that $\int_\Omega d^n x \, p(\mathbf{x}) = 1$, and clearly identified as the mean value of the random variable $g(X)$, where X has law $p(\mathbf{x})$. The integral (2.6) can be therefore estimated as:

$$I_m = \frac{1}{m} \sum_{i=1}^{m} g(X_i) \tag{2.7}$$

2.2.1 Importance Sampling

The possibility of using (2.7) to estimate I is conditioned to the requirements listed in the previous paragraph. It is obvious from (2.6) that the estimator (2.7) has the desired expectation $E[I_m] = I$. On the other hand, as far as the variance is concerned, we find:

$$E[I_m^2] - E[I_m]^2 = \frac{1}{m} \left(\int_{\Omega} d^n x \, p(\mathbf{x}) \, g(\mathbf{x})^2 - I^2 \right) \tag{2.8}$$

Unlike I, the integral appearing in (2.8) depends on the specific representation $f(\mathbf{x}) = p(\mathbf{x}) \, g(\mathbf{x})$ of the integrand $f(\mathbf{x})$. In particular, it can be significantly reduced by choosing a distribution $p(\mathbf{x})$ that concentrates in the regions of Ω where $|f(\mathbf{x})|$ is large. The technique of choosing $p(\mathbf{x})$ in such a way as to reduce the variance (2.8) is an example of importance sampling.

The possibility of using (2.7) to estimate I is also conditioned to the ability of sampling the multi-dimensional probability distribution $p(\mathbf{x})$ efficiently. For some simple probability distributions, direct sampling methods are known: for instance, the uniform distribution can be sampled using suitable pseudorandom number generators [38], and Gaussian probability distributions relying on the Box-Muller transform [39].
The Metropolis-Hastings algorithm [40], [41] permits to draw samples from a probability distribution $p(\mathbf{x})$, by only assuming the ability to compute the value of a function $f(\mathbf{x})$ proportional to $p(\mathbf{x})$. The requirement that $f(\mathbf{x})$ should be merely proportional to $p(\mathbf{x})$, rather than exactly equal to it, makes the Metropolis-Hastings algorithm particularly useful since calculating the necessary normalization factor is often impossible. The Metropolis-Hastings algorithm rests upon a rigorous result of the theory of Markov chains, that will be reviewed in the forthcoming Subsection 2.2.2. In order to maintain the presentation as light as possible, the main results are just mentioned, and their proof is deferred to Appendix 9

2.2.2 The Metropolis-Hastings Algorithm

Let $(\Omega, \mathcal{F}, P)$ be a probability space, and E a set of N elements which, without loss of generality, will be put equal to $\{1 \dots N\}$. A generic random variable $X : \Omega \to E$ is completely and uniquely determined by the discrete probability distribution (or law):

$$\pi_k = P(X = k), \qquad 0 \leq \pi_k \leq 1 \quad \forall\, k \in E, \qquad \sum_{k=1}^{N} \pi_k = 1 \tag{2.9}$$

The set of discrete $\mathcal{S}_E$ laws on E is called the n-simplex: it is the subset of $\mathbb{R}^n$ obtained intersecting the first orthant (i.e. the set of all vectors with nonnegative entries) with the hyperplane consisting of all vectors whose entries sum to 1. $\mathcal{S}_E$ is a closed and bounded subset of $\mathbb{R}^n$ and consequently, by the Heine-Borel theorem, it is compact.
Moreover, let $\mathcal{P}$ be a transition matrix on E i.e. an $n \times n$ matrix with real-valued coefficients, such that:

$$0 \leq \mathcal{P}_{ij} \leq 1 \quad \forall\, i, j \in E, \qquad \sum_{j=1}^{N} \mathcal{P}_{ij} = 1 \quad \forall\, i \in E \tag{2.10}$$

Given a law π_0 on E and a transition matrix $\mathcal{P}$ on E, a homogeneous Markov chain with sample space E, initial law π_0 and transition matrix $\mathcal{P}$ is a family $\{X_n\}_{n=0}^{\infty}$ of random variables $X_n : \Omega \to E$ such that:

1. X_0 has law π_0, i.e. $P(X_0 = k) = (\pi_0)_k$

2. whenever conditional probabilities are well-defined:

$$P(X_{n+1} = j | X_n = i, X_{n-1} = i_{n-1}, \dots, X_0 = i_0) = \mathcal{P}_{ij} \tag{2.11}$$

The requirements (9.15) permit to interpret $\mathcal{P}_{ij}$ as the probability of moving from $i \in E$ to $j \in E$: the second one, in particular, guarantees that the probability of moving from i to any other state is 1.
The initial law and the transition matrix give an exhaustive knowledge of the corresponding homogeneous Markov chain. In fact, the condition (2.11) immediately implies

that the law of X_n is:

$$(\pi_n)_k = \sum_{j=1}^{N} (\pi_0)_j \, (\mathcal{P}^n)_{jk} \tag{2.12}$$

Given a homogeneous Markov chain with sample space E and a law $\pi \in \mathcal{S}_E$, we say that π is invariant provided that:

$$\pi_k = \sum_{j=1}^{N} \pi_j \mathcal{P}_{jk} \tag{2.13}$$

One of the most important properties of Markov chains is that, under certain conditions, they can converge towards a unique invariant law. The Metropolis algorithm, with the purpose of sampling a desired probability distribution π^*, takes advantage of this desirable property to construct a Markov chain having precisely π^* as unique invariant law.

Let us therefore detail the conditions under which a Markov chain converges towards a unique invariant law.

The very important Markov-Kakutani theorem [42, 43] ensures that any homogeneous Markov chain has at least an invariant law.

In principle, to determine the invariant laws of a homogeneous Markov chain, the eigenvalue problem $\pi^* = \pi^* \mathcal{P}$ should be solved. Since that, for large N, that may be a computationally demanding procedure, it is desirable to have a sufficient condition to conclude whether a given law is invariant. A sufficient condition for a law π^* to be invariant is the fulfilment of the following detailed balance condition:

$$\pi_i^* \, \mathcal{P}_{ij} = \pi_j^* \, \mathcal{P}_{ji} \quad , \qquad \forall i, j \in E \tag{2.14}$$

Indeed, if π^* satisfies (2.14), then:

$$\sum_{j=1}^{N} \pi_i^* \, \mathcal{P}_{ij} = \sum_{j=1}^{N} \pi_j^* \, \mathcal{P}_{ji} \tag{2.15}$$

whence:

$$\pi_i^* = \pi_i^* \left(\sum_{j=1}^{N} \mathcal{P}_{ij} \right) = \sum_{j=1}^{N} \pi_j^* \tag{2.16}$$

and π^* is invariant. Of course, the converse implication leading from (2.14) to (2.13) is in general not true. Notice that, unlike the very definition (2.13) of invariant law, (2.14) does not involve a computationally demanding summation over j.

A generic Markov chain has more than one invariant law. The uniqueness of the invariant law holds for the so-called regular Markov chains. A transition matrix $\mathcal{P}$ is irreducibile if for all $i, j \in E$ there exists a number $m = m(i, j)$ of steps in which j can be reached from i, i.e. $\mathcal{P}_{ij}^{(m)} > 0$. $\mathcal{P}$ is regular if there exists a number m of steps in which any state j can be reached from any other state i, i.e. $\mathcal{P}_{ij}^{(m)} > 0$ independently on i, j.

The fundamental Markov's theorem [44, 45] ensures that if a homogeneous Markov chain with regular transition matrix starts at a generic initial law v, it converges exponentially fast to a unique law π^*.

In 1953, N. Metropolis *et al.* [40] proved the possibility of designing an irreducible ho-

mogeneous Markov chain having a desired probability distribution as unique invariant law. This possibility has deep implications in the field of simulations: for instance, the archetipal problem (2.5) of computing a definite integral has already been reduced to that of efficiently sampling a generic probability distribution. The Metropolis theorem provides an algorithmic procedure for efficiently simulating an irreducible Markov chain converging to that probability distribution, and therefore to compute (2.5).
Given a symmetric and irreducible transition matrix, $\mathcal{T}_{ij} = \mathcal{T}_{ji}$, subject to no other restrictions, the Metropolis theorem defines the following transition matrix:

$$\mathcal{P}_{ij} = \begin{cases} \mathcal{T}_{ij} & i \neq j,\ \pi_j \geq \pi_i \\ \mathcal{T}_{ij} \frac{\pi_j}{\pi_i} & i \neq j,\ \pi_j < \pi_i \\ 1 - \sum_{j \neq i} \mathcal{P}_{ij} & i = j \end{cases} \tag{2.17}$$

For all the initial laws v the Markov chain $\{X_n\}_n$ with initial law v and transition matrix $\mathcal{P}$ is regular, and has π as unique invariant law. This result is proved in detail in Appendix 9.
Usually (2.17) is written, for $i \neq j$, in the form:

$$\mathcal{P}_{ij} = \mathcal{T}_{ij}\, \mathcal{A}_{ij} = \mathcal{T}_{ij}\ \min\left(1, \frac{\pi_j}{\pi_i}\right) \tag{2.18}$$

$\mathcal{T}_{ij}$ is a trial move that is accepted or refused depending on the outcome of a Metropolis test controlled by the term $\mathcal{A}_{ij}$. The requirement that $\mathcal{T}$ be symmetric, i.e. $\mathcal{T}_{ij} = \mathcal{T}_{ji}$ for all i, j, can be removed provided that $\mathcal{T}_{ji} > 0$ whenever $\mathcal{T}_{ij} > 0$; in such situation, the Metropolis theorem still holds for the Markov chain:

$$\mathcal{P}_{ij} = \mathcal{T}_{ij}\, \mathcal{A}_{ij} = \min\left(1, \frac{\pi_j\, \mathcal{T}_{ji}}{\pi_i\, \mathcal{T}_{ij}}\right) \quad i \neq j \tag{2.19}$$

where it is meant that $\mathcal{P}_{ij} = 0$ if $\mathcal{T}_{ij} = 0$, whereas $\mathcal{P}_{ii}$ is defined as in (2.17).
The Metropolis theorem translates in the following algorithmic procedure for sampling a desired probability distribution π and computing a definite integral $I = \sum_{x \in E} g(x)\, \pi(x)$:

1. start from m samples $x_1^{(0)} \ldots x_m^{(0)} \in E$ of the initial law v
2. for each sample $x_l^{(k)} \equiv i$:
   - sample a point $j \in E$ from $\mathcal{T}_{ij}$
   - compute $\frac{\pi_j\, \mathcal{T}_{ji}}{\pi_i\, \mathcal{T}_{ij}}$
   - accept the move $i \to j$ with probability $\min\left(1, \frac{\pi_j\, \mathcal{T}_{ji}}{\pi_i\, \mathcal{T}_{ij}}\right)$
3. iterate point (2) until the Markov chain has converged onto π^*
4. after convergence, calculate the partial sum $\overline{I}_k = \frac{1}{m} \sum_{l=1}^{m} g\left(x_l^{(k)}\right)$, $k \geq k_0$
5. the estimate for I is $\frac{1}{n} \sum_{k=k_0}^{k_0+n} \overline{I}_k$ where n is the number of iterations after the Markov chain has converged onto π^*

In principle the transition probability distribution $\mathcal{T}_{ij}$ is only subject to the requirements of Theorem 9.4. Its accurate choice, though, determines the length of the transient after

which the sampled distribution is π^*, the efficiency of the algorithm and the strength of the correlations between a partial sum and the consecutive ones. Qualitatively, small moves determine a high acceptance ratio but intense correlations between consecutive moves; on the other hand, large moves determine modest correlations between consecutive moves but a low acceptance ratio. On empirical basis, a good compromise between such competing issues is obtained with an acceptance ratio around 50%.

2.3 Variational Monte Carlo Method

The Variational Monte Carlo (VMC) is the simplest QMC method. It is used to compute expectation values of quantum mechanical operators on a given trial wavefunction. VMC was first employed by W. L. McMillan [46] to calculate the ground-state properties of liquid ^{4}He and then generalized to fermionic systems by D. M. Ceperley *et al.* [47]. VMC derives its name from Ritz's variational theorem [48], which states that, given a trial wave function $\Psi(\mathcal{R})$, the expectation value of the Hamiltonian over $\Psi(\mathcal{R})$ is an upper bound for the ground-state energy:

Theorem 2.1 (W. Ritz)**.** *Let $\mathcal{H}$ be a separable Hilbert space, $\hat{H}$ a self-adjoint Hamiltonian operator with compact resolvent on $\mathcal{H}$. If the ground state energy of $\hat{H}$ is $\epsilon_0 > -\infty$, the energy functional:*

$$\Psi \mapsto \mathcal{E}(\Psi) = \frac{\langle \Psi | \hat{H} | \Psi \rangle}{\langle \Psi | \Psi \rangle} \tag{2.20}$$

satisfies the inequality $\mathcal{E}(\Psi) \geq \epsilon_0$ for all trial wavefunctions $\Psi \in \mathcal{H}$. Moreover, the equality is attained if and only if $\hat{H} |\Psi\rangle = \epsilon_0 |\Psi\rangle$.

Proof. *Since $\hat{H}$ is a self-adjoint operator with compact resolvent, its spectrum is a discrete subset $\{\epsilon_n\}_{n=0}^{\infty}$ of $\mathbb{R}$, and the set of orthogonal projectors $\{\hat{\Pi}_n\}_{n=0}^{\infty}$ on the eigenspaces of $\hat{H}$ is complete. Therefore:*

$$\hat{H} = \sum_{n=0}^{\infty} \epsilon_n \hat{\Pi}_n \tag{2.21}$$

and for a generic wavefunction $\Psi \in \mathcal{H}$:

$$|\Psi\rangle = \sum_{n=0}^{\infty} \hat{\Pi}_n |\Psi\rangle \tag{2.22}$$

The energy $\mathcal{E}(\Psi)$ therefore admits the following expression:

$$\mathcal{E}(\Psi) = \frac{\sum_{n=0}^{\infty} \epsilon_n \langle \Psi | \hat{\Pi}_n | \Psi \rangle}{\sum_{n=0}^{\infty} \langle \Psi | \hat{\Pi}_n | \Psi \rangle} = \frac{\sum_{n=0}^{\infty} \epsilon_n p_n}{\sum_{n=0}^{\infty} p_n} \tag{2.23}$$

The stationary points of eq. (2.23) *are identified by the condition $\mathcal{E}(\Psi) = \epsilon_m$, which is clearly satisfied if and only if $|\Psi\rangle = \Pi_m |\Psi\rangle$. Among the stationary points of eq.* (2.23)*, the one minimizing the energy corresponds to $\epsilon_0 = \min_m \epsilon_m$.*

It is worth noticing that Theorem 2.1 has been proved under rather conservative assumptions about the nature of the Hamiltonian operator, in order to avoid technical difficulties, but it holds under milder conditions [49, 50, 51].
Given a trial wavefunction $\Psi(\mathcal{R})$, the expectation value of an operator $\hat{O}$ over $\Psi(\mathcal{R})$ can

be expressed as:

$$\mathcal{O}(\Psi) = \frac{\langle\Psi|\hat{O}|\Psi\rangle}{\langle\Psi|\Psi\rangle} = \frac{\int d\mathcal{R}\,\Psi^*(\mathcal{R})\left(\hat{O}\Psi\right)(\mathcal{R})}{\int d\mathcal{R}\,|\Psi(\mathcal{R})|^2} = \int d\mathcal{R}\,O_{L,\Psi}(\mathcal{R})\,\frac{|\Psi(\mathcal{R})|^2}{\int d\mathcal{R}'\,|\Psi(\mathcal{R}')|^2} \tag{2.24}$$

and interpreted as the mean value of the random variable:

$$O_{L,\Psi}(\mathcal{R}) = \frac{\left(\hat{O}\Psi\right)(\mathcal{R})}{\Psi(\mathcal{R})} \tag{2.25}$$

over the probability distribution

$$p(\mathcal{R}) = \frac{|\Psi(\mathcal{R})|^2}{\int d\mathcal{R}'\,|\Psi(\mathcal{R}')|^2} \tag{2.26}$$

In particular, the energy $\mathcal{E}(\Psi)$ is the mean value of the local energy:

$$E_{L,\Psi}(\mathcal{R}) = \frac{\hat{H}\Psi(\mathcal{R})}{\Psi(\mathcal{R})} = -\sum_i \frac{\hbar^2}{2m_i}\frac{\triangle_i\Psi(\mathcal{R})}{\Psi(\mathcal{R})} + \mathcal{V}(\mathcal{R}) \tag{2.27}$$

VMC uses the Metropolis-Hastings algorithm, Theorem 9.4, to sample the probability distribution $p(\mathcal{R})$, and computes $\mathcal{O}(\Psi)$ as sample average of $O_{L,\Psi}(\mathcal{R})$. A possible choice for the transition probability distribution $\mathcal{T}(\mathcal{R}\to\mathcal{R}')$ is a Gaussian function in the configuration space:

$$\mathcal{T}(\mathcal{R}\to\mathcal{R}') = \frac{e^{-\frac{|\mathcal{R}-\mathcal{R}'|^2}{4\delta\tau}}}{(4\pi\delta\tau)^{\frac{dN}{2}}} \tag{2.28}$$

characterized by a positive parameter $\delta\tau$, called VMC time step, that must be calibrated to optimize the acceptance probability (2.19). Due to the symmetry of the transition matrix (2.28), the latter reduces to:

$$\mathcal{A}(\mathcal{R}\to\mathcal{R}') = \min\left(1, \frac{|\Psi(\mathcal{R}')|^2}{|\Psi(\mathcal{R})|^2}\right) \tag{2.29}$$

It is worth noticing that the distribution $|\Psi(\mathcal{R})|^2$ does not have to be normalized since only ratios enter in the acceptance. Therefore, it is possible to sample the square of a complex wavefunction whose normalization is not known.

2.3.1 Slater-Jastrow Wavefunctions

The quality of the trial wavefunction used in a VMC calculation controls its statistical efficiency and limits the final accuracy of its results. The repeated evaluation of the trial wavefunction and of its spatial derivatives is also the most demanding part of the computation. Therefore, trial wavefunctions sholud be both accurate and efficiently computable. To the lowest perturbative order in the interaction Hamiltonian, the ground state of a many-fermion system is the following product of Slater determinants (one per particle type t) of single-particle orbitals:

$$\Psi_S(\mathcal{R}) = \prod_{t=1}^{T} \det\left(\varphi_{t,i}(\mathbf{x}_j)\right) \tag{2.30}$$

where the indexes i, j label particles of type t only. As proved in Appendix 10.1.1, for spin-independent Hamiltonian operators and for the QMC evaluation of spin-independent operators, the single Slater determinant of $\varphi_{t,i}(\mathbf{x}_j)$ can be replaced by a product of determinants (one per spin polarization). That replacement is computationally advantageous because the determinant of the large matrix is replaced by a product of determinants of smaller matrices. With harmless abuse of notation, particles with different spin polarization will be hencefort treated as particles of different types.

The ground state of a many-boson system, on the other hand, is the following product of permanents:

$$\Psi_S(\mathcal{R}) = \prod_{t=1}^{T} \text{perm}\left(\varphi_{t,i}(\mathbf{x}_j)\right) \tag{2.31}$$

Despite the apparent similarity of the definitions of determinant and permanent, the calculation of the latter is notoriously [52] more cumbersome. Fortunately, in the ground state of a spin-independent Hamiltonian, all particles of a given type t occupy the same orbital $\varphi_t(\mathbf{r}_j)$ and (2.31) reduces to:

$$\Psi_S(\mathcal{R}) = \prod_{t=1}^{T} \prod_{j=1}^{N_t} \varphi_t(\mathbf{r}_j) \tag{2.32}$$

The Ansätze (2.30), (2.32) prove quite poor for most applications. Following the proposal of [53, 54, 55], (2.30),(2.32) are multiplied by a symmetric Jastrow factor encompassing two-body and three-body correlations:

$$\Psi_{SJ3B}(\mathcal{R}) = \Psi_S(\mathcal{R})\, e^{-Z_{2B}(\mathcal{R})}\, e^{-Z_{3B}(\mathcal{R})} \tag{2.33}$$

with:

$$\begin{aligned} Z_{2B}(\mathcal{R}) &= \sum_{i<j} u_{ij}(r_{ij}) \\ Z_{3B}(\mathcal{R}) &= \sum_{i<j} \tilde{\xi}_{ij}(r_{ij}) - \frac{1}{2}\sum_{l} \mathbf{G}_l(\mathcal{R}) \cdot \mathbf{G}_l(\mathcal{R}) \end{aligned} \tag{2.34}$$

for some radial functions $u_{ij}(r), \tilde{\xi}_{ij}(r)$ which depend on the types of the particles ij. Notice that two-body and three-body correlations give rise to a roto-translationally invariant wavefunction if and only if these functions are radial. In (2.34) $r_{ij} = |\mathbf{r}_i - \mathbf{r}_j|$ and:

$$\begin{aligned} \mathbf{G}_l(\mathcal{R}) &= \sum_{i \neq l} \xi_{il}(r_{il})\,(\mathbf{r}_l - \mathbf{r}_i) \\ \tilde{\xi}_{ij}(r) &= \xi^2_{ij}(r) r^2 \end{aligned} \tag{2.35}$$

which considerably improves the quality of the wavefunction [46, 56, 57, 58, 59, 60]. For many-fermion ground states and many-boson excited states, the use of Feynman-Cohen backflow correlations [61, 62] has proved to considerably improve the Ansatz (2.33) in homogeneous and molecular systems [56, 60, 63, 64]. The Feynman-Cohen procedure consists in replacing the single-particle orbitals $\varphi_{t,i}(\mathbf{r}_j)$ by functions:

$$\varphi_{t,i}(\mathbf{r}_j) \to \varphi_{t,i}(\mathbf{x}_j) \qquad \mathbf{x}_j = \mathbf{r}_j + \sum_{l \neq j} \eta_{jl}(r_{jl})\,(\mathbf{r}_j - \mathbf{r}_l) \tag{2.36}$$

of the collective coordinates $\mathbf{x}_j$ including hydrodynamic backflow effects.

2.3.2 Theoretical Justification

A key requisite for the development of VMC is the design of an accurate and efficiently computable trial wavefunction $\Psi_T(\mathcal{R})$: this issue requires to incorporate relevant interparticle correlations in the structure of $\Psi_T(\mathcal{R})$. Recent years have witnessed great progress in the theoretical justification and definition of Jastrow-Feenberg and backflow correlations [65, 66] on the basis of the generalized Feynman-Kac formula [67, 68, 69]. In particular, in 2003 M. Holzmann *et al.* [66] have justified and evaluated backflow and three-body correlations for a two-component system of electrons and protons. Very recently, M. Taddei *et al.* [70] have proposed a novel class of correlated trial wavefunctions, based on iterative backflow transformations, and used them to study liquid ^{3}He in two dimensions, observing a systematic lowering of the energy and its variance.
The starting point of the systematic procedure for incorporating interparticle correlations in the functional form of the trial wavefunction is [67, 68, 69, 66] the following observation:

Theorem 2.2. *Let $\mathcal{H}$ be a separable Hilbert space and $\hat{H}$ a self-adjoint Hamiltonian operator with compact resolvent on $\mathcal{H}$. Then, the formal solution $|\Psi_\tau\rangle = e^{-\tau\hat{H}}|\Psi_T\rangle$ of the imaginary-time evolution equation:*

$$-\partial_\tau |\Psi_\tau\rangle = \hat{H}|\Psi_\tau\rangle \tag{2.37}$$

where $|\Psi_T\rangle \in \mathcal{H}$ is a trial state subject to the only constraint that $\hat{\Pi}_0|\Psi_T\rangle \neq 0$, satisfies the following relation:

$$|\Psi_\tau\rangle = e^{-\tau\epsilon_0}\hat{\Pi}_0|\Psi_T\rangle + o\left(e^{-\tau\epsilon_0}\right) \tag{2.38}$$

Proof. *As in the proof of Ritz's variational theorem 2.1, since $\hat{H}$ has compact resolvent its spectrum is a discrete subset $\{\epsilon_n\}_{n=0}^{\infty}$ of $\mathbb{R}$, and the set of orthogonal projectors $\{\hat{\Pi}_n\}_{n=0}^{\infty}$ on the eigenspaces of $\hat{H}$ is complete. Therefore:*

$$|\Psi_T\rangle = \sum_{n=0}^{\infty}\hat{\Pi}_n|\Psi_T\rangle \tag{2.39}$$

and:

$$e^{-\tau\hat{H}}|\Psi_T\rangle = \sum_{n=0}^{\infty}e^{-\tau\epsilon_n}\Pi_n|\Psi_T\rangle = e^{-\tau\epsilon_0}\hat{\Pi}_0|\Psi_T\rangle + e^{-\tau\epsilon_0}\sum_{n=1}^{\infty}e^{-\tau(\epsilon_n-\epsilon_0)}\hat{\Pi}_n|\Psi_T\rangle \tag{2.40}$$

The observation that: $\|\sum_{n=1}^{\infty}e^{-\tau(\epsilon_n-\epsilon_0)}\hat{\Pi}_n|\Psi_T\rangle\|^2 = \sum_{n=1}^{\infty}e^{-2\tau(\epsilon_n-\epsilon_0)}p_n = o(1)$ completes the proof.

Theorem 2.2 states that, given a trial state $|\Psi_T\rangle$, better and better approximations for the exact ground state $|\Phi_0\rangle$ of the system can be produced by projecting $|\Psi_T\rangle$ with the imaginary time evolution operator $e^{-\tau\hat{H}}$. For a system of N particles of T types in dimension d, whose dynamics is governed by the Hamiltonian operator:

$$\left(\hat{H}\Psi\right)(\mathcal{R}) = -\sum_i\frac{\hbar^2}{2m_i}\triangle_i\Psi(\mathcal{R}) + \frac{1}{2}\sum_{j\neq i}v_{ij}(r_{ij})\,\Psi(\mathcal{R}) \tag{2.41}$$

this requires to solve the partial differential equation:

$$-\partial_\tau \Psi_\tau(\mathcal{R}) = -\sum_i \frac{\hbar^2}{2m_i} \triangle_i \Psi_\tau(\mathcal{R}) + \frac{1}{2} \sum_{j \neq i} v_{ij}(r_{ij})\, \Psi_\tau(\mathcal{R}) \tag{2.42}$$

with the initial condition $\Psi_0(\mathcal{R}) = \Psi_T(\mathcal{R})$. For the purpose of the forthcoming discussion, it will prove useful write $\Psi_\tau(\mathcal{R}) = \Psi_T(\mathcal{R}) f_\tau(\mathcal{R})$, thus translating (2.42) in the following partial differential equation for the function $f_\tau(\mathcal{R})$:

$$-\partial_\tau f_\tau(\mathcal{R}) = -\sum_i \frac{\hbar^2}{2m_i} \triangle_i f_\tau(\mathcal{R}) - \sum_{i\alpha} \frac{\hbar^2}{m_i} \frac{\partial_{r_{i\alpha}} \Psi_T(\mathcal{R})}{\Psi_T(\mathcal{R})}\, \partial_{r_{i\alpha}} f_\tau(\mathcal{R}) + E_{L,\Psi_T}(\mathcal{R})\, f_\tau(\mathcal{R}) \tag{2.43}$$

with the initial condition $f_0(\mathcal{R}) = 1$. There exists a deep and truly fascinating relationship between imaginary-time evolution and stochastic processes, taking advantage of which an insight into the properties of $f_\tau(\mathcal{R})$ can be gained. This relationship is captured by the Feynman-Kac formula [71, 72], which we state below and prove in Appendix 9. According to the Feynman-Kac formula, the solution $u(x,t)$ of the parabolic partial differential equation:

$$\begin{cases} -\partial_t u(x,t) + \mathcal{L}_t u(x,t) - V(x) u(x,t) = f(x,t) \quad (x,t) \in \mathbb{R}^n \times (0,T) \\ u(x,0) = \phi(x) \quad x \in \mathbb{R}^n \end{cases} \tag{2.44}$$

where the differential operator $\mathcal{L}_t$ reads:

$$\mathcal{L}_t = \frac{1}{2} \sum_{ij} a_{ij}(x,t) \frac{\partial^2}{\partial x_i \partial x_j} + \sum_i b_i(x,t) \frac{\partial}{\partial x_i} \tag{2.45}$$

can be written as:

$$u(x,T) = E[\phi(X_T) Z_T] - E\left[\int_0^T f(X_t, T-t)\, Z_t dt\right] \tag{2.46}$$

where X_t is the solution of the stochastic differential equation:

$$\begin{aligned} dX_t &= b(X_t,t)\, dt + \sigma(X_t,t)\, dB_t \\ X_0 &= x \end{aligned} \tag{2.47}$$

with $a(x,t) = \sigma(x,t)\, \sigma(x,t)^T$, and:

$$Z_t = e^{-\int_0^t V(X_s) ds} \tag{2.48}$$

is the *path integral* of the function $V(x)$.
The Feynman-Kac formula (2.46) establishes a link between a broad class of parabolic partial differential equations and stochastic processes. In particular, it permits to solve certain partial differential equations by simulating random paths of suitable stochastic processes.
Applying equation (2.46) to the imaginary-time Schrödinger equation (2.43) yields:

$$f_\tau(\mathcal{R}) = E\left[e^{-\int_0^\tau d\tau' E_{L,\Psi_T}(\mathcal{R}_{\tau'})}\right] \tag{2.49}$$

or equivalently:

$$\Psi_\tau(\mathcal{R}) = \Psi_T(\mathcal{R})\, E\left[e^{-\int_0^\tau d\tau'\, E_{L,\Psi_T}(\mathcal{R}_{\tau'})}\right] \tag{2.50}$$

where $\mathcal{R}_\tau$ is the solution of the following drift-diffusion stochastic differential equation:

$$\begin{aligned} d\mathcal{R}_{\tau,i\alpha} &= \frac{\hbar^2}{m_i}\frac{\partial_{r_{i\alpha}}\Psi_T(\mathcal{R}_\tau)}{\Psi_T(\mathcal{R}_\tau)}d\tau + \frac{\hbar^2}{2m_i}dB_\tau \\ \mathcal{R}_0 &= \mathcal{R} \end{aligned} \tag{2.51}$$

In (2.49) and (2.50), $E[\cdot]$ stands for the expectation of the functional $e^{-\int_0^\tau d\tau'\, E_{L,\Psi_T}(\mathcal{R}_{\tau'})}$ over the trajectories of the stochastic process (2.51), and defines the functional integral:

$$\Psi_\tau(\mathcal{R}) = \Psi_T(\mathcal{R}) \int_{\mathcal{C}(0,\tau)} \mathcal{D}[\mathcal{R}_{\tau'}] e^{-\int_0^\tau d\tau' E_{L,\Psi}(\mathcal{R}_{\tau'})} \tag{2.52}$$

where $\mathcal{C}(0,\tau)$ denotes the Wiener space of continuous trajectories starting at imaginary time τ in $\mathcal{R}$, and $\mathcal{D}[\mathcal{R}_{\tau'}]$ the diffusion measure associated with the stochastic process (2.51).

So far, no mention of the symmetry of the wavefunction $\Psi_\tau(\mathcal{R})$ has been made. Since the antisymmetrization (symmetrization) operator $\hat{S}_-$ ($\hat{S}_+$):

$$\left(\hat{S}_\pm \Psi\right)(\mathbf{r}_1 \dots \mathbf{r}_N) = \sum_{\sigma \in S_N} \frac{(\pm 1)^\sigma}{N!} \Psi(\mathbf{r}_{\sigma(1)} \dots \mathbf{r}_{\sigma(N)}) \tag{2.53}$$

commutes with the imaginary-time evolution, a many-fermion (boson) wavefunction is produced applying $\hat{S}_-$ ($\hat{S}_+$) to $\Psi_\tau(\mathcal{R})$.

Equation (2.52) provides a systematic procedure for improving trial wavefunctions used in VMC calculations. Let us choose $\Psi_T(\mathcal{R})$ to be a product of plane waves:

$$\Psi_T(\mathcal{R}) = e^{i\mathbf{k}_1\cdot\mathbf{r}_1} \dots e^{i\mathbf{k}_n\cdot\mathbf{r}_n} \tag{2.54}$$

whose image through $\hat{S}_-$ ($\hat{S}_+$) is the ground state of a non-interacting system, for a suitable choice of the wavevectors $\mathbf{k}_i$. If the imaginary time τ in (2.52) is sufficiently small, the functional integral can be approximated assuming $\mathcal{R}_{\tau'} \simeq \mathcal{R}$, and since:

$$E_{L,\Psi_T}(\mathcal{R}) = \sum_i \frac{\hbar^2 |\mathbf{k}_i|^2}{2m_i} + \frac{1}{2}\sum_{j\neq i} v_{ij}(r_{ij}) \tag{2.55}$$

we obtain the following approximation for $\Psi_{\delta\tau}(\mathcal{R})$:

$$\Psi_{\delta\tau}(\mathcal{R}) \propto \prod_i e^{i\mathbf{k}_i\cdot\mathbf{r}_i}\, e^{-\frac{1}{2}\sum_{j\neq i} u_{ij}^{(\delta\tau)}(r_{ij})} \qquad u_{ij}^{(\delta\tau)}(r_{ij}) = \delta\tau\, v_{ij}(r_{ij}) \tag{2.56}$$

Interestingly, the imaginary-time propagation has brought into stage two-body correlations. The image of $\Psi_{\delta\tau}(\mathcal{R})$ through $\hat{S}_-$ ($\hat{S}_+$) is called a Slater-Jastrow (Jastrow) wavefunction. The approximation (2.56) is quite crude, and should be refined applying at least another propagation step, in which $\Psi_T(\mathcal{R})$ could be substituted with $\Psi_{\delta\tau}(\mathcal{R})$. As before, the functional integral could be approximated assuming $\mathcal{R}_{\tau'} \simeq \mathcal{R}$ but since the

local energy of the wavefunction (2.56) reads:

$$E_{L,\Psi_{\delta\tau}}(\mathcal{R}) = \sum_i \frac{\hbar^2 |\mathbf{k}_i|^2}{2m_i} + \sum_i \frac{\hbar^2 \delta\tau}{2m_i} \sum_{j\neq i} \left(v''_{ij}(r_{ij}) - v'_{ij}(r_{ij}) \frac{d-1}{r_{ij}} \right) +$$
$$+ \sum_i i\,\mathbf{k}_i \cdot \sum_{j\neq i} \frac{\hbar^2 \delta\tau}{2m_i} \left(v'_{ij}(r_{ij}) \frac{\mathbf{r}_i - \mathbf{r}_j}{r_{ij}} \right) - \sum_i \frac{\hbar^2 \delta\tau^2}{2m_i} \left| v'_{ij}(r_{ij}) \frac{\mathbf{r}_i - \mathbf{r}_j}{r_{ij}} \right|^2 + \frac{1}{2} \sum_{i\neq j} v(r_{ij}) \tag{2.57}$$

we are left with the following approximation for $\Psi_{2\delta\tau}(\mathcal{R})$:

$$\Psi_{2\delta\tau}(\mathcal{R}) \propto \prod_i e^{i\mathbf{k}_i \cdot \mathbf{x}_i^{(2\delta\tau)}}\, e^{-\frac{1}{2}\sum_{j\neq i} u_{ij}^{(2\delta\tau)}(r_{ij})} e^{\sum_i \mathbf{G}_i^{(2\delta\tau)} \cdot \mathbf{G}_i^{(2\delta\tau)}} \tag{2.58}$$

where:

$$\mathbf{x}_i^{(2\delta\tau)} = \mathbf{r}_i + \sum_{j\neq i} \eta_{ij}^{(2\delta\tau)}(r_{ij})\,(\mathbf{r}_i - \mathbf{r}_j) \qquad \eta_{ij}^{(2\delta\tau)}(r) = -\frac{\hbar^2 \delta\tau^2}{2m_i} \frac{v'_{ij}(r_{ij})}{r_{ij}}$$

$$u_{ij}^{(2\delta\tau)}(r_{ij}) = \delta\tau\, v_{ij}(r_{ij}) + \left(\frac{\hbar^2 \delta\tau^2}{2m_i} + \frac{\hbar^2 \delta\tau^2}{2m_j} \right) \left(v''_{ij}(r_{ij}) - v'_{ij}(r_{ij}) \frac{d-1}{r_{ij}} \right) \tag{2.59}$$

$$\mathbf{G}_i^{(2\delta\tau)} = \sum_{j\neq i} \xi_{ij}^{(2\delta\tau)}(r_{ij})(\mathbf{r}_i - \mathbf{r}_j) \qquad \xi_{ij}^{(2\delta\tau)}(r_{ij}) = \sqrt{\frac{\hbar^2 \delta\tau^3}{2m_i}}\, \frac{v'_{ij}(r_{ij})}{r_{ij}}$$

A further step of imaginary-time propagation has modified the previously existing two-body correlations, and has brought into stage three-body and backflow correlations. Three-body correlations come from the contribution $\sum_i \mathbf{G}_i^{(2\delta\tau)} \cdot \mathbf{G}_i^{(2\delta\tau)}$ which involves a sum over three distinct particle indexes. Backflow correlations substitute the single-particle coordinates $\mathbf{r}_i$ with the collective quasi-coordinates $\mathbf{x}_i$. The inclusion of backflow correlations is relevant only for fermionic ground states and bosonic excited states (for bosonic ground states, $\mathbf{k}_i = \mathbf{0}$ for all i).
In view of the approximations introduced to produce the Ansatz (2.58), we cannot expect the two-body, three-body and backflow correlation functions $u^{(2\delta\tau)}, \xi^{(2\delta\tau)}, \eta^{(2\delta\tau)}$ in (2.59) to be satisfactory. In fact, while the functional form (2.58) of $\Psi_{2\delta\tau}(\mathcal{R})$ is assumed, the two-body, three-body and backflow correlation functions are chosen relying on suitable optimization procedures.

2.3.3 Shadow wavefunctions

Approximating the action of the imaginary-time evolution operator onto Slater determinants (2.30) or permanents of single-particle orbitals (2.32) leads to Slater-Jastrow wavefunction, which have a fixed and explicit functional form characterized by one or more variational parameters.
Other ways of approximating the imaginary-time evolution lead to other classes of trial wavefunctions. The Shadow Wave Functions (SWF) [73, 74, 75, 76, 77] do not attempt at an explicit functional form, but take into account correlations between more than two

particles by introducing auxiliary variables, called *shadows* and denoted $\mathcal{S}$, and coupling them with the real positions $\mathcal{R}$ of the particles. For a homogeneous system of spinless N bosons, SWFs have the form:

$$\Psi_{SWF}(\mathcal{R}) = \Psi_{J,r}(\mathcal{R}) \int d\mathcal{S}\, \Theta(\mathcal{R},\mathcal{S})\, \Psi_{J,s}(\mathcal{S}) \tag{2.60}$$

where $\mathcal{R} = (\mathbf{r}_1 \dots \mathbf{r}_N)$ denotes the positions of the particles, and $\mathcal{S} = (\mathbf{s}_1 \dots \mathbf{s}_N)$ the shadow auxiliary variables. $\Psi_{J,r}(\mathcal{R}), \Psi_{J,s}(\mathcal{S})$ are Jastrow wavefunctions encompassing two-body correlations, and:

$$\Theta(\mathcal{R},\mathcal{S}) = \prod_{i=1}^{N} e^{-C|\mathbf{r}_i - \mathbf{s}_i|^2} \qquad C \geq 0 \tag{2.61}$$

is a Gaussian kernel that couples real positions and shadow auxiliary variables.
The integration in (2.60) can be regarded to as approximating the action of the imaginary-time evolution operator on the Jastrow wavefunction $\Psi_{J,s}(\mathcal{S})$. The parameters in the Jastrow wavefunction $\Psi_{J,r}(\mathcal{R}), \Psi_{J,s}(\mathcal{S})$ and the width C of the Gaussian kernel are variational parameters, to be optimized in such a way as to approach the exact ground-state wavefunction as much as possible. The integration over the shadow auxiliary variables cannot be carried out explicitly, whence SWFs is given in implicit form only.
SWFs are particularly flexible, and capable of describing both a liquid phase and a solid phase, depending on the form of the real, shadow and real-shadow correlations [76, 73]. SWFs have also been successfully applied to the investigation of excited states of ^{4}He [78, 79, 80, 81].

2.3.4 Details of the VMC algorithm for Slater-Jastrow wavefunctions

In the present Subsection, we describe the calculation of the logarithm, gradient and laplacian of SJ3BB wavefunctions, following the notation of [60]. The present Subsection also introduces the novel results presented in Section 2.4.
The trial wavefunction (2.33),(2.36) has the form:

$$\Psi_T(\mathcal{R}) = e^{-Z(\mathcal{R})} \tag{2.62}$$

The gradient of (2.62) is:

$$\partial_{i\alpha}\Psi_T(\mathcal{R}) = -\partial_{i\alpha}Z(\mathcal{R})\, \Psi_T(\mathcal{R}) \tag{2.63}$$

and the laplacian of (2.62) is readily obtained from:

$$-\partial^2_{i\alpha}\Psi_T(\mathcal{R}) = \left(\partial^2_{i\alpha}Z(\mathcal{R}) - \left(\partial_{i\alpha}Z(\mathcal{R})\right)^2\right)\Psi_T(\mathcal{R}) \tag{2.64}$$

The knowledge of (2.63), (2.64) leads immediately to the local energy (2.27). The contributions to $\partial_{i\alpha}Z(\mathcal{R})$, $\partial^2_{i\alpha}\Psi_T(\mathcal{R})$ coming from two-body, three-body and backflow correlations will be now fully detailed.

Two-body correlations. The gradient of the two-body term $Z_{2B}(\mathcal{R})$ in (2.34) is:

$$\partial_{i\alpha}Z_{2B}(\mathcal{R}) = \sum_{k\neq i} u'_{ik}(r_{ik})\, \frac{r_{ik,\alpha}}{r_{ik}} \tag{2.65}$$

and its laplacian is readily obtained from:

$$\partial^2_{i\alpha} Z_{2B}(\mathcal{R}) = \sum_{k\neq i} u''_{ik}(r_{ik})\,\frac{r^2_{ik,\alpha}}{r^2_{ik}} + \frac{u'_{ik}(r_{ik})}{r_{ik}}\,\frac{r^2_{ik} - r^2_{ik,\alpha}}{r^2_{ik}} \tag{2.66}$$

whence:

$$\sum_\alpha \partial^2_{i\alpha} Z_{2B}(\mathcal{R}) = \sum_{k\neq i} u''_{ik}(r_{ik}) + (d-1)\,\frac{u'_{ik}(r_{ik})}{r_{ik}} \tag{2.67}$$

Three-Body correlations. The three-body term $Z_{3B}(\mathcal{R})$ in (2.34) yields the following contributions to (2.63), (2.64):

$$\partial_{i\alpha} Z_3(\mathcal{R}) = \lambda_T \sum_{l\beta} G_{l\beta}(\mathcal{R})\,\partial_{i\alpha} G_{l\beta}(\mathcal{R}) \tag{2.68}$$

where:

$$\begin{aligned}\partial_{i\alpha} G_{l\beta}(\mathcal{R}) = \delta_{il} \sum_{p\neq l} \left[\delta_{\alpha\beta}\,\xi_{lp}(r_{lp}) + \frac{\xi'(r_{lp})}{r_{lp}}\,r_{lp,\alpha}\,r_{lp,\beta}\right] - \\ (1-\delta_{il})\left[\delta_{\alpha\beta}\,\xi_{li}(r_{li}) + \frac{\xi'_{li}(r_{li})}{r_{li}}\,r_{il,\alpha}\,r_{il,\beta}\right]\end{aligned} \tag{2.69}$$

so that:

$$\partial_{i\alpha} Z_3(\mathcal{R}) = \lambda_T \sum_{l\neq i} G_{\alpha i}(\mathcal{R})\xi_{il}(r_{il}) + \sum_{l\neq i,\beta} G_{\beta i}(\mathcal{R})\,\frac{\xi'_{il}(r_{il})}{r_{il}}\,r_{il,\alpha} r_{il,\beta} \tag{2.70}$$

Moreover:

$$\partial^2_{i\alpha} Z_3(\mathcal{R}) = \lambda_T \textstyle\sum_{l\beta} \Big(\,\partial_{i\alpha} G_{l\beta}(\mathcal{R})\,\partial_{i\alpha} G_{l\beta}(\mathcal{R}) + G_{l\beta}(\mathcal{R})\,\partial^2_{i\alpha} G_{l\beta}(\mathcal{R})\,\Big) \tag{2.71}$$

is defined through:

$$\begin{aligned}\partial^2_{i\alpha} G_{l\beta}(\mathcal{R}) = \delta_{il} \sum_{p\neq i} \left[\delta_{\alpha\beta}\,\xi'(r_{lp})\,\frac{r_{lp,\alpha}}{r_{lp}} + \frac{\xi''(r_{lp})}{r^2_{lp}}\,r^2_{lp,\alpha}\,r_{lp,\beta} + \xi'(r_{lp})\,\partial_{i\alpha}\left(\frac{r_{lp,\alpha}\,r_{lp,\beta}}{r_{lp}}\right)\right] + \\ (1-\delta_{il})\,\left[\delta_{\alpha\beta}\,\xi'(r_{il})\,\frac{r_{il,\alpha}}{r_{il}} + \frac{\xi''(r_{il})}{r^2_{il}}\,r^2_{il,\alpha}\,r_{il,\beta} - \xi'(r_{il})\,\partial_{i\alpha}\left(\frac{r_{il,\alpha}\,r_{il,\beta}}{r_{il}}\right)\right]\end{aligned} \tag{2.72}$$

and reads:

$$\begin{aligned}\sum_\alpha \partial^2_{i\alpha} G_{l\beta}(\mathcal{R}) = \delta_{il} \sum_{p\neq i} \left[\xi''_{lp}(r_{lp})\,r_{lp,\beta} + (d+1)\,\frac{\xi'_{lp}(r_{lp})}{r_{lp}}\,r_{lp,\beta}\right] + \\ (1-\delta_{il})\left[\xi''_{li}(r_{li})\,r_{li} + (d+1)\,\frac{\xi'_{li}(r_{li})}{r_{li}}\,r_{li\,\beta}\right]\end{aligned} \tag{2.73}$$

Backflow correlations. Let us now consider a Slater determinant $\det(\varphi_t)$ of single-particle orbitals of a given type t, in presence of backflow correlations. For the purpose of

computing the first derivatives of (2.36) it will be useful to recall the following properties of matrix-valued functions:

Lemma 2.1. *Let Ω be an open subset of $\mathbb{R}^n$, and $A : \Omega \to M_{k\times k}(\mathbb{C})$ be a matrix-valued function. If A is a differentiable map, and $A(\mathbf{x})$ is invertible for all $\mathbf{x} \in \Omega$, then:*

$$\partial_{x_i} \det\big(A(\mathbf{x})\big) = \det\big(A(\mathbf{x})\big)\, \mathrm{Tr}\left[A^{-1}(\mathbf{x})\, \partial_{x_i} A(\mathbf{x})\right] \tag{2.74}$$

and:

$$\partial_{x_i} A^{-1}(\mathbf{x}) = -A^{-1}(\mathbf{x}) \partial_{x_i} A(\mathbf{x}) A^{-1}(\mathbf{x}) \tag{2.75}$$

Proof. *First, let us observe that $A(\mathbf{x}+\delta\mathbf{x}) = A(\mathbf{x}) + \sum_i \delta x_i B_i(\mathbf{x})$ up to terms of order $O\left(|\delta\mathbf{x}|^2\right)$. Therefore:*

$$\det(A(\mathbf{x}+\delta\mathbf{x})) = det(A(\mathbf{x}))\det\Big(I + \sum_i \delta x_i A(\mathbf{x})^{-1} B_i(\mathbf{x})\Big) + O\left(|\delta\mathbf{x}|^2\right) \tag{2.76}$$

by the properties of the characteristic polynomial:

$$\det(A(\mathbf{x}+\delta\mathbf{x})) = \det(A(\mathbf{x})) + \det(A(\mathbf{x}))\sum_i \delta x_i \mathrm{Tr}\left[A^{-1}(\mathbf{x})\, B_i(\mathbf{x})\right] + O\left(|\delta\mathbf{x}|^2\right) \tag{2.77}$$

whence (2.74) *is obtained. Equation* (2.75) *follows from the observation that:*

$$0 = \partial_{x_i}\left(A^{-1}(\mathbf{x})A(\mathbf{x})\right) = \left(\partial_{x_i} A^{-1}(\mathbf{x})\right)\, A(\mathbf{x}) + A^{-1}(\mathbf{x})\left(\partial_{x_i} A(\mathbf{x})\right) \tag{2.78}$$

and also to introduce the follwing intermediate tensors (whose calculation requires $\mathcal{O}(d^2N^2)$ operations):

$$\begin{aligned} A^{\alpha\beta}_{il} &= \partial_{i\alpha} x_{l\beta} \qquad & B^{\alpha\beta}_{il} &= \partial^2_{i\alpha} x_{l\beta} \\ \varphi^{\alpha}_{t,pl} &= \frac{\partial \varphi_{t,pl}}{\partial x_{l\alpha}} \qquad & \varphi^{\alpha\beta}_{t,pl} &= \frac{\partial^2 \varphi_{t,pl}}{\partial x_{l\beta}\partial x_{l\alpha}} \end{aligned} \tag{2.79}$$

where the indexes l, p label particles of type t only, and the derivatives in $\varphi^{\alpha}_{t,pl}$ and $\varphi^{\alpha\beta}_{t,pl}$ are computed with respect to the collective coordinate $\mathbf{x}_l$. In the light of the definitions (2.79), a straightforward application of Lemma 2.1 and of the chain rule yields:

$$\partial_{i\alpha} \det(\varphi_t) = \sum_{j\beta} \frac{\partial \det(\varphi_t)}{\partial x_{j\beta}} A^{\alpha\beta}_{ij} = \det(\varphi_t) \sum_{j\beta} F^{\beta}_{jj} A^{\alpha\beta}_{ij} \tag{2.80}$$

where $F^{\beta}_{jk} = \sum_l \varphi^{-1}_{t,jl}\varphi^{\alpha}_{t,lk}$. Therefore:

$$\partial_{i\alpha} \log(\det(\varphi_t)) = \sum_{j\beta} F^{\beta}_{jj} A^{\alpha\beta}_{ij} \tag{2.81}$$

To compute the second derivative of $\det(S)$, we can take advantage of the fact that:

$$\partial^2_{i\alpha} \log(\det(\varphi_t)) = \frac{\partial^2_{i\alpha} \det(\varphi_t)}{\det(\varphi_t)} - \left(\frac{\partial_{i\alpha} \det(\varphi_t)}{\det(\varphi_t)} \right)^2 \tag{2.82}$$

and:

$$\partial^2_{i\alpha} \det(\det(\varphi_t)) = \sum_{jk} \sum_{\beta\gamma} \partial_{x_{k\gamma}} \left(\frac{\partial \det(\det(\varphi_t))}{\partial x_{j\beta}} \right) A^{\alpha\gamma}_{ik} A^{\alpha\beta}_{ij} + \sum_{j\beta} F^{\beta}_{jj} B^{\alpha\beta}_{ij} \det(\det(\varphi_t)) \tag{2.83}$$

In fact, a straightforward application of Lemma 2.1 and of the chain rule yields:

$$\partial_{x_{k\gamma}} \left(\frac{\partial \det(\varphi_t)}{\partial x_{j\beta}} \right) = \det(\varphi_t) \left[\sum_l \delta_{kj} \varphi^{\gamma\beta}_{t,lj} \varphi^{-1}_{t,jl} + F^{\gamma}_{kk} F^{\beta}_{jj} - F^{\gamma}_{jk} F^{\beta}_{kj} \right] \tag{2.84}$$

and joining (2.81), (2.82) and (2.83) we obtain:

$$\partial^2_{i\alpha} \log(\det(\varphi_t)) = \sum_{j\beta} F^{\beta}_{jj} B^{\alpha\beta}_{ij} + \sum_{jk} \sum_{\beta\gamma} A^{\alpha\gamma}_{ik} A^{\alpha\beta}_{ij} \left[\delta_{kj} \sum_l \varphi^{\gamma\beta}_{t,lj} \varphi^{-1}_{t,jl} - F^{\gamma}_{jk} F^{\beta}_{kj} \right] \tag{2.85}$$

Smart Sampling. In the basic VMC algorithm, the transition probability distribution $\mathcal{T}(\mathcal{R} \to \mathcal{R}')$ is typically a Gaussian in the configuration space, (2.28). Writing $\mathcal{R}' = \mathcal{R} + \delta\mathcal{R}$ and expanding the acceptance probability around the current configuration we find:

$$\mathcal{A}(\mathcal{R} \to \mathcal{R} + \delta\mathcal{R}) = 1 + O(\delta\mathcal{R}) \tag{2.86}$$

Since the first deviation from unity comes at order $O(\delta\mathcal{R})$, the performance of the algorithm can be improved changing the transition probability distribution.
Following [82], let us substitute the Gaussian transition probability distribution of the basic VMC algorithm with the transition probability distribution:

$$\mathcal{P}(\mathcal{R} \to \mathcal{R}') = \frac{e^{-\frac{|\mathcal{R} - \mathcal{R}' + \delta\tau\, F(\mathcal{R})|^2}{4\delta\tau}}}{(4\pi\tau)^{\frac{dN}{2}}} \tag{2.87}$$

In (2.87), the quantity:

$$F(\mathcal{R}) = \partial_{i\alpha} \log \left(|\Psi_T(\mathcal{R})|^2 \right) \tag{2.88}$$

called *quantum force*, acts as a drift term that guides configurations towards regions where $|\Psi_T(\mathcal{R})|^2$ is large; the diffusion term, on the other hand, allows the exploration of regions where $|\Psi_T(\mathcal{R})|^2$ is small. The transition probability distribution (2.87) is not symmetric, and the acceptance probanility takes the general form:

$$\mathcal{A}(\mathcal{R} \to \mathcal{R}') = \min \left(1, \frac{|\Psi_T(\mathcal{R}')|^2}{|\Psi_T(\mathcal{R})|^2} \frac{\mathcal{T}(\mathcal{R}' \to \mathcal{R})}{\mathcal{T}(\mathcal{R} \to \mathcal{R}')} \right) \tag{2.89}$$

Writing $\mathcal{R}' = \mathcal{R} + \delta\mathcal{R}$ and expanding the acceptance probability around the current configuration we find:

$$\mathcal{A}(\mathcal{R} \to \mathcal{R} + \delta\mathcal{R}) = 1 + O(\delta\mathcal{R}^2) \tag{2.90}$$

Since the first deviation from unity comes at order $O(\delta\mathcal{R}^2)$, the transition probability distribution (2.87) significantly improves the performance of the algorithm. The choice of the transition probability distribution (2.87) is motivated by a mathematical argument that will be presented in Appendix 9.

2.4 Optimization of Jastrow-Feenberg and Backflow correlations

As discussed in Subsection 2.3.2, for a given Hamiltonian a functional form for the many-body wavefunction is typically guessed combining physical intuition and mathematical arguments based on the imaginary-time evolution [67, 66]. In general, some parameters $\mathbf{p} \in \mathcal{P} \subseteq \mathbb{R}^n$, usually called variational parameters, remain to be determined. We therefore need to choose an approximation for the actual ground state within a family of wavefunctions:

$$\mathbf{p} \mapsto |\Psi(\mathbf{p})\rangle, \quad \langle\mathcal{R}|\Psi(\mathbf{p})\rangle = \Psi(\mathbf{p},\mathcal{R}) \tag{2.91}$$

It is therefore very useful to devise and implement systematic and efficient procedures to find optimal parameters. This is achieved choosing a suitable *cost function* to be optimized, typically the expectation value of the Hamiltonian, the *energy*:

$$\mathcal{E}(\mathbf{p}) = \frac{\langle\Psi(\mathbf{p})|\hat{H}|\Psi(\mathbf{p})\rangle}{\langle\Psi(\mathbf{p})|\Psi(\mathbf{p})\rangle} \tag{2.92}$$

or the *energy variance* [83]:

$$\mathcal{S}(\mathbf{p}) = \frac{\langle\Psi(\mathbf{p})|\left(\hat{H}-\mathcal{E}(\mathbf{p})\right)^2|\Psi(\mathbf{p})\rangle}{\langle\Psi(\mathbf{p})|\Psi(\mathbf{p})\rangle} \tag{2.93}$$

One of the most widely employed schemes to improve the variational parameters is the *correlated sampling* (CS) method [84], in which a set of configurations distributed according to $|\Psi(\mathbf{p}_0,\mathcal{R})|^2$ is generated, $\mathbf{p}_0$ being the current parameter configuration. With the purpose of minimizing the *energy*, such configurations are used to estimate $\mathcal{E}(\mathbf{p})$ relying on the expression:

$$\mathcal{E}(\mathbf{p}) = \frac{\int d\mathcal{R}|\Psi(\mathbf{p}_0,\mathcal{R})|^2\mathcal{W}(\mathcal{R})E_L(\mathbf{p},\mathcal{R})}{\int d\mathcal{R}|\Psi(\mathbf{p}_0,\mathcal{R})|^2\mathcal{W}(\mathcal{R})} \tag{2.94}$$

where:

$$\mathcal{W}(\mathcal{R}) = \frac{|\Psi(\mathbf{p},\mathcal{R})|^2}{|\Psi(\mathbf{p}_0,\mathcal{R})|^2} \quad E_L(\mathbf{p},\mathcal{R}) = \frac{\hat{H}\Psi(\mathbf{p},\mathcal{R})}{\Psi(\mathbf{p},\mathcal{R})} \tag{2.95}$$

The main advantage of the CS technique is that the sampling of $|\Psi(\mathbf{p}_0,\mathcal{R})|^2$ for a single parameter configuration $\mathbf{p}_0$ gives access to the value of the $\mathcal{E}(\mathbf{p})$, in principle, for any parameter configuration $\mathbf{p}$. $\mathcal{E}(\mathbf{p})$ is then minimized with respect to $\mathbf{p}$ computing the energy gradient within the forward difference approximation and updating $\mathbf{p}$.
The correlated sampling algorithm can also be used to minimize the energy variance $\mathcal{S}(\mathbf{p})$. In such situation [83], the parameter update can be realized with the Levenberg-Marquardt method [85, 86].
Although minimization of $\mathcal{E}(\mathbf{p})$ using the CS method has often been successful, in some cases the procedure can exhibit a numerical instability [87]: it is well known, in particular, that the CS method may give inaccurate results when the nodal surface of a many-fermion trial wavefunction is allowed to change during the optimization process.

In fact, unless the nodal surfaces of $\Psi(\mathbf{p}_0, \mathcal{R})$ and $\Psi(\mathbf{p}, \mathcal{R})$ coincide, massive fluctuations in the weights occur on configurations close to the zeros of $|\Psi(\mathbf{p}_0, \mathcal{R})|^2$, determining drastic statistical errors in the CS estimate of $\mathcal{E}(\mathbf{p})$. In such situations, the recursion to alternative optimization schemes [88, 89, 90, 91, 92, 93, 94, 95] is advisable.

2.4.1 The linear method

The Linear Method (LM) was first conceived by Nightingale and Melik-Alaverdian [94] and later generalized by Toulouse and Umrigar [95] and Umrigar et al. [92]. Within the LM, the optimization of the *energy* (2.92) is pursued by iteratively:

1. expanding the normalized wavefunction:

$$|\tilde{\Psi}(\mathbf{p})\rangle = \frac{|\Psi(\mathbf{p})\rangle}{\langle\Psi(\mathbf{p})|\Psi(\mathbf{p})\rangle^{\frac{1}{2}}} \tag{2.96}$$

around the current parameter configuration $\mathbf{p}_0$ to first order in the parameter variation $\Delta\mathbf{p} = \mathbf{p} - \mathbf{p}_0$:

$$|\overline{\Psi}(\mathbf{p})\rangle = |\overline{\Psi}_0\rangle + \sum_{j=1}^{M} \Delta p_j \; |\overline{\Psi}_j\rangle \tag{2.97}$$

with $|\overline{\Psi}_0\rangle = |\overline{\Psi}(\mathbf{p}_0)\rangle$ and:

$$|\overline{\Psi}_j\rangle = \frac{|\Psi_j\rangle}{\langle\Psi_0|\Psi_0\rangle^{\frac{1}{2}}} - \frac{\langle\Psi_j|\Psi_0\rangle}{\langle\Psi_0|\Psi_0\rangle} \frac{|\Psi_0\rangle}{\langle\Psi_0|\Psi_0\rangle^{\frac{1}{2}}} \tag{2.98}$$

where $|\Psi_0\rangle = |\Psi(\mathbf{p}_0)\rangle$ and $|\Psi_j\rangle = |\frac{\partial\Psi}{\partial p_j}(\mathbf{p}_0)\rangle$. The normalization constraint:

$$0 = \partial_{p_j} \langle\tilde{\Psi}(\mathbf{p})|\tilde{\Psi}(\mathbf{p})\rangle = 2\,\langle\partial_{p_j}\tilde{\Psi}(\mathbf{p})|\tilde{\Psi}(\mathbf{p})\rangle \tag{2.99}$$

results in the orthogonality between $|\overline{\Psi}_0\rangle$ and $|\overline{\Psi}_i\rangle$.

2. minimizing the expectation value of the Hamiltonian operator $\hat{H}$ over the wavefunction (2.97):

$$\mathcal{E}(\mathbf{p}) = \frac{\langle\overline{\Psi}(\mathbf{p})|\hat{H}|\overline{\Psi}(\mathbf{p})\rangle}{\langle\overline{\Psi}(\mathbf{p})|\overline{\Psi}(\mathbf{p})\rangle} \tag{2.100}$$

with respect to the parameter variation $\Delta\mathbf{p}$. Inserting (2.97) into (2.100) leads to:

$$\mathcal{E}(\mathbf{p}) = \frac{\begin{pmatrix}1 & \Delta\mathbf{p}^T\end{pmatrix}\begin{pmatrix}\mathcal{E}(\mathbf{p}_0) & \mathbf{g}^T \\ \mathbf{g} & \overline{\mathcal{H}}\end{pmatrix}\begin{pmatrix}1 \\ \Delta\mathbf{p}\end{pmatrix}}{\begin{pmatrix}1 & \Delta\mathbf{p}^T\end{pmatrix}\begin{pmatrix}1 & 0 \\ 0 & \overline{\mathcal{S}}\end{pmatrix}\begin{pmatrix}1 \\ \Delta\mathbf{p}\end{pmatrix}} \tag{2.101}$$

where $\mathcal{E}(\mathbf{p}_0)$ is the current value of the energy and:

$$g_j = \frac{\langle\overline{\Psi}_0|\hat{H}|\overline{\Psi}_j\rangle}{\langle\overline{\Psi}_0|\overline{\Psi}_0\rangle} \tag{2.102}$$

is related to the gradient of the energy by:

$$\partial_{p_j}\mathcal{E}(\mathbf{p}_0) = 2g_j \tag{2.103}$$

which is easily derived computing $\partial_{p_i}\mathcal{E}(\mathbf{p})$ and recalling (2.99). Finally:

$$\overline{\mathcal{H}}_{ij} = \frac{\langle\overline{\Psi}_i|\hat{H}|\overline{\Psi}_j\rangle}{\langle\overline{\Psi}_0|\overline{\Psi}_0\rangle} \qquad \overline{\mathcal{S}}_{ij} = \frac{\langle\overline{\Psi}_i|\overline{\Psi}_j\rangle}{\langle\overline{\Psi}_0|\overline{\Psi}_0\rangle} \tag{2.104}$$

In published literature, the matrices appearing at the numerator and denominator of (2.101) are referred to, respectively, as *energy* and *overlap* matrices [90, 92, 94].

3. choosing the parameter variation $\Delta\mathbf{p}$ in such a way to minimize (2.101). The global minimum of (2.101) is necessarily a stationary point, where $\partial_{\mathbf{p}}\mathcal{E}(\mathbf{p}) = 0$; the stationarity condition translates into the following generalized eigenvalue equation:

$$\begin{pmatrix}\mathcal{E}(\mathbf{p}_0) & \mathbf{g}^T\\ \mathbf{g} & \overline{\mathcal{H}}\end{pmatrix}\begin{pmatrix}1\\ \Delta\mathbf{p}\end{pmatrix} = \mathcal{E}\begin{pmatrix}1 & 0\\ 0 & \overline{\mathcal{S}}\end{pmatrix}\begin{pmatrix}1\\ \Delta\mathbf{p}\end{pmatrix} \tag{2.105}$$

We notice that, in principle, the generalized eigenvalue equation (2.105) might admit solutions whose first component is zero; equation (2.101) shows that such solution corresponds to parameter variations that are orthogonal to the energy gradient and thus remain tangent to the hypersurface of constant energy, bringing no improvements. We thus consider only solutions having the form in (2.105).

There are $M+1$ possible parameter variations $\{\Delta\mathbf{p}^{(i)}\}_{i=1}^{M+1}$, M being the number of parameters, corresponding to properly rescaled solutions $\begin{pmatrix}1\\ \Delta\mathbf{p}^{(i)}\end{pmatrix}$ of the generalized eigenvalue equation (2.105) with eigenvalues $\{\mathcal{E}^{(i)}\}_{i=1}^{M+1}$. Such parameter variations are stationary points of the energy expectation (2.101). Moreover, inserting $\Delta\mathbf{p}^{(i)}$ in (2.101) and recalling (2.105) leads to:

$$\mathcal{E}(\mathbf{p}_0 + \Delta\mathbf{p}^{(i)}) = \mathcal{E}^{(i)} \tag{2.106}$$

clearly implying that the global minimum of the energy expectation (2.101) corresponds to the solution of (2.105) relative to the lowest eigenvalue. It is worth noticing that, for large parameter variations $\Delta\mathbf{p}^{(i)}$, the expanded wavefunction (2.97) might not be an accurate approximation for the actual normalized wavefunction (2.96). This could induce to unphysically low eigenvalues $\mathcal{E}^{(i)}$, that should be regarded to as unreliable estimates for the energy functional and rejected.

VMC estimators of Energy and Overlap Matrices. The elements of the energy and overlap matrices are estimated in VMC calculations. We introduce the symbol $\langle f\rangle$ to denote the average:

$$\langle f\rangle = \int d\mathcal{R}\,\frac{|\Psi_0(\mathcal{R})|^2}{\int d\mathcal{R}'|\Psi_0(\mathcal{R}')|^2}\,f(\mathcal{R}) = \int d\mathcal{R}\,p(\mathcal{R})\,f(\mathcal{R}) \tag{2.107}$$

of $f(\mathcal{R})$ over the probability distribution $p(\mathcal{R})$. It is readily found that:

$$\overline{\mathcal{S}}_{ij} = \left\langle\left(\frac{\Psi_i}{\Psi_0} - \left\langle\frac{\Psi_i}{\Psi_0}\right\rangle\right)\left(\frac{\Psi_j}{\Psi_0} - \left\langle\frac{\Psi_j}{\Psi_0}\right\rangle\right)\right\rangle \tag{2.108}$$

and that:

$$\begin{aligned}
\mathcal{E}(\mathbf{p}_0) &= \langle E_L \rangle \\
g_j &= \langle E_{L,j} \rangle + \left\langle E_L \frac{\Psi_j}{\Psi_0} \right\rangle - \langle E_L \rangle \left\langle \frac{\Psi_j}{\Psi_0} \right\rangle \\
g_i^T &= \left\langle \frac{\Psi_i}{\Psi_0} E_L \right\rangle - \left\langle \frac{\Psi_i}{\Psi_0} \right\rangle \langle E_L \rangle \\
\overline{\mathcal{H}}_{ij} &= \left\langle \left(\frac{\Psi_i}{\Psi_0} - \left\langle \frac{\Psi_i}{\Psi_0} \right\rangle \right) \left(\frac{\Psi_j}{\Psi_0} - \left\langle \frac{\Psi_j}{\Psi_0} \right\rangle \right) E_L \right\rangle + \left\langle \frac{\Psi_i}{\Psi_0} E_{L,j} \right\rangle - \left\langle \frac{\Psi_i}{\Psi_0} \right\rangle \langle E_{L,j} \rangle
\end{aligned} \tag{2.109}$$

where the symbols $E_L(\mathcal{R}) = \frac{\hat{H}\Psi_0(\mathcal{R})}{\Psi_0(\mathcal{R})}$ and $E_{L,j}(\mathcal{R}) = \frac{\hat{H}\Psi_j(\mathcal{R})}{\Psi_0(\mathcal{R})} - E_L(\mathcal{R})\frac{\Psi_j(\mathcal{R})}{\Psi_0(\mathcal{R})}$ have been introduced. The estimators (2.108), (2.109) are written in form of covariances rather than mean values of products to highlight their adequateness to numerical simulation. Indeed, it is well-known [90, 92, 35] that fluctuations of covariances are typically smaller than those of products.
The estimators for the elements $\overline{\mathcal{H}}_{ij}$ of the energy matrix are not symmetric in i and j when approximated by averages over finite Monte Carlo samples, whereas $\overline{\mathcal{H}}$ itself is of course symmetric. The hermiticity of the energy matrix is not exploited to symmetrize the estimator (2.108) since, as discussed in [94, 92], using a non-symmetric estimator results in considerably smaller fluctuations in the parameter variations.
We remark that, despite the solution of a non-symmetric eigenvalue equation can lead to complex eigenvalues, it turns out [94, 92] that parameter variations $\Delta\mathbf{p}_i$ corresponding to wavefunctions $\Psi(\mathbf{p}_0 + \Delta\mathbf{p}_i)$ having large overlap with the current wavefunction $\Psi(\mathbf{p}_0)$ correspond to eigenvalues with small imaginary part. Moreover, the leading divergences in (2.109) near the nodal surface of Ψ_0, contained in $\frac{\Psi_i(\mathcal{R})}{\Psi_0(\mathcal{R})}\frac{\Psi_j(\mathcal{R})}{\Psi_0(\mathcal{R})}E_L(\mathcal{R})$ and $\frac{\Psi_i(\mathcal{R})}{\Psi_0(\mathcal{R})}E_{L,j}(\mathcal{R})$, cancel exactly [95]. Thanks to this favorable property, the LM works for optimizing fermionic wavefunctions.

Alternative Normalization. We remark that the choice (2.96) is very natural but not unique. In fact, a differently normalized wavefunction:

$$|\tilde{\tilde{\Psi}}(\mathbf{p})\rangle = N(\mathbf{p})\,|\tilde{\Psi}(\mathbf{p})\rangle \tag{2.110}$$

with $N(\mathbf{p}_0) = 1$ has the first-order expansion:

$$|\overline{\overline{\Psi}}(\mathbf{p})\rangle = |\overline{\Psi}_0\rangle + \sum_{j=1}^{M} \Delta p_j\,|\overline{\overline{\Psi}}_j\rangle \tag{2.111}$$

with:

$$|\overline{\overline{\Psi}}_j\rangle = |\overline{\Psi}_j\rangle + \frac{\partial N}{\partial p_j}(\mathbf{p}_0)\,|\overline{\Psi}_0\rangle \tag{2.112}$$

The expansions (2.97) and (2.111) lie in the subspace of the Hilbert space spanned by the current wavefunction $|\Psi_0\rangle$ and its derivatives $|\Psi_j\rangle$, implying that the parameter variations $\Delta\mathbf{p}$ and $\Delta\overline{\overline{\mathbf{p}}}$ corresponding to the energy minimum are proportional [92]:

$$\Delta\overline{\overline{\mathbf{p}}} = \frac{\Delta\mathbf{p}}{1 - \sum_{j=1}^{M} \frac{\partial N}{\partial p_j}(\mathbf{p}_0)\Delta p_j} \tag{2.113}$$

the derivatives $\frac{\partial N}{\partial p_j}(\mathbf{p}_0)$ of the normalization function should be adjusted in such a way as to improve the performance of the algorithm. The empirical evidence that a good choice for nonlinear parameters is represented by:

$$\frac{\partial N}{\partial p_j}(\mathbf{p}_0) = -\frac{(1-\xi)\sum_k \overline{\mathcal{S}}_{jk}\Delta p_k}{(1-\xi)+\xi\sqrt{1+\sum_{jk}\Delta p_j \overline{\mathcal{S}}_{jk}\Delta p_k}} \tag{2.114}$$

has been signaled in literature [96, 92]. The constant $\xi \in [0,1]$ there appearing is meant to be adjusted by hand during each iteration. To understand the rationale behind its choice, it is worth inserting (2.114) into (2.113) obtaining:

$$\Delta\overline{\overline{\mathbf{p}}} = \frac{\Delta\mathbf{p}}{1+\frac{(1-\xi)Q}{(1-\xi)+\xi\sqrt{1+Q}}} \tag{2.115}$$

where $Q = \sum_{jk}\Delta p_j \overline{\mathcal{S}}_{jk}\Delta p_k$ is a positive quantity, since the overlap matrix (2.108) is positive-definite:

$$\sum_{jk} v_j \overline{\mathcal{S}}_{jk} v_k = \left\langle \sum_j v_j \left(\frac{\Psi_j}{\Psi_0} - \left\langle \frac{\Psi_j}{\Psi_0} \right\rangle \right) \sum_k v_k \left(\frac{\Psi_k}{\Psi_0} - \left\langle \frac{\Psi_k}{\Psi_0} \right\rangle \right) \right\rangle \geq 0 \tag{2.116}$$

The denominator at the right member of (2.115) is a monotonically decreasing function of ξ, ranging from $1+Q$ to 1. Therefore, smaller values of ξ decrease the parameter variations. In some cases the choice $\xi = 1$ can result in excessively large parameter variations that must be rejected; the safer choice $\xi = 0$, on the other hand, can lead to excessively small parameter variations that slow down the convergence of the algorithm. The choice $\xi = \frac{1}{2}$ typically represents a good compromise between these two competing effects.

Regularization. If the current parameter configuration $\mathbf{p}_0$ is not sufficiently close to the minimum for the quadratic approximation of the energy to hold, or if the number of VMC samples employed to estimate the elements of the energy and overlap matrices is too small, and the latter are insufficiently accurate, the parameter variations $\Delta\mathbf{p}^{(i)}$ proposed by the LM may lead us towards worse wavefunctions. In such situation, it is convenient to apply a Tikhonov regularization [97, 90] to the energy matrix (2.105) by making the substitution:

$$\begin{pmatrix} \mathcal{E}(\mathbf{p}_0) & \mathbf{g}^T \\ \mathbf{g} & \overline{\mathcal{H}} \end{pmatrix} \rightarrow \begin{pmatrix} \mathcal{E}(\mathbf{p}_0) & \mathbf{g}^T \\ \mathbf{g} & \overline{\mathcal{H}} + \alpha\mathbb{I} \end{pmatrix} \tag{2.117}$$

α being a real positive number, for large values of which the parameter variations $\Delta\mathbf{p}_i$ are easily shown to either diverge as $\Delta\mathbf{p}_i = \alpha\mathbf{v} + \mathcal{O}(1)$, $\mathbf{v}$ being solution of the nonlinear system $\mathbf{v} = (\mathbf{g}\cdot\mathbf{v})\,S\mathbf{v}$, or vanish as $\Delta\mathbf{p}_i = \alpha^{-1}\mathbf{w} + \mathcal{O}(\alpha^{-2})$, being $\mathbf{w} = -\mathbf{g}$. Therefore, vanishing parameter variations rotate from their original direction to the steepest descent direction in a nontrivial way. The parameter $\alpha \in (0,\infty)$ is meant to be adjusted by hand before each iteration. The criterion of choice is discussed in [95]: for several values of α, the parameter variation associated to the lowest physically reasonable eigenvalue (2.106) is used as an input to a VMC calculation; then, either the value of α yielding the lowest VMC energy is chosen, or an interpolation is carried out to identify the best value

of α.

2.4.2 Application to Slater-Jastrow wavefunctions

Typical calculations in condensed matter Physics involve wavefunctions containing two-body and three-body correlations for Bose systems [56, 59], and backflow correlations for Fermi systems [57, 58, 60, 59, 64]. In the case of Fermi system, $\Psi(\mathbf{p},\mathcal{R})$ is positive-definite; nevertheless, it is well-known [98, 99] that in VMC calculations the Monte Carlo sampling can be restricted, without introducing any bias, to subsets of the configuration space where the sign of the trial wavefunction is fixed, for instance positive. Within such regions the trial wavefunction can always be written as:

$$\begin{aligned}\Psi(\mathbf{p},\mathcal{R}) &= e^{-Z(\mathbf{p},\mathcal{R})} \\ Z(\mathbf{p},\mathcal{R}) &= \begin{cases} Z_{2B}(\mathbf{p},\mathcal{R}) + Z_{3B}(\mathbf{p},\mathcal{R}) \\ Z_{2B}(\mathbf{p},\mathcal{R}) + Z_{3B}(\mathbf{p},\mathcal{R}) + Z_{BF}(\mathbf{p},\mathcal{R}) \end{cases}\end{aligned} \tag{2.118}$$

where the upper (lower) line refers to Bosons (Fermions). We first observe that:

$$\frac{\Psi_j(\mathbf{p},\mathcal{R})}{\Psi(\mathbf{p},\mathcal{R})} = -\partial_{p_j} Z(\mathbf{p},\mathcal{R}) \tag{2.119}$$

is a sum of contributions, each coming from a specific part of the wavefunction. Moreover:

$$\begin{aligned} E_{L,j}(\mathbf{p},\mathcal{R}) &= -\frac{\hbar^2}{2m}\sum_i \left(\frac{\triangle_i \Psi_j(\mathbf{p},\mathcal{R})}{\Psi(\mathbf{p},\mathcal{R})} - \frac{\Psi_j(\mathbf{p},\mathcal{R})}{\Psi(\mathbf{p},\mathcal{R})}\frac{\triangle_i \Psi(\mathbf{p},\mathcal{R})}{\Psi(\mathbf{p},\mathcal{R})} \right) = \\ &= \frac{\hbar^2}{2m}\sum_i \left(\triangle_i \partial_{p_j} Z(\mathbf{p},\mathcal{R}) + 2\frac{\nabla_i \Psi(\mathbf{p},\mathcal{R})}{\Psi(\mathbf{p},\mathcal{R})}\cdot \nabla_i \partial_{p_j} Z(\mathbf{p},\mathcal{R}) \right) \end{aligned} \tag{2.120}$$

In order to construct the VMC estimators of the energy and overlap matrices, we need to compute the quantities $\partial_{p_j} Z(\mathbf{p},\mathcal{R})$, $\nabla_i \partial_{p_j} Z(\mathbf{p},\mathcal{R})$ and $\sum_i \triangle_i \partial_{p_j} Z(\mathbf{p},\mathcal{R})$. As the logarithm $-Z(\mathbf{p},\mathcal{R})$ of the trial wavefunction is additive in the terms corresponding to Jastorw-Feenberg and backflow correlations, its derivatives with respect to the variational parameters can be treated separately. In the forthcoming calculations, for all radial functions $f(\mathbf{p},r)$ the notation $\partial_{p_j} f^{(i)}(\mathbf{p},r)$ will be employed to indicate the i-th radial derivative of $\partial_{p_j} f(\mathbf{p},r)$.

Two-Body Correlations. The contribution to the quantity $Z(\mathbf{p},\mathcal{R})$ brought by the two-body Jastrow factor reads:

$$Z(\mathbf{p},\mathcal{R}) = \sum_{k<l} u(\mathbf{p}_{2B}, r_{kl}) \tag{2.121}$$

so that:

$$\partial_{p_j} Z(\mathbf{p},\mathcal{R}) = \sum_{k<l} \partial_{p_j} u(\mathbf{p}_{2B}, r_{kl}) \tag{2.122}$$

and:

$$\partial_{r_{i\alpha}} \partial_{p_j} Z(\mathbf{p},\mathcal{R}) = \sum_{k\neq i} \partial_{p_j} u^{(1)}(\mathbf{p}_{2B}, r_{ik}) \frac{r_{ik,\alpha}}{r_{ik}} \tag{2.123}$$

The laplacian reads:

$$\sum_i \triangle_i \partial_{p_j} Z(\mathbf{p},\mathcal{R}) = 2\left(\sum_{i<k} \partial_{p_j} u^{(2)}(\mathbf{p}_{2B}, r_{ik}) + (d-1)\,\frac{\partial_{p_j} u^{(1)}(\mathbf{p}_{2B}, r_{ik})}{r_{ik}}\right) \tag{2.124}$$

Backflow Correlations. The contribution to the quantity $Z(\mathbf{p},\mathcal{R})$ brought by the backflow correlations reads:

$$Z(\mathbf{p},\mathcal{R}) = -\log(\det(\varphi)) \tag{2.125}$$

where $\varphi_{ki} = \varphi_k(\mathbf{p}_{BF}, \mathbf{x}_i)$. In order to construct the VMC estimators of the energy and overlap matrices we use Lemma 2.1, that leads us to:

$$\partial_{p_j} Z(\mathbf{p},\mathcal{R}) = -\text{tr}\left(\varphi^{-1}\partial_{p_j}\varphi\right) \tag{2.126}$$

to:

$$\partial_{r_{i\alpha}}\partial_{p_j} Z(\mathbf{p},\mathcal{R}) = \text{tr}\left(\varphi^{-1}\partial_{r_{i\alpha}}\varphi\,\varphi^{-1}\partial_{p_j}\varphi\right) - \text{tr}\left(\varphi^{-1}(\partial_{r_{i\alpha}}\partial_{p_j}\varphi)\right) \tag{2.127}$$

and to:

$$\begin{aligned}\partial^2_{r_{i\alpha}}\partial_{p_j} Z(\mathbf{p},\mathcal{R}) = \text{tr}\Big(\partial_{r_{i\alpha}}\left(\varphi^{-1}\partial_{r_{i\alpha}}\varphi\varphi^{-1}\right)\partial_{p_j}\varphi\Big) + \text{tr}\Big(\left(\varphi^{-1}\partial_{r_{i\alpha}}\varphi\varphi^{-1}\right)(\partial_{r_{i\alpha}}\partial_{p_j}\varphi)\Big)\\ - \text{tr}\Big(\partial_{r_{i\alpha}}\varphi^{-1}\,\partial_{r_{i\alpha}}\partial_{p_j}\varphi\Big) - \text{tr}\Big(\varphi^{-1}\partial^2_{r_{i\alpha}}\partial_{p_j}\varphi\Big)\end{aligned} \tag{2.128}$$

Thanks to Lemma 2.1, it is also clear that the second and third terms of (2.128) are equal and opposite. Therefore:

$$\partial^2_{r_{i\alpha}}\partial_{p_j} Z(\mathbf{p},\mathcal{R}) = \text{tr}\Big(\partial_{r_{i\alpha}}\left(\varphi^{-1}\partial_{r_{i\alpha}}\varphi\varphi^{-1}\right)\partial_{p_j}\varphi\Big) - 2\text{tr}\Big(\partial_{r_{i\alpha}}\varphi^{-1}(\partial_{r_{i\alpha}}\partial_{p_j}\varphi)\Big) - \text{tr}\Big(\varphi^{-1}\partial^2_{r_{i\alpha}}\partial_{p_j}\varphi\Big) \tag{2.129}$$

Observing that:

$$\partial_{r_{i\alpha}}\left(\varphi^{-1}\partial_{r_{i\alpha}}\varphi\varphi^{-1}\right) = \varphi^{-1}\partial^2_{r_{i\alpha}}\varphi\varphi^{-1} - 2\varphi^{-1}\partial_{r_{i\alpha}}\varphi\varphi^{-1}\partial_{r_{i\alpha}}\varphi\varphi^{-1} \tag{2.130}$$

we find the following estimator for $\partial^2_{r_{i\alpha}}\partial_{p_j} Z(\mathbf{p},\mathcal{R})$:

$$\begin{aligned}\partial^2_{r_{i\alpha}}\partial_{p_j} Z(\mathbf{p},\mathcal{R}) = \text{tr}\Big((\varphi^{-1}\partial^2_{r_{i\alpha}}\varphi)\varphi^{-1}\partial_{p_j}\varphi\Big) - 2\text{tr}\Big((\varphi^{-1}\partial_{r_{i\alpha}}\varphi)(\varphi^{-1}\partial_{r_{i\alpha}}\varphi)(\varphi^{-1}\partial_{p_j}\varphi)\Big)\\ + 2\text{tr}\Big((\varphi^{-1}\partial_{r_{i\alpha}}\varphi)(\varphi^{-1}\partial_{r_{i\alpha}}\partial_{p_j}\varphi)\Big) - \text{tr}\Big(\varphi^{-1}\partial^2_{r_{i\alpha}}\partial_{p_j}\varphi\Big)\end{aligned} \tag{2.131}$$

Despite their slightly intricate appearance, the estimators (2.126), (2.127) and (2.131) *determine a total computational cost of the optimization procedure scaling as* $\mathcal{O}(N^3)$. This result is non-trivial and useful since, in presence of backflow correlations, even the evaluation of the wavefunction (at the basis of the VMC and optimization algorithms) involves $\mathcal{O}(N^3)$ operations. This is because each backflow coordinate $\mathbf{x}_i$ depends on all the coordinates $\mathbf{r}_i$, preventing the use of the Sherman-Morrison method to evaluate the wavefunction at the cost of $\mathcal{O}(N^2)$ operations. The explicit expression of the estimators (2.126), (2.127) and (2.131), as long as their computational cost, is derived in detail in Appendix 10.2.

Three-Body Correlations. The contribution to the quantity $Z(\mathbf{p},\mathcal{R})$ brought by the three-body correlations reads:

$$Z(\mathbf{p},\mathcal{R}) = \frac{\lambda_T}{2}\sum_{l=1}^{N}\mathbf{G}(l)\cdot\mathbf{G}(l) - \lambda_T\sum_{j<k}\tilde{\xi}(r_{jk}) \tag{2.132}$$

If $p_j = \lambda_T$, the quantity $\partial_{p_j} Z(\mathbf{p},\mathcal{R})$ is simply $\frac{1}{\lambda_T} Z(\mathbf{p},\mathcal{R})$ so that:

$$\partial_{r_{i\alpha}}\partial_{p_j} Z(\mathbf{p},\mathcal{R}) = \sum_l \partial_{r_{i\alpha}}\mathbf{G}(l)\cdot\mathbf{G}(l) - \sum_{k\neq i}\frac{r_{ik,\alpha}}{r_{ik}}\,\tilde{\xi}^{(1)}(r_{ik}) \tag{2.133}$$

and:

$$\begin{aligned}\sum_\alpha \partial^2_{r_{i\alpha}}\partial_{p_j} Z(\mathbf{p},\mathcal{R}) = &\sum_{l,\alpha}\left(\partial_{r_{i\alpha}}\mathbf{G}(l)\cdot\partial_{i\alpha}\mathbf{G}(l) + \partial^2_{r_{i\alpha}}\mathbf{G}(l)\cdot\mathbf{G}(l)\right)\\ &-\sum_{p\neq i}\left(\tilde{\xi}^{(2)}(r_{ip}) + (d-1)\frac{\tilde{\xi}^{(1)}(r_{ip})}{r_{ip}}\right)\end{aligned} \tag{2.134}$$

For all other parameters $p_j \in \mathbf{p}_{3B}$:

$$\partial_{p_j} Z(\mathbf{p},\mathcal{R}) = \lambda_T\sum_l \partial_{p_j}\mathbf{G}(l)\cdot\mathbf{G}(l) - \lambda_T\sum_{l<k}\partial_{p_j}\tilde{\xi}(r_{lk}) \tag{2.135}$$

where:

$$\partial_{p_j}\mathbf{G}(l) = \sum_{k\neq l}\partial_{p_j}\xi(r_{lk})\,(\mathbf{r}_l - \mathbf{r}_k) \tag{2.136}$$

Moreover:

$$\partial_{r_{i\alpha}}\partial_{p_j} Z(\mathbf{p},\mathcal{R}) = \lambda_T\sum_{l\beta}\left(\partial_{r_{i\alpha}}\partial_{p_j}\mathbf{G}(l)\cdot\mathbf{G}(l) + \partial_{r_{i\alpha}}\mathbf{G}(l)\cdot\partial_{p_j}\mathbf{G}(l)\right) - \lambda_T\sum_{k\neq i}\frac{r_{ik,\alpha}}{r_{ik}}\,\partial_p\tilde{\xi}^{(1)}(r_{ik}) \tag{2.137}$$

with:

$$\begin{aligned}\partial_{r_{i\alpha}}\partial_{p_j} G_\beta(l) = &\,\delta_{li}\sum_{p\neq l}\left(\delta_{\alpha\beta}\partial_{p_j}\xi(r_{lp}) + \frac{\partial_{p_j}\xi^{(1)}(r_{lp})}{r_{lp}}\,r_{lp,\alpha}r_{lp,\beta}\right)\\ &-(1-\delta_{li})\left(\delta_{\alpha\beta}\partial_{p_j}\xi(r_{li}) + \frac{\partial_{p_j}\xi^{(1)}(r_{li})}{r_{li}}\,r_{li,\alpha}r_{li,\beta}\right)\end{aligned} \tag{2.138}$$

The only remaining quantity is:

$$\begin{aligned}\sum_\alpha \partial^2_{r_{i\alpha}}\partial_{p_j} Z(\mathbf{p},\mathcal{R}) = &\lambda_T\sum_{l\alpha}\left(2\,\partial_{r_{i\alpha}}\partial_{p_j}\mathbf{G}(l)\cdot\partial_{r_{i\alpha}}\mathbf{G}(l) + \partial^2_{r_{i\alpha}}\partial_{p_j}\mathbf{G}(l)\cdot\mathbf{G}(l) + \partial^2_{r_{i\alpha}}\mathbf{G}(l)\cdot\partial_{p_j}\mathbf{G}(l)\right)\\ &-\lambda_T\sum_{p\neq i}\left(\partial_{p_j}\tilde{\xi}^{(2)}(r_{ip}) + (d-1)\frac{\partial_{p_j}\tilde{\xi}^{(1)}(r_{ip})}{r_{ip}}\right)\end{aligned} \tag{2.139}$$

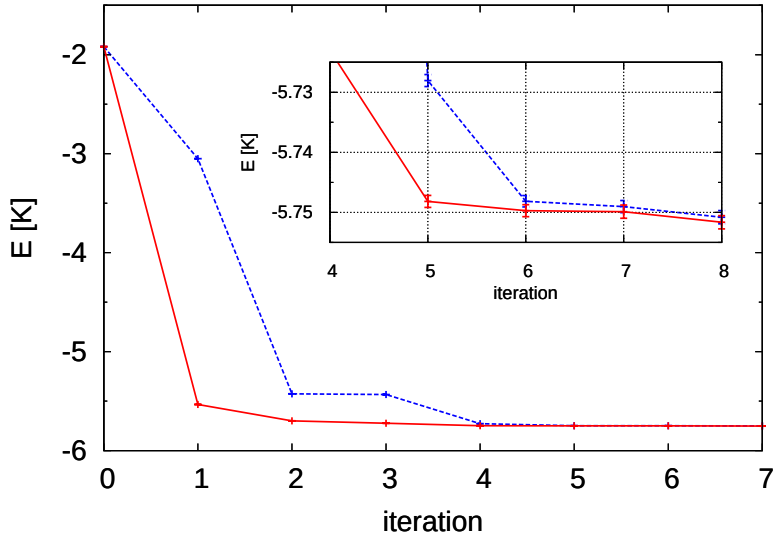

Figure 2.1: Convergence of the VMC total energy of $N = 64$ ^{4}He atoms at equilibrium density during the optimization of the Jastrow-McMillan factor with (solid) and without (dashed) regularization.

with:

$$\begin{aligned}\partial_{p_j} \sum_{\alpha} \partial^2_{r_{i\alpha}} G_\beta(l) = \delta_{il} \sum_{p \neq l} \left((d+1) \partial_{p_j} \xi^{(1)}(r_{lp}) \frac{r_{lp,\beta}}{r_{lp}} + \partial_{p_j} \xi^{(2)}(r_{lp}) r_{lp,\beta} \right) \\ + (1 - \delta_{il}) \left((d+1) \partial_{p_j} \xi^{(1)}(r_{li}) \frac{r_{li,\beta}}{r_{li}} + \partial_{p_j} \xi^{(2)}(r_{li}) r_{li,\beta} \right)\end{aligned} \tag{2.140}$$

2.4.3 Results

The performance of the algorithm has been benchmarked simulating a 3D system of $N = 64$ ^{4}He atoms interacting through the HFDHE2 potential [100] near the equilibrium density $\rho = 0.02186\,\text{Å}^{-3}$, and a $2D$ system of $N = 26$ electrons at Wigner-Seitz radius $r_s = 1$ [6].

3D ^{4}He. In our study of 3D ^{4}He atoms, we have used a wavefunction encompassing Jastrow-McMillan two-body correlations [46]:

$$u(r) = \frac{1}{2} \left(\frac{b}{r} \right)^m \tag{2.141}$$

and Gaussian three-body correlations [58, 59]:

$$\xi(r) = e^{-w_T^2 (r - r_T)^2} \tag{2.142}$$

The Jastrow-McMillan factor has been first optimized in absence of three-body correlations: the convergence of the VMC energy is illustrated in Figure 2.1, and the flow in the parameter space resulting from the optimization algorithm is illustrated in Fig-

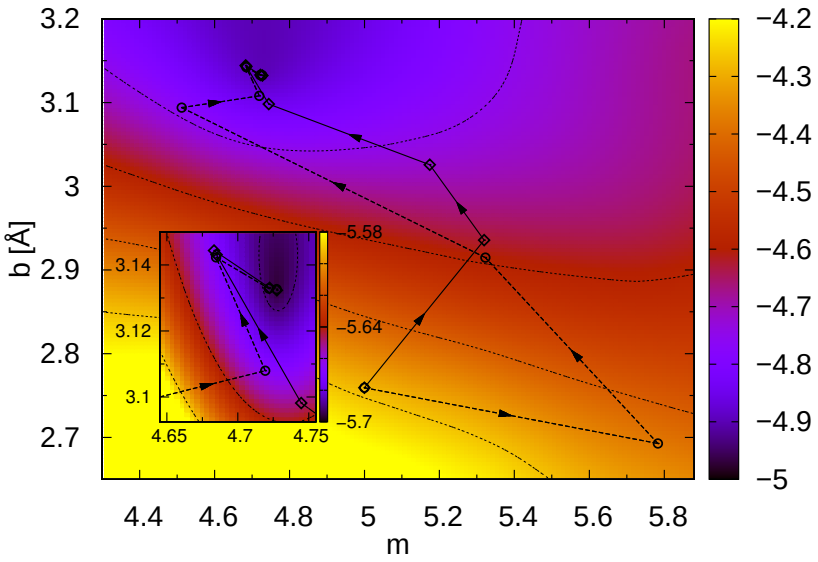

Figure 2.2: Convergence of the Jastrow-McMillan factor of $N = 64$ ^{4}He atoms at equilibrium density with (solid arrows) and without (dashed arrows) regularization. To show the improvement brought by the regularization, the flows in the parameter space resulting from the two algorithms are superposed to a contour plot of the energy landscape $\mathcal{E}(\mathbf{p})$ obtained via several VMC calculations; dotted lines represent level curves of the energy landscape.

ure (2.2). In both figures, two distinct series have been obtained by applying the basic parameter update algorithm described in Section 2.4.1, and by improving it with the alternative normalization and regularization procedures. Figures 2.1 and 2.2 show that the use of alternative normalization and regularization results in a more rapid convergence of the algorithm. We obtain an energy $-5.752(1)\,K$, in good agreement with the value $-5.72(2)\,K$ reported in [101]. The Gaussian factor has been subsequently optimized keeping the Jastrow-McMillan factor fixed at the parameter values $\mathbf{p}_{2B} = (b, m)$ corresponding to the last step of Figure 2.2. The convergence of the VMC energy is illustrated in Figure 2.3, and the flow in the parameter space in Figure (2.4). A simultaneous optimization of the two-body and three-body correlations has been then carried out, starting from the parameters in the last step of Figures 2.2 and 2.4. It led to the results in figures 2.5 and 2.6. We obtain an energy $-6.675(1)\,K$, in good agreement with the value $-6.65(2)\,K$ reported in [101].

2D electrons. In our study of 2D electrons, we have measured energies in Rydberg units and lengths in Bohr radii. We have used a wavefunction encompassing parameter-free RPA two-body correlations [102, 103, 104, 60]:

$$2nu(\mathbf{q}) = \sqrt{\frac{1}{S_0^2(\mathbf{q})} + \frac{4v(\mathbf{q})m\rho}{\hbar^2|\mathbf{q}|^2}} - \frac{1}{S_0(\mathbf{q})} \tag{2.143}$$

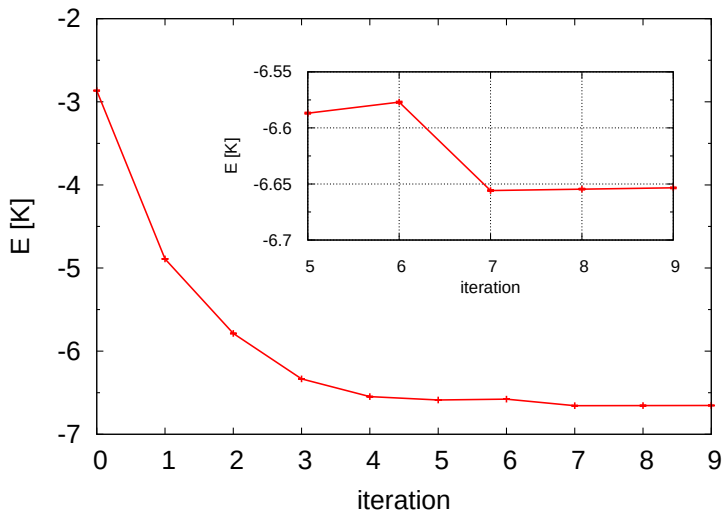

Figure 2.3: Convergence of the VMC total energy of $N = 64$ ^{4}He atoms at equilibrium density during the optimization of the Gaussian three-body factor in a wave function composed of a three-body part multiplied by a previously-optimized Jastrow-McMillan factor.

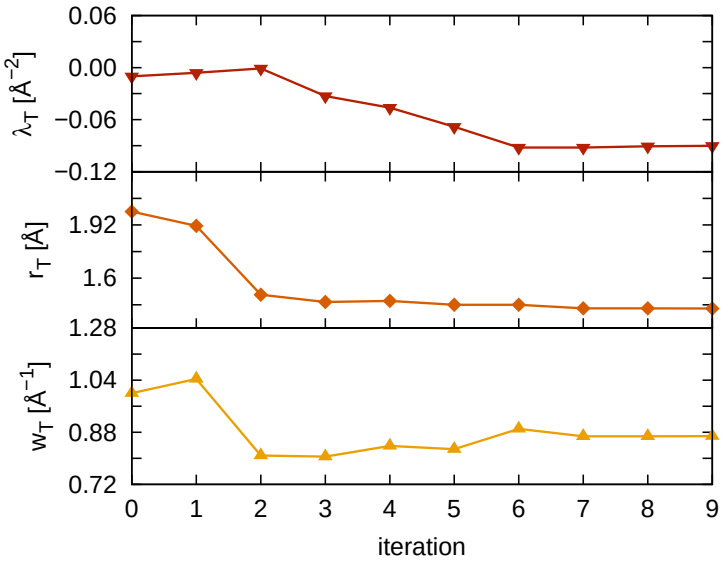

Figure 2.4: Convergence of the Gaussian three-body factor of $N = 64$ ^{4}He atoms at equilibrium density.

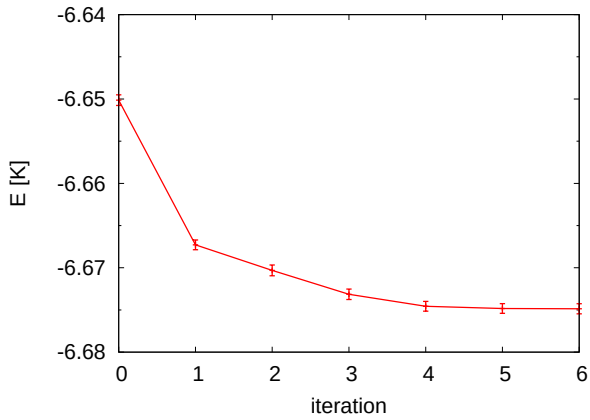

Figure 2.5: Convergence of the VMC total energy of $N = 64$ ^{4}He atoms at equilibrium density during the optimization of a wave function composed of a Jastrow-McMillan factor and of a Gaussian three-body factor.

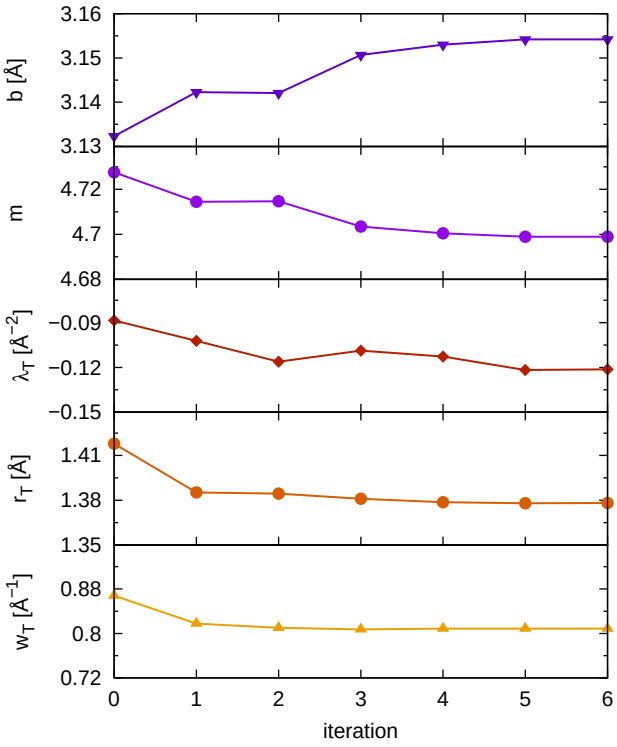

Figure 2.6: Convergence of Jastrow-McMillan (upper panels) and Gaussian three-body (lower panels) factors of $N = 64$ ^{4}He atoms at equilibrium density.

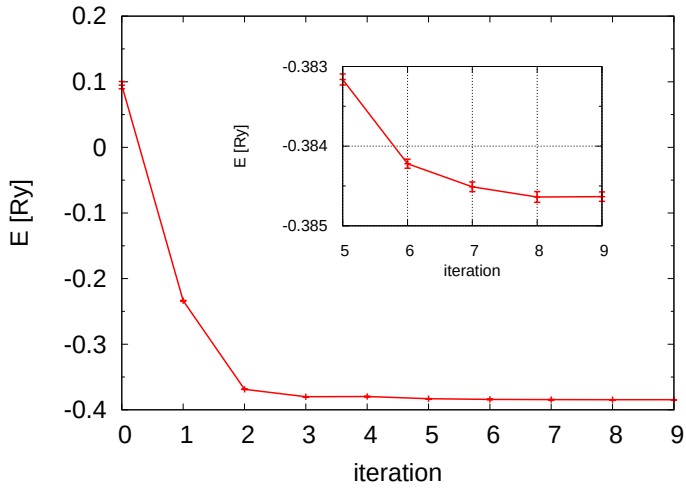

Figure 2.7: Convergence of the VMC total energy of a 2D system of $N = 26$ electrons at $r_s = 1$ during the optimization of the backflow correlations of a wavefunction composed of a parameter-free Jastrow-RPA factor and a Slater-backflow determinant.

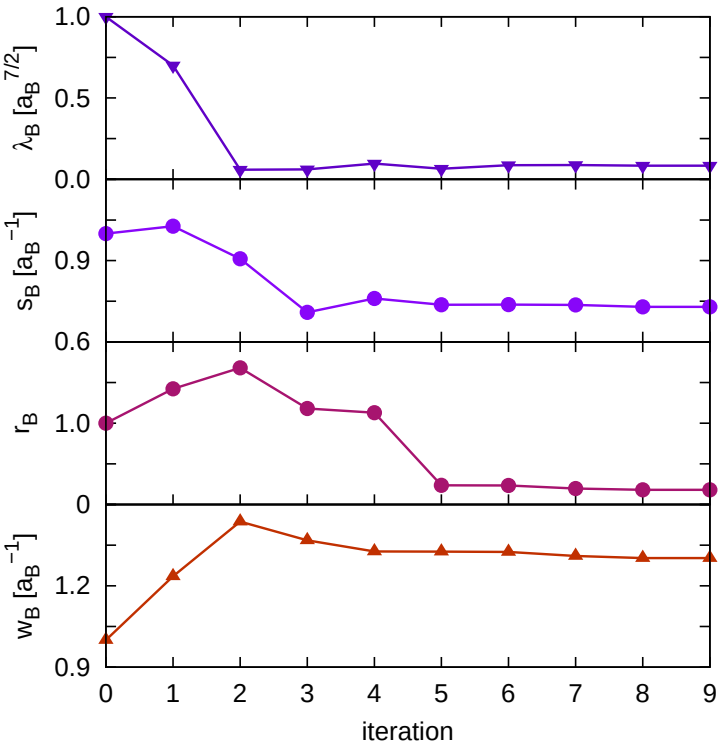

Figure 2.8: Convergence of backflow correlations of a 2D system of $N = 26$ electrons at $r_s = 1$ during the optimization of the backflow correlations of a wavefunction composed of a parameter-free Jastrow-RPA factor and a Slater-backflow determinant.

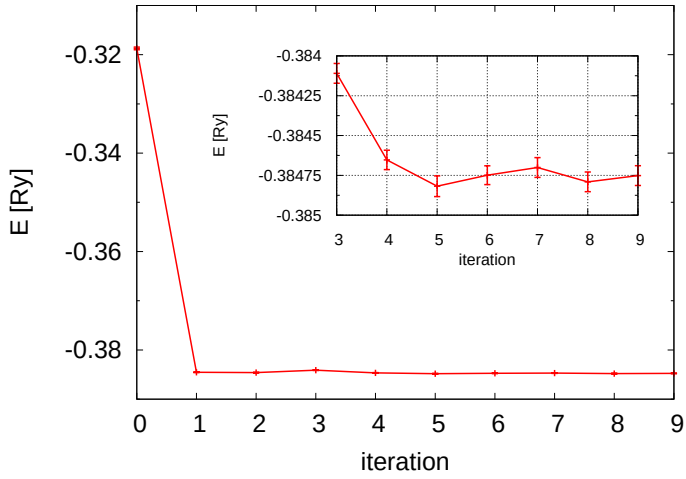

Figure 2.9: Convergence of the VMC total energy of a 2D system of $N = 26$ electrons at $r_s = 1$ during the optimization of a Gaussian three-body factor of a wavefunction composed of a parameter-free Jastrow-RPA factor, a previously-optimized Slater-backflow determinant and a Gaussian three-body factor.

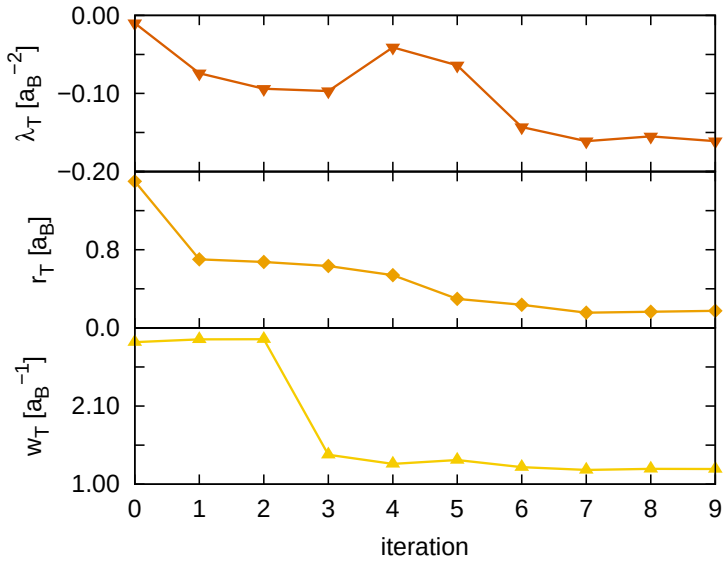

Figure 2.10: Convergence of the Gaussian three-body factor of a 2D system of $N = 26$ electrons at $r_s = 1$ during the optimization of the Gaussian three-body factor of a wavefunction composed of a parameter-free Jastrow-RPA factor, a previously-optimized Slater-backflow determinant and a Gaussian three-body factor.

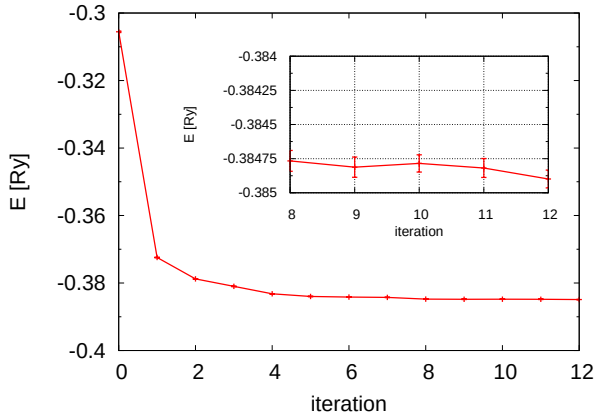

Figure 2.11: Convergence of the VMC total energy of a 2D system of $N = 26$ electrons at $r_s = 1$ during the simultaneous optimization of backflow and three-body correlations.

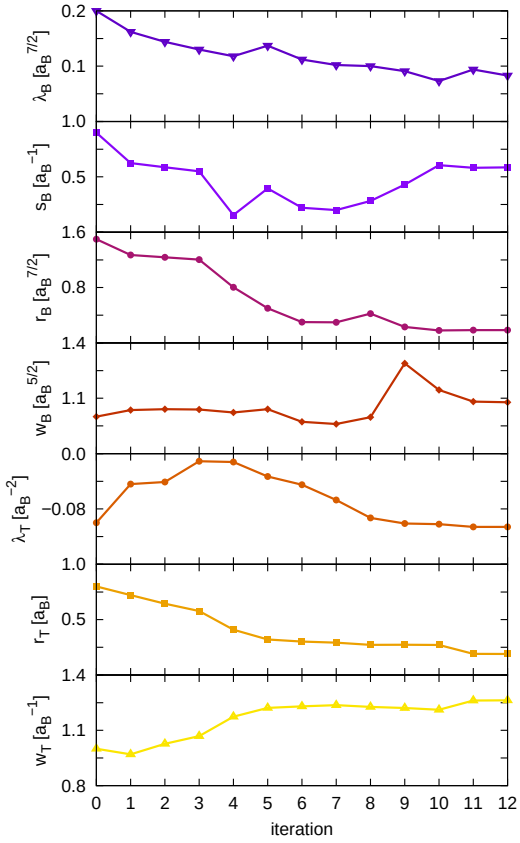

Figure 2.12: Convergence of the backflow and three-body correlations of a 2D system of $N = 26$ electrons at $r_s = 1$ during their simultaneous optimization.

N	t (sec)
2	0.15
10	0.55
26	5.90
42	22.50
58	56.97
72	108.00
98	264.54
162	1141.35
242	3727.22

Table 2.1: Duration per core t (seconds) of 100 optimization blocks, each of 10 VMC steps, for several numbers N of electrons. The polynomial $t(N) = a_2N^2 + a_3N^3$, with $a_2 = 2.72226 \times 10^{-3}$ and $a_3 = 2.51738 \times 10^{-4}$ fits the data with reduced chi squared 0.72. Attempting to fit a quartic polynomial $t(N) + a_4N^4$, we find $a_4 \sim 10^{-10}$ confirming the scaling of the algorithm.

here detailed in Fourier space with $v(\mathbf{q}) = \frac{2\pi e^2}{|\mathbf{q}|}$ and:

$$\frac{\pi}{2} S_0(\mathbf{q}) = \sin^{-1}\left(\frac{|\mathbf{q}|}{2k_F}\right) + \frac{|\mathbf{q}|}{2k_F}\sqrt{1 - \left(\frac{|\mathbf{q}|}{2k_F}\right)^2} \tag{2.144}$$

along with rational backflow correlations parametrized as in [60]:

$$\eta(r) = \lambda_B \frac{1 + s_B r}{r_B + w_B r + r^{\frac{7}{2}}} \tag{2.145}$$

and Gaussian three-body correlations [58, 60, 59]:

$$\xi(r) = e^{-w_T^2 (r - r_T)^2} \tag{2.146}$$

This wavefunction is better described and theoretically justified in Appendix 10.

The backflow correlations have been first optimized in absence of three-body correlations: the convergence of the VMC energy is illustrated in Figure 2.7, and the flow in the parameter space in Figure (2.8). We obtain the energy $-0.3846(2)\, Ry$, in good agreement with the value $-0.3839(4)\, Ry$ reported in [63].

The Gaussian factor has been subsequently optimized keeping the backflow correlations fixed at the parameter values $\mathbf{p}_{BF} = (\lambda_B, s_B, r_B, w_B)$ corresponding to the last step of Figure 2.7. The convergence of the VMC energy is illustrated in Figure 2.9, and the flow in the parameter space in Figure 2.10. A simultaneous optimization of the three-body and backflow correlations has been finally carried out, starting from a randomly chosen parameter configuration, leading to the results illustrated in Figures 2.11 and 2.12. We remark that, although a more rapid convergence of the backflow parameters is attained in absence of the three-body correlations, at least for the system under study, the algorithm proves able to simultaneously handle parameters with different orders of

magniture and pertaining to different parts of the wavefunction.
In Table 2.1 we provide estimates of the duration of optimization runs, confirming the cubic scaling of the methodology in the number of particles. The duration estimates were obtained using the WTIME function of the MPI library, monitoring runs in which solely backflow correlations were optimized. In the caption we show that the execution time per CPU scales as N^3.

CHAPTER 3

Projective configurational quantum Monte Carlo methods

In the present Chapter, some of the most important projective configurational QMC methods are reviewed. Those methods make use of the imaginary-time evolution to systematically improve a trial wavefunction, and permit the calculation of imaginary-time correlation functions.

3.1 Introduction

The VMC method presented in Sections 2.3 and 2.4 is a very elegant and efficient algorithm. However, it provides estimates of static properties which are inherently biased by the choice of the trial wavefunction.
Projective QMC methods are based on the observation (Theorem 2.2) that the ground state of a many-body system is the asymptotic solution of the imaginary-time Schrödinger equation:

$$-\partial_\tau |\Psi_\tau\rangle = \hat{H} |\Psi_\tau\rangle \tag{3.1}$$

with the initial condition $|\Psi_0\rangle = |\Psi_T\rangle$. Therefore, a trial state Ψ_T used in a VMC calculation can be propagated in imaginary time to yield a better approximation to the ground state. Operatively, a projective QMC method relates the imaginary-time evolution (3.1) to a stochastic process taking values in a suitable manifold. The mapping of the imaginary time evolution (3.1) onto a stochastic process is by no means obvious, and can be realized in many different ways, each giving rise to a distinct projective QMC method. For configurational methods, such manifold is the configurational space of the system while for determinantal methods, that will be presented in Chapter 5, it is the set of N-particle Slater determinants. Expectation values of hermitian operators are represented as stochastic averages over random paths in the manifold, which are sampled using Monte Carlo methods.
To delve into the topic of projective QMC methods, let us consider an introductory example.

3.1.1 Imaginary-time evolution and classical stochastic dynamics

Consider a classical particle subject to the action of a force field $\mathbf{F}(\mathbf{r}) = -\nabla U(\mathbf{r})$, and immersed in a viscous medium exerting the friction force $-\gamma\mathbf{v}$, γ being a phenomenological friction coefficient. For a constant force field $\mathbf{F}(\mathbf{r}) \equiv \mathbf{F}_0$, Newton's equation:

$$m\mathbf{r}_t'' = \mathbf{F}(\mathbf{r}_t) - \gamma\mathbf{r}_t' \tag{3.2}$$

has the particular solution $\mathbf{r}_t = \mathbf{r}_0 + \frac{\mathbf{F}_0}{\gamma}\, t$, and any other solution converges to $\mathbf{r}_t$ in the long time limit. For a slowly-varying force field, a good approximation to the solution of

Newton's equation is still provided by the trajectory satisfying $\gamma \mathbf{r}'_t = \mathbf{F}(\mathbf{r})$. We can thus approximate Newton's equation with:

$$\gamma \mathbf{r}'_t = \mathbf{F}(\mathbf{r}_t) \tag{3.3}$$

The interaction with the medium does not ehxaust to the friction force, but provoques random collisions. To take them into account, we substitute Newton's equation with the following Langevin stochastic differential equation:

$$\gamma dR_t = \mathbf{F}(R_t) + \sigma dB_t \tag{3.4}$$

with the initial condition $R_{t=0} = R_0$, R_0 being a random variable with probability distribution $p_0(\mathbf{r})$. It is well-known, and it is proved in detail in Appendix 9, that the probability distribution $p_t(\mathbf{r})$ of the random variable R_t is the unique solution of the Fokker-Planck parabolic partial differential equation:

$$-\partial_t p_t(\mathbf{r}) = -\frac{\sigma^2}{2} \triangle p_t(\mathbf{r}) + \nabla \left(\mathbf{F}(\mathbf{r}) \cdot \nabla p_t(\mathbf{r}) \right) \tag{3.5}$$

with the initial condition $p_{t=0}(\mathbf{r}) = p_0(\mathbf{r})$. By direct inspection, it is easy to show that:

$$p_\infty(\mathbf{r}) = \frac{e^{-\Phi(\mathbf{r})}}{\int d\mathbf{r}' \, e^{-\Phi(\mathbf{r}')}} \tag{3.6}$$

is a stationary solution of the Fokker-Planck equation if $\sigma^2 \mathbf{F}(\mathbf{r}) = -2\nabla\Phi(\mathbf{r})$, i.e. if $\Phi(\mathbf{r}) = \frac{\sigma^2}{2} U(\mathbf{r})$. Writing:

$$p_t(\mathbf{r}) = \Phi_0(\mathbf{r}) \psi_t(\mathbf{r}) \quad , \qquad \Phi_0(\mathbf{r}) = e^{-\frac{1}{2}\Phi(\mathbf{r})} \tag{3.7}$$

we find that $p_t(\mathbf{r})$ solves the Fokker-Planck equation if $\psi_t(\mathbf{r})$ solves the following partial differential equation:

$$-\partial_t \psi_t(\mathbf{r}) = -\frac{\sigma^2}{2} \triangle \psi_t(\mathbf{r}) + \frac{\sigma^2}{2} \frac{\triangle \Phi_0(\mathbf{r})}{\Phi_0(\mathbf{r})} \psi_t(\mathbf{r}) \tag{3.8}$$

which, introducing the definitions $\frac{\sigma^2}{2} = \frac{\hbar^2}{2m}$, $\frac{\sigma^2}{2} \frac{\triangle \psi_0(\mathbf{r})}{\psi_0(\mathbf{r})} = V(\mathbf{r})$, takes the form:

$$-\partial_t \psi_t(\mathbf{r}) = \hat{H}_{FP} \psi_t(\mathbf{r}) \quad , \qquad \hat{H}_{FP} = -\frac{\hbar^2}{2m} \triangle + V(\mathbf{r}) \tag{3.9}$$

of an imaginary-time Schrödinger equation. By direct inspection, it is easy to verify that:

$$\hat{H}_{FP} \Phi_0(\mathbf{r}) = 0 \tag{3.10}$$

Moreover $\Phi_0(\mathbf{r})$ has constant sign, and thus it is the ground state of $\hat{H}_{FP}$ as proved by R. P. Feynman using a clever variational argument [105]. Therefore:

$$\psi_t = e^{-t\hat{H}_{FP}} \psi_0 \quad , \qquad \lim_{t \to \infty} \psi_t \propto \Phi_0 \tag{3.11}$$

In the light of this observation, we conclude that:

$$\lim_{t\to\infty} p_t(\mathbf{r}) = \Phi_0^2(\mathbf{r}) = \frac{e^{-\Phi(\mathbf{r})}}{\int d\mathbf{r}'\, e^{-\Phi(\mathbf{r}')}} = \frac{e^{-\beta U(\mathbf{r})}}{\int d\mathbf{r}'\, e^{-\beta U(\mathbf{r})}} \quad , \qquad \beta = \frac{\sigma^2}{2} = \frac{\hbar^2}{2m} \tag{3.12}$$

which has the form of a Gibbs probability distribution with inverse temperature β.

We have seen that the stochastic diffusion of a classical particle is in rigorous connection with the imaginary-time dynamics of a quantum particle. With this heuristic example, we have catched a glimpse of the more deep and general connection between real-time stochastic classical dynamics and imaginary-time quantum dynamics. Despite the large number of projective configurational QMC methods, and the fundamental differences between them, this connection is their common inspiring paradigm [84, 106].

3.2 Path Integral Ground State

We know that the imaginary-time Schrödinger equation admits the formal solution:

$$|\Psi_\tau\rangle = e^{-\tau\hat{H}}\,|\Psi_T\rangle \tag{3.13}$$

whence the wavefunction $\Psi_\tau(\mathcal{R})$ has the implicit expression:

$$\Psi_\tau(\mathcal{R}_1) = \int d\mathcal{R}_0\, \langle\mathcal{R}_1|e^{-\tau\hat{H}}|\mathcal{R}_0\rangle\, \Psi_T(\mathcal{R}_0) = \int d\mathcal{R}_0\, G_\tau(\mathcal{R}_1,\mathcal{R}_0)\, \Psi_T(\mathcal{R}_0) \tag{3.14}$$

where the object $G_\tau(\mathcal{R}_1,\mathcal{R}_0) = \langle\mathcal{R}_1|e^{-\tau\hat{H}}|\mathcal{R}_0\rangle$ is called the propagator $G_\tau(\mathcal{R}_1,\mathcal{R}_0)$ of the Hamiltonian operator $\hat{H}$ relative to the imaginary-time interval τ. The use of a finite imaginary time τ is the first approximations characterizing the PIGS method. Except for some special models, propagators are unknown mathematical objects, and thus (3.14) appears not manageable. However, the Trotter formula [107] permits to exactly write (3.13) as:

$$|\Psi_\tau\rangle = \left(e^{-\delta\tau\hat{H}}\right)^m |\Psi_T\rangle \tag{3.15}$$

where m is an integer number and $\delta\tau = \frac{\tau}{m}$ is called time step. Correspondingly:

$$\begin{aligned}\Psi_\tau(\mathcal{R}_m) &= \int d\mathcal{R}_{m-1}\ldots d\mathcal{R}_0\, \langle\mathcal{R}_m|e^{-\delta\tau\hat{H}}|\mathcal{R}_{m-1}\rangle\ldots\langle\mathcal{R}_1|e^{-\delta\tau\hat{H}}|\mathcal{R}_0\rangle\, \Psi_T(\mathcal{R}_0) = \\ &= \int d\mathcal{R}_{m-1}\ldots d\mathcal{R}_0 \prod_{i=0}^{m-1} G_{\delta\tau}(\mathcal{R}_{i+1},\mathcal{R}_i)\, \Psi_T(\mathcal{R}_0)\end{aligned} \tag{3.16}$$

Even if (3.14) appears much more complicated than its counterpart (3.14) it involves propagators $G_{\delta\tau}(\mathcal{R}_{i+1},\mathcal{R}_i)$ relative to the small imaginary-time interval $\delta\tau$, for which extremely useful and accurate approximations exist. The adoption of one of these analytic but approximate forms is the second approximation characterizing the PIGS method. The most simple approximations are the primitive approximation:

$$e^{-\tau\hat{H}} \simeq e^{-\tau\hat{T}}e^{-\tau\hat{V}} \tag{3.17}$$

and the Trotter-Suzuki or symmetrized primitive approximation:

$$e^{-\tau\hat{H}} \simeq e^{-\frac{\tau}{2}\hat{V}} e^{-\tau\hat{T}} e^{-\frac{\tau}{2}\hat{V}} \tag{3.18}$$

Their accuracy is assessed by the following:

Theorem 3.1 ([107, 108, 109])**.** *Let $\hat{A}, \hat{B}$ be two bounded operators. Then:*

$$e^{-\tau(\hat{A}+\hat{B})} = e^{-\tau\hat{A}} e^{-\tau\hat{B}} + \mathcal{O}(\tau^2) \tag{3.19}$$

and:

$$e^{-\tau(\hat{A}+\hat{B})} = e^{-\frac{\tau}{2}\hat{A}} e^{-\tau\hat{B}} e^{-\frac{\tau}{2}\hat{A}} + \mathcal{O}(\tau^3) \tag{3.20}$$

Proof. *Since the operators $\hat{A}, \hat{B}$ are bounded, the exponential $e^{-\tau(\hat{A}+\hat{B})}$ can be written as sum of the Taylor series:*

$$e^{-\tau(\hat{A}+\hat{B})} = \sum_{n=0}^{\infty} \frac{(-\tau)^n}{n!} (\hat{A}+\hat{B})^n \tag{3.21}$$

whence:

$$e^{-\tau(\hat{A}+\hat{B})} = I - \tau(\hat{A}+\hat{B}) + \frac{\tau^2}{2}(\hat{A}+\hat{B})^2 + \mathcal{O}(\tau^3) = I - \tau\hat{A} - \tau\hat{B} + \frac{\tau^2}{2}\left(\hat{A}^2 + \hat{B}^2 + \{\hat{A}, \hat{B}\}\right) \tag{3.22}$$

readily follows. Expressing also the product $e^{-\tau\hat{A}} e^{-\tau\hat{B}}$ in terms of the Taylor series of $e^{-\tau\hat{A}}$ and $e^{-\tau\hat{B}}$ reveals that:

$$e^{-\tau\hat{A}} e^{-\tau\hat{B}} = I - \tau\hat{A} - \tau\hat{B} + \frac{\tau^2}{2}\left(\hat{A}^2 + \hat{B}^2\right) + \tau^2\hat{A}\hat{B} + \mathcal{O}(\tau^3) \tag{3.23}$$

comparing (3.22) *and* (3.23) *we conclude that* (3.19) *holds. Performing a similar study we easily verify that also* (3.20) *holds. The approximation* (3.20) *is considerably more accurate than* (3.19)*, its error scaling as $\mathcal{O}(\tau^3)$.*

The (3.19) has been proved under the simplifying assumption that the operators $\hat{A}, \hat{B}$ are bounded, but holds under milder assumptions. In particular, it applies to the kinetic energy and to a broad class of potential energies, which are not bounded. Naturally, there exist other approximations besides (3.19), like the pair-product [110, 111]:

$$G_{\delta\tau}(\mathcal{R}, \mathcal{R}') = \langle \mathcal{R} | e^{-\delta\tau\hat{T}} | \mathcal{R}' \rangle \prod_{i<j=1}^{N} G_{2,\delta\tau}(\mathbf{r}_{ij}, \mathbf{r}'_{ij}) \tag{3.24}$$

where $G_{2,\delta\tau}(\mathbf{r}_{ij}, \mathbf{r}'_{ij})$ a the two-body effective-potential propagator, which depends on the relative coordinates $\mathbf{r}_{ij} = \mathbf{r}_i - \mathbf{r}_j$. Various methods exist to obtain the two-body propagator, one of these is to solve exactly the Schrödinger equation for two interacting particles, determining an exact two-body propagator. Other relevant approximations of the short-time many-body propagator are the pair Suzuki-Chin approximation [112], which is a pair approximation of the fourth order Suzuki-Chin density matrix [113], the multiproduct expansion [114, 115] and the pair multiproduct expansion [116].
The usefulness of Theorem 3.1 is immediately understood: since, as we will see in a moment, the propagators of the kinetic and potential energies $\hat{T}, \hat{V}$ can be computed analytically, the main difficulty in computing the propagator of the complete Hamiltonian

$\hat{H}$ comes from the non-commutativity between $\hat{T}$ and $\hat{V}$. The use of approximations like (3.20) removes this difficulty, reducing the propagator of the complete Hamiltonian $\hat{H}$ to a combination of the propagators of the kinetic and potential energies at the cost of an error which drops as $\mathcal{O}(\delta\tau^n)$ for some n (in the case of (3.20), $n = 3$).

Let us now compute the Trotter-Suzuki decomposition of the propagator. First we take the matrix element of $e^{-\delta\tau\hat{V}}$ over two configurations $|\mathcal{R}\rangle, |\mathcal{R}'\rangle$ having neither Bose nor Fermi symmetry. As we will see in a moment this choice, even if not rigorous, leads to a much simpler functional form of the propagator and to a propagated wavefunction with the desired symmetry. Since:

$$\langle\mathcal{R}|e^{-\delta\tau\hat{V}}|\mathcal{R}'\rangle = \delta(\mathcal{R}-\mathcal{R}')\, e^{-\delta\tau V(\mathcal{R})} \tag{3.25}$$

then:

$$\langle\mathcal{R}|e^{-\delta\tau\hat{H}}|\mathcal{R}'\rangle = e^{-\frac{\delta\tau}{2}V(\mathcal{R})}\, \langle\mathcal{R}|e^{-\delta\tau\hat{T}}|\mathcal{R}'\rangle\, e^{-\frac{\delta\tau}{2}V(\mathcal{R}')} \tag{3.26}$$

For a system of N particles in PBC, the propagator of the kinetic energy is:

$$\begin{aligned}
&\langle\mathcal{R}|e^{-\delta\tau\hat{T}}|\mathcal{R}'\rangle = \langle\mathbf{r}_1\dots\mathbf{r}_N|e^{-\delta\tau\hat{T}}|\mathbf{r}'_1\dots\mathbf{r}'_N\rangle = \\
&= \sum_{\mathbf{k}_1\dots\mathbf{k}_N} \langle\mathbf{r}_1\dots\mathbf{r}_N|\mathbf{k}_1\dots\mathbf{k}_N\rangle e^{-\delta\tau\sum_i\lambda_i|\mathbf{k}_i|^2}\langle\mathbf{k}_1\dots\mathbf{k}_N|\mathbf{r}'_1\dots\mathbf{r}'_N\rangle = \\
&= \prod_{i=1}^{N}\prod_{\alpha=1}^{d}\sum_{k_{i,\alpha}} \frac{e^{ik_{i,\alpha}(r_{i,\alpha}-r'_{i,\alpha})}}{L}\, e^{-\delta\tau\lambda_i k_{i,\alpha}^2} = \prod_{i=1}^{N}\prod_{\alpha=1}^{d} g_{\delta\tau\lambda_i}(r_{i,\alpha}-r'_{i,\alpha})
\end{aligned} \tag{3.27}$$

where $\lambda_i = \frac{\hbar^2}{2m}$, and:

$$g_{\delta\tau\lambda_i}(r) = \frac{1}{L}\sum_{n\in\mathbb{Z}} e^{i\frac{2\pi n}{L}r} e^{-\delta\tau\lambda_i\left(\frac{2\pi n}{L}\right)^2} \tag{3.28}$$

This function is readily evaluated, recalling that:

$$\sum_{n\in\mathbb{Z}} e^{bn}\, e^{-an^2} = \frac{e^{\frac{b^2}{4a}}}{\sqrt{a}}\,\vartheta_3\left(-\frac{b\pi}{2a}, e^{-\frac{\pi^2}{a}}\right) \qquad b\in\mathbb{C}\,,\ a>0 \tag{3.29}$$

$\vartheta_3(u,v)$ denoting Jacobi's theta function. For large systems, the propagator of the kinetic energy considerably simplifies due to the Euler-MacLaurin formula:

$$g_{\delta\tau\lambda_i}(r) \simeq \frac{1}{2\pi}\int_{-\infty}^{\infty} dk\, e^{irk}\, e^{-\delta\tau\lambda_i k^2} = \frac{e^{-\frac{r^2}{4\delta\tau\lambda_i}}}{\sqrt{4\pi\delta\tau\lambda_i}} \tag{3.30}$$

which gives the following expression:

$$\langle\mathcal{R}|e^{-\delta\tau\hat{T}}|\mathcal{R}'\rangle = \prod_{j=1}^{N}\frac{e^{-\sum_{i=0}^{2m-1}\frac{|\mathbf{r}_{j,i+1}-\mathbf{r}_{j,i}|^2}{4\delta\tau\lambda_j}}}{(4\pi\delta\tau\lambda_j)^{\frac{d}{2}}} \tag{3.31}$$

for the propagator of the kinetic energy. It is evident from (3.26) and (3.31) that the propagator has neither Bose nor Fermi symmetry, but only the following property:

$$G_{\delta\tau}(\sigma\mathcal{R},\sigma\mathcal{R}') = G_{\delta\tau}(\mathcal{R},\mathcal{R}') \qquad \sigma\in S_N \tag{3.32}$$

holding for any permutation σ of the set $\{1 \dots N\}$. Thanks to this property, the wavefunction (3.16) has the same symmetry of the trial wavefunction. Indeed:

$$\begin{aligned}\Psi_\tau(\sigma\mathcal{R}_1) &= \int d\mathcal{R}_0\, G_{\delta\tau}(\sigma\mathcal{R}_1, \mathcal{R}_0)\, \Psi_T(\mathcal{R}_0) = \int d\mathcal{R}_0\, G_{\delta\tau}(\mathcal{R}_1, \sigma^{-1}\mathcal{R}_0)\, \Psi_T(\mathcal{R}_0) = \\ &= \int d\mathcal{R}_0\, G_{\delta\tau}(\mathcal{R}_1, \mathcal{R}_0)\, \Psi_T(\sigma\mathcal{R}_0) = (\pm 1)^\sigma \int d\mathcal{R}_0\, G_{\delta\tau}(\mathcal{R}_1, \mathcal{R}_0)\, \Psi_T(\mathcal{R}_0) = \\ &= (\pm 1)^\sigma \Psi_\tau(\mathcal{R}_1)\end{aligned} \tag{3.33}$$

and (3.33) trivially extends to more than one propagation step. The expression (3.14) of the propagated wavefunction yields the following formula for the average of a local operator $\hat{O}$ over the wavefunction $\Psi_\tau(\mathcal{R})$:

$$\begin{aligned}\langle \hat{O} \rangle_\tau &= \frac{\langle \Psi_\tau | \hat{O} | \Psi_\tau \rangle}{\langle \Psi_\tau | \Psi_\tau \rangle} = \\ &= \frac{\int d\mathcal{R}_0 \dots d\mathcal{R}_{2m} \prod_{i=0}^{2m-1} G_{\delta\tau}(\mathcal{R}_{i+1}, \mathcal{R}_i)\, \Psi_T(\mathcal{R}_{2m})\, O(\mathcal{R}_m)\, \Psi_T(\mathcal{R}_0)}{\int d\mathcal{R}_0 \dots d\mathcal{R}_{2m} \Psi_T(\mathcal{R}_{2m}) \prod_{i=0}^{2m-1} G_{\delta\tau}(\mathcal{R}_{i+1}, \mathcal{R}_i)\, \Psi_T(\mathcal{R}_0)} = \\ &= \frac{\int d\mathcal{X} \Pi(\mathcal{X})\, O(\mathcal{X})}{\int d\mathcal{X} \Pi(\mathcal{X})} = \int d\mathcal{X} \frac{\Pi(\mathcal{X})}{\int d\mathcal{X}' \Pi(\mathcal{X}')}\, O(\mathcal{X})\end{aligned} \tag{3.34}$$

where the locality assumption $\langle \mathcal{R} | \hat{O} | \mathcal{R}' \rangle = O(\mathcal{R})\, \delta(\mathcal{R} - \mathcal{R}')$ has been used. In the last member of equation (3.34), the average $\langle \hat{O} \rangle_\tau$ has been expressed, as illustrated in Figure 3.2, as the ratio between two integrals over discretized paths:

$$\mathcal{X} = (\mathcal{R}_{2m} \dots \mathcal{R}_0) \in \mathcal{C}^n \tag{3.35}$$

with respect to the measure:

$$\Pi(\mathcal{X}) = \Psi_T(\mathcal{R}_{2m}) \prod_{i=0}^{2m-1} G_{\delta\tau}(\mathcal{R}_{i+1}, \mathcal{R}_i)\, \Psi_T(\mathcal{R}_0) \tag{3.36}$$

Expressions of the form (3.34) are called *path integrals* after the seminal work by R. P. Feynman [117]. To prove computationally useful, a path integral must involve a positive and normalized measure (3.36) that, by virtue of such properties, can be sampled using the Metropolis algorithm. Since the propagators $G_{\delta\tau}(\mathcal{R}_{i+1}, \mathcal{R}_i)$ are positive, requiring that $\Pi(\mathcal{X}) > 0$ over all paths $\mathcal{X}$ means requiring that the trial state $\Psi_T(\mathcal{R})$ be non-negative. For Bose systems, Jastrow-Feenberg trial wavefunctions fulfil such requirement, permitting to devise an algorithmic procedure for computing ground-state averages of local operators by stochastically sampling the measure (3.36).

This algorithm was first introduced by D. M. Ceperley [3] under the name of Variational Path Integral. It inspired several other methods, based on different strategies for sampling the path space $\mathcal{C}^n$, like the Reptation Monte Carlo [118] and the Path Integral Ground State (PIGS) method, introduced by A. Sarsa, K. Schmidt and W. Magro [119]. Being based on Feynman's path *real-space imaginary-time* formulation of quantum mechanics, path integral methods have long been the paradigmatic approaches to simulating Bose systems at zero temperature.

The PIGS method is *exact* whenever the two approximations underlying it, namely the

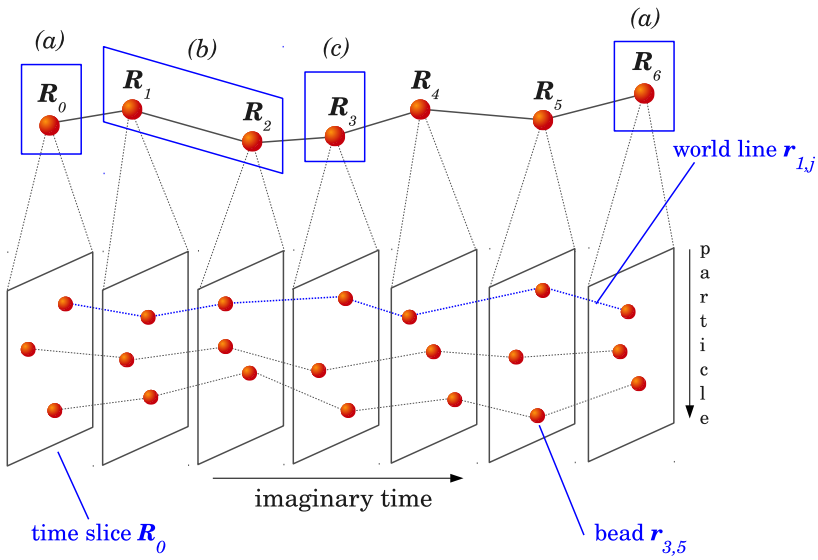

Figure 3.1: Top: Schematic representation of the integrals in (3.34). (a) At the extrema of the path, the trial wavefunction is computed. (b) Between all pairs of adjacent configurations, the propagator is computed. The product of these objects efines the measure (3.36). (c) At the center of the path, where the ground-state has been reached, the estimator of the observable $\mathcal{O}$ is computed. Bottom: Schematic representation of the PIGS terminology.

choice of a finite projection time τ and of a finite time step $\delta\tau$, affect the computed expectation values to an extent which is below their statistical uncertainty. Such a regime is always attainable by using a large enough M and a small enough $\delta\tau$ [119].

Extension to non-local observables. For the sake of simplicity, only the PIGS estimator for local observables $\hat{O}$ like the potential energy and the static structure factor has been worked out in (3.34). The algorithm, however, can be extended to non-local observables like the total energy and the OBDM. The ground-state average of the total energy is obtained exploiting the commutation between $\hat{H}$ and $e^{-\tau\hat{H}}$:

$$\langle\hat{H}\rangle_\tau = \frac{\langle\Psi_\tau|\hat{H}|\Psi_\tau\rangle}{\langle\Psi_\tau|\Psi_\tau\rangle} = \frac{\langle\Psi_{2\tau}|\hat{H}|\Psi_T\rangle}{\langle\Psi_{2\tau}|\Psi_T\rangle} \tag{3.37}$$

and the expression (3.16) to obtain:

$$\langle\hat{H}\rangle_\tau = \frac{\int d\mathcal{X}\,\Pi(\mathcal{X})\,E(\mathcal{X})}{\int d\mathcal{X}\,\Pi(\mathcal{X})} \tag{3.38}$$

where $E(\mathcal{X}) = E_L(\mathcal{R}_0)$. The ground-state average $\langle\hat{T}\rangle_\tau$ of the kinetic energy can be easily obtained as the difference $\langle\hat{T}\rangle_\tau = \langle\hat{H}\rangle_\tau - \langle\hat{V}\rangle_\tau$ between the ground-state averages of the total and potential energies.

3.2.1 The fermion sign problem

The positivity of the measure $\Pi(\mathcal{X})$ is an essential requisite for constructing the PIGS algorithm. For Fermi system, any trial wavefunction $\Psi_T(\mathcal{R})$ must be an antisymmetric under the exchange of two or more particles, and thus it cannot be a non-negative object. The measure $\Pi(\mathcal{X})$ is therefore non-positive, and the question whether the PIGS algorithm can actually be applied to the investigation of Fermi systems rises. To address this delicate issue, let us write the trial wavefunction as:

$$\Psi_T(\mathcal{R}) = |\Psi_T(\mathcal{R})|\,\mathrm{sgn}\,(\Psi_T(\mathcal{R})) \tag{3.39}$$

obtaining the decomposition:

$$\Pi(\mathcal{X}) = |\Pi(\mathcal{X})|\,\mathcal{S}(\mathcal{X}) \tag{3.40}$$

for the measure $\Pi(\mathcal{X})$, where $\mathcal{S}(\mathcal{X}) = \mathrm{sgn}\,(\Pi(\mathcal{X})) = \mathrm{sgn}\,(\Psi_T(\mathcal{R}_{2m})\,\Psi_T(\mathcal{R}_0))$. In the light of the decomposition (3.40), the PIGS estimator (3.34) takes the form:

$$\langle\hat{O}\rangle_\tau = \frac{\int d\mathcal{X}\,|\Pi(\mathcal{X})|\,\mathcal{S}(\mathcal{X})\,O(\mathcal{X})}{\int d\mathcal{X}\,|\Pi(\mathcal{X})|\,\mathcal{S}(\mathcal{X})} = \frac{\int d\mathcal{X}\,\frac{|\Pi(\mathcal{X})|}{\int d\mathcal{X}'\,|\Pi(\mathcal{X}')|}\,\mathcal{S}(\mathcal{X})\,O(\mathcal{X})}{\int d\mathcal{X}\,\frac{|\Pi(\mathcal{X})|}{\int d\mathcal{X}'\,|\Pi(\mathcal{X}')|}\,\mathcal{S}(\mathcal{X})} \tag{3.41}$$

of a ratio between path integrals. Each of the path integrals appearing in (3.41) can be stochastically sampled, since $|\Pi(\mathcal{X})|$ is by construction a positive quantity. Unfortunately, either in the thermodynamic limit $N \to \infty$ or in the long imaginary time limit $\tau \to \infty$, (3.41) is a $\frac{0}{0}$ indeterminate form. To verify this fact, let us cast the denominator

of (3.41) in the following form:

$$\int d\mathcal{X}\, \frac{|\Pi(\mathcal{X})|}{\int d\mathcal{X}'\, |\Pi(\mathcal{X}')|}\, \mathcal{S}(\mathcal{X}) = \frac{\langle \Psi_T | e^{-2\tau \hat{H}} | \Psi_T \rangle}{\langle \tilde{\Psi}_T | e^{-2\tau \hat{H}} | \tilde{\Psi}_T \rangle} \tag{3.42}$$

where $\tilde{\Psi}_T(\mathcal{R}) = |\Psi_T(\mathcal{R})|$ is a Bose wavefunction. In order to estimate (3.42), let us then expand $\Psi_T(\mathcal{R})$ and $|\Psi_T(\mathcal{R})|$ on a complete set of Bose and Fermi eigenstates of the Hamiltonian $\hat{H}$ respectively:

$$\Psi_T(\mathcal{R}) = \sum_\mu c_\mu\, \varphi_\mu^{(F)}(\mathcal{R}) \qquad\qquad \tilde{\Psi}_T(\mathcal{R}) = |\Psi_T(\mathcal{R})| = \sum_\mu \tilde{c}_\mu\, \varphi_\mu^{(B)}(\mathcal{R}) \tag{3.43}$$

and substitute (3.43) into (3.42) to find:

$$\int d\mathcal{X}\, \frac{|\Pi(\mathcal{X})|}{\int d\mathcal{X}'\, |\Pi(\mathcal{X}')|}\, \mathcal{S}(\mathcal{X}) = \frac{\sum_\mu |c_\mu|^2\, e^{-2\tau \epsilon_\mu^{(F)}}}{\sum_\mu |\tilde{c}_\mu|^2\, e^{-2\tau \epsilon_\mu^{(B)}}} \tag{3.44}$$

In order to understand the behavior of (3.44), it is important to observe that the energies $\epsilon_\mu^{(F)}, \epsilon_\mu^{(B)}$ are extensive quantities, and that the Fermi ground state $\varphi_\mu^{(F)}(\mathcal{R})$ has higher energy than the Bose ground state $\varphi_\mu^{(B)}(\mathcal{R})$, i.e. $\epsilon_0^{(F)} > \epsilon_0^{(B)}$. In the light of these observations, we conclude that (3.44) drops as:

$$\int d\mathcal{X}\, \frac{|\Pi(\mathcal{X})|}{\int d\mathcal{X}'\, |\Pi(\mathcal{X}')|}\, \mathcal{S}(\mathcal{X}) \simeq \frac{|c_\mu|^2}{|\tilde{c}_\mu|^2}\, e^{-2\tau \left(\epsilon_0^{(F)} - \epsilon_0^{(B)} \right)} \tag{3.45}$$

either in the thermodynamic limit $N \to \infty$ or in the long imaginary time limit $\tau \to \infty$. The appearance of an indeterminate form in the PIGS estimator (3.42) is the infamous *fermion sign problem*, first discovered by R. P. Feynman and A. R. Hibbs at pages 292-293 of [2] where, after describing the path integral theory for superfluid ^{4}He, the authors noted:

The path integral expression for Fermi particles, such as ^{3}He, is also easily written down. However, in the case of liquid ^{3}He, the effect of the potential is very hard to evaluate quantitatively in an accurate manner. The reason for this is that the contribution of a cycle to the sum over permutations is either positive or negative depending on whether the cycle has an odd or even number of atoms in its length L. At very low temperature, the contributions of cycles such as $L = 51$ and $L = 52$ are very nearly equal but opposite in sign, and therefore they very nearly cancel. It is necessary to compute the difference between such terms, and this requires very careful calculation of each term separately. It is very difficult to sum an alternating series of large terms which are decreasing slowly in magnitude when a precise analytic formula for each term is not available. Progress could be made in this problem if it were possible to arrange the mathematics describing a Fermi system in a way that corresponds to a sum of positive terms. Some such schemes have been tried, but the resulting terms appear to be much too hard to evaluate even qualitatively. The (explanation) of the superconducting state was first answered in a convincing way by Bardeen, Cooper, and Schrieffer. The path integral approach played no part in their analysis, and in fact has never proved useful for degenerate Fermi systems. [2]

As Feynman and Hibbs argued, for the calculation of any ground state average by the direct Fermi PIGS there is a tremendous loss of efficiency over the Bose case. As we will

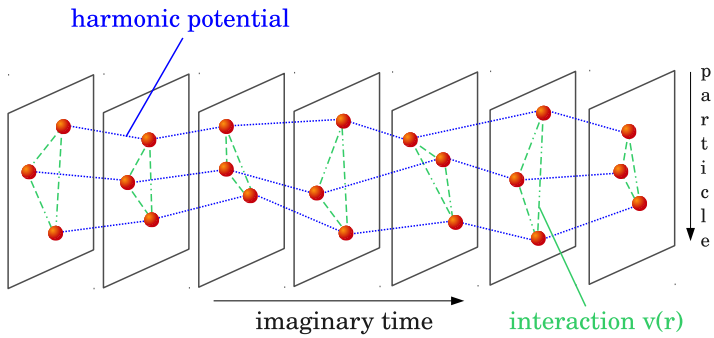

Figure 3.2: (a) Schematic representation of the quantum-classical isomorphism. World lines of the PIGS algorithm are in one-to-one correspondence with classical polymers. Blue dotted lines represent the harmonic interaction between adjacent beads in the same world line, while green dashed lines represent the actual interaction between beads in the same configuration.

see in Sections 3.3, 3.4, the simulation of Fermi particles with projective configurational QMC methods requires the implementation of suitable approximation schemes.

3.2.2 The quantum-classical isomorphism

The paths $\mathcal{X}$ are collections $\mathcal{X} = (\mathcal{R}_0 \dots \mathcal{R}_{2m})$ of configurations, and each configuration is a snapshot $\mathcal{R}_i = (\mathbf{r}_{1,i} \dots \mathbf{r}_{N,i})$ of the system. In the PIGS literature, the generic configuration $\mathbf{r}_{j,i}$ is called *beads*, and the set of configurations $\{\mathbf{r}_{j,i}\}_{i=0}^{2m}$ relative to the j-th paricle is called its *world line*. These terms are illustrated in Figure 3.2.
The probability distribution (3.36) has a surprising and suggestive physical meaning. For the sake of simplicity, we use the primitive approximation and write:

$$\Pi(\mathcal{X}) = \left(\prod_{j=1}^{N} \frac{e^{-\sum_{i=0}^{2m-1} \frac{|\mathbf{r}_{j,i+1} - \mathbf{r}_{j,i}|^2}{4\delta\tau\lambda_j}}}{(4\pi\delta\tau\lambda_j)^{\frac{d}{2}}} \right) \left(\prod_{i=0}^{2m} e^{-\sum_{j<k} v(\mathbf{r}_{j,i} - \mathbf{r}_{k,i})} \right) \Psi_T(\mathcal{R}_0)\, \Psi_T(\mathcal{R}_{2m}) \tag{3.46}$$

we realize that quantum ground-state averages are equivalent to canonical averages of a classical system of special interacting linear polymers. Each polymer, in particular, corresponds to a world line. The first factor reveals that beads along the same world line, i.e. particles in the same polymer, interact with a harmonic potential, while beads in the same configuration interact with the interparticle potential $v(\mathbf{r})$. At the extrema $\mathcal{R}_0, \mathcal{R}_{2m}$ of the polymers, the interaction is modified by the presence of the trial wavefunction, typically encompassing two-body Jastrow correlations.

At the beginning of the present Section, we saw that the stochastic diffusion of a purely classical particle is in rigorous connection with the imaginary-time dynamics of a quantum particle. The quantum-classical isomorphism expressed by (3.46) corroborates and generalizes that observation, and allows to foresee its practical implications. In fact, the somewhat unfamiliar concept of imaginary-time dynamics enters as a fascinating link between classical and quantum Physics, which permits to interpret quantum mechanical phenomena in terms of classical and more intuitive concepts, and to simulate the intriguing properties of quantum systems by means of auxiliary classical problems.
In the case of PIGS, the imaginary-time projection has been mapped onto the thermodynamics of a canonical ensemble of classical polymers. In the case of Diffusion Monte Carlo, we will be brought to study the real-time stochastic dynamics of a classical system.

3.2.3 Details of the PIGS algorithm.

The PIGS method relies on the Metropolis-Hastings algorithm to sample the probability distribution $\Pi(\mathcal{X})$, and computes the ground-state average of an operator $\hat{O}$ as sample average of a suitable estimator $O(\mathcal{X})$. Defining a good transition probability distribution $\mathcal{T}(\mathcal{X} \to \mathcal{X}')$ is an essential requisite for developing an efficient algorithm. Unlike in the VMC method, where the transition probability distribution $\mathcal{T}(\mathcal{R} \to \mathcal{R}')$ has the form (2.28) or (2.87), signifying that only one move is tried, in the PIGS method the transition probability distribution is a convex linear combination:

$$\mathcal{T}(\mathcal{X} \to \mathcal{X}') = \sum_i p_i \, \mathcal{T}_i(\mathcal{X} \to \mathcal{X}') \tag{3.47}$$

of elementary transition probability distributions $\mathcal{T}_i(\mathcal{X} \to \mathcal{X}')$, each corresponding to an elementary move which is tried with probability p_i. The most common moves are listed below:

- *uniform translation*: a polymer $\mathbf{p}_i = (\mathbf{r}_{i,2m} \dots \mathbf{r}_{i,0})$ is chosen randomly and shifted of an amount $\delta\mathbf{r}$:
$$\mathbf{r}_{i,j} \to \mathbf{r}'_{i,j} = \mathbf{r}_{i,j} + \delta\mathbf{r} \tag{3.48}$$
which is typically normally distributed with mean $\mathbf{0}$ and variance σ_T.

- *tail move*: a polymer $\mathbf{p}_i = (\mathbf{r}_{i,2m} \dots \mathbf{r}_{i,0})$ is chosen randomly, all the beads $\mathbf{r}_{i,j}$ with j after (or before) a randomly chosen extremum m_1, i.e. $j > m_1$ (or $j < m_1$) are removed and substituted with a Brownian motion starting at $\mathbf{r}_{i,m_1}$. For $j > m_1$, in particular:
$$\mathbf{r}_{i,j} \to \mathbf{r}'_{i,j} = \mathbf{r}_{i,m_1} + \sigma_B \, B_{\frac{j-m_1}{m_2-m_1}} \tag{3.49}$$

- *brownian bridge move*: a polymer $\mathbf{p}_i = (\mathbf{r}_{i,2m} \dots \mathbf{r}_{i,0})$ is chosen randomly, all the beads $\mathbf{r}_{i,j}$ with j between two randomly chosen extrema m_1, m_2 ($m_1 < j < m_2$) are removed, and substituted with a Brownian bridge connecting $\mathbf{r}_{i,m_1}$ and $\mathbf{r}_{i,m_2}$:

$$\mathbf{r}_{i,j} \to \mathbf{r}'_{i,j} = \mathbf{r}_{i,m_1} + \frac{j-m_1}{m_2-m_1} \, (\mathbf{r}_{i,m_2} - \mathbf{r}_{i,m_1}) + \sigma_{\tilde{B}} \, \tilde{B}_{\frac{j-m_1}{m_2-m_1}} \tag{3.50}$$

The probabilities p_i and the parameters $\sigma_T, \sigma_W, \sigma_B$ have to be adjusted in such a way as to maintain the acceptance of the algorithm close to the optimal $50\,\%$ value.

3.2.4 Imaginary-time correlations and the PIGS method

For simplicity, let us consider operators $\hat{O}_i$, $\hat{O}_j$ that are diagonal in the coordinare representation, like the density flutuation operator. The imaginary-time correlation function (1.28) is given by:

$$F_{ij}(k\delta\tau) = \frac{\langle \Psi_T | e^{-(m-k)\delta\tau\hat{H}} \hat{O}_i e^{-k\delta\tau\hat{H}} \hat{O}_j^\dagger e^{-m\delta\tau\hat{H}} | \Psi_T \rangle}{\langle \Psi_T | e^{-2m\delta\tau\hat{H}} | \Psi_T \rangle} \tag{3.51}$$

Using (3.34), (3.51) is transformed into an integral over discretized paths $\mathcal{X}$:

$$F_{ij}(k\delta\tau) = \int d\mathcal{X} O_{ij}(\mathcal{X}) \Pi(\mathcal{X}) \tag{3.52}$$

the estimator $O_{ij}(\mathcal{X}) = \mathcal{O}_i(\mathcal{R}_{m+k})\mathcal{O}_j^*(\mathcal{R}_m)$ requires the evalutation of the operators $\hat{O}_i$, $\hat{O}_j$ at two configurations displaced by k imaginary-time steps. The inverse Laplace transform of the ITFS output by a PIGS calculation must be computed, in order to obtain the DSF $S_{ij}(\omega)$. This delicate issue will be dealt with in Appendix 12.

3.3 Diffusion Monte Carlo

One of the most efficient and widely used projective QMC methods is the Diffusion Monte Carlo (DMC), introduced R. C. Grimm and R. G. Storer [120] and J. Anderson [121, 122] and refined by several authors, including P. J. Reynolds *et al.* [123] and R. Assaraf *et al.* [124]. The DMC method had a spectacular debut [125] in a paper by D. M. Ceperley and B. J. Alder, which provided density functional calculations of molecules and solids with the well-known LDA functional. Since then, the DMC method has been extensively used to investigate electronic properties of molecules and solids [99]. The DMC method, used in Chapter 7, is reviewed in the present Section, with the purpose of making the present thesis more self-contained, and of preparing the description of the phaseless AFQMC method in Chapter 5, which bears some relationship with the DMC method.

3.3.1 Pure Diffusion Monte Carlo

DMC provides a stochastic solution of the imaginary-time Schrödinger equation:

$$-\partial_\tau \Psi_\tau(\mathcal{R}) = -\sum_i \frac{\hbar^2 \triangle_i}{2m_i} \Psi_\tau(\mathcal{R}) + V(\mathcal{R})\Psi_\tau(\mathcal{R}) \tag{3.53}$$

relating it to a suitable stochastic process. As sketched in the introduction of 3, this mapping could be quite naturally accomplished if (3.53) had the form (3.5) of a Fokker-Planck equation. Even if (3.53) has some remarkable resemblance with a Fokker-Planck equation, there are two important differences:

- wavefunctions $\Psi_\tau(\mathcal{R})$ are in principle complex-valued, while the Fokker-Planck equation only applies to positive functions. This problem is absent in Bose systems with time-reversal symmetry, whose ground state is non-degenerate and has a non-negative wavefunction (as discussed in 3.2).

- equation (3.53) contains a multiplicative term $V(\mathcal{R})\Psi_\tau(\mathcal{R})$ which is absent in a Fokker-Planck equation. Due to such term, the integral over the configurational space of $\Psi_\tau(\mathcal{R})$ acquires a non-trivial time dependence, which is absent in the Fokker-Planck equation.

Despite these apparent difficulties, it is possible to simulate (3.53) by means of stochastic processes. Indeed, the Feynman-Kac formula (2.46) gives the following representation:

$$\begin{aligned}\Psi_\tau(\mathcal{R}) &= E[\Psi_T(\mathcal{R}_\tau)e^{-\int_0^\tau d\tau' V(\mathcal{R}_{\tau'})}] = \\ &= \lim_{m\to\infty}\int d\mathcal{R}_m \dots d\mathcal{R}_0 \prod_{i=0}^{m} G_{\delta\tau}(\mathcal{R}_{i+1},\mathcal{R}_i)\, e^{-\sum_{i=0}^{m+1}\delta\tau V(\mathcal{R}_i)}\,\Psi_T(\mathcal{R}_0)\end{aligned} \tag{3.54}$$

for the solution of (3.53). In (3.54) $\delta\tau = \frac{\tau}{m}$, $\mathcal{R}_{m+1} = \mathcal{R}$ and the expectation is taken over the trajectories of the dN-dimensional Brownian motion ending at $\mathcal{R}$, whence:

$$G_{\delta\tau}(\mathcal{R},\mathcal{R}') = \frac{e^{-\frac{(\mathcal{R}-\mathcal{R}')^2}{2\delta\tau}}}{(2\pi\delta\tau)^{\frac{dN}{2}}} \tag{3.55}$$

is the propagator of the kinetic energy operator. The stochastic representation (3.54) of $\Psi_\tau(\mathcal{R})$ holds for Bose and Fermi wavefunctions, and gives access to mixed estimates of physical observables:

$$\mathcal{O}_{mix}(\tau) = \frac{\langle\Psi_T|\hat{O}|\Psi_\tau\rangle}{\langle\Psi_T|\Psi_\tau\rangle} = \frac{\int d\mathcal{R}\,\mathcal{O}_L(\mathcal{R})\Psi_T(\mathcal{R})\Psi_\tau(\mathcal{R})}{\int d\mathcal{R}\,\Psi_T(\mathcal{R})\Psi_\tau(\mathcal{R})} \quad , \qquad \mathcal{O}_L(\mathcal{R}) = \frac{\big(\hat{O}\Psi_T\big)(\mathcal{R})}{\Psi_T(\mathcal{R})} \tag{3.56}$$

which have the form of averages over the function $\Psi_\tau(\mathcal{R})$ instead of its square modulus. Notice that $\mathcal{O}_{mix}(0)$ is the variational estimate of $\hat{O}$. Moreover, for an observable described by an operator $\hat{O}$ commuting with $\hat{H}$, in the long-imaginary time limit $\mathcal{O}_{mix}(\tau)$ converges to an exact ground-state average. Merging (3.54) and (3.56), leads to an algorithmic procedure for computing mixed estimates:

1. Initialize a large number N_w of configurations $\{\mathcal{R}_{w,0}\}_{w=1}^{N_w}$ sampling them from the positive function $\Psi_T(\mathcal{R})$. The configurations $\mathcal{R}_{w,0}$ are called *walkers*. Assign to each walker a weight $\mathfrak{W}_{w,0} = 1$

2. Evolve the walker configurations as:

$$\mathcal{R}_{w,i+1} = \mathcal{R}_{w,i} + \eta_{w,i} \tag{3.57}$$

   where the vectors $\eta_{w,i}$ are sampled from independent normal random variables with mean 0 and variance $\frac{\hbar^2\delta\tau}{2m}$. Update the walker weights as:

$$\mathfrak{W}_{w,i+1} = \mathfrak{W}_{w,i}\, e^{-\delta\tau V(\mathcal{R}_{w,i})} \tag{3.58}$$

3. estimate $\mathcal{O}_{mix}(i\delta\tau)$ as:

$$\mathcal{O}_{mix}(i\delta\tau) \simeq \frac{\sum_{w=1}^{N_w} O_L(\mathcal{R}_{w,i})\,\Psi_T(\mathcal{R}_{w,i})\,\mathfrak{W}_{w,i}}{\sum_{w=1}^{N_w}\Psi_T(\mathcal{R}_{w,i})\,\mathfrak{W}_{w,i}} \tag{3.59}$$

4. iterate the previous two steps until convergence to the ground state

This basic form of the DMC algorithm, the *pure DMC without importance sampling* [99], cleverly exploits the stochastic representation of the imaginary-time Schrödinger equation to compute mixed estimates of physical properties. The use of the Feynman-Kac formula reveals that the problematic multiplicative term in (3.53) is not incompatible with the stochastic solution of the imaginary-time Schrödinger equation, but determines the appearence of positive weights in the mixed estimators (3.59) of physical properties.

3.3.2 Importance Sampling

The pure DMC without importance sampling can be spectaculaly unstable in the long imaginary-time limit. For Fermi systems, where the trial wavefunction has non-constant sign, it suffers from a form of sign problem analogous to that discussed in Section 3.2. Moreover, the behavior of the weights $\mathfrak{W}_{w,i}$ is quite pathological for two reasons:

- the weights undergo massive fluctuations in systems with singular interaction potentials $V(\mathcal{R})$, like the Coulomb potential.

- since:
$$\Psi_\tau(\mathcal{R}) \simeq \langle \Phi_0 | \Psi_T \rangle \, \Phi_0(\mathcal{R}) e^{-\tau \epsilon_0} \tag{3.60}$$
in the long imaginary-time limit, ϵ_0 being the ground-state energy of the system, the numerator and the denominator of (3.59) either go to 0 (∞) for $\epsilon_0 > 0$ ($\epsilon_0 < 0$). This undesirable behavior reflects in the exponential decrease (increase) of the weights $\mathfrak{W}_{w,i}$, and makes the estimator (3.59) a $0/0$ (∞/∞) indeterminate form.

The stability and the efficiency of the algorithm can be significantly improved, and the first problem practically solved, if additional information about the ground-state wavefunction is used [120, 121, 68]. The idea, quite naturally suggested by the presence of the product $\Psi_T(\mathcal{R})\Psi_\tau(\mathcal{R})$ in (3.56), is to consider the modified wavefunction:

$$f_\tau(\mathcal{R}) = \Psi_T(\mathcal{R})\Psi_\tau(\mathcal{R}) \quad , \qquad f_0(\mathcal{R}) = \Psi_T(\mathcal{R})^2 \tag{3.61}$$

where $\Psi_T(\mathcal{R})$ is a trial wavefunction, as close as possible to the ground state. If $\Psi_\tau(\mathcal{R})$ obeys the imaginary-time Schrödinger equation (3.53), $f_\tau(\mathcal{R})$ obeys the following equation:

$$-\partial_\tau f_\tau(\mathcal{R}) = -\sum_i \frac{\hbar^2 \triangle_i}{2m_i} f_\tau(\mathcal{R}) + \sum_i \frac{\hbar^2 \nabla_i}{m_i} \cdot \Big(F_i(\mathcal{R}) f_\tau(\mathcal{R}) \Big) + E_L(\mathcal{R}) f_\tau(\mathcal{R}) \tag{3.62}$$

In (3.62), the quantum force:

$$F_i(\mathcal{R}) = \frac{\nabla_i \Psi_T(\mathcal{R})}{\Psi_T(\mathcal{R})} \tag{3.63}$$

introduces a drift term, and $E_L(\mathcal{R})$ is the local energy of the trial wavefunction $\Psi_T(\mathcal{R})$. With a judicious choice of the trial wavefunction, one can make $E_L(\mathcal{R})$ a smooth function close to the ground-state energy. In this respect, it is essential that the trial wavefunction incorporates all the *a priori* knowledge of the actual ground state of the system, e.g. Kato's cusp conditions for many-electron wavefunctions (see Appendix 10).The role of the quantum force is to cause configurations to drift away from regions where the trial wavefunction is small.

Equation (3.62) can be obtained either by direct calculation or, following [68, 126], with an argument that will prove useful later, in the proof of the generalized Feynman-Kac formula. Writing the Hamiltonian as:

$$\hat{H} = \hat{H}_0 + E_L(\mathcal{R}) \quad , \qquad \hat{H}_0(f) = -\sum_i \frac{\hbar^2}{2m_i} \triangle_i f + \sum_i \frac{\hbar^2}{2m_i} \frac{\triangle_i \Psi_T}{\Psi_T} f \tag{3.64}$$

we find, with a straightforward calculation, that:

$$-\Psi_T \hat{H}_0 \left(\frac{f}{\Psi_T} \right) = \mathcal{L}(f) \tag{3.65}$$

where the Fokker-Planck operator $\mathcal{L}$ reads:

$$\mathcal{L}(f) = \sum_i \frac{\hbar^2 \triangle_i}{2m_i} f - \sum_i \frac{\hbar^2}{m_i} \nabla_i \left(F_i \, f \right) \tag{3.66}$$

In the light of (3.66), we easily find the imaginary-time evolution equation of $f_\tau(\mathcal{R})$:

$$-\partial_\tau f_\tau = -\Psi_T \partial_\tau \Psi_\tau = \Psi_T \left(\hat{H}_0 + E_L \right) \Psi_\tau = \Psi_T \hat{H}_0 \left(\frac{f_\tau}{\Psi_T} \right) + E_L f_\tau = -\mathcal{L}(f_\tau) + E_L f_\tau \tag{3.67}$$

With the aid of (3.66), we can prove that $f_\tau(\mathcal{R})$ is a positive function, and represent mixed estimates of physical properties as stochastic averages. To prove this result we don't rely on the usual Feynman-Kac representation formula, devised for a different class of partial differential equations, but the following generalized Feynman-Kac representation formula, introduced in [68, 126] and proved in Appendix 9.2.4. Thanks to this formula, the solution $f_\tau(\mathcal{R})$ of (3.62) can be written as:

$$f_\tau(\mathcal{R}) = E \left[\Psi_T^2(\mathcal{R}_0) Z_\tau \right] \tag{3.68}$$

where the expectation is computed along the trajectories of the stochastic process:

$$\begin{cases} dR_{i,\tau'} = F_i(R_{\tau'}) \, d\tau' + \frac{\hbar^2}{2m_i} dB_{i,\tau'} \\ R_\tau = R \end{cases} \tag{3.69}$$

associated to the Fokker-Planck equation:

$$\partial_\tau p_\tau = -\sum_i \frac{\hbar^2}{2m_i} \triangle_i p_\tau + \sum_i \frac{\hbar^2}{m_i} \nabla_i \cdot \left(F_i \, p_\tau \right) = -\mathcal{L}(p_\tau) \tag{3.70}$$

and:

$$Z_\tau = e^{-\int_0^\tau d\tau' \, E_L(\mathcal{R}_{\tau'})} \tag{3.71}$$

is the path integral of the local energy. In the light of (9.55) and (3.71), $f_\tau(\mathcal{R}) \geq 0$ for all configurations.

The generalized Feynman-Kac formula leads [123, 106, 68, 126] to an importance-sampled version of the pure DMC method of Subsection 3.3.1. In the importance-sampled version, the walker configurations are evolved as:

$$\mathcal{R}_{w,i+1} = \mathcal{R}_{w,i} + \delta\tau F(\mathcal{R}_{w,i}) + \eta_{w,i} \tag{3.72}$$

weights are updated according to:

$$\mathfrak{W}_{w,i+1} = \mathfrak{W}_{w,i} e^{-\delta\tau E_L(\mathcal{R}_{w,i})} \tag{3.73}$$

and mixed estimates take the form:

$$\mathcal{O}_{mix}(i\delta\tau) \simeq \frac{\sum_{w=1}^{N_w} O_L(\mathcal{R}_{w,i})\,\mathfrak{W}_{w,i}}{\sum_{w=1}^{N_w} \mathfrak{W}_{w,i}} \tag{3.74}$$

The incorporation of the importance sampling transformation (3.61) sets the starting point of the pure DMC algorithm to the trial wavefunction $\Psi_T(\mathcal{R})$, potentially very close to the actual ground state, and mitigates the fluctuations in the walker weights. Moreover, as we will see later, the introduction of importance the sampling DMC algorithm is quite naturally conductive towards the fixed-node DMC method for Fermi systems. However, it does not solve the first problem associated with walker weights, namely their tendency to increase exponentially as the excited eigenstates in the trial wavefunction are projected out. This issue will be dealt with in the forthcoming Subsections.

3.3.3 Adaptive estimate of the ground-state energy

The long imaginary time behavior of the weights $\mathfrak{W}_{w,i}$ is essentially determined by the sign of the unknown ground-state energy ϵ_0 even in the importance-sampled DMC method. In particular, as made evident by (3.73), for $\epsilon_0 > 0$ ($\epsilon_0 < 0$) the weights exponentially decrease (increase). Only for $\epsilon_0 = 0$ they remain finite. Intuitively, it would be desirable to have an estimate of ϵ_0 to control the increase of the weights. To this purpose, let us observe that the normalized state:

$$\tilde{\Psi}_\tau(\mathcal{R}) = \frac{\Psi_\tau(\mathcal{R})}{\|\Psi_\tau\|} \tag{3.75}$$

satisfies the following modified imaginary-time Schrödinger equation:

$$-\partial_\tau \tilde{\Psi}_\tau = \Big(\hat{H} - E(\tau)\Big)\,\tilde{\Psi}_\tau \tag{3.76}$$

where:

$$\mathcal{E}(\tau) = \frac{\langle\Psi_\tau|H|\Psi_\tau\rangle}{\langle\Psi_\tau|\Psi_\tau\rangle} = \epsilon_0 + o\,(1) \tag{3.77}$$

provides an adaptive estimate of the ground-state energy, subtracting which to the Hamiltonian operator in the imaginary-time Schrödinger equation permits to control the normalization of the wavefunction $\tilde{\Psi}_\tau$, and thus the long imaginary-time behavior of the weights.

3.3.4 The branching process

Instead of accumulating the product of the weight factors $\mathfrak{W}_{w,i}$ as in (3.73), it is more efficient numerically to replicate the walkers after each evolution step (3.72). Indeed, weights taking small values give essentially no contribution to the estimate (3.74).
In the replication or branching process [123], each walker is replaced by a number:

$$m_w = \text{int}\,(\mathfrak{W}_{w,i} + u) \tag{3.78}$$

of copies, where int(x) stands for the integer part of the real number x and u is a random number, uniformly distributed in the interval $[0,1]$. In the case $m_w = 0$, the walker is deleted. In case $m_w = 1$ the walker is unaffected and continues with the next evolution step (3.72). In case $m_w > 1$, the walker continues with the next diffusion step, but also begins a new series of $m_w - 1$ diffusive displacements starting at the present configuration $\mathcal{R}_{w,i}$. After the branching process, the weights of the surviving walkers and of their copies are set equal to 1.
The fluctuations in the weights then translate into fluctuations in the number of walkers, that should be kept constant in such a way as to avoid the extinction of the population (small weights) or the occurrence of memory overflows (large weights). This control on the replication rate of the walkers is expecially necessary at the beginning of the DMC simulation.
One possibility is to perform a simulation with a fixed number of walkers [124]. There are of course many ways to satisfy this requirement. One possibility is to modify the branching process as detailed below:

1. rescale all the weights $\mathfrak{W}_{w,i}$ as:

$$\mathfrak{W}_{w,i} \to \tilde{\mathfrak{W}}_{w,i} = \frac{N_w}{\sum_w \mathfrak{W}_{w,i}} \mathfrak{W}_{w,i} \tag{3.79}$$

   so that $\sum_w \tilde{\mathfrak{W}}_{w,i} = N_w$.

2. deterministically duplicate each walker int$\big(\tilde{\mathfrak{W}}_{w,i}\big)$ times.

3. $k = \sum_w \tilde{\mathfrak{W}}_{w,i} - \text{int}\big(\tilde{\mathfrak{W}}_{w,i}\big)$ walkers still need to be created. To this purpose, observe that the scaled residual weights:

$$p_w = \frac{\tilde{\mathfrak{W}}_{w,i} - \text{int}\big(\tilde{\mathfrak{W}}_{w,i}\big)}{k} \tag{3.80}$$

   define a multinomial random variable with N_w possible outcomes. Sample the multinomial random variable (3.80) k times, and duplicate the outcome walkers $w_1 \dots w_k$. This procedure is called *residual resampling* method.

The residual sampling produces a collection of N_w walkers, whose weights are then put equal to 1. The control exerted on the population of walkers produces a systematic bias, called the population control bias. This phenomenon can be very easily understood already on an intuitive basis: if a fluctuation increases the fraction of walkers in a region where $E_L(\mathcal{R})$ is very small, the total weight, or equivalently the population size, increases. Controlling the number of walkers moderates this trend, decreasing the equilibrium distribution relative to $f_\tau(\mathcal{R})$. In other words, the DMC equilibrium distribution $f_\tau(\mathcal{R})$ is too small for low $E_L(\mathcal{R})$ and, similarly, too large in regions of high $E_L(\mathcal{R})$. Both effects increase the DMC estimate of the energy. This reasoning suggests [127] that the expectation value of the energy will be biased by an amount inversely proportional to N_w. It is possible to eliminate the population control error by performing calculations for different population sizes N_w, and extrapolating to infinite N_w.

3.3.5 The DMC algorithm

Below is detailed the DMC algorithm resulting from the incorporation of the importance sampling, adaptive energy estimation and branching procedures. The algorithm is also

illustrated in Figure 3.3

1. Generate a large number N_w of walkers $\{\mathcal{R}_{w,0}\}_{w=1}^{N_w}$ by sampling $\Psi_T(\mathcal{R})^2$ with the Metropolis algorithm. Set the weights $\{\mathfrak{W}_{w,0}\}_{w=1}^{N_w}$ of the walkers to 1 and produce the initial estimate of the ground-state energy with the formula:

$$E(0) = \frac{\sum_{w=1}^{N_w} E_L(\mathcal{R}_{w,0})}{N_w} \tag{3.81}$$

2. diffuse each walker using (3.72), and update its weight using:

$$\mathfrak{W}_{w,i+1} = \mathfrak{W}_{w,i} \exp\left(-\delta\tau \left(\frac{E_L(\mathcal{R}_{w,i+1}) + E_L(\mathcal{R}_{w,i})}{2} - E(i\delta\tau)\right)\right) \tag{3.82}$$

3. perform the branching process described in Subsection 3.3.4

4. adjust the adaptive estimate of the ground-state energy with the formula:

$$E((i+1)\delta\tau) = \frac{\sum_{w=1}^{N_w} E_L(\mathcal{R}_{w,i})}{N_w} \tag{3.83}$$

   $\mathcal{R}_{w,i}$ denoting the configuration of the walker w after the branching process.

5. iterate points 2, 3, 4 until convergence

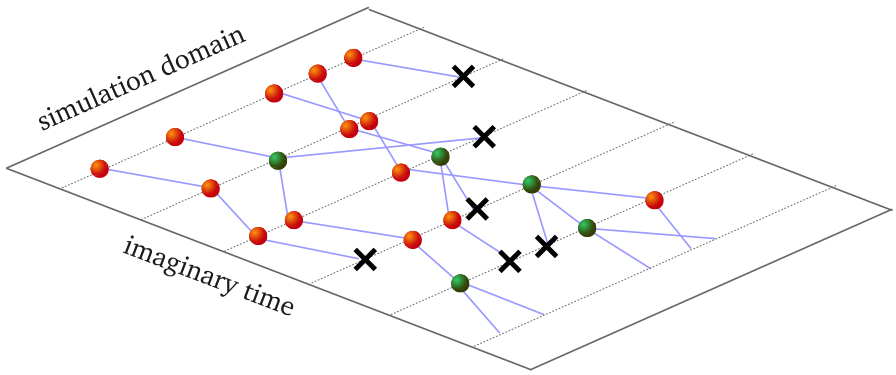

Figure 3.3: Pictorial representation of the DMC algorithm. At each time step, the walkers (represented by spheres) are updated using (3.72). The branching process then duplicates (green spheres) or deletes (black crosses) the updated walkers according to their weight.

The DMC method is characterized by several approximations. The population control bias has already been discussed. The DMC method gives access to mixed estimates of physical properties. Only in the case of operators $[\hat{O}, \hat{H}] = 0$ the corresponding mixed estimator can be exact (a relevant example is provided by $\hat{O} = \hat{H}$, which makes the DMC method particularly indicated for the calculation of energies). In general the mixed

estimator is an approximation of the pure one [128]. A better approximation can be produced assuming that $\Phi_0 = \alpha\Psi_T + \beta\delta\Psi$, with $|\beta| \ll 1$, and writing the pure estimator as:

$$\mathcal{O}_{pure} = \frac{\langle\Phi_0|\hat{O}|\Phi_0\rangle}{\langle\Phi_0|\Phi_0\rangle} \simeq 2\mathcal{O}_{mix} - \mathcal{O}_{vmc} = \mathcal{O}_{ext} \tag{3.84}$$

where $\mathcal{O}_{vmc}$ denotes the variational estimator:

$$\mathcal{O}_{vmc} = \frac{\langle\Psi_T|\hat{O}|\Psi_T\rangle}{\langle\Psi_T|\Psi_T\rangle} \tag{3.85}$$

There are of course many ways of approximating the pure estimator, all equivalent to each other up to terms of orfer $|\beta|^2$. In particular, for positive operators $\hat{O} \geq 0$, it can be advisable to substitute (3.84) with:

$$\mathcal{O}'_{ext} \simeq \frac{\mathcal{O}^2_{mix}}{\mathcal{O}_{vmc}} \tag{3.86}$$

since it is possible that $\mathcal{O}_{ext} < 0$ even if $\mathcal{O}_{mix}, \mathcal{O}_{vmc} > 0$, while necessary $\mathcal{O}_{mix} \geq 0$. Naturally, the accuracy of the extrapolated estimator depends on the trial wavefunction as well as on the DMC ground state. This is a significant drawback, but alternative estimators exist like the forward walking [106]. Another possibility is to use the Reptation QMC method [118], presented in the forthcoming Section.

There is another approximation underlying the DMC algorithm, which is related to the stochastic representation of the imaginary-time evolution equation (3.62). The generalized Feynman-Kac formula (9.55) has very naturally suggested to split the unknown Green's function $G'_{\delta\tau}(\mathcal{R}', \mathcal{R})$ of the imaginary-time evolution equation (3.62) into a drift-diffusion and a branching part. While the drift-diffusion part $\langle\mathcal{R}'|e^{\delta\tau\mathcal{L}}|\mathcal{R}\rangle$ controls the displacement of the walkers across the configuration space, the branching part $e^{-\delta\tau E_L(\mathcal{R})}$ $\delta(\mathcal{R} - \mathcal{R}')$ gives them positive weights, that the branching process converts into multiplicities. However, since:

$$G_{\delta\tau}(\mathcal{R}', \mathcal{R}) = \langle\mathcal{R}'|e^{-\delta\tau(-\mathcal{L}+E_L)}|\mathcal{R}\rangle = e^{-\delta\tau E_L(\mathcal{R}')}\,\langle\mathcal{R}'|e^{\delta\tau\mathcal{L}}|\mathcal{R}\rangle + \mathcal{O}(\delta\tau^2) \tag{3.87}$$

this is a primitive approximation. It has been shown that a Green's function with an error of order $\delta\tau^2$ produces an estimated energy with a linear time-step dependence [129]. It is very natural to ask whether the primitive approximation can be replaced with another approximation, giving rise to a more desirable time-step dependence for the estimated energy.

To this purpose, the incorporation of the accept-reject procedure, typical of the Metropolis algorithm and of the VMC method, in the DMC algorithm with importance sampling, proves surprisingly useful [121, 130]. Let us recall the relation between the Green's functions for the original and for the importance-sampled imaginary-time Schrödinger equations:

$$\begin{aligned} G_{\delta\tau}(\mathcal{R}', \mathcal{R}) &= \langle\mathcal{R}'|e^{-\delta\tau\hat{H}}|\mathcal{R}\rangle = \langle\mathcal{R}'|e^{-\delta\tau(\hat{H}_0+E_L)}|\mathcal{R}\rangle = \\ &= \langle\mathcal{R}'|e^{-\delta\tau\frac{1}{\Psi_T}(-\mathcal{L}+E_L)\Psi_T}|\mathcal{R}\rangle = \frac{\Psi_T(\mathcal{R})}{\Psi_T(\mathcal{R}')}\,G'_{\delta\tau}(\mathcal{R}', \mathcal{R}) \end{aligned} \tag{3.88}$$

Since $G_{\delta\tau}(\mathcal{R}', \mathcal{R})$ is symmetric, from (3.88) it is immediate to derive:

$$\Psi_T(\mathcal{R})^2 \, G'_{\delta\tau}(\mathcal{R}', \mathcal{R}) = \Psi_T^2(\mathcal{R}') G'_{\delta\tau}(\mathcal{R}, \mathcal{R}') \tag{3.89}$$

which closely resembles the detailed-balance equation for homogeneous Markov chains. This resemblance is purely suggestive, for at least three reasons: the DMC algorithm is not based on the formalism of Markov chains; moreover, $\Psi_T(\mathcal{R})^2$ is not the probability distribution the DMC method is aiming to sample; finally, the Green's function $G'_{\delta\tau}(\mathcal{R}', \mathcal{R})$ contains a branching factor, and thus it cannot be interpreted as the transition probability distribution of a Markov chain.
However, (3.88) is an exact property that any approximation to $G'_{\delta\tau}(\mathcal{R}', \mathcal{R})$ should respect. One way to enforce (3.88) in the importance-sampled algorithm, in order to improve the time-step dependence of estimated energy, is to perform the substitution:

$$\mathcal{G}_{dd}(\mathcal{R}', \mathcal{R}) = \langle \mathcal{R}' | e^{\delta\tau \mathcal{L}} | \mathcal{R} \rangle \to \mathcal{A}(\mathcal{R}', \mathcal{R}) \mathcal{G}_{dd}(\mathcal{R}', \mathcal{R}) \tag{3.90}$$

where A is an accept-reject probability such that (3.88) is fulfilled. A possible choice is:

$$\mathcal{A}(\mathcal{R}', \mathcal{R}) = \min \left(1, \frac{|\Psi_T(\mathcal{R}')|^2}{|\Psi_T(\mathcal{R})|^2} \frac{\mathcal{G}_{dd}(\mathcal{R}', \mathcal{R})}{\mathcal{G}_{dd}(\mathcal{R}, \mathcal{R}')} \right) \tag{3.91}$$

If the acceptance probability is 1, then the approximate move $\mathcal{R} \to \mathcal{R}'$ proposed by the drift-diffusion part is used, which is correct up to first order in $\delta\tau$. Otherwise, the accept-reject step changes the drift-diffusion part of the Green's function. In the end, adding the acceptance-reject step results in changing the dependence of the estimated energy and observables on the time step, in a not completely predictable way. Experience shows that, for sufficiently good trial wavefunctions, a less steep dependence of the estimated energy on the time step is observed. This permits to use higher time steps, thus reducing the convergence time of the algorithm. It is worth pointing out that unlike in the VMC algorithm, where the time step should be tuned in such a way as the average acceptance probability is around 50%, in the DMC algorithm it should be as small as possible, because a finite time step is responsible for a bias. Experience shows that sufficiently small time steps correspond to acceptances larger than 99%.

3.3.6 DMC for fermions: the fixed-node approximation

The DMC method is optimal for studying the ground state of a Bose system, which can be taken real and everywhere positive. For Fermi systems, importance-samples DMC solves an associate bosonic problem, having no meaningful relation with the original fermionic problem. For instance, as proved by the generalized Feynman-Kac formula, $f_\tau(\mathcal{R}) \geq 0$ but in general this property is not shared by $\Psi_T(\mathcal{R})\Phi_0(\mathcal{R}) \geq 0$, since the signs of the fermionic wavefunctions $\Psi_T(\mathcal{R})$, $\Phi_0(\mathcal{R})$ not necessarily agree. The sign of the wavefunction $\Psi_T(\mathcal{R})$ has to be taken into account, otherwise the DMC algorithm converges to a $\lim_{\tau\to\infty} f_\tau(\mathcal{R})$ unrelated to the Fermi ground state.
Many approaches to this problem have been proposed [131, 132, 133, 134, 135], even if it has been demonstrated [136] that fermionic QMC does not have a general solution, i.e. an algorithm both exact and convergent in a time which is polynomial in the number of degrees of freedom of the problem.
The so-called fixed-node approximation [121, 137, 125, 123], enables to devise an adaptation of the DMC algorithm which is widely used for dealing with the fermion antisymmetry. Althought it is not exact, it gives ground-state energies that satisfy a variational

principle and are usually very precise.

The nodal surface. Given a fermionic trial wavefunction $\Psi_T(\mathcal{R})$, we call *nodal surface of* $\Psi_T(\mathcal{R})$ the region $\mathcal{N}$ in the configuration space where it takes value 0:

$$\mathcal{N} = \{\mathcal{R} \in \mathcal{C} : \Psi_T(\mathcal{R}) = 0\} \tag{3.92}$$

Due to Dini's implicit function theorem [138], the nodal surface is a $(dN-1)$-dimensional manifold. For a system of spinless particles, $\Psi_T(\mathcal{R})$ must be zero whenever two particles coincide. This coincidence condition defines the $(N-1)$-dimensional *coalescence surface of* $\Psi_T(\mathcal{R})$. For $d > 1$, by trivially comparing the dimensionalities of the two manifolds, we see that the coalescence surface is no more than a subset of the nodal surface. On the other hand, the two objects coincide for the ground-state of several system of spinless particles in $d = 1$, as discussed by D. M. Ceperley [98]. Apart from this special case no simple characterization of the nodal surface, which is a very intricated manifold expecially in large systems, can be achieved.
Given a configuration $\mathcal{R}$ not in the nodal surface, $\mathcal{R} \notin \mathcal{N}$, we call the *nodal pocket* around $\mathcal{R}$ the set $\Omega(\mathcal{R})$ of all points that can be reached from $\mathcal{R}$ with a continuous curve that doesn't cross the nodal surface. A nodal pocket is thus a connected region in the confguration space, whose boundary is a part of the nodal surface $\mathcal{N}$.
We say that the wavefuncion $\Psi_T(\mathcal{R})$ has the *tiling property* if for any point $\mathcal{R}'$ not in the nodal surface, $\mathcal{R}' \notin \mathcal{N}$, there exist a point $\mathcal{R}'' \in \Omega(\mathcal{R})$ and a permutation $\sigma \in S_N$ such that $\mathcal{R}' = \sigma\mathcal{R}''$. In this case, the configurational space is tiled by the nodal surface and by the images of $\Omega(\mathcal{R})$ under permutations:

$$\bigcup_{\sigma \in S_N} \Omega(\sigma\mathcal{R}) = \mathcal{C} - \mathcal{N} \tag{3.93}$$

Examples of wavfunctions with and without the tiling property are illustrated in Figure 3.4.
If $\Psi_T(\mathcal{R})$ has the tiling property, it can be written as:

$$\Psi_T(\mathcal{R}') = (-1)^\sigma \Psi_T^{(0)}(\mathcal{R}'') \tag{3.94}$$

where $\mathcal{R}' = \sigma\mathcal{R}''$ as before and $\Psi_T^{(0)}(\mathcal{R})$ is the restriction of $\Psi_T(\mathcal{R})$ on the nodal pocket $\Omega(\mathcal{R})$:

$$\Psi_T^{(0)}(\mathcal{R}'') = \begin{cases} \Psi_T(\mathcal{R}'') & \mathcal{R}'' \in \Omega(\mathcal{R}) \\ 0 & \text{otherwise} \end{cases} \tag{3.95}$$

Equation (3.94) can also be written as:

$$\Psi_T(\mathcal{R}) = \frac{1}{N!} \sum_{\sigma \in S_N} (-1)^\sigma \Psi_T^{(0)}(\sigma\mathcal{R}) = \left(\hat{S}_- \Psi_T^{(0)}\right)(\mathcal{R}) \tag{3.96}$$

Thanks to the tiling property and the antisymmetry, knowledge of $\Psi_T(\mathcal{R})$ inside the nodal pocket grants the ability to extend it to the whole $\mathcal{C}$.

The fixed-node DMC algorithm. As proved by D. M. Ceperley [98], using a clever variational argument, a broad class of Fermi ground states have the tiling property. In order to find the ground-state wavefunction, it is therefore sufficient to know the ground-

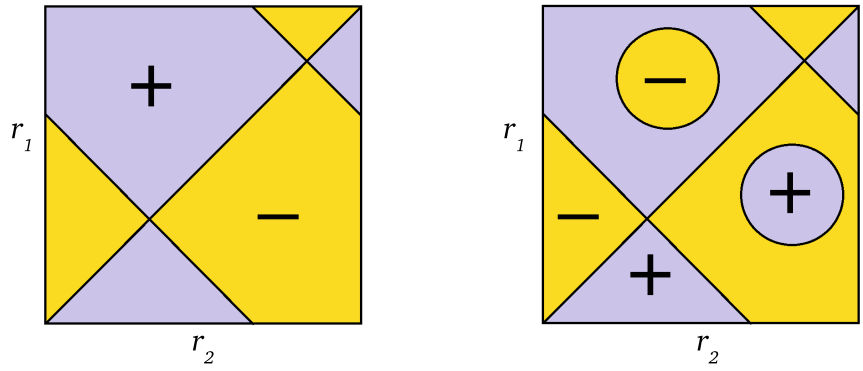

Figure 3.4: Nodal pockets and surfaces of two wavefunctions $\Psi(r_1, r_2)$ of two 1D spinless fermions in PBC. Left: the configurational space is the union of the nodal pocket Ω_+ (mauve) and of its permutation Ω_- (yellow). This wavefunction has the tiling property. Right: the configurational space is the union of two nodal pockets $\Omega_+^{(1)}$, $\Omega_+^{(2)}$ (mauve) and of their permutations $\Omega_-^{(1)}$, $\Omega_-^{(2)}$ (yellow). This wavefunction does not have the tiling property.

state nodal surface and to solve the imaginary-time Schrödinger equation inside a nodal pocket, where the ground-state wavefunction has constant sign.

The fixed-node approximation constrains the nodal surface of the ground-state wavefunction Φ_0 to be equal to that of a trial wavefunction Ψ_T having the tiling property, so that the nodal pockets of the two wavefunctions coincide. Then, the importance sampling algorithm is employed to find the distribution $\Psi_T(\mathcal{R})\Phi_0(\mathcal{R})$. The latter is everywhere positive, except on the nodal surface, and thus the usual DMC algorithm for Bose particles can be applied, provided that the nodal srface is never crossed.

We thus endow the walkers with a sign $\sigma_{w,i} = \mathrm{sgn}(\Psi_T(\mathcal{R}_{w,i}))$ and, after a drift-diffusion move $\mathcal{R}_{w,i} \to \mathcal{R}_{w,i+1}$ has been proposed according to (3.72), we impose the fixed-node constraint by checking the sign $\mathrm{sgn}(\Psi_T(\mathcal{R}_{w,i+1}))$ of the trial wavefunction at the updated configuration and rejecting the move if the walker has crossed the nodal surface, i.e. if $\mathrm{sgn}(\Psi_T(\mathcal{R}_{w,i+1})) \neq \sigma_{w,i}$. The only communication between walkers in different nodal pockets is provided by the adaptive estimate of the ground-state energy.

It has been proved by Moskowitz *et al.* and by Reynolds *et al.* [137, 123] that the fixed-node DMC methods provides a variational estimate of the ground-state energy. Denote $\lim_{\tau\to\infty} f_\tau^{(0)}(\mathcal{R}) = \Psi_T(\mathcal{R})\Phi^{(0)}(\mathcal{R})$ the asymptotic DMC distribution inside the nodal pocket Ω and $\mathcal{E}^{(0)}$ the corresponding energy:

$$\mathcal{E}^{(0)} = \frac{\langle \Phi^{(0)} | \hat{H} | \Phi^{(0)} \rangle}{\langle \Phi^{(0)} | \Phi^{(0)} \rangle} \tag{3.97}$$

We now show that $\mathcal{E}^{(0)}$ is the energy of the wavefunction:

$$\Phi(\mathcal{R}) = \left(\hat{S}_- \Phi_T^{(0)} \right)(\mathcal{R}) \tag{3.98}$$

In fact:

$$\begin{aligned}\frac{\langle\Phi|\hat{H}|\Phi\rangle}{\langle\Phi|\Phi\rangle} = \frac{\langle\Phi|\hat{H}|\hat{S}_-\Phi^{(0)}\rangle}{\langle\Phi|\hat{S}_-\Phi^{(0)}\rangle} = \frac{\langle\Phi|\hat{H}|\Phi^{(0)}\rangle}{\langle\Phi|\Phi^{(0)}\rangle} = \frac{\int_{\mathcal{C}} d\mathcal{R}\,\Phi(\mathcal{R})\big(\hat{H}\Phi^{(0)}\big)(\mathcal{R})}{\int_{\mathcal{C}} d\mathcal{R}\,\Phi(\mathcal{R})\Phi^{(0)}(\mathcal{R})} = \\ = \frac{\int_{\Omega} d\mathcal{R}\,\Phi(\mathcal{R})\big(\hat{H}\Phi^{(0)}\big)(\mathcal{R})}{\int_{\Omega} d\mathcal{R}\,\Phi(\mathcal{R})\Phi^{(0)}(\mathcal{R})} = \frac{\int_{\Omega} d\mathcal{R}\,\Phi^{(0)}(\mathcal{R})\big(\hat{H}\Phi^{(0)}\big)(\mathcal{R})}{\int_{\Omega} d\mathcal{R}\,\Phi^{(0)}(\mathcal{R})\Phi^{(0)}(\mathcal{R})} = \mathcal{E}^{(0)}\end{aligned} \tag{3.99}$$

Due to the variational principle 2.1:

$$\mathcal{E}^{(0)} = \frac{\langle\Phi|\hat{H}|\Phi\rangle}{\langle\Phi|\Phi\rangle} \geq \frac{\langle\Phi_0|\hat{H}|\Phi_0\rangle}{\langle\Phi_0|\Phi_0\rangle} = \epsilon_0 \tag{3.100}$$

Unfortunately, the fixed-node approximation is an *uncontrolled approximation*, unlike e.g. the use of finite time step, projection time and number of walkers. Those approximations are controllable, in the sense that they depend on a small number of parameters ($\delta\tau$, m, N_w) and fade as the parameters approach a certain limit ($\delta\tau \to 0$, $m \to \infty$, $N_w \to \infty$). On the other hand, no simple parametrization of nodal surfaces is available, hence the fixed-node approximation is said to be uncontrolled. Nevertheless, as remarkably accurate trial wavefunctions are available, it provides reliable estimates of ground-state properties in a broad range of extremely relevant physical contexts [99].

3.4 Reptation Monte Carlo

The Reptation QMC (RQMC) method is based on the path-integral representation (3.34) of the imaginary-time evolution, like the PIGS mthod.
Such representation reduces the calculation of ground-state expectation values and ITCFs to the average of suitable estimators over a space of discretized paths. As long as Bose systems are concerned, as discussed in Section 3.2, the PIGS method relies on the sampling of $\mathcal{X}$ through an appropriate Metropolis algorithm, and gives access to unbiased estimates of ground-state properties and ITCFs. However, the straightforward application of the PIGS method to Fermi systems is hampered by the fermion sign problem, described in Subsection 3.2.1.
The fixed-node approximation, discussed in Section 3.3, provides a way to circumvent the fermion sign problem. It can be incorporated in the PIGS method initializing paths $\{\mathcal{X}_j\}_j$, $\mathcal{X}_j = (\mathcal{R}_{0,j} \dots \mathcal{R}_{2m,j})$ along which the sign of a trial wavefunction $\Psi_T(\mathcal{R})$ is constant, and rejecting moves that carry a configuration across the nodal surface of $\Psi_T(\mathcal{R})$. Due to such constraint the typical PIGS moves, illustrated in Section 3.2, are most likely rejected even for very small values of the time step, resulting in a considerable loss of efficiency over the Bose case.
The versatility of the RQMC method comes from the very special way in which the probability distribution $\Pi(\mathcal{X})$ in (3.36) is sampled.
In the original RQMC method, conceived by S. Baroni and S. Moroni [118], the path space is sampled relying on a reptation algorithm, of the type introduced by A. K. Kron [139] and F. T. Wall and F. Mandel [140] to sample the configurational space of linear polymer chains. Given a path $\mathcal{X} = (\mathcal{R}_0 \dots \mathcal{R}_{2m})$, a growth direction is chosen at random. In particular, a variable $d = \pm 1$ is introduce, which is sampled with probability p_d. If $d = 1$ ($d = -1$), $\mathcal{R}_d = \mathcal{R}_0$ ($\mathcal{R}_d = \mathcal{R}_{2m}$) is chosen to be the growth end. For the time being, let us consider generic probabilities p_d: we will see in a moment that only the choice $p_d = \frac{1}{2}$ leads to a correct exploration of the path space.

A trial move $\mathcal{X} \to \mathcal{X}'$ is proposed, towards a path:

$$\begin{aligned} \mathcal{X}' &= (\mathcal{R}'\mathcal{R}_0 \dots \mathcal{R}_{2m-1}) \qquad & d = 1 \\ \mathcal{X}' &= (\mathcal{R}_1 \dots \mathcal{R}_{2m}\mathcal{R}') \qquad & d = -1 \end{aligned} \tag{3.101}$$

In other words, a time slice is added to the *head* $\mathcal{R}_d$ and removed from the *tail* $\mathcal{R}_{-d}$. This type of move, illustrated in Figure 3.5, is called reptation, being reminescent of the creeping of a reptile. In (3.101), $\mathcal{R}'$ is a new configuration proposed according to a suitable transition probability $\mathcal{T}_d(\mathcal{X} \to \mathcal{X}') = \mathcal{G}(\mathcal{R}_d, \mathcal{R}')$. The transition probability $\mathcal{P}_d(\mathcal{X} \to \mathcal{X}')$, given the growth direction d, is the product of $\mathcal{T}_d(\mathcal{X} \to \mathcal{X}')$ and of the acceptance probability:

$$\mathcal{A}_d(\mathcal{X} \to \mathcal{X}') = \min\left(1, \frac{\Pi(\mathcal{X}')}{\Pi(\mathcal{X})} \frac{\mathcal{T}_{-d}(\mathcal{X}' \to \mathcal{X})}{\mathcal{T}_d(\mathcal{X} \to \mathcal{X}')}\right) \tag{3.102}$$

which ensures that $\mathcal{P}_d(\mathcal{X} \to \mathcal{X}')$ satisfies the detailed balance condition:

$$\Pi(\mathcal{X})\mathcal{P}_d(\mathcal{X} \to \mathcal{X}') = \Pi(\mathcal{X}')\mathcal{P}_{-d}(\mathcal{X}' \to \mathcal{X}) \tag{3.103}$$

This desirable property is shared by the transition probability:

$$\mathcal{P}(\mathcal{X} \to \mathcal{X}') = \sum_d p_d \, \mathcal{P}_d(\mathcal{X} \to \mathcal{X}') \tag{3.104}$$

only if $p_d = \frac{1}{2}$. In fact:

$$\begin{aligned} \Pi(\mathcal{X})P(\mathcal{X} \to \mathcal{X}') &= \sum_d p_d \, \Pi(\mathcal{X})\mathcal{P}_d(\mathcal{X} \to \mathcal{X}') = \\ = \sum_d p_d \, \Pi(\mathcal{X}')\mathcal{P}_{-d}(\mathcal{X}' \to \mathcal{X}) &= \Pi(\mathcal{X}') \sum_d p_{-d} \, \mathcal{P}_d(\mathcal{X}' \to \mathcal{X}) \end{aligned} \tag{3.105}$$

and the last member coincides with $\Pi(\mathcal{X}')\mathcal{P}(\mathcal{X}' \to \mathcal{X})$ only if $p_{-d} = p_d = \frac{1}{2}$. The autocorrelation time of the original RQMC method scales as $\mathcal{O}(m^2)$, an unfavorable scaling whenever it is necessary to project the trial wavefunction for a large number m of time steps [141]. Fortunately, a minimal modification of the original RQMC algorithm, resulting in the bounce RQMC algorithm [141, 142], helps solving these problems.

The growth direction is randomly set at the beginning of the simulation, and reversed upon rejection only, hence the name *bounce*. The bounce RQMC method does not satisfy detailed balance (2.14), but satisfies the more general stationarity condition (2.13) required for sampling the correct probability distribution. To prove this result, let us enlarge the path space with the direction variable d. In the enlarged path space $\{\mathcal{X}, d\}$, $\mathcal{X} \in \mathcal{C}^{2m+1}$, $d \in \{-1, 1\}$, the transition probability distribution $\mathcal{P}(\mathcal{X}, d \to \mathcal{X}', d')$ is non-zero only for $d = d'$, $\mathcal{X} \neq \mathcal{X}'$ (the move is accepted and the growth direction remains unaltered) and $d \neq d'$, $\mathcal{X} = \mathcal{X}'$ (the move is rejected and the growth direction changes). The desired probability distribution $\Pi(\mathcal{X}, d) = \frac{1}{2}\,\Pi(\mathcal{X})$ is the unique stationary distribution of the bounce RQMC random walk. In fact, it solves the eigenvalue equation:

$$\int d\mathcal{X} \sum_d \Pi(\mathcal{X}, d)\mathcal{P}(\mathcal{X}, d \to \mathcal{X}', d') = \Pi(\mathcal{X}', d') \tag{3.106}$$

since:

$$2\int d\mathcal{X}\sum_{d}\Pi(\mathcal{X},d)\mathcal{P}(\mathcal{X},d\to\mathcal{X}',d')=\Pi(\mathcal{X}')+\int d\mathcal{X}\,\Pi(\mathcal{X})\mathcal{P}(\mathcal{X},d'\to\mathcal{X}',d')= \\ =\Pi(\mathcal{X}')+\int d\mathcal{X}\,\Pi(\mathcal{X}')\mathcal{P}(\mathcal{X}',d'\to\mathcal{X},d')=2\,\Pi(\mathcal{X}') \tag{3.107}$$

having observed, in the first passage, that $\mathcal{P}(\mathcal{X},d\to\mathcal{X}',-d)=\delta(\mathcal{X}'-\mathcal{X})$ and, in the last passage, that $\int d\mathcal{X}\mathcal{P}(\mathcal{X}',d'\to\mathcal{X},d')=1$ since the integration exhausts all possibilities for a move from the path $\mathcal{R}$.
The passage to the bounce algorithm significantly decreases [141] the autocorrelation time of the RQMC, and also tames occasional ergodicity problems that hamper the ergodic exploration of the path space. The fixed-node approximation can be incorporated in the RQMC by rejecting moves that carry configurations across the nodal surface, and bouncing the corresponding path. The RQMC is appealing for at least two reasons: it gives access to ground-state expectation values without recurring to mixed or extrapolated estimates, and yields static properties and imaginary-time correlations as natural by-products of ground-state simulations.

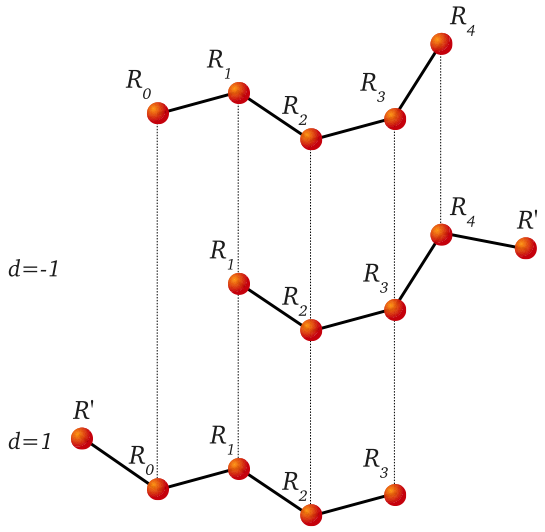

Figure 3.5: Pictorial representation of the RQMC move (3.101) for a polymer of 5 configurations: if $d=1$ ($d=-1$), $\mathcal{R}_4$ ($\mathcal{R}_0$) is cancelled and $\mathcal{R}'$ is sampled from $G(\mathcal{R}_0,\mathcal{R}')$ ($G(\mathcal{R}_4,\mathcal{R}')$)

CHAPTER 4

One-dimensional ^{4}He: Luttinger liquid theory and beyond.

In the present Chapter, the recent studies [143, 144] of the dynamical structure factor of 1D ^{4}He atoms and hard rods are presented. The Tomonaga-Luttinger liquid (TLL) theory [145, 146, 147, 148, 149] and the nonlinear Tomonaga-Luttinger liquid (NL-TLL) theory [150, 151, 152, 153], that provide the most successful extant paradigm for the interpretation of 1D quantum substances, are briefly reviewed in Sections 4.2 and 4.3.
The exactly solvable ideal Fermi gas, Lieb-Liniger [154] and hard-rods [155, 156] models are presented in Section 4.4. The dynamical structure factors $S(q,\omega)$ of 1D ^{4}He atoms and hard rods, which we computed using the PIGS and GIFT methods, are then presented and discussed in Sections 4.4.3 and 4.7, on the basis of the TLL and NL-TLL theories.

4.1 Introduction

One-dimensional (1D) quantum systems exhibit some of the most diverse and fascinating phenomena seen in all of condensed matter Physics [157, 149, 153]. The combined effect of quantum fluctuations, interparticle interaction and reduced dimensionality gives rise to features which are absent in their higher-dimensional counterparts. Bose systems in 2D and 3D can undergo a transition [158, 159] to a superfluid phase with spontaneous breaking of the continuous $U(1)$ symmetry and the appearence of the related Goldstone modes. This determines a dynamical structure factor $S(\mathbf{q},\omega)$ largerly dominated by the well-known phonon-maxon-roton collective excitation, illustrated in Figure 4.1.
For Fermi systems in 2D and 3D, unless strong correlations rising from an intense interaction (e.g. crystallization) or a BCS pairing mechanism are present, Landau's Fermi liquid theory predicts individual long-lived excitations obeying the Fermi-Dirac statistics, the Landau quasiparticles. The presence of quasiparticles determines a spectral function $A(\mathbf{k},\omega)$ largerly dominated by quasiparticle excitations. The DSF, on the other hand, features a coherent excitation (a plasmon in the electron gas, a phonon in neutral systems like ^{3}He) that gets damped as soon as its approaches the particle-hole band illustrated in Figure 4.1.
For both Bose and Fermi systems, another possibility is a phase transition [158, 159, 6] to a solid phase with spontaneous breaking of the continuous translational symmetry. In such case, $S(\mathbf{q},\omega)$ is largerly dominated by a phononic collective excitation, describing vibrations of particles around their equilibrium positions.
These well-established paradigms break down in 1D.
For Bose systems with short-range interactions, no spontaneous breaking of the continuous $U(1)$ symmetry can occur, due to the Hohenberg-Mermin-Wagner theorem [162, 163, 164, 165]. This circumstance rules out the possibility of Bose-Einstein condensation,

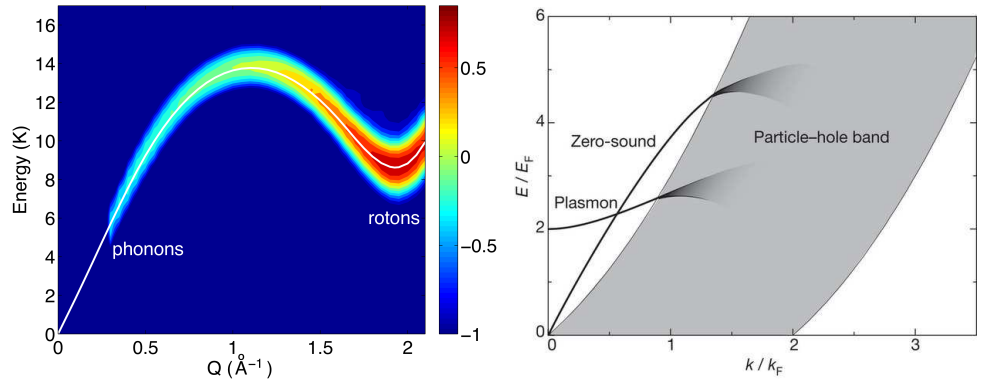

Figure 4.1: (a) DSF of superfluid 3D ^{4}He at saturated vapor pressure and temperature $T = 1.3\,K$, as a function of the transferred wavevector $\mathbf{q}$ and energy (taken from [160]). (b) The gray area corresponds to the particle-hole band, i.e. to the range of excitation energy E as a function of the transferred wavevector $\mathbf{q}$ accessible by promoting a particle below the Fermi level to an empty stat above it. In addition, an interacting Fermi system displays collective density modes, called plasmons in charged systems and phonons in neutral systems. With increasing wavevector, the collective modes enter the particle–hole band, where they decay (taken from [161]).

and hampers the possibility of a DSF dominated by a phonon-maxon-roton excitation. As we will see in Section 4.2, the SDF still features a collective excitation, at least in the low-energy limit, but such excitation does not originate from the breaking of a continuous symmetry unless the system is crystalline. The transition to a crystalline phase, however, is possible only in presence of long-range interactions [6].

For Fermi systems, already on a qualitative level, it can be easily understood that the notion of individual excitation must be contradictory in 1D. If a particle moves amidst an interacting 1D liquid, in a finite amount of time it collides with its neighbouring particle, and transmit momentum to it; that neighbouring particle collides with its neighbouring particle transmitting momentum to it and so on. In this way, a particle moving in the 1D liquid pushes a macroscopic number of its neighbors away and momentum is transferred by collective excitations rather than individual excitations. As a consequence, we might expect that the Fermi liquid theory breaks down in 1D. Indeed, when constructing a perturbative estimate of the Green's function one encounters divergences [153] which are interpretable as manifestations of the fact that the very notion of an individual excitation is fundamentally flawed in 1D.

The low-energy dynamical properties of both Bose and Fermi systems in 1D are predicted by the phenomenological TLL theory, briefly reviewed in the forthcoming Section.

4.2 The Tomonaga-Luttinger liquid theory

The concept of collective excitations is of fundamental importance for understanding the properties of 1D liquids, but it is also a very delicate and subtle issue. The present Section provides a brief review of the phenomenological bosonization, a way of deriving

the effective Hamiltonian describing the low-energy excitations of a broad class of 1D systems. This introduction has the purpose of making the discussion more complete as no *a priori* knowledge of the TLL theory is required to understand the results of the present Chapter. Details of the calculations are deferred to Appendix 11.

Let us start [148, 157] from the following representation of the density operator $\hat{\rho}(x)$:

$$\hat{\rho}(x) = \frac{\partial_x \hat{\theta}(x)}{\pi} \sum_{p \in \mathbb{Z}} e^{i2p\hat{\theta}(x)} \qquad x \in \mathbb{R} \tag{4.1}$$

where the field operator $\hat{\theta}(x)$ is hermitian, and satisfies the boundary condition $\hat{\theta}(x + L) = \hat{\theta}(x) + \pi N$, N being an integer. Thanks to those properties, the operator $\hat{\rho}(x)$ in (4.1) is hermitian and satisfies the periodic boundary condition $\hat{\rho}(x + L) = \hat{\rho}(x)$. The integral of the operator $\hat{\rho}(x)$ on the interval $[x_0, x_0 + L]$:

$$\int_{x_0}^{x_0+L} \hat{\rho}(x) = N \tag{4.2}$$

is the number N of particles in the interval $[x_0, x_0 + L]$, suggesting that the field operator $\hat{\Theta}(x) = \frac{\hat{\theta}(x)}{\pi}$ might be regarded to as a sort of integrated density, which can be used to count particles. This intuition is confirmed by the following exact equality:

$$\hat{\rho}(x) = \frac{\partial_x \hat{\theta}(x)}{\pi} \sum_{n \in \mathbb{Z}} \delta\left(\frac{\hat{\theta}(x)}{\pi} - n\right) \tag{4.3}$$

resulting from a simple calculation reported in Appendix 11. Since the operators $\hat{\rho}(x)$ and $\delta\big(\frac{\hat{\theta}(x)}{\pi} - n\big)$ in (4.3) are positive, we conclude that:

$$\frac{\partial_x \hat{\theta}(x)}{\pi} \geq 0 \tag{4.4}$$

so that $\hat{\Theta}(x)$ is monotonically increasing, as expected for an integrated density. Moreover, it is well-known that:

$$\hat{\rho}(x) = \sum_{n \in \mathbb{Z}} \delta\big(x - \hat{x}_n\big) \tag{4.5}$$

where $\hat{x}_{n+N} = \hat{x}_n + L$ by virtue of the periodic boundary conditions. Comparing (4.3) and (4.5) we conclude that $\hat{\Theta}(x)$ attains the value n at the position $\hat{x}_n$ of the n-th particle. The operator $\hat{\Theta}(x)$ interpolates between those values, and thus it can admit fluctuations, which are described by the oscillatory terms in (4.1). Notice that, in order to interpret $\hat{\Theta}(x)$ as an integrated density, the particles composing the system need to be labeled in a unique way, and this can only be achieved in 1D systems [157]. If the density operator $\hat{\rho}(x)$ is averaged over distances large compared to the typical interparticle distance $d = \frac{L}{N} = \frac{1}{\rho_0}$, the oscillating terms in (4.1) vanish leaving a smeared density:

$$\hat{\rho}_s(x) = \frac{\partial_x \hat{\theta}(x)}{\pi} = \rho_0 + \frac{\partial_x \hat{\phi}(x)}{\pi} \tag{4.6}$$

having defined $\hat{\phi}(x) = \hat{\theta}(x) - \rho_0 x$.

In the low-momentum regime, the density fluctuations in (4.1) control the dynamics of the system. To this purpose it is necessary to write the single-particle creation operator $\hat{\Psi}^{\dagger}_{B,F}(x)$, where the subscripts B and F refer to bosons and fermions respectively, in terms of collective field operators. It can be proved (see Appendix 11 for details) that the most general expression for $\hat{\Psi}^{\dagger}_{B,F}(x)$ compatible with the condition:

$$\hat{\Psi}^{\dagger}_{B,F}(x)\hat{\Psi}_{B,F}(x) = \hat{\rho}(x) \tag{4.7}$$

is:

$$\hat{\Psi}^{\dagger}_{B,F}(x) = \sqrt{\hat{\rho}(x)}\, e^{i\hat{\eta}_{B,F}(x)} \tag{4.8}$$

For bosons, the operator $\hat{\eta}_B(x)$ must be self-adjoint, and such that:

$$[\hat{\eta}_B(x), \hat{\eta}_B(y)] = 0 \tag{4.9}$$

and:

$$\Big[\, \partial_x\hat{\phi}(x), \hat{\eta}_B(y) \,\Big] = -i\pi\, \delta(x-y) \tag{4.10}$$

Equation (4.10) means that $\partial_x\hat{\phi}(x)$ and $\hat{\eta}(y)$ are canonically conjugate. With a simple calculation, it is possible to show that $\hat{\Psi}^{\dagger}_{B}(x)$ has the representation:

$$\hat{\Psi}^{\dagger}_{B}(x) = \sqrt{\frac{\partial_x\hat{\theta}(x)}{\pi}} \sum_{p\in\mathbb{Z}} e^{i2p\,\hat{\theta}(x)}\, e^{i\hat{\eta}_B(x)} \tag{4.11}$$

The possibility of expressing the single-particle creation operator in terms of field operators describing collective excitations is the heart of the representation (4.11), and the manifestation of the fact that excitations in interacting 1D systems are necessarily collective.

The fermionic single-particle creation operator is obtained [157] applying a Wigner-Jordan transformation to the bosonic single-particle creation operator:

$$\hat{\Psi}^{\dagger}_{F}(x) = \hat{\Psi}^{\dagger}_{B}(x)\, e^{i\hat{\theta}(x)} \tag{4.12}$$

With the knowledge of the single-particle creation operators (4.11), (4.12) and of the density operator (4.1), it is possible to write the Hamiltonian of the system:

$$\hat{H} = \frac{\hbar^2}{2m} \int dx\, \partial_x\hat{\Psi}^{\dagger}_{B,F}(x)\, \partial_x\hat{\Psi}_{B,F}(x) + \frac{1}{2}\int dx \int dy\, v(x-y)\hat{\rho}(x)\hat{\rho}(y) \tag{4.13}$$

in terms of collective field operators only. Clearly, such representation do not solve the many-body Schrödinger equation, but simply permit to reformulate it in terms of collective field operators. However, since the collective field operators $\hat{\phi}(x)$, $\hat{\eta}_{B,F}(y)$ describe the natural excitations of the system, the new expression of the Hamiltonian operator (4.13) permits the complete solution of the many-body Schrödinger equation in the long-wavelength limit. Using (4.11), the kinetic energy becomes:

$$\int dx\, \partial_x\hat{\Psi}^{\dagger}_{B,F}(x)\, \partial_x\hat{\Psi}_{B,F}(x) \simeq \frac{\hbar^2\rho_0}{2m} \int dx\, \partial_x\hat{\eta}_{B,F}(x)^2 \tag{4.14}$$

up to terms of higher order in $\hat{\eta}_{B,F}(x)$, $\hat{\phi}(x)$. Similarly, the potential energy becomes:

$$\frac{1}{2}\int dx \int dy\, v(x-y)\hat{\rho}(x)\hat{\rho}(y) \simeq \frac{1}{2\pi^2}\int dx \int dy\, v(x-y)\partial_x\hat{\phi}(x)\partial_x\hat{\phi}(y) \tag{4.15}$$

up to terms of higher order in $\hat{\theta}(x)$. In the long wavelength limit, the spatial scale on which the short-range interaction potential $v(x-y)$ decays to 0 is irrelevant, and the approximation $v(x-y) \simeq v_0\,\delta(x-y)$ can be safely inserted in (4.16), leading to:

$$\frac{1}{2}\int dx \int dy\, v(x-y)\hat{\rho}(x)\hat{\rho}(y) \simeq \frac{v_0}{2\pi^2}\int dx\, \partial_x\hat{\phi}(x)^2 \tag{4.16}$$

whence, writing:

$$\frac{\pi\hbar\rho_0}{m} = cK_L \quad , \qquad \frac{v_0}{\hbar\pi} = \frac{c}{K_L} \tag{4.17}$$

we obtain the effective TLL Hamiltonian operator [145, 148]:

$$\hat{H}_{LL} = \frac{\hbar c}{2\pi}\int dx\, \left(K_L\partial_x\hat{\eta}_{B,F}(x)^2 + \frac{1}{K_L}\,\partial_x\hat{\phi}(x)^2\right) \tag{4.18}$$

which captures the behavior of the system in the long-wavelength limit. In (4.18), the positive number K_L is called *Luttinger parameter*. Remarkably, the Hamiltonian (4.18) does not rest on a peculiar microscopic model but results from general considerations. To diagonalize the TLL Hamiltonian, it is convenient to express the field operators $\partial_x\hat{\eta}_{B,F}(x)$, $\partial_x\hat{\phi}(x)$ in Fourier space:

$$\hat{\eta}_{B,F}(x) = \eta_0 + \sum_{k\neq 0}\frac{e^{-ikx}}{\sqrt{L}}\,\hat{\eta}_{B,F}(k) \qquad \hat{\phi}(x) = \sum_{k\neq 0}\frac{e^{-ikx}}{\sqrt{L}}\,\hat{\phi}(k) \tag{4.19}$$

obtaining:

$$\hat{H}_{LL} = \frac{\hbar c}{2\pi}\left(K_L\sum_k k^2\,\hat{\eta}_{B,F}(k)\hat{\eta}_{B,F}(-k) + \frac{1}{K_L}\sum_k k^2\,\hat{\phi}(k)\hat{\phi}(-k)\right) \tag{4.20}$$

up to the irrelevant constant term $\frac{c\rho_0^2}{K_L}\,L$. The fields (4.19) can be expressed in terms of canonical Bose operators $[\hat{a}_k, \hat{a}^\dagger_{k'}] = \delta_{k,k'}$ performing the substitutions:

$$\hat{\eta}_{B,F}(k) = i\sqrt{\frac{\pi|k|}{2K_L}}\,\frac{1}{k}\,\left(\hat{a}_k + \hat{a}^\dagger_{-k}\right) \qquad \hat{\phi}(k) = i\,\sqrt{\frac{\pi K_L|k|}{2}}\,\frac{1}{|k|}\,\left(\hat{a}_k - \hat{a}^\dagger_{-k}\right) \tag{4.21}$$

a very simple calculation proves that (4.21) preserves the commutation relation (4.10), and gives to (4.20) the more expressive form:

$$\hat{H}_{LL} = \sum_k \hbar c|k|\,\left(\hat{a}^\dagger_k\hat{a}_k + \frac{1}{2}\right) \tag{4.22}$$

In the light of (4.22), the long-wavelength excitations of the system are collective density

oscillations, i.e. phonons, with dispersion relation $\epsilon_k = \hbar c|k|$. The sound velocity is:

$$c = \sqrt{\frac{\rho_0 v_0}{m}} \tag{4.23}$$

and the compressibility κ_s is:

$$\kappa_s^{-1} = m\rho_0\, c^2 = v_0 \rho_0^2 \tag{4.24}$$

The Luttinger parameter K_L is related to the compressibility κ_s by:

$$K_L^2 = \frac{\hbar^2 \pi^2 \rho_0^3}{m}\, \kappa_s \tag{4.25}$$

and to the sound velocity by:

$$K_L = \frac{v_F}{c} \tag{4.26}$$

where $v_F = \frac{\hbar\pi\rho_0}{m}$ is the Fermi velocity of a 1D ideal Fermi gas of particles with mass m and density ρ_0. In the long wavelength limit, the Physics of the system is universal, i. e. it is completely characterized by the Luttinger parameter K_L independent of details of the interaction and particle statistics. In particular:

- the limit $K_L \to 0$ is signalled by a large sound velocity and a small compressibility, and thus it is realized in rigid systems (e.g. dense systems with strong repulsive hard-core interactions)
- the limit $K_L \to \infty$, signalled by a small sound velocity and a large compressibility, is realized in soft systems (e.g. dilute systems with soft-core interactions)

It is worth pointing out that in deriving the Hamiltonian (4.22), we have restricted our consideration to Galilean invariant systems. The relation (4.26), in particular, is a peculiar prerogative of Galilean-invariant systems [148, 166, 157]. In Appendix 11, the correlation functions of the TLL are calculated in detail, following the approach of [148, 167]. We report here the long-distance asymptotic form of the radial distribution function:

$$g(r) \simeq 1 - \frac{K_L}{2(k_F r)^2} + \sum_{m=1}^{\infty} C_m \frac{\cos\left(m(2k_F r)\right)}{(2k_F r)^{2m^2 K_L}} \quad , \qquad r \gg k_F^{-1} \tag{4.27}$$

where $k_F = \pi\rho_0$ is the Fermi wavevector of a 1D ideal Fermi gas at the same density of the system, and the coefficients C_m are model-dependent [148, 168]. Despite those two limitations, the functional form of (11.27) reflects the physical properties and the universality of the TLL paradigm: it encompasses a constant value of uncorrelated particles, a power-law decay due to density fluctuations (with the amplitude fully fixed by the Luttinger parameter), and oscillations with a power-law envelope.
These features determine the salient properties of the static structure factor: the power-law decay due to density fluctuation essentially determines the low-momentum behavior:

$$S(q) \simeq \frac{\hbar|q|}{2mc} = \frac{v_F}{c}\,\frac{|q|}{2k_F} = K_L\,\frac{|q|}{2k_F} \quad , \qquad |q| \ll 2k_F \tag{4.28}$$

while the oscillations with a power-law envelope determine the shape of the static structure factor close to the wavevectors $q = 2mk_F$. Such oscillations, in particular, might

determine peaks at the multiples $q = 2mk_F$ of the momentum $2k_F$, with height:

$$S(q = 2mk_F) = S_{smooth}(2mk_F) + C_m\, N^{1-2m^2K_L} \tag{4.29}$$

In particular, a peak is present at $q = 2mk_F$ if $K_L < \frac{1}{2m^2}$; there are no diverging peaks for $K_L > 1/2$, one diverging peak for $1/8 < K_L < 1/2$, two for $1/18 < K_L < 1/8$ and so on. This regime has been referred to as quasi-crystalline in literature [168], because there are a number of difference with a crystal. A crystal has diagonal long-range order, as the density oscillations remain in phase at large distances. Instead, in 1D the coherence of density oscillations fades with power-law decay. In a crystal, the Bragg peaks grow linearly with the number of particles, while in a quasi-crystal the exponent of the peaks in (4.29) is smaller than unity and depends on K_L. Moreover, in a crystal the number of diverging peaks is infinite, while in 1D quasi-crystals the number of peaks depend on K_L. Finally, the DSF has the following expression [169, 167]:

$$S(q,\omega) = \sum_{m=1}^{\infty} S_m\, \omega^{2m^2(K_L-1)} \frac{f\left(\frac{c(q-2mk_F)}{\omega}\right) + f\left(\frac{c(q+2mk_F)}{\omega}\right)}{2} \tag{4.30}$$

where:

$$f(x) = \begin{cases} (1-x^2)^{m^2K_L-1} & |x| < 1 \\ 0 & \text{otherwise} \end{cases} \tag{4.31}$$

Care must be taken in interpreting those results, since the TLL theory is accurate only in the long-wavelength limit, and for low-energy excitations. The correlation functions of the TLL therefore approximate those of an actual 1D liquid only in the limit of large distance or, equivalently, of low momentum and energy.

4.2.1 Ground-state wavefunction of a Tomonaga-Luttinger liquid.

In 1967, L. Reatto and G. V. Chester [170] proposed a trial ground-state wavefunction for a strongly interacting system of bosons, under the basic assumption that the system can support long-wavelength phonons and that these can propagate independently of any other mode of motion. Their proposal parallels the approach by T. Gaskell to homogeneous Fermi systems [102].

In the previous Subsection 4.2 we saw that the TLL satisfies those requisites, whence the Reatto-Chester wavefunction desribes its ground-state wavefunction [6]. The starting point is applying, to the TLL Hamiltonian (4.22), the transformation:

$$\hat{P}_q = \frac{\hat{a}^\dagger_{-q} + \hat{a}_q}{\sqrt{2}} \qquad \hat{X}_q = \frac{\hat{a}^\dagger_{-q} - \hat{a}_q}{\sqrt{2}i} \tag{4.32}$$

obtaining:

$$\hat{H}_{LL} = \frac{1}{2}\sum_{q\neq 0} \hbar c|q| \left(\hat{P}_{-q}\hat{P}_q + \hat{X}_{-q}\hat{X}_q\right) \tag{4.33}$$

$\hat{X}_q$ is closely related to the density fluctuation operator, since:

$$\begin{aligned}\hat{\rho}_q &= \int dx\, e^{iqx}\, \hat{\rho}(x) \simeq \int dx\, e^{iqx}\, \frac{\partial_x \hat{\phi}(x)}{\pi} = \\ &= \sum_k \int dx\, \frac{-ik}{\pi}\, \frac{e^{i(q-k)x}}{\sqrt{L}}\, \hat{\phi}(k) = iq \sqrt{\frac{K_L}{\pi|q|}}\, \hat{X}_q\end{aligned} \tag{4.34}$$

for $q \neq 0$, having recalled (4.19). We conclude that the configurations $|\mathcal{R}\rangle$ are joint eigenfunctions of all the operators $\hat{X}_q$ with eigenvalues:

$$\hat{X}_q|\mathcal{R}\rangle = X_q|\mathcal{R}\rangle \qquad X_q = \frac{1}{iq}\sqrt{\frac{\pi|q|}{K_L}}\sum_{i=1}^{N} e^{iqr_i} \tag{4.35}$$

The operators $\hat{X}_q, \hat{P}_q$, despite being non-hermitian, obey the canonical commutation relations:

$$[\hat{X}_q, \hat{X}_{q'}] = [\hat{P}_q, \hat{P}_{q'}] = 0 \quad , \qquad [\hat{X}_q, \hat{P}_{-q'}] = i\delta_{q,q'} \tag{4.36}$$

so that we can write $\hat{P}_q = -i\frac{\partial}{\partial X_{-q}}$. The requirement that the TLL ground state be annihilated by the operator $\hat{a}_q$ translates in the following equality:

$$\hat{a}_q|\Phi_0\rangle = \frac{\hat{P}_q - i\hat{X}_q}{\sqrt{2}}|\Phi_0\rangle = 0 \tag{4.37}$$

which, in the representation of the $\hat{X}_q$ operators, takes the more explicit form:

$$-\frac{\partial}{\partial X_{-q}}\Phi_0(\{X_q\}_q) - X_q\Phi_0(\{X_q\}_q) = 0 \tag{4.38}$$

which is solved by:

$$\Phi_0(\{X_q\}_q) = \mathcal{N}\, e^{-\frac{1}{2}\sum_{q\neq 0} X_{-q}X_q} \tag{4.39}$$

In view of the relation (4.35), we find:

$$X_{-q}X_q = |X_q|^2 = \frac{\pi}{|q|K_L L}\sum_{ij} e^{iqr_{ij}} \tag{4.40}$$

Combining (4.39) and (4.40), we find:

$$\Phi_0(\mathcal{R}) \propto \exp\left(-\sum_{i<j}\sum_{q\neq 0}\frac{\pi}{|q|K_L L}\, e^{iqr_{ij}}\right) \tag{4.41}$$

The summation over q can be evaluated recalling that $q = \frac{2\pi}{L}\, n$, with $n \in \mathbb{Z}$, and that $\sum_{n=1}^{\infty}\frac{t^n}{n} = -\log(1-t)$ when $|t| \leq 1$, $t \neq 1$, leading to the Reatto-Chester wavefunction:

$$\Phi_0(\mathcal{R}) \propto \prod_{i<j}\left|\sin\left(\frac{\pi r_{ij}}{L}\right)\right|^{\frac{1}{g}} \tag{4.42}$$

where $g = K_L$. When applying the Reatto-Chester wavefunction (4.42) to a realistic

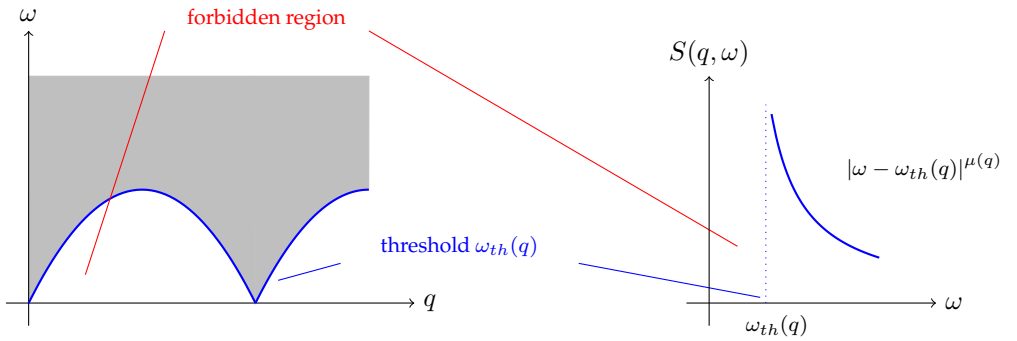

Figure 4.2: Left: the basic assumption of the nonlinear Luttinger liquid theory is the existence of a low-energy threshold $\omega_{th}(q)$ above which the DSF is supported, thus $S(q,\omega) \equiv 0$ for $\omega < \omega_{th}(q)$. Close to the low-energy threshold, the DSF develops a power-law singularity $S(q,\omega) \simeq |\omega - \omega_{th}(q)|^{\mu(q)}$ with an exponent $\mu(q)$ completely determined by the Luttinger parameter K_L and the low-energy threshold $\omega_{th}(q)$.

system, in view of the approximate nature of the TLL theory and of the phenomenologic nature of K_L, g should be treated as a variational parameter.

4.3 Nonlinear Tomonaga-Luttinger liquid theory

The TLL theory is an effective low-energy theory, capable to describe the low-momentum and low-energy excitations of a 1D liquid. After the development of the TLL theory, the search for an effective theory capable of describing the DSF of a 1D system has been pursued by several authors [150, 171, 172], most notably A. Imambekov and L. Glazman, who recently extended the TLL theory beyond the low-momentum regime [152, 153]. Their extension is called nonlinear TLL theory. The main assumption underlying the nonlinear TLL theory is that the DSF has a sharp edge of support $\omega_{th}(q)$, illustrated in Figure 4.2.
The threshold $\omega_{th}(q)$ is a model-dependent, and therefore non-universal, quantity. Only in the low-momentum region, $\omega_{th}(q)$ is well-approximated by the linear dispersion relation $c|q|$, corresponding to phononic excitations. The most natural starting point, that is considering the curvature in the dispersion relation $\omega_{th}(q)$ and therefore going beyond the linear approximation of the TLL theory, is rather difficult to control mathematically: reason being that the additional term is not appropriate for a perturbative analysis [153]. Instead, the idea behind the nonlinear TLL theory is to treat an excitation with energy close to the low-energy threshold as an impurity in an otherwise usual Luttinger liquid. The field operator $\hat{\Psi}(x)$ is written as the sum of two terms:

$$\hat{\Psi}(x) = \hat{\Psi}_{LL}(x) + e^{iqx}\,\hat{d}(x) \tag{4.43}$$

where $\hat{\Psi}_{LL}(x)$, given by (11.4), destroys a particle in the TLL, and $\hat{d}(x)$ destroys an impurity. The impurity has momentum q and its dispersion relation follows the low-energy threshold $\omega_{th}(q)$. Linearizing the dispersion around q leads to a new velocity $v_d = \partial_q \omega_{th}(q)$. The Physics of the system is described by the effective Hamiltonian operator [150, 171, 172, 152]:

$$\hat{H} = \hat{H}_{LL} + \hat{H}_d + \hat{H}_{int} \tag{4.44}$$

where $\hat{H}_{LL}$ is the TLL Hamiltonian (4.18), $\hat{H}_d$ is given by:

$$\hat{H}_d = \int dx\, \hat{d}^\dagger(x)\left(\hbar\omega_{th}(q) - i\hbar v_d \partial_x\right)\hat{d}(x) \tag{4.45}$$

and describes the kinetics of the impurity, while:

$$\hat{H}_{imp} = \int dx\, \left(V_\phi(q)\frac{\partial_x\hat{\phi}(x)}{2\pi} + V_\eta(q)\frac{\partial_x\hat{\eta}(x)}{2\pi}\right)\hat{d}^\dagger(x)\hat{d}(x) \tag{4.46}$$

describes the interaction of the impurity with the TLL. The impurity Hamiltonian was first introduced by K. D. Schotte and U. Schotte for the study of the threshold singularities exhibited by X-ray spectra in 1D metals [151]. It was applied by S. Sorella and A. Parola [173, 174], and later by M. Pustilnik *et al.*, M. Khodas *et al.* and G. Pereira *et al.*, to the study of spectral functions of interacting 1D fermions [171, 172, 150]. Using quite general arguments [152], it is possible to show that the potentials $V_\phi(q)$, $V_\eta(q)$ are in turn related to the Luttinger parameter and the derivatives of the threshold energy by:

$$\begin{aligned}\frac{V_\phi(q)}{2\pi} &= \frac{1}{\pi}\,\partial_\rho\omega_{th}(q) + \frac{c}{K_L}\\ \frac{V_\eta(q)}{2\pi} &= \partial_q\omega_{th}(q) - \frac{q}{m}\end{aligned} \tag{4.47}$$

The usefulness of the description provided by the operators (4.18), (4.45), (4.46) comes from the observation that the unitary transformation:

$$\hat{U} = \exp\left(i\int dx\, \left(\sqrt{K_L}\,\frac{\delta_+(q)-\delta_-(q)}{2\pi}\,\hat{\eta}(x) - \frac{1}{\sqrt{K_L}}\,\frac{\delta_+(q)+\delta_-(q)}{2\pi}\,\hat{\phi}(x)\right)\hat{d}^\dagger(x)\hat{d}(x)\right) \tag{4.48}$$

decouples the impurity from the Luttinger liquid, provided that the phase shifts $\delta_\pm(q)$ are related to the interaction potentials $V_{\phi,\eta}(q)$ by:

$$\begin{aligned}-\frac{V_\eta(q)}{\sqrt{K_L}} &= -\delta_-(q)\,(v_d + c) + \delta_+(q)\,(v_d - c)\\ -V_\phi(q)\,\sqrt{K_L} &= -\delta_-(q)\,(v_d + c) - \delta_+(q)\,(v_d - c)\end{aligned} \tag{4.49}$$

This result can be verified by direct inspection, through a lengthy but straightforward calculation in Appendix 11.

$$\delta_\pm(q) = \frac{-\frac{1}{\sqrt{K_L}}V_\eta(q) \pm \sqrt{K_L}V_\phi(q)}{2\,(\pm\partial_q\omega_{th}(q) - c)} \tag{4.50}$$

The solution of the Hamiltonian (4.18) (4.45), (4.46) allows us to understand the shape of the DSF in the vicinity of the low-energy threshold. For $2nk_F < q < 2(n+1)k_F$, this quantity is given by [152]:

$$S(q,\omega) = S_0(q)(\omega - \omega_{th}(q))^{-\mu_n(q)} \tag{4.51}$$

with:

$$\mu_n(q) = 1 - \frac{1}{2}\left((2n+1)\sqrt{K_L} + \frac{\delta_+(q_n^*) + \delta_-(q_n^*)}{2\pi}\right)^2 - \frac{1}{2}\left(\frac{1}{\sqrt{K_L}} + \frac{\delta_+(q_n^*) - \delta_-(q_n^*)}{2\pi}\right)^2 \tag{4.52}$$

and $q_n = (2n+1)k_F - q$. The DSF exhibits a power-law singularity, with an exponent defined by the Luttinger parameter and by the low-energy threshold. While there is no proof that (4.51) holds for any strongly interacting Galilean-invariant system, it has been argued [152] that it should be valid as long as the low-energy threshold satisfies the stability condition:

$$|\partial_q \omega_{th}(q)| < c \tag{4.53}$$

and interactions decay faster than $1/x$. Equation (4.53) guarantees that phases $\delta_\pm(q)$ are continuous functions of the momentum.

TLL theories are very powerful and elegant phenomenological theories, which express several static and dynamical properties in terms of a few phenomenologic quantities (the Luttinger parameter and the low-energy threshold) that must be determined with numerical calculations or QMC simulations. TLL theories, however, have limits of applicability, and thus they do not exhaust our understanding of 1D substances. Several salient features of the DSF are predicted, but only the recursion of numerical calculations or QMC simulation can unveil the whole DSF.

4.4 Exactly solvable models

Remarkably, several 1D many-body systems of considerable conceptual and experimental relevance are exactly solvable [154, 156, 155], and provide a precious support for understanding static and dynamic properties of interacting 1D systems in suitable regimes [175, 176, 177]. In the forthcoming Subsections 4.4.1, 4.4.2, 4.4.3 the exactly-solvable models of relevance for the 1D ^{4}He are presented.

4.4.1 The ideal Fermi gas

As discussed in Section 4.1, even a weak interaction provoques a strong alteration in the ground-state of a 1D many-fermion system, which is driven away from the normal phase, described by Landau's Fermi liquid theory, to the strongly correlated Luttinger liquid phase. At first sight, then, the ideal Fermi gas (IFG) might appear a somewhat inadequate model of actual 1D systems. However, it is brought back into stage in a very surprising and amazing way: as we will see in detail in Subsection 4.4.2, 1D bosons with repulsive interaction share a number of properties with ideal fermions. The analogy between one-dimensional repulsive bosons and fermions is called fermionization in published literature [178, 179]. On a very intuitive and heuristic way, this is because the repulsive interaction, preventing particles from tunneling across each other, mimicks the Pauli exclusion principle [178].

A brief review of the properties of the spinless 1D IFG is thus useful in order to facilitate the understanding of the fermionization phenomenon and of the static and dynamical properties of repulsive bosons.

Static properties. Consider an ideal Fermi gas of N spinless particles, inside a region $[0, L]$ with PBC. The eigenfunctions of the IFG Hamiltonian:

$$\hat{H} = -\frac{\hbar^2}{2m} \sum_{i=1}^{N} \frac{\partial^2}{\partial r_i^2} \tag{4.54}$$

are the following Slater determinants:

$$\Phi_{k_1 \dots k_N}(r_1 \dots r_N) = \det\left(\frac{e^{ik_i r_j}}{L}\right) \tag{4.55}$$

with $k_i = \frac{2\pi}{L} n_i$, $n_i \in \mathbb{Z}$ in order to comply with PBC. Due to the Pauli exclusion principle, made manifest by the determinant in (4.55), the integer numbers n_i must be distinct. Without loss of generality, we can assume that they are in ascending order, i.e. $n_i < n_{i+1}$ for all $i = 1 \dots N$. The corresponding eigenvalues are:

$$\mathcal{E} = \frac{\hbar^2}{2m} \sum_i k_i^2 = \frac{\hbar^2}{2m} \left(\frac{2\pi}{L}\right)^2 \sum_i n_i^2 \tag{4.56}$$

For N odd, the ground-state Φ_0 of the system is non-degenerate and specified by the integer numbers $n_i = -n_F + (i-1)$, with $n_F = \frac{N-1}{2}$. The ground-state energy per particle reads:

$$\mathcal{E}_N = \frac{1}{N} \frac{\hbar^2}{2m} \left(\frac{2\pi}{L}\right)^2 \frac{N(N^2-1)}{12} = \frac{\hbar^2 k_F^2}{6m} \left(1 - \frac{1}{N^2}\right) \xrightarrow{N\to\infty} \frac{\hbar^2 k_F^2}{6m} \tag{4.57}$$

where $k_F = \pi\rho$ is the Fermi wavevector of the IFG. The compressibility of the system is readily computed from $\mathcal{E}_N$ using formula (1.34). Formula (4.25) then shows that $K_L = 1$. The static structure factor of the system is readily computed using Wick's theorem:

$$\begin{aligned} S(q) &= \langle\Phi_0|\hat{\rho}_q \hat{\rho}_{-q}|\Phi_0\rangle = \sum_{kp} \langle\Phi_0|\hat{a}_{k+q}^\dagger \hat{a}_k \hat{a}_{p-q}^\dagger \hat{a}_p|\Phi_0\rangle = \sum_{kp} \langle\Phi_0|\hat{a}_{k+q}^\dagger \hat{a}_p|\Phi_0\rangle \langle\Phi_0|\hat{a}_k \hat{a}_{p-q}^\dagger|\Phi_0\rangle = \\ &= \sum_{kp} \Theta(k_F - |p|)\delta_{p,k+q}\, \Theta(|k| - k_F)\delta_{k,p-q} = \sum_p \Theta(k_F - |p|)\Theta(|p-q| - k_F) \end{aligned} \tag{4.58}$$

The straightforward evaluation of the last sum leads to:

$$S(q) = \begin{cases} \frac{q}{2k_F} & 0 < q < 2k_F \\ 1 & q > 2k_F \end{cases} \tag{4.59}$$

Equation (1.55) then gives the following exact expression of the radial distribution function:

$$g(r) = 1 - \frac{1}{2(k_F r)^2} + \frac{\cos(2k_F r)}{(k_F r)^2} \tag{4.60}$$

in which we recognize (11.27) with $K_L = 1$ and $C_m = \delta_{m1}$.

Dynamical structure factor. We compute the DSF (1.26) for $q > 0$ with the aid of the Lehmann representation (1.23):

$$S(q,\omega) = \frac{1}{N}\sum_n \delta(\omega-\omega_n)\,|\langle\Phi_n|\hat{\rho}_{-q}|\Phi_0\rangle|^2 \tag{4.61}$$

Since $\hat{\rho}_{-q} = \sum_k \hat{a}^\dagger_{k-q}\hat{a}_k$, the summation is restricted to all the excited states of the form $|\Phi_n\rangle = \hat{a}^\dagger_{k-q}\hat{a}_k|\Phi_0\rangle$, with $|k| \le k_F$ and $|k-q| > k_F$. The energy gap between Φ_n and Φ_0 is:

$$\hbar\omega_n = \frac{\hbar^2(k-q)^2}{2m} - \frac{\hbar^2k^2}{2m} = \frac{\hbar^2 q}{2m}(q-2k) \tag{4.62}$$

whence:

$$S(q,\omega) = \frac{1}{N}\sum_k \Theta(k_F-|k|)\Theta(|k-q|-k_F)\delta\left(\omega - \frac{\hbar q}{2m}(q-2k)\right) \tag{4.63}$$

In the thermodynamic limit, the DSF converges [6] to a flat distrubution:

$$S(q,\omega) = \frac{S(q)}{\omega_I(q)-\omega_{II}(q)}\begin{cases} 1 & \omega_{II}(q) \le \omega \le \omega_I(q) \\ 0 & \text{otherwise}\end{cases} \tag{4.64}$$

The DSF has support inside the particle-hole band $\omega_{II}(q) \le \omega \le \omega_I(q)$ of the (q,ω) plane, comprised between the branches:

$$\hbar\omega_I(q) = \frac{\hbar^2q^2}{2m} + \hbar v_F q \qquad \hbar\omega_{II}(q) = \left|\hbar v_F q - \frac{\hbar^2q^2}{2m}\right| \tag{4.65}$$

illustrated in Figure 4.3. A straightforward calculation shows that the branches $\hbar\omega_I(q)$, $\hbar\omega_{II}(q)$ correspond to elementary single particle-hole excitations:

$$n_{i,PH} = n_{i,GS} + (p - n_{h,GS})\delta_{i,h} \qquad i = 1\dots N \tag{4.66}$$

called Type-I and Type-II respectively [154, 180]. In the Type-I excitation a particle is taken from the Fermi level, $h = N$ and $n_h = n_F$, to some high-energy state $p > n_F \in \mathbb{N}$, while in the Type-II excitation a particle is taken from a low-energy state, $h < N$ and $n_h < n_F$, and brought just above the Fermi level $p = n_F + 1$. The elementary Type-I and Type-II excitations are illustrated in Figure 4.3.

4.4.2 The Lieb-Liniger model

The Lieb-Liniger model (LLM) describes 1D bosons with contact interaction in periodic boundary conditions, and is defined by the Hamiltonian operator:

$$\hat{H} = -\frac{\hbar^2}{2m}\sum_{i=1}^N \frac{\partial^2}{\partial r_i^2} + \frac{\hbar^2 c}{2m}\sum_{i\neq j}\delta(r_i - r_j) \tag{4.67}$$

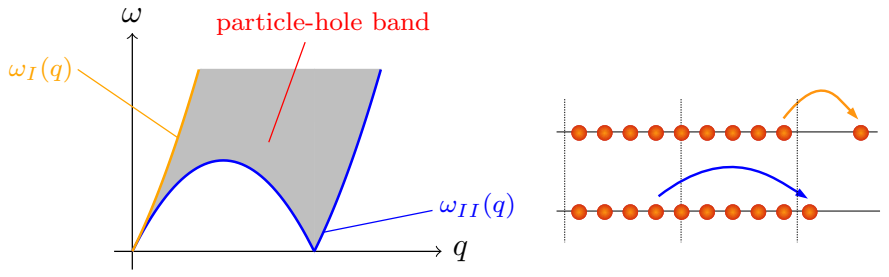

(a) (b)

Figure 4.3: (a) The DSF of the IFG has support in the particle-hole band of the (q, ω) plane (gray region), which is bounded by the branches $\omega_I(q)$ (orange line) and $\omega_{II}(q)$ (blue line). (b) pictorial representation of the Type I excitation (upper line) with $p = 3$ and of the Type-II excitation with $h = 4$ for a system of $N = 9$ particles.

where the parameter $c \in \mathbb{R}$ measures the strength of the interaction. Measuring lengths in units of ρ^{-1}, i.e. performing the substitution $r_i \to x_i = \rho r_i$, and energies in units of:

$$\frac{\hbar^2 \rho^2}{2m} = \frac{1}{\pi^2} \frac{\hbar^2 (\pi\rho)^2}{2m} = \frac{\epsilon_F}{\pi^2} \tag{4.68}$$

where ϵ_F is the Fermi energy of an IFG at the same density of the LLM, we obtain:

$$\hat{H} = -\sum_{i=1}^{N} \frac{\partial^2}{\partial x_i^2} + \gamma \sum_{i \neq j} \delta(x_i - x_j) \tag{4.69}$$

where $\gamma = \frac{c}{\rho}$ is a dimensionless parameter. The domain of the Hamiltonian (4.69) is the set of wavefunctions $\Psi(x_1 \dots x_N) \in \mathcal{L}^2(\mathbb{R}^N)$ such that:

$$\begin{aligned} &\Psi(x_1 \dots x_i + L \dots x_N) = \Psi(x_1 \dots x_i \dots x_N) \\ &\Psi(x_1 \dots x_i \dots x_j \dots x_N) = \Psi(x_1 \dots x_j \dots x_i \dots x_N) \\ &\lim_{x_{i+1} \to x_i^+} \left(\frac{\partial}{\partial x_{i+1}} - \frac{\partial}{\partial x_i} \right) \Psi(x_1 \dots x_N) = 2\gamma \lim_{x_{i+1} \to x_i^+} \Psi(x_1 \dots x_N) \end{aligned} \tag{4.70}$$

where the first equation imposes PBC, the second one imposes Bose symmetry and the third one imposes that $\langle \Psi | \hat{H} | \Psi \rangle < \infty$. The interaction in (4.69) is repulsive (attractive) for $\gamma > 0$ ($\gamma < 0$) and vanishes for $\gamma = 0$. The hard-core limit $\gamma = \infty$ is known as the Tonks-Girardeau system [178, 149]. Notice that $L = N$ is measured in units of ρ^{-1}.

Solution by Bethe Ansatz. The LLM is an analytically solvable model, which captures the essential physical properties of 1D particles with short range interaction, and proves a very powerful tool for the interpretation of experimental results [177, 181]. The main limitation in describing actual experiments applying the LLM is the translational invariance of the Hamiltonian operator (4.69), which is spoiled by the trapping used in experimental setups to confine the system.
In order to solve the LLM, let us concentrate on the sector of the configurational space where $x_1 < \dots < x_N$. In that sector, the wavefunction Ψ is an eigenfunction of the

free Hamiltonian operator. It is therefore very natural to consider a set of real numbers $(k_1, \dots, k_N)$, called *quasimomenta*, and formulate the following Bethe Ansatz [182, 154]:

$$\Psi(x_1 \dots x_N) = \sum_{\sigma \in S_n} A_\sigma e^{ik_{\sigma(1)}x_1 + \dots + k_{\sigma(N)}x_N} \tag{4.71}$$

where the coefficients A_σ depend on the permutation $\sigma \in S_N$. The wavefuncion (4.71) is an eigenfunction of the Hamiltonian operator (4.69) with eigenvalue:

$$E = \sum_{i=1}^{N} k_i^2 \tag{4.72}$$

and of the momentum operator $\hat{P} = -i \sum_{i=1}^{N} \frac{\partial}{\partial r_i}$ with eigenvalue:

$$K = \sum_{i=1}^{N} k_i \tag{4.73}$$

in units of $\hbar\rho^{-1}$. Moreover, in all other sectors of the configurational space it is sufficient to define:

$$\Psi(x_1 \dots x_N) = \Psi\left(\min(x_1 \dots x_N) \dots \max(x_1 \dots x_N)\right) \tag{4.74}$$

in such a way as to obtain a bosonic wavefunction. Let us now discuss for which values of the coefficients A_σ the last of conditions (4.70) is satisfied. Consider two permutations σ, ρ which differ from each other by the exchange of two adjacent particles $i, i+1$ i.e. $\rho(i) = \sigma(i+1)$, $\sigma(i) = \rho(i+1)$ and $\sigma(k) = \rho(k)$ otherwise. We might expect the existence of a relation between A_σ and A_ρ involving $k_{\sigma(i)}$ and $k_{\sigma(i+1)}$, and not all other A_τ coefficients. In particular, (4.70) holds if:

$$i\left(k_{\sigma(i+1)} - k_{\sigma(i)}\right)\left(A_\sigma - A_\rho\right) = \gamma\left(A_\sigma + A_\rho\right) \tag{4.75}$$

implying:

$$A_\rho = A_\sigma \frac{k_{\sigma(i+1)} - k_{\sigma(i)} + i\gamma}{k_{\sigma(i+1)} - k_{\sigma(i)} - i\gamma} = -A_\sigma\, e^{i\theta_{\sigma(i),\sigma(i+1)}} \qquad \theta_{i,j} = -2\arctan\left(\frac{k_i - k_j}{\gamma}\right) \tag{4.76}$$

Since a generic permutation σ can be expressed as composition of elementary permutations exchanging two adjacent indexes we have:

$$A_\sigma = A_1(-1)^{\mathrm{sgn}(\sigma)} \prod_{i<j} e^{i\theta_{\sigma(i),\sigma(j)}} \tag{4.77}$$

Equation (4.77) determines the coefficients A_σ appearing in the wavefunction eq. (4.71) once the quasimomenta $k_1 \dots k_N$ are given. It also imposes a constraint of great conceptual and physical relevance on the quasimomenta $k_1 \dots k_N$, namely that they must be all distinct. In fact, suppose that $k_i = k_j$ for some i, j and consider the quantities:

$$\Psi(\dots x_i \dots x_j \dots) = \sum_{\sigma} A_\sigma\, e^{ik_{\sigma(1)}x_1 + \dots + ik_{\sigma(i)}x_i + \dots + ik_{\sigma(j)}x_j + \dots + ik_{\sigma(N)}x_N} \tag{4.78}$$

and:

$$\Psi(\dots x_j \dots x_i \dots) = \sum_\rho A_\rho \, e^{ik_{\rho(1)}x_1 + \dots + ik_{\rho(j)}x_j + \dots + ik_{\rho(i)}x_i + \dots + ik_{\rho(N)}x_N} \tag{4.79}$$

which, for the Bose symmetry constraint to be satisfied, should be equal. Writing $\rho = \sigma \circ \tau$, where τ is the permutation that exchanges i and j, we find:

$$\Psi(\dots x_j \dots x_i \dots) = \sum_\sigma -A_\sigma e^{ik_{\sigma(1)}x_1 + \dots + ik_{\sigma(i)}x_j + \dots + ik_{\sigma(j)}x_i + \dots + ik_{\rho(N)}x_N} \tag{4.80}$$

Comparing (4.78) and (4.80) we easily find that:

$$\Psi(\dots x_i \dots x_j \dots) = -\Psi(\dots x_j \dots x_i \dots) \tag{4.81}$$

but since $\Psi(x_1 \dots x_N)$ is symmetric, then $\Psi(x_1 \dots x_N) \equiv 0$. We have thus proven that the quasimomenta must be all distinct: the presence of a repulsive interaction brings into stage an effective exclusion principle [178, 154, 179]. The emergence of such effective exclusion principle confers a fermionic nature to the wavefunction (4.71), even if the underlying system is composed by bosons. To complete the solution of the LLM, we need to find the quasimomenta. To this purpose, let us observe that the wavefunction (4.71) satisfies the periodic boundary conditions if:

$$(-1)^{N-1} e^{-ik_j L} = e^{i\sum_{s=1}^N \theta_{sj}} \quad \forall\, j = 1 \dots N \tag{4.82}$$

In fact, consider the quantities:

$$\Psi(0, x_2, \dots, x_N) = \sum_{\rho \in S_N} A_\rho e^{i\sum_{n=2}^N k_{\rho(n)} x_n} \tag{4.83}$$

and:

$$\Psi(x_2, \dots, x_N, L) = \sum_{\sigma \in S_N} A_\sigma \, e^{i\sum_{n=1}^{N-1} k_{\sigma(n)} x_{n+1}} e^{ik_{\sigma(N)} L} \tag{4.84}$$

which, for the periodic boundary conditions to be satisfied, should be equal. Since the permutation ρ can be expressed as $\rho = \sigma \circ \tau$ where τ is the permutation such that $\tau(n) = n - 1$ for all $n = 2 \dots N$ and $\tau(1) = N$, we can write:

$$\Psi(0, x_2, \dots, x_N) = \sum_{\sigma \in S_N} \frac{A_{\sigma\circ\tau}}{A_\sigma} \, A_\sigma \; e^{i\sum_{n=1}^{N-1} k_{\sigma(n)} x_{n+1}} \tag{4.85}$$

whence the quantities (4.83) and (4.84) are equal if and only if:

$$\exp\left(ik_{\sigma(N)} L\right) = \frac{A_{\sigma\circ\tau}}{A_\sigma} = (-1)^{N-1} \exp\left(i \sum_{s=1}^N \theta_{s,\sigma(N)}\right) \tag{4.86}$$

This equation should hold for all permutations σ, and thus we can write:

$$\exp\left(ik_j L\right) = (-1)^{N-1} \exp\left(i \sum_{s=1}^N \theta_{s,j}\right) \tag{4.87}$$

Taking the logarithm of both members of eq. (4.87) we are left with:

$$Lk_j - 2\sum_{s=1}^{N} \arctan\left(\frac{k_s - k_j}{\gamma}\right) + \xi(N) = 2\pi n_j \tag{4.88}$$

where $n_j \in \mathbb{Z}$ for all j, and:

$$\xi(N) = \begin{cases} \pi & \text{if } N \text{ is even.} \\ 0 & \text{if } N \text{ is odd.} \end{cases} \tag{4.89}$$

The system of coupled non-linear equations (4.88) is called the Bethe system. It has been shown [180] that (4.88) admits a unique solution, given the values of the integers $n_1 \dots n_N$, and that [183] the eigenfunctions (4.71) are a complete and orthonormal set. In particular, the norm of a state (4.71) is the determinant of a Gaudin matrix [184, 185]. Multiplying the N equations (4.87) we obtain:

$$(-1)^{N(N-1)} e^{-iL\sum_j k_j} = e^{i\sum_{sj}\theta_{s,j}} \tag{4.90}$$

which, since $N(N-1)$ is an even number and the arctangent is an odd function, implying that $\theta_{s,i} + \theta_{i,s} = 0$ for all s and i, reduces to:

$$\sum_j k_j = \frac{2\pi}{L}\sum_j n_j - \frac{N\xi(N)}{L} \tag{4.91}$$

where $N\xi(N) = 0$ is an integer multiple of 2π for both N even and odd. The total momentum $K = \sum_j k_j$ of the system is therefore an integer mutliple of $\frac{2\pi}{L}$. Moreover, it is easy to verify that if $(k_1 \dots k_N)$ is a solution of the Bethe system (4.88), so is $(k'_1 \dots k'_N)$ with:

$$k'_i = k_i + \frac{2\pi}{L} n_0 \tag{4.92}$$

for some integer $n_0 \in \mathbb{Z}$. The transformation (4.92) changes the total wavevector by an amount:

$$\Delta K = 2\pi\rho n_0 = 2k_F n_0 \tag{4.93}$$

$k_F = \pi\rho$ being the Fermi wavevector of an ideal Fermi gas at the same density of the system, and the total energy by an amount:

$$\Delta E = \frac{(\Delta K)^2}{N} + \frac{2\Delta K}{N} \tag{4.94}$$

in agreement with the Galilean invariance of the system.

Static properties. In order to find the quasimomenta $k_1 \dots k_n$, the Bethe system (4.88) should be solved. An analytic solution can be found only in the limit $c \to \infty$, i.e. in the Tonks-Girardeau system, where the approximation:

$$\arctan\left(\frac{k_j - k_l}{\gamma}\right) \simeq 0 \tag{4.95}$$

is accurate and the Bethe system is solved by:

$$k_j = \frac{2\pi}{L}\, n_j \tag{4.96}$$

Remarkably, the quasimomenta of the system coincide with those of a 1D IFG. For N odd, the ground state is specified by a set of quasimomenta k_j such that the integers n_j are symmetrically distributed around 0, i.e. $n_j = -\frac{N-1}{2} + (j-1)$ for $j = 1 \dots N$. For N even, the ground state is still non-degenerate in agreement with Feynman's argument [105] and it is specified by a set of quasimomenta k_j such that the half-integers $n_j - \xi(N)$ are symmetrically distributed around 0, i.e. $n_j - \xi(N) = -\frac{N}{2} + (j-1)$ for $j = 1 \dots N$. This is in striking contrast with the IFG, which has a 2-fold degenerate ground state with N even: while the momenta in (4.55) are true quantum numbers labelling single-particle orbitals occupied by the particles, in the context of the LLM they are collective parameters that must comply with the bosonic nature of the system, and in particular with the non-degeneracy of the ground state. This result is also true for finite interaction strength $\gamma < \infty$: to understand it, we could remind that if $n_j < n_l$ then $k_j < k_l$, and thus any state with a different set of integers has higher energy [154].

We might wish to investigate the thermodynamic limit of the LLM. To this purpose, let us consider an observable $\mathcal{O}$ described by a function $f(\hat{P})$ of the momentum operator. Its ground-state average has the form:

$$\langle \Psi | f(\hat{P}) | \Psi \rangle = \frac{1}{N} \sum_j f(k_j) \tag{4.97}$$

(for instance, the kinetic energy has $f(k) = k^2$). In the thermodynamic limit, we might expect the quasimomenta k_j to eventually form a continuum, in the sense that:

$$\lim_{L,N\to\infty} \frac{1}{N} \sum_i f(k_i) = \frac{1}{\rho} \int dk\, \rho(k)\, f(k) \tag{4.98}$$

for a suitable quasimomentum density $\rho(k)$. To find $\rho(k)$, let us observe that since $k_{i+1} - k_i = \mathcal{O}\left(\frac{1}{L}\right)$ as it is evident from the Bethe system (4.88), we can write:

$$\theta_{s,i} - \theta_{s,i+1} = -\frac{2c}{c^2 + (k_s - k_i)^2}\, (k_{i+1} - k_i) + \mathcal{O}\left(\frac{1}{L^2}\right) \tag{4.99}$$

so that, summing over s and recalling (4.88), we obtain:

$$k_{i+1} - k_i = \frac{2\pi}{L} - \frac{1}{L} \sum_s \frac{2c}{c^2 + (k_s - k_i)^2}\, (k_{i+1} - k_i) + \mathcal{O}\left(\frac{1}{L^2}\right) \tag{4.100}$$

Defining $k_{i+1} - k_i = \frac{1}{L\,\rho(k_i)}$ we find:

$$\frac{1}{N} \sum_i f(k_i) = \frac{1}{N} \sum_i f(k_i)\, \frac{k_{i+1} - k_i}{k_{i+1} - k_i} = \frac{1}{n} \sum_i f(k_i)\, (k_{i+1} - k_i)\, \rho(k_i) \tag{4.101}$$

and therefore:

$$\lim_{L,N\to\infty} \frac{1}{N} \sum_i f(k_i) = \frac{1}{\rho} \int dk\, \rho(k)\, f(k) \tag{4.102}$$

by the Euler-MacLaurin formula. The last step towards the full solution of the LLM in the thermodynamic limit is the calculation of the quasimomentum density $\rho(k)$. To this purpose, let us recall that, by virtue of the definition $k_{i+1} - k_i = \frac{1}{L\,\rho(k_i)}$, the quasimomentum density $\rho(k)$ has support on a compact set $[-K, K]$. Moreover:

$$\frac{1}{L\rho(k_i)} = \frac{2\pi}{L} - \frac{1}{L^2\rho(k_i)} \sum_s \frac{2\gamma}{\gamma^2 + (k_s - k_i)^2} \frac{k_{s+1} - k_s}{k_{s+1} - k_s} + \mathcal{O}\left(\frac{1}{L^2}\right) \tag{4.103}$$

and thus:

$$1 = 2\pi\,\rho(k_i) - \sum_s \frac{2\gamma}{\gamma^2 + (k_s - k_i)^2}\,(k_{s+1} - k_s)\,\rho(k_s) + \mathcal{O}\left(\frac{1}{L}\right) \tag{4.104}$$

which, in the thermodynamic limit, converges to:

$$\rho(k) = \frac{1}{2\pi} + \frac{1}{2\pi} \int_{-K}^{K} \frac{2\gamma}{\gamma^2 + (k - k')^2}\ \rho(k')\,dk' \tag{4.105}$$

In the thermodynamic limit, the ground-state energy per particle reads:

$$\mathcal{E}_N = \frac{1}{\rho} \int_{-K}^{K} dk\,\rho(k)\,k^2 \tag{4.106}$$

and the condition that the total momentum be equal to 0 translates in:

$$\int_{-K}^{K} dk\,\rho(k)\,k = 0 \tag{4.107}$$

while, choosing $f(k) \equiv 1$ we find a subsidiary condition on the quasimomentum density:

$$\rho = \int_{-K}^{K} dk\,\rho(k) \tag{4.108}$$

that completes (4.105). Performing the change of coordinates $k = Kx$, $\rho(k) = \rho(Kx) = g(x)$, $\gamma = K\lambda$, equations (4.105), (4.106) and (4.108) become:

$$g(x) = \frac{1}{2\pi} + \frac{1}{2\pi} \int_{-1}^{1} \frac{2\lambda}{\lambda^2 + (x - y)^2}\,g(y)\,dy \tag{4.109}$$

and:

$$\mathcal{E}_N = \frac{K^3}{\rho} \int_{-1}^{1} dx\,g(x)\,x^2 \qquad \rho = K \int_{-1}^{1} dx\,g(x) \tag{4.110}$$

The numeric solution of (4.105) for the quasimomentum density, which we carry out following the the procedure explained by Z. Ristivojevic [186], leads to the static properties of the LLM in the thermodynamic limit. The ground-state energy per particle and the Luttinger parameter of the LLM are illustrated in Figure 4.4. Following [180], we write the ground-state energy per particle as:

$$\mathcal{E}_\infty = \lim_{N\to\infty} \mathcal{E}_N = \rho^2 e(\gamma) \tag{4.111}$$

Using the relation (4.25), it is readily found [180, 186] that the Luttinger parameter is related to $e(\gamma)$ by the exact expression:

$$K_L = \frac{\pi}{\sqrt{3e(\gamma) - \gamma \frac{de}{d\gamma}(\gamma) + \frac{\gamma^2}{2}\frac{d^2e}{d\gamma^2}(\gamma)}} \tag{4.112}$$

Also the Luttinger parameter of the LLM is shown in Figure 4.4. Remarkably, the LLM explores all possible values of $K_L \geq 1$ by only varying the parameter γ, i.e. either the interaction strength c or the linear density ρ.
The ground-state energy per particle has the following asymptotic forms [187, 186]:

$$\begin{aligned} \mathcal{E}_\infty &= \frac{\hbar^2\rho^2}{2m}\left(\gamma - \frac{4}{3\pi}\gamma^{\frac{3}{2}} + \mathcal{O}(\gamma^2)\right) \qquad \gamma \ll 1 \\ \mathcal{E}_\infty &= \frac{\hbar^2\rho^2}{2m}\left(\frac{\pi^2}{3} - \frac{4\pi^2}{3\gamma} + \frac{4\pi^2}{\gamma^2} + \mathcal{O}(\gamma^{-3})\right) \qquad \gamma \gg 1 \end{aligned} \tag{4.113}$$

Whence the Luttinger parameter (4.25) reads, in the weak-coupling regime $\gamma \ll 1$:

$$K_L = \frac{\pi}{\sqrt{\gamma - \frac{1}{2\pi}\gamma^{\frac{3}{2}}}} \tag{4.114}$$

The asymptotic expansion (4.114) will prove quite important in the study of 1D ^{4}He.

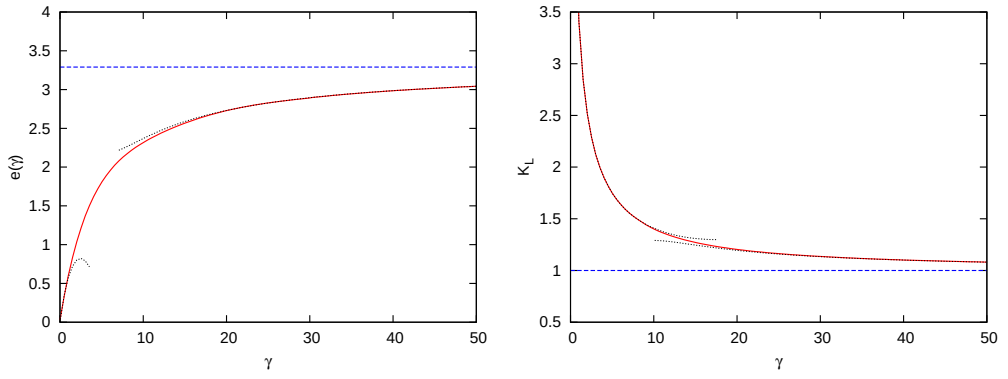

(a) (b)

Figure 4.4: (a) equation of state and (b) Luttinger parameter of the LLM as function of the parameter γ, measuring the strength of the interaction. Red lines correspond to the numeric solution of (4.105), blue dashed lines to asymptotic values $e(\infty) = \frac{\pi^2}{3}$, $K_L(\infty) = 1$ in the Tonks-Girardeau limit, and black dotted lines to the asymptotic forms (4.113).

Dynamical structure factor. The zero-temperature DSF of the LLM has been numerically investigated by J. S. Caux and P. Calabrese [188], by exactly evaluating the matrix elements of the density fluctuation operator $\hat{\rho}_q$ with the algebraic Bethe Ansatz [189]

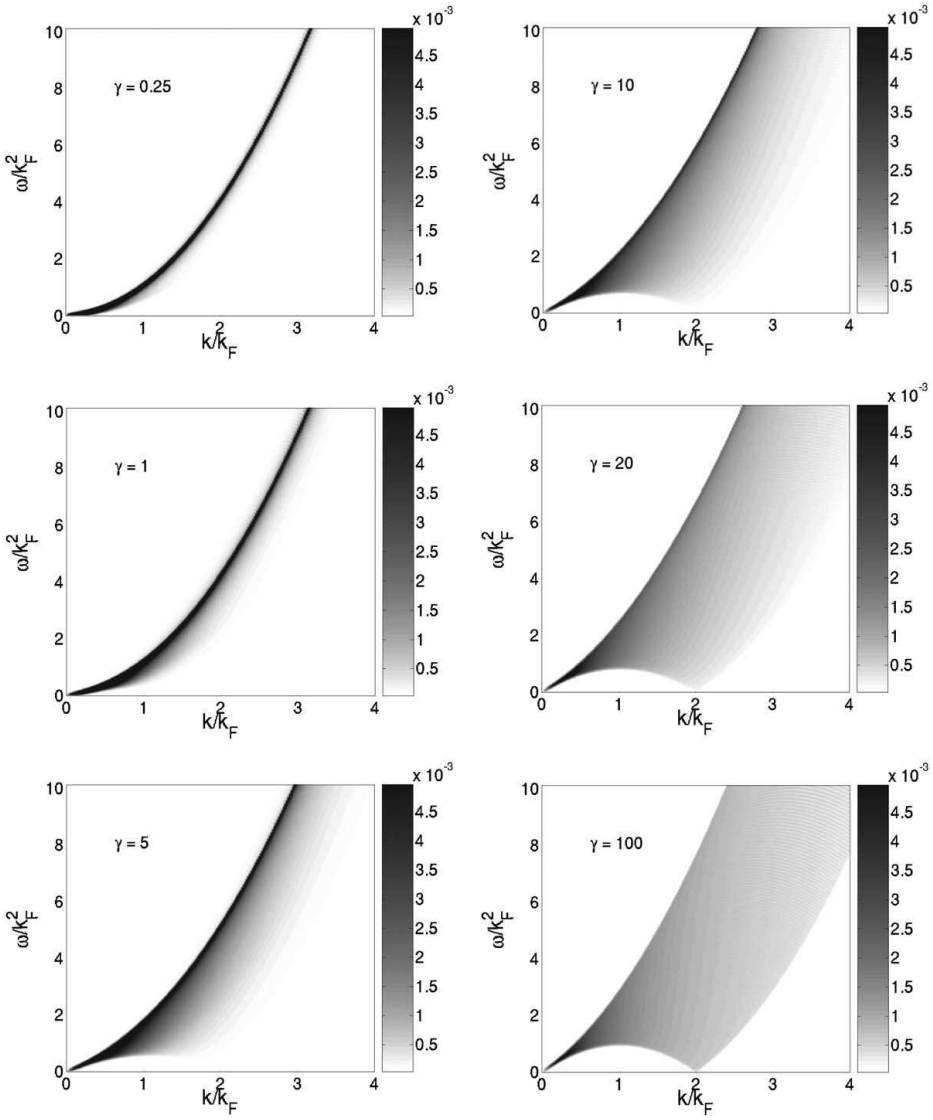

Figure 4.5: Density plots of the DSF of the LLM as function of interaction strength γ. The horizontal axis is the transferred wavevector, running up to $4k_F$, and the vertical axis the transferred energy $\hbar\omega$. Data are relative to a system of $N = 100$ particles with density $\rho = 1$ and $\gamma = 0.25, 1, 5, 10, 20, 100$. Taken from [188].

and performing the summation in the Lehmann representation (1.23) numerically, with a dedicated algorithm. The main result of their study is illustrated in Figure 4.5. The shape of the DSF is best understood recalling the elementary excitations of the LLM which, as in the case of the IFG, come in two types [154, 180]. Type-I excitations are Bogoliubov-like quasiparticles, that exist for any momentum q and represent states with one quantum numbers n_j displaced outside the ground-state interval. Type-II excitations are associated to holes in the ground-state interval. They exist in the interval $|k| \leq 2k_F$, and their

dispersion relation coincides with the low-energy threshold of the DSF. Type-II modes have been identified with dark solitons [190].

The dispersion relation of Type-I excitations is described, in the thermodynamic limit, by an integral equation [180] yielding a curve interpolating between the asymptotic limits $\epsilon_I(q) = \frac{\hbar^2 q^2}{2m}$ ($\gamma \to 0$) and $\epsilon_I(q) = \hbar\omega_I(q)$ ($\gamma \to \infty$). At small γ, the DSF is concentrated at the Type-I excitation, whose analytic form is well-approximated [191] by the Bogoliubov dispersion relation:

$$\epsilon_I(q) = \hbar v_S |q| \sqrt{1 + \frac{q^2}{q_0^2}} \qquad q_0 = 2\frac{m v_S}{\hbar} \tag{4.115}$$

with sound velocity:

$$v_S = \frac{\hbar\rho}{m}\frac{1}{K_L} \simeq v_F\sqrt{\gamma} \tag{4.116}$$

in agreement with (4.26), in light of the estimate (4.114). As γ increases, the DSF flattens but the spectral weight remains concentrated near the Type-I excitation. Increasing γ further towards the Tonks-Girardeau limit, for any given momentum q the DSF approaches a constant value over a finite frequency interval. For all values of γ, the signal mostly lies between the continuum defined by convolution of the Type-I and Type-II dispersion relations.

4.4.3 The hard-rods model

The behavior of several 1D systems with a hard-core repulsive interaction, like ^{4}He or other gases adsorbed in carbon nanotubes [192, 175, 193, 194, 143], can be understood making the assumption that the particles behave like a gas of impenetrable or hard rods.

In fact, at high density, the principal effect of the short-range hard-core repulsive interaction is volume exclusion, and therefore a reasonable schematization of the actual microscale behavior of the system can be obtained by taking into account the volume exclusion phenomenon only, and neglecting all other details of the interaction: within this approach, the system under study is approximated with an assembly of hard rods of a suitable length a.

The recognition that volume exclusion is the most important factor in analyzing short-range hard-core repulsive interactions in classical systems dates back to the seminal work by J. D. van der Waals [195] and J. H. Jeans [196]. It was later recognized [197, 198] that the statistical mechanics of a system of classical hard rods is exactly solvable. In 1940 T. Nagamiya proved [155] that also a system of quantum hard rods is exactly solvable using the Bethe Ansatz technique, and imposing a special system of boundary conditions. T. Nagamiya's treatment was later adapted by B. Sutherland [156] to the more familiar periodic boundary conditions.

Solution by Bethe Ansatz Hard rods are the 1D counterpart of 3D hard spheres [193, 194]. The interparticle hard-rod potential is:

$$V_{HR}(r) = \begin{cases} \infty & |r| \le a \\ 0 & |r| > a \end{cases} \tag{4.117}$$

where a is the size of the rods. The Hamiltonian of a system of N particles inside an interval $[0, L]$ of length L with interparticle hard-rod potential is:

$$\hat{H} = -\frac{\hbar^2}{2m} \sum_{i=1}^{N} \frac{\partial^2}{\partial r_i^2} + \sum_{i<j=1}^{N} V_{HR}(r_i - r_j) \tag{4.118}$$

where m is the mass of the particles, and $(r_1 \dots r_N)$ their coordinates, lying in the configuration space $\mathcal{C} = [0, L]^N$. The domain of the Hamiltonian operator (4.118) is the set of wavefunctions $\Psi(r_1 \dots r_N) \in \mathcal{L}^2(\mathcal{C})$ such that:

$$\begin{aligned} &\Psi(r_1 \dots r_i \dots r_j \dots r_N) = \pm\, \Psi(r_1 \dots r_j \dots r_i \dots r_N) \\ &\Psi(r_1 \dots r_i + L \dots r_N) = \quad \Psi(z_1 \dots r_i \dots r_N) \\ &\Psi(r_1 \dots r_i \dots r_j \dots r_N) = 0 \quad \text{if } |r_i - r_j| \leq a \end{aligned} \tag{4.119}$$

As in the LLM, the first of the conditions (4.119) imposes Bose or Fermi symmetry, the second imposes periodic boundary conditions (PBC) and the third guarantees that $\langle \Psi | \hat{H} | \Psi \rangle < \infty$.

In order to solve the hard-rods Hamiltonian (4.118), following [155], let us concentrate on the sector $\mathcal{S}$ of the configuration space $\mathcal{C}$ where $r_1 < r_2 - a < r_3 - 2a < \dots < r_N - (N-1)a$, which is related to all other sectors of the configuration space by a simple permutation of the particles, and eliminate the rod size a by the transformation:

$$x_i = r_i - (i-1)a \tag{4.120}$$

illustrated in Figure 4.6.

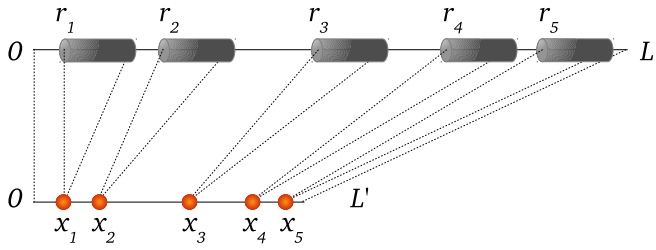

(a)

Figure 4.6: (a) pictorial representation of the transformation (4.120) for $N = 5$ rods. The position of the first rod is left unchanged by (4.120), that of the second rod is shifted of an amount $-a$ (thus eliminating the length of the first rod), and so on. The rod coordinates lie between 0 and the unexcluded volume $L' = L - Na$, from which the length of all the N rods is eliminated.

The rod coordinates x_i lie in the interval $[0, L']$, where $L' = L - Na$ is called the unexcluded volume, and satisfy the conditions $x_1 < x_2 < x_3 < \dots < x_N$. The hard-rod

Hamiltonian (4.118) then takes the form:

$$\hat{H} = -\frac{\hbar^2}{2m} \sum_{i=1}^{N} \frac{\partial^2}{\partial x_i^2} \tag{4.121}$$

and the third condition (4.119), which imposes that the particle collide with each other as impenetrable elastic rods, can be correspondingly expressed as:

$$\Psi(x_1 \dots x_i \dots x_j \dots x_N) = 0 \quad \text{if } x_i = x_j \tag{4.122}$$

Eigenfunctions of (4.121) satisfying the condition (4.122) have the form [155]:

$$\Psi(x_1 \dots x_N) = \frac{1}{\sqrt{N!}} \det\left(\frac{e^{ik_i x_j}}{\sqrt{L'}}\right) \tag{4.123}$$

where $k_1 \dots k_N$ are a set of quantum numbers called quasi-wavevectors, that will be identified later. The eigenvalue corresponding to (4.124) is $E = \frac{\hbar^2}{2m} \sum_{i=1}^{N} k_i^2$. Moreover, (4.123) is identically zero if and only if any two quasi-wavevectors coincide. The values of the quasi-wavevectors $k_1 \dots k_N$ are fixed imposing PBC to the wavefunctions (4.123). Practically, imposing PBC means requiring that:

$$\Psi(0\, r_2 \dots r_N) = \Psi(L\, r_2 \dots r_N) \tag{4.124}$$

for all strings of coordinates $(r_2 \dots r_N)$ such that $(0\, r_2 \dots r_N), (r_2 \dots r_N\, L) \in \mathcal{S}$. Merging (4.123) and (4.124) we find that PBC are satisfied if, for all quasi-wavevectors k_i, the following condition holds:

$$(k_i - K)\, a = k_i(L - (N-1)a) - 2\pi n_i + \xi^{B,F}(N) \tag{4.125}$$

where $i = 1 \dots N$, $K = \sum_{i=1}^{N} k_i$, $n_i \in \mathbb{Z}$ is an integer number, $\xi^F(N) = 0$ and:

$$\xi^B(N) = \begin{cases} 0 & \text{for } N \text{ odd} \\ \pi & \text{for } N \text{ even} \end{cases} \tag{4.126}$$

Equation (4.125) leads easily to:

$$k_i = \frac{2\pi}{L'} n_i + \frac{1}{L'} \xi^{B,F}(N) - \frac{aK}{L'} \tag{4.127}$$

Remarkably, even if the quasi-wavevectors k_i are constructed with both L and L', the total momentum K is an integer multiple:

$$K = \frac{2\pi}{L} \sum_{i=1}^{N} n_i + \frac{N\xi^{B,F}(N)}{L} \tag{4.128}$$

of $\frac{2\pi}{L}$. The eigenfunctions of the HR Hamiltonian are in one-to-one correspondence with strings $n_1 < \dots < n_N$ of ascending integer numbers.

Static properties. For a system of N bosonic hard rods, with N odd, the ground-state wavefunction is characterized by quasi-wavevectors symmetrically distributed around

0:

$$k_{i,GS} = \frac{2\pi}{L'} n_{i,GS} \qquad n_{i,GS} = -n_F + (i-1) \tag{4.129}$$

with $n_F = (N-1)/2$. The corresponding ground-state energy reads [155, 193]:

$$E_{GS} = \frac{\hbar^2}{2m}\left(\frac{2\pi}{L'}\right)^2 \sum_{i=1}^{N} n_{i,GS}^2 = \frac{\hbar^2}{2m}\left(\frac{2\pi}{L'}\right)^2 \sum_{n=-n_F}^{n_F} n^2 = \frac{\hbar^2}{2m}\left(\frac{2\pi}{L'}\right)^2 \frac{n_F(n_F+1)(2n_F+1)}{3} \tag{4.130}$$

$\rho = N/L$ being the linear density of the system. The ground-state wavevector is naturally $K = 0$. In the thermodynamic limit of large system size N at constant density ρ, the ground-state energy per particle converges to:

$$\mathcal{E}_\infty = \lim_{N\to\infty} \mathcal{E}_N = \frac{\hbar^2 k_F^2}{6m(1-\rho a)^2} \tag{4.131}$$

whence the Luttinger parameter K_L [148, 199] can be computed from the compressibility (1.34) through (4.26). The resulting exact expression, $K_L = (1-\rho a)^2$, provides a Luttinger parameter always smaller than 1, in contrast with the LLM for which $K_L \geq 1$, and converging to 0 as the excluded volume Na converges to the total volume L.

The reduced dimensionality is again responsible for the fermionization of impenetrable Bose particles. In the case of hard rods, we can see that eigenfunctions of both Bose and Fermi systems have the same functional form in the sector $\mathcal{S}$ of the configurational space; away from $\mathcal{S}$, they differ from each other only by a sign associated to a permutation of the particles [178]. Therefore, the matrix elements of local operators like the density fluctuation operator are identical for Bose and Fermi particles. This, in particular, implies that the static structure factor and the dynamical structure factor are independent of the statistics.

Excited states. We have seen that the ground-state wavefunction of the hard-rod system, once expressed in terms of the rod coordinates, has the functional form of a Fermi sea with renormalized wavevectors $k_{i,GS}$, specified in terms of integer numbers $n_{i,GS}$. The excitations of the hard rods system have the form of multiple particle-hole excitations on top of this renormalized Fermi sea. Like in the IFG, the simplest excitations consist in the creation of a single particle-hole pair:

$$n_{i,PH} = n_{i,GS} + (p - n_{h,GS})\delta_{i,h} \tag{4.132}$$

where $h \in \{1 \dots N\}$ and $p > n_F$ are integer numbers. Among single particle-hole excitations, we find again Type-I:

$$n_{i,I} = n_{i,GS} + (p_I - n_{N,GS})\,\delta_{i,N} \tag{4.133}$$

and Type-II:

$$n_{i,II} = n_{i,GS} + (n_F + 1 - n_{h_{II},GS})\,\delta_{i,N} \tag{4.134}$$

modes, which are reminescent of the corresponding excitations of the LLM [154] and IFG. In both cases, in view of the collective nature of the quasimomenta k_i, the excitation of a single rod (i.e. the change of an integer number n_i) provoques a recoil of all the other ones, according to (4.127).

A simple calculation shows that the dispersion relation of the Lieb-I excitation is given

by:

$$\frac{E_I - E_{GS}}{\epsilon_F} = 4 \left(\frac{L}{L'}\right)^2 \left[\frac{K_I}{2k_F} + \left(\frac{K_I}{2k_F}\right)^2\right] + \mathcal{O}\left(\frac{1}{N}\right) \tag{4.135}$$

where $K_I \geq 0$ is the wavevector of the Lieb-I excitation, and $\epsilon_F = \frac{\hbar^2 k_F^2}{2m}$. Since:

$$\left(\frac{L}{L'}\right)^2 = \frac{1}{(1-\rho a)^2} = \frac{1}{K_L} \tag{4.136}$$

we obtain the expression:

$$\frac{E_I - E_{GS}}{\epsilon_F} = \frac{4}{K_L} \left[\frac{K_I}{2k_F} + \left(\frac{K_I}{2k_F}\right)^2\right] + \mathcal{O}\left(\frac{1}{N}\right) \tag{4.137}$$

A similar calculation shows that the dispersion relation of the Lieb-II excitation is given by:

$$\frac{E_{II} - E_{GS}}{\epsilon_F} = \frac{4}{K_L} \left[\frac{K_{II}}{2k_F} - \left(\frac{K_{II}}{2k_F}\right)^2\right] + \mathcal{O}\left(\frac{1}{N}\right) \tag{4.138}$$

where $0 \leq K_{II} \leq 2k_F$ is the momentum of the Lieb-II excitation. In the thermodynamic limit, the $\mathcal{O}(1/N)$ corrections vanishing, the Lieb-I and Lieb-II excitations have the same functional form of the ideal Fermi gas, except for the substitution of the bare mass m with the *dressed or renormalized mass* $m^* = mK_L < m$. This exact relation is in agreement with the general expression for m^* within the nonlinear TLL theory [200, 152, 153].
Both Lieb-I and Lieb-II excitations approach $k = 0$ with slope equal to the sound velocity $v_s = \frac{v_F}{K_L}$. v_s is larger than the Fermi velocity, in view of the small compressibility of the system. Other relevant excitations are those producing *supercurrent states* [154, 6, 201]:

$$n_{i,SC} = n_{i,GS} + s \qquad s \in \mathbb{N} \tag{4.139}$$

with momenta $K_{SC} = 2k_F\, s$ and excitation energies:

$$E_{SC} - E_{GS} = \frac{\hbar^2}{2m} \frac{K_{SC}^2}{N} \tag{4.140}$$

independent of the rod length a, and vanishing in the thermodynamic limit. Supercurrent states correspond to Galilean transformations of the ground state with velocities $v_{SC} = \frac{2\hbar k_F}{m} \frac{s}{N}$. The first supercurrent state, in particular, is called umklapp excitation [154, 6, 201].

4.5 Dynamic structure factor of a system of hard rods.

4.5.1 Introduction

Even if the eigenfunctions and eigenvalues of the hard-rods Hamiltonian can be determined exactly, so far numerical methods have been the only systematic way to obtain a complete description of its static correlation functions. Recently, the VMC method has been successfully used to compute the ground-state properties of the hard-rods model [193, 194]. In particular, in [193] the authors have computed the static structure factor over a broad range of transferred wavevectors, $k \leq 12k_F$. Despite the ground-state

wavefunction is known, no simple analytical expression can be easily derived for $S(q)$ at arbitrary q, although some properties can be inferred.

- since the system is a realization of a Luttinger liquid with $K_L = (1-\rho a)^2$, low-momentum excitations are dominated by phonons:

$$S(q) = (1-\rho a)^2 \frac{q}{2k_F} + \mathcal{O}(q^2) \tag{4.141}$$

- at $q = 2mk_F$, and for $1 - 2m^2K_L > 0$, $S(q)$ exhibits a quasi-Bragg peak with heigth proportional to $N^{1-2m^2K_L}$:

$$S(2mk_F) = S_{smooth}(2mk_F) + C_m N^{1-2m^2K_L} \tag{4.142}$$

Away from these points, not many exact properties of the static structure factor are known. Reason being that the passage to the collective rod coordinates (4.120) has a weak influence on the ground state (4.123) (it has the same functional form of the ground-state wavefunction of an IFG at increased density $\rho' = \rho/(1-\rho a) = \rho/\sqrt{K_L}$) but also a strong influence on local operators like the density fluctuation operator:

$$\rho_q(\mathcal{R}) = \sum_{j=1}^{N} e^{iqr_j} = \sum_{j=1}^{N} e^{iqx_j}\, e^{iq(j-1)a} \tag{4.143}$$

which, in the representation of rod coordinates, is no longer a bosonic operator (i.e. invariant under permutations of the particles) unless q is a multiple of $\frac{2\pi}{a}$. We denote as $\mathcal{Q}_n = \frac{2\pi}{a}\, n$ such special wavevectors. When $q = \mathcal{Q}_n$, the phase factors $e^{i\mathcal{Q}_n(j-1)a} = 1$ are absent, and the passage to rod coordinates has no influence on $\rho_q(\mathcal{R})$. As a consequence:

$$S(\mathcal{Q}_n) = \int_{\mathcal{C}} d\mathcal{R} |\rho_{\mathcal{Q}_n}(\mathcal{R})\, \Phi_0(\mathcal{R})|^2 = N! \int_{\mathcal{S}} d\mathcal{R} |\rho_{\mathcal{Q}_n}(\mathcal{R})\, \Phi_0(\mathcal{R})|^2 \tag{4.144}$$

can be exactly rewritten as [193]:

$$S(\mathcal{Q}_n) = N! \int_0^{L'} dx_1 \ldots \int_{n_{n-1}}^{L'} dx_N |\rho_{\mathcal{Q}_n}(x_1 \ldots x_N)\, \Phi_0(x_1 \ldots x_N)|^2 \tag{4.145}$$

and thus takes the same value of the static structure factor of an IFG at density ρ':

$$S(\mathcal{Q}_n) = \begin{cases} \frac{|\mathcal{Q}_n|}{2k'_F} & |\mathcal{Q}_n| \leq 2k'_F \\ 1 & \text{otherwise} \end{cases} \tag{4.146}$$

This property has been directly observed in [193]. The authors also discussed the possibility that the analogy (4.146) extends to the DSF. To prove this result, in view of the Lehmann representation (1.23):

$$S(q,\omega) = \frac{1}{N} \sum_n \delta(\omega - \omega_n)\, |\langle \Phi_n | \hat{\rho}_{-q} | \Phi_0 \rangle|^2 \tag{4.147}$$

it is necessary to analyze the matrix elements of the density fluctuation operator. Since:

$$\langle \Phi_n | \hat{\rho}_{-\mathcal{Q}_n} | \Phi_0 \rangle = \int_{\mathcal{C}} d\mathcal{R} \Phi_n^*(\mathcal{R}) \rho_{-\mathcal{Q}_n}(\mathcal{R}) \Phi_0(\mathcal{R}) = N! \int_{\mathcal{S}} d\mathcal{R} \Phi_n^*(\mathcal{R}) \rho_{-\mathcal{Q}_n}(\mathcal{R}) \Phi_0(\mathcal{R}) \quad (4.148)$$

and $\rho_{-\mathcal{Q}_n}(r_1 \dots r_N) = \rho_{-\mathcal{Q}_n}(x_1 \dots x_N)$, the matrix elements:

$$\langle \Phi_n | \hat{\rho}_{-\mathcal{Q}_n} | \Phi_0 \rangle = N! \int_0^{L'} dx_1 \dots \int_{n_{n-1}}^{L'} dx_N \Phi_n^*(x_1 \dots x_N) \rho_{-\mathcal{Q}_n}(x_1 \dots x_N) \Phi_0(x_1 \dots x_N) \quad (4.149)$$

have the same form (4.58) of an IFG at density ρ'. Hence, the DSF has the exact intriguing expression:

$$S(\mathcal{Q}_n, \omega) = \frac{S(\mathcal{Q}_n)}{\omega_I(\mathcal{Q}_n^*) - \omega_{II}(\mathcal{Q}_n^*)} \begin{cases} 1 & \omega_{II}(\mathcal{Q}_n^*) \leq \omega \leq \omega_I(\mathcal{Q}_n^*) \\ 0 & \text{otherwise} \end{cases} \quad (4.150)$$

where $\mathcal{Q}_n^* = (1 - \rho a)\mathcal{Q}_n$. At different momenta $q \neq \mathcal{Q}_n$, $S(q, \omega)$ differs from the IFG prediction.

4.5.2 QMC evaluation of the dynamic structure factor

The hard rods model is an extremely useful schematization that permits to understand static and dynamic properties of strongly correlated 1D systems with strong repulsive interactions at short distances. The study of the hard-rods DSF thus provides a benchmark for interpreting that of $1D$ Helium or other gases in the high-density regime.
In our study, we have resorted to the PIGS algorithm, described in Section 3.2, to exactly compute the ITCF of the density fluctuation operator, and to the GIFT method, described in Appendix 12, to perform the inverse Laplace transform giving access to the DSF. As trial wavefunction, we have chosen the exact ground-state wavefunction (4.123) of the hard-rods Hamiltonian. In view of the singular nature of the potential (4.118) at short distances, we have not used the standard symmetrized primitive approximation (3.18) but the pair-product approximation:

$$G_{\delta\tau}(\mathcal{R}, \mathcal{R}') = \langle \mathcal{R} | e^{-\delta\tau \hat{T}} | \mathcal{R}' \rangle \prod_{i<j=1}^{N} G_{2,\delta\tau}(\mathbf{r}_{ij}, \mathbf{r}'_{ij}) \quad (4.151)$$

where $G_{2,\delta\tau}(\mathbf{r}_{ij}, \mathbf{r}'_{ij})$ has been found solving the the Schrödinger equation for two hard rods.
Here, we show results relative to the simulation of $N = 25$ hard rods at density $\rho a = 0.642$, corresponding to $K_L = 0.128$. The resulting DSF is shown in Figure 4.7.
To interpret those data, let us observe that the low-energy threshold $\omega_{th}(k)$ of the hard-rods model reads, in the thermodynamic limit, $\hbar\omega_{th}(q) = E_{II}(q) - E_{GS}$ for $0 < q < 2k_F$. Away from this region, i.e. for $2nk_F < q < 2(n+1)k_F$ it is just:

$$\hbar\omega_{th}(q) = E_{II}(q - 2nk_F) - E_{GS} \quad (4.152)$$

thanks to the invariance of the system under Galilean boosts in the thermodynamic limit. For $n = 1$, the lowest excited state with momentum $2nk_F < q < 2(n+1)k_F$ corresponds to a Lieb-II excitation on top of an umklapp excitation: it is therefore a state with 2 particle-hole excitations. Similarly, for $n > 0$ the lowest excited state with momentum

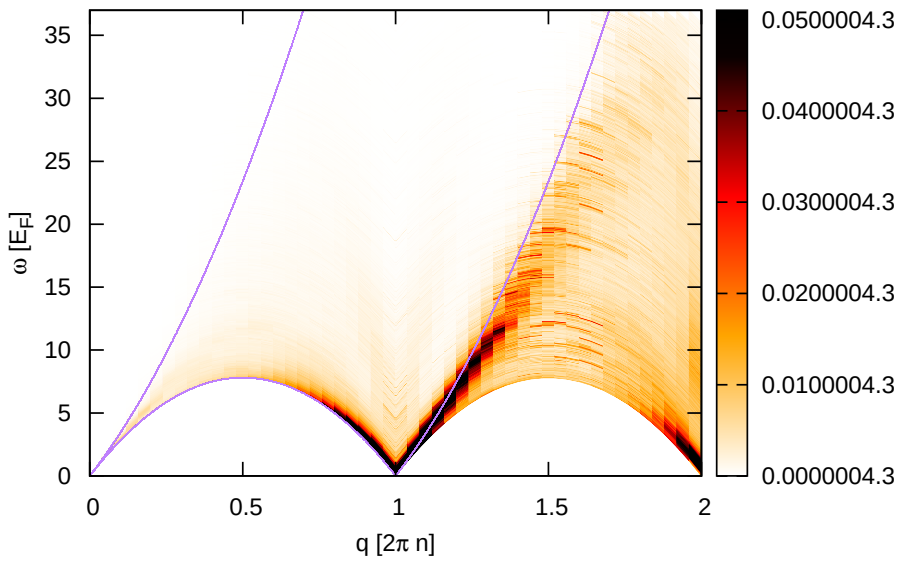

Figure 4.7: Dynamical structure factor of $N = 25$ hard rods at $\rho a = 0.642$, $K_L = 0.128$. Wavevectors are measued in units of $2k_F$, energies in units of E_F.

$2nk_F < q < 2(n+1)k_F$ is obtained performing n suitable particle-hole excitations [202, 153, 201].
From the analytic expression (4.152) of the low-energy threshold, and of the Luttinger parameter of the hard-rods Hamiltonian, we can extract the universal exponent $\mu(q)$ characterizing the power-law singularity predicted by the nonlinear Luttinger theory in vicinity of the low-energy threshold. To this purpose, it is sufficient to perform the very easy calculations (4.51), (4.52). For $2nk_F < q < 2(n+1)k_F$, the result is the surprisingly compact expression:

$$\mu(q) = -2(\tilde{q} - n)(\tilde{q} - (n+1)) \qquad \tilde{q} = \frac{qa}{2\pi} \tag{4.153}$$

which we plot, in Figure 4.8, for a system of hard rods with $\rho a = 0.642$ and Luttinger parameter $K_L = 0.128$.
$\mu(q)$ is a piecewise continuous function of q, which the peculiar dependence on n makes discontinuous at $q = 2nk_F$. Its details shade light on the behavior of $S(q, \omega)$ close to the low-energy threshold. In particular:

- for $q < 2k_F$, $\mu(q) > 0$ whence the DSF diverges close to the low-energy threshold.
- at $q = 2k_F$, $\mu(q)$ changes sign whence the DSF drops to zero close to the low-energy threshold.
- at the special wavevector $\mathcal{Q}_1 = \frac{2\pi}{a} \simeq 1.558$, $\mu(\mathcal{Q}_1) = 0$ in agreement with the prediction [193] of a flat spectrum.
- for $\mathcal{Q}_1 < q < 4k_F$, $\mu(q) > 0$ whence the DSF again diverges close to the low-energy threshold.

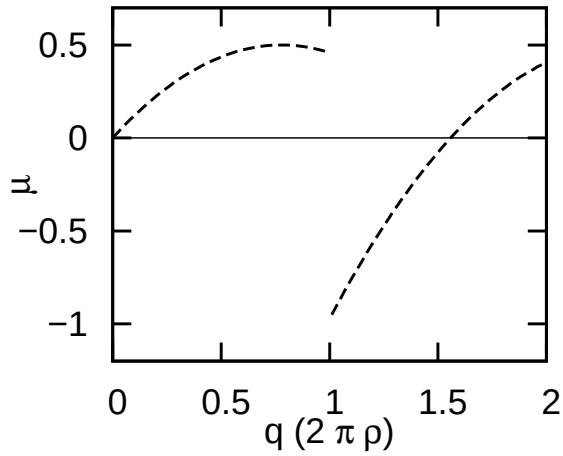

Figure 4.8: Exponent $\mu(q)$ of the power-law singularity (4.51) predicted by the nonlinear Luttinger liquid theory in the DSF of a system of hard-rods at $\rho a = 0.642$.

All these features are in appreciable agreement with Figure 4.7, where we observe a concentration of the spectral weight close to $\omega_{th}(q)$ for $q < 2k_F$. At $2k_F < q < \mathcal{Q}_1$ the spectral weight remains concentrated, but departs from the low-energy threshold. Close to $\mathcal{Q}_1$, the DSF abruptly and considerably broadens, in agreement with the prediction of a flat spectrum [193]. After $\mathcal{Q}_1$, the spectral weight concentrates again, and remains close to the low-energy threshold.

In performing the inverse Laplace transform that led to Figure 4.7, we have only imposed that the DSF has a low-energy threshold of the form (4.152), up to a scaling factor that we adjusted in such a way as to maximize the agreement with the ITCFs output by the PIGS algorithm.

No *a priori* information about the behavior of the DSF close to the low-energy threshold has been exploited by the GIFT method. The nonlinear TLL theory has not been assumed, but found in agreement with independently-derived data.

We remark that, while the low-energy properties of the DSF are quite universal and can be described by Luttinger liquid theories, with which we have compared our results, high-energy properties depend explicitly on the shape of the interaction potential, and lie in a regime currently beyond the reach of those theories, but accessible to QMC simulations.

4.5.3 Quantification of finite-size effects

We have simulated $N = 25$ of particles, a number already used in published literature for the simulation of 1D systems [203, 204]. It has been our care to verify that the properties of $N = 25$ hard rods are indeed representative of the thermodynamic limit, given the accuracy of our calculations. The expression (4.130) of the ground-state energy per particle shows that:

$$\mathcal{E}_N = \mathcal{E}_\infty \left(1 - \frac{1}{N^2}\right) \tag{4.154}$$

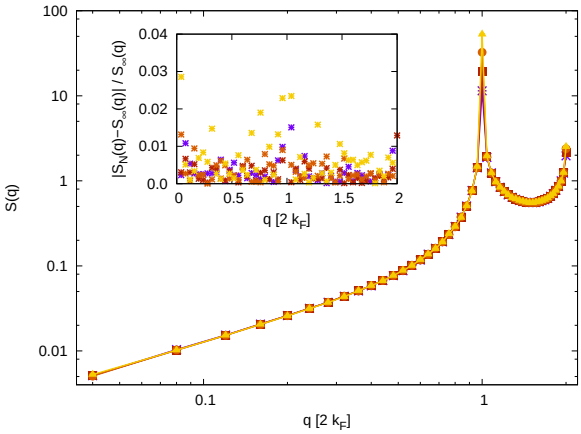

Figure 4.9: Static structure factor of $N = 25, 50, 100, 200$ (purple, red, orange and yellow symbols) hard rods at $\rho = 0.642a$. Away from $q = 2k_F, 4k_F$ the data are compatible with each other within the error bars of the simulations. Inset: we measure the relative accuracy of the static structure factor $S(q)$ computing the relative error $\frac{|S_N(q) - \lim_{N\to\infty} S_N(q)|}{\lim_{N\to\infty} S_N(q)}$ which, away from the points $q = 2k_F, 4k_F$, is below 3%.

whence $\mathcal{E}_{25} = 0.9984\,\mathcal{E}_\infty$. The scaling of the static structure factor with the number of particles is more delicate. Equation (4.29) shows that for $q = 2mk_F$ the static structure factor might display peaks of diverging weight. In presence of those peaks, i.e. for $2m^2K_L < 1$, only the ratio:

$$\frac{S(2mk_F)}{N^{1-2m^2K_L}} = \frac{S_{smooth}(2mk_F)}{N^{1-2m^2K_L}} + \frac{S_{peak}(2mk_F)}{N^{1-2m^2K_L}} = \frac{S_{smooth}(2mk_F)}{N^{1-2m^2K_L}} + C_m \tag{4.155}$$

has a finite $N =\!\!\rightarrow \infty$ limit. Away from those problematic points, we found that the static structure factor converges very rapidly to the thermodynamic limit performing simulations of $N = 25, 50, 100, 200$ hard rods at $\rho = 0.642a$. The results are reported in Figure 4.9. Our estimates of the static structure factor have relative error between 0.3% and 1%, i.e. $0.003 \leq \frac{\sigma_{S(q)}}{S(q)} \leq 0.01$ for all N and q. Figure 4.9 confirms the very moderate size effects affecting the static structure factor. The possibility of computing the low-energy threshold of the hard-rods model exactly for all numbers N of particles grants the ability of quantifying the finite-size effects of the DSF. Going through the straightforward calculation (4.138), we find this interesting result:

$$\omega_{th,N}(q) = \frac{\hbar^2 k^2}{2m^* N} + \left(1 + \frac{1}{N}\right) \omega_{th,\infty}(q) \tag{4.156}$$

The relative error of $\omega_{th,N}(q) - \frac{\hbar^2 k^2}{2m^* N}$ is therefore $\frac{1}{N} = 4\%$ at $N = 25$. The finite-size effects on the low-energy threshold are more severe than those affecting the static structure factor but still acceptable, since the DSF is obtained from the imaginary-time density-density response functions from an ill-posed inverse Laplace transform. While the finite-size effects on the low-energy threshold can be corrected exactly, the DSF might exhibit other finite-size effects which, to the best of our knowledge, cannot be predicted given

the Bethe Ansatz solution of the hard-rods Hamiltonian.

4.6 ^{4}He: equation of state and Luttinger parameter

Recent years have witnessed a growing interest in the experimental realization [205, 206, 207] and theoretical characterization of 1D ^{4}He systems, either confined inside nanopores [208, 209] or moving inside dislocation lines in crystalline samples [210, 211, 212]. Our most accurate knowledge of 1D liquids comes from Bragg scattering experiments, whose differential cross section is proportional to the DSF of the system. We have studied the DSF of a collection of ^{4}He atoms strictly confined along a segment of length L in PBC, and interacting through the phenomenologic HFDHE2 Aziz potential [100].
The use of the HFDHE2 Aziz potential, which is the interaction potential for particles in 3D, is legitimated by the strict confinement. Suppose that the atoms are moving inside a cylindrical structure or under the action of a transverse confining potential $v(\mathbf{r}_\perp)$, where $\mathbf{r}_\perp$ is the component of the position perpendicular to the structure. If the confinement is sufficiently sharp, the atoms reside in the lowest subband $\phi(\mathbf{r}_\perp)$ of transverse motion, the higher subbands being so high in energy as to be practically irrelevant [6]. Thus, the only relevant single-particle wavefunctions lie in the Hilbert space:

$$\mathcal{H} = \left\{\Psi(\mathbf{r}_\perp, r_\parallel) : \Psi(\mathbf{r}_\perp, r_\parallel) = \phi(\mathbf{r}_\perp) f(r_\parallel), f \in \mathcal{L}^2(\mathbb{R})\right\} \tag{4.157}$$

f being subject to PBC. $\mathcal{H}$ is trivially isomorphic to the single-particle Hilbert space $\mathcal{L}^2(\mathbb{R})$ of a spinless particle strictly confined in 1D, and the matrix elements of the kinetic energy read:

$$\langle\Psi_1|\hat{T}|\Psi_2\rangle = \langle\phi|\hat{T}_\perp|\phi\rangle\,\langle f_1|f_2\rangle + \langle\phi|\phi\rangle\,\langle f_1|\hat{T}_\parallel|f_2\rangle \tag{4.158}$$

whence the restriction of the kinetic energy $\hat{T}$ to $\mathcal{H}$ is $\frac{\hbar^2}{2m}\frac{\partial^2}{\partial r_\parallel^2}$ up to an irrelevant constant correction. On the other hand, the matrix elements of the potential energy can be significantly influenced by the subband $\phi(\mathbf{r}_\perp)$ since:

$$\langle\Psi_1\Psi_2|\hat{V}|\Psi_3\Psi_4\rangle = \langle f_1 f_2|\hat{V}_\parallel|f_3 f_4\rangle \tag{4.159}$$

with:

$$V_\parallel(r_{1,\parallel} - r_{2,\parallel}) = \int d\mathbf{r}_{1,\perp} \int d\mathbf{r}_{2,\perp} |\phi(\mathbf{r}_{1,\perp})|^2 |\phi(\mathbf{r}_{2,\perp})|^2 V\left(\sqrt{|\mathbf{r}_{1,\perp} - \mathbf{r}_{2,\perp}|^2 + |r_{1,\parallel} - r_{2,\parallel}|^2}\right) \tag{4.160}$$

We have investigated a system of strictly confined atoms, i.e. $|\phi(\mathbf{r}_\perp)|^2 \simeq \delta(\mathbf{r}_\perp)$. In such case:

$$V_\parallel(r_{1,\parallel} - r_{2,\parallel}) = V(r_{1,\parallel} - r_{2,\parallel}) \tag{4.161}$$

the effective interaction $V_\parallel(r)$ has the same analytic form of the bare interaction $V(r)$.
In our study of 1D ^{4}He, we have resorted to the PIGS method described in Section 3.2. As trial wavefunction, we have chosen a shadow wavefunction (2.60), with a shadow-shadow Jastrow factor in the Reatto-Chester form (4.42). The so-defined shadow wavefunction has two variational parameters, C and g in (2.60) and (4.42) respectively. The parameters C, g have been optimized using the simulated annealing method [213], choosing as cost function a linear combination of the VMC energy and of the distance between the VMC $g(r)$ and the $g(r)$ output by a preliminary SPIGS calculation.

The use of the PIGS method gives access to exact estimates of static and dynamic observables. We have simulated systems of $N = 25$ up to 160 particles at densities ranging from $\rho = 0.020$ Å^{-1} to $\rho = 0.300$ Å^{-1}.

The Aziz potential, illustrated in Figure 4.10 has a very diverse landscape, featuring a hard repulsive core of radius $R_{core} \simeq 2.5$ Åand a weak attractive tail. The mass of ^{4}He atoms is sufficiently large as to allow the existence of a two-body bound state with a binding energy of about $1.3mK$ and a large scattering length $a_S \simeq 100$ Å[214]. These two competing properties effects are responsible for a surprisingly rich equation of state, illustrated in Figure 4.10.

The ground-state energy per particle starts from $\mathcal{E} \simeq 0$ at very low density $\rho \simeq 0$, then it decreases towards the minimum value $\mathcal{E} = -1.980(1)\, mK$, attained at the equilibrium density $\rho_{eq} = 0.037(1)$ Å^{-1}. As the density is further increased, $\mathcal{E}$ rapidly increases due to the hard repulsive core of the Aziz potential. Starting from the EoS, we evaluated the compressibility of the system using (1.34), and from the compressibility we obtained K_L applying (4.25). We have also inferred the value of K_L from the low-momentum behavior (4.28) of the static structure factor $S(q)$. The procedure is illustrated in Figure 4.11: we fit the low-momentum part of $S(q)$ to a linear function of $\frac{q}{2k_F}$. In all situations, we observe the passage of the line through the origin of the plane $q, S(q)$, and thus we infer K_L from its slope. The static structure factor offers a third way of estimating K_L. The linear Luttinger theory predicts the occurrence of peaks (4.29) in $S(2mk_F)$, with height related to K_L by:

$$\log(S(2mk_F)) = \log\left(S_{smooth}(2mk_F) + S_{peak}(2mk_F)\right) \simeq \log(C_m) + (1-2m^2)K_L \log(N) \tag{4.162}$$

The good agreement between the two estimations confirms their robustness.

The main information conveyed by Figure 4.10 is that, by only varying the linear density ρ, 1D ^{4}He attains all possible values of the Luttinger parameter. The relationship between K_L and the compressibility permits to grasp the physical mechanism underlying this behavior. At high density, particles essentially experience the repulsive core of the interaction, whence the compressibility attains very small values [215, 216, 203]. As the density is decreased, the effect of the repulsive core becomes weaker and the compressibility increases. At the critical density $\rho_{sp} = 0.026(2)$ Å^{-1}, we observe a divergence in the compressibility, signalling that 1D ^{4}He manifests a spinodal decomposition [217]. In this context, the term spinodal decomposition indicates a liquid-gas phase separation, ilustrated in Figure 4.12, accompanied by the formation of dense droplets immersed in a rarefied gas.

The mechanism behind this phase separation can be easily guessed, already on an intuitive level: at density $\rho < \rho_{eq}$, the energy of a phase in which a fracion $x = \frac{\rho}{\rho_{eq}} < 1$ of the volume is occuped by particles at equilibrium density and the remaining fraction is empty reads, neglecting interfacial effects:

$$\mathcal{E}_x(\rho) = (1-x)\mathcal{E}(0) + x\mathcal{E}(\rho_{eq}) = \frac{\rho}{\rho_{eq}}\,\mathcal{E}(\rho_{eq}) \tag{4.163}$$

and is represented by the straight line connecting the points $(0,0)$ and $(\rho_{eq}, \mathcal{E}(\rho_{eq}))$ in Figure 4.12. The separated phase can thus be energetically favored over the liquid phase. For density between ρ_{sp} and ρ_{eq}, a liquid phase could be realized with an adiabatic reduction of ρ, since the compressibility of the system is finite, and thus it is stable against density fluctuations. Once the critical density ρ_{sp} is reached, the spinodal decomposition takes place because the divergence of the compressibility makes the system thermody-

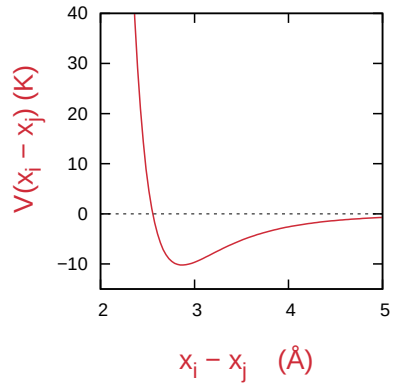

(a)

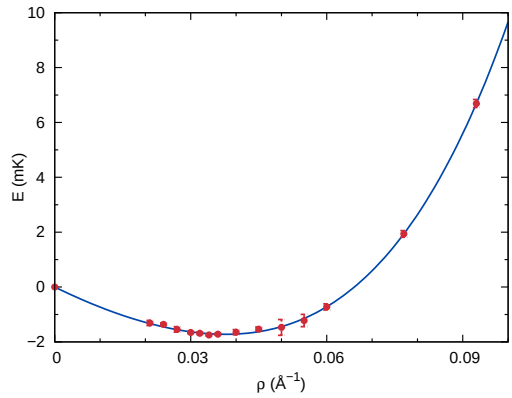

(b)

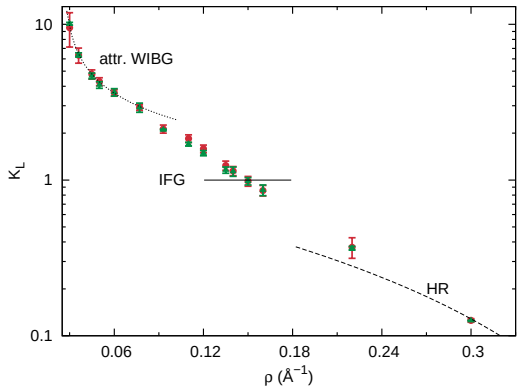

(c)

Figure 4.10: (a) Aziz potential. (b) EoS of 1D ^{4}He over the density range $\rho \leq 0.09$ Å^{-1}. QMC data are the red points, while the blue line is a fourth-order polynomial fit. (c) Luttinger parameter K_L of 1D ^{4}He, extracted from the compressibility (1.34) (red triangles) and from the low-momentum behavior (4.28) of the static structure factor (green circles). Superimposed lines, described in the text, correspond to the Luttinger parameters of the Lieb-Liniger (attr. WIBG), ideal Fermi gas (IFG) and hard-rods (HR) model.

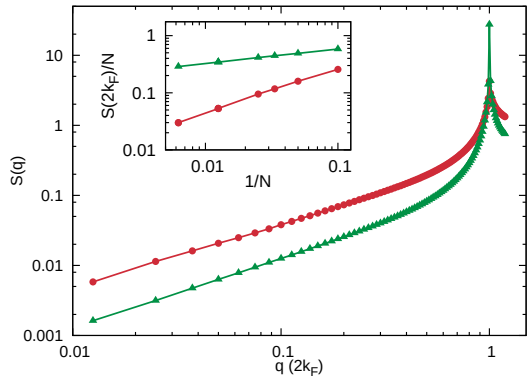

Figure 4.11: Static structure factor $S(q)$ at $\rho = 0.220$ Å^{-1} (red circles) and $\rho = 0.300$ Å^{-1} (green triangles) In the low-momentum region, $S(q) \simeq K_L \frac{q}{2k_F}$. Inset: the scaling of the main peak at $q = 2k_F$ versus the number of particles N at the same two densities provides an alternative way of extracting K_L. For $\rho = 0.220$ Å^{-1} ($\rho = 0.300$ Å^{-1}), $K_L = 0.354(5)$ ($K_L = 0.123(2)$).

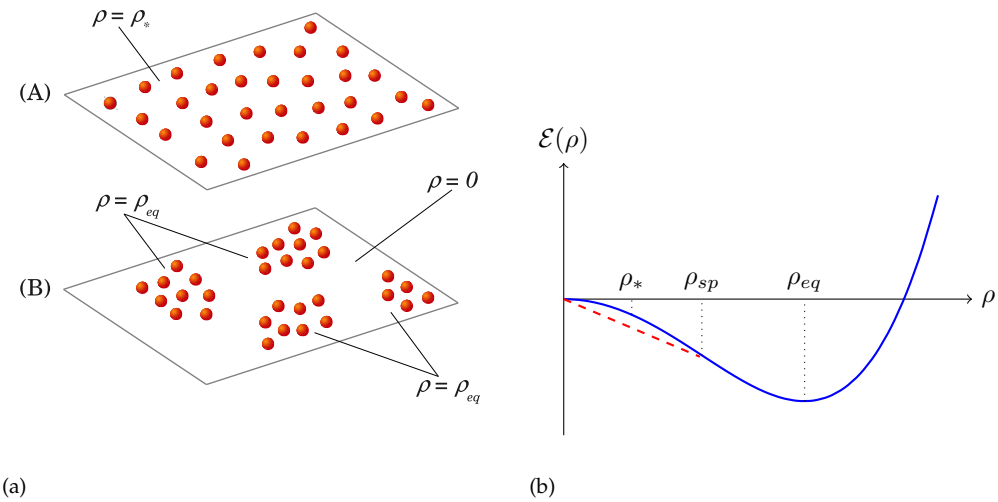

Figure 4.12: Left: (A) a typical configuration reflecting the spatial arrangment of particles in the liquid phase of a 2D system. (B) a typical configuration reflecting the spatial arrangment of particles in the liquid-gas separated phase of a 2D system: its fingerprint is the presence of droplets at equilibrium density ρ_{eq} surrounded by a rarefied gas. Right: Equation of state of the liquid phase (blue solid line) and of the separated phase (red dashed line). At low density, the separated phase is energetically favored over the liquid phase.

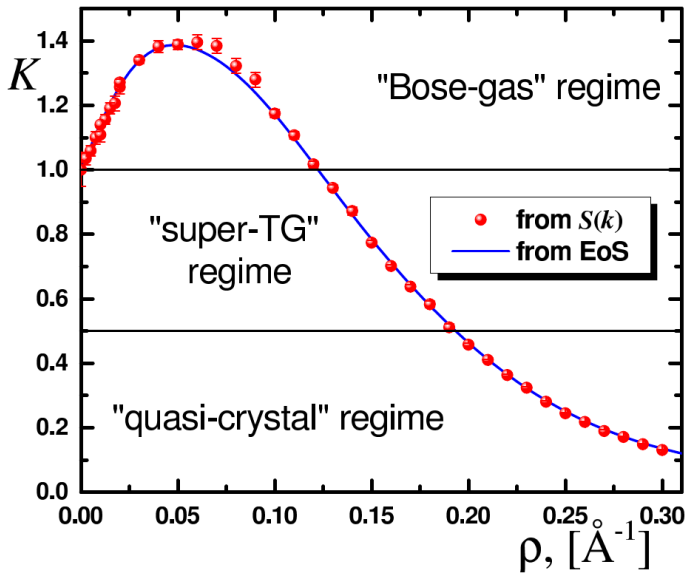

Figure 4.13: (a) Luttinger parameter K_L of 1D ^{3}He as a function of the linear density ρ, from the speed of sound (blue line) and the compressibility (red points). Taken from [168]

namically unstable against density fluctuations. The rich phenomenology of 1D ^{4}He is a peculiar consequence of the interplay between the hard repulsive core and the weak attractive tail in the Aziz potential, but also of the mass of ^{4}He. The latter is sufficiently large to permit the existence of a two-body bound state and the occurrence of the spinodal decomposition, which is anticipated by the divergence of the Luttinger parameter. It has been recently recognized [168] that ^{3}He has a non-trivial dependence of K_L on the linear density, illustrated in Figure 4.13. In the high-density regime, $K_L < 1$ like in ^{4}He. However, in the low-density regime, the lighter isotope attains $K_L \simeq 1.4$ at $\rho \simeq 0.05$ Å^{-1}, and then tends to $K_L = 1$ in the $\rho \to 0$ limit, not displaying the $K_L \gg 1$ behavior of ^{4}He essentially because of the smaller mass, which prevents the spinodal decomposition to take place.
It is worth pointing out that:

- in the low-density regime $K_L \gg 1$, the dependence of K_L on the density is well captured by the formula $K_L \simeq \frac{\alpha}{\sqrt{\rho-\rho_{sp}}}$, α being a fit parameter (the dotted line in Figure 4.10). This behavior is reminiscent of the relation (4.114), holding in the weakly-interacting regime for the repulsive LLM. We are thus led to compare the ^{4}He system with a LLM having $\gamma \propto (\rho - \rho_{sp})$

- at density $\rho \simeq 0.150$ Å^{-1}, the Luttinger parameter attains the same value, $K_L = 1$, of an IFG.

- in the high-density regime $K_L \ll 1$, the dependence of K_L on the density is well captured by the hard-rods formula $K_L = (1 - \rho a)^2$ of Subsection 4.4.3, once the hard-rod length is put equal to the scattering length $a = 2.139$ Åof 1D ^{4}He [218, 167].

At least in the low-momentum and energy regime, 1D ^{4}He shares some features with the three exactly solvable models presented in Section 4.4. In wiev of the discussion of Sections (4.2), (4.3), pinpointing the universality of 1D systems in suitable regimes, we might expect that these similarities do not exhaust to the Luttinger parameter, but estend to dynamical properties like the DSF.

4.7 ^{4}He: dynamical structure factor

We have studied the DSF of $N = 25$ atoms at the representative densities $\rho = 0.036$, 0.060, 0.093, 0.150, 0.220, 0.300 Å^{-1}, for transferred wavevectors up to $|q| = 2.25k_F$. We have tackled the issue of computing the full DSF via an analytic continuation of the ITCF of the density fluctuation operator, calculated with the SPIGS method as explained in Section 3.2. We use an inversion strategy devised refining and making more efficient [219] the Genetic Inversion via Falsification of Theories (GIFT) method [220], which has provided robust results for the DSF of several quantum liquids [220, 221, 222]
At all densities, for small q and ω, the DSF is peaked around $\hbar c|q|$ within our resolution, with a sound velocity c consistent with our estimate of K_L. The behavior at higher energies is strikingly different, and extremely surprising.

4.7.1 Low-density regime

At the lowest density $\rho = 0.036$ Å^{-1}, as shown in Figure 4.14, the spectral weight of the SDF is peaked around the Bogoliubov dispersion relation:

$$\epsilon_B(q) = \frac{\hbar}{m\xi^2}\sqrt{2(q\xi)^2 + (q\xi)^4} \qquad \xi = \frac{\hbar K_L}{\sqrt{2}mv_F} \tag{4.164}$$

well beyond the limits of applicability of the TLL theory. The same behavior is observed for the weakly-interacting Lieb Liniger model [188] (see Figure 4.5). In both cases, it is very interesting and surprising to see that the system obeys Bogoliubov's paradigm of the weakly-interacting Bose [223, 4] like superfluid 2D and 3D systems, even if the main assumption leading to this phenomenon, the occurrence of Bose-Einstein condensation, is ruled out in 1D by the Hohenberg-Mermin-Wagner theorem [162, 163, 164, 165].
We also notice that the DSF, which in the low-momentum region develops a single sharp peak at very low energy (due to the low sound velocity), broadens as soon as it enters in the particle-hole band of an IFG at the same density.
Following [224], we interpret this broadening as the manifestation of the finite lifetime of Bogoliubov quasiparticles, resulting from weak perturbations to the TLL Hamiltonian.
As the density is increased and the Luttinger parameter decreases towards 1, the broadening of the DSF becomes more and more pronounced as shown in Figure 4.14 At high energies, the spectral weight of the DSF partially fills the particle-hole band (4.65) of an IFG at the same density.

4.7.2 Intermediate-density regime

At the special density $\rho = 0.150$ Å^{-1} ($K_L \simeq 1$) for which the Luttinger parameter attains the same value of the IFG, the situation changes dramatically as illustrated in Figure 4.15. In the low-momentum region, the SDF develops a sharp peak and the sound velocity equals the Fermi velocity: 1D ^{4}He is thus mimicking an IFG, a further signature of the fascinating fermionization phenomenon.

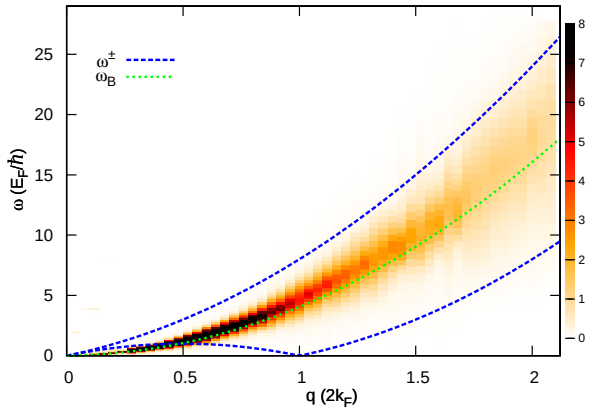

(a)

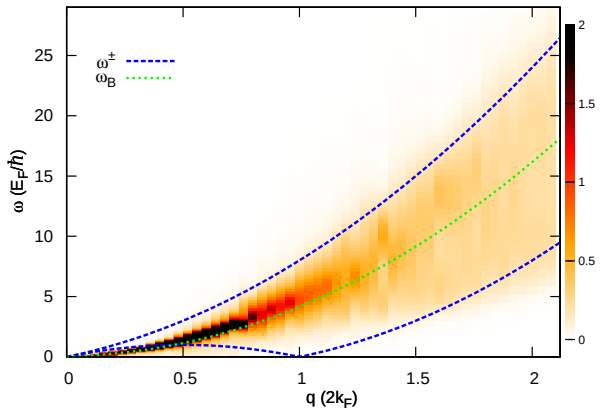

(b)

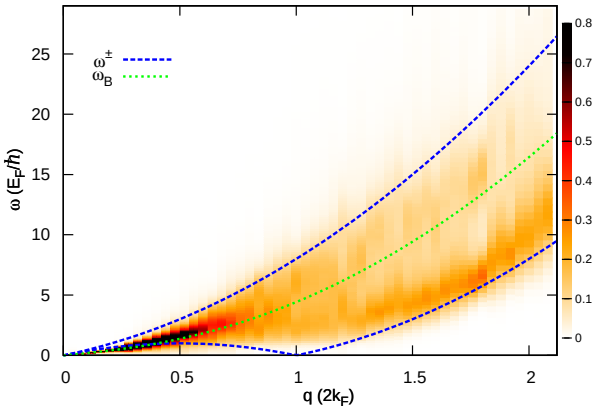

(c)

Figure 4.14: (a) DSF of 1D ^{4}He at $\rho = 0.036$ Å^{-1}, $K_L \simeq 6.3$. Wavevectors are measued in units of $2k_F$, energies in units of E_F. The green dashed line is the Bogoliubov dispersion relation (4.164), and the blue dashed line delimits the particle-hole band (4.65) of an IFG at the same density. (b) DSF of 1D ^{4}He at $\rho = 0.060$ Å^{-1}, $K_L \simeq 3.6$. (c) DSF of 1D ^{4}He at $\rho = 0.093$ Å^{-1}, $K_L \simeq 2.1$.

At higher momentum and energy, however, the spectral weight concentrates in a region of width a few Fermi energies, which we call *lower mode*. This is in contrast with the IFG and the LLM, which at $K_L = 1$ develops a flat DSF [188]. We interpret this difference as a strong non-universality effect, since in the high-momentum and energy region the THH is no longer applicable.

4.7.3 High-density region

As the density is further increased, the Luttinger parameter decreases below 1, and the of the DSF changes again as illustrated in Figure 4.15. Indeed, the physical behavior of the system is now largely shaped by the hard repulsive core of the Aziz potential, responsible for a volume exclusion phenomenon.
Let us begin analyzing the DSF at $\rho = 0.220$ Å^{-1}, $K_L \simeq 0.348$: we notice that the particle-hole band into which the DSF has support for $q < 2k_F$ is renormalized by the substitution of the bare mass m with the effective mass $m^* = K_L m < m$ in the expression (4.65). This is in agreement with the observation (4.137), (4.138) that the Lieb-I and Lieb-II excitations of the hard-rods Hamiltonian have the same functional form of their counterparts in the IFG and Tonks-Girardeaus systems, the only difference being, in the thermodynamic limit, the replacement $m \to m^*$.
The hard-rod character of 1D ^{4}He, which is already emerging at $\rho = 0.220$ Å^{-1}, more strikingly manifests at $\rho = 0.300$ Å^{-1}, $K_L \simeq 0.123$. To verify this fact, it is sufficient to compare Figures 4.7 and 4.15: in fact, Figure 4.7 is relative to a system of hard-rods with the same Luttinger parameter.
Both the hard-rods spectrum and the ^{4}He spectrum agree with the predictions of the nonlinear TLL theory, which are relative to the hard-rods system. In the light of this observation, we are led to argue that the unknown low-energy threshold of 1D ^{4}He should be quite close to that of hard rods, in agreement with the intuition that volume exclusion is the main effect of the interaction in the high-density regime.
In particular, for $q < 2k_F$ ($\mu(q) > 0$) we observe a concentration of the spectral weight close to $\omega_{th}(q)$. For $2k_F < q < \mathcal{Q}_1$ ($\mu(q) < 0$) the spectral wright remains concentrated but departs from the low-energy threshold. Close to $q = \mathcal{Q}_1$ ($\mu(q) = 0$), illustrated in Figure 4.15 with a red arrow, we observe a flattening of the DSF in agreement with the prediction of [193]. For $\mathcal{Q}_1 < q < 4k_F$ ($\mu(q) > 0$) the spectral weight again concentrates close to the low-energy threshold, which is illustrated in Figure 4.15 as a double-dotted green line. In the high-density regime, thus, the hard-rods model almost fully characterizes the spectrum at low energies. Nevertheless, in the high-energy region we observe quantitative differences between the two models, due to the details of the interaction.

4.8 ^{4}He: drag force exerted on a soft impurity

Interacting Bose systems in 2D and 3D display a complex of transport phenomena, ranging from frictionless flow through thin capillaries, suppression of the classical inertial moment, metastable currents, quantized circulation (vortices) and coherent tunneling (Josephson effect), that can be inferred from the occurrence of Bose-Einstein condensation, and the existence of an order parameter representing the wavefunction of the condensate [225, 226, 227, 228, 229].
By contrast, in 1D systems with short-range velocity-independent interaction there is no BEC even at zero temperature [165]. Nevertheless, the existence of BEC is neither a sufficient nor necessary condition for superfluidity, and a 1D system of bosons may be superfluid under some conditions [225, 226, 227, 228, 229].

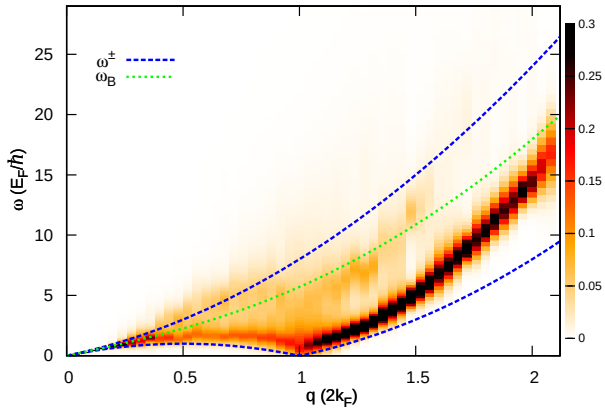

(a)

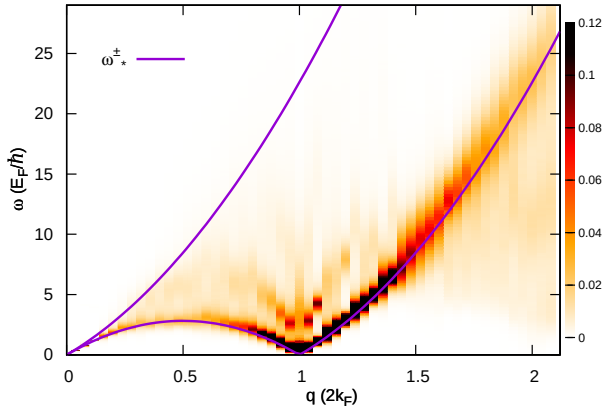

(b)

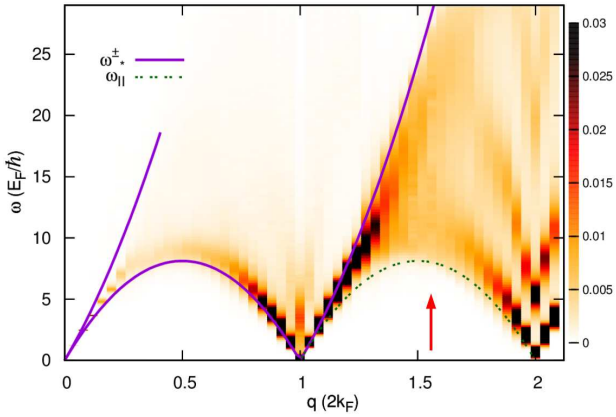

(c)

Figure 4.15: (a) DSF of 1D ^{4}He at density $\rho = 0.150$ Å^{-1}, $K_L \simeq 1$. (b) DSF of 1D ^{4}He at density $\rho = 0.220$ Å^{-1}, $K_L \simeq 0.348$. (c) DSF of 1D ^{4}He at density $\rho = 0.300$ Å^{-1}, $K_L \simeq 0.123$.

We have studied superfluidity in 1D ^{4}He studying the friction or drag force exerted on a particle of mass m moving with velocity v inside the system. The notion of drag force is theoretically important, because it generalizes Landau's celebrated criterion of superfluidity. According to Landau, an obstacle in a gas, moving with velocity v, may cause transitions from the ground state of the gas to excited states lying on the line $\epsilon(k) = \hbar v\, k$ in the energy-momentum space. If all the spectrum is above this line, the motion cannot excite the system, and the flow of the impurity is superfluid. However, even when the line intersects the spectrum, the transition probabilities to these states can be strongly suppressed due to the interaction or to the external perturbing potential. In this case, the drag force provides a quantitative measure of superfluidity. A physical realization of an impurity moving inside a 1D system can be either a particle interacting with the system through a soft-core interaction [230], or a moving optical lattice [231, 232, 233].

The drag force exerted on a moving impurity can be computed relying on Fermi's golden rule, with a suitable adaptation of the discussion in Section (1.1). An impurity moving inside a medium, with velocity $\mathbf{v}$, is scattered by the medium particles, and that the scattering leads to transitions with momentum and energy transfer. Scattering processes are then responsible for the existence of a finite value of energy loss per unit time:

$$\frac{d\mathcal{E}}{dt}(\mathbf{v}) = -\mathbf{F}(\mathbf{v}) \cdot \mathbf{v} \tag{4.165}$$

In the right member of (4.165), the energy loss has been expressed as the power dissipated by the drag force $\mathbf{F}(\mathbf{v})$. The wavevector is connected to the initial velocity by the familiar relation $\mathbf{v} = \frac{\hbar \mathbf{k}_i}{m}$, where m is the mass of the impurity. Assuming the usual form (1.24) for the interaction Hamiltonian between the impurity and the medium, the rate for the scattering process is given to lowest order in the impurity interaction, by Fermi's golden rule:

$$p(\mathbf{k}_{in} \to \mathbf{k}_f) = 2\pi \frac{|V_{\mathbf{q}}|^2}{\Omega^2} N S(\mathbf{q}, \omega) \tag{4.166}$$

where the momentum and energy transfer are given by:

$$\hbar\mathbf{q} = \hbar\left(\mathbf{k}_i - \mathbf{k}_f\right) \qquad \hbar\omega = E_{\mathbf{k}_i} - E_{\mathbf{k}_f} = \hbar\mathbf{q}\cdot\mathbf{v} - \frac{\hbar^2|\mathbf{q}|^2}{2m} \tag{4.167}$$

where $E_{\mathbf{k}} = \frac{\hbar^2|\mathbf{k}|^2}{2m}$ is the dispersion relation for the impurity. In order to obtain the energy loss per unit time, we need to sum up the energy transfer (4.167) weighted with the rate (4.168) over all the final states:

$$\frac{d\mathcal{E}}{dt} = -\sum_{\mathbf{q}} p(\mathbf{k}_{in} \to \mathbf{k}_f) \left(\hbar\mathbf{q}\cdot\mathbf{v} - \frac{\hbar^2|\mathbf{q}|^2}{2m}\right) \tag{4.168}$$

Replacing the sum by the integral in the thermodynamic limit and using (4.168):

$$\frac{d\mathcal{E}}{dt} = -\int \frac{d\mathbf{q}}{(2\pi)^{d-1}} |V_{\mathbf{q}}|^2 \rho\left(\hbar\mathbf{q}\cdot\mathbf{v} - \frac{\hbar^2|\mathbf{q}|^2}{2m}\right) S\left(\mathbf{q}, \mathbf{q}\cdot\mathbf{v} - \frac{\hbar|\mathbf{q}|^2}{2m}\right) \tag{4.169}$$

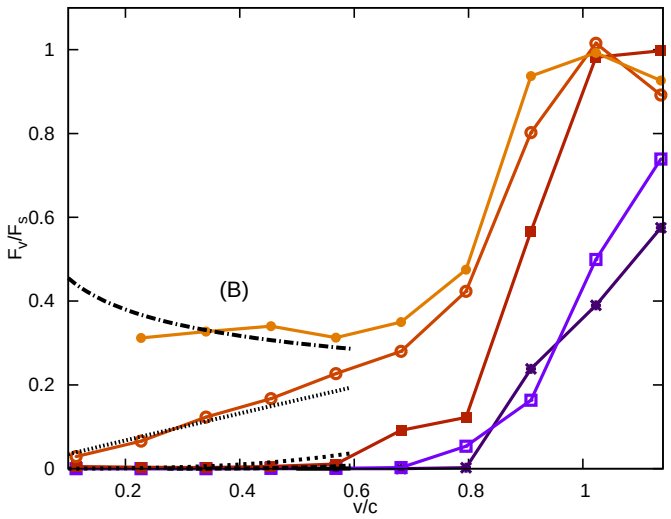

Figure 4.16: Drag force $F(v)$ as a function of the ratio $\frac{v}{c}$, compared to the Luttinger liquid theory prediction (black lines) and normalized to the maximum value F_{max}. Curves correspond to densities $\rho = 0.060, 0.093, 0.150, 0.220 \mathring{A}^{-1}$ (purple crosses, mauve empty squares, red filled squares, dark red empty circles, orange filled circles marked with a B).

For a heavy impurity, $|\mathbf{v}| \gg \frac{\hbar|\mathbf{q}|}{m}$, inside a 1D medium, (4.169) simplifies to:

$$\frac{d\mathcal{E}}{dt} = -\left(\int_0^\infty dq |V_q|^2 \rho\, \hbar q\, S(q, qv)\right) v = -F(v)v \tag{4.170}$$

Formula (4.170) reveals that knowledge of the DSF and of the impurity-medium interaction potential grants the ability of computing the drag force. The relationship between the concept of drag force and Landau's criterion for superfluidity is readily understood: if the DSF is concentrated above the straight line $\hbar v_0 q$ in the momentum-energy plane, then $F(v) \equiv 0$ for all velocities $v < v_0$. On the other hand, the integral can be very small or vanish even if the spectrum lies below the line $\hbar v_0 q$, but the excitation probabilities are suppressed [201], for instance because the interaction V_q takes non-zero values only in a finite region of the momentum space.

However, in a broad class of 1D system, like the IFG, ^{4}He at high density and hard rods, the DSF touches the $\omega = 0$ line at $2k_F$, whence the possibility of a dissipationless flow is by no means obvious.

For the sake of simplicity, we have assumed a contact interaction $V_q \equiv g$, and we have used our estimate of the DSF in Figures 4.14,4.15 to compute the drag force using (4.170). The resulting expression is reported in Figure 4.16.

We observe a power-law increase of $F(v)$ with the velocity, and a saturation to a maximum value F_{max} at $v \simeq c$. The power-law increase is consistent with the Luttinger liquid theory [234, 201]. For a slow impurity $v \ll c$, as we have just observed, the most important contibution to (4.170) comes from the region $q \simeq 2k_F$. Equations (11.33), (11.34)

show that, close to $q = 2k_F, \omega = 0$ the DSF has the power-law behavior:

$$S(q,\omega) \simeq \frac{S_1}{2}\omega^{2(K_L-1)}\left(1-\frac{c^2(k-2k_F)^2}{\omega^2}\right)^{K_L-1} \quad , \qquad -1 \leq \frac{c^2(k-2k_F)^2}{\omega^2} \leq 1 \tag{4.171}$$

Inserting (4.171) into (4.170) and performing the change of variables $x = \frac{c(q-2k_F)}{\omega}$ yields the following expression for the drag force:

$$F(v) \propto \int_0^\infty dqqS(q,qv) \propto \int_{-1}^{\min\left(\frac{c}{v},1\right)} \frac{dx}{\left(1-\frac{v}{c}x\right)^3}\left(\frac{\frac{v}{c}}{1-\frac{v}{c}x}\right)^{2(K_L-1)}(1-x^2)^{K_L-1} \tag{4.172}$$

for $v \ll c$, the approximation $1-\frac{v}{c}x \simeq 1$ is accurate and we find:

$$F(v) = F_0\left(\frac{v}{c}\right)^{2K_L-1} \tag{4.173}$$

that compares satisfactory with our estimates at all densities, except $\rho = 0.330\mathring{A}^{-1}$. At the highest density, a reliable estimate of the drag force is hampered by finite-size effects. We remark that the drag force is non-vanishing at any v, but for $K_L > 1$ its power-law behavior determines a quasi-superfluid response of the system, allowing for impurities flowing with very small dissipation [235]. Our estimate of $F(v)$ is perturbative, therefore it is relevant for soft impurities such as small geometry deformations in quasi-1D systems, while already on an intuitive level it is clear that for hard-core impurities the superfluid response is completely suppressed.

CHAPTER 5

The phaseless Auxiliary Field Quantum Monte Carlo

In the present Chapter, we observe [236] that the FN approximation can significantly bias RQMC estimates of imaginary–time correlation functions $F(\mathbf{q}, \tau)$ (ITCFs). We review the phaseless AFQMC method by S. Zhang et al. *[237, 238], an innovative QMC method based on a very peculiar representation of the imaginary-time evolution, which is mapped onto a stochastic process in the manifold of Slater determinants. Within the phaseless AFQMC, control of the sign problem is achieved implementing a radically different approximation scheme. The methodology thus provides a valid alternative to FN-DMC and FN-RQMC for the calculation of static properties, and a promising candidate for the calculation of ITCFs.*

5.1 Imaginary-time correlations and the fixed-node approximation

The configurational QMC methods illustrated in Chapter 2 relate the imaginary-time Schrödinger equation:

$$-\partial_\tau |\Psi_\tau\rangle = \hat{H} |\Psi_\tau\rangle \tag{5.1}$$

to a stochastic process in the configurational space of the system, based on the relations between partial differential equations and Markov processes unraveled by the theory of stochastic calculus. For Bose systems, projective methods like PIGS and RQMC give access to exact estimates of imaginary-time correlation functions.

On the other hand, the exact simulation of Fermi systems with configurational QMC methods is hampered by the sign problem, described in Subection 3.2.1. Due to the sign problem, the variances of the QMC estimators grow exponentially with the number N of particles and the imaginary time τ of projection. The sign problem can be mitigated implementing suitable approximation schemes, like the fixed-node (FN) approximation discussed in Subection 3.3.6. The FN approximation restricts the stochastic sampling of the configurational space to regions where the sign of a reasonable approximation for the ground-state wavefunction, the trial wavefunction, remains constant. It decreases the variance of the QMC estimators, but introduces a bias in their mean value. In particular, the FN approximation provides very accurate estimates of the ground-state energy and correlation functions [121, 123], but it may give inaccurate results for imaginary-time correlation functions even when the nodal structure of the ground-state wavefunction is exactly known.

As an example, in Figure 5.1 we consider a system of $N = 5$ noninteracting spinless fermions in 2D, and we compare the exact imaginary-time density-density correlation function with the FN-RQMC estimate. The RQMC calculation uses exact ground state of the system, i.e. the Slater determinant with lowest kinetic energy, as trial wavefunction. This choice restricts the stochastic sampling (3.101) to paths $\mathcal{X}$ along which the sign

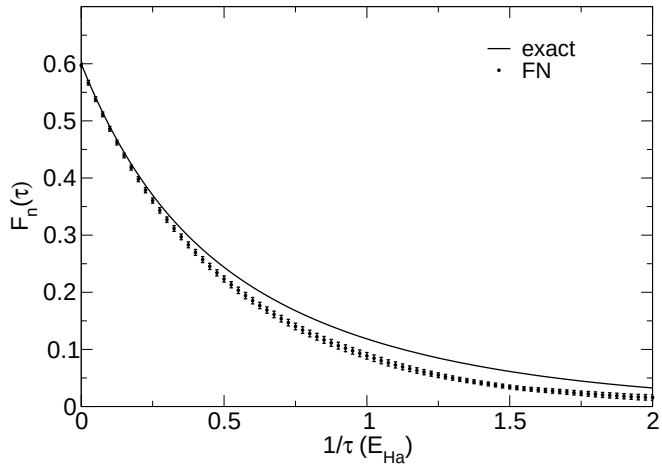

Figure 5.1: FN result (points) and exact value (line) of the imaginary time correlation function of $\hat{\rho}_{\boldsymbol{q}}$ with $\boldsymbol{q} = \frac{2\pi}{L}(0,1)$ for a 2D system of 5 noninteracting spinless fermions. Details of the calculation are presented in [236].

of the ground-state wavefunction is constant, and thus provides unbiased estimates of ground-state properties like $S(\mathbf{q})$.

There is a significant mismatch between the two quantities, that can only rise from the imposition of the ground-state nodal surface as a subset of the nodal surface of all excited states.

Since the FN approximation can significantly bias the QMC estimates of ITCFs, it is very interesting to investigate the accuracy of the ITCFs calculated by QMC using restrictions different from the FN. In recent years alternative QMC methods have been conceived, which simulate the imaginary-time evolution with a suitable stochastic process taking place in the manifold of Slater determinants [239, 237, 238, 240, 241], and thus are called *determinantal QMC methods*.

Determinantal QMC methods are a broad class of methodologies. Just to cite a few examples, the Hirsch-Fye QMC was conceived for solving quantum impurity problems [242] and later applied to the solution of the Dynamical Mean-Field theory problem [243]. The full configuration interaction quantum Monte Carlo (FCIQMC) [240, 244, 245] has enabled highly-accurate studies of many challenging systems [246, 241]. The auxiliary fields QMC (AFQMC) method, the technique of using the Hubbard-Stratonovich transformation to introduce auxiliary fields into an interacting problem in oder to reduce it to a class of non-interacting problems, was introduced by R. Blankenbecler *et al.* and G. Sugiyama and S. E. Koonin [247, 239]. The constrained path QMC [248, 249] and the phaseless AFQMC [237, 238], conceived by S. Zhang *et al.*, are refined and powerful methodologies combining important advantages of the Green's function QMC, DMC and AFQMC methods. The constrained path QMC and the phaseless QMC methodologies have been successfully applied to significant problems in condensed matter Physics [250, 251, 252], quantum chemistry [253, 254, 255, 256] and material Physics [257, 258, 259].

In this thesis, we have resorted to the phaseless AFQMC method to compute ITCFs of many-fermion systems in order circumvent the significant bias introduced by the FN approximation. As the phaseless AFQMC method maps the imaginary-time evolution

onto a stochastic process in the manifold of Slater determinants, the salient properties of those many-fermion states are briefly reviewed in Section 5.2. The phaseless AFQMC methodology then is presented in Section 5.3.

5.2 Properties of Slater determinants

Let us consider a single particle, whose quantum-mechanical description takes place in a Hilbert space $\mathcal{H}$. Let M be the dimension of $\mathcal{H}$, and $\{\varphi_i\}_{i=1}^{M}$ be an orthonormal complete set of single-particle basis states. These single-particle orbitals can be spin-definite plane waves in homogeneous systems, lattice sites in the Hubbard model, or molecular orbitals in quantum-chemical systems. Often the Hilbert space $\mathcal{H}$ is separable but non-finitely generated: in such situations, the single-particle basis states are truncated to some finite number M. Wavefunctions $\psi \in \mathcal{H}$ are linear combinations:

$$|\psi\rangle = \sum_{i=1}^{M} |\varphi_i\rangle \langle\varphi_i|\psi\rangle \tag{5.2}$$

of single-particle basis states, with complex-valued coefficients $\langle\varphi_i|\psi\rangle$.
The quantum-mechanical description of N distinguishable particles, each described in $\mathcal{H}$, takes place in the Hilbert space:

$$\mathcal{H}^{(N)} = \bigotimes_{i=1}^{N} \mathcal{H} \tag{5.3}$$

with dimension M^N. $\mathcal{H}^{(N)}$ is generated by factored wavefunctions:

$$|\psi_1 \dots \psi_N\rangle = |\psi_1\rangle \otimes \cdots \otimes |\psi_N\rangle \quad , \qquad \psi_1 \dots \psi_N \in \mathcal{H} \tag{5.4}$$

In quantum mechanics we assume that elementary particles, such as the electrons or photons, are indistinguishable: this requirement implies [260, 261] that the states of N indistinguishable particles be eigenfunctions of the alternating operator:

$$\hat{S}_{\pm} |\psi_1 \dots \psi_N\rangle = \sum_{\sigma \in S_N} \frac{(\pm 1)^{\sigma}}{N!} |\psi_{\sigma(1)} \dots \psi_{\sigma(N)}\rangle \tag{5.5}$$

with eigenvalue either 1 (bosons) or -1 (fermions). For now on we will consider only fermionic systems, whose quantum-mechanical description is set in the Hilbert space $\mathcal{H}_{-}^{(N)} = \hat{S}_{-}\mathcal{H}^{(N)}$. Factored states are turned into *Slater determinants*:

$$|\Psi\rangle = |\psi_1 \dots \psi_N\rangle_{-} = \hat{S}_{-} |\psi_1 \dots \psi_N\rangle \tag{5.6}$$

by the alternating operator $\hat{S}_{-}$. The set of N-particle Slater determinants will be denoted $\mathfrak{D}(N)$. Notice that while the set of Slater determinants of single-particle orbitals $\{\varphi_i\}$:

$$|i_1 \dots i_N\rangle = \hat{S}_{-} |\varphi_{i_1} \dots \varphi_{i_N}\rangle \quad , \qquad i_1 < \cdots < i_N = 1 \dots M \tag{5.7}$$

forms a complete set in $\mathcal{H}_{-}^{(N)}$, with dimension $\binom{M}{N}$, a generic many-fermion wavefunction is a linear superposition of those Slater determinants and typically it cannot be writ-

ten as a single Slater determinant. The Slater determinant in (5.6) can be conveniently parametrized by the rectangular complex-valued matrix $\Psi \in \mathcal{M}_{M\times N}(\mathbb{C})$:

$$\Psi = \begin{pmatrix} \langle\varphi_1|\psi_1\rangle & \dots & \langle\varphi_1|\psi_N\rangle \\ \dots & \dots & \dots \\ \langle\varphi_M|\psi_1\rangle & \dots & \langle\varphi_M|\psi_N\rangle \end{pmatrix} \tag{5.8}$$

The i-th column of Ψ represents a single-particle orbital ψ_i, that is completely specified by the M-dimensional vector $\langle\varphi_j|\psi_i\rangle$. For a d-dimensional homogeneous systems of spin-$\frac{1}{2}$ particles with spin-independent Hamiltonians, a very natural choice for the single-particle orbitals φ_i is represented by the spin-definite plane waves introduced in Appendix 13.1:

$$\varphi_i(\mathbf{r},\omega) = \frac{e^{i\mathbf{k}\cdot\mathbf{r}}}{\sqrt{\Omega}}\chi_\sigma(\omega) \quad \frac{L}{2\pi}\mathbf{k} \in \mathbb{Z}^d,\ \sigma = \uparrow,\downarrow \tag{5.9}$$

whence $i = (\mathbf{k},\sigma)$. In such systems, a relevant role is played by Slater determinants of the form:

$$|\Psi\rangle = \hat{S}_- \, |u_1,\uparrow\rangle \otimes \cdots \otimes |u_{N_\uparrow},\uparrow\rangle \otimes |v_1,\downarrow\rangle \otimes \cdots \otimes |v_{N_\downarrow},\downarrow\rangle \tag{5.10}$$

which have a well-defined number $N_\uparrow$ ($N_\downarrow$) of spin-up (spin-down) particles. Notice that the elements $|u_i\rangle$, $|v_i\rangle$ are linear combinations of plane waves only. Arranging the single-particle orbitals φ_i so that for $i \leq \frac{M}{2}$ φ_i has spin up (and, for $i > \frac{M}{2}$ φ_i spin down), the elements of $\Psi \in M_{M\times N}(\mathbb{C})$ read:

$$\Psi_{ij} = \langle\varphi_i|\psi_j\rangle = \begin{cases} \langle\mathbf{k}_i|u_j\rangle & \text{if } i \leq \frac{M}{2},\ j \leq N_\uparrow \\ 0 & \text{if } i > \frac{M}{2},\ j > N_\uparrow \\ 0 & \text{if } i \leq \frac{M}{2},\ j \leq N_\uparrow \\ \langle\mathbf{k}_{i-M_k}|v_{j-N_\uparrow}\rangle & \text{if } i > \frac{M}{2},\ j > N_\uparrow \end{cases} \tag{5.11}$$

whence Ψ takes the block form:

$$\Psi = \begin{bmatrix} U_\Psi & 0 \\ 0 & V_\Psi \end{bmatrix} \tag{5.12}$$

with $U_\Psi \in M_{\frac{M}{2}\times N_\uparrow}(\mathbb{C})$ and $V_\Psi \in M_{\frac{M}{2}\times N_\downarrow}(\mathbb{C})$ defined by:

$$(U_\Psi)_{ij} = \langle\mathbf{k}_i|u_j\rangle \tag{5.13a}$$

$$(V_\Psi)_{ij} = \langle\mathbf{k}_i|v_j\rangle \tag{5.13b}$$

A Slater determinant can be efficiently parametrized with an $M \times N$ complex matrix (5.8) or, in the case of spin-$\frac{1}{2}$ particles with a spin-independent Hamiltonian, by two $\frac{M}{2} \times N_\uparrow$, $\frac{M}{2} \times N_\downarrow$ complex matrices (5.13). The block form (5.12) can be regarded to as a counterpart of the possibility, discussed in Appendix 10.1.1 of replacing a Slater determinant of spin-orbitals with two Slater determinants of configurational orbitals, one per spin polarization. From a computational point of view, working with block-diagonal matrices is always preferential to working with dense matrices. Indeed, block-diagonal matrices lend themselves to more efficient computations, as well as in more efficient utilization of computer storage.

It is worth mentioning several properties, thanks to which overlaps between Slater determinants and matrix elements of one-body and two-body operators can be efficiently

computed performing linear algebra operations. Moreover, it will be proved that the manifold $\mathfrak{D}(N)$ is closed under the action of exponentials of single-particle operators, a result of fundamental importance for the implementation of the phaseless AFQMC method.

5.2.1 Scalar products

For any two non-orthogonal Slater determinants, the overlap $\langle\Phi|\Psi\rangle$ is given by:

$$\langle\Phi|\Psi\rangle = \langle\phi_1 \dots \phi_N|\hat{S}_-|\psi_1 \dots \psi_N\rangle = \sum_{\sigma\in S_N} \frac{(-1)^\sigma}{N!} \langle\phi_1 \dots \phi_N|\psi_{\sigma(1)} \dots \psi_{\sigma(N)}\rangle \tag{5.14}$$

Since $\langle\phi_1 \dots \phi_N|\psi_{\sigma(1)} \dots \psi_{\sigma(N)}\rangle = \prod_{i=1}^N \langle\phi_i|\psi_{\sigma(N)}\rangle = \prod_{i=1}^N A_{i,\sigma(i)}$ we have:

$$\langle\Phi|\Psi\rangle = \frac{\det(A)}{N!} = \frac{\det(\Phi^\dagger\Psi)}{N!} \tag{5.15}$$

where the $N \times N$ matrix A has been expressed as:

$$A_{ij} = \langle\phi_i|\psi_j\rangle = \sum_{k=1}^N \langle\phi_i|\varphi_k\rangle \langle\varphi_k|\psi_j\rangle = (\Phi^\dagger\Psi)_{ij} \tag{5.16}$$

The calculation of $\langle\Phi|\Psi\rangle$ requires $\mathcal{O}(N^2M)$ operations for computing $\Phi^\dagger\Psi$ and $\mathcal{O}(N^3)$ operations for computing $\det(\Phi^\dagger\Psi)$.

5.2.2 Matrix elements of one-body operators

Let $\hat{O} = \sum_{i,j=1}^M O_{ij}\ \hat{a}_i^\dagger\hat{a}_j$ be a one-body operator, with the creation and destruction operators relative to the single-particle orbitals φ_i. To calculate the matrix element:

$$\frac{\langle\Phi|\hat{O}|\Psi\rangle}{\langle\Phi|\Psi\rangle} = \sum_{i,j=1}^M O_{ij}\ \frac{\langle\Phi|\hat{a}_i^\dagger\hat{a}_j|\Psi\rangle}{\langle\Phi|\Psi\rangle} \tag{5.17}$$

it is necessary to evaluate $\hat{a}_i^\dagger\hat{a}_j\,|\Psi\rangle$. This can be done recalling that:

$$\begin{aligned}\hat{a}_i^\dagger\hat{a}_j\,|\Psi\rangle = \hat{a}_i^\dagger\hat{a}_j\,|\psi_1 \dots \psi_N\rangle_- = \hat{a}_i^\dagger \sum_{k=1}^N \frac{(-1)^{k+1}}{\sqrt{N}} \langle\varphi_j|\psi_k\rangle\,|\psi_1 \dots \not{\psi}_k \dots \psi_N\rangle_- = \\ = \sum_{k=1}^N (-1)^{k+1} \langle\varphi_j|\psi_k\rangle\,|\varphi_i\psi_1 \dots \not{\psi}_k \dots \psi_N\rangle_- = \sum_{k=1}^N \langle\varphi_j|\psi_k\rangle\,|\psi_1 \dots \varphi_i \dots \psi_N\rangle_-\end{aligned} \tag{5.18}$$

where $|\psi_1 \dots \not{\psi}_k \dots \psi_N\rangle_-$ denotes $|\psi_1 \dots \psi_{k-1}\psi_{k+1} \dots \psi_N\rangle_-$ and $|\psi_1 \dots \varphi_i \dots \psi_N\rangle_-$ denotes $|\psi_1 \dots \psi_{k-1}\varphi_i\psi_{k+1} \dots \psi_N\rangle_-$. Inserting (5.18) in (5.17) and recalling (5.15) yields:

$$\frac{\langle\Phi|\hat{a}_i^\dagger\hat{a}_j|\Psi\rangle}{\langle\Phi|\Psi\rangle} = \sum_{k=1}^N \langle\varphi_j|\psi_k\rangle\,\frac{\det(B_i)}{\det(A)} \tag{5.19}$$

where $B_i \in M_{N\times N}(\mathbb{C})$ is the following matrix:

$$B_i = \begin{pmatrix} \langle\phi_1|\psi_1\rangle & \dots & \langle\phi_1|\psi_{k-1}\rangle & \langle\phi_1|\varphi_i\rangle & \langle\phi_1|\psi_{k+1}\rangle & \dots & \langle\phi_1|\psi_N\rangle \\ \dots & \dots & \dots & \dots & \dots & \dots & \dots \\ \langle\phi_N|\psi_1\rangle & \dots & \langle\phi_N|\psi_{k-1}\rangle & \langle\phi_N|\varphi_i\rangle & \langle\phi_N|\psi_{k+1}\rangle & \dots & \langle\phi_N|\psi_N\rangle \end{pmatrix} \tag{5.20}$$

$\det(B)_i$ can be evaluated remembering that Cramer's Rule [262] implies:

$$\frac{\det(B)}{\det(A)} = \sum_{l=1}^{N} \left(A^{-1}\right)_{kl} \langle\phi_l|\varphi_i\rangle \quad \rightarrow \quad \det(B) = \det(A) \sum_{l=1}^{N} \left((\Phi^\dagger\Psi)^{-1}\right)_{kl} \langle\phi_l|\varphi_i\rangle \tag{5.21}$$

with $A = \Phi^\dagger\Psi$ as in (5.15). Hence:

$$\begin{aligned} \mathcal{G}_{ji} = \frac{\langle\Phi|\hat{a}_i^\dagger\hat{a}_j|\Psi\rangle}{\langle\Phi|\Psi\rangle} = \sum_{k,l=1}^{N} \langle\varphi_j|\psi_k\rangle \left((\Phi^\dagger\Psi)^{-1}\right)_{kl} \langle\phi_l|\varphi_i\rangle = \\ = \sum_{k,l=1}^{N} (\Psi)_{jk} \left((\Phi^\dagger\Psi)^{-1}\right)_{kl} (\Phi^\dagger)_{li} = \left(\Psi\left((\Phi^\dagger\Psi)^{-1}\right)\Phi^\dagger\right)_{ji} \end{aligned} \tag{5.22}$$

he matrix $\mathcal{G}$ will be called normally ordered Green's matrix. Inserting (5.22) in (5.17) leads immediately to:

$$\frac{\langle\Phi|\hat{O}|\Psi\rangle}{\langle\Phi|\Psi\rangle} = \sum_{ij=1}^{M} O_{ij}\mathcal{G}_{ji} = \mathrm{Tr}[O\mathcal{G}] \tag{5.23}$$

The calculation of the Green's matrix, given $\Phi^\dagger\Psi$, requires $\mathcal{O}(N^3)$ operations, and the trace (5.23) requires $\mathcal{O}(M^2)$ further operations.

5.2.3 Matrix elements of two-body operators

Let us now consider a two-body operator $\hat{O} = \sum_{i,j=1}^{M} O_{ijlk}\, \hat{a}_i^\dagger\hat{a}_j^\dagger\hat{a}_k\hat{a}_l$. To evaluate the matrix element:

$$\langle\Phi|\hat{O}|\Psi\rangle = \sum_{ijkl=1}^{M} O_{ijlk}\ \langle\Phi|\hat{a}_i^\dagger\hat{a}_j^\dagger\hat{a}_k\hat{a}_l|\Psi\rangle \tag{5.24}$$

we can rely on the generalized Wick's Theorem by R. Balian and E. Brezin [263], thanks to which:

$$\frac{\langle\Phi|\hat{a}_i^\dagger\hat{a}_j^\dagger\hat{a}_k\hat{a}_l|\Psi\rangle}{\langle\Phi|\Psi\rangle} = \frac{\langle\Phi|\hat{a}_i^\dagger\hat{a}_l|\Psi\rangle}{\langle\Phi|\Psi\rangle}\frac{\langle\Phi|\hat{a}_j^\dagger\hat{a}_k|\Psi\rangle}{\langle\Phi|\Psi\rangle} - \frac{\langle\Phi|\hat{a}_i^\dagger\hat{a}_k|\Psi\rangle}{\langle\Phi|\Psi\rangle}\frac{\langle\Phi|\hat{a}_j^\dagger\hat{a}_l|\Psi\rangle}{\langle\Phi|\Psi\rangle} = \mathcal{G}_{li}\mathcal{G}_{kj} - \mathcal{G}_{ki}\mathcal{G}_{lj} \tag{5.25}$$

Equation (5.25) leads to:

$$\frac{\langle\Phi|\hat{O}|\Psi\rangle}{\langle\Phi|\Psi\rangle} = \sum_{ijkl=1}^{M} O_{ijlk}\ (\mathcal{G}_{li}\mathcal{G}_{kj} - \mathcal{G}_{ki}\mathcal{G}_{lj}) \tag{5.26}$$

In principle, the evaluation of (5.26) requires $\mathcal{O}(M^4)$ operations. Further simplifications, however, are possible if either O or $\mathcal{G}$ have a simple structure.

5.2.4 Exponentials of one-body operators

We now prove a result known as Thouless theorem, because it was first discovered by D. J. Thouless [264] and restated in the present form by D. R. Hamann and S. B. Fahy [265]. The Thouless theorem states that the manifold $\mathfrak{D}(N)$ is closed under the action of exponentials of one-body operators: as discussed in the forthcoming Section, the ability of mapping the imaginary-time Schrödinger equation onto a stochastic process in the manifold of Slater determinants rests upon the combined use of the Hubbard-Stratonovich transformation [266, 267] and of this result.

In order to prove the Thouless theorem, let us consider a one-body operator $\hat{O}$ and a Slater determinant $\Psi \in \mathfrak{D}(N)$. To evaluate $e^{\hat{O}} |\Psi\rangle$, it proves useful to observe that:

$$\begin{aligned} |\Psi\rangle = |\psi_1 \dots \psi_N\rangle_- &= \sum_{i_1 \dots i_N = 1}^{M} \langle \varphi_{i_1} | \psi_1 \rangle \dots \langle \varphi_{i_N} | \psi_N \rangle \;\; |\varphi_{i_1} \dots \varphi_{i_N}\rangle_- = \\ &= \sum_{i_1 \dots i_N = 1}^{M} \psi_{i_1 1} \dots \psi_{i_N N} \; \frac{\hat{a}^\dagger_{i_1} \dots \hat{a}^\dagger_{i_N}}{\sqrt{N!}} |0\rangle \end{aligned} \tag{5.27}$$

Thanks to (5.27), we see that calculating $e^{\hat{O}} \hat{a}^\dagger_{i_1} \dots \hat{a}^\dagger_{i_N} |0\rangle$ permits to calculate also $e^{\hat{O}} |\Psi\rangle$. With this in mind, let us oserve that:

$$\hat{O} \; \hat{a}^\dagger_k = \sum_{i,j=1}^{M} O_{ij} \; \hat{a}^\dagger_i \hat{a}_j \hat{a}^\dagger_k = \sum_{i,j=1}^{M} O_{ij} \; \hat{a}^\dagger_i \left\{ \hat{a}_j, \hat{a}^\dagger_k \right\} - \sum_{i,j=1}^{M} O_{ij} \; \hat{a}^\dagger_i \hat{a}^\dagger_k \hat{a}_j = \sum_{i=1}^{M} \hat{a}^\dagger_i \left(O_{ik} + \delta_{ik} \hat{O} \right) \tag{5.28}$$

Equation (5.28) can be generalized to an arbitrary integer power $\hat{O}^n$ of $\hat{O}$ yielding:

$$\hat{O}^n \; \hat{a}^\dagger_k = \sum_{i=1}^{M} \; \hat{a}^\dagger_i \; \sum_{s=0}^{n} \binom{n}{s} \left(O^s\right)_{ik} \hat{O}^{n-s} \tag{5.29}$$

Equation (5.29) can be easily proved by induction: for $n = 1$ it reduces to (5.28) and, assuming it holds for some $n > 0$:

$$\begin{aligned} \hat{O}^{n+1} \; \hat{a}^\dagger_k = \hat{O} \; \hat{O}^n \; \hat{a}^\dagger_k &= \sum_{i=1}^{M} \; \hat{O} \; \hat{a}^\dagger_i \; \sum_{s=0}^{n} \binom{n}{s} \left(O^s\right)_{ik} \hat{O}^{n-s} = \\ &= \sum_{i=1}^{M} \; \hat{a}^\dagger_j \; \left(\sum_{s=0}^{n} \binom{n}{s} \left(O^{s+1}\right)_{ik} \hat{O}^{n-s} + \sum_{s=0}^{n} \binom{n}{s} \left(O^s\right)_{ik} \hat{O}^{n+1-s} \right) = \\ &= \sum_{i=1}^{M} \; \hat{a}^\dagger_j \; \left(\sum_{s=1}^{n+1} \binom{n}{s-1} \left(O^s\right)_{ik} \hat{O}^{n+1-s} + \sum_{s=0}^{n} \binom{n}{s} \left(O^s\right)_{ik} \hat{O}^{n+1-s} \right) = \\ &= \sum_{i=1}^{M} \; \hat{a}^\dagger_j \; \sum_{s=0}^{n+1} \binom{n+1}{s} \left(O^s\right)_{ik} \hat{O}^{n+1-s} \end{aligned} \tag{5.30}$$

In the third passage (5.28)) has been recalled, and in the last passage the properties $\binom{n}{n} =$

$1 = \binom{n+1}{n+1}$, $\binom{n}{0} = 1 = \binom{n+1}{0}$ and $\binom{n}{s-1} + \binom{n}{s} = \binom{n+1}{s}$ have been used. Thanks to (5.29):

$$\begin{aligned} e^{\hat{O}} \hat{a}_k^\dagger &= \sum_{n=0}^{\infty} \frac{\hat{O}^n}{n!} \hat{a}_k^\dagger = \sum_i \hat{a}_i^\dagger \sum_{n=0}^{\infty} \sum_{s=0}^{n} \frac{1}{n!} \binom{n}{s} (O^s)_{ik} \hat{O}^{n-s} = \\ &= \sum_i \hat{a}_i^\dagger \sum_{n=0}^{\infty} \sum_{r=0}^{\infty} \sum_{s=0}^{\infty} \delta_{r+s,n} \frac{1}{n!} \binom{n}{s} (O^s)_{ik} \hat{O}^{n-s} = \\ &= \sum_i \hat{a}_i^\dagger \sum_{r=0}^{\infty} \sum_{s=0}^{\infty} \frac{(O^s)_{ik}}{s!} \frac{\hat{O}^r}{r!} = \sum_i \hat{a}_i^\dagger \left(e^O\right)_{ik} e^{\hat{O}} \end{aligned} \tag{5.31}$$

In the left term of (5.31) $e^{\hat{O}}$ appears at the left of a creation operator, in the right one it appears at the right of a linear combination of creation operators, with coefficients given by the matrix elements of e^O. Inserting (5.31) into $e^{\hat{O}} \hat{a}_{i_1}^\dagger \dots \hat{a}_{i_N}^\dagger |0\rangle$ leads to:

$$\begin{aligned} e^{\hat{O}} \frac{\hat{a}_{i_1}^\dagger \dots \hat{a}_{i_N}^\dagger}{\sqrt{N!}} |0\rangle &= \sum_{j_1 \dots j_n} \hat{a}_{j_1}^\dagger \dots \hat{a}_{j_N}^\dagger \left[e^O\right]_{j_1 i_1} \dots \left[e^O\right]_{j_N i_N} \frac{e^{\hat{O}}}{\sqrt{N!}} |0\rangle = \\ &= \sum_{j_1 \dots j_N} \left[e^O\right]_{j_1 i_1} \dots \left[e^O\right]_{j_N i_N} |\varphi_{j_1} \dots \varphi_{j_N}\rangle_- \end{aligned} \tag{5.32}$$

which, together with (5.27), gives [265]:

$$e^{\hat{O}} |\psi_1 \dots \psi_N\rangle_- = |e^O \psi_1 \dots e^O \psi_N\rangle_- \tag{5.33}$$

showing that $e^{\hat{O}} |\Psi\rangle$ is simply another Slater determinant.

5.2.5 Simplifications for spin-independent systems

No assumptions regarding either the structure of the Slater determinants involved or the single-particle basis have been made in deriving formulae (5.22), (5.33) and (5.26). It is interesting to particularize them to the case of a system of spin-$\frac{1}{2}$ particles with spin-independent Hamiltonian. In such case:

$$\begin{aligned} \Psi \left((\Phi^\dagger \Psi)^{-1}\right) \Phi^\dagger &= \begin{bmatrix} U_\Psi & 0 \\ 0 & V_\Psi \end{bmatrix} \begin{bmatrix} \left[U_\Phi^\dagger U_\Psi\right]^{-1} & 0 \\ 0 & \left[V_\Phi^\dagger V_\Psi\right]^{-1} \end{bmatrix} \begin{bmatrix} U_\Phi^\dagger & 0 \\ 0 & V_\Phi^\dagger \end{bmatrix} = \\ &= \begin{bmatrix} U_\Psi \left[U_\Phi^\dagger U_\Psi\right]^{-1} U_\Phi^\dagger & 0 \\ 0 & V_\Psi \left[V_\Phi^\dagger V_\Psi\right]^{-1} V_\Phi^\dagger \end{bmatrix} \end{aligned} \tag{5.34}$$

and thus the normally-ordered Green matrix takes the following block form:

$$\frac{\langle \Phi | \hat{a}_{\mathbf{k},\uparrow}^\dagger \hat{a}_{\mathbf{p},\uparrow} | \Psi \rangle}{\langle \Phi | \Psi \rangle} = \left(U_\Psi \left(U_\Phi^\dagger U_\Psi \right)^{-1} U_\Phi^\dagger \right)_{\mathbf{pk}} \quad \frac{\langle \Phi | \hat{a}_{\mathbf{k},\downarrow}^\dagger \hat{a}_{\mathbf{p},\downarrow} | \Psi \rangle}{\langle \Phi | \Psi \rangle} = \left(V_\Psi \left(V_\Phi^\dagger V_\Psi \right)^{-1} V_\Phi^\dagger \right)_{\mathbf{pk}} \tag{5.35}$$

all other elements being 0. Equation (5.33) takes a particularly interesting form when single-particle spin-independent operators:

$$\hat{O} = \sum_{\mathbf{k},\mathbf{p}} \sum_{\sigma} O_{\mathbf{k},\mathbf{p}} \hat{a}^{\dagger}_{\mathbf{k},\sigma} \hat{a}_{\mathbf{p},\sigma} \tag{5.36}$$

are involved. With an easy calculation, we see that the Slater determinant $e^{\hat{O}} |\Psi\rangle$ is described by the block matrix:

$$\begin{bmatrix} e^{O} & 0 \\ 0 & e^{O} \end{bmatrix} \begin{bmatrix} U_{\Psi} & 0 \\ 0 & V_{\Psi} \end{bmatrix} = \begin{bmatrix} e^{O} U_{\Psi} & 0 \\ 0 & e^{O} V_{\Psi} \end{bmatrix} \tag{5.37}$$

5.3 The Hubbard-Stratonovich transformation

The phaseless AFQMC is an *ab initio* method, meaning that the starting point of its construction is the Hamiltonian operator of the system under study, which we take of the general form:

$$\hat{H} = \hat{T} + \hat{V} = \hat{H} = \sum_{il=1}^{M} T_{il}\, \hat{a}^{\dagger}_{i} \hat{a}_{l} + \sum_{ijkl=1}^{M} \gamma_{ijlk}\, \hat{a}^{\dagger}_{i} \hat{a}^{\dagger}_{j} \hat{a}_{k} \hat{a}_{l} \tag{5.38}$$

where M is the dimensionality of the single–particle Hilbert space. It is a projector QMC method, which retrieves the ground-state Φ_0 of the system as long-imaginary time limit of:

$$\lim_{\tau \to \infty} e^{-\tau \left(\hat{H} - \epsilon_0 \right)} |\Psi_T\rangle = |\Phi_0\rangle \langle \Phi_0 | \Psi_T \rangle \tag{5.39}$$

where the unknown ground-state energy ϵ_0 is replaced with an *adaptive* estimate, according to a common procedure in Diffusion Monte Carlo (DMC) calculations [99]. In AFQMC, the association between the imaginary-time evolution (5.39) and a stochastic process in $\mathfrak{D}(N)$ begins with a discretization of the propagator:

$$e^{-\tau \left(\hat{H} - \epsilon_0 \right)} = \left(e^{-\delta\tau \left(\hat{H} - \epsilon_0 \right)} \right)^{n} \tag{5.40}$$

with $\delta\tau = \frac{\tau}{n}$. The treatment of the short-imaginary time propagator $e^{-\delta\tau \left(\hat{H} - \epsilon_0 \right)}$ requires to express the Hamiltonian (5.38) in a very peculiar way. It is easy to show that the coefficients γ_{ijlk} in the interaction part of (5.38) satisfy the relation:

$$\gamma^{*}_{ijlk} = \gamma_{lkij} \tag{5.41}$$

and thus can be cast in the hermitian matrix $\Gamma_{(ki)(jl)} = \gamma_{ijlk}$, of order M^2. Due to the spectral theorem:

$$\Gamma_{(ki)(jl)} = \sum_{\zeta=1}^{M^2} \mathcal{U}^{*}_{\zeta(ki)}\, \Gamma_{\zeta}\, \mathcal{U}_{\zeta(jl)} \tag{5.42}$$

for some real-valued coefficients Γ_{ζ} and some unitary matrix U of order M^2. Using (5.42) and:

$$\hat{a}^{\dagger}_{i} \hat{a}^{\dagger}_{j} \hat{a}_{k} \hat{a}_{l} = \hat{a}^{\dagger}_{i} \left\{ \hat{a}^{\dagger}_{j} \hat{a}_{k} \right\} \hat{a}_{l} + \hat{a}^{\dagger}_{i} \hat{a}_{k} \hat{a}^{\dagger}_{j} \hat{a}_{l} = \tag{5.43}$$

we see that (5.38) can be put in the form:

$$\hat{H} = \hat{H}_0 - \sum_{\zeta=1}^{M^2} \hat{O}_\zeta^\dagger \hat{O}_\zeta \tag{5.44}$$

which, recalling:

$$\hat{O}_\zeta^\dagger \hat{O}_\zeta = \frac{1}{2}\left((\hat{O}_\zeta + \hat{O}_\zeta^\dagger)^2 + (i\hat{O}_\zeta - i\hat{O}_\zeta^\dagger)^2\right) \tag{5.45}$$

leads to:

$$\hat{H} = \hat{H}_0 - \sum_{\zeta=1}^{M^2} \Gamma_\zeta \left(\frac{(\hat{O}_\zeta + \hat{O}_\zeta^\dagger)^2}{2} + \frac{(i\hat{O}_\zeta - i\hat{O}_\zeta^\dagger)^2}{2}\right) \tag{5.46}$$

with:

$$\hat{H}_0 = \sum_{il}\left(\beta_{il} + \sum_{j=1}^{M}\gamma_{ijlj}\right)\hat{a}_i^\dagger \hat{a}_l \quad , \qquad \hat{O}_\zeta = \sum_{jl} U_{\zeta(jl)}\ \hat{a}_j^\dagger \hat{a}_l \tag{5.47}$$

Notice that the interaction part of (5.38) has been replaced with a sum of squares of one-body hermitian operators [268]. Inserting such expression in $e^{-\delta\tau\left(\hat{H}-\epsilon_0\right)}$ and applying a primitive decomposition yields:

$$e^{-\delta\tau\left(\hat{H}-\epsilon_0\right)} = e^{-\delta\tau(\hat{H}_0-\epsilon_0)}\prod_{\zeta=1}^{M^2} e^{\frac{\delta\tau}{2}\Gamma_\zeta(\hat{O}_\zeta+\hat{O}_\zeta^\dagger)^2} e^{\frac{\delta\tau}{2}\Gamma_\zeta(i\hat{O}_\zeta-i\hat{O}_\zeta^\dagger)^2} + \mathcal{O}(\delta\tau^2) \tag{5.48}$$

To each of the factors appearing in (5.48), we can apply the following Hubbard-Stratonovich transformation:

Theorem 5.1 ([267, 266])**.** *Let $\mathcal{H}$ be a finitely-generated single-particle Hilbert space, λ a complex number and $\hat{O}$ a hermitian operator acting on $\mathcal{H}_-^{(N)}$. Then:*

$$e^{\frac{\lambda^2}{2}\hat{O}^2} = \int_{-\infty}^{\infty} d\eta\ \frac{e^{-\frac{\eta^2}{2}}}{\sqrt{2\pi}}\ e^{\eta\lambda\hat{O}} \tag{5.49}$$

Proof. *Since the Hilbert space $\mathcal{H}_-^{(N)}$ is finitely-generated like $\mathcal{H}$, the operator $\hat{O}$ is bounded and can be represented as:*

$$\hat{O} = \sum_n o_n \hat{\Pi}_n \tag{5.50}$$

where $\{o_n\}_n$ denotes the spectrum of $\hat{O}$ and $\{\hat{\Pi}_n\}_n$ the set of orthogonal projectors on the eigenspaces of $\hat{O}$. Then:

$$e^{\frac{\lambda^2}{2}\hat{O}^2} = \sum_n e^{\frac{\lambda^2}{2}o_n^2}\hat{\Pi}_n \tag{5.51}$$

Recalling the identity:

$$e^{\frac{\lambda^2}{2}x^2} = \int_{-\infty}^{\infty} d\eta\ \frac{e^{-\frac{\eta^2}{2}}}{\sqrt{2\pi}}\ e^{\eta\lambda x} \tag{5.52}$$

we can write:

$$e^{\frac{\lambda^2}{2}\hat{O}^2} = \sum_n \int_{-\infty}^{\infty} d\eta \frac{e^{-\frac{\eta^2}{2}}}{\sqrt{2\pi}}\; e^{\eta\lambda o_n}\hat{\Pi}_n \tag{5.53}$$

and interchange the summation, which is made on a finite number of indices n, and the integral operations obtaining:

$$e^{\frac{\lambda^2}{2}\hat{O}^2} = \int_{-\infty}^{\infty} d\eta \frac{e^{-\frac{\eta^2}{2}}}{\sqrt{2\pi}}\; \sum_n e^{\eta\lambda o_n}\hat{\Pi}_n \tag{5.54}$$

The proof of (5.49) *is completed observing that:*

$$\sum_n e^{\eta\lambda o_n}\hat{\Pi}_n = e^{\eta\lambda\hat{O}} \tag{5.55}$$

Application of (5.49) yields:

$$\begin{aligned} e^{-\delta\tau\left(\hat{H}-\epsilon_0\right)} = e^{-\delta\tau(\hat{H}_0-\epsilon_0)} \prod_{\zeta=1}^{M^2} \int_{-\infty}^{\infty} d\eta_{\zeta,1} \frac{e^{-\frac{\eta_{\zeta,1}^2}{2}}}{\sqrt{2\pi}} \int_{-\infty}^{\infty} d\eta_{\zeta,2} \frac{e^{-\frac{\eta_{\zeta,2}^2}{2}}}{\sqrt{2\pi}} \times \\ \times\; e^{\eta_{\zeta,1}\sqrt{\delta\tau\Gamma_\zeta}(\hat{O}_\zeta+\hat{O}_\zeta^\dagger)} e^{\eta_{\zeta,2}\sqrt{\delta\tau\Gamma_\zeta}(i\hat{O}_\zeta-i\hat{O}_\zeta^\dagger)} + \mathcal{O}(\delta\tau^2) \end{aligned} \tag{5.56}$$

which, up to terms of order $\mathcal{O}(\delta\tau^2)$, is equal to:

$$\begin{aligned} e^{-\delta\tau\left(\hat{H}-\epsilon_0\right)} = \prod_{\zeta=1}^{M^2} \int_{-\infty}^{\infty} d\eta_{\zeta,1} \frac{e^{-\frac{\eta_{\zeta,1}^2}{2}}}{\sqrt{2\pi}} \int_{-\infty}^{\infty} d\eta_{\zeta,2} \frac{e^{-\frac{\eta_{\zeta,2}^2}{2}}}{\sqrt{2\pi}} \times \\ e^{-\delta\tau(\hat{H}_0-\epsilon_0)+\sum_\zeta \eta_{\zeta,1}\sqrt{\delta\tau\Gamma_\zeta}(\hat{O}_\zeta+\hat{O}_\zeta^\dagger)+\eta_{\zeta,2}\sqrt{\delta\tau\Gamma_\zeta}(i\hat{O}_\zeta-i\hat{O}_\zeta^\dagger)} + \mathcal{O}(\delta\tau^2) \end{aligned} \tag{5.57}$$

We can write (5.57):

$$e^{-\delta\tau\left(\hat{H}-\epsilon_0\right)} = \int dg(\boldsymbol{\eta})\, \hat{G}(\boldsymbol{\eta}) + \mathcal{O}(\delta\tau^2) \tag{5.58}$$

where $dg(\boldsymbol{\eta})$ is the standard $2M^2$-dimensional normal probability measure, $\hat{G}(\boldsymbol{\eta}) = e^{\hat{A}(\boldsymbol{\eta})}$ and $\hat{A}(\boldsymbol{\eta}) = \sum_{ij=1}^{M} \mathcal{A}(\boldsymbol{\eta})_{ij}\hat{a}_i^\dagger\hat{a}_j$ the one-body operator:

$$\hat{A}(\boldsymbol{\eta}) = -\delta\tau(\hat{H}_0-\epsilon_0) + \sum_\zeta \sqrt{\delta\tau\Gamma_\zeta}\,(\eta_{\zeta,1}+i\eta_{\zeta,2})\hat{O}_\zeta + h.c. \tag{5.59}$$

which can be compactly written as:

$$\hat{A}(\boldsymbol{\eta}) = -\delta\tau(\hat{H}_0-\epsilon_0) + \sqrt{\delta\tau}\, i\, \hat{\boldsymbol{B}}\cdot\boldsymbol{\eta} \tag{5.60}$$

where:

$$i\hat{B}_{\zeta,k} = \begin{cases} \hat{O}_\zeta + \hat{O}_\zeta^\dagger \\ i\hat{O}_\zeta - i\hat{O}_\zeta^\dagger \end{cases} \tag{5.61}$$

Comparing (5.46) and (5.60), we see that $\hat{\boldsymbol{B}}$ is related to the Hamiltonian operator by:

$$\hat{H} = \hat{H}_0 + \frac{1}{2}\hat{\boldsymbol{B}}\cdot\hat{\boldsymbol{B}} \tag{5.62}$$

Notice that the Hubbard-Stratonovich transformation is an exact operator identity. The time-step error $\mathcal{O}(\delta\tau^2)$ comes from the Trotter-Suzuki decomposition (5.48).
Equation (5.58) establishes a formal correspondence between an interacting fermion system and an ensemble of *non-interacting* fermion systems subject to *fluctuating external potentials*. The coupling with these external potentials is controlled by normally-distributed parameters $\boldsymbol{\eta}$, called *auxiliary fields*, the integration over which recovers the interaction. The practical importance of (5.58) stems from the remarkable properties of Slater determinants. Let us consider a trial state $\Psi_T \in \mathfrak{D}(N)$ in the manifold of Slater determinants. The most natural choice of the trial function $|\Psi_T\rangle$, which is used throughout the present work, is the Hartree-Fock ground state of the Hamiltonian, i.e. the lowest energy Slater determinant. The interaction term in $\hat{H}$ causes a departure of the propagated state $e^{-\delta\tau\hat{H}}|\Psi_T\rangle$ from $\mathfrak{D}(N)$, as illustrated in Figure 5.2. On the other hand:

$$e^{-\delta\tau(\hat{H}-\epsilon_0)}|\Psi_T\rangle = \int dg(\boldsymbol{\eta})\,\hat{G}(\boldsymbol{\eta})\,|\Psi_T\rangle + \mathcal{O}(\delta\tau^2) \tag{5.63}$$

Since the operator $\hat{G}(\boldsymbol{\eta})$ is the exponential of a one-body operator, and $\mathfrak{D}(N)$ is closed under the action of such operators, as proved in (5.33), we conclude that:

$$\hat{G}(\boldsymbol{\eta})\,|\Psi_T\rangle \in \mathfrak{D}(N) \qquad \text{for all } \boldsymbol{\eta} \in \mathbb{R}^{2M^2} \tag{5.64}$$

The analytically intractable state $e^{-\delta\tau\left(\hat{H}-\epsilon_0\right)}|\Psi_T\rangle$ is then retrieved as the average of the Slater determinants $\hat{G}(\boldsymbol{\eta})\,|\Psi_T\rangle$ over the normally-distributed auxiliary fields $\boldsymbol{\eta}$. Iterating this calculation for a number n of imaginary-time steps such that $n\delta\tau = \tau$, we find:

$$e^{-\tau(\hat{H}-\epsilon_0)}|\Psi_T\rangle = \lim_{n\to\infty}\int dg(\boldsymbol{\eta}_{n-1})\ldots dg(\boldsymbol{\eta}_0)\hat{G}(\boldsymbol{\eta}_{n-1})\ldots\hat{G}(\boldsymbol{\eta}_0)\,|\Psi_T\rangle = \int \mathcal{D}\boldsymbol{\eta}\;|\Psi(\boldsymbol{\eta})\rangle \tag{5.65}$$

meaning that the exact imaginary-time evolution is recovered through the stochastic average of Brownian trajectories in the manifold of Slater determinants. The evolution of the orbitals ψ_i such that $|\Psi_T\rangle = |\psi_1\ldots\psi_N\rangle_-$ is governed by the following [269] stochastic differential equation:

$$d\psi_i(\tau) = -(\hat{H}_0 - \epsilon_0)\psi_i(\tau)d\tau - i\,\hat{\boldsymbol{B}}\psi_i(\tau)\cdot d\boldsymbol{\eta}_\tau \tag{5.66}$$

where $d\boldsymbol{\eta}_\tau$ is the stochastic differential of a $2M^2$-dimensional Wiener process. The numerical sampling of such stochastic process provides a stochastic linear combination of Slater determinants, which estimates the ground state of (5.38) in the long imaginary-time limit.

5.4 The phaseless auxiliary fields quantum Monte Carlo method

Despite its formal simplicity, the straightforward numerical implementation of (5.65) leads in general to an exponential increase in statistical errors with the imaginary time, due to the appearence of complex random phases during the evolution (5.65).
The overlap between the ground-state wavefunction and the trial wavefunction is the long-imaginary time limit of:

$$\langle\Psi_T|\,e^{-\tau(\hat{H}-\epsilon_0)}\,|\Psi_T\rangle = \int \mathcal{D}\boldsymbol{\eta}\;\langle\Psi_T|\Psi(\boldsymbol{\eta})\rangle \tag{5.67}$$

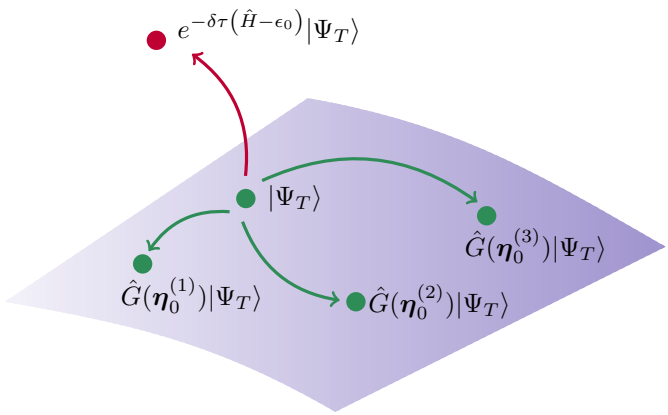

Figure 5.2: (color online) pictorial representation of the random walk in the manifold of N-particle Slater determinants $\mathfrak{D}(N)$ (lavender surface). The figure points out that the imaginary-time propagator $e^{-\delta\tau(\hat{H}-\epsilon_0)}$ drives a Slater determinant $|\Psi_T\rangle$ away from $\mathfrak{D}(N)$, while the one-body propagators $\hat{G}(\eta)$ preserve $\mathfrak{D}(N)$. This permits to retrieve the analytically intractable state $e^{-\delta\tau(\hat{H}-\epsilon_0)}|\Psi_T\rangle$ as a stochastic linear combination of Slater determinants $\hat{G}(\eta_0^{(w)})|\Psi_T\rangle$ according to (5.94).

In presence of random phases, most trajectories opposive overlaps $\langle\Psi_T|\Psi(\boldsymbol{\eta})\rangle$ that cancel each other in the average leading to $\langle\Phi_0|\Psi_T\rangle$. Already on an intutive level, it is easy to understand that such trajectories are useless for reconstructing the ground-state wavefunction, and severely degrade the signal-to-noise ratio of QMC estimators, because they only increase statistical uncertainties giving no conribution to the mean value.

S. Zhang *et al.* invented a modification of the stochastic process (5.65) through the introduction of an importance sampling transformation [268] that guides the random walk, closely resembling the typical scheme adopted [123] in DMC simulations.

First we introduce in the expression (5.65) n arbitrary and possibly complex-valued shift parameters $\boldsymbol{\xi}_0 \dots \boldsymbol{\xi}_{n-1}$ obtaining:

$$e^{-n\delta\tau(\hat{H}-\epsilon_0)}|\Psi_T\rangle \simeq \int dg(\boldsymbol{\eta}_{n-1}-\boldsymbol{\xi}_{n-1})\dots dg(\boldsymbol{\eta}_0-\boldsymbol{\xi}_0)\,|\Psi_n\rangle \tag{5.68}$$

where we have written $|\Psi_n\rangle = \hat{G}(\boldsymbol{\eta}_{n-1}-\boldsymbol{\xi}_{n-1})\dots\hat{G}(\boldsymbol{\eta}_0-\boldsymbol{\xi}_0)\,|\Psi_T\rangle$ for maintaining the notation as simple as possible. Naturally, the determinants $|\Psi_k\rangle$ satisfy the recursion relation $|\Psi_{k+1}\rangle = \hat{G}(\boldsymbol{\eta}_k-\boldsymbol{\xi}_k)\,|\Psi_{k-1}\rangle$ with $|\Psi_0\rangle = |\Psi_T\rangle$. Then, we recall that:

$$dg(\boldsymbol{\eta}-\boldsymbol{\xi}) = dg(\boldsymbol{\eta})\,e^{-\frac{\boldsymbol{\xi}\cdot\boldsymbol{\xi}}{2}+\boldsymbol{\eta}\cdot\boldsymbol{\xi}} \tag{5.69}$$

and write Ψ_n in terms of a telescopic product:

$$|\Psi_n\rangle = \frac{|\Psi_n\rangle}{\langle\Psi_T|\Psi_n\rangle}\prod_{k=2}^{n}\frac{\langle\Psi_T|\Psi_k\rangle}{\langle\Psi_T|\Psi_{k-1}\rangle}\,\frac{\langle\Psi_T|\Psi_1\rangle}{\langle\Psi_T|\Psi_T\rangle} \tag{5.70}$$

Inserting (5.70) in (5.68), we obtain:

$$e^{-n\delta\tau\left(\hat{H}-\epsilon_0\right)}\left|\Psi_T\right\rangle \simeq \int dg(\boldsymbol{\eta}_{n-1})\ldots dg(\boldsymbol{\eta}_0)\mathfrak{W}\left[\boldsymbol{\eta}_{n-1},\boldsymbol{\xi}_{n-1}\ldots\boldsymbol{\eta}_0\boldsymbol{\xi}_0\right]\frac{\left|\Psi_n\right\rangle}{\left\langle\Psi_T|\Psi_n\right\rangle} \tag{5.71}$$

In equation (5.71) appear complex-valued shift parameters $\boldsymbol{\xi}_{n-1}\ldots\boldsymbol{\xi}_0$ and a weight function $\mathfrak{W}\left[\boldsymbol{\eta}_{n-1},\boldsymbol{\xi}_{n-1}\ldots\boldsymbol{\eta}_0,\boldsymbol{\xi}_0\right]$ satisfying the recursion relation:

$$\mathfrak{W}\left[\boldsymbol{\eta}_n,\boldsymbol{\xi}_n\ldots\boldsymbol{\eta}_0,\boldsymbol{\xi}_0\right]=\mathfrak{W}\left[\boldsymbol{\eta}_{n-1},\boldsymbol{\xi}_{n-1}\ldots\boldsymbol{\eta}_0,\boldsymbol{\xi}_0\right]\,\mathfrak{I}\left[\boldsymbol{\eta}_n,\boldsymbol{\xi}_n;\left|\Psi_n\right\rangle\right] \tag{5.72}$$

where the following *importance function*:

$$\mathfrak{I}\left[\boldsymbol{\eta},\boldsymbol{\xi};\left|\Psi\right\rangle\right]=e^{-\frac{\boldsymbol{\xi}\cdot\boldsymbol{\xi}}{2}+\boldsymbol{\eta}\cdot\boldsymbol{\xi}}\frac{\left\langle\Psi_T|\hat{G}(\boldsymbol{\eta}-\boldsymbol{\xi})|\Psi\right\rangle}{\left\langle\Psi_T|\Psi\right\rangle} \tag{5.73}$$

appears. So far, the shift parameters are arbitrary. We subsequently fix their values to contain fluctuations in the importance function and therefore in the weight function. To this purpose, we expand $\hat{G}(\boldsymbol{\eta}-\boldsymbol{\xi})$ up to $\sqrt{\delta\tau}$ obtaining:

$$\hat{G}(\boldsymbol{\eta}-\boldsymbol{\xi})=\mathbb{I}+i\sqrt{\delta\tau}\,(\boldsymbol{\eta}-\boldsymbol{\xi})\cdot\hat{\boldsymbol{B}}+\mathcal{O}(\delta\tau) \tag{5.74}$$

Introducing this approximation in (5.73) leads to:

$$\log\left(\mathfrak{I}\left[\boldsymbol{\eta},\boldsymbol{\xi};\left|\Psi\right\rangle\right]\right)=-\frac{\boldsymbol{\xi}\cdot\boldsymbol{\xi}}{2}+\boldsymbol{\eta}\cdot\boldsymbol{\xi}+i\sqrt{\delta\tau}\,\frac{\left\langle\Psi_T|\hat{\boldsymbol{B}}|\Psi\right\rangle}{\left\langle\Psi_T|\Psi\right\rangle}\cdot(\boldsymbol{\eta}-\boldsymbol{\xi}) \tag{5.75}$$

where the operation $\frac{\langle\Psi_T|\cdot|\Psi\rangle}{\langle\Psi_T|\Psi\rangle}$ will be henceforth abbreviated with $\langle\cdot\rangle$.

Imposing $\partial_{\boldsymbol{\eta}}\log\left(\mathfrak{I}\left[\boldsymbol{\eta},\boldsymbol{\xi};\left|\Psi\right\rangle\right]\right)=0$ fixes the value of the shift parameter to:

$$\boldsymbol{\xi}_{opt}=-i\sqrt{\delta\tau}\langle\hat{\boldsymbol{B}}\rangle \tag{5.76}$$

Insertion of (5.76) into (5.73) yields the stabilized expression for the importance function:

$$\mathfrak{I}\left[\boldsymbol{\eta},\boldsymbol{\xi}_{opt};\left|\Psi\right\rangle\right]=e^{-\frac{\boldsymbol{\xi}_{opt}\cdot\boldsymbol{\xi}_{opt}}{2}+\boldsymbol{\eta}\cdot\boldsymbol{\xi}_{opt}}\,\langle\hat{G}(\boldsymbol{\eta}-\boldsymbol{\xi}_{opt})\rangle=e^{-\frac{\boldsymbol{\xi}_{opt}\cdot\boldsymbol{\xi}_{opt}}{2}+\boldsymbol{\eta}\cdot\boldsymbol{\xi}_{opt}}\,\frac{\left\langle\Psi_T|\hat{G}(\boldsymbol{\eta}-\boldsymbol{\xi}_{opt})|\Psi\right\rangle}{\left\langle\Psi_T|\Psi\right\rangle} \tag{5.77}$$

The two factors have the following expansions in powers of $\sqrt{\delta\tau}$:

$$e^{-\frac{\boldsymbol{\xi}_{opt}\cdot\boldsymbol{\xi}_{opt}}{2}+\boldsymbol{\eta}\cdot\boldsymbol{\xi}_{opt}}=1-i\sqrt{\delta\tau}\langle\hat{\boldsymbol{B}}\rangle+\frac{\delta\tau}{2}\langle\hat{\boldsymbol{B}}\rangle\cdot\langle\hat{\boldsymbol{B}}\rangle-\frac{\delta\tau}{2}\left(\boldsymbol{\eta}\cdot\langle\hat{\boldsymbol{B}}\rangle\right)^2+\mathcal{O}(\delta\tau^{\frac{3}{2}}) \tag{5.78}$$

$$\langle\hat{G}(\boldsymbol{\eta}-\boldsymbol{\xi}_{opt})\rangle=1+i\sqrt{\delta\tau}(\boldsymbol{\eta}-\boldsymbol{\xi}_{opt})\cdot\langle\hat{\boldsymbol{B}}\rangle-\delta\tau(\langle\hat{H}_0\rangle-\epsilon_0)-\frac{\delta\tau}{2}\langle(\boldsymbol{\eta}\cdot\hat{\boldsymbol{B}})^2\rangle \tag{5.79}$$

whence the expansion of the importance function is:

$$\mathfrak{I}\left[\boldsymbol{\eta},\boldsymbol{\xi}_{opt};\left|\Psi\right\rangle\right]=1-\delta\tau(\langle\hat{H}_0\rangle-\epsilon_0)-\frac{\delta\tau}{2}\left(\langle(\boldsymbol{\eta}\cdot\langle\hat{\boldsymbol{B}}\rangle)^2\rangle+\langle\hat{\boldsymbol{B}}\rangle\cdot\langle\hat{\boldsymbol{B}}\rangle-\langle(\boldsymbol{\eta}\cdot\hat{\boldsymbol{B}})^2\rangle\right)+\mathcal{O}(\delta\tau^{3/2}) \tag{5.80}$$

The importance function is still complex-valued, and thus the problematic random phases responsible for the occurrence of the sign problem in AFQMC have not been eliminated

by the importance sampling transformation. We now observe that the average of the importance function (5.84) over the auxiliary fields configurations has the following simple and suggestive expression:

$$\int dg(\boldsymbol{\eta})\, \mathfrak{I}\left[\boldsymbol{\eta}, \boldsymbol{\xi}_{opt}; |\Psi\rangle\right] = 1 - \delta\tau(\langle \hat{H}\rangle - \epsilon_0) + \mathcal{O}(\delta\tau^{3/2}) \tag{5.81}$$

which we easily retrieve observing that:

$$\int dg(\boldsymbol{\eta})(\boldsymbol{\eta}\cdot\langle\hat{\boldsymbol{B}}\rangle)^2 = \sum_{\substack{\zeta i \\ \zeta' i'}} \langle \hat{B}_{\zeta,i}\rangle \langle \hat{B}_{\zeta',i'}\rangle \int dg(\boldsymbol{\eta})\eta_{\zeta,i}\eta_{\zeta',i'} = \sum_{\zeta i}\left(\langle \hat{B}_{\zeta,i}\rangle\right)^2 = \langle\hat{\boldsymbol{B}}\rangle\cdot\langle\hat{\boldsymbol{B}}\rangle \tag{5.82}$$

and similarly:

$$\int dg(\boldsymbol{\eta})\langle(\boldsymbol{\eta}\cdot\hat{\boldsymbol{B}})^2\rangle = \langle\hat{\boldsymbol{B}}\cdot\hat{\boldsymbol{B}}\rangle \tag{5.83}$$

leading to:

$$\int dg(\boldsymbol{\eta})\, \mathfrak{I}\left[\boldsymbol{\eta}, \boldsymbol{\xi}_{opt}; |\Psi\rangle\right] = 1 - \delta\tau(\langle \hat{H}\rangle - \epsilon_0) - \frac{\delta\tau}{2}\langle\hat{\boldsymbol{B}}\cdot\hat{\boldsymbol{B}}\rangle + \mathcal{O}(\delta\tau^{3/2}) \tag{5.84}$$

in which we recognize (5.84) since $\hat{H} = \hat{H}_0 + \frac{1}{2}\hat{\boldsymbol{B}}\cdot\hat{\boldsymbol{B}}$. The real local energy approximation, motivated by the observation (5.84), consists in neglecting all terms of order $\delta\tau$ in the importance function except for the real part of $\langle\hat{H}\rangle$, and translates in the following approximation for the importance function:

$$\mathfrak{I}\left[\boldsymbol{\eta}, \boldsymbol{\xi}; |\Psi\rangle\right] \simeq e^{-\delta\tau(\epsilon_{loc}(\Psi)-\epsilon_0)} \tag{5.85}$$

where:

$$\epsilon_{loc}(\Psi) = \mathrm{Re}\langle\hat{H}\rangle = \mathrm{Re}\left(\frac{\langle\Psi_T|\hat{H}|\Psi\rangle}{\langle\Psi_T|\Psi\rangle}\right) \tag{5.86}$$

The real local energy approximation (5.85) turns (5.73) into a *real quantity*, avoiding typical phase problems arising from complex weights. It turns the stochastic representation of the ground-state wavefunction into:

$$e^{-\tau\hat{H}}|\Psi_T\rangle = \int \mathcal{D}\boldsymbol{\eta}\, \mathfrak{W}_\tau \frac{|\Psi(\boldsymbol{\eta})\rangle}{\langle\Psi_T|\Psi(\boldsymbol{\eta})\rangle} \tag{5.87}$$

where:

$$\mathfrak{W}_\tau = e^{-\int_0^\tau(\epsilon_{loc}(\Psi(\boldsymbol{\eta}))-\epsilon_0)} \tag{5.88}$$

meaning that, within the real local energy approximation, the imaginary-time evolution is recovered through a stochastic weighted average of scaled Slater determinants, whose orbitals evolve according to the stochastic differential equation [269]:

$$d\psi_i(\tau) = -\left(\hat{H}_0 - \epsilon_0 - \langle\hat{\boldsymbol{B}}\rangle\cdot\hat{\boldsymbol{B}}\right)\psi_i(\tau)d\tau - i\,\hat{\boldsymbol{B}}\psi_i(\tau)\cdot d\boldsymbol{\eta}_\tau \tag{5.89}$$

that now contains an additional drift term, due to the shift parameters. In the weight $\mathfrak{W}_\tau$, we easily recognize the path integral of the local energy along the trajectories of the stochastic process.

The phase problem is not completely eliminated by the real local energy approximation. To elucidate this problem, let us consider the function $f : \mathfrak{D}(N) \to \mathbb{C}$ mapping a determinant Ψ onto the overlap $f(\Psi) = \langle \Psi_T | \Psi \rangle$. As illustrated in Figure at the beginning of the stochastic process (5.87) the overlap takes value $f(\Psi_T) = 1$ with probability 1, and then spreads in the complex plane. As the imaginary time increases, the determinants $\Psi(\boldsymbol{\eta})$ populate the complex plane symmetrically, independent of their initial position $f(\Psi_T) = 1$. In particular, a finite density of walkers develops at the origin, where the local energy diverges, and this causes diverging fluctuations in the weights of the walkers. To prevent this possibility, S. Zhang *et al.* have devised the phaseless approximation [237, 238], where the importance function is constrained to evolve, according to the dephasing:

$$\Delta\theta = \mathrm{Im}\left[\log\left[\langle \hat{G}(\boldsymbol{\eta} - \boldsymbol{\xi})\rangle\right]\right] = \mathrm{Im}\left[\log\left[\frac{\langle \Psi_T | \hat{G}(\boldsymbol{\eta} - \boldsymbol{\xi}) | \Psi \rangle\rangle}{\langle \Psi_T | \Psi \rangle}\right]\right] \tag{5.90}$$

of the overlap with the trial state, as:

$$\mathfrak{I}\left[\boldsymbol{\eta}, \boldsymbol{\xi}; |\Psi\rangle\right] \simeq e^{-\delta\tau(\epsilon_{loc}(\Psi) - \epsilon_0)} \max(0, \cos(\Delta\theta)) \tag{5.91}$$

Since the angle $\Delta\theta$ corresponds to the flip in the phase of a determinant during a step of the random walk, the term $\max(0, \cos(\Delta\theta))$ is meant to suppress determinants whose phase undergoes an abrupt change, under the assumption [238, 268] that such behaviour indicates the vanishing of the overlap with the trial state. In this way, the determinants are maintained far from the origin $f(\Psi) = 0$ of the complex plane. This constraint offers a compromise between the need to control the phase problem, in order to produce QMC estimators with small variance, and the conservation of the initial form for the probability distribution, in order to produce unbiased QMC estimators. The beneficial impact of the phaseless approximation is illustrated in Figure 5.3.
Equation (5.71), together with the choice (5.85), (5.91) for the evolution of the weights attached to the Slater determinants, gives rise to the so-called *phaseless AFQMC method*.
The implementation of the real local energy and phaseless approximations allows the reconstruction, without the phase problem, of an approximate ground state for the Hamiltonian $\hat{H}$, and removes the risk of a diverging variance of the difference $\Phi_0 - \Psi(\boldsymbol{\eta})$, which which would result from an accumulation of determinants close to $f(\Psi(\boldsymbol{\eta})) = 0$. The real local energy and phaseless approximations considerably diminuish the variance of the AFQMC estimator (5.65) of the ground-state wavefunction, but introduce a bias in its mean value. Unlike the finite time-step approximation leading to (5.58) these are uncontrollable approximations, that do not fade as one or more parameters approach a certain limit. Experience, however, shows that it is a reasonable and accurate approximation. Indeed, the phaseless QMC method described above has been successfully applied to significant problems in condensed matter [250, 251, 252], quantum chemistry [253, 254, 255, 256] and materials Physics [257, 258, 259], in most situations with a simple Hartree-Fock determinant as trial state.

5.4.1 The algorithm

The observations introduced in Sections 5.2, 5.3 give rise to a polynomially complex algorithm for numerically sampling the ground state (5.39). The efficiency of the algorithm is granted by the possibility of parametrizing and manipulating Slater determinants with $M \times N$ and $M \times M$ complex-valued matrices respectively. The algorithm can be resumed in the following sequence of operations:

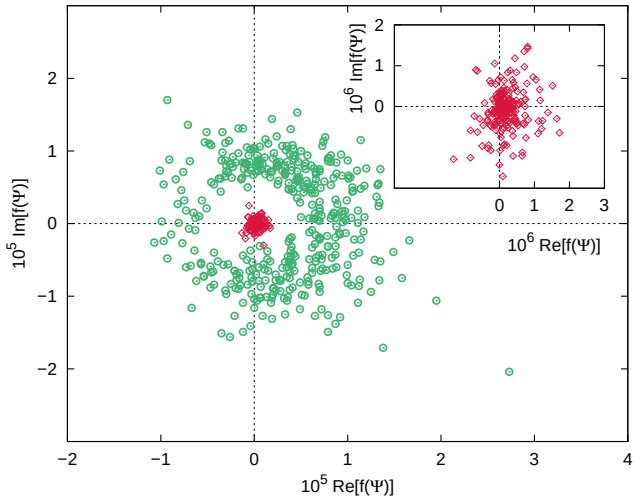

(a)

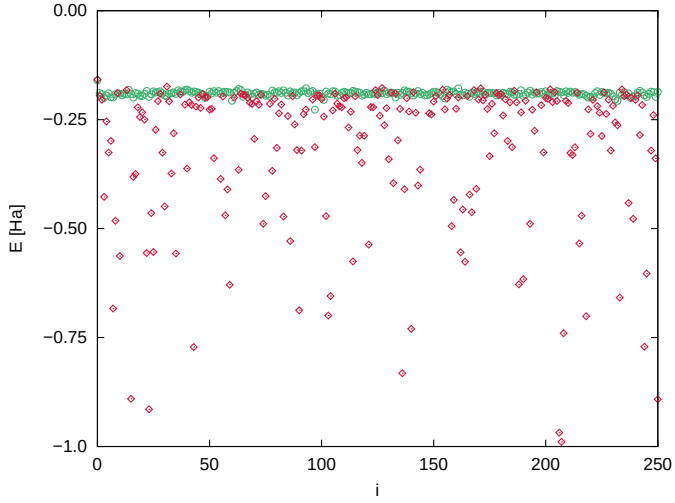

(b)

Figure 5.3: (a) Walker distribution in the complex plane $f(\Psi) = \langle \Psi_T | \Psi \rangle$, for a system of $N = 26$ 2D electrons at Seitz radius $r_s = 1$. In absence of the phaseless constraint (red symbols), walkers uniformly distribute close to the origin of the complex plane. In presence of the phaseless constraint (green symbols) are kept away from the origin of the complex plane. (b) Ground-state energy per particle, for a system of $N = 26$ 2D electrons at Seitz radius $r_s = 1$. Massive fluctuations are observed in absence of the phaseless constraint (red symbols), when the walkers can approach the origin of the complex plane. In presence of the phaseless constraint (green symbols) the fluctuations are considerably reduced. The estimates of the ground-state energy yield by the two calculations are $\mathcal{E}_N = -1.4(9)$ Ha and $\mathcal{E}_N = -0.192(5)$ Ha respectively.

1. Generate a large number N_w of Slater determinants $|\Psi_0^{(1)}\rangle \dots |\Psi_0^{(N_w)}\rangle$, called walkers, to a trial state $|\Psi_T\rangle$.

2. for $k = 0 \dots n-1$:

   - produce an adaptive estimate of the ground-state energy according to the formula:
   $$\epsilon_0 \simeq \frac{1}{\sum_{w=1}^{N_w} \mathfrak{W}_k^{(w)}} \sum_{w=1}^{N_w} \mathfrak{W}_k^{(w)} \frac{\langle \Psi_T | \hat{H} | \Psi_k^{(w)} \rangle}{\langle \Psi_T | \Psi_k^{(w)} \rangle} \tag{5.92}$$

   - sample normally distributed auxiliary field configurations $\boldsymbol{\eta}_k^{(1)} \dots \boldsymbol{\eta}_k^{(N_w)}$ are sampled, and update walkers and weights according to:
   $$\begin{aligned} |\Psi_{k+1}^{(w)}\rangle &= \hat{G}(\boldsymbol{\eta}_k^{(w)} - \boldsymbol{\xi}_k^{(w)}) \, |\Psi_k^{(w)}\rangle \\ \mathfrak{W}_{k+1}^{(w)} &= \mathfrak{W}_k^{(w)} \, \mathfrak{I}\left[\boldsymbol{\eta}_k^{(w)}, \boldsymbol{\xi}_k^{(w)}; |\Psi_k^{(w)}\rangle\right] \end{aligned} \tag{5.93}$$

   where $\boldsymbol{\xi}_k^{(w)}$ is the optimal shifts parameter (5.76). Moreover, the objects in (5.93) contain the adaptive estimate (5.92) of the ground-state energy.

3. as in the DMC algorithm, in order to avoid the inefficiencies connected with the accumulation of the weights $\mathfrak{W}_k^{(w)}$, perform the branching process described in Subsection 3.3.4.

4. estimate $e^{-n\delta\tau\left(\hat{H}-\epsilon_0\right)} |\Psi_T\rangle$ as:
   $$e^{-n\delta\tau\left(\hat{H}-\epsilon_0\right)} |\Psi_T\rangle \simeq \sum_{w=1}^{N_w} \mathfrak{W}_n^{(w)} \frac{|\Psi_n^{(w)}\rangle}{\langle \Psi_T | \Psi_n^{(w)} \rangle} \tag{5.94}$$

The estimate (5.94) gives access to the following *mixed estimate* of an observable $\mathcal{O}$:

$$\mathcal{O}_{mix} = \frac{\langle \Psi_T | \hat{O} e^{-n\delta\tau\left(\hat{H}-\epsilon_0\right)} | \Psi_T \rangle}{\langle \Psi_T | e^{-n\delta\tau\left(\hat{H}-\epsilon_0\right)} | \Psi_T \rangle} \tag{5.95}$$

which is computed as:

$$\mathcal{O}_{mix} \simeq \frac{\sum_{w=1}^{N_w} \mathfrak{W}_n^{(w)} \frac{\langle \Psi_T | \hat{O} | \Psi_n^{(w)} \rangle}{\langle \Psi_T | \Psi_n^{(w)} \rangle}}{\sum_{w=1}^{N_w} \mathfrak{W}_n^{(w)}} \tag{5.96}$$

with:

$$|\Psi_n^{(w)}\rangle = \hat{G}(\boldsymbol{\eta}_{n-1}^{(w)} - \boldsymbol{\xi}_{n-1}^{(w)}) \dots \hat{G}(\boldsymbol{\eta}_0^{(w)} - \boldsymbol{\xi}_0^{(w)}) |\Psi_T\rangle \tag{5.97}$$

For example, the mixed estimator for the ground-state energy per particle is:

$$\mathcal{E}_N^{(mix)} = \frac{1}{N} \frac{\sum_{w=1}^{N_w} \mathfrak{W}_n^{(w)} \epsilon_{loc}(\Psi_n^{(w)})}{\sum_{w=1}^{N_w} \mathfrak{W}_n^{(w)}} \tag{5.98}$$

For a generic determinant Ψ, the local energy can be easily evaluated using the following mixed estimator of the Green's function:

$$\mathcal{G}_{ji}^{(mix)} = \frac{\langle \Psi_T | \hat{a}_i^\dagger \hat{a}_j | \Psi \rangle}{\langle \Psi_T | \Psi \rangle} = \left(\Psi \left((\Psi_T^\dagger \Psi)^{-1} \right) \Psi_T^\dagger \right)_{ji} \tag{5.99}$$

In Appendix 13.4, we discuss how the numeric stability of the mixed Green's function can be significantly improved using a modified Gram-Schmidt reorthonormalization. Since:

$$\frac{\langle \Psi_T | \hat{a}_i^\dagger \hat{a}_j^\dagger \hat{a}_k \hat{a}_l | \Psi \rangle}{\langle \Psi_T | \Psi \rangle} = \mathcal{G}_{li}^{(mix)} \mathcal{G}_{kj}^{(mix)} - \mathcal{G}_{ki}^{(mix)} \mathcal{G}_{lj}^{(mix)} \tag{5.100}$$

by (5.26), the expression of the local energy becomes:

$$\begin{aligned} \epsilon_{loc}(\Psi) &= \sum_{il} T_{il} \mathcal{G}_{li}^{(mix)} + \sum_{ijkl} \gamma_{ijlk} \left(\mathcal{G}_{li}^{(mix)} \mathcal{G}_{kj}^{(mix)} - \mathcal{G}_{ki}^{(mix)} \mathcal{G}_{lj}^{(mix)} \right) = \\ &= \sum_{ij} T_{il} \mathcal{G}_{li}^{(mix)} + \sum_{ijkl} \left(\gamma_{ijlk} - \gamma_{jilk} \right) \mathcal{G}_{li}^{(mix)} \mathcal{G}_{kj}^{(mix)} \end{aligned} \tag{5.101}$$

In general, the calculation of the one-body part requires $\mathcal{O}(M^2)$ operations and that of the two-body part requires $\mathcal{O}(M^4)$ operations. Of course, (5.104) can be considerably simplified. First, let us assume that the one-body part $\hat{T}$ of the Hamiltonian is diagonal in the single- particle basis φ_i, i.e. $T_{il} = T_i \, \delta_{il}$, and that $|\Psi_T\rangle$ is the Hartree-Fock ground state of $\hat{T}$. Ordering the orbitals φ_i in ascending order of energy, we see that the matrices associated to Ψ_T and Ψ take the block form:

$$\Psi_T = \begin{pmatrix} I \\ O \end{pmatrix} \qquad \Psi = \begin{pmatrix} \Psi_1 \\ \Psi_2 \end{pmatrix} \tag{5.102}$$

where I denotes the $N \times N$ identity matrix. Thanks to (5.102) the mixed Green's function considerably simplifies. In fact, $(\Psi_T^\dagger \Psi)^{-1} = \Psi_1^{-1}$ and:

$$\mathcal{G}^{(mix)} = \begin{pmatrix} I & \Psi_2 \Psi_1^{-1} \\ O & O \end{pmatrix} \tag{5.103}$$

i.e. $\mathcal{G}_{ij}^{(mix)} = 0$ whenever $i > N$, and $\mathcal{G}_{ij}^{(mix)} = \delta_{ij}$ whenever $i, j < N$. Thanks to this simplification, (5.104) reduces to:

$$\epsilon_{loc}(\Psi) = \sum_{i=1}^{N} T_i + \sum_{ij=1}^{M} \sum_{lk}^{N} \left(\gamma_{ijlk} - \gamma_{jilk} \right) \mathcal{G}_{li}^{(mix)} \, \mathcal{G}_{kj}^{(mix)} \tag{5.104}$$

and the computational cost of the one-body and two-body part drops to $\mathcal{O}(N)$, $\mathcal{O}(N^2 M^2)$ respectively. Further simplifications are possible given a particular form of the two-body part $\hat{V}$.

A drawback of the mixed estimator is that the ground-state energy obtained in AFQMC under the phaseless approximation is not variational [268].

5.4.2 The backpropagation technique

The mixed estimator coincides with the exact estimator only for observables such that $\hat{O}$ commutes with the Hamiltonian $\hat{H}$. It is possible to correct the systematic error due to the non-commutativity combining the mixed estimator and the variational estimator:

$$\mathcal{O}_{vmc} = \frac{\langle \Psi_T | \hat{O} | \Psi_T \rangle}{\langle \Psi_T | \Psi_T \rangle} \tag{5.105}$$

in the extrapolated estimator (3.84), already presented in the DMC method:

$$\mathcal{O}_{ext} = 2\mathcal{O}_{mix} - \mathcal{O}_{vmc} \tag{5.106}$$

The extrapolation, however, is good only if the trial wavefunction is close to the ground state. A more systematic and refined approach is provided by the backpropagation technique, devised by S. Zhang *et al.* [248, 270].

The rationale behind the backpropagation technique is the observation that the ground-state average $\langle \Phi_0 | \hat{O} | \Phi_0 \rangle$ of a many-body observable $\hat{O}$ not commuting with $\hat{H}$ is the $m, n \to \infty$ limit of the following formula:

$$\mathcal{O}_{bp} = \frac{\langle \Psi_T | e^{-m\delta\tau\left(\hat{H}-\epsilon_0\right)} \hat{O} e^{-n\delta\tau\left(\hat{H}-\epsilon_0\right)} | \Psi_T \rangle}{\langle \Psi_T | e^{-(m+n)\delta\tau\left(\hat{H}-\epsilon_0\right)} | \Psi_T \rangle} \tag{5.107}$$

where the trial wavefunction has been propagated on both the right- and the left-hand side of the operator. Expressing the imaginary-time propagators appearing in (5.107) with (5.68) yields the following representations for the numerator and the denominator of (5.107):

$$\begin{aligned}
&\langle \Psi_T | e^{-(m+n)\delta\tau\left(\hat{H}-\epsilon_0\right)} | \Psi_T \rangle = \int dg(\boldsymbol{\eta}_{m+n-1}) \dots dg(\boldsymbol{\eta}_0) \, \langle \Psi_T | \prod_{i=0}^{m+n-1} \hat{G}(\boldsymbol{\eta}_i) | \Psi_T \rangle \\
&\langle \Psi_T | e^{-m\delta\tau\left(\hat{H}-\epsilon_0\right)} \hat{O} e^{-n\delta\tau\left(\hat{H}-\epsilon_0\right)} | \Psi_T \rangle = \int dg(\boldsymbol{\eta}_{m+n-1}) \dots dg(\boldsymbol{\eta}_0) \times \\
&\times \langle \Psi_T | \prod_{i=n}^{m+n-1} \hat{G}(\boldsymbol{\eta}_i) \hat{O} \prod_{i=0}^{n-1} \hat{G}(\boldsymbol{\eta}_i) | \Psi_T \rangle
\end{aligned} \tag{5.108}$$

where the symbol $\prod_{i=i_1}^{i_2} \hat{G}(\boldsymbol{\eta}_i)$ stands for the product $\hat{G}(\boldsymbol{\eta}_{i_2}) \dots \hat{G}(\boldsymbol{\eta}_{i_1})$. Further application of the importance sampling transformation and of identity (5.70) yields:

$$\begin{aligned}
&\langle \Psi_T | e^{-(m+n)\delta\tau\left(\hat{H}-\epsilon_0\right)} | \Psi_T \rangle = \int dg(\boldsymbol{\eta}_{m+n-1}) \dots dg(\boldsymbol{\eta}_0) \mathfrak{W}\left[\boldsymbol{\eta}_{m+n-1}, \boldsymbol{\xi}_{m+n-1} \dots \boldsymbol{\eta}_0, \boldsymbol{\xi}_0\right] \\
&\langle \Psi_T | e^{-m\delta\tau\left(\hat{H}-\epsilon_0\right)} \hat{O} e^{-n\delta\tau\left(\hat{H}-\epsilon_0\right)} | \Psi_T \rangle = \int dg(\boldsymbol{\eta}_{m+n-1}) \dots dg(\boldsymbol{\eta}_0) \\
&\mathfrak{W}\left[\boldsymbol{\eta}_{m+n-1}, \boldsymbol{\xi}_{m+n-1} \dots \boldsymbol{\eta}_0, \boldsymbol{\xi}_0\right] \times \frac{\langle \Psi_{BP,m} | \hat{O} | \Psi_n \rangle}{\langle \Psi_{BP,m} | \Psi_n \rangle}
\end{aligned} \tag{5.109}$$

where the symbol $|\Psi_{BP,m}\rangle$ stands for $\hat{G}^\dagger(\boldsymbol{\eta}_n - \boldsymbol{\xi}_n) \dots \hat{G}^\dagger(\boldsymbol{\eta}_{n+m-1} - \boldsymbol{\xi}_{n+m-1}) | \Psi_T \rangle$. The

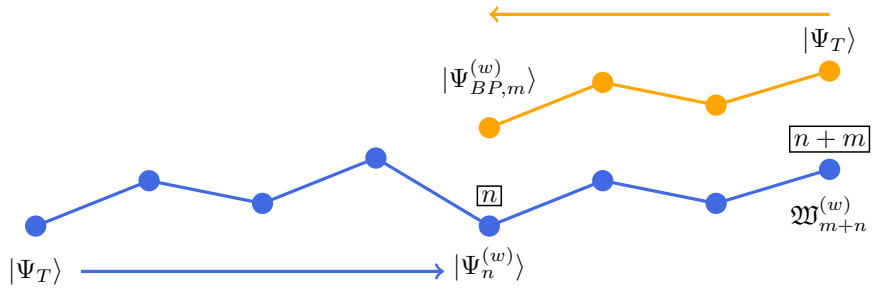

Figure 5.4: Pictorial representation of the backpropagation technique (5.110), with $n = 5$ propagation steps and $m = 3$ backpropagation steps. $|\Psi^{(w)}_n\rangle$ is computed at the time step n, while the determinant $|\Psi^{(w)}_{BP,m}\rangle$ is computed between the time steps n and $n+m$, and the weight $\mathfrak{W}^{(w)}_{m+n}$ is computed at the time step $m+n$.

estimator of $\mathcal{O}_{bp}$ is therefore:

$$\mathcal{O}_{bp} \simeq \frac{\sum_{w=1}^{N_w} \mathfrak{W}^{(w)}_{n+m} \frac{\langle \Psi^{(w)}_{BP,m} | \hat{O} | \Psi^{(w)}_n \rangle}{\langle \Psi^{(w)}_{BP,m} | \Psi^{(w)}_n \rangle}}{\sum_{w=1}^{N_w} \mathfrak{W}^{(w)}_{n+m}} \tag{5.110}$$

with:

$$\begin{aligned} |\Psi^{(w)}_n\rangle &= \hat{G}(\boldsymbol{\eta}^{(w)}_{n-1} - \boldsymbol{\xi}^{(w)}_{n-1}) \dots \hat{G}(\boldsymbol{\eta}^{(w)}_0 - \boldsymbol{\xi}^{(w)}_0) |\Psi_T\rangle \\ |\Psi^{(w)}_{BP,m}\rangle &= \hat{G}^\dagger(\boldsymbol{\eta}^{(w)}_n - \boldsymbol{\xi}^{(w)}_n) \dots \hat{G}^\dagger(\boldsymbol{\eta}^{(w)}_{n+m-1} - \boldsymbol{\xi}^{(w)}_{n+m-1}) |\Psi_T\rangle \end{aligned} \tag{5.111}$$

The backpropagation technique, illustrated in Figure 5.4 makes use of sequences of auxiliary fields from different segments of the random walk to project the trial wavefunction also at the left of the operator $\hat{O}$. This estimator approaches the exact expectation value as the number m of backpropagation steps is increased. However, it is well-known [248] that raising m requies repeated matrix multiplication in order to compute $\Psi^{(w)}_{BP,m}$ which can lead to numerical instability.

CHAPTER 6

Imaginary-time correlations and the phaseless AFQMC

In the present Chapter, the novel study [236] proposing to compute imaginary-time correlation functions (ITCFs) with the phaseless AFQMC is presented.
In Chapter 1, we have seen that the dynamical structure factor $S_{\hat{A},\hat{B}}(\omega)$ (see equation (1.23)) of two operators $\hat{A}$, $\hat{B}$ can be recovered from their ITCF:

$$F_{\hat{A},\hat{B}}(\tau) = \langle \Phi_0 | \hat{A}(\tau) \hat{B} | \Phi_0 \rangle = \langle \Phi_0 | \hat{A} e^{-\tau \left(\hat{H} - \epsilon_0 \right)} \hat{B} | \Phi_0 \rangle \tag{6.1}$$

though an inverse Laplace transform. In the present Chapter, it is proved that the ITCF of the one-body operators $\hat{A}$, $\hat{B}$ can be computed efficiently and accurately within the phaseless AFQMC. The methodology is tested against exact results for few-fermions systems amenable of exact numeric diagonalization of the Hamiltonian operator.

6.1 Phaseless AFQMC estimator of imaginary-time correlations

Being constructed with the imaginary-time evolution operator, the ITCF (6.1) is a natural quantity to be evaluated in QMC calculations. Its evaluation in determinantal QMC methods, however, is not as simple as in configurational QMC methods as discussed in Subsection (3.2.4). The static correlation function:

$$F_{\hat{A},\hat{B}}(0) = \langle \Phi_0 | \hat{A} \hat{B} | \Phi_0 \rangle \tag{6.2}$$

of the operators $\hat{A}$, $\hat{B}$ can be computed with the backpropagation estimator introduced in Section 5.4.2. A straightforward extension of that methodology to the ITCF (6.1) is prevented, because the operator $\hat{B}$ does not preserve $\mathfrak{D}(N)$. To overcome this difficulty, we generalize the clever approach to the calculation of dynamical Green's functions conceived by F. F. Assaad and M. Imada [271] and by M. Feldbacher and F. Assaad [272]. We introduce the Hubbard-Stratonovich representation (5.58) of the imaginary-time propagator in (6.1), and move the operators $\hat{G}(\boldsymbol{\eta})$ to the right of $\hat{B} = \sum_{ij=1}^{M} \mathcal{B}_{ij} \, \hat{a}_i^\dagger \hat{a}_j$ commuting them with the operators $\hat{a}_i^\dagger$, $\hat{a}_j$.
Given the need of moving $\hat{G}(\boldsymbol{\eta})$ to the right of $\hat{a}_i^\dagger \hat{a}_j$, the first step to express (6.1) in a form more adequate for AFQMC is to evaluate:

$$\hat{a}_k^\dagger(\tau) = e^{\tau \hat{F}} \hat{a}_k^\dagger e^{-\tau \hat{F}} \tag{6.3}$$

where $\hat{F} = \sum_{ij=1}^{M} \mathcal{F}_{ij} \; \hat{a}_i^\dagger \hat{a}_j$ is a one-body operator. The operator (6.3) obeys the differen-

tial equation:

$$\frac{d}{d\tau}\hat{a}_k^\dagger(\tau) = e^{\tau\hat{F}}\hat{F}\hat{a}_k^\dagger e^{-\tau\hat{F}} - e^{\tau\hat{F}}\hat{a}_k^\dagger\hat{F}e^{-\tau\hat{F}} = \left[\hat{F}, \hat{a}_k^\dagger(\tau)\right]_- \tag{6.4}$$

Recalling:

$$\left\{\hat{A}, \hat{B}\hat{C}\right\}_- = \hat{A}\hat{B}\hat{C} - \hat{B}\hat{C}\hat{A} = \left\{\hat{A}, \hat{B}\right\}\hat{C} - \hat{B}\hat{A}\hat{C} - \hat{B}\hat{C}\hat{A} = \left\{\hat{A}, \hat{B}\right\}\hat{C} - \hat{B}\left\{\hat{A}, \hat{C}\right\} \tag{6.5}$$

we see that:

$$\left[\hat{F}, \hat{a}_k^\dagger\right](\tau) = \sum_{ij=1}^{M} \mathcal{F}_{ij}\left[\hat{a}_i^\dagger\hat{a}_j, \hat{a}_k^\dagger\right] = \sum_i \mathcal{F}_{ik}\hat{a}_i^\dagger \tag{6.6}$$

whence (6.4) takes the more explicit form:

$$\frac{d}{d\tau}\hat{a}_k^\dagger(\tau) = \sum_i \mathcal{F}_{ik}\hat{a}_i^\dagger \tag{6.7}$$

The differential equation (6.7) is solved, together with the initial condition $\hat{a}_k^\dagger(0) = \hat{a}_k^\dagger$, by:

$$\hat{a}_k^\dagger(\tau) = \sum_{i=1}^{M}\left(e^{\tau\mathcal{F}}\right)_{ik}\hat{a}_i^\dagger \tag{6.8}$$

$e^{\tau\mathcal{F}}$ denoting the exponential of the matrix $\tau\mathcal{F}$. An analogous calculation shows that:

$$\hat{a}_l(\tau) = \sum_{j=1}^{M}\left[e^{-\tau F}\right]_{lj}\hat{a}_j \tag{6.9}$$

An immediate consequence of (6.8), (6.9) is that:

$$e^{\tau\hat{F}}\hat{a}_k^\dagger\hat{a}_l e^{-\tau\hat{F}} = \hat{a}_k^\dagger(\tau)\hat{a}_l(\tau) = \sum_{ij}\left(e^{\tau\mathcal{F}}\right)_{ik}\hat{a}_i^\dagger\hat{a}_j\left(e^{-\tau\mathcal{F}}\right)_{lj} \tag{6.10}$$

showing that the exponential of the one-body operator $\hat{F}$ can be moved to the right of a product $\hat{a}_k^\dagger\hat{a}_l$ at the cost of introducing the matrix $e^{\tau\mathcal{F}}$ and its inverse. Formula (6.10) can be applied to the operator $\hat{G}(\boldsymbol{\eta}_{n-r})\hat{a}_k^\dagger\hat{a}_l$ (the reason for this notation will become clear in a moment) yielding:

$$\hat{G}(\boldsymbol{\eta}_{n-r})\hat{a}_k^\dagger\hat{a}_l = \sum_{ij}\left(e^{\mathcal{A}(\boldsymbol{\eta}_{n-r})}\right)_{ik}\left(e^{-\mathcal{A}(\boldsymbol{\eta}_{n-r})}\right)_{lj}\hat{a}_i^\dagger\hat{a}_j\hat{G}(\boldsymbol{\eta}_{n-r}) \tag{6.11}$$

multiplying both members on the left by $\hat{G}(\boldsymbol{\eta}_{n-r+1})$ and applying (6.10) yields:

$$\hat{G}(\boldsymbol{\eta}_{n-r+1})\hat{G}(\boldsymbol{\eta}_{n-r})\hat{a}_k^\dagger\hat{a}_l = \sum_{ij}\left(e^{\mathcal{A}(\boldsymbol{\eta}_{n-r+1})}e^{\mathcal{A}(\boldsymbol{\eta}_{n-r})}\right)_{ik}\left(e^{-\mathcal{A}(\boldsymbol{\eta}_{n-r})}e^{-\mathcal{A}(\boldsymbol{\eta}_{n-r+1})}\right)_{lj} \\ \hat{a}_i^\dagger\hat{a}_j\hat{G}(\boldsymbol{\eta}_{n-r+1})\hat{G}(\boldsymbol{\eta}_{n-r}) \tag{6.12}$$

Iterated application of formula (6.10) to the product $\hat{G}(\boldsymbol{\eta}_{n-1})\ldots\hat{G}(\boldsymbol{\eta}_{n-r})\hat{a}_k^\dagger\hat{a}_l$ then yields:

$$\hat{G}(\boldsymbol{\eta}_{n-1})\dots\hat{G}(\boldsymbol{\eta}_{n-r})\hat{a}_k^\dagger\hat{a}_l = \sum_{ij}\mathcal{D}(\boldsymbol{\eta}_{n-1},\dots,\boldsymbol{\eta}_{n-r})_{ik}\mathcal{D}^{-1}(\boldsymbol{\eta}_{n-1},\dots,\boldsymbol{\eta}_{n-r})_{lj}$$
$$\hat{a}_i^\dagger\hat{a}_j\hat{G}(\boldsymbol{\eta}_{n-1})\dots\hat{G}(\boldsymbol{\eta}_{n-r}) \tag{6.13}$$

where $\mathcal{D}(\boldsymbol{\eta}_{n-1},\dots,\boldsymbol{\eta}_{n-r}) = e^{\mathcal{A}(\boldsymbol{\eta}_{n-1})}\dots e^{\mathcal{A}(\boldsymbol{\eta}_{n-r})}$. The observation (6.13) leads to the following representation for the ITCF:

$$\begin{aligned}F_{\hat{A},\hat{B}}(r\delta\tau) &= \sum_{kl}\mathcal{B}_{kl}\int dg(\boldsymbol{\eta}_{n-1})\dots dg(\boldsymbol{\eta}_{n-r})\langle\Phi_0|\hat{A}\hat{G}(\boldsymbol{\eta}_{n-1})\dots\hat{G}(\boldsymbol{\eta}_{n-r})\hat{a}_k^\dagger\hat{a}_l|\Phi_0\rangle = \\ &= \sum_{ijkl}\mathcal{B}_{kl}\int dg(\boldsymbol{\eta}_{n-1})\dots dg(\boldsymbol{\eta}_{n-r})\langle\Phi_0|\hat{A}\hat{a}_i^\dagger\hat{a}_j\hat{G}(\boldsymbol{\eta}_{n-1})\dots\hat{G}(\boldsymbol{\eta}_{n-r})|\Phi_0\rangle\times \\ &\times\ \mathcal{D}(\boldsymbol{\eta}_{n-1},\dots,\boldsymbol{\eta}_{n-r})_{ik}\,\mathcal{D}^{-1}(\boldsymbol{\eta}_{n-1},\dots,\boldsymbol{\eta}_{n-r})_{lj}\end{aligned} \tag{6.14}$$

To obtain the AFQMC estimator of the ITCF we observe, as in the backpropagation technique, that $F_{\hat{A},\hat{B}}(r\delta\tau)$ is well-approximated by:

$$F_{\hat{A},\hat{B}}(r\delta\tau) \simeq \frac{\langle\Psi_T|e^{-m\delta\tau\left(\hat{H}-\epsilon_0\right)}\hat{A}e^{-r\delta\tau\left(\hat{H}-\epsilon_0\right)}\hat{B}e^{-(n-r)\delta\tau\left(\hat{H}-\epsilon_0\right)}|\Psi_T\rangle}{\langle\Psi_T|\,e^{-(m+n-r)\delta\tau\left(\hat{H}-\epsilon_0\right)}\,|\Psi_T\rangle} \tag{6.15}$$

for large m,n. We introduce the Hubbard-Stratonovich transformation (5.58) in the numerator and denominator of (6.15) obtaining:

$$\begin{aligned}&\langle\Psi_T|e^{-(m+n-r)\delta\tau\left(\hat{H}-\epsilon_0\right)}|\Psi_T\rangle = \int dg(\boldsymbol{\eta}_{m+n-1})\dots dg(\boldsymbol{\eta}_n)dg(\boldsymbol{\eta}_{n-r})\dots dg(\boldsymbol{\eta}_0)\times \\ &\times\ \langle\Psi_T|\prod_{i=n}^{m+n-1}\hat{G}(\boldsymbol{\eta}_i)\prod_{i=0}^{n-r-1}\hat{G}(\boldsymbol{\eta}_i)|\Psi_T\rangle\end{aligned} \tag{6.16}$$

and:

$$\begin{aligned}&\langle\Psi_T|e^{-m\delta\tau\left(\hat{H}-\epsilon_0\right)}\hat{A}e^{-r\delta\tau\left(\hat{H}-\epsilon_0\right)}\hat{B}e^{-n\delta\tau\left(\hat{H}-\epsilon_0\right)}|\Psi_T\rangle = \sum_{ijkl}\mathcal{B}_{kl}\int dg(\boldsymbol{\eta}_{m+n-1})\dots dg(\boldsymbol{\eta}_0)\times \\ &\times\ \langle\Psi_T|\prod_{i=n}^{m+n-1}\hat{G}(\boldsymbol{\eta}_i)\hat{A}\hat{a}_i^\dagger\hat{a}_j\prod_{i=0}^{n-1}\hat{G}(\boldsymbol{\eta}_i)|\Psi_T\rangle\,\mathcal{D}(\boldsymbol{\eta}_{n-1}\dots\boldsymbol{\eta}_{n-r})_{ik}\mathcal{D}^{-1}(\boldsymbol{\eta}_{n-1}\dots\boldsymbol{\eta}_{n-r})_{lj}\end{aligned} \tag{6.17}$$

Further application of the importance sampling transformation and of identity (5.70) yields:

$$F_{\hat{A},\hat{B}}(r\delta\tau) \simeq$$
$$\frac{\int dg(\boldsymbol{\eta}_{m+n-1})\dots dg(\boldsymbol{\eta}_0)\mathfrak{W}\left[\boldsymbol{\eta}_{m+n-1},\boldsymbol{\xi}_{m+n-1}\dots\boldsymbol{\eta}_0,\boldsymbol{\xi}_0\right]\sum_{ijkl}\mathcal{D}_{ik}\mathcal{B}_{kl}\mathcal{D}^{-1}_{lj}\frac{\langle\Psi_{BP,m}\hat{A}\hat{a}_i^\dagger\hat{a}_j|\Psi_n\rangle}{\langle\Psi_{BP,m}|\Psi_n\rangle}}{\int dg(\boldsymbol{\eta}_{m+n-1})\dots dg(\boldsymbol{\eta}_n)dg(\boldsymbol{\eta}_{n-r})\dots dg(\boldsymbol{\eta}_0)\tilde{\mathfrak{W}}\left[\boldsymbol{\eta}_{m+n-1},\boldsymbol{\xi}_{m+n-1}\dots\boldsymbol{\eta}_0,\boldsymbol{\xi}_0\right]} \tag{6.18}$$

where:

$$\mathcal{D}_{ik} = \mathcal{D}(\boldsymbol{\eta}_{n-1} - \boldsymbol{\xi}_{n-1}, \ldots, \boldsymbol{\eta}_{n-r} - \boldsymbol{\xi}_{n-r})_{ik} \tag{6.19}$$

The numerator and the denominator of (6.18) involve integrations over $n+m$ and $n+m-r$ auxiliary fields configurations respectively. Therefore, while the weights appearing in the numerator coincide with those in (5.110), the weights appearing in the denominator read:

$$\tilde{\mathfrak{W}}\left[\boldsymbol{\eta}_{m+n-1}, \boldsymbol{\xi}_{m+n-1} \cdots \boldsymbol{\eta}_0, \boldsymbol{\xi}_0\right] = \prod_{k=n}^{n+m-1} \prod_{k=0}^{n-r-1} \mathfrak{I}\left[\boldsymbol{\eta}_k, \boldsymbol{\xi}_k; |\Psi_k\rangle\right] \tag{6.20}$$

The AFQMC estimator of (6.18) is:

$$F_{\hat{A},\hat{B}}(r\delta\tau) \simeq \frac{1}{\sum_{w=1}^{N_w} \mathfrak{W}_{m+n-r}^{(w)}} \sum_{w=1}^{N_w} \mathfrak{W}_{m+n}^{(w)} \sum_{ijkl} \mathcal{D}_{ik} \mathcal{B}_{kl} \mathcal{D}_{lj}^{-1} \frac{\langle \Psi_{BP,m}^{(w)} | \hat{A} \hat{a}_i^\dagger \hat{a}_j | \Psi_n^{(w)} \rangle}{\langle \Psi_{BP,m}^{(w)} | \Psi_n^{(w)} \rangle} \tag{6.21}$$

where the Slater determinants $\Psi_{BP,m}^{(w)}, \Psi_n^{(w)}$ are those appearing in (5.111), the matrix $\mathcal{D}$ is:

$$\mathcal{D}_{ik} = \mathcal{D}(\boldsymbol{\eta}_{n-1}^{(w)} - \boldsymbol{\xi}_{n-1}^{(w)}, \ldots, \boldsymbol{\eta}_{n-r}^{(w)} - \boldsymbol{\xi}_{n-r}^{(w)})_{ik} \tag{6.22}$$

and the weights $\mathfrak{W}_{m+n-r}^{(w)}$ are constructed with the slightly modified recursion relation:

$$\mathfrak{W}_{k+1}^{(w)} = \begin{cases} \mathfrak{W}_k^{(w)} & \text{if } n-r \leq k \leq n-1 \\ \mathfrak{W}_k^{(w)}\, \mathfrak{I}\left[\boldsymbol{\eta}_k^{(w)}, \boldsymbol{\xi}_k^{(w)}; |\Psi_k^{(w)}\rangle\right] & \text{otherwise} \end{cases} \tag{6.23}$$

By application of (6.12) and of the backpropagation technique [237, 268], it is possible to estimate the ITCF from the mean value of a random variable over the random path followed by the walkers in the manifold of Slater determinants.
The estimator (6.21) is essentially a weighted average of suitably-constructed matrix elements; each walker w constructs the matrix element and the weights $\mathfrak{W}_{m+n-r}^{(w)}$, $\mathfrak{W}_{m+n}^{(w)}$ involved in the weighted average (6.21) from two Slater determinants $|\Psi_n^{(w)}\rangle$, $|\Psi_{BP,m}^{(w)}\rangle$ and two matrices $\mathcal{D}$, $\mathcal{D}^{-1}$. These objects are functions of the auxiliary fields configurations $\boldsymbol{\eta}^{(w)}$ defining the random path followed by the walker in the manifold of Slater determinants, and their calculation is pictorially illustrated in Fig. 6.1.

6.2 Computational Cost

The AFQMC estimator of ITCFs should join numeric stability and low computational cost. The aim of the present Section is to show that the computational cost of (6.21) is $\mathcal{O}(M^3)$, M being the number of orbitals constituting the single-particle basis. The contribution F_w to (6.21) brought by a single walker of index w reads:

$$F_w = \sum_{ijklrs} \mathcal{A}_{rs}\, \mathcal{D}_{ik} \mathcal{B}_{kl} \mathcal{D}_{lj}^{-1}\, \langle \hat{a}_r^\dagger \hat{a}_s \hat{a}_i^\dagger \hat{a}_j \rangle_w \tag{6.24}$$

where the abbreviation:

$$\langle \cdot \rangle_w = \frac{\langle \Psi_{BP,m}^{(w)} | \cdot | \Psi_n^{(w)} \rangle}{\langle \Psi_{BP,m}^{(w)} | \Psi_n^{(w)} \rangle} \tag{6.25}$$

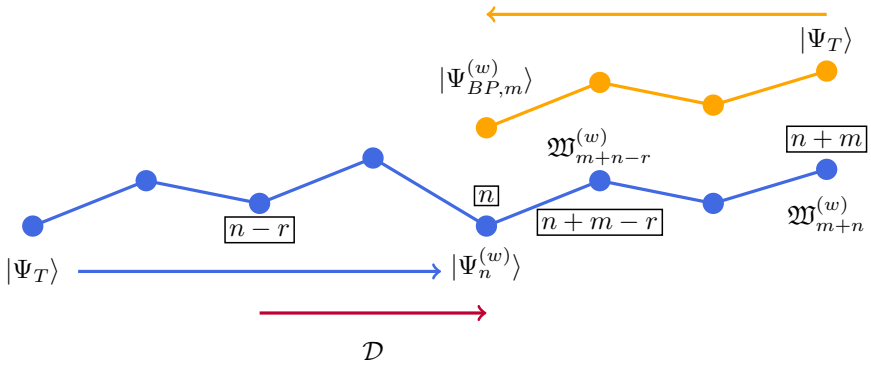

Figure 6.1: Pictorial representation of the phaseless AFQMC estimator for $F_{\hat{A},\hat{B}}(\tau)$, equation (6.21); $F_{\hat{A},\hat{B}}(\tau)$ is computed at $\tau = r\,\delta\tau$ with $r = 2$, with $n = 5$ propagation steps and $m = 3$ backpropagation steps. The matrix $\mathcal{D}$ appearing in (7.5) is computed between the time steps $n - r$ and n (at which $|\Psi^{(w)}_n\rangle$ is computed); the determinant $|\Psi^{(w)}_{BP,m}\rangle$ is computed between the time steps n and $n + m$, and the weights $\mathfrak{W}^{(w)}_{m+n-r}$ and $\mathfrak{W}^{(w)}_{m+n}$ are computed at the time steps $m + n - r$ and $m + n$.

has been inserted. The generalized Wick's theorem [263] implies that:

$$\langle \hat{a}^\dagger_r \hat{a}_s \hat{a}^\dagger_i \hat{a}_j \rangle_w = \langle \hat{a}^\dagger_r \hat{a}_s \rangle_w \langle \hat{a}^\dagger_i \hat{a}_j \rangle_w + \langle \hat{a}^\dagger_r \hat{a}_j \rangle_w \langle \hat{a}_s \hat{a}^\dagger_i \rangle_w = \mathcal{G}_{sr}\mathcal{G}_{ji} + \mathcal{G}_{jr}\left(\delta_{si} - \mathcal{G}_{si}\right) \tag{6.26}$$

Combining (6.24) and (6.26) yields:

$$F_w = \sum_{ijklrs} \mathcal{A}_{rs}\,\mathcal{B}_{kl}\,\mathcal{G}_{sr}\mathcal{G}_{ji}\mathcal{D}_{ik}\mathcal{D}^{-1}_{lj} + \sum_{ijklr} \mathcal{A}_{ri}\,\mathcal{B}_{kl}\,\mathcal{G}_{jr}\mathcal{D}_{ik}\mathcal{D}^{-1}_{lj} - \sum_{ijklrs} \mathcal{A}_{rs}\,\mathcal{B}_{kl}\,\mathcal{G}_{jr}\mathcal{G}_{si}\mathcal{D}_{ik}\mathcal{D}^{-1}_{lj} \tag{6.27}$$

Despite its cumbersome appearance, (6.27) can be efficiently evaluated computing the intermediate tensors $\mathcal{D}\mathcal{B}$, $\mathcal{A}\mathcal{G}^T$ and $\mathcal{D}^{-1}\mathcal{G}^T$ at the cost of $\mathcal{O}(M^3)$ operations, and subsequently computing F_w as:

$$F_w = \left[\sum_r (\mathcal{A}\mathcal{G})_{rr}\right] \sum_{il} (\mathcal{D}\mathcal{B})_{il} \left(\mathcal{D}^{-1}\mathcal{G}\right)_{li} + \sum_{ilr} (\mathcal{D}\mathcal{B})_{il} \left[\left(\mathcal{D}^{-1}\mathcal{G}\right)_{lr} \mathcal{A}_{ri} - \left(\mathcal{D}^{-1}\mathcal{G}\right)_{li} (\mathcal{A}\mathcal{G})_{ri}\right] \tag{6.28}$$

at the cost of $\mathcal{O}(M^3)$ more operations. The calculation of F_w further simplifies for operators $\hat{A}$ such that $\mathcal{A}_{ij} = \mathcal{A}_j\,\delta_{i,a(j)}$ for some function $a : \{1 \dots M\} \to \{1 \dots M\}$.
The complexity $\mathcal{O}(M^3)$ is the best allowed by the phaseless AFQMC methodology: in fact, the calculation of ITCFs requires at least $\mathcal{O}(M^3)$ operations to accumulate the matrix $\mathcal{D}$, and the contractions in (6.27) do not compromise this favorable scaling with the number of single-particle orbitals.

6.3 Assessment of accuracy

The approximations underlying the phaseless AFQMC method are known to be very good for the ground state, but ITCFs require sampling of excited states, related to the fluctuations around the asymptotic distribution of the random walk: this issue is largely unexplored and, in the present thesis, its accuracy has been addressed. There is no *a priori* motivation for concluding that the approximation (5.85) is better than the FN for

the exploration of the manifold of excited states. In the present section, this important point is verified for a model system, by comparison with exact results.

6.3.1 A class of solvable systems

We test the accuracy of the AFQMC results on a class of simple systems for which exact numeric expression for the spectral decomposition:

$$\hat{H} = \sum_{\alpha} \epsilon_{\alpha} \left|\Phi_{\alpha}\right\rangle \left\langle\Phi_{\alpha}\right| \tag{6.29}$$

of the Hamiltonian can be given. $\hat{H}$ reads:

$$\hat{H} = \sum_{m,\sigma} \frac{2\pi}{N} \frac{|\boldsymbol{n}_m|^2}{r_s^2} \hat{a}^{\dagger}_{m,\sigma} \hat{a}_{m,\sigma} + \sum_{\sigma,\sigma'} \sum_{mnrs} \frac{1}{\sqrt{4N\pi}\, r_s} \frac{\delta_{\boldsymbol{n}_r - \boldsymbol{n}_m, \boldsymbol{n}_n - \boldsymbol{n}_s}}{|\boldsymbol{n}_r - \boldsymbol{n}_m|} \hat{a}^{\dagger}_{m,\sigma} \hat{a}^{\dagger}_{n,\sigma'} \hat{a}_{s,\sigma'} \hat{a}_{r,\sigma} \tag{6.30}$$

up to an irrelevant constant factor. The single-particle Hilbert space $\mathcal{H}$ is spanned by spin-definite plane waves $|\boldsymbol{n}_i\sigma\rangle$ with $\boldsymbol{n}_i \in \mathbb{Z}^2$, $|\boldsymbol{n}_i|^2 \leq n_{max}$ for some integer n_{max} and $\sigma = \pm 1$. The parameter $r_s \in (0, \infty)$ controls the relevance of the interaction part and N stands for the number of particles. For small number of particles N and low kinetic energy cutoff n_{max} the above Hamiltonian defines a simple model which can be solved exactly.
Knowledge of eigenvalues $\{\epsilon_{\alpha}\}_{\alpha}$ and eigenvectors $\{|\Phi_{\alpha}\rangle\}_{\alpha}$ of $\hat{H}$, that we achieved relying on the Lapack DSYEV routine [273], allows exact calculation of the imaginary-time propagator:

$$e^{-\tau\left(\hat{H}-\epsilon_0\right)} = \sum_{\alpha} e^{-\tau(\epsilon_{\alpha}-\epsilon_0)} \left|\Phi_{\alpha}\right\rangle \left\langle\Phi_{\alpha}\right| \quad , \tag{6.31}$$

of the projector $|\Phi_0\rangle \langle\Phi_0|$ onto the minimum energy eigenspace, of backpropagated ground-state averages:

$$\mathcal{O}_{bp} = \frac{\langle\Psi_T|e^{-m\delta\tau\left(\hat{H}-\epsilon_0\right)}\hat{O}|\Phi_0\rangle}{\langle\Psi_T|e^{-m\delta\tau\left(\hat{H}-\epsilon_0\right)}|\Phi_0\rangle} = \frac{\sum_{\alpha}\langle\Psi_T|\Phi_{\alpha}\rangle e^{-m\delta\tau(\epsilon_{\alpha}-\epsilon_0)}\langle\Phi_{\alpha}|\hat{O}|\Phi_0\rangle}{\langle\Psi_T|\Phi_0\rangle} \tag{6.32}$$

and of backpropagated ITCFs (6.1):

$$\begin{aligned} F_{\hat{A},\hat{B}}(\tau) &= \frac{\langle\Psi_T|e^{-m\delta\tau\left(\hat{H}-\epsilon_0\right)}\hat{A}e^{-r\delta\tau\left(\hat{H}-\epsilon_0\right)}\hat{B}|\Phi_0\rangle}{\langle\Psi_T|e^{-m\delta\tau\left(\hat{H}-\epsilon_0\right)}|\Phi_0\rangle} = \\ &= \frac{\sum_{\alpha,\beta}\langle\Psi_T|\Phi_{\alpha}\rangle e^{-m\delta\tau(\epsilon_{\alpha}-\epsilon_0)-r\delta\tau(\epsilon_{\beta}-\epsilon_0)}\langle\Phi_{\alpha}|\hat{A}|\Phi_{\beta}\rangle\langle\Phi_{\beta}|\hat{B}|\Phi_0\rangle}{\langle\Psi_T|\Phi_0\rangle} \end{aligned} \tag{6.33}$$

and the comparison of such quantities with AFQMC results.
We focus on the ITCF $F_{\boldsymbol{n}}(\tau) = \frac{1}{N}\langle\Psi_0|\hat{\rho}_{\boldsymbol{n}}(\tau)\hat{\rho}_{-\boldsymbol{n}}|\Psi_0\rangle$ of the density fluctuation operator $\hat{\rho}_{\boldsymbol{n}}$ and of its adjoint $\hat{\rho}^{\dagger}_{\boldsymbol{n}} = \hat{\rho}_{-\boldsymbol{n}}$.

6.3.2 Results

The phaseless AFQMC method represents the ground state as a stochastic linear combination of Slater determinants, (5.94), from which accurate estimates of the ground-state

energy can be obtained [237, 254, 256]. However, much more information can be obtained from the simulation. Here we present results for the components of the ground state on the chosen basis of the Hilbert space and for the ITCFs.

Each of the simulations presented below is characterized by two sets of parameters: $(N_\uparrow, N_\downarrow, r_s, M)$ define the system under study, whereas $(\delta\tau, m, N_w)$ control the details of the simulation. In particular, $N_\uparrow$ ($N_\downarrow$) is the number of spin-up (spin-down) fermions, r_s controls the strength of the interaction, M fixes the order of the matrices with which the algorithm deals, while m corresponds to the number of backpropagation steps.

Apart from the basis set size M, which we keep small to allow comparison with exact diagonalization, and we extrapolate to the joint limit $\delta\tau \to 0$, $N_w \to \infty$ [127] and $m \to \infty$ to eliminate sources of systematic errors. As an example, we show in Figure 6.2 the extrapolations for a calculation with $(N_\uparrow, N_\downarrow, r_s, M) = (1, 1, 1, 49)$. Discrepancies with respect to the exact results are therefore due to the only uncontrolled approximations of the method, namely the real local energy and the phaseless approximations (5.85).

In Figure 6.3 we show results relative to the simulation of systems with $r_s = 1$, $M = 13$, for some values of $N_\uparrow$ and $N_\downarrow$. The left panels of the figure show the components of the stochastic solution on the Hilbert space basis functions. The little statistical fluctuations around the x axis show that the random walk visits a large number of states, while the significant components of the AFQMC solution match those of the exact ground state with good accuracy. The ITCF $F_{\boldsymbol{n}}(\tau)$ of the density fluctuation operator for $\mathbf{n} = (1, 0)$ is reported in the right column of Figure 6.3. The wave vector $\mathbf{n}$ has been chosen in the lowest energy shell since it gives rise to non-vanishing ITCFs even for small M. The agreement with exact values is remarkable, in particular if compared with the discrepancy observed for the FN result, Figure 5.1.

For all these systems we computed also the ground state energy per particle, and the overlap between exact and reconstructed ground state: the results are listed in table Table 6.1, the bias of the energy resulting of the order of 10^{-3}Ha, which is smaller than the FN bias using a Slater-Jastrow trial function with plane-wave nodes.

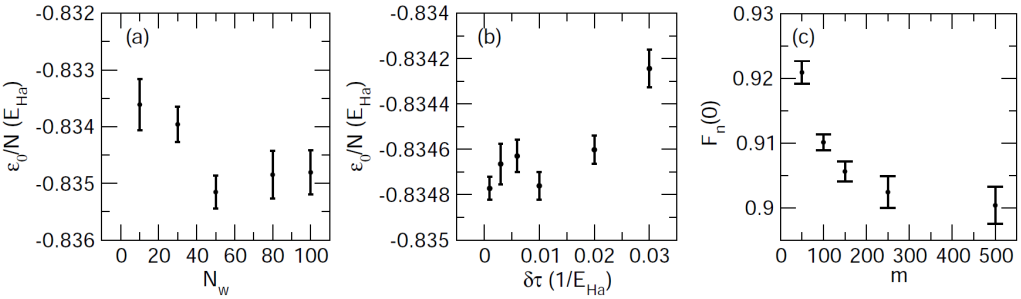

Figure 6.2: Steps of the convergence procedure for $(N_\uparrow, N_\downarrow, r_s, M) = (1, 1, 1, 49)$: (a) AFQMC estimate of the ground state energy per particle for several values of N_w at fixed $\delta\tau = 0.001$: N_w can be safely set to 80 (b) AFQMC estimate of the ground state energy per particle for several values of $\delta\tau$ at fixed $N_w = 80$: $\delta\tau$ can be safely set to 0.003 (c) AFQMC estimate of $F_{\mathbf{n}}(0)$ for several values of m at fixed $N_w = 80$, $\delta\tau = 0.003$: m can be safely set to $m = 250$

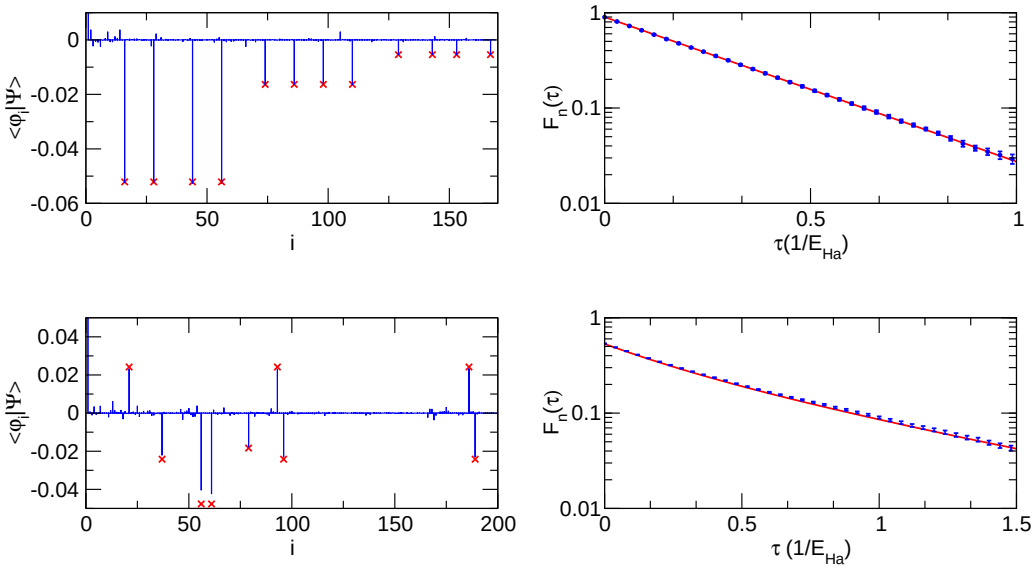

Figure 6.3: Left column: exact nonvanishing (red crosses) and reconstructed (blue columns) components of the ground state for systems with $N_\uparrow, N_\downarrow = (1,1), (5,0)$ (top to bottom), relative to all elements of the basis except $|\varphi_1\rangle = |\Psi_T\rangle$. Exact and reconstructed values of $\langle\varphi_1|\Psi\rangle$ are respectively $0.9937, 0.9939(2)$ and $0.9926, 0.9885(3)$. Right column: exact (red line) and reconstructed (circles) imaginary time correlation function of the density fluctuation operator with $\mathbf{n} = (1,0)$ for systems with $N_\uparrow, N_\downarrow = (1,1), (5,0)$ (top to bottom). When not visible, error bars are smaller than the symbol size.

6.3.3 Computational Issues

Although our primary interest is the assessment of the accuracy of AFQMC in calculating the ITCFs addressed in the previous section, we explored the behavior of the method for larger values of r_s and M.
As r_s increases, the interaction becomes more and more important, and the overlap of the exact wavefunction with the trial function becomes smaller. Also the increase in M, which is required for the study of realistic models, makes the stochastic exploration of the Hilbert space more difficult: in particular, the calculation of ITCFs is further complicated by the need of multiplying many exponentials of large matrices, see (6.21), which induces instabilities at large imaginary time. This problem is already known [271, 272, 274].
In Figure 6.4 appear results relative to systems with $N_\uparrow = 1$, $N_\downarrow = 1$, showing that AFQMC estimations of static and dynamic properties remain in satisfactory agreement with exact values even if M is raised to 49. Also for $M = 49$, the data in Figure 6.4 and Table 6.1 show that we are in good agreement with RQMC calculations, providing the exact result in the limit $M \to +\infty$, which cannot be explored via exact diagonalization.
The algorithm is able to reproduce exact values even at $r_s = 2, 3, 4$ and $M = 21$, as shown in Figure 6.5. Since it is known that the degree of correlation in the uniform electron gas is significantly higher in 2D than in 3D for given r_s, the range of densities covered well represents the typical realistic density values in 3D (up to $r_s \sim 5$).
We complete the study with calculations relative to systems with $N_\uparrow, N_\downarrow = (5, 0)$. Results are shown in Figure 6.6. For $M = 9$ the quality of AFQMC calculations is still satisfactory, even if we observe a small overestimate of $F_{\mathbf{n}}(\tau)$. Finally for $M = 97$ we compared our results with FN calculations. We observe good agreement between the estimates of the static property $F_{\mathbf{n}}(0)$ yield by both algorithms. As far as finite τ ITCFs are concerned, we found that the discrepancy between the two results qualitatively resembles the discrepancy between exact solution and FN in the case of non interacting particles in Fig. 5.1: an encouraging result.
To quantify the quality of the presented results, the reader may refer to Table 6.1, where we report an average reduced chi-squared:

$$\chi^2 = \frac{1}{N_\tau} \sum_{i=1}^{N_\tau} \frac{|F_n^{(AFQMC)}(\tau_i) - F_n(\tau_i)|^2}{\sigma_i^2} \tag{6.34}$$

N_τ being the number of imaginary times at which the ITCF is computed.

6.4 Numeric Stabilization

We have tested our extenstion of the phaseless AFQMC methodology to the calculation of ITCFs against exact diagonalization for interacting few-fermion systems. Such tests revealed that it is actually possible to compute ITCFs with satifactory accuracy, at least for systems with moderate number of particles and interaction strength. This is a very interesting result since it is known that there exist situations when the well-established and widely employed FN approximation scheme provides inaccurate results for ITCFs. Our analysis indicates that the AFQMC algorithm can become an accurate tool to calculate dynamical properties of few-body systems. However, the estimator (6.21) is negatively-conditioned by a form of numeric instability caused by the large number of matrix multiplications and exponentiations. The aim of the present Section is to elucidate the origin of such phenomenon and to propose a method for stabilizing the calculation of ITCFs

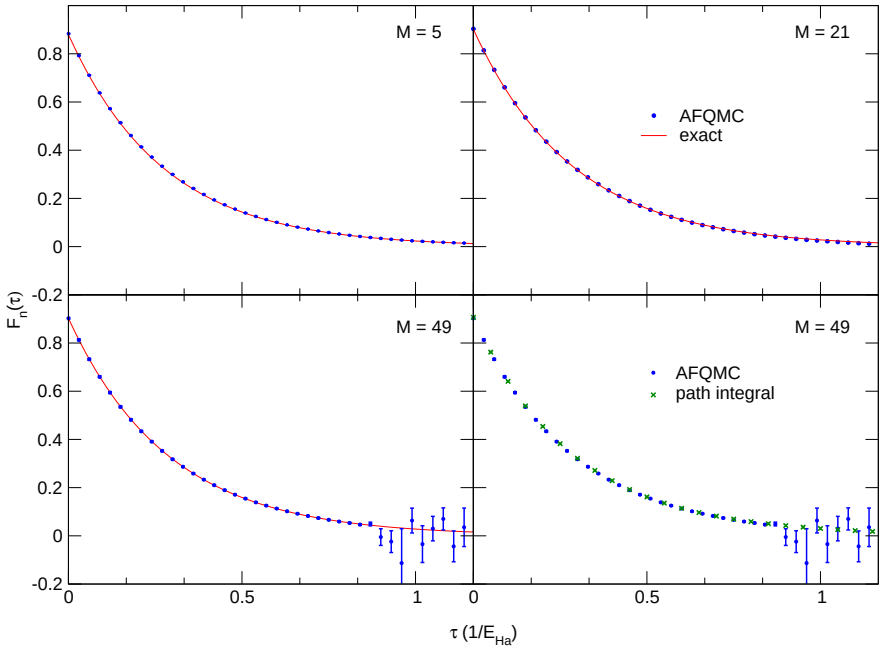

Figure 6.4: density-density ITCF relative to $M = 5, 21, 49$ at $r_s = 1$ for $N_\uparrow = 1, N_\downarrow = 1$. In the right lower box, comparison between AFQMC and exact RQMC calculations is given. When not visible, error bars are smaller than the symbol size.

$N_\uparrow$	$N_\downarrow$	r_s	M	$\epsilon_0/N(AFQMC)$	$\epsilon_0/N(exact)$	$\langle\Phi_0\|\Psi\rangle$	χ^2
1	1	1	5	-0.82255(5)	-0.82259	0.99999(5)	1.02
1	1	1	13	-0.8315(1)	-0.8313	0.9999(1)	0.02
1	1	1	21	-0.83338(6)	-0.83307	0.9989(7)	0.09
1	1	1	49	-0.83476(7)	-0.83441	0.9882(4)	0.04
1	1	2	5	-0.4282(1)	-0.4282	0.9629(3)	0.97
1	1	2	13	-0.4351(1)	-0.4330	0.9650(2)	0.87
1	1	2	21	-0.4359(3)	-0.4339	0.9586(2)	0.90
1	1	2	49	-0.4362(3)	-0.4345	0.9594(5)	0.32
1	1	3	21	-0.3020(3)	-0.2972	0.9253(8)	0.05
1	1	4	21	-0.2320(4)	-0.2272	0.904(1)	0.70
5	0	1	9	0.11327(2)	0.11247	0.99185(1)	0.69
5	0	1	13	0.10726(3)	0.10591	0.98600(7)	2.87
5	0	2	9	-0.19485(1)	-0.19751	0.9863(4)	1.09
5	0	2	13	-0.19878(2)	-0.20311	0.9683(3)	1.02

Table 6.1: Exact (column 6) and calculated (column 5) ground-state energy per particle in Hartree units, and overlap between exact and reconstructed ground state (column 7) for various systems (parameters are listed in columns 1 to 4). Values (column 8) of χ^2 (6.34).

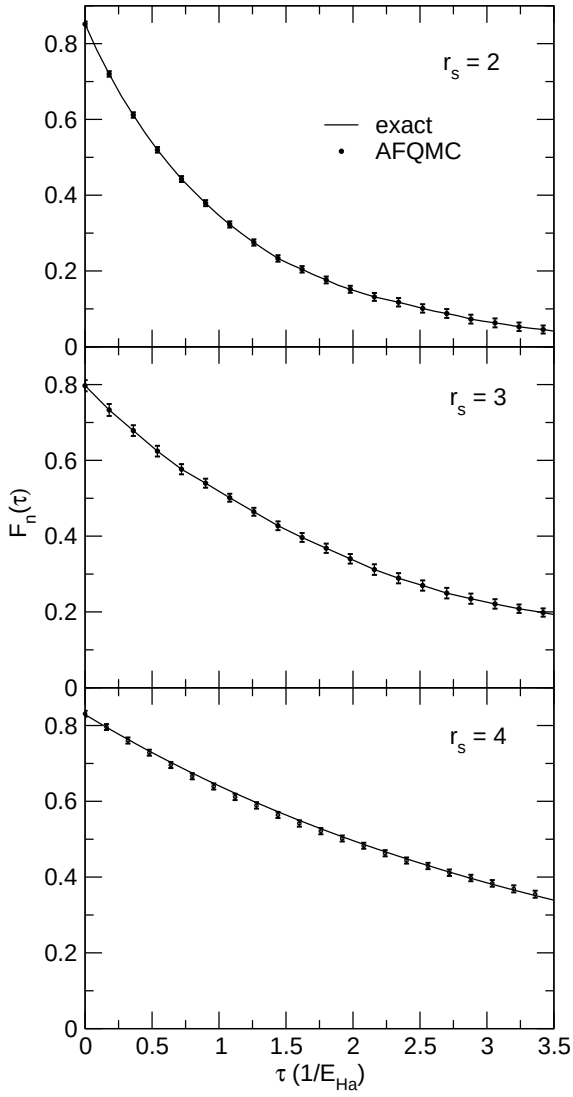

Figure 6.5: density-density ITCF relative to $r_s = 2, 3, 4$ (top to bottom) for $N_\uparrow = 1, N_\downarrow = 1$ at $M = 21$. When not visible, error bars are smaller than the symbol size.

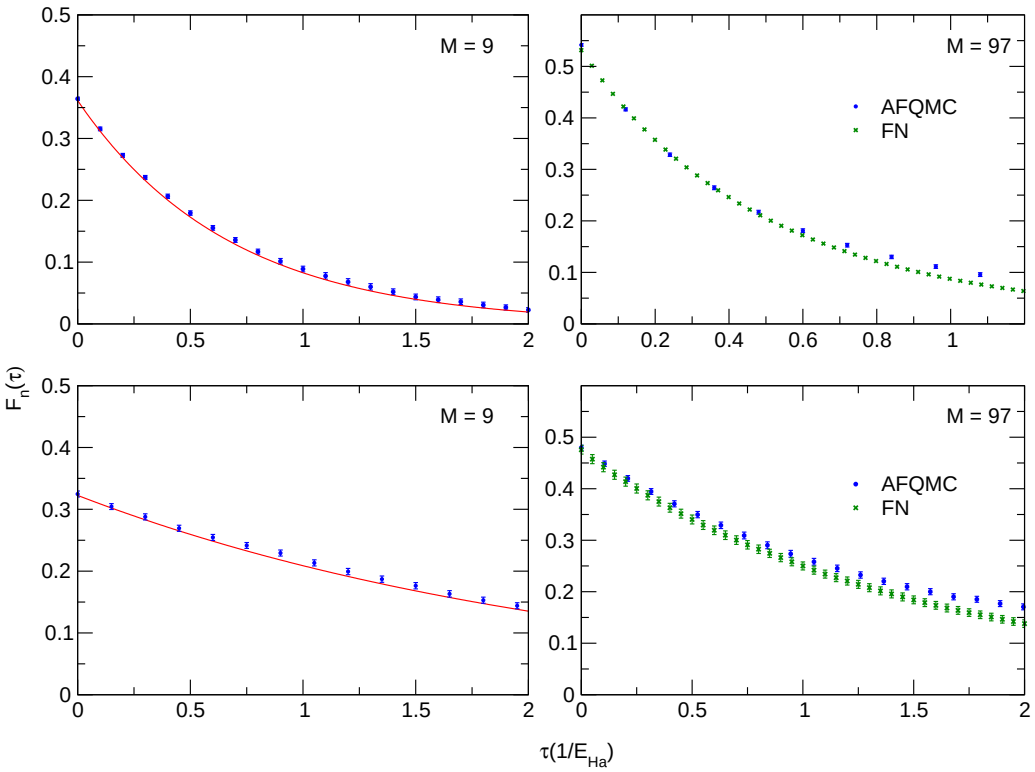

Figure 6.6: Density-density ITCF relative to $M = 9, 97$ at $r_s = 1$ (upper panel) and to $M = 13, 97$ at $r_s = 2$ (lower panel) for $N_\uparrow = 5, N_\downarrow = 0$. In the right box of each panel comparison between AFQMC and FN calculations (green crosses) is given. When not visible, error bars are smaller than the symbol size.

in AFQMC. The AFQMC estimator (6.21) of the ITCF $F_{\hat{A},\hat{B}}(\tau)$ involves a weighted average, over the random paths followed by the N_w walkers employed in the simulation, of a quantity in which the matrix elements of $\mathcal{D}$ and $\mathcal{D}^{-1}$ appear. $\mathcal{D}$ and $\mathcal{D}^{-1}$ need to be computed numerically, respectively as product of r matrices and inverse of $\mathcal{D}$. It is well-known, and better explained in Appendix 13.4.2, that the numerical computation of $\mathcal{D}$ and $\mathcal{D}^{-1}$ introduces rounding-off errors [275], which accumulate as r increases with detrimental impact on the results of the computation.

Rounding-off errors are particularly severe when the ∞-norm condition number:

$$\kappa(\mathcal{D}) = \|\mathcal{D}\|_\infty \|\mathcal{D}^{-1}\|_\infty \tag{6.35}$$

of the matrix $\mathcal{D}$, in which $\|A\|_\infty = \max_{ij} |A_{ij}|$ denotes the ∞-norm on the space of $M \times M$ complex-valued matrices, is large. For the systems under study, we observe a condition number roughly increasing as $\kappa(\mathcal{D}) \simeq C_1^r$ for some constant C_1. The rapid increase of $\kappa(\mathcal{D})$ indicates that the numeric matrix inversion $\mathcal{I}(\mathcal{D})$ used to estimate $\mathcal{D}^{-1}$ might be ill-conditioned, an intuition that can be confirmed by studying the figure of merit:

$$\|E\|_\infty = \|\mathbb{I} - \mathcal{D}\mathcal{I}(\mathcal{D})\|_\infty \tag{6.36}$$

For small r, $\frac{\|E\|_\infty}{M}$ is comparable with the machine precision $\epsilon = 10^{-16}$; it then increases as C_2^r for some constant C_2 and eventually saturates around 1. In Appendix (13.4.2) a qualitative explanation of the power-law increase of $\frac{\|E\|_\infty}{M}$ is provided. The gradual corruption of data revealed by the increase of $\|E\|_\infty$ reflects, as illustrated in figure (6.7), on the quality of the AFQMC estimates of ITCFs, which combine the matrix elements of $\mathcal{D}$ and $\mathcal{I}(\mathcal{D})$ as prescribed by (6.21). We propose to mitigate the numeric instability of the ITCF estimator by performing a Tikhonov regularization [97] of the numeric inverse $\mathcal{I}(\mathcal{D})$. Practically, the SVD of $\mathcal{D}$ is computed:

$$\mathcal{D} = U \mathrm{diag}(\sigma_1 \dots \sigma_M) V^\dagger \tag{6.37}$$

and $\mathcal{I}(\mathcal{D})$ is obtained as:

$$\mathcal{I}(\mathcal{D}) = V \mathrm{diag}(\tilde{\sigma}_1 \dots \tilde{\sigma}_M) U^\dagger \tag{6.38}$$

where $\tilde{\sigma}_i = \frac{\sigma_i}{\lambda^2 + \sigma_i^2}$ is defined by a regularization parameter λ. Large singular values $\sigma_i \gg \lambda$ are mapped to $\tilde{\sigma}_i \simeq \frac{1}{\sigma_i}$, while small singular values $\sigma_i \ll \lambda$ are kept below the threshold $\frac{1}{2\lambda}$. Particular care must be taken in choosing the regularization parameter λ, since for small λ the Tikhonov regularization is clearly ineffective, while for large λ it provokes a severe alteration in $\mathcal{I}(\mathcal{D})$. On the other hand, an intermediate value of λ prevents small errors in $\mathcal{D}$, associated to small singular values σ_i, to be dramatically amplified by the numeric inversion.

The effect of the Tikhonov regularization has been probed considering the model systems of 2 particles introduced earlier in the present Chapter, for which exact numeric solution of the Hamiltonian eigenvalue problem is feasible, and thus the ITCFs is exactly known. In Figure 6.7 we show the effect of the Tikhonov regularization (6.38) on the ITCFs. The results show the existence of a broad interval of λ, comprising the machine precision $\epsilon = 10^{-16}$, for which the Tikhonov regularization mitigates the numeric instability affecting the AFQMC estimator of ITCFs without introducing any appreciable bias besides that introduced by the real local energy and phaseless approximations. The figure displays, in the upper and lower panel respectively, the statistical errors of the AFQMC estimations and the discrepancies with respect to the exact results for three

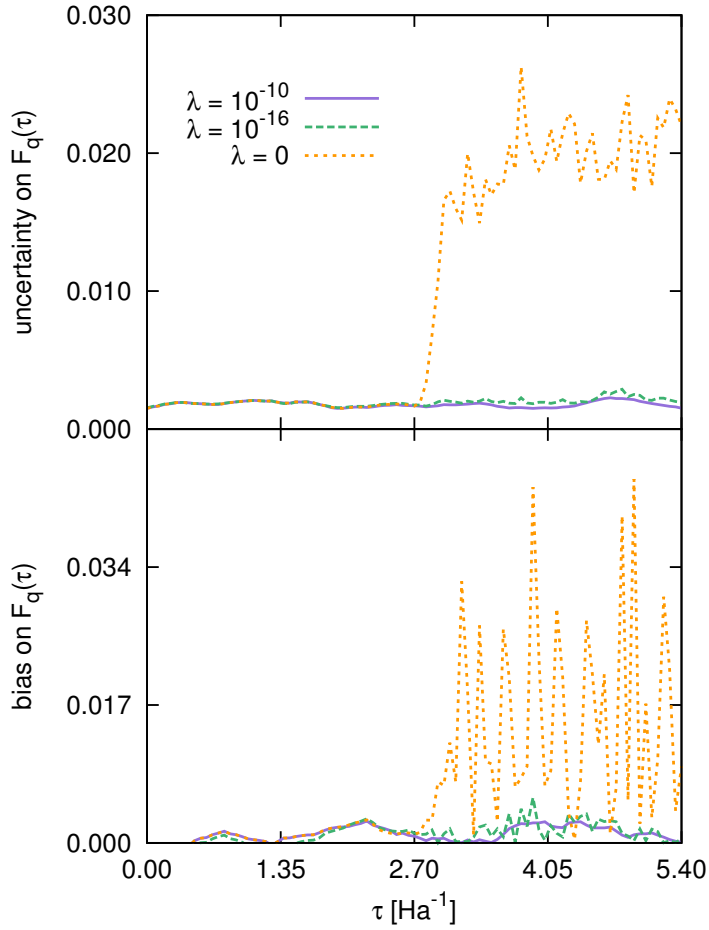

Figure 6.7: Effect of the Tykhonoff regularization (6.38) on the ITCF relative to a system of $N = 2$ electrons with $M = 21$ basis set elements. Upper panel: statistical uncertainty affecting the AFQMC estimate of $F(q, \tau)$ with $\lambda = 10^{-10}$ (lavender solid lines), $\lambda = 10^{-16}$ (green dashed lines) and $\lambda = 0$ (orange dotted lines). Lower panel: bias affecting the AFQMC estimate of $F(\mathbf{q}, \tau)$.

different values of λ. It is evident that, as the imaginary time becomes large, the effect of the regularization is very important.

CHAPTER 7

Imaginary-time correlations of high-density two-dimensional electron gases

In the present Chapter, the recent work [276] is presented. We pursue our study of imaginary-time correlation applying the phaseless AFQMC to 2D homogeneous electron gases of up to 42 particles, assessing the ability of the methodology to accurately compute ITCFs for medium-sized fermion systems.

7.1 Introduction

The study performed in Chapter 6 has shown that the phaseless AFQMC method can provide very accurate estimations of ITCFs for few-body systems.
This encouraging results, however, does not grant that the methodology is able to provide accurate quantitative results for larger systems. In the present Chapter, the phaseless AFQMC method is applied to the calculation of ITCFs for much larger systems. We evaluate density-density correlation functions $F(\mathbf{q}, \tau)$ for two-dimensional homogeneous electron gases (HEGs) of up to 42 particles and we perform their inverse Laplace transform to extract information about the excitations of the system.
We finally assess the accuracy of the calculations comparing AFQMC results with predictions within the random phase approximation (RPA) for finite systems [4, 277], and results of FN DMC calculations [123, 99], performed with a nodal surface specified by backflow correlations optimized with the Linear Method presented in Section 2.4.
The calculation of ITCFs is much more difficult than the calculation of ground-state properties. Indeed, in the long imaginary time limit, the estimates of ITCFs are affected by a form of numerical instability that becomes more and more severe as the number of particles is increased. We therefore employ the stabilization technique introduced in Chapter 6, that proved unnecessary for few-fermions systems, for improving the quality of ITCFs output by AFQMC calculations.
The difficulties related to the stabilization of ITCFs, and the need of simulating finite systems with a finite basis set in the single-particle Hilbert space, clearly provide some limitations. In the particular case of the HEG calculations become more demanding as the density is decreased. First, decreasing the density, the number of plane waves required to reach convergence in the basis set size increases. Moreover, density-density ITCFs decay in a typical time τ^* which increases with density: these circumstance make the calculation of ITCFs more demanding. Therefore, we focus on the high-density regime, which is nevertheless extremely interesting as the presence of the interaction leads to important correlation effects, enhanced by the low dimensionality.

7.2 The two-dimensional homogeneous electron gas

The homogeneous electron gas (HEG) is one of the most widely studied systems in condensed matter Physics [278, 279, 280, 125, 6, 281]. It represents a model of recognized importance, which offers the opportunity to explore the quantum behavior of many-body systems on a fundamental basis and provides a ground test for several quantum chemistry [282], many-body [4] and quantum Monte Carlo (QMC) [125, 104, 60, 283] methodologies. Furthermore, recent years have witnessed the realization of increasingly high-quality two-dimensional (2D) HEGs in devices of considerable experimental interest such as quantum-well structures [284, 285] and field-effect transistors [286].

The 2D HEG is a system of charged spin-$\frac{1}{2}$ fermions interacting with the Coulomb potential and immersed in a uniform positively-charged background. For the purpose of studying the 2D HEG we simulate a system of N particles moving inside a square region $\mathcal{R}$ of surface $\Omega = L^2$, employing periodic boundary conditions (PBC) at the boundaries of the simulation domain, in conjunction with an Ewald summation procedure [287], described in greater detail in Appendix 13.1. We measure energies in Hartree units E_{Ha}, and lengths in Bohr radii a_B. The Hamiltonian of the system reads, in such units:

$$\hat{H} = \sum_{\mathbf{k}\sigma} \frac{|\mathbf{k}|^2}{2} \hat{a}^\dagger_{\mathbf{k}\sigma} \hat{a}_{\mathbf{k}\sigma} + \frac{1}{2\Omega} \sum_{\mathbf{q}\neq 0} \frac{2\pi}{|\mathbf{q}|} \sum_{\substack{\mathbf{k}\sigma \\ \mathbf{p}\varsigma}} \hat{a}^\dagger_{\mathbf{k}+\mathbf{q}\sigma} \hat{a}^\dagger_{\mathbf{p}-\mathbf{q}\varsigma} \hat{a}_{\mathbf{p}\varsigma} \hat{a}_{\mathbf{k}\sigma} \tag{7.1}$$

where spin-definite plane waves:

$$\varphi_{\mathbf{k}\sigma}(\mathbf{r}, \omega) = \frac{e^{i\mathbf{k}\cdot\mathbf{r}}}{\sqrt{\Omega}} \chi_\sigma(\omega) \quad \frac{L}{2\pi}\mathbf{k} \in \mathbb{Z}^2, \ \sigma = \uparrow, \downarrow \tag{7.2}$$

are used as a basis for the single-particle Hilbert space. Naturally, in a numeric calculation the wavevectors (7.2) must be truncated to some cutoff level $|\mathbf{k}| \leq k_{cut}$. We denote $\mathcal{B}$ the set of such wavevectors. The number N_b of elements in $\mathcal{B}$ can be roughly estimated using the Euler-Maclaurin integration formula:

$$N_b = \sum_{|\mathbf{k}|\leq k_{cut}} 1 \simeq \left(\frac{L}{2\pi}\right)^2 \pi \int_0^{k_{cut}} dk k = \frac{\pi}{2} \left(\frac{L}{2\pi} k_{cut}\right)^2 \tag{7.3}$$

Also the set of transferred wavevectors $\mathbf{q}$ must be truncated. If the summation over $\mathbf{k}, \mathbf{p}$ in (7.1) is restricted to $\mathcal{B}$, and we require that also $\mathbf{k}+\mathbf{q}, \mathbf{p}-\mathbf{q}$ are in $\mathcal{B}$, only wavevectors $\mathbf{q}$ in the set $\mathcal{T}$ defined by:

$$\mathcal{T} = \left\{ \mathbf{q} : \frac{L}{2\pi}\mathbf{q} \in \mathbb{Z}^2 \text{ and } \mathbf{k}+\mathbf{q} \in \mathcal{B} \text{ for some } \mathbf{k} \in \mathcal{B} \right\} \tag{7.4}$$

give non-zero contributions to the summation in (7.1). If $\mathbf{q} \in \mathcal{T}$, by the triangle inequality:

$$|\mathbf{q}| = |\mathbf{k}+\mathbf{q}-\mathbf{k}| \leq |\mathbf{k}+\mathbf{q}| + |\mathbf{k}| \leq 2k_{cut} \tag{7.5}$$

whence the number N_t of elements in $\mathcal{T}$ can be roughly estimated as:

$$N_t \simeq \sum_{|\mathbf{k}|\leq 2k_{cut}} 1 \simeq \frac{\pi}{2} \left(\frac{L}{2\pi} 2k_{cut}\right)^2 \simeq 4N_b \tag{7.6}$$

The ground-state energy per particle of the system is obtained adding, to the mean value of (7.1), the corrective constant term:

$$\xi = \frac{1}{2L}\left[2\sum_{\substack{\mathbf{n}\in\mathbb{Z}^2\\ \mathbf{n}\neq\mathbf{0}}}\frac{\mathrm{erfc}\,(\sqrt{\pi}|\mathbf{n}|)}{|\mathbf{n}|} - 4\right] = -3.900265\,\frac{1}{2L} \tag{7.7}$$

arising from the Ewald summation procedure employed [287]. The Hamiltonian (7.1) can be parametrized in terms of the dimensionless Seitz radius r_s, defined by:

$$\frac{\Omega}{N} = \frac{1}{\rho} = \pi r_s^2 a_B^2 \tag{7.8}$$

where ρ is the density of the system and a_B the Bohr radius. This parametrization shows that the matrix elements of the kinetic energy roughly scale as $|\mathbf{k}|^2 \simeq r_s^{-2}$, and those of the potential energy as $1/\Omega|\mathbf{q}| \simeq r_s^{-1}$. Thus, for increasing Seitz radius, the interaction part of $\hat{H}$ plays a more and more relevant role.

This intuition is confirmed considering the ground-state energy per particle of the Hartree-Fock Slater determinant:

$$|\Psi_T\rangle = \prod_{\sigma=\uparrow,\downarrow}\prod_{|\mathbf{k}|\leq k_F}\hat{a}^\dagger_{\mathbf{k}\sigma}\,|0\rangle \tag{7.9}$$

which is derived in detail in [6]. Since:

$$\mathcal{T} = \lim_{N\to\infty}\mathcal{T}_N = \lim_{N\to\infty}\frac{1}{N}\langle\Psi_T|\hat{T}|\Psi_T\rangle = \frac{\alpha_d}{r_s^2}\,E_{Ha} \tag{7.10}$$

where $\alpha_d = 0.500$ (1.105) for a 2D (3D) system, and:

$$\mathcal{V} = \lim_{N\to\infty}\mathcal{V}_N = \lim_{N\to\infty}\frac{1}{N}\langle\Psi_T|\hat{V}|\Psi_T\rangle = \frac{\beta_d}{r_s}\,E_{Ha} \tag{7.11}$$

where $\beta_d = -0.600$ (0.458) for a 2D (3D) system, the ratio between kinetic and potential energy per particle, which provides a rough measure of their relative importance, reads:

$$\frac{\mathcal{V}}{\mathcal{T}} = \frac{\beta_d}{\alpha_d}r_s \tag{7.12}$$

since $\frac{\beta_d}{\alpha_d} = 1.200$ (0.415) for a 2D (3D) system, the low dimensionality enhances the relevance of the potential energy. A 2D system at $r_s = 1$ (2) is roughly correlated as a 3D system with $r_s = 2.9$ (5.8).

7.3 Hubbard-Stratonovich Transformation in the plane-wave basis set

For a very general Hamiltonian like (5.38), the operator $\hat{G}(\eta)$ is given by (5.58), (5.59), and its structure is specified through a procedure that might result lengthy and computationally expensive.

When spin-definite plane waves are used as a basis for the single-particle Hilbert space,

and the interaction part of the Hamiltonian has the form:

$$\hat{H} = \sum_{\mathbf{k}\sigma} t_{\mathbf{k}}\, \hat{a}^{\dagger}_{\mathbf{k}\sigma}\hat{a}_{\mathbf{k}\sigma} + \frac{1}{2\Omega}\sum_{\mathbf{q}\neq 0}\phi_{\mathbf{q}}\hat{a}^{\dagger}_{\mathbf{k}+\mathbf{q}\sigma}\hat{a}^{\dagger}_{\mathbf{p}-\mathbf{q}\varsigma}\hat{a}_{\mathbf{p}\varsigma}\hat{a}_{\mathbf{k}\sigma} = \hat{H}_0 + \frac{1}{2\Omega}\sum_{\mathbf{q}\neq 0}\phi_{\mathbf{q}}\hat{a}^{\dagger}_{\mathbf{k}+\mathbf{q}\sigma}\hat{a}^{\dagger}_{\mathbf{p}-\mathbf{q}\varsigma}\hat{a}_{\mathbf{p}\varsigma}\hat{a}_{\mathbf{k}\sigma} \tag{7.13}$$

which reduces to (7.1) when $t_{\mathbf{k}} = \frac{|\mathbf{k}|^2}{2}$ and $\phi_{\mathbf{q}} = \frac{2\pi}{|\mathbf{q}|}$, a remarkable simplification occurs.

In fact, by a straightforward application of the canonical anticommutation relations, the Hamiltonian (7.1) can be exactly rewritten as:

$$\hat{H} = \sum_{\mathbf{k}\sigma}\left(\frac{|\mathbf{k}|^2}{2} - \mu(\mathbf{k})\right)\hat{a}^{\dagger}_{\mathbf{k}\sigma}\hat{a}_{\mathbf{k}\sigma} + \frac{1}{2\Omega}\sum_{\mathbf{q}}\frac{2\pi}{|\mathbf{q}|}\hat{\rho}_{\mathbf{q}}\hat{\rho}_{-\mathbf{q}} \tag{7.14}$$

where:

$$\mu(\mathbf{k}) = \frac{1}{2\Omega}\sum_{\mathbf{p}\neq\mathbf{k}}\frac{2\pi}{|\mathbf{p}-\mathbf{k}|} \tag{7.15}$$

and $\hat{\rho}_{\mathbf{q}} = \sum_{\mathbf{k}\sigma}\hat{a}^{\dagger}_{\mathbf{k}-\mathbf{q}\sigma}\hat{a}_{\mathbf{k}\sigma}$ is the density fluctuation operator. Recalling the parity of $\frac{2\pi}{|\mathbf{q}|}$ and the anticommutation relation:

$$[\hat{\rho}_{\mathbf{q}}, \hat{\rho}_{-\mathbf{q}}]_+ = \frac{(\hat{\rho}_{\mathbf{q}} + \hat{\rho}_{-\mathbf{q}})^2}{2} + \frac{(i\hat{\rho}_{\mathbf{q}} - i\hat{\rho}_{-\mathbf{q}})^2}{2} \tag{7.16}$$

one eventually finds:

$$\hat{H} = \hat{H}_0 + \frac{1}{2}\sum_{\mathbf{q}}\left(\hat{A}_1(\mathbf{q})^2 + \hat{A}_2(\mathbf{q})^2\right) \tag{7.17}$$

with:

$$\hat{H}_0 = \sum_{\mathbf{k}\sigma}\left(\frac{|\mathbf{k}|^2}{2} - \mu(\mathbf{k})\right)\hat{a}^{\dagger}_{\mathbf{k}\sigma}\hat{a}_{\mathbf{k}\sigma} \tag{7.18}$$

and:

$$\hat{A}_1(\mathbf{q}) = \sqrt{\frac{2\pi}{\Omega|\mathbf{q}|}}\,\frac{\hat{\rho}_{\mathbf{q}} + \hat{\rho}_{-\mathbf{q}}}{2} \quad \hat{A}_2(\mathbf{q}) = \sqrt{\frac{2\pi}{\Omega|\mathbf{q}|}}\,\frac{i\hat{\rho}_{\mathbf{q}} - i\hat{\rho}_{-\mathbf{q}}}{2} \tag{7.19}$$

which, since $\hat{\rho}_{-\mathbf{q}} = \hat{\rho}^{\dagger}_{\mathbf{q}}$, are hermitian operators. Applying the Hubbard-Stratonovich transformation to the propagator of the Hamiltonian (7.21) yields:

$$\hat{G}(\boldsymbol{\eta}) = e^{-\frac{\delta\tau}{2}\hat{H}_0}e^{-i\sqrt{\delta\tau}\sum_{\mathbf{q}\neq 0}\eta_{1\mathbf{q}}\hat{A}_1(\mathbf{q}) + \eta_{2\mathbf{q}}\hat{A}_2(\mathbf{q})}e^{-\frac{\delta\tau}{2}\hat{H}_0} \tag{7.20}$$

with:

$$\hat{H}_0 = \sum_{\mathbf{k}\sigma}\left(\frac{|\mathbf{k}|^2}{2} - \frac{1}{2\Omega}\sum_{\mathbf{p}\neq\mathbf{k}}\frac{2\pi}{|\mathbf{p}-\mathbf{k}|}\right)\hat{a}^{\dagger}_{\mathbf{k}\sigma}\hat{a}_{\mathbf{k}\sigma} = \sum_{\mathbf{k}\sigma}\left(\mathcal{H}_0\right)_{\mathbf{k}}\,\hat{a}^{\dagger}_{\mathbf{k}\sigma}\hat{a}_{\mathbf{k}\sigma} \tag{7.21}$$

and:

$$\hat{A}_1(\mathbf{q}) = \sqrt{\frac{2\pi}{\Omega|\mathbf{q}|}}\,\frac{\hat{\rho}_{\mathbf{q}} + \hat{\rho}_{-\mathbf{q}}}{2} \quad \hat{A}_2(\mathbf{q}) = \sqrt{\frac{2\pi}{\Omega|\mathbf{q}|}}\,\frac{i\hat{\rho}_{\mathbf{q}} - i\hat{\rho}_{-\mathbf{q}}}{2} \tag{7.22}$$

The operators (7.22) will be henceforth written as:

$$\hat{A}_s(\mathbf{q}) = \sum_{\mathbf{kp}\sigma} \left(\mathcal{A}_s(\mathbf{q})\right)_{\mathbf{kp}} \hat{a}^\dagger_{\mathbf{k}\sigma}\hat{a}_{\mathbf{p}\sigma} \tag{7.23}$$

with:

$$\left(\mathcal{A}_1(\mathbf{q})\right)_{\mathbf{kp}} = \sqrt{\frac{2\pi}{\Omega|\mathbf{q}|}}\,\frac{\delta_{\mathbf{k},\mathbf{p}+\mathbf{q}} + \delta_{\mathbf{k},\mathbf{p}-\mathbf{q}}}{2} \quad , \qquad \left(\mathcal{A}_2(\mathbf{q})\right)_{\mathbf{kp}} = \sqrt{\frac{2\pi}{\Omega|\mathbf{q}|}}\,\frac{i\delta_{\mathbf{k},\mathbf{p}+\mathbf{q}} - i\delta_{\mathbf{k},\mathbf{p}-\mathbf{q}}}{2} \tag{7.24}$$

We remind that formulae (7.20),(7.21) and (7.22) result from an exact calculation. The number of auxiliary fields involved in (7.20) is $2N_t \simeq 8N_b = 4M$. For large systems, this is a considerable decrease in comparison with the general case, when the number of auxiliary fields is $2M^2 \gg 4M$.

7.4 Evaluation of the local energy

In Section we have seen that the calculation of the local energy can require up to $\mathcal{O}(N^2M^2)$ operations. For the Hamiltonian (7.25), it is possible to push the complexity of that operation down to $\mathcal{O}(N^2M)$. Let us first write (7.25) as:

$$\hat{H} = \sum_\sigma \hat{H}_\sigma + \sum_\sigma \hat{H}_{\sigma,\overline{\sigma}} \tag{7.25}$$

with:

$$\begin{aligned}
\hat{H}_\sigma &= \sum_{\mathbf{k}} t_{\mathbf{k}}\,\hat{a}^\dagger_{\mathbf{k}\sigma}\hat{a}_{\mathbf{k}\sigma} + \frac{1}{2\Omega}\sum_{\mathbf{k},\mathbf{p}}\sum_{\mathbf{q}\neq 0}\phi_{\mathbf{q}}\hat{a}^\dagger_{\mathbf{k}+\mathbf{q}\sigma}\hat{a}^\dagger_{\mathbf{p}-\mathbf{q}\sigma}\hat{a}_{\mathbf{p}\sigma}\hat{a}_{\mathbf{k}\sigma} \\
\hat{H}_{\sigma,\overline{\sigma}} &= \frac{1}{2\Omega}\sum_{\mathbf{q}\neq 0}\phi_{\mathbf{q}}\sum_{\mathbf{k},\mathbf{p}}\hat{a}^\dagger_{\mathbf{k}+\mathbf{q}\sigma}\hat{a}^\dagger_{\mathbf{p}-\mathbf{q}\overline{\sigma}}\hat{a}_{\mathbf{p}\overline{\sigma}}\hat{a}_{\mathbf{k}\sigma}
\end{aligned} \tag{7.26}$$

The term $\sum_\sigma \hat{H}_\sigma$ is a summation over the spin polarizations $\sigma = \uparrow, \downarrow$; in the second term $\overline{\uparrow} = \downarrow$, $\overline{\uparrow} = \downarrow$, and thus it mixes different spin polarizations.

The most natural choice of the trial state is the Hartree-Fock determinant, which is the tensor product of two Fermi spheres with radii $k_{F,\uparrow}, k_{F,\downarrow}$ corresponding to the lowest-energy $N_\uparrow$, $N_\downarrow$ plane waves respectively. The matrix describing Ψ_T has the block form (5.12), with:

$$U = \begin{pmatrix} 1 \\ 0 \end{pmatrix} \quad , \qquad V = \begin{pmatrix} 1 \\ 0 \end{pmatrix} \tag{7.27}$$

the identity matrices having orders $N_\uparrow, N_\downarrow$ respectively. Since $\hat{H}_{\sigma,\overline{\sigma}} = \hat{H}_{\overline{\sigma},\sigma}$, the contribution to the local energy brought by the second term of (7.25) reads:

$$\langle \sum_\sigma \hat{H}_{\sigma,\overline{\sigma}} \rangle = \frac{1}{\Omega}\sum_{|\mathbf{k}|\leq k_{F,\uparrow}}\sum_{|\mathbf{p}|\leq k_{F,\downarrow}}\sum_{\mathbf{q}\neq 0}\phi_{\mathbf{q}}\mathcal{G}^{(mix)}_{\mathbf{k}\uparrow,\mathbf{k}+\mathbf{q}\uparrow}\,\mathcal{G}^{(mix)}_{\mathbf{p}\downarrow,\mathbf{p}-\mathbf{q}\downarrow} \tag{7.28}$$

requiring $\mathcal{O}(N_t N_\uparrow N_\downarrow) = \mathcal{O}(MN^2)$ operations. Similarly:

$$\langle \hat{H}_\sigma \rangle = \sum_{|\mathbf{k}|\leq k_{F,\sigma}} t_{\mathbf{k}} + \frac{1}{2\Omega} \sum_{|\mathbf{k}|\leq k_{F,\sigma}} \sum_{|\mathbf{p}|\leq k_{F,\sigma}} \left(\mathcal{G}^{(mix)}_{\mathbf{k}\sigma,\mathbf{k}+\mathbf{q}\sigma} \mathcal{G}^{(mix)}_{\mathbf{p}\sigma,\mathbf{p}-\mathbf{q}\sigma} - \mathcal{G}^{(mix)}_{\mathbf{k}\sigma,\mathbf{p}-\mathbf{q}\sigma} \mathcal{G}^{(mix)}_{\mathbf{p}\sigma,\mathbf{k}+\mathbf{q}\sigma} \right) \quad (7.29)$$

requiring $\mathcal{O}(N_t N_\sigma^2) = \mathcal{O}(MN^2)$ operations. Since the interaction part of $\hat{H}_\sigma$ is a symmetric function of $\mathbf{k}, \mathbf{p}$ that vanishes for $\mathbf{k} = \mathbf{p}$, the summation over $\mathbf{k}, \mathbf{p}$ below $k_{F,\sigma}$ can be further restricted, leading to a more efficient estimator.

7.5 Evaluation of the density-fluctuation ITCF

The estimator of the density-density ITCF $F(\mathbf{q}, \tau)$ has the general form derived in Section (6.1), but with some simplifications due to the simple structure of the density fluctuation operator. With the choice:

$$\hat{A} = \hat{\rho}_{\mathbf{q}} \sum_{\mathbf{k},\mathbf{p}} \sum_{\sigma} \delta_{\mathbf{k},\mathbf{p}-\mathbf{q}} \hat{a}^\dagger_{\mathbf{k}\sigma} \hat{a}_{\mathbf{p}\sigma} \quad (7.30)$$

the estimator of $F(\mathbf{q}, r\delta\tau)$ takes the form:

$$F(\mathbf{q}, r\delta\tau) \simeq \frac{1}{N} \frac{\sum_{w=1}^{N_w} \mathfrak{W}^{(w)}_{(n+m)\delta\tau}}{\sum_{w=1}^{N_w} \mathfrak{W}^{(w)}_{(n+m-r)\delta\tau}} \sum_{w=1}^{N_w} \frac{\mathfrak{W}^{(w)}_{(n+m)\delta\tau}}{\sum_{w=1}^{N_w} \mathfrak{W}^{(w)}_{(n+m)\delta\tau}} F_w = \sum_w \mathcal{P}_w F_w \quad (7.31)$$

with:

$$F_w = \sum_{\mathbf{k},\mathbf{k}',\mathbf{k}''} \sum_{\mathbf{p},\mathbf{p}',\mathbf{p}''} \sum_{\sigma\sigma''} \delta_{\mathbf{k},\mathbf{p}-\mathbf{q}} \; \delta_{\mathbf{k}',\mathbf{p}'+\mathbf{q}} \; \mathcal{D}_{\mathbf{k}'',\mathbf{k}'} \mathcal{D}^{-1}_{\mathbf{p}',\mathbf{p}''} \langle \hat{a}^\dagger_{\mathbf{k}\sigma} \hat{a}_{\mathbf{p}\sigma} \hat{a}^\dagger_{\mathbf{k}'',\sigma''} \hat{a}_{\mathbf{p}'',\sigma''} \rangle_w \quad (7.32)$$

The abbreviations , (6.25) have been used. Elimination of the Kronecker deltae yields:

$$F_w = \sum_{\mathbf{k},\mathbf{k}''} \sum_{\mathbf{p}',\mathbf{p}''} \sum_{\sigma\sigma''} \mathcal{D}_{\mathbf{k}'',\mathbf{p}'+\mathbf{q}} \mathcal{D}^{-1}_{\mathbf{p}',\mathbf{p}''} \langle \hat{a}^\dagger_{\mathbf{k}\sigma} \hat{a}_{\mathbf{k}+\mathbf{q}\sigma} \hat{a}^\dagger_{\mathbf{k}'',\sigma''} \hat{a}_{\mathbf{p}'',\sigma''} \rangle_w \quad (7.33)$$

using the generalized Wick's theorem, we obtain:

$$\langle \hat{a}^\dagger_{\mathbf{k}\sigma} \hat{a}_{\mathbf{k}+\mathbf{q}\sigma} \hat{a}^\dagger_{\mathbf{k}'',\sigma''} \hat{a}_{\mathbf{p}'',\sigma''} \rangle_w = \mathcal{G}_{\mathbf{k}+\mathbf{q}\sigma,\mathbf{k}\sigma} \mathcal{G}_{\mathbf{p}''\sigma'',\mathbf{k}''\sigma''} + \delta_{\sigma,\sigma''} \left(\delta_{\mathbf{k}'',\mathbf{k}+\mathbf{q}} - \mathcal{G}_{\mathbf{k}+\mathbf{q}\sigma,\mathbf{k}''\sigma} \right) \quad (7.34)$$

inserting which in (7.33) yields the estimator:

$$\begin{aligned} F_w = & \left(\sum_{\mathbf{k}\sigma} \mathcal{G}^{(\sigma)}_{\mathbf{k}+\mathbf{q},\mathbf{k}} \right) \left(\sum_{\sigma} \sum_{\mathbf{k}'',\mathbf{p}'} \mathcal{D}_{\mathbf{k}'',\mathbf{p}'+\mathbf{q}} \mathcal{M}^{(\sigma)}_{\mathbf{p}',\mathbf{k}''} \right) + \\ & + \sum_{\sigma} \sum_{\mathbf{k},\mathbf{p}'} \mathcal{D}_{\mathbf{k}+\mathbf{q},\mathbf{p}'+\mathbf{q}} \mathcal{M}^{(\sigma)}_{\mathbf{k},\mathbf{p}'} - \sum_{\sigma} \sum_{\mathbf{k},\mathbf{p}'} \mathcal{N}^{(\sigma)}_{\mathbf{p}'+\mathbf{q},\mathbf{k}+\mathbf{q}} \mathcal{M}^{(\sigma)}_{\mathbf{k},\mathbf{p}'} \end{aligned} \quad (7.35)$$

where the intermediate matrices $\mathcal{M}^{(\sigma)}, \mathcal{N}^{(\sigma)}$ read:

$$\mathcal{M}^{(\sigma)}_{\mathbf{k},\mathbf{p}'} = \sum_{\mathbf{p}''} \mathcal{D}^{-1}_{\mathbf{p}',\mathbf{p}''} \mathcal{G}_{\mathbf{p}''\sigma'',\mathbf{k}''\sigma''} \quad , \qquad \mathcal{N}^{(\sigma)}_{\mathbf{p}'+\mathbf{q},\mathbf{k}+\mathbf{q}} = \sum_{\mathbf{k}''} \mathcal{D}_{\mathbf{k}'',\mathbf{p}'+\mathbf{q}} \mathcal{G}_{\mathbf{k}+\mathbf{q}\sigma,\mathbf{k}''\sigma} \quad (7.36)$$

The calculation of the intermediate matrices requires $\mathcal{O}(M^3)$ operations, and all the contractions in (7.35) require at most $\mathcal{O}(M^2)$ operations.

7.6 Results

The central results of this Chapter are: (i) the practical verification of the possibility of accurately calculating *ab initio* ITCFs of medium-sized homogeneous electron gases and (ii) the understanding of the computational cost and limitations of the procedure. We have simulated paramagnetic systems of $N = 18, 26, 42$ electrons at $r_s = 0.1, 0.5, 1$; we show also results for $N = 18$ particles at $r_s = 2$. The complexity scales as M^3 (M being the number of basis sets elements), and the absolute statistical error of $F(\mathbf{q}, \tau)$ can be kept at the level $10^{-3} - 2.5\,10^{-3}$ with moderate computational resources even at values of $\tau \simeq 3/E_F$ for $r_s = 0.1, 0.5, 1$ and $\tau \simeq 2.5/E_F$ for $r_s = 2$, $E_F = 1/r_s^2$ being the Fermi energy.
The imaginary time steps used in our calculations were $\delta\tau = 0.003, 0.004, 0.006, 0.008$ E_{Ha}^{-1} at $r_s = 0.1, 0.5, 1, 2$ respectively. For each simulation, the number of plane-waves constituting the single-particle Hilbert space has been raised up to $M = 300$ according to the number of particles and to the strength of the interaction. For all calculations, it was verified that decreasing the time step and increasing the number of plane waves had a negligible effect on the ground-state energy per particle, which we illustrate in Table 7.1, in comparison with RPA and configurational QMC.
The configurational QMC evaluation of the ground state energy per particle has been performed using DMC, with a nodal structure encompassing backflow correlations optimized by means of the Linear Method [35, 144].
At $r_s = 0.1$ the three methods give compatible results. As r_s increases, AFQMC estimates are always closer to FN than RPA, lying between them. It is well-known that FN calculations with optimized nodal structures yield highly accurate estimates of the ground-state energy, as confirmed by comparison with Full Configuration Interaction QMC calculations [288, 289]: this result, therefore, confirms the great accuracy of the phaseless approximation in the sampling of the ground-state wavefunction.
To obtain correct estimates of ITCFs, it is necessary to perform a sufficiently large number m of backpropagation steps. However, as discussed in 5.4.2, raising m can increase the variance of the back-propagated estimator, limiting the possibility of extracting physical information from the long imaginary-time tails of the ITCFs. We have used a number of backpropagation steps in the range $m = 200 - 600$. When $m = 600$ has proved insufficient, to avoid the increases in variance mentioned above, AFQMC estimates have been extrapolated to the $m \to \infty$ limit (data obtained by extrapolation will be henceforth marked with an asterisk).

7.6.1 Imaginary time correlation functions and excitation energies

For all the values of N and r_s, an AFQMC estimate of the density-density ITCF (1.31) is produced according to the procedure sketched in Chapter 6. The obtained $F(\mathbf{q}, \tau)$ is shown in the upper panel of Figures 7.1, 7.2, 7.3 and 7.4. It is evident from the plots that the stabilization technique prevents an uncontrollable increase of the statistical error with imaginary time.
As it is well-known [220], it is highly non-trivial to extract physical information from ITCFs. In the case of the HEG, the finite size of the systems under study induces to expect, for all the considered wave vectors, contributions to $F(\mathbf{q}, \tau)$ coming from particle–hole excitations. The dynamical structure factor $S(\mathbf{q}, \omega)$, the inverse Laplace transform

of $F(\mathbf{q},\tau)$, is thus expected to display multiple peaks corresponding to the excitation energies. This picture is confirmed by RPA calculations for finite systems, reported in Appendix 13.5.

The presence of multiple peaks complicates the task of performing the analytic continuation leading to $S(\mathbf{q},\omega)$. Therefore, since the number of peaks grows rapidly with $|\mathbf{q}|$, we have limited our attention to the wavevectors $\mathbf{q}_1 = (2\pi/L)\,(1,0)$ and $\mathbf{q}_2 = (2\pi/L)\,(1,1)$. Notice that $|\mathbf{q}_1|/k_F = 0.707, 0.5, 0.447$ and $|\mathbf{q}_2|/k_F = 1, 0.707, 0.632$ for $N = 18, 26, 42$ respectively. Naturally, $k_F = \sqrt{2}/r_s$ is the Fermi wavevector.

For finite systems, the ITCF $F(\mathbf{q},\tau)$ is a sum of exponentials:

$$F(\mathbf{q},\tau) = \sum_{i=1}^{N_w} s_i e^{-\tau\omega_i} \tag{7.37}$$

with positive frequencies ω_i and weights s_i. In particular, ω_i are the excitation frequencies of the system.

To extract information about those excitation energies, it is in general necessary to compute $F(\mathbf{q},\tau)$ up to a sufficiently long imaginary time τ^*. To study the scaling of τ^* with r_s we now make the assumption that $F(\mathbf{q},\tau)$ is equal to a single exponential:

$$F(\mathbf{q},\tau) \simeq S(\mathbf{q})\, e^{-\tau\hbar\omega(\mathbf{q})} \tag{7.38}$$

with energy $\hbar\omega(\mathbf{q})$ equal to the plasmon dispersion relation that, for a 2D HEG, is [6]:

$$\hbar\omega(\mathbf{q}) = \sqrt{\frac{2\pi e^2\hbar^2}{m}\rho|\mathbf{q}|} \tag{7.39}$$

writing $\rho = \frac{N}{\Omega}$ and $\mathbf{q} = \frac{2\pi}{L}\mathbf{n}$, we find that $F(\mathbf{q},\tau)$ decays on a time scale τ^* proportional to $r_s^{3/2}$ and $N^{1/2}$. This qualitative estimate shows that the calculation of $F(\mathbf{q},\tau)$ becomes more and more demanding as r_s, N are increased. The assumption that $F(\mathbf{q},\tau)$ is equal to a single exponential is adequate only for small $|\mathbf{q}|$ and for a very large system. Otherwise, $F(\mathbf{q},\tau)$ is a sum of several exponentials, some of which correspond to excitations in the particle-hole band and, for $|\mathbf{q}| \leq 2k_F$, can have very low energy. Therefore, our argument provides a lower bound for the scaling of τ^*.

Given the AFQMC estimates of $F(\mathbf{q},\tau)$ we can only compute the DSF of the finite systems under study. For this reason, we do not attempt to predict the DSF in the thermodynamic limit, but just extract the excitations energies and weights by fitting the evaluated ITCF to a sum of exponentials with the well-established Levenberg-Marquardt curve-fitting method [85]. In all cases, the number $N_w \leq 3$ of frequencies and weights is that leading to the best fit.

In Figures 7.1, 7.2, 7.3 and 7.4 we show results relative to the simulation of paramagnetic systems at $r_s = 0.1, 0.5, 1, 2$ respectively. Each figure contains data relative to the particle numbers $N = 18, 26, 42$ and wavevectors $\mathbf{q}_1, \mathbf{q}_2$. In the upper panel we show the estimated $F(\mathbf{q},\tau)$, while in the middle and lower panels we show, for $\mathbf{q}_1$ and $\mathbf{q}_2$ respectively, the obtained frequencies and weights, together with the RPA results. The AFQMC estimations of the quantities s_i, ω_i are displayed as points with both horizontal and vertical statistical errors: the horizontal ones provide the uncertainties on the frequencies ω_i of the excitations, while the vertical ones gives the error bars on the weights s_i. The coordinates of the points give, naturally, the mean frequencies and weights. The statistical uncertainties on the quantities s_i, ω_i are those yield by the fit procedure. The frequencies

predicted by the RPA are represented as impulses with height equal to the corresponding weights. Figures 7.1, 7.2, 7.3 and 7.4 reveal that, for increasing r_s, $F(\mathbf{q},\tau)$ decays more and more slowly. In particular, as long as $\mathbf{q}_2$ is considered, the dynamical structure factor exhibits an excitation with energy roughly proportional to r_s^{-2}. In order to extend this calculation to $r_s = 3$, we should compute $F(\mathbf{q},\tau)$ up to $\tau \simeq 25 E_{Ha}^{-1}$. Moreover, at $r_s = 2$ a calculation without numerical stabilization provides a reliable estime of $F(\mathbf{q},\tau)$ for $\tau \leq 5.5 E_{Ha}^{-1}$, and a stabilization with $\lambda = 10^{-16}$ brings this threshold to $\tau \leq 10.0 E_{Ha}^{-1}$. On the basis of these observations, we expect that the calculation of $F(\mathbf{q},\tau)$ at $r_s > 3$ would be much more demanding and problematic, requiring a more aggressive stabilization. As a reference value, the calculations at $N = 18$ and $r_s = 1(2)$ required 6×10^3 (5×10^4) core hours on a Blue Gene/Q (Power BQC 1.6 GHz). The difference stems from the number of plane waves, of backpropagation steps and of imaginary time instants on which $F(\mathbf{q},\tau)$ has been computed.

We see that, at $r_s = 0.1$, there is a close agreement between AFQMC and RPA predictions of both frequencies and spectral weights. Since it is known that, for small r_s, RPA predictions are very accurate, such agreement provides a robust check for the reliability of AFQMC methodology in providing information about the manifold of excited states of the system. It is well-known [236] that, in the same situation, calculations of $F(\mathbf{q},\tau)$ based on the Fixed-Node approximation would give inaccurate results even if the nodal structure of the ground state wavefunction is known with very high accuracy. As r_s increases, discrepancies appear between the two approaches. The presence of such discrepancies is naturally expected: none of the methodologies used in the present work is free from approximations. The approximations underlying RPA and AFQMC, in particular, are quite different in nature and are expected to agree only in the limit of high density (very low r_s).

In order to further assess the quality of our estimates of $F(\mathbf{q},\tau)$, we consider the momenta:

$$\mathcal{M}_j = \int_0^\infty d\omega\, \omega^j\, S(\mathbf{q},\omega) \qquad j \in \mathbb{Z} \tag{7.40}$$

of the DSF. As proved in Appendix 12.0.6, the exact values of several momenta $\mathcal{M}_n$ are fixed by sum rules [6], and the AFQMC estimate of those quantities can be compared with exact values or static properties. In particular:

$$\mathcal{M}_0 = S(\mathbf{q}) \tag{7.41}$$

while $\mathcal{M}_1$ obeys the continuity sum rule:

$$\mathcal{M}_1 = \frac{\hbar^2 |\mathbf{q}|^2}{2m} \tag{7.42}$$

and $\mathcal{M}_{-1}$ obeys the compressibility sum rule:

$$\mathcal{M}_{-1} = -\frac{\chi(\mathbf{q})}{2n} \tag{7.43}$$

where $\chi(\mathbf{q})$ denotes the static density response function.

In Table 7.2 we compute the momentum (7.42) using the dynamical structure factors in Figs. 7.1, 7.2, 7.3 and 7.4 and we compare it with the exact value $|\mathbf{q}|^2/2$. In most cases, the AFQMC estimate of (12.33) is less than 2 standard deviations away from the exact result. We remark that, unlike in the case of RPA, there is no *a priori* motivation for expecting that AFQMC estimators of density-density ITCFs provide accurate estimates of the first

momentum.
In order to further assess the quality of our results, in Tables 7.3 and 7.4 we detail the comparison with the RPA and configurational QMC results for the static structure factor $S(\mathbf{q}) = F(\mathbf{q}, 0)$ and the static density response function:

$$\tilde{\chi}(\mathbf{q}) = -\frac{\chi(\mathbf{q})}{2\rho} = \int_0^{+\infty} d\tau \, F(\mathbf{q}, \tau) = \mathcal{M}_{-1} \tag{7.44}$$

In the AFQMC calculations, $\tilde{\chi}(\mathbf{q})$ is obtained using the parameters yield by the fitting procedure of the density-density correlations $F(\mathbf{q}, \tau)$. In absence of exact results for ITCFs, the comparison between QMC extimates of static properties related to the momenta of $S(\mathbf{q}, \omega)$ is a practical way of assessing the quality of ITCFs from AFQMC calculations.
The configurational QMC evaluation of the static structure factor $S(\mathbf{q})$ has been obtained via FN DMC calculations with the nodal structure described above. The DMC estimates are calculated using the extrapolated estimator [99]. We observe that, increasing r_s above 0.1, the AFQMC predictions remain, in general, closer to the configurational QMC ones than to the RPA ones: this is a strong indication about the quality of AFQMC results, since the QMC calculations include correlations beyond the RPA level.
Even more significant is the comparison between AFQMC estimates of the static density response function $\tilde{\chi}(\mathbf{q})$, which we obtain from the momentum (7.43) of the dynamical structure factor, with RPA and Fixed-Node estimations. In principle, the Fixed-Node evaluation of the static density response function $\tilde{\chi}(\mathbf{q})$ is highly non trivial, involving the manifold of excited states. It is well-kown [283], and explained in Appendix 10.3, that such difficulty can be circumvented extracting $\tilde{\chi}(\mathbf{q})$ from the ground-state energy per particle of a system subject to an external periodic potential of amplitude $v_{\mathbf{q}}$ in the $v_{\mathbf{q}} \to 0$ limit. Again, increasing r_s above 0.1, the AFQMC predictions remain, in general, closer to the configurational Monte Carlo ones than to the RPA ones: this is a strong indication about the quality of AFQMC results, since the Monte Carlo calculations include correlations beyond the RPA level.
This result is remarkable, since the AFQMC evaluation of $\tilde{\chi}(\mathbf{q})$ is considerably influenced by the low-energy excitations which, if predicted inaccurately, can significantly bias the result. We notice that knowledge of the momenta (7.41), (7.42), (7.43) was not enforced in the fitting procedure that led us to the dynamical structure factor: instead, those quantities have been computed from the dynamical structure factor and found in satisfactory agreement, at least for $r_s \leq 1$, with independently derived quantities.
The study of the momenta (7.41), (7.43) leads to argue that the deviations from the RPA observed at $r_s \leq 1$ indicate the better accuracy of the AFQMC dynamical structure factor. Indeed, the configurational QMC includes correlations beyond the RPA level, and thus its estimate of the momenta (7.41), (7.43) should be considered more accurate than RPA estimates. Since the AFQMC dynamical structure factor leads to estimates of (7.41), (7.43) which are in better agreement with FN QMC, at least for $r_s \leq 1$, we argue that AFQMC provides more accurate estimates of $F(\mathbf{q}, \tau)$ and thus $S(\mathbf{q}, \omega)$ than RPA. This result shows that, remarkably, in the high-density regime the accuracy of AFQMC for the imaginary time dynamics is comparable to that of the ground state energy.
As r_s further increases, however, the agreement decreases. We have verified that the number of plane-waves and the number of backpropagation steps are sufficiently large to extrapolate the results and to filter the excited states contributions from the trial wavefunction. Hence, the origin of the discrepancies between the estimations yield by the three methodologies used in the present work has to be sought in the approximation

schemes underlying them.

N	r_s	$\mathcal{E}_N$ (RPA)	$\mathcal{E}_N$ (AF)	$\mathcal{E}_N$ (FN)
18	0.1	40.14	40.14(2)	40.13(1)
26	0.1	45.84	45.82(1)	45.81(1)
42	0.1	42.18	42.18(1)	42.17(1)
18	0.5	0.5065	0.5007(2)	0.5012(2)
26	0.5	0.7520	0.7360(2)	0.7326(8)
42	0.5	0.6031	0.6002(1)	0.5922(9)
18	1.0	-0.2489	-0.2562(1)	-0.2580(1)
26	1.0	-0.1847	-0.1921(1)	-0.1961(1)
42	1.0	-0.2215	-0.2283(1)	-0.2309(2)
18	2.0	-0.2661	-0.2695(1)	-0.2717(1)

Table 7.1: RPA (column 3), AFQMC (column 4) and FN-DMC (column 5) estimates of the ground-state energy per particle for various systems (parameters are listed in columns 1-3); energies are measured in E_{Ha}. The RPA ground state energy is calculated on the Gaskell trial wavefunction described in Section 10.1.3 and in [103].

N	r_s	$\lvert\mathbf{q}\rvert$	$\Delta\mathcal{M}_1$
18	0.1	8.355427	0.015(9)
18	0.1	11.81636	0.000(1)
26	0.1	6.952136	0.001(1)
26	0.1	9.831805	0.002(2)
42	0.1	5.469911	0.003(4)
42	0.1	7.735622	0.000(2)
18	0.5	1.671085	0.015(21)
18	0.5	2.363271	0.018(14)
26	0.5	1.390427	0.006(6)
26	0.5	1.966361	0.019(9)
42	0.5	1.093982	0.023(38)
42	0.5	1.547124	0.033(27)
18	1.0	0.835543	0.020(11)
18	1.0	1.181636	0.019(8)
26	1.0	0.695214	0.036(16)
26	1.0	0.983181	0.022(12)
42	1.0	0.546991	0.002(10)
42	1.0	0.773562	0.030(25)
18	2.0	0.417771	0.078(21)
18	2.0	0.590818	0.12(6)

Table 7.2: Relative error (column 4) $\Delta\mathcal{M}_1 = |\mathcal{M}_1^{(\text{AFQMC})} - \mathcal{M}_1^{(\text{EXACT})}|/\mathcal{M}_1^{(\text{EXACT})}$ on the first momentum.

N	r_s	$\|\mathbf{q}\|$	$S(\mathbf{q})$ (RPA)	$S(\mathbf{q})$ (AF)	$S(\mathbf{q})$ (FN)
18	0.1	8.355427	0.3105	0.314(2)	0.319(4)
18	0.1	11.81636	0.5150	0.525(4)	0.521(4)
26	0.1	6.952136	0.3326	0.342(2)	0.343(4)
26	0.1	9.831805	0.3623	0.367(6)	0.370(5)
42	0.1	5.469911	0.2101	0.212(7)	0.217(4)
42	0.1	7.735622	0.3045	0.310(6)	0.306(5)
18	0.5	1.671085	0.2511	0.258(1)	0.266(4)
18	0.5	2.363271	0.4137	0.440(3)	0.448(5)
26	0.5	1.390427	0.2225	0.254(3)*	0.238(4)
26	0.5	1.966361	0.3009	0.313(2)	0.322(4)
42	0.5	1.093982	0.1533	0.161(2)	0.146(5)
42	0.5	1.547124	0.2366	0.247(2)	0.264(4)
18	1.0	0.835543	0.2098	0.231(2)	0.218(5)
18	1.0	1.181636	0.3451	0.395(3)	0.386(4)
26	1.0	0.695214	0.1746	0.227(2)*	0.192(5)
26	1.0	0.983181	0.2558	0.289(2)	0.281(4)
42	1.0	0.546991	0.1219	0.141(1)	0.126(5)
42	1.0	0.773562	0.1938	0.219(2)	0.208(5)
18	2.0	0.417771	0.1657	0.172(2)*	0.176(4)
18	2.0	0.590818	0.2732	0.304(3)*	0.305(4)

Table 7.3: RPA (column 4), AFQMC (column 5) and FN-DMC (column 6) estimates of the static structure factor $S(\mathbf{q})$ for various systems and wave-vectors (parameters are listed in columns 1-3); wave-vectors are measured in a_B^{-1}. AFQMC estimates marked with an asterisk are extrapolated.

7.7 Conclusions

We have shown the possibility to provide accurate first principles calculations of imaginary time correlations for medium–sized fermionic systems in the continuum, using the phaseless AFQMC method.

We have simulated a $2D$ homogeneous electron gas of up to $N = 42$ electrons using a plane-waves basis set of up to $M = 300$ elements. We have shown that the density-density ITCFs can be calculated with a polynomially complex algorithm having the favorable scaling $\mathcal{O}(M^3)$. In order to achieve a good accuracy level in the calculations, we propose stabilization procedures to deal with matrix inversion, which can be used in combination with well-established stabilization procedures for matrix exponentiation and multiplication [290, 274]: in particular, we suggest a Tikhonov regularization that allows to maintain a good accuracy level even for imaginary time values of the order of $3/E_F$. We have yielded also comparisons with predictions of the static structure factor and the static density response obtained via the RPA approximation and via FN-QMC calculations.

At small r_s the AFQMC correctly reproduces the RPA results. At larger r_s on the other hand, it provides quantitative estimates of the deviations from the RPA, as the comparison with FN calculations reveals. We believe this is a relevant result for QMC simulations: it is known, in fact, that the widely employed FN approximation fails to properly

N	r_s	$\|\mathbf{q}\|$	$\tilde{\chi}(\mathbf{q})$ (RPA)	$\tilde{\chi}(\mathbf{q})$ (AF)	$\tilde{\chi}(\mathbf{q})$ (FN)
18	0.1	8.355427	0.00276	0.0028(4)	0.00287(1)
18	0.1	11.81636	0.00449	0.0046(1)	0.00469(1)
26	0.1	6.952136	0.00598	0.0065(2)	0.00653(4)
26	0.1	9.831805	0.00282	0.0028(1)	0.00287(4)
42	0.1	5.469911	0.00311	0.0032(4)	0.00325(4)
42	0.1	7.735622	0.00330	0.0034(2)	0.00335(2)
18	0.5	1.671085	0.04516	0.048(1)	0.0484(4)
18	0.5	2.363271	0.06992	0.081(2)	0.0788(4)
26	0.5	1.390427	0.06298	0.085(6)*	0.069(2)
26	0.5	1.966361	0.04827	0.051(1)	0.0504(4)
42	0.5	1.093982	0.04074	0.043(5)	0.042(2)
42	0.5	1.547124	0.04903	0.051(3)	0.049(2)
18	1.0	0.835543	0.12612	0.152(3)	0.143(2)
18	1.0	1.181636	0.18979	0.301(6)	0.226(1)
26	1.0	0.695214	0.14601	0.22(2)*	0.162(2)
26	1.0	0.983181	0.13872	0.188(6)	0.161(2)
42	1.0	0.546991	0.10212	0.158(7)	0.14(1)
42	1.0	0.773562	0.13014	0.176(9)	0.16(1)
18	2.0	0.417771	0.31451	0.34(1)*	0.374(4)
18	2.0	0.590818	0.46238	0.89(1)*	0.590(2)

Table 7.4: RPA (column 4), AFQMC (column 5) and FN-DMC (column 6) estimates of the compressibility $\tilde{\chi}(\mathbf{q})$ for various systems and wave-vectors (parameters are listed in columns 1-3); wave-vectors are measured in a_B^{-1}, and $\tilde{\chi}(\mathbf{q})$ in E_{Ha}^{-1}. AFQMC estimates marked with an asterisk are extrapolated.

sample the imaginary-time propagator, due to the imposition of the ground-state nodal structure to excited states[236]. AFQMC, on the other hand, appears to provide a useful tool to explore, from first principles, the manifold of the excited states of a fermionic system. In particular, our calculations qualify the phaseless AFQMC as a practical and useful methodology for the accurate evaluation of $F(\mathbf{q}, \tau)$, for homogeneous systems of $N = \mathcal{O}(10^2)$ correlated fermions in the continuum. Calculations are lighter and more accurate when ITCFs decay rapidly, as in the case of 2D HEGs in the high–density regime. To further assess the performance of the metodology, it would be relevant to compute other ITCFs for both homogenous and non–homogeneous systems, such as chemical systems.

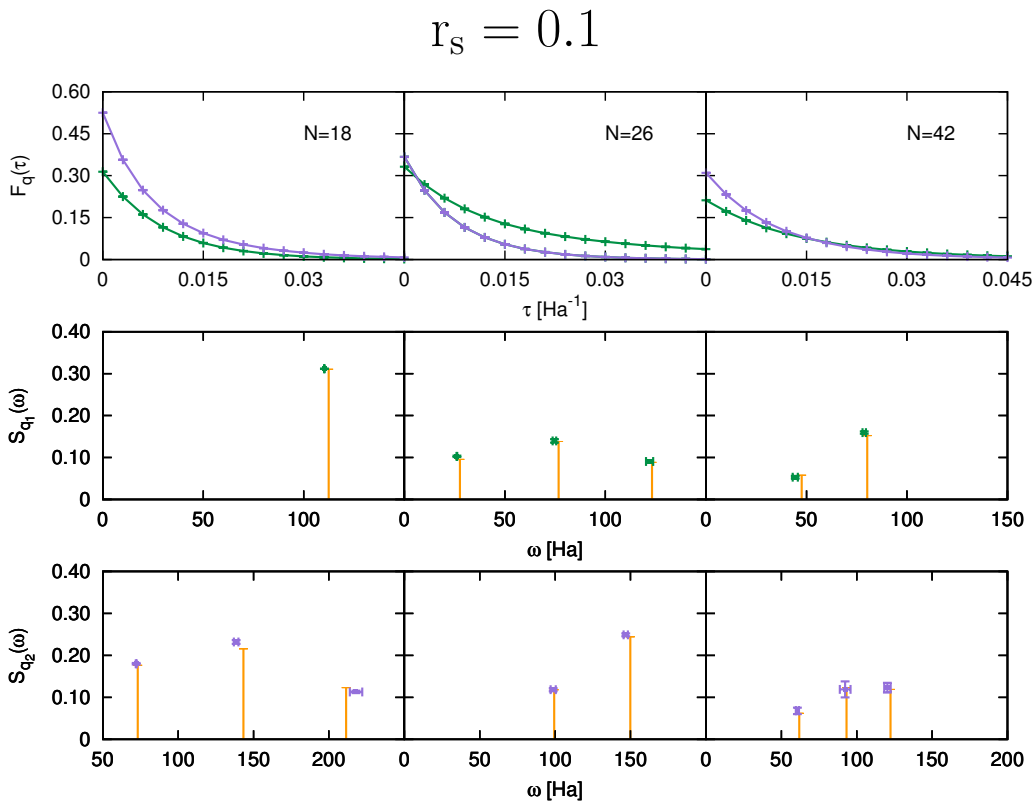

Figure 7.1: (color online) Upper panel: imaginary time correlation functions of the density fluctuation operator $\hat{\rho}_{\mathbf{q}}$ for paramagnetic systems of $N = 18, 26$ and 42 particles (left to right) at $r_s = 0.1$, with transferred momenta $\mathbf{q}_1$ (green lines) and $\mathbf{q}_2$ (lavender lines). When not visible, errors are below the symbol size. Lines are only a guide for eyes. Central panel: dynamical structure factor for $N = 18, 26$ and 42 particles (left to right) with transferred momentum $\mathbf{q}_1$ (RPA: orange impulses, AFQMC: green symbols). Lower panel: dynamical structure factor for $N = 18, 26$ and 42 particles (left to right) with transferred momentum $\mathbf{q}_2$ (RPA: orange impulses, AFQMC: lavender symbols).

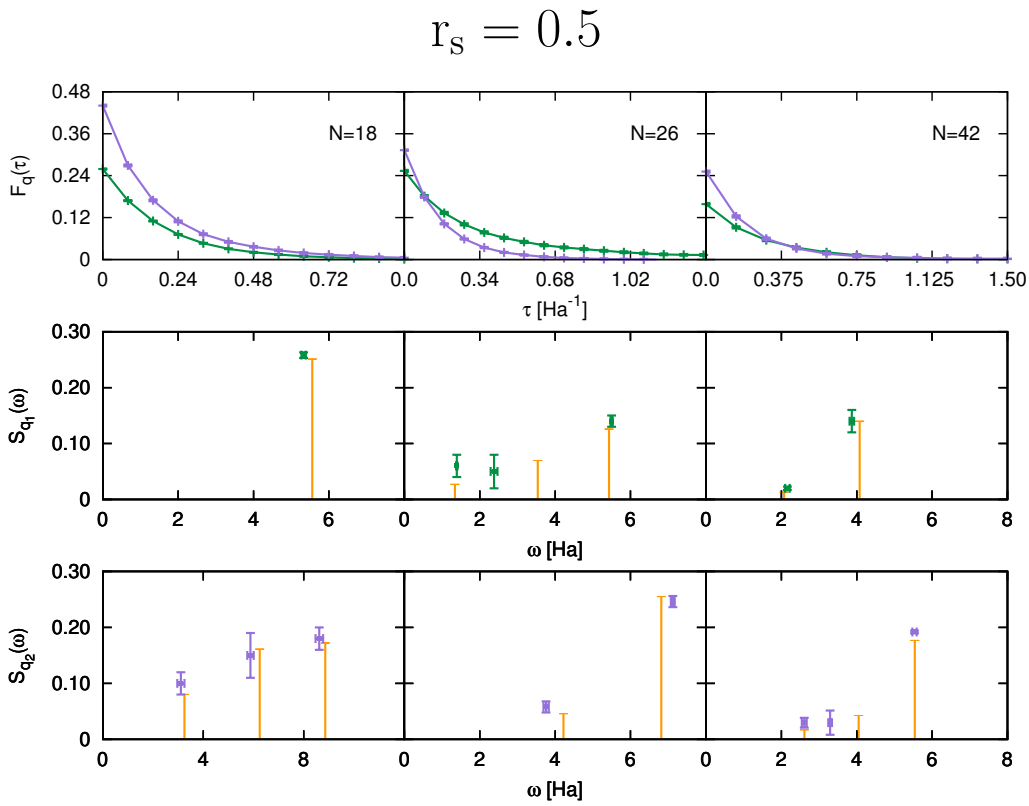

Figure 7.2: (color online) Upper panel: imaginary time correlation functions of the density fluctuation operator $\hat{\rho}_{\mathbf{q}}$ for paramagnetic systems of $N = 18, 26$ and 42 particles (left to right) at $r_s = 0.5$, with transferred momenta $\mathbf{q}_1$ (green lines) and $\mathbf{q}_2$ (lavender lines). When not visible, errors are below the symbol size. Lines are only a guide for eyes. Central panel: dynamical structure factor for $N = 18, 26$ and 42 particles (left to right) with transferred momentum $\mathbf{q}_1$ (RPA: orange impulses, AFQMC: green symbols). Lower panel: dynamical structure factor for $N = 18, 26$ and 42 particles (left to right) with transferred momentum $\mathbf{q}_2$ (RPA: orange impulses, AFQMC: lavender symbols).

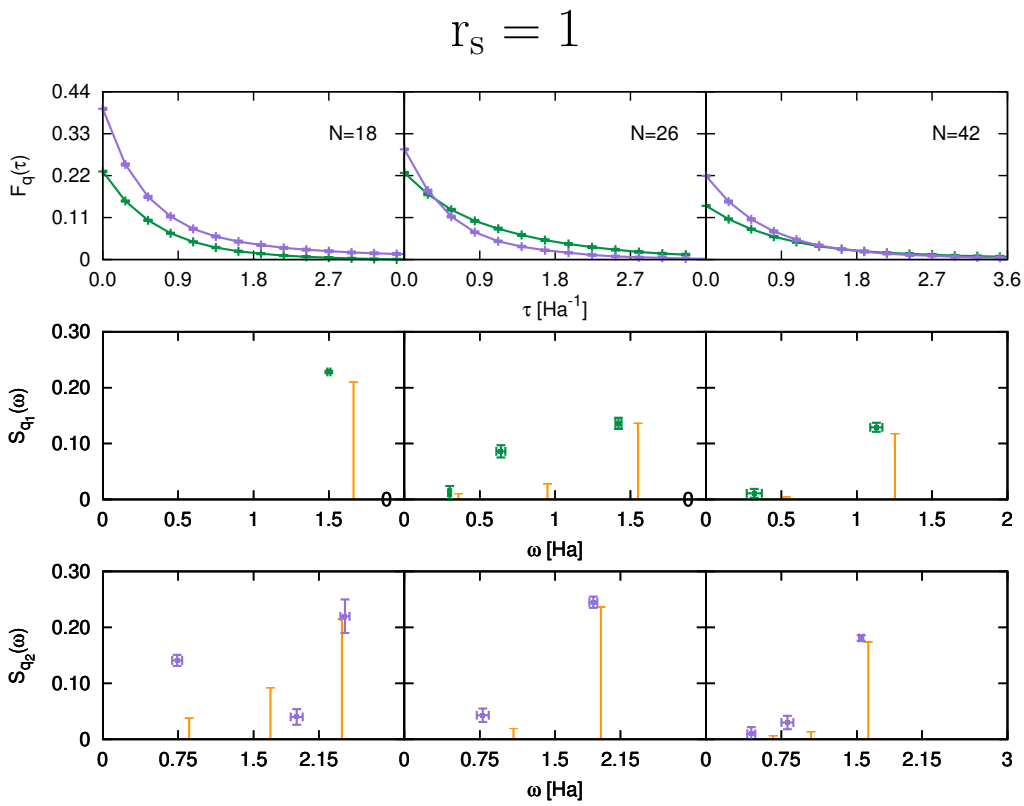

Figure 7.3: (color online) Upper panel: imaginary time correlation functions of the density fluctuation operator $\hat{\rho}_{\mathbf{q}}$ for paramagnetic systems of $N = 18, 26$ and 42 particles (left to right) at $r_s = 1$, with transferred momenta $\mathbf{q}_1$ (green lines) and $\mathbf{q}_2$ (lavender lines). When not visible, errors are below the symbol size. Lines are only a guide for eyes. Central panel: dynamical structure factor for $N = 18, 26$ and 42 particles (left to right) with transferred momentum $\mathbf{q}_1$ (RPA: orange impulses, AFQMC: green symbols). Lower panel: dynamical structure factor for $N = 18, 26$ and 42 particles (left to right) with transferred momentum $\mathbf{q}_2$ (RPA: orange impulses, AFQMC: lavender symbols).

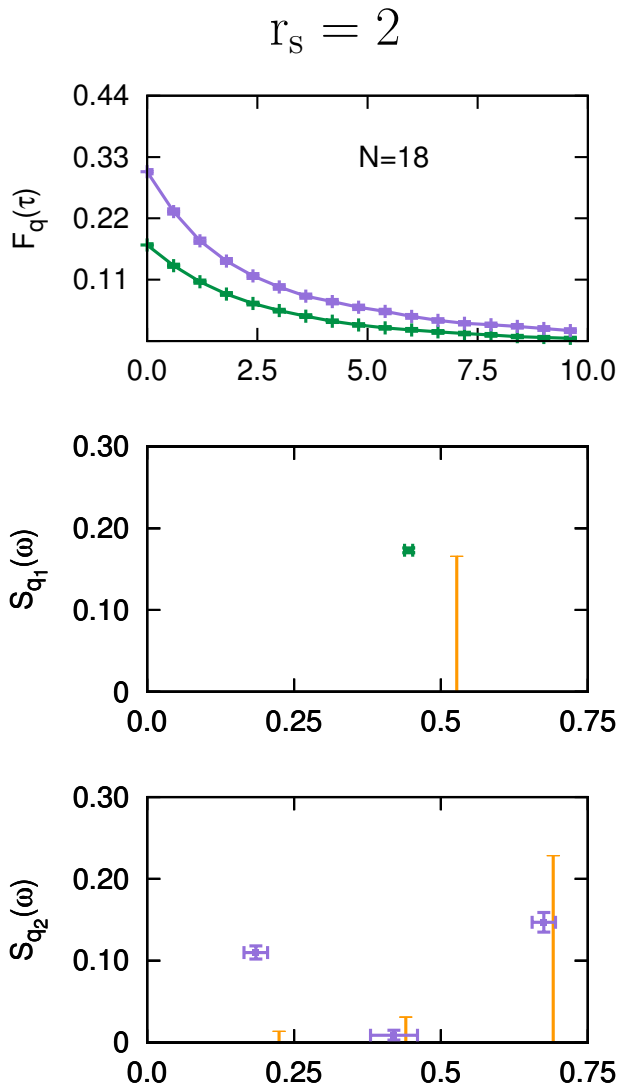

Figure 7.4: (color online) Upper panel: imaginary time correlation functions of the density fluctuation operator $\hat{\rho}_{\mathbf{q}}$ for paramagnetic systems of $N = 18, 26$ and 42 particles (left to right) at $r_s = 2$, with transferred momenta $\mathbf{q}_1$ (green lines) and $\mathbf{q}_2$ (lavender lines). When not visible, errors are below the symbol size. Lines are only a guide for eyes. Central panel: dynamical structure factor for $N = 18, 26$ and 42 particles (left to right) with transferred momentum $\mathbf{q}_1$ (RPA: orange impulses, AFQMC: green symbols). Lower panel: dynamical structure factor for $N = 18, 26$ and 42 particles (left to right) with transferred momentum $\mathbf{q}_2$ (RPA: orange impulses, AFQMC: lavender symbols).

CHAPTER 8

Effective mass of high-density two-dimensional electron gases from AFQMC

In the present Chapter we present preliminary results about the phaseless AFQMC calculation of the electronic band and effective mass of high-density two-dimensional electron gases [291]. In Section 8.1, the concept of imaginary-time Green's function is briefly reviewed, in connection with experimentally measurable properties like the spectral function. In Section 8.2, some basic notions of Landau's Fermi liquid theory are recalled, and the concepts of electronic band and effective mass are presented. In Section 8.3, the AFQMC estimate of imaginary-time Green's functions is described along with the stabilization technique conceived by F. F. Assaad, and preliminary results of simulations in periodic and twist-averaged boundary conditions are presented in Section 8.4.

8.1 Introduction

Detailed knowledge of electronic properties of materials is obtained from spectroscopy, i.e. the study of the emission, absorption and scattering of electromagnetic and matter radiation accompanying transitions among many-body states.
Photoelectron spectroscopy is a general term that refers to all those techniques based on the application of the photoelectric effect, originally observed by H. Hertz [292] and later explained as a manifestation of the quantum nature of matter by A. Einstein [293]. Angle-resolved photoemission spectroscopy (ARPES) is one of the most advanced methods of studying the electronic band structure of solids. By measuring the kinetic energy and the angular distribution of the electrons photoemitted from a sample illuminated with photons at momentum $\hbar\mathbf{k}_\gamma$ and energy $\hbar\omega_\gamma$, it is possible to gain information on both the energy and momentum of the electrons propagating inside a material [294].
To develop a formal description of the photoemission process, one has to calculate the transition probability for an optical excitation between the N-electron ground state $\Psi_i = \Phi_0^{(N)}$ and all possible $(N-1)$-electron final states Ψ_f. The transition probability is approximated using Fermi's golden rule [19]:

$$W_{if} = \frac{2\pi}{\hbar} |\langle \Psi_f | \hat{H}' | \Psi_i \rangle|^2 \delta(E_f - E_i - \hbar\omega_\gamma) \tag{8.1}$$

where E_f, E_i are the initial and final energies of the system. The interaction with the electromagnetic field is described by the Hamiltonian:

$$\hat{H} = \sum_{i=1}^{N} \frac{1}{2m} \left(\hat{\mathbf{p}}_i - \frac{e}{c}\mathbf{A}(\hat{\mathbf{r}}_i) \right)^2 + \sum_{i<j} V(\hat{\mathbf{r}}_i - \hat{\mathbf{r}}_j) = \hat{H}_0 + \hat{H}' \tag{8.2}$$

where $\mathbf{p}_i$ is the momentum of the i-th electron, and $\mathbf{A}(\mathbf{r})$ is the electromagnetic vector potential (the scalar electromagnetic potential is removed with a suitable gauge transformation). Notice that:

$$\hat{H}' = \sum_{i=1}^{N} \frac{e^2}{2mc^2} |\mathbf{A}(\hat{\mathbf{r}}_i)|^2 + \frac{e}{2mc} \left(\hat{\mathbf{p}}_i \cdot \mathbf{A}(\hat{\mathbf{r}}_i) + \mathbf{A}(\hat{\mathbf{r}}_i) \cdot \hat{\mathbf{p}}_i \right) \tag{8.3}$$

is a one-body operator, that is commonly approximated by dropping the quadratic term in $\mathbf{A}(\hat{\mathbf{r}}_i)$ and taking advantage of the commutation relation:

$$\hat{\mathbf{p}}_i \cdot \mathbf{A}(\hat{\mathbf{r}}_i) = \mathbf{A}(\hat{\mathbf{r}}_i) \cdot \hat{\mathbf{p}}_i - i\hbar \nabla_i \cdot \mathbf{A}(\hat{\mathbf{r}}_i) \simeq \mathbf{A}(\hat{\mathbf{r}}_i) \cdot \hat{\mathbf{p}}_i \tag{8.4}$$

where the last term has been neglected because the electromagnetic vector potential is slowly-varying over atomic dimensions. The result is the so-called dipole approximation:

$$\hat{H}' = \frac{e}{mc} \sum_{i=1}^{N} \mathbf{A}(\hat{\mathbf{r}}_i) \cdot \hat{\mathbf{p}}_i = \sum_{\mathbf{p},\mathbf{r}} \sum_{\varsigma} \Delta_{\mathbf{p},\mathbf{r}} \hat{a}^\dagger_{\mathbf{p}\varsigma} \hat{a}_{\mathbf{r}\varsigma} \tag{8.5}$$

for the interaction Hamiltonian. In evaluating the transition rate W_{fi}, the possible final states are selected relying on the so-called sudden approximation, i.e. disregarding the many-body interactions as well as the relaxation of the system during the photoemission.

The sudden approximation consists in writing $|\Psi_f\rangle = \hat{a}^\dagger_f |\Phi^{(N-1)}_\mu\rangle$, where $|\Phi^{(N-1)}_\mu\rangle$ is an $(N-1)$-particle eigenstate of the unperturbed Hamiltonian. By making this choice, it is assumed that a photoelectron is emitted in the single-particle state f with a possible excitation of the remaining $N-1$ electrons, that we take uncorrelated with the photoelectron. We take f to be a spin-definite plane wave, $\hat{a}^\dagger_f = \hat{a}^\dagger_{\mathbf{k}\sigma}$, and assume that $\hat{a}_{\mathbf{k}\sigma} |\Phi^{(N)}_0\rangle = 0$. The transition rate then takes the form:

$$W_{if} = \frac{2\pi}{\hbar} \sum_{\mathbf{r},\mathbf{r}'} \Delta_{\mathbf{k},\mathbf{r}} \Delta^*_{\mathbf{k},\mathbf{r}'} \langle \Phi^{(N)}_0 | \hat{a}^\dagger_{\mathbf{r}'\sigma} | \Phi^{(N-1)}_\mu \rangle \langle \Phi^{(N-1)}_\mu | \hat{a}_{\mathbf{r}\sigma} | \Phi^{(N)}_0 \rangle \delta(\epsilon^-_\mu + t_{\mathbf{k}} - \hbar\omega_\gamma) \tag{8.6}$$

since:

$$\langle \Psi_f | \hat{H}' | \Psi_i \rangle = \sum_{\mathbf{p},\mathbf{r}} \sum_{\varsigma} \Delta_{\mathbf{p},\mathbf{r}} \langle \Phi^{(N-1)}_\mu | \hat{a}_{\mathbf{k}\sigma} \hat{a}^\dagger_{\mathbf{k}\varsigma} \hat{a}_{\mathbf{r}\varsigma} | \Phi^{(N)}_0 \rangle = \sum_{\mathbf{r}} \Delta_{\mathbf{k},\mathbf{r}} \langle \Phi^{(N-1)}_\mu | \hat{a}_{\mathbf{r}\sigma} | \Phi^{(N)}_0 \rangle \tag{8.7}$$

The Dirac delta permits to retrieve $\epsilon^-_\mu = \epsilon_\mu(N-1) - \epsilon_0(N)$ as the difference between the photon energy and the photoelectron kinetic energy $t_{\mathbf{k}}$. Since the N-particle ground state is an eigenstate of spin-z and momentum with eigenvalue 0, the transition rate is non-zero only for $\Phi^{(N-1)}_\mu$ with momentum $\hbar\mathbf{k}' = \hbar\mathbf{k}_\gamma - \hbar\mathbf{k}$ and spin $-\sigma$ along the z-axis, whence:

$$W_{if} = \frac{2\pi}{\hbar} |\Delta_{\mathbf{k},\mathbf{k}'}|^2 \langle \Phi^{(N)}_0 | \hat{a}^\dagger_{\mathbf{k}'\sigma} | \Phi^{(N-1)}_\mu \rangle \langle \Phi^{(N-1)}_\mu | \hat{a}_{\mathbf{k}'\sigma} | \Phi^{(N)}_0 \rangle \delta(\epsilon^-_\mu + t_{\mathbf{k}} - \hbar\omega_\gamma) \tag{8.8}$$

The probability that a photoelectron is emitted with momentum $\hbar\mathbf{k}$ and energy $\hbar\omega = t_{\mathbf{k}}$ is:

$$I(\mathbf{k}, \omega) = \frac{2\pi}{\hbar} |\Delta_{\mathbf{k},\mathbf{k}'}|^2 A(\mathbf{k}', \omega') \tag{8.9}$$

with $\hbar\omega' = \hbar\omega_\gamma - \hbar\omega$ and:

$$A(\mathbf{k}', \omega') = \sum_\mu \sum_\sigma \langle \Phi_0^{(N)} | \hat{a}^\dagger_{\mathbf{k}'\sigma} | \Phi_\mu^{(N-1)} \rangle \langle \Phi_\mu^{(N-1)} | \hat{a}_{\mathbf{k}'\sigma} | \Phi_0^{(N)} \rangle \delta(\epsilon_\mu^- - \hbar\omega') \tag{8.10}$$

We now recall that the distribution $A(\mathbf{k}', \omega')$ is related to the time-ordered Green's function [4]:

$$\begin{aligned} iG_{\mathbf{k}\sigma}(t,t') &= \langle \Phi_0^{(N)} | \hat{a}_{\mathbf{k}\sigma}(t) \hat{a}^\dagger_{\mathbf{k}\sigma}(t') | \Phi_0^{(N)} \rangle \, \Theta(t-t') - \langle \Phi_0^{(N)} | \hat{a}^\dagger_{\mathbf{k}\sigma}(t') \hat{a}_{\mathbf{k}\sigma}(t) | \Phi_0^{(N)} \rangle \, \Theta(t'-t) = \\ &= iG^>_{\mathbf{k}\sigma}(t,t') \, \Theta(t-t') - iG^<_{\mathbf{k}\sigma}(t,t') \, \Theta(t'-t) \end{aligned} \tag{8.11}$$

The greater Green's function $G^>_{\mathbf{k}}(t,t')$ can be interpreted as the probability amplitude that a particle added to the system at time t' with momentum $\mathbf{k}$ and spin σ is still in the same state at time t. The Källén-Lehmann representation of the greater and lesser Green's function is readily obtained recalling that $\hat{a}_{\mathbf{k}\sigma}(t) = e^{it\hat{H}} \hat{a}_{\mathbf{k}\sigma} e^{-it\hat{H}}$. We obtain:

$$iG^>_{\mathbf{k}\sigma}(t,t') = \langle \Phi_0^{(N)} | \hat{a}_{\mathbf{k}\sigma}(t) \hat{a}^\dagger_{\mathbf{k}\sigma}(t') | \Phi_0^{(N)} \rangle = \sum_\mu A_\mu e^{-i(t-t')\epsilon_\mu^+} \tag{8.12}$$

with $\epsilon_\mu^+ = \epsilon_\mu(N+1) - \epsilon_0(N) = \epsilon_\mu(N+1) - \epsilon_0(N+1) + \mu$ and:

$$A_\mu = |\langle \Phi_0^{(N)} | \hat{a}_{\mathbf{k}\sigma} | \Phi_\mu^{(N+1)} \rangle|^2 \tag{8.13}$$

Similarly:

$$iG^<_{\mathbf{k}\sigma}(t,t') = \langle \Phi_0^{(N)} | \hat{a}^\dagger_{\mathbf{k}\sigma}(t) \hat{a}_{\mathbf{k}\sigma}(t') | \Phi_0^{(N)} \rangle = \sum_\mu B_\mu e^{i(t-t')\epsilon_\mu^-} \tag{8.14}$$

with $\epsilon_\mu^- = \epsilon_\mu(N-1) - \epsilon_0(N) = \epsilon_\mu(N-1) - \epsilon_0(N-1) - \mu$ and:

$$B_\mu = |\langle \Phi_0^{(N)} | \hat{a}^\dagger_{\mathbf{k}\sigma} | \Phi_\mu^{(N-1)} \rangle|^2 \tag{8.15}$$

Since both the patches $G^>_{\mathbf{k}\sigma}(t,t')$, $G^<_{\mathbf{k}\sigma}(t,t')$ depend on t, t' only through the difference $t - t'$, we can define the Fourier transform of the Green's function as:

$$G_{\mathbf{k}\sigma}(\omega) = \int d(t-t') e^{i\omega(t-t')} G_{\mathbf{k}\sigma}(t-t') = \int dt e^{i\omega t} G_{\mathbf{k}\sigma}(t) \tag{8.16}$$

which is most conveniently computed considering the greater and lesser Green's functions separately:

$$\int_0^\infty dt e^{i\omega t} iG^>_{\mathbf{k}\sigma}(t) = \sum_\mu A_\mu \int_0^\infty dt e^{i(\omega - \epsilon_\mu^+)t} = \lim_{\eta \to 0^+} \sum_\mu A_\mu \frac{1}{\eta - i(\omega - \epsilon_\mu^+)} \tag{8.17}$$

$$\int_{-\infty}^0 dt e^{i\omega t} iG^<_{\mathbf{k}\sigma}(t) = \sum_\mu B_\mu \int_{-\infty}^0 dt e^{i(\omega + \epsilon_\mu^-)t} = \lim_{\eta \to 0^+} \sum_\mu B_\mu \frac{1}{\eta + i(\omega + \epsilon_\mu^-)} \tag{8.18}$$

obtaining:

$$G_{\mathbf{k}\sigma}(\omega) = \lim_{\eta\to 0^+} \sum_\mu A_\mu \frac{1}{(\omega - \epsilon_\mu^+) + i\eta} - B_\mu \frac{1}{-(\omega + \epsilon_\mu^-) + i\eta} \tag{8.19}$$

The Plemelij-Sokhotskij theorem $\lim_{\eta\to 0^+} \frac{1}{\omega \pm i\eta} = \mathcal{P}(\omega) \pm i\pi\delta(\omega)$ ensures that:

$$A(\mathbf{k},\omega) = -\frac{1}{\pi} \sum_\sigma \mathrm{Im}\left(G_{\mathbf{k}\sigma}(\omega)\right) = A^>(\mathbf{k},\omega) + A^<(\mathbf{k},-\omega) \tag{8.20}$$

where:

$$\begin{aligned} A^>(\mathbf{k},\omega) &= \sum_\mu \sum_\sigma |\langle \Phi_0^{(N)} | \hat{a}_{\mathbf{k}\sigma} | \Phi_\mu^{(N+1)} \rangle|^2 \, \delta(\omega - \epsilon_\mu^+) \\ A^<(\mathbf{k},\omega) &= \sum_\mu \sum_\sigma |\langle \Phi_0^{(N)} | \hat{a}_{\mathbf{k}\sigma}^\dagger | \Phi_\mu^{(N-1)} \rangle|^2 \, \delta(\omega - \epsilon_\mu^-) \end{aligned} \tag{8.21}$$

$A^>(\mathbf{k},\omega)$, $A^<(\mathbf{k},\omega)$ are called addition and removal spectral functions, and can be probed with inverse and direct photoemission spectroscopy respectively [294]. The addition spectral function $A^>(\mathbf{k},\omega)$ is the inverse Laplace transform of the imaginary-time greater Green's function:

$$G^>_{\mathbf{k}\sigma}(\tau) = \langle \Phi_0^{(N)} | \hat{a}_{\mathbf{k}\sigma}(\tau) \hat{a}_{\mathbf{k}\sigma}^\dagger | \Phi_0^{(N)} \rangle \quad , \qquad \tau \geq 0 \tag{8.22}$$

with $\hat{a}_{\mathbf{k}\sigma}(\tau) = e^{\tau \hat{H}} \hat{a}_{\mathbf{k}\sigma} e^{-\tau \hat{H}}$. Similarly, the removal spectral function $A^<(\mathbf{k},\omega)$ is the inverse Laplace transform of the imaginary-time lesser Green's function:

$$G^<_{\mathbf{k}\sigma}(\tau) = \langle \Phi_0^{(N)} | \hat{a}_{\mathbf{k}\sigma}^\dagger(\tau) \hat{a}_{\mathbf{k}\sigma} | \Phi_0^{(N)} \rangle \quad , \qquad \tau \geq 0 \tag{8.23}$$

8.2 Landau's Fermi liquid theory

For systems called *Fermi liquids*, the collective evolution described by the Green's function can be identified, in a certain energy range, with the creation of a single *quasiparticle*, the effect of the other particles being a renormalization of the bare quantum numbers. The concept of quasiparticle was introduced on a phenomenological basis by L. D. Landau [295] and successfully applied to the study of the electron gas and of liquid ^{3}He [296, 297]. Normal metals like sodium and potassium are also Fermi liquids [298], and to some extent they can thus be described in terms of non-interacting quasiparticles.

A microscopic justification in many-body theory was provided later by V. M. Galitskii, who evaluated self-energy corrections by resumming ladder diagrams for two-particle scattering processes [299].

As the interaction is adiabatically turned on, the single-particle excitations of the ideal Fermi gas evolve into quasiparticles of a Fermi liquid. The origin of this simple picture is that in Fermi liquids the interaction preserves a Fermi surface, wherein most particles are frozen at low energy. However, the identification of quasiparticles is by no means obvious, and involves the notions of lifetime and weight.

The first requirement that defines quasiparticles is to be a pole of the propagator:

$$G_{\mathbf{k}}(\omega) = \frac{1}{\hbar\omega - \frac{\hbar^2 k^2}{2m} - \Sigma(k, \hbar\omega)} \tag{8.24}$$

i.e. a solution of the equation:

$$\hbar\omega - \frac{\hbar^2 k^2}{2m} - \Sigma(k, \hbar\omega) = 0 \tag{8.25}$$

which will be henceforth denoted as $\epsilon(k) + i\hbar\gamma(k)$. The propagator gains the form:

$$G_{\mathbf{k}}(\omega) = \frac{Z_k}{\hbar\omega - \epsilon(k) - i\hbar\gamma(k)} + G_{smooth}(\omega) \tag{8.26}$$

of a quasiparticle propagator plus a regular part $G_{smooth}(k, \omega)$. The latter is unknown, but has no poles by definition. The many-body time-ordered Green's function can therefore be expressed as:

$$i\, G_{\mathbf{k}}(t) = Z_k e^{-i\frac{\epsilon(k)}{\hbar}t} e^{-\gamma(k)t} + G_{smooth}(t) \quad t > 0 \tag{8.27}$$

and the spectral function as:

$$A(\mathbf{k}, \omega) = Z_k \frac{1}{\pi} \frac{\gamma(k)}{\left(\omega - \frac{\epsilon(k)}{\hbar}\right)^2 + \gamma(k)^2} + A_{smooth}(\omega) \tag{8.28}$$

Therefore, the concept of quasiparticle is useful if we require that $\hbar\gamma(k) \ll \epsilon(k)$, and $Z_k \gg 0$. Inserting the first condition in (8.25) leads to the following expressions for $\epsilon(k), \gamma(k)$ and Z_k:

$$\begin{aligned} \epsilon(k) &= \frac{\hbar^2 k^2}{2m} + \mathrm{Re}\Sigma\left(k, \epsilon(k)\right) \\ Z_k^{-1} &= 1 - \partial_{\hbar\omega}\mathrm{Re}\Sigma\left(k, \epsilon(k)\right) \\ \hbar\gamma(k) &= Z_k\, \mathrm{Im}\Sigma\left(k, \epsilon(k)\right) \end{aligned} \tag{8.29}$$

As shown by Luttinger [300], $\gamma(k)$ is small if $\epsilon(k)$ is close to the Fermi energy $\mu = \epsilon(k_F)$. Away from the Fermi level, where $\hbar\gamma(k) \ll \epsilon(k)$, $Z_k \gg 0$ and the concept of of quasiparticle is meaningful, the spectral function still features narrow peaks at positions $\epsilon(k)$, which define the so-called electronic band. However, in a Fermi liquid the electronic band and the quasiparticle dispersion relation should agree at the Fermi level [301, 302].

Close to the chemical potential μ, the quasiparticle dispersion relation has the expansion:

$$\epsilon(k) = \mu + \frac{\hbar^2 k_F}{m^*}(k - k_F) \tag{8.30}$$

whence:

$$\frac{m}{m^*} = \frac{m}{\hbar^2 k_F}\,\partial_k \epsilon(k_F) = \frac{1 + \frac{m}{\hbar^2 k_F}\,\partial_k \mathrm{Re}\Sigma\left(k_F, \mu\right)}{1 - \partial_{\hbar\omega}\mathrm{Re}\Sigma\left(k_F, \mu\right)} = Z_{k_F}\left(1 + \frac{m}{\hbar^2 k_F}\,\partial_k \mathrm{Re}\Sigma\left(k_F, \mu\right)\right) \tag{8.31}$$

The imaginary part $\gamma(k)$ defines the quasiparticle lifetime, which is finite due to the scattering processes, and diverges close to the Fermi level.
Since the effective mass can be computed from the quasiparticle dispersion relation, and this quantity agrees with the electronic band around k_F, it is possible to provide an estimate of m^* from the derivatives of the electronic band [301, 302].

8.3 AFQMC evaluation of the greater Green's function

With the purpose of estimating the Green's function:

$$\mathcal{G}_{ij}(\tau) = \frac{\langle \Phi_0 | \hat{a}_i e^{-\tau(\hat{H}-\epsilon_0)} \hat{a}_j^\dagger | \Phi_0 \rangle}{\langle \Phi_0 | \Phi_0 \rangle} \quad \tau \geq 0 \tag{8.32}$$

with the phaseless AFQMC method, let us write:

$$\hat{a}_i e^{-\tau(\hat{H}-\epsilon_0)} \hat{a}_j^\dagger = \int dg(\boldsymbol{\eta}_{n-1}) \dots dg(\boldsymbol{\eta}_{n-1-r})\, \hat{a}_i \hat{G}(\boldsymbol{\eta}_{n-1}) \dots \hat{G}(\boldsymbol{\eta}_{n-1-r}) \hat{a}_j^\dagger \tag{8.33}$$

and recall the identity (6.8), thanks to which:

$$\hat{G}(\boldsymbol{\eta})\, \hat{a}_j^\dagger = \sum_k \left[e^{\mathcal{A}(\boldsymbol{\eta})} \right]_{kj} \hat{a}_k^\dagger\, \hat{G}(\boldsymbol{\eta}) \tag{8.34}$$

Equation (8.34) leads to:

$$\mathcal{G}_{ij}(\tau) = \int dg(\boldsymbol{\eta}_{n-1}) \dots dg(\boldsymbol{\eta}_{n-1-r}) \sum_k \mathcal{D}_{kj} \frac{\langle \Phi_0 | \hat{a}_i \hat{a}_k^\dagger \hat{G}(\boldsymbol{\eta}_{n-1}) \dots \hat{G}(\boldsymbol{\eta}_{n-1-r}) | \Phi_0 \rangle}{\langle \Phi_0 | \Phi_0 \rangle} \tag{8.35}$$

where:

$$\mathcal{D} = e^{\mathcal{A}(\boldsymbol{\eta}_{n-1})} \dots e^{\mathcal{A}(\boldsymbol{\eta}_{n-1-r})} \tag{8.36}$$

Application of the importance sampling technique yields the estimator:

$$\mathcal{G}_{ij}(\tau) \sim \frac{\sum_{w=1}^{N_w} \mathfrak{W}_{n+m}^{(w)}}{\sum_{w=1}^{N_w} \mathfrak{W}_{n+m-r}^{(w)}} \sum_{w=1}^{N_w} \frac{\mathfrak{W}_{n+m}^{(w)}}{\sum_{w=1}^{N_w} \mathfrak{W}_{n+m}^{(w)}} \sum_k \mathcal{D}_{kj} \frac{\langle \Psi_{BP,m\delta\tau}^{(w)} | \hat{a}_i \hat{a}_k^\dagger | \Psi_{n\delta\tau}^{(w)} \rangle}{\langle \Psi_{BP,m\delta\tau}^{(w)} | \Psi_{n\delta\tau}^{(w)} \rangle} \tag{8.37}$$

where $\Psi_{n\delta\tau}^{(w)}$ and $\Psi_{BP,m\delta\tau}^{(w)}$ are given by (5.111).

8.3.1 Numeric Stabilization

In the long imaginary time limit, the estimator (8.37) is affected by a form of numeric instability, stemming from the need of multiplying more and more matrices to compute (8.36). The estimator (8.37) can be stabilized relying on the technique introduced by F. F. Assaad and M. Imada [271] and by M. Feldbacher and F. F. Assaad [272].
The first step is expressing (8.37) as:

$$\mathcal{G}(\tau) = \sum_w \mathcal{P}_w\, \left(I - \mathcal{G}_w(\tau_n, \tau_n) \right) B_w(\tau_n, \tau_n - \tau) = \sum_w \mathcal{P}_w\, \mathcal{H}_w(\tau_n, \tau_n - \tau) \tag{8.38}$$

where $\tau_n = n\delta\tau$, $\mathcal{P}_w$ is the same weight in (7.31) and:

$$\mathcal{G}_w(\tau_n,\tau_n)_{ik} = \frac{\langle \Psi^{(w)}_{BP,m\delta\tau} | \hat{a}^\dagger_k \hat{a}_i | \Psi^{(w)}_{n\delta\tau} \rangle}{\langle \Psi^{(w)}_{BP,m\delta\tau} | \Psi^{(w)}_{n\delta\tau} \rangle} \tag{8.39}$$

Moreover:

$$B_w(\tau_n,\tau_m) = \begin{cases} e^{\mathcal{A}(\boldsymbol{\eta}_{n-1})} \dots e^{\mathcal{A}(\boldsymbol{\eta}_{m-1})} & \text{if } n > m \\ 1 & \text{if } n = m \\ e^{-\mathcal{A}(\boldsymbol{\eta}_{m-1})} \dots e^{-\mathcal{A}(\boldsymbol{\eta}_{n-1})} & \text{if } n < m \end{cases} \tag{8.40}$$

Thanks to (5.22), the matrix (8.39) can be written as:

$$\mathcal{G}_w(\tau_n,\tau_n) = B_w(\tau_n,0)\Psi_T \left(\Psi_T\, B_w(T,0)\, \Psi_T\right)^{-1} \Psi_T B_w(T,\tau_n) \tag{8.41}$$

where $\tau_m = m\delta\tau$ and $T = \tau_n + \tau_m$.

As discussed in [272, 303], (8.39) is a projector:

$$\mathcal{G}_w(\tau_n,\tau_n) = \mathcal{G}_w(\tau_n,\tau_n)^2 \tag{8.42}$$

To prove this important result, it is useful to observe that the matrices B_w obey:

$$B_w(\tau_1,\tau_3) = B_w(\tau_1,\tau_2)B_w(\tau_2,\tau_3) \tag{8.43}$$

for all τ_1,τ_2,τ_3. Therefore:

$$\begin{aligned} \mathcal{G}_w(\tau_n,\tau_n)^2 =& B_w(\tau_n,0)\Psi_T \left(\Psi_T\, B_w(T,0)\, \Psi_T\right)^{-1} \Big[\Psi_T B_w(T,\tau_n)\times \\ &\times B_w(\tau_n,0)\Psi_T\Big] \left(\Psi_T\, B_w(T,0)\, \Psi_T\right)^{-1} \Psi_T B_w(T,\tau_n) = \\ =& B_w(\tau_n,0)\Psi_T \left(\Psi_T\, B_w(T,0)\, \Psi_T\right)^{-1} \Psi_T B_w(T,\tau_n) = G_w(\tau_n,\tau_n) \end{aligned} \tag{8.44}$$

Equation (8.42) and the following relation:

$$\mathcal{G}_w(\tau_2,\tau_2) = B_w(\tau_2,\tau_3)G_w(\tau_3,\tau_3)B_w(\tau_3,\tau_2) \tag{8.45}$$

which is a straightforward consequence of (8.41) and (8.43), have a great importance in the stabilization of (8.37). Thanks to (8.42) and (8.45), indeed, the matrices $\mathcal{H}_w$ obey the multiplication relation:

$$\mathcal{H}_w(\tau_3,\tau_1) = \mathcal{H}_w(\tau_3,\tau_2)\mathcal{H}_w(\tau_2,\tau_1) \tag{8.46}$$

for all τ_1,τ_2,τ_3. Equation (8.46) can be proved observing that:

$$\mathcal{H}_w(\tau_3,\tau_2)\mathcal{H}_w(\tau_2,\tau_1) = (1-\mathcal{G}_w(\tau_3,\tau_3))B_w(\tau_3,\tau_2)(1-\mathcal{G}_w(\tau_2,\tau_2))B_w(\tau_2,\tau_1) \tag{8.47}$$

which, since:

$$\begin{aligned} 1-\mathcal{G}_w(\tau_2,\tau_2) &= B_w(\tau_2,\tau_3)B_w(\tau_3,\tau_2) - B_w(\tau_2,\tau_3)G_w(\tau_3,\tau_3)B_w(\tau_3,\tau_2) = \\ &= B_w(\tau_2,\tau_3)\left(1-\mathcal{G}_w(\tau_3,\tau_3)\right)B_w(\tau_3,\tau_2) \end{aligned} \tag{8.48}$$

takes the form:

$$\mathcal{H}_w(\tau_3,\tau_2)\mathcal{H}_w(\tau_2,\tau_1) = (1-\mathcal{G}_w(\tau_3,\tau_3))^2 B_w(\tau_3,\tau_1) \tag{8.49}$$

and equals the left member of (8.46) by (8.42). Equation (8.46) trivially generalizes to:

$$\mathcal{H}_w(\tau_k,\tau_1) = \prod_{j=1}^{k-1} \mathcal{H}_w(\tau_{j+1},\tau_j) \tag{8.50}$$

For $\tau_k \gg \tau_1$, the left member of (8.46) can be numerically unstable, resulting from the product of many matrices. On the other hand, the factors in the right member are numerically more stable objects that can be multiplied safely.
Thanks to (8.46), it is possible to write the estimator (8.37) of $\mathcal{G}_{ij}(\tau)$ as:

$$\mathcal{G}(\tau) = \sum_w \mathcal{P}_w\, \mathcal{H}_w(\tau_n,\tau_n-\tau) = \mathcal{G}(\tau) = \sum_w \mathcal{P}_w\, \mathcal{H}_w(\tau_n,\tau_n-\tau')\mathcal{H}_w(\tau_n-\tau',\tau_n-\tau) \tag{8.51}$$

where $\tau' = s\delta\tau < \tau$ and:

$$\begin{aligned}
\mathcal{H}_w(\tau_n,\tau_n-\tau') &= \Big(1 - B_w(\tau_n,0)\Psi_T \left(\Psi_T\, B_w(T,0)\, \Psi_T\right)^{-1} \Psi_T B_w(T,\tau_m)\Big) \times \\
&\times \left(D(\boldsymbol{\eta}_{n-1})\ldots D(\boldsymbol{\eta}_{n-1-s})\right) \\
\mathcal{H}_w(\tau_n-\tau',\tau_n-\tau) &= \Big(1 - B_w(\tau_n-\tau',0)\Psi_T \left(\Psi_T\, B_w(T,0)\, \Psi_T\right)^{-1} \Psi_T B_w(T,\tau_m+\tau')\Big) \times \\
&\times \Big(D(\boldsymbol{\eta}_{n-1-(s+1)})\ldots D(\boldsymbol{\eta}_{n-1-r})\Big)
\end{aligned} \tag{8.52}$$

The estimator (8.51) is computationally more demanding than (8.37) but involves numerically more stable objects, and it trivially generalizes to more than two matrices $\mathcal{H}_w$.

8.4 Results

The main result of the present Chapter is the calculation of the effective mass and electronic band of high-density 2D HEGs with the phaseless AFQMC method.

8.4.1 Simulations with periodic boundary conditions

We have simulated paramagnetic systems of $N = 10,\ 18,\ 26,\ 42$ electrons in PBC, at $r_s = 0.25,\ 0.5,\ 1,\ 1.5,\ 2$. We focus on the high-density regime, where the methodology provides reliable results with moderate computational resources.
For all the studied systems, we have computed the ground-state energy per particle $\mathcal{E}_N$ simulating N particles inside a square region of surface $\Omega = N\pi r_s^2 a_B^2$ in PBC.
Moreover, we have computed the ground-state energy per particle $\mathcal{E}_{N+1}$ simulating $N+1$ particles inside a square region of surface Ω, i.e. at Seitz radius:

$$r_s' = \sqrt{\frac{N}{N+1}}\, r_s \tag{8.53}$$

The difference:

$$\mu_N = \mathcal{E}_{N+1} - \mathcal{E}_N \tag{8.54}$$

provides an estimate of the chemical potential.
For all the studied systems, we have also computed the imaginary-time greater Green's function:

$$\mathcal{G}_{\mathbf{k}}(\tau) = \frac{\mathcal{G}_{\mathbf{k}\uparrow}(\tau) + \mathcal{G}_{\mathbf{k}\downarrow}(\tau)}{2} \tag{8.55}$$

which is reported in Figure 8.1 for $N = 42$.
We have fitted the AFQMC estimates of $\mathcal{G}_{\mathbf{k}}(\tau)$ to a single exponential:

$$\mathcal{G}_{\mathbf{k}}(\tau) \simeq (1 - n_{\mathbf{k}})\ e^{-\tau\epsilon^{+}_{\mathbf{k}}} \tag{8.56}$$

and, recalling that $\epsilon^{+}_{\mathbf{k}} = \epsilon_{\mathbf{k}} + \mu$, we have obtained the electronic bands reported in Figure 8.1. For all N, r_s, we have fitted the electronic band to a quartic function:

$$\frac{\epsilon_{\mathbf{k}}}{\epsilon_F} = a + b\left(\frac{k}{k_F}\right)^2 + c\left(\frac{k}{k_F}\right)^4 \tag{8.57}$$

and computed the effective mass of the HEG with formula (8.31):

$$\frac{m^*}{m} = \frac{k_F}{\partial_k \frac{\epsilon(k_F)}{E_F}} \tag{8.58}$$

The effective masses obtained with this procedure are listed in Table 8.1 for all N, r_s. Error bars on the ratio m^*/m are obtained from those on the fit parameters a, b, c in (8.57) by standard error propagation.
The data in Figure 8.1 and Table 8.1 confirm the good accuracy of our calculations, but they also reveal the great difficulty of computing the effective mass of the 2D HEG with QMC calculations:

1. First, the Fermi liquid properties of the HEG are well-defined in the thermodynamic limit of large system size, and in QMC simulations we can study only small numbers of electrons.

2. Moreover, for a HEG in a finite simulation cell subject to PBC, momentum quantization limits the available wavevectors $\mathbf{k}$ to a discrete lattice. The energy band is well-defined for all wavevectors, but agrees with the quasiparticle dispersion relation (giving access to the effective mass) only close to the Fermi surface, which is directly inaccessible due to the finite size of the systems under study. In particular, as discussed in [304, 305, 306, 307], finite-size effects on the Fermi liquid properties are particularly severe.

3. Finally, the long-range Coulomb and correlation effects cannot be treated exactly in a finite cell, giving rise to finite-size errors in the energy band and hence in the effective mass [301, 302].

The data presented in Figures 8.1 and Table 8.1 illustrate the presence of finite-size effects on the electronic band and effective mass on a quantitative basis. Indeed, due to the finite size of the systems under study, wavevectors in Figure 8.1 are always greater than $k_{min} = 1.09\,k_F$ and thus the Fermi wavevector k_F is not approached. Moreover the estimates of m^*, despite being very precise, exhibit a very slow and in most cases non-monotonic convergence to the thermodynamic limit.
These observation clearly indicate the need of estimating the electronic band and effective mass with a more refined and reliable technique.

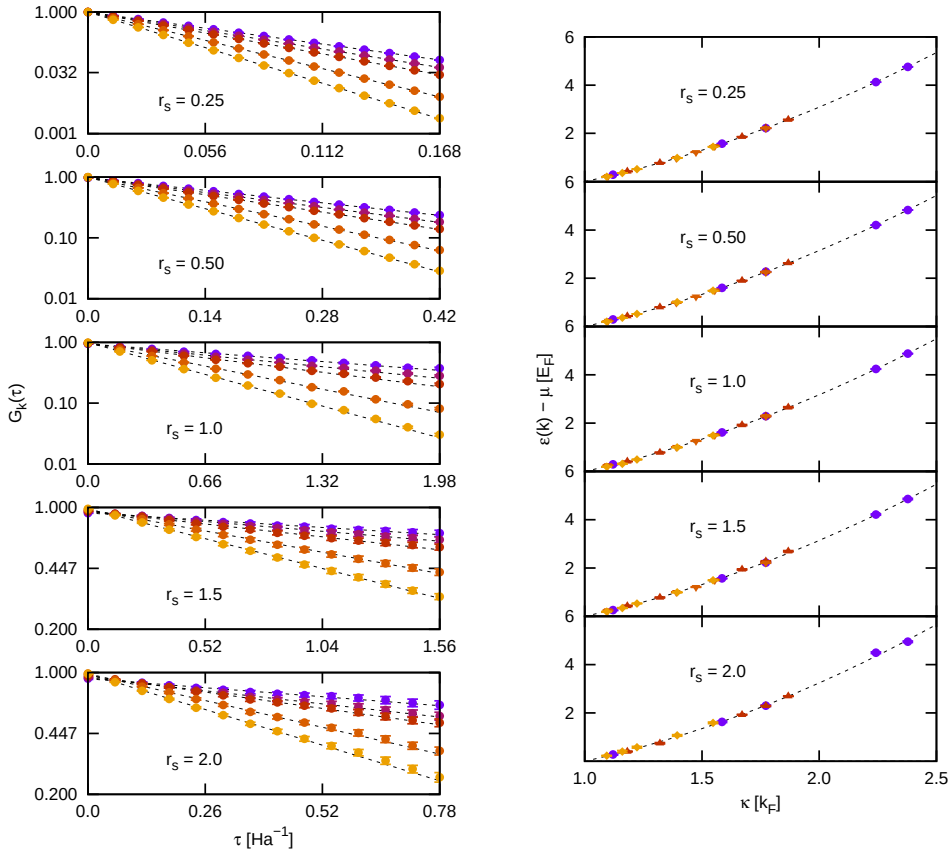

(a) (b)

Figure 8.1: Left: imaginary-time Green's functions for systems of $N = 42$ particles at $r_s = 0.25$, 0.5, 1, 1.5, 2 (top to bottom) and $\frac{|\mathbf{q}|}{k_F} = 1.09, 1.16, 1.22, 1.39, 1.55$ (mauve, purple, red, orange, yellow). $k_F = \sqrt{2}/r_s$ is the Fermi wavevector at the thermodynamic limit. Dashed lines are the results of the fit (8.56). Right: electronic bands $\epsilon(k)$ for systems at $r_s = 0.25, 0.5, 1, 1.5, 2$ (top to bottom), and $N = 10, 18, 26, 42$ (mauve circles, red upward-pointing triangles, orange downward-pointing triangles, yellow diamonds). Dashed lines, resulting from the fit (8.57), are just guides for the eye.

8.4.2 Calculations with twist-averaged boundary conditions

We mitigate the two major difficulties of the calculation, namely the extrapolations to $N \to \infty$ and $k \to k_F$, replacing PBC with twist-averaged boundary conditions (TABC) [308], briefly described in Appendix 13.1.3.

We already observed in Chapter 7 the presence of considerable finite-size and shell effects in dynamical properties like the DSF. Extrapolating the SDF to the thermodynamic limit appears a rather delicate operation, due to the presence of multiple excitation energies even at the smallest wavevectors $\mathbf{q}$.

On the other hand, the imaginary-time Green's function is dominated by a single excitation energy corresponding to the electronic band $\epsilon(k)$. In the light of this observation,

N	r_s	$\frac{m^*}{m}$	$\sigma_{\frac{m^*}{m}}$
10	0.25	0.982	0.003
18	0.25	0.974	0.001
26	0.25	0.970	0.002
42	0.25	0.956	0.004
10	0.5	0.970	0.004
18	0.5	0.951	0.002
26	0.5	0.956	0.002
42	0.5	0.929	0.002
10	1.0	0.956	0.003
18	1.0	0.936	0.006
26	1.0	0.957	0.007
42	1.0	0.902	0.007
10	1.5	0.956	0.006
18	1.5	0.919	0.009
26	1.5	0.985	0.012
42	1.5	0.923	0.006
10	2.0	0.940	0.004
18	2.0	0.912	0.008
42	2.0	0.886	0.006

Table 8.1: Effective mass (column 3) of the systems under study, as function of the number of particle (column 1) and of the Seitz radius (column 2).

TABC appear a very natural choice for mitigating the shell effects on $\epsilon(k)$ and m^*.
For several twists $\boldsymbol{\theta}$, placed on a grid $\mathcal{G}$ of 15 points:

1. we construct the basis of the single-particle Hilbert space applying the twist $\boldsymbol{\theta}$ to the spin-definite plane waves (7.2):

$$\varphi_{\mathbf{k}'\sigma}(\mathbf{r},\omega) = \frac{e^{i\left(\mathbf{k}+\frac{\boldsymbol{\theta}}{L}\right)\cdot\mathbf{r}}}{\sqrt{\Omega}}\chi_\sigma(\omega) \tag{8.59}$$

2. we sort the single-particle orbitals in ascending order of energy and construct the lowest-energy Slater determinant $|\Psi_T(\boldsymbol{\theta})\rangle$.

3. we perform a phaseless AFQMC calculation, with trial determinant equal to $|\Psi_T(\boldsymbol{\theta})\rangle$, of $\mathcal{E}_N(\boldsymbol{\theta})$, $\mathcal{E}_{N+1}(\boldsymbol{\theta})$ and:

$$G_{\mathbf{k}'}(\tau) \simeq (1-n_{\mathbf{k}'})\; e^{-\tau\epsilon^+_{\mathbf{k}'}} \tag{8.60}$$

thus extracting the electronic band $\epsilon_{\mathbf{k}'} = \epsilon^+_{\mathbf{k}'} - \mu(\boldsymbol{\theta})$ relative to the twist $\boldsymbol{\theta}$, where

$\mu(\boldsymbol{\theta}) = \mathcal{E}_{N+1}(\boldsymbol{\theta}) - \mathcal{E}_N(\boldsymbol{\theta})$. The imaginary-time Green's functions relative to $\boldsymbol{\theta} = (2,2)$ are illustrated in Figure 8.2, to illustrate the accuracy of the calculation in presence of twists.

4. we fit the electronic band to a quartic function, computing the effective mass $\frac{m^*(\boldsymbol{\theta})}{m}$ relative to the twist $\boldsymbol{\theta}$ with (8.31).

At the end of the simulation, we average $m^*(\boldsymbol{\theta})$ over the twists $\boldsymbol{\theta}$:

$$\frac{m^*}{m} = \frac{\sum_{\boldsymbol{\theta}\in\mathcal{G}} w_{\boldsymbol{\theta}} \frac{m^*(\boldsymbol{\theta})}{m}}{\sum_{\boldsymbol{\theta}\in\mathcal{G}} w_{\boldsymbol{\theta}}} \tag{8.61}$$

$w_{\boldsymbol{\theta}}$ being a weight that takes into account the multiplicity of the twist $\boldsymbol{\theta}$ (resulting from the symmetry of the Brillouin zone under reflections of the x and y axes) and the statistical uncertainty on $m^*(\boldsymbol{\theta})/m$. We also gather the excitation energies $\epsilon_{\mathbf{k}'}$ to produce a TABC estimate of the electronic band.
Electronic bands at $r_s = 0.25, 0.5, 1.0$ are shown in Figures 8.3 and 8.4. Comparing Figure 8.1 with Figures 8.3 and 8.4, we see that TABC considerably help approaching the Fermi surface.
Effective masses obtained with the TABC estimator (8.61) are illustrated in Figure 8.6. In all cases the effective masses decrease monotonically with the number N of particles. With the purpose of extrapolating the effective mass to the thermodynamic limit, and of investigating the behavior of the effective mass as a function of N, we fit the the function:

$$\frac{m^*}{m}(N) = a + \frac{b}{N^c} \tag{8.62}$$

to the data illustrated in Figure 8.6. In (8.62) a,b and c are fitting parameters, with $c > 0$ and $a = \lim_{N\to\infty} \frac{m^*}{m}(N)$. Results of the fit procedure are detailed in Table 8.2.
In all cases, the convergence to the thermodynamic limit is slow, since the fitting functions (8.62) feature an optimal exponent $c < 1$. This is in qualitative agreement with the $N^{-1/4}$ behavior predicted by M. Holzmann *et al.* [305, 306] for excitations near the Fermi surface. It should be noted that a more quantitative comparison would be difficult to make, because the exponent c is a very sensitive quantity, featuring larger relative errors than the parameters a, b. Moreover, the estimates $m^*(\boldsymbol{\theta})$ of the effective mass in (8.61) result from a fit of the electronic band over the range $k_F < |\mathbf{k}| < 2k_F$, that can mask the behavior of the band near the Fermi surface [301, 302]. Finally, the finite-size effects on m^* might also be modelled by the real local energy and phaseless approximations: indeed, recent DMC calculations provide qualitatively different finite-size effects [302].
The parameter a, corresponding to the thermodynamic limit of the effective mass, is a less sensitive parameter. To verify this fact, we have fitted also the function $\frac{m^*}{m}(N) = a + \frac{b}{N} + \frac{c}{N^2}$ to the data illustrated in Figure 8.6, obtaining $m^*/m = 0.958(5)$, $0.936(8)$, $0.904(5)$ in good agreement with the results in Table 8.2.
It is also possible to compute the effective mass fitting the electronic bands in Figures 8.3 and 8.4 to a quartic function (8.57). Results of the fit procedure are detailed in Table 8.2.
The two estimates are based on different approaches. In the first one, equation (8.61), the estimates $m^*(\boldsymbol{\theta})$, each relative to a specific twist $\boldsymbol{\theta}$, are averaged over all twists. In the second one, electronic bands relative to various twists $\boldsymbol{\theta}$ are gathered to form the estimates in Figures 8.3, 8.4 and then fitted to a quartic function. Due to the inherent difference between between the two approaches, results are only in qualitative agreement

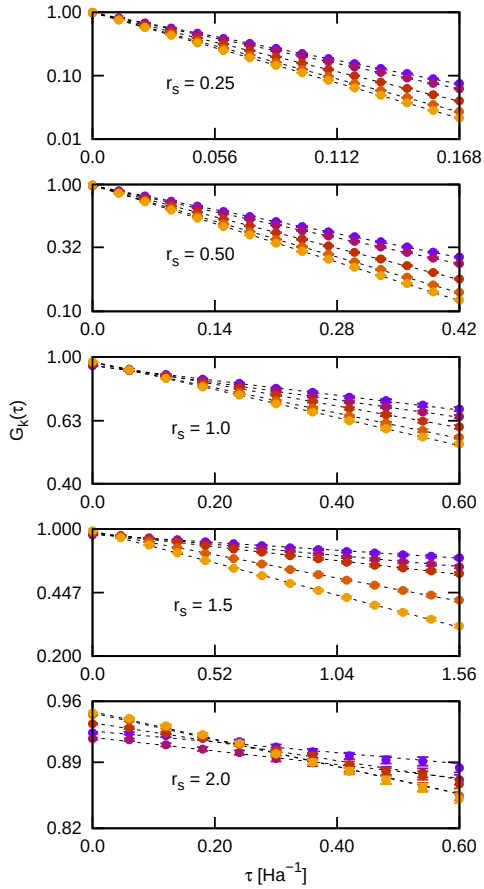

Figure 8.2: Imaginary-time Green's functions for systems of $N = 42$ particles at $r_s = 0.25$, 0.5, 1, 1.5, 2 (top to bottom) and $\frac{|\mathbf{q}|}{k_F} = 1.06$, 1.10, 1.17, 1.23, 1.26 (mauve, purple, red, orange, yellow), under the twist $\boldsymbol{\theta} = (2, 2)$. Dashed lines are the results of the fit (8.56).

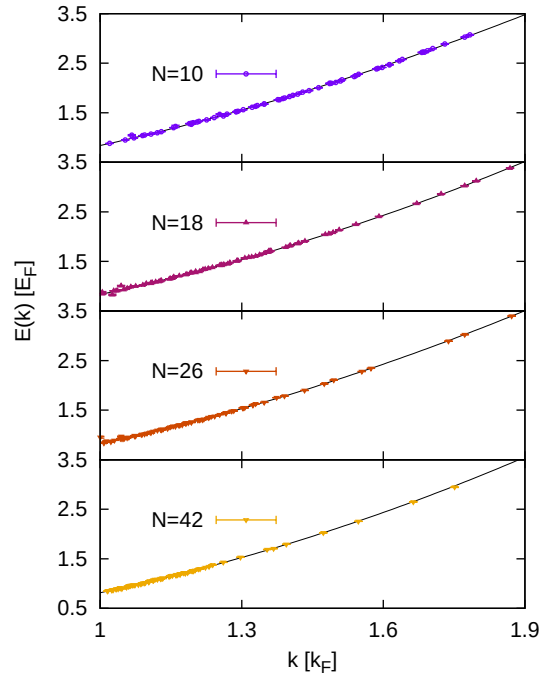

(a)

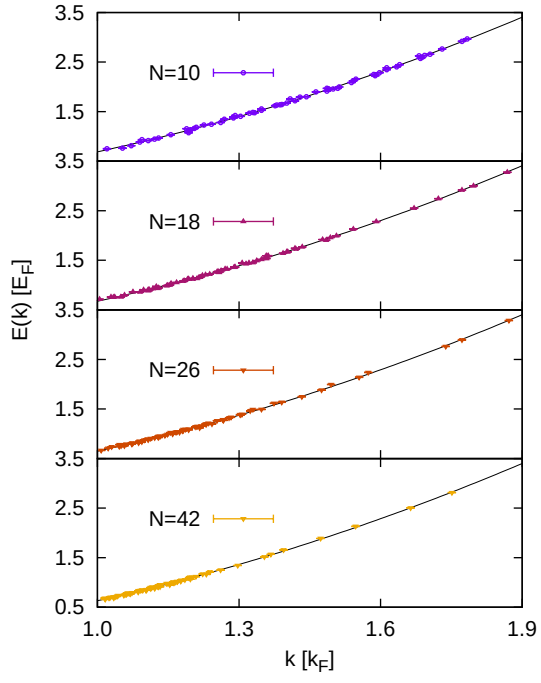

(b)

Figure 8.3: TABC estimate of the electronic band for systems of $N = 10, 18, 26, 42$ (top to bottom) particles at $r_s = 0.25$ (a), 0.5 (b). Black solid lines result from the fit (8.57).

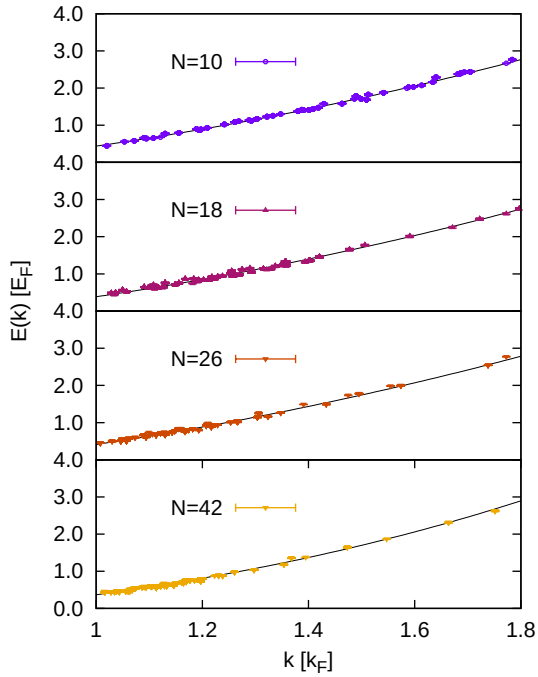

Figure 8.4: TABC estimate of the electronic band for systems of $N = 10, 18, 26, 42$ (top to bottom) particles at $r_s = 1.0$. Black solid lines result from the fit (8.57)

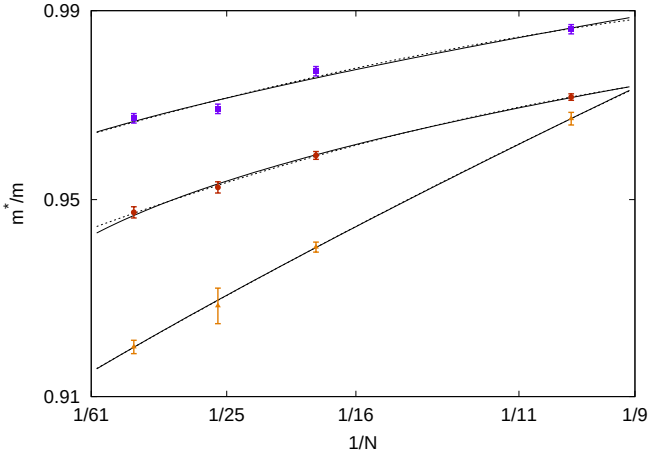

Figure 8.5: TABC estimates of the effective mass for systems of $N = 10, 18, 26, 42$ particles at $r_s = 0.25, 0.5, 1.0$ (mauve, red, orange). Black solid lines result from the fit (8.62) to a power law, black dashed lines from the fit to $a + \frac{b}{N} + \frac{c}{N^2}$.

r_s	c	χ^2
0.25	0.25	2.07
	0.50	1.81
	0.75	1.73
	1.00	1.84
0.5	0.25	0.79
	0.40	0.60
	0.50	0.64
	0.75	1.12
	1.00	1.72
1.0	0.25	3.06
	0.50	2.08
	0.75	1.25
	0.80	1.14
	0.90	1.26

r_s	c_{opt}	$\frac{m^*}{m}$
0.25	0.73	0.955(5)
0.5	0.42	0.919(8)
1.0	0.92	0.906(6)

r_s	N	$\frac{m^*}{m}$
0.25	10	0.953(18)
	18	0.986(16)
	26	0.970(15)
	42	0.977(29)
0.50	10	0.973(27)
	18	0.966(20)
	26	0.954(26)
	42	0.942(27)
1.00	10	0.964(10)
	18	0.943(31)
	26	0.932(35)
	42	0.993(35)

Table 8.2: Left: χ^2 value for several values of the exponent c in the finite-size fitting formula (8.62). Center: optimal exponent c and extrapolated effective mass $\lim_{N\to\infty} m^*(\boldsymbol{\theta})/m = a$. Right: effective masses obtained from the fit of the electronic bands in Figures 8.3, 8.4 to a quartic function.

with each other. Moreover, the effective masses obtained fitting the electronic bands exhibit larger statistical uncertainties.
These observations lead to consider the estimates (8.61) more robust.

8.4.3 Comparison with previous results

Our results for the effective mass of the 2D HEG as function of the Seitz radius are shown in Figure 8.6, in comparison with previous eperimental results [309, 286] and theoretical predictions from many-body calculations [6, 310] and QMC simulations [311, 63, 301, 302, 305].
The main information conveyed by Figure 8.6 is probably the great difficulty of computing the Fermi-liquid parameters of the 2D HEG, and their extreme sensitivity to the approximations employed in the calculations.
The effective mass is the most important parameter in Landau's phenomenological Fermi-liquid theory. All many-body calculations predict a decrease of the effective mass at $r_s \sim 0$ [312]. For instance, the RPA gives [237] the asymptotic expression:

$$\frac{m^*}{m} = 1 - \frac{r_s}{\sqrt{8}} \ln\left(\frac{\sqrt{2}}{r_s}\right) \quad , \qquad r_s \ll 1 \tag{8.63}$$

However, away from $r_s \sim 0$, the behavior of this fundamental physical property is far from being understood and established, and it is the subject of an ongoing debate.
Our results are in good agreement with VMC calculations by Y. Kwon *et al.* [311], later

confirmed by transient-estimate calculations [63] and, at $r_s = 1$, with recent DMC calculations by N. D. Drummond and J. R. Needs [301, 302].
Our estimates of the effective mass are also in reasonable agreement with experimental data by Y. Tan *et al.* [286]. However, it should be noted that the 2D electron gases studied in experiments are unavoidably different from the ideal 2D HEGs assumed in many-body calculations and QMC simulations, in that experimental systems are embedded in quasi-2D structures and are unavoidably subject to disorder [301]. In particular, results by Y. Tan *et al.* have been performed in 2D GaAs/AlGaAs heterostructures. Therefore, a precise quantitative comparison with existing experimental results would be inappropriate. However, experimental and QMC data mentioned above share the same qualitative behavior, featuring a decrease towards a global minimum and a subsequent increase.
On the other hand, many-body calculations illustrated in Figure 8.6, experimental data by J. L. Smith and P. J. Stiles [309], and VMC calculations by M. Holzmann *et al.* predict a steep increase in the effective mass as the Seitz radius is increased. For many-body calculations, in particular, m^* attains the minimum value at $r_s < 0.5$ and returns equal to m around $r_s \sim 1$. Our calculations, which we have fitted to the formula:

$$\frac{m^*}{m} = 1 - a\, r_s \ln\left(\frac{b}{r_s}\right) \quad , \qquad \begin{array}{l} a = 0.091(5) \\ b = 2.8(1) \end{array} \tag{8.64}$$

give much lower values of the effective mass over the range $r_s \leq 2$. Moreover, based on the fit (8.64), we predict that m^* returns equal to 1 at $r_s = 2.8(1)$, in qualitative agreement with QMC data by Y. Kwon *et al.* [311, 63].
It should be noted that all the methodologies represented in Figure 8.6, including the phaseless AFQMC method, are based on approximation schemes influencing their results. As clearly expained in [312], many-body calculations are based on a suitable simplification of the exact Ward's identity, in which the irreducible electron-hole interaction diagram is replaced by an effective electronic interaction. This simplification enables the self-consistent or on-shell calculation of the electronic band [312, 6], and thus of the effective mass. Results naturally depend on the choice of the effective electronic interaction and whether or not calculations are performed self-consistently [302].
Similarly, results of QMC simulations bear a dependence on the approximations underlying them, and of the techniques used to extrapolate results in the limit $N \to \infty$, $k \to k_F$.
Our calculations are being performed with the phaseless AFQMC method, that relies on approximation schemes different than the FN of DMC. Indeed, it exhibits different finite-size effects and provides a different estimate of this fundamental parameter of Landau's Fermi-liquid theory. The *a priori* unexpected agreement with VMC estimates by Y. Kwon *et al.* [311, 63] and DMC estimates by N. D. Drummond and R. J. Needs [301, 302] is therefore a remarkable circumstance, since the three methodologies rest upon indepedent approximation schemes (the variational Ansatz, FN and phaseless approximations respectively).
We hope that our estimate of the effective mass of high-density 2D HEGs, once completed, can provide a useful contribution to the investigation of Landau's Fermi-liquid parameters of the 2D HEG.

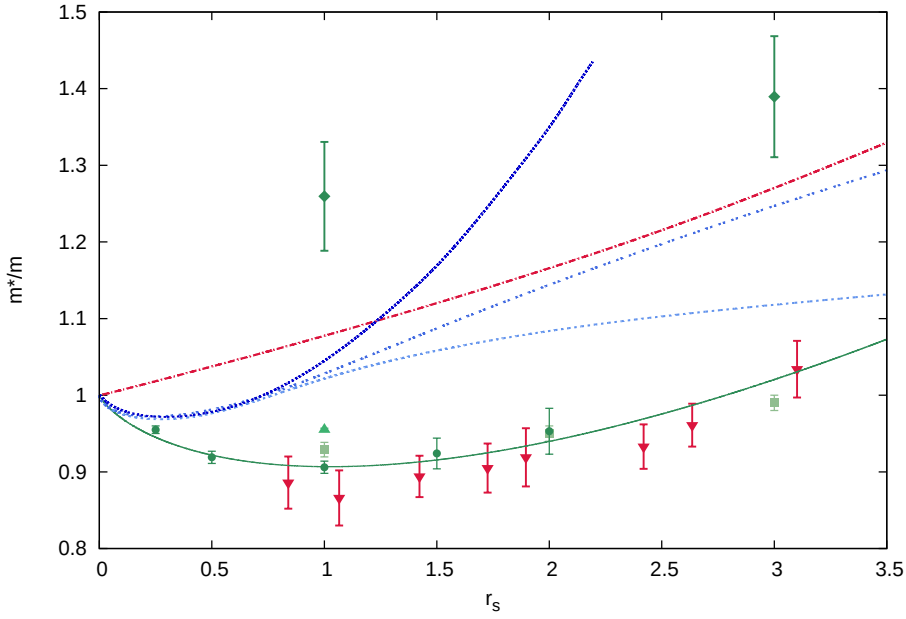

Figure 8.6: Quasiparticle effective mass m^* as function of the Seitz radius for paramagnetic 2D HEGs, as calculated or measured by several authors. Red dot-dashed line: experimental results by J. L. Smith and P. J. Stiles [309]. Red down-pointing triangles: experimental results by Y. Tan *et al.* [286].
Light blue dashed line: GW calculation with RPA effective interaction [6]. Medium blue double-dotted line: on-shell GW calculation with Kukkonen-Overhauser effective interaction and on-shell approximation [310]. Dark blue dotted line: self-consistent GW calculation with Kukkonen-Overhauser effective interaction [310].
Light green squares: VMC estimates by Y. Kwon *et al.* [311]. Medium green up-pointing triangles: DMC estimates by N. D. Drummond and R. J. Needs [302]. Dark green diamonds: VMC estimates by M. Holzmann *et al.* [305]. Dark green circles: AFQMC estimates (present work). Dark solid line: fit (8.64) of the AFQMC estimates.

Appendices

CHAPTER 9

Some results about time-dependent random phenomena

The purpose of the present Appendix is to provide the proofs of the propositions and theorems presented in Chapter 2, that were not included in the main text in order make the presentation as light as possible. The presentation of such results has the purpose of making the present Thesis as more self-consistent as possible. Formal and exhaustive presentations of the theory of Markov chains and stochastic processes can be found in [44, 313, 37, 45, 44, 72].

9.1 Markov chains

The following theorem, due to A. Markov and S. Kakutani [42, 43], ensures the existence of invariant laws for homogeneous Markov chains:

Theorem 9.1 (Markov-Kakutani)**.** *Any transition matrix $\mathcal{P}$ admits at least an invariant law.*
Proof. *Given a generic point $\pi \in \mathcal{S}_E$, consider the following sequence of Césaro averages:*

$$\pi_n = \frac{1}{n} \sum_{k=0}^{n-1} \pi \, \mathcal{P}^k \tag{9.1}$$

Obviously $\pi_n \in \mathcal{S}_E \; \forall \, n \geq 0$. Now, since $\mathcal{S}_E$ is a compact set, by virtue of the Bolzano-Weierstrass theorem the sequence (9.1) *has a subsequence $\{\pi_{n_k}\}_{n_k}$ converging to a point $\pi^* \in \mathcal{S}_E$. We observe that:*

$$\begin{aligned} \pi^* \mathcal{P} &= \lim_{k \to \infty} \pi_{n_k} \mathcal{P} = \lim_{k \to \infty} \frac{1}{n_k} \sum_{j=1}^{n_k} \pi \mathcal{P}^{j+1} \\ \pi^* \mathcal{P} &= \lim_{k \to \infty} \frac{1}{n_k} \sum_{j=2}^{n_k+1} \pi \mathcal{P}^{j} = \lim_{k \to \infty} \frac{1}{n_k} \left(\sum_{j=1}^{n_k} \pi \mathcal{P}^{j} + \pi \mathcal{P}^{n_k+1} - \pi \mathcal{P} \right) = \lim_{k \to \infty} \pi_{n_k} = \pi^* \end{aligned} \tag{9.2}$$

In the light of the definitions of irreducibility and regularity, given in Chapter 2, it is possible to prove Markov's theorem. Let us begin with an intermediate result:

Theorem 9.2. *If a transition matrix $\mathcal{P}$ has all strictly positive entries, it admits a unique invariant law π^* and, for all initial laws v:*

$$\pi^*_j = \lim_{n \to +\infty} \left(v \, \mathcal{P}^n \right)_j \tag{9.3}$$

Proof. *By virtue of Theorem 9.1, $\mathcal{P}$ admits invariant law π^* exists. By definition, it is a fixed point of the map:*

$$\mathcal{C} : \mathcal{S}_E \to \mathcal{S}_E v \mapsto \mathcal{C}(v) = v\mathcal{P} \tag{9.4}$$

It will now be shown that $\mathcal{C}$ is a strict contraction on $\mathcal{S}_E$ relative to the following distance:

$$d(v, w) = \frac{1}{2} \sum_{i \in E} |v_i - w_i| \tag{9.5}$$

First, since all the entries of $\mathcal{P}$ are strictly positive, there exists some number ϵ such that $\epsilon < \frac{1}{N}$ and $\mathcal{P}_{ij} \geq \epsilon \, \forall \, i, j \in E$. It is simple to show that $\mathcal{Q}_{ij} = \frac{\mathcal{P}_{ij} - \epsilon}{1 - N\epsilon}$ is a transition matrix on $\mathcal{S}_E$. The distance $d\left(\mathcal{C}(v), \mathcal{C}(w)\right)$ between the images of two generic laws $v, w \in \mathcal{S}_E$ through the map $\mathcal{C}$ can be expressed as:

$$\frac{1}{2} \sum_j \left| \left(v\,\mathcal{P}\right)_j - \left(w\,\mathcal{P}\right)_j \right| = \frac{1}{2} \sum_j \left| \sum_i \left(v_i - w_i\right) \left(1 - N\epsilon\right) \mathcal{Q}_{ij} \right| \tag{9.6}$$

and since:

$$\left| \sum_i \left(v_i - w_i\right) \left(1 - N\epsilon\right) \mathcal{Q}_{ij} \right| \leq \left(1 - N\epsilon\right) \sum_i |v_i - w_i| \; \mathcal{Q}_{ij} \tag{9.7}$$

and $\mathcal{Q}$ is a transition matrix, the distance (9.6) *is bounded by:*

$$d\left(\mathcal{C}(v), \mathcal{C}(w)\right) \leq \left(1 - N\epsilon\right) \sum_i |v_i - w_i| \sum_j \mathcal{Q}_{ij} = \left(1 - N\epsilon\right) \sum_i |v_i - w_i| = \left(1 - N\epsilon\right) d(v, w) \tag{9.8}$$

Equation (9.8) *ensures that $\mathcal{C}$ is a contraction. Hence the uniqueness of the invariant law π^* and its expression* (9.9) *follow from Banach's fixed point theorem [314].*

Theorem 9.2 has been proved under the strict requirement that all the entries of $\mathcal{P}$ are positive. Such condition can be relaxed, leading to the following fundamental result:

Theorem 9.3 (Markov)**.** *If a transition matrix $\mathcal{P}$ is regular, it admits a unique invariant law π^* and, for all initial laws v:*

$$\pi^*_j = \lim_{n \to +\infty} \left(v\,\mathcal{P}^n\right)_j \tag{9.9}$$

Proof. *The regularity condition implies the existence of an integer $m > 0$ such that $\mathcal{P}^m$ has all entries strictly positive. Hence, by Banach's fixed point theorem there exists a unique law π^* such that:*

$$\pi^* = \pi^* \mathcal{P}^m \qquad \lim_{n \to \infty} v\,\mathcal{P}^{mn} = \pi^* \quad \forall \, v \in \mathcal{S}_E \tag{9.10}$$

the second of (9.10) *can be extended to all laws of the form $v\,\mathcal{P}^k$ with $k < m - 1$. Now, if a sequence $\{v_n\}_n$ has the property that all the subsequences $\{v_{k+mn}\}_n$, with $k < m - 1$, converge to the same limit v^*, then it converges to v^*. Therefore:*

$$\lim_{n \to \infty} v\,\mathcal{P}^n = \pi^* \quad \forall \, v \in \mathcal{S}_E \tag{9.11}$$

π^* is also invariant since, by the continuity of the matrix product:

$$\pi^* \mathcal{P} = \left(\lim_{n \to \infty} v\,\mathcal{P}^n \right) \mathcal{P} = \lim_{n \to \infty} v\,\mathcal{P}^{n+1} = \pi^* \tag{9.12}$$

In the light of Markov's theorem, we can prove the following Metropolis theorem.

Theorem 9.4 (Metropolis *et al.*)**.** *Let $\pi \in \mathcal{S}_E$ be a non-uniform law with strictly positive components $\pi_j > 0 \, \forall \, i \in E$. Let $\mathcal{T}$ be a symmetric and irreducible transition matrix, $\mathcal{T}_{ij} = \mathcal{T}_{ji}$, subject to no other restrictions, and define:*

$$\mathcal{P}_{ij} = \begin{cases} \mathcal{T}_{ij} & i \neq j, \ \pi_j \geq \pi_i \\ \mathcal{T}_{ij} \frac{\pi_j}{\pi_i} & i \neq j, \ \pi_j < \pi_i \\ 1 - \sum_{j \neq i} \mathcal{P}_{ij} & i = j \end{cases} \tag{9.13}$$

For all the initial laws v the Markov chain $\{X_n\}_n$ with initial law v and transition matrix $\mathcal{P}$ is regular, and has π as unique invariant law.

Proof. *Let us first show that* (2.17) *is regular. If $i \neq j$ and $\mathcal{T}_{ij} > 0$, by construction $\mathcal{P}_{ij} > 0$; therefore, $\mathcal{P}$ is irreducible. To prove that* (2.17) *is regular, it is sufficient to show that there exists $i_0 \in E$ such that $\mathcal{P}_{i_0 \to i_0} > 0$. Since π is not uniform, there exists $M \subset E, M \neq E$ on which π takes maximum value; due to the irreducibility of $\mathcal{T}$ the chain can move outside M, and therefore there exist $i_0 \in M$ and $j_0 \in M^c$ such that $\mathcal{T}_{i_0 j_0} > 0$ and, by construction, $\pi_{i_0} > \pi_{j_0}$. Moreover, $\mathcal{P}_{ij} \leq \mathcal{T}_{ij}$ if $i \neq j$. These intermediate results imply:*

$$\begin{gathered} \mathcal{P}_{i_0 i_0} = 1 - \sum_{j \neq i_0} \mathcal{P}_{i_0 j} = 1 - \sum_{j \neq i_0, j_0} \mathcal{P}_{i_0 j} - \mathcal{P}_{i_0 j_0} \geq \\ \geq 1 - \sum_{j \neq i_0, j_0} \mathcal{T}_{i_0 j} - \mathcal{T}_{i_0 j_0} \frac{\pi_{j_0}}{\pi_{i_0}} = \\ = 1 - \sum_{j \neq i_0} \mathcal{T}_{i_0 j} + \mathcal{T}_{i_0 j_0} \left(1 - \frac{\pi_{j_0}}{\pi_{i_0}}\right) = \mathcal{T}_{i_0 i_0} + \mathcal{T}_{i_0 j_0} \left(1 - \frac{\pi_{j_0}}{\pi_{i_0}}\right) \geq \\ \geq \mathcal{T}_{i_0 j_0} \left(1 - \frac{\pi_{j_0}}{\pi_{i_0}}\right) > 0 \end{gathered} \tag{9.14}$$

thus ensuring the regularity of (2.17)*.*

In the light of Markov's theorem 9.3 it remains to show that π is invariant. Chosen a couple of states (i, j) such that, without loss of generality, $\pi_j \leq \pi_i$, $\mathcal{P}_{ij} = \mathcal{T}_{ij} \frac{\pi_j}{\pi_i}$ whereas $\mathcal{P}_{ji} = \mathcal{T}_{ji}$ and thus:

$$\pi_i \mathcal{P}_{ij} = \pi_i \mathcal{T}_{ij} \frac{\pi_j}{\pi_i} = \mathcal{T}_{ij} \pi_j = \pi_j \mathcal{P}_{ji} \tag{9.15}$$

where the hypothesis that $\mathcal{T}$ is symmetric has been used. As a consequence of (9.15) *π is invariant.*

9.2 Stochastic processes

Given a probability space $(\Omega, \mathcal{F}, P)$ and a measurable space $(E, \mathcal{E})$, an $\mathcal{E}$-valued stochastic process is a collection of random variables $X_t : \Omega \to E$, indexed by a parameter $t \in T \subseteq \mathbb{R}$. E is called the state space of the process and, if $E \subseteq \mathbb{R}^m$, X_t is called an mD stochastic process. Similarly, If $T = [0, T]$ is an interval, X_t is called a continuous-time stochastic process.

One of the most important continuous time stochastic process is the 1D Wiener process or Brownian motion, characterized by the following properties:

1. $B_0 = 0$ almost surely
2. the function $t \to B_t$ is almost surely everywhere continuous

3. for all $r < s < t$, the increment $B_t - B_s$ is independent of B_r and normally distributed: $B_t - B_s \sim N(0, t-s)$. Therefore, $B_t \sim N(0,t)$.

The 1D Brownian bridge is the stochastic process:

$$\tilde{B}_t = B_t - tB_1 \quad , \qquad 0 \leq t \leq 1 \tag{9.16}$$

The Brownian bridge satistfies $\tilde{B}_0 = \tilde{B}_1 = 0$ almost surely, and thus its trajectories depart and converge to the origin, the intermediate points being not restricted. The Brownian bridge starting at a and ending at b reads:

$$\tilde{B}_t \to \tilde{B}_t + \frac{t - t_1}{t_2 - t_1}(b - a) \tag{9.17}$$

Brownian motions and bridges are easily extended to higher dimensions writing $B_t = (B_{1,t} \dots B_{m,t})$, where $B_{i,t}$ are independent 1D Brownian motions.
Itō calculus, named after K. Itō [315], extends the methods of ordinary calculus to stochastic processes. The central concept of Itō calculus are stochastic integrals, which generalize the notion of Riemann integral to stochastic processes. Given a 1D stochastic process X_t, stochastic integrals constructed with X_t come in two types, depending on whether integration is made with respect to time or to a Brownian motion B_t:

$$\int_0^t X_s \, ds = \lim_{N\to\infty} \sum_{i=0}^{N-1} \Delta t \, X_{t_i} \quad , \quad \int_0^t X_s \, dB_s = \lim_{N\to\infty} \sum_{i=0}^{N-1} X_{t_i} \left(B_{t_{i+1}} - B_{t_i} \right) \tag{9.18}$$

where $t_i = \frac{it}{N}$, $i = 0 \dots N$ and $\Delta t = \frac{t}{N}$.
In the design and improvement of QMC methods, a role of considerable importance is played by Itō processes, i.e. all stochastic processes that can be expressed as the sum of an integral with respect to a Brownian motion and an integral with respect to time:

$$X_t = X_0 + \int_0^t \mu_s \, ds + \int_0^t \sigma_s \, dB_s \tag{9.19}$$

Whenever a process X_t is an Itō process, we say that X_t has stochastic differential:

$$dX_t = \mu_t \, dt + \sigma_t \, dB_t \tag{9.20}$$

Stochastic differential equations (9.20) can be regarded to as generalizing ordinary differential equations, like Newton's equations, to situations in which the observable described by X_t is subject to a noisy evolution. An instrument of fundamental theoretical and practical interest in Itō calculus is the following Itō's lemma [315, 316, 72], which we state without proof:

Lemma 9.1. *Let X_t be a process taking values in $E = \mathbb{R}^m$ with stochastic differential:*

$$dX_t = F(X_t, t)dt + G(X_t, t)dB_t \tag{9.21}$$

where dB_t is an rD Brownian motion and $F : E \times T \to E$ is a vector-valued integrable function and $G : E \times T \to \mathcal{M}_{m\times r}(\mathbb{R})$ is a matrix-valued square-integrable function. Let also $f : E \times T\mathbb{R}$ be a measurable function, continuous in every point $(\mathbf{x}, t)$, $\mathbf{x} = (x_1, \dots, x_m)$, continuously differentiable twice in $\mathbf{x}$ and once in t. Then, the process $Y_t = f(X_t, t)$ is an Itō process with

differential:

$$dY_t = \partial_t f(X_t,t)\,dt + \sum_{i=1}^{m} \partial_{x_i} f(X_t,t)\,dX_{i,t} + \frac{1}{2}\sum_{ij=1}^{m} \partial_{x_i x_j} f(X_t,t) \sum_{h=1}^{r} G_{ih}(X_t,t) G_{jh,t}(X_t,t) dt \tag{9.22}$$

In the remainder of the present Appendix, Itō's lemma will be used to prove the Fokker-Planck equation and the Feynman-Kac representation formulae.

9.2.1 Fokker-Planck equation

Let us consider a stochastic process $\mathcal{R}_t$ on $\mathbb{R}^d$, solution of the stochastic differential equation:

$$\begin{cases} dR_t = b(R_t,t)dt + \sigma(R_t,t)dB_t \\ R_0 = R \end{cases} \tag{9.23}$$

where R is a random variable with probability distribution $p_0(\mathbf{x})$, and a function $f : \mathbb{R}^d \to \mathbb{R}$. Under very mild assumptions [72] about the stochastic differential equation (9.23) and about f, the expectation $E[f(R_t)]$ of the random variable $f(R_t)$ is:

$$E[f(R_t)] = \int d\mathbf{y}\, f(\mathbf{y})\, p_t(\mathbf{y}) = \int d\mathbf{y} \int d\mathbf{x}\, f(\mathbf{y})\, p(\mathbf{y},t;\mathbf{x},0)\, p_0(\mathbf{x}) \tag{9.24}$$

where $p_t(\mathbf{y})$ is the probablity distribution of R_t, and $p(\mathbf{y},t;\mathbf{x},0)$ is the transition probability distribution of the stochastic process. We provide an alternative expression for (9.24) applying Itō's lemma to the stochastic process $S_t = f(R_t)$:

$$\begin{aligned} dS_t &= \sum_{i=1}^{d} \partial_i f(R_t)\cdot (dR_t)_i + \frac{1}{2}\sum_{ij=1}^{d} \partial_{ij} f(R_t) a_{ij}(R_t,t) dt = \\ &= \left(\mathcal{L}_t f\right)(R_t)\, dt + \sum_{ij=1}^{d} \partial_i f(R_t)\sigma_{ij}(R_t,t) dB_j(t) \end{aligned} \tag{9.25}$$

where the differential operator :

$$\left(\mathcal{L}_t f\right)(x) = \frac{1}{2}\sum_{ij=1}^{d} a_{ij}(x,t)\,\partial_{ij} f(x) + \sum_{i=1}^{d} b_i(x,t)\,\partial_i f(x) \tag{9.26}$$

Since:

$$S_t = f(R) + \int_0^t dS_t \tag{9.27}$$

and the Itō integral $\int_0^t \partial_i f(R_t)\,\sigma_{ij}(R_t,t)\,dB_j(t)$ has zero mean [72], we can write:

$$E[f(R_t)] = E[f(R)] + \int_0^t dt'\, E\left[\left(\mathcal{L}_{t'} f\right)(R_{t'})\right] \tag{9.28}$$

The time derivative:

$$\partial_t E[f(R_t)] = E\left[\left(\mathcal{L}_t f\right)(R_t)\right] \tag{9.29}$$

of (9.28) is most conveniently expressed recalling that:

$$\begin{aligned} \partial_t E[f(R_t)] &= \int d\mathbf{y} \int d\mathbf{x} f(\mathbf{y})\, \partial_t p(\mathbf{y}t;\mathbf{x}0)\, p_0(\mathbf{x}) \\ E\left[(\mathcal{L}_t f)\,(R_t)\right] &= \int \left(\frac{1}{2} \sum_{ij=1}^{d} a_{ij}(\mathbf{x},t)\, \partial_{ij} f(\mathbf{x}) + \sum_{i=1}^{d} b_i(\mathbf{x},t)\, \partial_i f(\mathbf{x}) \right) p(\mathbf{y}t;\mathbf{x}0)\, p_0(\mathbf{x}) \end{aligned} \tag{9.30}$$

Integrating by parts the right member of the equality, and recalling that R and f are arbitrary objects, we onclude that the transition probability distribution of the stochastic process R_t satisfies the following Fokker-Planck equation:

$$\partial_t p(\mathbf{y},t;\mathbf{x},0) = \frac{1}{2} \sum_{ij=1}^{d} \partial_{ij} \Big(a_{ij}(\mathbf{y},t) p(\mathbf{y},t;\mathbf{x},0) \Big) - \sum_{i=1}^{d} \partial_i \Big(b_i(\mathbf{y},t) p(\mathbf{y},t;\mathbf{x},0) \Big) \tag{9.31}$$

the association between the Fokker-Planck equation for $p(\mathbf{y},t;\mathbf{x},0)\Big)$ and the stochastic process R_t is the key for constructing an algorithmic procedure to compute the average $E[f(R_t)]$. First, observe that:

$$R_t = R + \int_0^t dR_{t'} \tag{9.32}$$

is approximated by the discretized stochatic process:

$$R_{i+1} = R_i + b(R_i,t_i)\Delta t + \sigma(R_i,t_i) dB_i \tag{9.33}$$

with $R_0 = R$, $t_i = i\Delta t$. Then, starting from a large number N_w of configurations $\{x_{0,w}\}_{w=1}^{N_w}$ sampled from the random variable R, and evolving them according to:

$$x_{i+1,w} = x_{i,w} + b(x_{i,w},t_i)\Delta t + \sigma(x_{i,w},t_i)\eta_{i,w} \tag{9.34}$$

where $\eta_{i,w}$ are sampled from independent and identically distributed Gaussian random variables with mean 0 and variance Δt, we can estimate $E[f(R_i)]$ as:

$$E[f(R_i)] \simeq \sum_{w=1}^{N_w} f(x_{i,w}) \tag{9.35}$$

by virtue of the central limit theorem.

9.2.2 Smart Sampling

The possibility of simulating the stochastic process associated to a Fokker-Planck equation is the theoretical justification of the smart sampling procedure [82]. Let us start from the observation that the Fokker-Planck equation:

$$-\partial_\tau p(\mathcal{R},\tau) = -\sum_i \frac{\hbar^2}{2m_i} \triangle_i p(\mathcal{R},\tau) + \sum_{i\alpha} \frac{\hbar^2}{m_i} \partial_{i\alpha} \Big(p(\mathcal{R},\tau) F_{i\alpha}(\mathcal{R}) \Big) \tag{9.36}$$

where the function:

$$F_{i\alpha}(\mathcal{R}) = \partial_{i\alpha} \log \Big(|\Psi_T(\mathcal{R})|^2 \Big) \tag{9.37}$$

is called *quantum force*, admits the unique stationary distribution:

$$p(\mathcal{R}) = \frac{|\Psi_T(\mathcal{R})|^2}{\int d\mathcal{R}' \, |\Psi_T(\mathcal{R}')|^2} \tag{9.38}$$

In order to verify that $|\Psi_T(\mathcal{R})|^2$ is a stationary solution of (9.36), it is sufficient to insert the reputed solution $|\Psi_T(\mathcal{R})|^2$ into (9.36). The solution is unique under very mild assumptions on the quantum force [317]. Suppose that $p_0(\mathcal{R})$ is a positive function, such that $\int d\mathcal{R}\, p_0(\mathcal{R}) = 1$. Then, $p_0(\mathcal{R})$ can be regarded to as the probability distribution of a suitable random variable $\mathcal{R}_0$. The solution $p(\mathcal{R}, \tau)$ of (9.36) with initial condition $p_0(\mathcal{R})$ can be interpreted as the probability distribution of stochastic process $\mathcal{R}_t$, solving the stochastic differential equation:

$$d\mathcal{R}_{\tau,i\alpha} = \frac{\hbar^2}{m_i} F_{i\alpha}(\mathcal{R}_\tau) d\tau + \frac{\hbar^2}{2m_i} dB_{\tau,i\alpha} \tag{9.39}$$

In the long imaginary time limit, $p(\mathcal{R}, \tau)$ converges to (9.37).

Since the stochastic process $\mathcal{R}_\tau$ is given by the stochastic integral:

$$\mathcal{R}_{\tau,i\alpha} = \mathcal{R}_{0,i\alpha} + \int_0^\tau \frac{\hbar^2}{m_i} F_{i\alpha}(R_{\tau'}) d\tau' + \int_0^\tau \frac{\hbar^2}{2m_i} dB_{\tau',i\alpha} \tag{9.40}$$

it can be approximated, at discrete times $\tau_n = n\delta\tau$, as:

$$\mathcal{R}_{\tau_{n+1},i\alpha} \simeq \mathcal{R}_{\tau_n,i\alpha} + \frac{\hbar^2}{m_i} F_{i\alpha}(\mathcal{R}_{\tau_n})\delta\tau + \frac{\hbar^2}{2m_i} \left(B_{\tau_{n+1},i\alpha} - B_{\tau_n,i\alpha} \right) \tag{9.41}$$

which is the sum between $\mathcal{R}_{\tau_n}$ and a normally distributed random variable with mean $\frac{\hbar^2}{m_i} F_{i\alpha}(\mathcal{R}_{\tau_n})\delta\tau$ and variance $\frac{\hbar^2}{2m_i}\delta\tau$.

This suggests to replace the Gaussian transition probability distribution (2.28) of the basic VMC algorithm with the transition probability distribution of the stochastic process (9.40), having the following form:

$$G_\tau(\mathcal{R}, \mathcal{R}') = \frac{e^{-\frac{\left(\mathcal{R} - \mathcal{R}' - \delta\tau \frac{F(\mathcal{R}')}{2}\right)^2}{2\delta\tau}}}{(2\pi\delta\tau)^{\frac{dN}{2}}} \tag{9.42}$$

which is non-symmetric $G_\tau(\mathcal{R}, \mathcal{R}') \neq G_\tau(\mathcal{R}', \mathcal{R})$.

9.2.3 Feynman-Kac representation formula

The following identity, due to R. P. Feynman and M. Kac [71], permits to express the solution of a parabolic partial differential equation as the average of a suitable functional over the trajectories or paths of a suitable stocastic process. The Feynman-Kac formula established a link between apparently disjoint fields of applied mathematics, and its usefulness is twofold. First, it offers a method of solving certain partial differential equation by simulating random paths of a stochastic process. Conversely, it offers a way of computing expectations of random processes by deterministic methods.

Theorem 9.5. *The solution $u(x,t)$ of the parabolic partial differential equation:*

$$\begin{cases} -\partial_t u(x,t) + \mathcal{L}_t u(x,t) - V(x)u(x,t) = f(x,t) \quad (x,t) \in \mathbb{R}^n \times (0,T) \\ u(x,0) = \phi(x) \quad x \in \mathbb{R}^n \end{cases} \tag{9.43}$$

where the differential operator $\mathcal{L}_t$ reads:

$$\mathcal{L}_t = \frac{1}{2}\sum_{ij} a_{ij}(x,t)\frac{\partial^2}{\partial x_i \partial x_j} + \sum_i b_i(x,t)\frac{\partial}{\partial x_i}$$

can be written as:

$$u(x,T) = E[\phi(X_T)Z_T] - E\left[\int_0^T f(X_t, T-t)\, Z_t dt\right] \tag{9.44}$$

where X_t is the solution of the stochastic differential equation:

$$\begin{aligned} dX_t &= b(X_t,t)\, dt + \sigma(X_t,t)\, dB_t \\ X_0 &= x \end{aligned} \tag{9.45}$$

where $a(x,t) = \sigma(x,t)\,\sigma(x,t)^T$, and:

$$Z_t = e^{-\int_0^t V(X_s)ds} \tag{9.46}$$

is the path integral *of the function $V(x)$.*

Proof. *The partial differential equation* (2.44) *has a unique solution $u(x,t) \in C^2(\mathbb{R}^n \times (0,T))$ under very mild assumptions about the differential operator $\mathcal{L}_t$ [317]. Assuming these hypotheses, let us define the stochastic process:*

$$t \mapsto \Phi_t = Z_t\, u(X_t, T-t) \tag{9.47}$$

where $u(x,t)$ is the exact, but unknown, solution of (2.44)*. The stochastic differential $d\Phi_t$ of the stochastic process Φ_t can be evaluated observing that $\Phi_t = F(Z_t, X_t, t)$ where:*

$$F(z,x,t) = z\, u(x, T-t), \tag{9.48}$$

that

$$dZ_t = -Z_t\, V(X_t)\, dt \tag{9.49}$$

and using Itō's lemma (9.1)*. The result is:*

$$\begin{aligned} d\Phi_t = Z_t\,(-\partial_t + \mathcal{L}_t)\, u(X_t, T-t)dt + u(X_t, T-t)dZ_t + \\ + \sum_{ij} \partial_{x_i} u(X_t, T-t)\sigma_{ij}(X_t, T-t)dB_{jt} \end{aligned} \tag{9.50}$$

Since, by construction, u is a solution of the partial differential equation (2.44)*, we get:*

$$\begin{aligned} d\Phi_t &= Z_t \left(V(X_t)u(X_t, T-t) + f(X_t, T-t)\right) dt + u(X_t, T-t)dZ_t + \\ &\sum_{ij} \partial_{x_i} u(X_t, T-t)\sigma_{ij}(X_t, T-t)dB_{jt} = \\ &= Z_t f(X_t, T-t)dt + \sum_{ij} \partial_{x_i} u(X_t, T-t)\sigma_{ij}(X_t, T-t)dB_{jt} \end{aligned} \tag{9.51}$$

recalling the explicit expression (9.49) *for dZ_t. We have thus:*

$$\Phi_T - \Phi_0 = \int_0^T Z_t f(X_t, T-t)dt + \int_0^T \sum_{ij} \partial_{x_i} u(X_t, T-t)\sigma_{ij}(X_t, T-t)dB_{jt} \tag{9.52}$$

Observing that:

$$\Phi_0 = u(x, T), \quad \Phi_T = Z_T u(X_T, 0) = Z_T \phi(X_T) \tag{9.53}$$

and taking the expectation of both members:

$$E\left[Z_T \phi(X_T)\right] - E\left[u(x, T)\right] = E\left[\int_0^T Z_t f(X_t, T-t)dt\right] \tag{9.54}$$

gives the Feynman-Kac representation formula (2.46)*.*

9.2.4 Generalized Feynman-kac formula

In the DMC method, a role of particular importance is played by the following generalization of the Feynman-Kac representation formula (2.46).

Theorem 9.6. *[65] The solution $f_\tau(\mathcal{R})$ of* (3.62) *can be written as:*

$$f_\tau(\mathcal{R}) = E\left[\Psi_T^2(\mathcal{R}_0) Z_\tau\right] \tag{9.55}$$

where the expectation is computed along the trajectories of the stochastic process:

$$\begin{cases} dR_{i,\tau'} = F_i(R'_\tau)\, d\tau' + \frac{\hbar^2}{2m_i} dB_{i,\tau'} \\ R_\tau = R \end{cases} \tag{9.56}$$

associated to the Fokker-Planck equation:

$$\partial_\tau p_\tau = -\sum_i \frac{\hbar^2}{2m_i} \triangle_i p_\tau + \sum_i \frac{\hbar^2}{m_i} \nabla_i \cdot \Big(F_i\, p_\tau\Big) = -\mathcal{L}(p_\tau) \tag{9.57}$$

and:

$$Z_\tau = e^{-\int_0^\tau d\tau'\, E_L(\mathcal{R}_{\tau'})} \tag{9.58}$$

is the path integral of the local energy.

Proof. *Using Trotter's formula, we readily find:*

$$f_\tau = e^{\tau(\mathcal{L} - E_L)} f_0 = \lim_{m\to\infty} \left(e^{\delta\tau(\mathcal{L} - E_L)}\right)^m f_0 \tag{9.59}$$

whence:

$$f_\tau(\mathcal{R}) = \lim_{m\to\infty} \int d\mathcal{R}_m \dots d\mathcal{R}_0 \prod_{i=0}^{m} G_{\delta\tau}(\mathcal{R}_{i+1}, \mathcal{R}_i)\, e^{-\sum_{i=0}^{m+1} \delta\tau E_L(\mathcal{R}_i)}\, \Psi_T^2(\mathcal{R}_0) \tag{9.60}$$

where $G_{\delta\tau}(\mathcal{R}_{i+1}, \mathcal{R}_i)$ *is the transition probability distribution of the stochastic process* (9.56)*:*

$$G_\tau(\mathcal{R}, \mathcal{R}') = \frac{e^{-\frac{\left(\mathcal{R}-\mathcal{R}'-\delta\tau\frac{F(\mathcal{R}')}{2}\right)^2}{2\delta\tau}}}{(2\pi\delta\tau)^{\frac{dN}{2}}} \tag{9.61}$$

and $\mathcal{R}_{m+1} = \mathcal{R}$*. In the* $m \to \infty$ *limit, the integration* (9.60) *is performed over the trajectories of the stochastic process* (9.56)*, and* (9.55) *is retrieved. Notice that, since in the integrand in the right member of* (9.60) *is positive,* $f_\tau(\mathcal{R}) \geq 0$ *for all configurations* $\mathcal{R}$ *and imaginary times* τ*. While the generalized Feynman-Kac formula is exact, the error made in approximating the limit* (9.60) *with a finite* m *is of order* $\left(\frac{\tau}{m}\right)^2 = \delta\tau^2$*. In fact, since the Green's function of* (3.62) *is:*

$$G_{\delta\tau}(\mathcal{R}', \mathcal{R}) = \langle \mathcal{R}' | e^{-\delta\tau(-\mathcal{L}+E_L)} | \mathcal{R} \rangle \tag{9.62}$$

the splitting:

$$G_{\delta\tau}(\mathcal{R}', \mathcal{R}) = e^{-\delta\tau E_L(\mathcal{R}')}\, \langle \mathcal{R}' | e^{\delta\tau\mathcal{L}} | \mathcal{R} \rangle + \mathcal{O}(\delta\tau^2) \tag{9.63}$$

is a primitive approximation to $G_{\delta\tau}(\mathcal{R}', \mathcal{R})$*.*

CHAPTER 10

Details of configurational QMC calculations for electronic systems

In the present Appendix, a succint description of the wavefunctions used in typical VMC and DMC simulations of the homogeneous electron gas is provided; the computational cost of optimizing backflow correlations with the Linear Method is discussed, and the DMC calculation of the static density susceptibility is briefly reviewed.

Its purpose is to complete the discussion of Chapters 2, 3, 6, 7 and to enhance the clarity and the reproducibility of the calculations there performed. The reader is deferred to [102, 318, 99] for further information.

10.1 Wavefunctions for homogeneous electronic systems

10.1.1 The treatment of spin

Suppose we want to use a wavefunction $\Psi(\mathbf{x}_1 \dots \mathbf{x}_N)$ to calculate the expectation value of a spin-independent operator $\hat{O}$. Recall that $\mathbf{x}_i = (\mathbf{r}_i, \omega_i)$ with $\omega_i = \uparrow, \downarrow$ for a spin-$\frac{1}{2}$ system. If $N_\uparrow$ particles have spin up, for each spatial configuration $\mathbf{r}_1 \dots \mathbf{r}_N$ we can write:

$$\Psi(\mathbf{r}_1\omega_1 \dots \mathbf{r}_N\omega_N) = \Psi(\mathbf{r}'_1 \uparrow \dots \mathbf{r}'_{N_\uparrow} \uparrow \mathbf{r}'_{N_\uparrow+1} \downarrow \dots \mathbf{r}'_N \downarrow) = F(\mathbf{r}'_1 \dots \mathbf{r}'_N) \tag{10.1}$$

applying a suitable permutation. The bosonic operator $\hat{O}$ is not affected by that permutation, and thus:

$$\mathcal{O} = \frac{\langle\Psi|\hat{O}|\Psi\rangle}{\langle\Psi|\Psi\rangle} = \frac{\langle F|\hat{O}|F\rangle}{\langle F|F\rangle} \tag{10.2}$$

The wavefunction $F(\mathbf{r}_1 \dots \mathbf{r}_N)$ is antisymmetric with respect to the exchange of the spatial coordinates of pairs of particles with the same spin, but has no specific symmetry on the exchange of the spatial coordinates of particles with different spin. As claimed in Section 2.3.1, we are thus able to treat particles with different spin polarizations as distinguishable from each other. We remark that, if $\Psi(\mathbf{x}_1 \dots \mathbf{x}_N)$ is the Slater determinant:

$$\Psi(\mathbf{x}_1 \dots \mathbf{x}_N) = \det\left(\frac{e^{i\mathbf{k}_i\mathbf{r}_j}}{\sqrt{\Omega}}\chi_{\sigma_i}(\omega_j)\right) \tag{10.3}$$

in which $\sigma_i = \uparrow$ for $i = 1 \dots N_\uparrow$, and $\sigma_i = \downarrow$ otherwise, the corresponding wavefunction is $F(\mathbf{r}'_1 \dots \mathbf{r}'_N)$ is the product:

$$F(\mathbf{r}'_1 \dots \mathbf{r}'_N) = F_\uparrow(\mathbf{r}'_1 \dots \mathbf{r}'_{N_\uparrow}) F_\downarrow(\mathbf{r}'_{N_\uparrow+1} \dots \mathbf{r}'_N) = \det\left(\frac{e^{i\mathbf{k}_i \mathbf{r}'_j}}{\sqrt{\Omega}}\right) \det\left(\frac{e^{i\mathbf{k}_i \mathbf{r}'_{N_\uparrow+j}}}{\sqrt{\Omega}}\right) \quad (10.4)$$

of two Slater determinants. The first (second) factor is relative to spin-up (spin-down) particles, and it is defined by wavevectors $\mathbf{k}_i$ in (10.3).

10.1.2 Kato's cusp condition

In the present Appendix, discussing a peculiar prerogative of electronic systems, lengths are measured in Bohr radii $a_B = \hbar^2/(2me^2)$ and energies are measured in Hartree units $E_{Ha} = e^2/a_B$ (conversion in these atomic units is equivalent to setting $\hbar = m = e = 1$).

Let us consider the time-independent Schrödinger equation for a many-electron system:

$$\left(\hat{H}\Psi\right)(\mathcal{R}) = -\sum_{i=1}^{N} \frac{1}{2} \triangle_i \Psi(\mathcal{R}) - \sum_{i=1}^{N} \frac{1}{r_{ij}} \Psi(\mathcal{R}) = E\Psi(\mathcal{R}) \quad (10.5)$$

where $\Psi(\mathcal{R})$ is an unknown exact wavefunction. The potential energy diverges whenever two particles approach each other. Since the local energy is constant and equal to E, there must be a cancelling divergence in the local kinetic energy. This property reflects in the shape of the exact wavefunction $\Psi(\mathcal{R})$, that has sharp cusps at the configurations in which two particles approach each other, i.e $r_{ij} = 0$. This result was rigorously proved by T. Kato in [319]. The Hartree-Fock determinant does not contain such cusps. Their absence gives rise to a singular local energy, which is responsible for the somewhat poor quality of that wavefunction. However, the missing cusps can be incorporated by carefully-devised Slater-Jastrow wavefunctions. Experience shows that enforcing the cusp condition reduces both the average energy and its variance [99].

Slater-Jastrow wavefunctions are not exact eigenfunctions, and thus their local energy is not constant and may diverge as $\mathbf{r}_i \to \mathbf{r}_j$. To study this possibility, let us write $\Psi_{SJ}(\mathcal{R})$ as:

$$\Psi_{SJ}(\mathcal{R}) = e^{-u_{ij}(r_{ij})} f(\mathbf{r}_{ij}, \tilde{\mathcal{R}}) \quad (10.6)$$

where $\mathbf{r}_{ij} = \mathbf{r}_i - \mathbf{r}_j$, $r_{ij} = |\mathbf{r}_{ij}|$ and $\tilde{\mathcal{R}}$ takes into account the center-of-mass coordinate $\mathbf{R}_{ij} = \frac{\mathbf{r}_i + \mathbf{r}_j}{2}$ and the remaining coordinates $\mathbf{r}_k$, $k \neq i, j$. Writing the Hamiltonian as:

$$\hat{H} = -\triangle_{\mathbf{r}_{ij}} + \frac{1}{r_{ij}} + \hat{H}' \quad (10.7)$$

where:

$$\hat{H}' = -\frac{\hbar^2}{4} \triangle_{\mathbf{R}_{ij}} - \sum_{k \neq i,j} \frac{1}{2} \triangle_{\mathbf{r}_k} + \sum_{k \neq j} \frac{1}{r_{ik}} + \sum_{k \neq i} \frac{1}{r_{jk}} + \sum_{k,l \neq i,j} \frac{1}{r_{kl}} \quad (10.8)$$

we can consider the behavior of the local energy as $r_{ij} \to 0$ while all the other coordinates $\tilde{\mathcal{R}}$ are kept fixed. If the particles i, j have different spins, the function $f(\mathbf{r}_{ij}, \tilde{\mathcal{R}})$ and its derivatives attain finite values for $r_{ij} \to 0$. Therefore, any divergence in the local energy arises from the action of the Laplace operator on the Jastrow factor $e^{-u_{ij}(r_{ij})}$. A

straightforward calculation shows that the local energy remains finite if:

$$\lim_{r\to 0}\frac{du_{ij}}{dr}(r) = -\frac{1}{2} \tag{10.9}$$

If the particles i, j have the same spin, the Pauli exclusion principle implies that f is an odd function of $\mathbf{r}_{ij}$, whence:

$$f(\mathbf{r}_{ij}, \tilde{\mathcal{R}}) = \mathbf{a}\cdot\mathbf{r}_{ij} + \mathcal{O}(r_{ij}^3) \tag{10.10}$$

A calculation analogous to the previous one shows that the local energy remains finite if:

$$\lim_{r\to 0}\frac{du_{ij}}{dr}(r) = -\frac{1}{4} \tag{10.11}$$

Equations (10.9) and (10.11) are called Kato's cusp conditions for parallel and antiparallel spins respectively.

10.1.3 The Gaskell trial wavefunction

A number of different trial wavefunctions have played an important role in unraveling the problem of electron correlations. An important example is the Jastrow function suggested by Gaskell [102] to describe correlations in homogeneous electron systems by including the zero-point fluctuations of plasmons.

In order to explain the physical origin and mathematical form of this wavefunction, following [318] we start from the decomposition $\hat{H} = \hat{H}_0 + \hat{H}_1$ of a generic Hamiltonian into a solvable part $\hat{H}_0$ with ground state $\Phi_0^{(0)}$ and an intractable perturbation part $\hat{H}_1$. We expand $\hat{H}_1$ in terms of eigenoperators $\hat{A}_\nu$ of the Liouvillean superoperator $\hat{L}_0$, given by:

$$\hat{L}_0[\hat{O}] = [\hat{H}_0, \hat{O}] \tag{10.12}$$

The eigenoperators $\hat{A}_\nu$ are specified by the condition $\hat{L}_0\hat{A}_\nu = a_\nu\hat{A}_\nu$ where $a_\nu \in \mathbb{C}$. Expressed in terms of the $\hat{A}_\nu$, the perturbation Hamiltonian reads:

$$\hat{H}_1 = \sum_\nu \mathrm{Tr}[\hat{H}_1\hat{A}_\nu^\dagger]\,\hat{A}_\nu = \sum_\nu \lambda_\nu\hat{A}_\nu \tag{10.13}$$

The ground state Φ_0 of $\hat{H}$ is related to the ground state of $\Phi_0^{(0)}$ of $\hat{H}_0$ by [318]:

$$\Phi_0 = \hat{\Omega}\,\Phi_0^{(0)} \tag{10.14}$$

where:

$$\hat{\Omega} = \lim_{z\to 0}\sum_{k=0}^{\infty}\left((z-\hat{L}_0)^{-1}\hat{H}_1\right)^k \tag{10.15}$$

Notice that:

$$\hat{L}_0[\hat{H}_1] = \sum_\nu \lambda_\nu a_\nu\hat{A}_\nu \tag{10.16}$$

by virtue of the expansion (10.13). Within the so-called *single-mode approximation* [318], the eigenvalues a_ν are replaced by a mean excitation energy $\hbar\omega_0$ that will be determined

later, so that:

$$\hat{L}_0[\hat{H}_1] \simeq \hbar\omega_0 \hat{H}_1 \tag{10.17}$$

With the help of (10.17), we rewrite (10.15) as:

$$\hat{\Omega} = \sum_{k=0}^{\infty} \frac{1}{k!} \left(-\frac{\hat{H}_1}{\hbar\omega_0} \right)^k = e^{-\frac{\hat{H}_1}{\hbar\omega_0}} \tag{10.18}$$

The single-mode approximation yields a very simple expression for $\hat{\Omega}$, in which the perturbing Hamiltonian, divided by the mean excitation energy $\hbar\omega_0$, appears in the form of an exponential function. Therefore:

$$\Phi_0 \simeq \hat{\Omega}\Phi_0^{(0)} = e^{-\frac{\hat{H}_1}{\omega_0}} \Phi_0^{(0)} \tag{10.19}$$

The yet unspecified energy $\hbar\omega_0$ is chosen as to minimize the energy of the wavefunction (10.19). Whenever:

$$\hat{H}_1 = \sum_i \hat{B}_i \qquad \hat{B}_i = \sum_\nu \lambda_{i,\nu} \hat{A}_\nu \tag{10.20}$$

with $[\hat{B}_i, \hat{B}_j] = 0$, the perturbing Hamiltonian is said to consist of a sum of independent excitation modes. From (10.18) we find that:

$$\hat{\Omega} = e^{-\sum_i \frac{\hat{B}_i}{\omega_i}} \tag{10.21}$$

where each mode has a specific mean excitation energy $\hbar\omega_i$. Gaskell's trial wavefunction for an interacting Fermi system belongs to this cathegory. The solvable part is the kinetic energy, with ground state $\Phi_S(R)$, and the perturbation is the interaction Hamiltonian. The latter reads:

$$\hat{H}_1 = \sum_{\mathbf{q}} \frac{v_{\mathbf{q}}}{2\Omega} \hat{\rho}_{\mathbf{q}} \hat{\rho}_{-\mathbf{q}} \tag{10.22}$$

We consider the contributions $\frac{v_{\mathbf{q}}}{2\Omega} \hat{\rho}_{\mathbf{q}} \hat{\rho}_{-\mathbf{q}}$ as independent excitation modes, and identify them with the $\hat{B}_i$ operators. Within the single-mode approximation:

$$\hat{\Omega} \simeq e^{-\sum_{\mathbf{q}} u_{\mathbf{q}} \hat{\rho}_{\mathbf{q}} \hat{\rho}_{-\mathbf{q}}} \tag{10.23}$$

where the coefficients $u_{\mathbf{q}}$ should be determined by energy minimization. Notice that:

$$\langle \mathcal{R}|\hat{\Omega}|\Phi_0^{(0)}\rangle = e^{-\sum_{\mathbf{q}} u_{\mathbf{q}} \rho_{\mathbf{q}}(\mathcal{R}) \rho^*_{\mathbf{q}}(\mathcal{R})} \langle \mathcal{R}|\Phi_0^{(0)}\rangle \tag{10.24}$$

After Fourier transform of the exponential in (10.24), the Gaskell ground-state wavefunction takes the form:

$$\Phi_0(\mathcal{R}) = e^{-\sum_{i\neq j} u(r_{ij})} \Phi_0^{(0)}(\mathcal{R}) \quad , \qquad u(\mathbf{r}) = \sum_{\mathbf{q}} u_{\mathbf{q}} e^{i\mathbf{q}\cdot\mathbf{r}} \tag{10.25}$$

of a Slater-Jastrow wavefunction (recall that $\Phi_0^{(0)}$ is a Slater determinant). The RPA approximation descibed in the forthcoming Subsection yields a parameter-free pseudopotential $u(r)$ satisfying Kato's cusp condition for antiparallel spins.

10.1.4 The RPA pseudopotential

Let us consider a classical system of N particles, whose equilibrium properties are controlled by the Hamiltonian functional:

$$\mathcal{H}(\mathcal{R}) = \mathcal{H}_0(\mathcal{R}) + \mathcal{H}_1(\mathcal{R}) = \mathcal{H}_0(\mathcal{R}) + \sum_{i<j} \phi(r_{ij}) \tag{10.26}$$

where $\mathcal{H}_0(\mathcal{R})$ is a solvable reference Hamiltonian and $\mathcal{H}_1(\mathcal{R})$ a weak perturbation, and focus on the average density $\rho(r)$ at a distance r from a certain particle. $\rho(r)$ is related to the radial distribution function $g(r)$ and to the average density ρ of the system by:

$$\rho(r) = \rho\, g(r) \tag{10.27}$$

so that the relative density fluctuation, also called total correlation function, is:

$$h(r) = \frac{\rho(r)}{\rho} - 1 = g(r) - 1 \tag{10.28}$$

The Fourier transform of $h(\mathbf{r})$ is related to the static structure factor by:

$$S_0(\mathbf{q}) = 1 + \rho \int d\mathbf{r}\, (g(r) - 1)\, e^{i\mathbf{q}\cdot\mathbf{r}} = 1 + \rho h(\mathbf{q}) \tag{10.29}$$

The following relation, due to L. Ornstein and F. Zernike [320], expresses the relative density fluctuation as:

$$\begin{aligned} h(r) &= c(r) + \rho \int d\mathbf{r}'\, c(r')\, h(|\mathbf{r} - \mathbf{r}'|) \\ h(\mathbf{q}) &= c(\mathbf{q}) + \rho c(\mathbf{q}) h(\mathbf{q}) \end{aligned} \tag{10.30}$$

where $c(r)$ is a suitable short-range correlation function. It is worth pointing out that the Ornstein-Zernike relation is an exact definition of $c(r)$, independent of the details of the Hamiltonian (10.26). In particular, it holds for the total correlation function $h_0(r)$ and the short-range correlation function $c_0(r)$ of the reference Hamiltonian:

$$\begin{aligned} h_0(r) &= c_0(r) + \rho \int d^d r'\, c(r')\, h(|\mathbf{r} - \mathbf{r}'|) \\ h_0(\mathbf{q}) &= c_0(\mathbf{q}) + \rho c_0(\mathbf{q}) h_0(\mathbf{q}) \end{aligned} \tag{10.31}$$

so that, joining (10.30) and (10.31), we obtain the exact relation:

$$\delta S(\mathbf{q}) = \frac{\delta c(\mathbf{q}) S_0^2(\mathbf{q})}{1 - \rho \delta c(\mathbf{q}) S_0(\mathbf{q})} \tag{10.32}$$

between $\delta S(\mathbf{q}) = S(\mathbf{q}) - S_0(\mathbf{q})$ and $\delta c(\mathbf{q}) = c(\mathbf{q}) - c_0(\mathbf{q})$, involving the static structure factor $S_0(\mathbf{q})$ of the reference Hamiltonian.

The Ornstein-Zernike equation needs to be solved for both the functions $h(r)$ and $c(r)$: this requires the introduction of an additional equation, known as a closure relation. Typical closures are the Percus-Yevick [321] approximation (adequate for hard-core potentials), the hypernetted-chain [33] equation (adequate for soft-core potentials) and the

random phase approximation (RPA):

$$c(r) = -\phi(r) \tag{10.33}$$

valid for weak perturbations. Under the RPA approximation, (10.32) becomes:

$$S(\mathbf{q}) = \frac{S_0(\mathbf{q})}{1 + \rho\phi(\mathbf{q})S_0(\mathbf{q})} \tag{10.34}$$

The equation (10.34) can be borrowed from the domain of classical Physics, to fix the Gaskell pseudopotential (10.25). In fact, the energy of the Slater-Jastrow wavefunction:

$$\mathcal{E} = \int d\mathcal{R}\, |\Psi_S(\mathcal{R})|^2\, |\Psi_J(\mathcal{R})|^2\, E_L(\mathcal{R}) \tag{10.35}$$

and can be interpreted as canonical ensemble average of $E_L(\mathcal{R})$ over the Gibbs probability distribution:

$$p(\mathcal{R}) = e^{-\hat{H}(\mathcal{R})} = e^{-\hat{H}_0(\mathcal{R})}\, e^{-\hat{H}_1(\mathcal{R})} \tag{10.36}$$

with $\hat{H}_0(\mathcal{R}) = -\log\left(|\Psi_S(\mathcal{R})|^2\right)$ and:

$$\hat{H}_1(\mathcal{R}) = 2\sum_{i<j} u(r_{ij}) \tag{10.37}$$

Recalling the arguments of Section 2.3.2, and neglecting the product of gradients $\nabla\Psi_S(\mathcal{R})\cdot\nabla\Psi_J(\mathcal{R})$, we readily find:

$$\begin{aligned} E_L(\mathcal{R}) = &\sum_{\mathbf{k}} \frac{\hbar^2|\mathbf{k}|^2}{2m} + \sum_{\mathbf{q}} \left(\frac{v_{\mathbf{q}}}{2} + \frac{\hbar^2|\mathbf{q}|^2}{2m} u_{\mathbf{q}}\right) (\rho_{\mathbf{q}}(\mathcal{R})\rho_{-\mathbf{q}}(\mathcal{R}) - N) + \\ &+ \sum_{\mathbf{q},\mathbf{q}'} \frac{\hbar^2\, \mathbf{q}\cdot\mathbf{q}'}{2m}\, u_{\mathbf{q}}\, u_{\mathbf{q}'} \rho_{\mathbf{q}+\mathbf{q}'}(\mathcal{R})\rho_{-\mathbf{q}}(\mathcal{R})\rho_{-\mathbf{q}'}(\mathcal{R}) \end{aligned} \tag{10.38}$$

Approximating the average of $\rho_{\mathbf{q}}(\mathcal{R})\rho_{-\mathbf{q}}(\mathcal{R}) - N$ as $N(S(\mathbf{q}) - 1)$ with $S(\mathbf{q})$ given by (10.34) and taking into account, in the last term of (10.38), only the terms with either $\mathbf{q} = 0, \mathbf{q}' = 0$ or $\mathbf{q} + \mathbf{q}' = 0$, we arrive at the final expression:

$$\mathcal{E} = \sum_{\mathbf{k}} \frac{\hbar^2|\mathbf{k}|^2}{2m} + \sum_{\mathbf{q}} N \left(\frac{v_{\mathbf{q}}}{2} + \frac{\hbar^2|\mathbf{q}|^2}{2m} u_{\mathbf{q}}\right) (S(\mathbf{q}) - 1) - \sum_{\mathbf{q}} \frac{\hbar^2\, |\mathbf{q}|^2}{2m}\, u_{\mathbf{q}}^2\, NS(\mathbf{q}) \tag{10.39}$$

The pseudopotential minimizing (10.39) reads:

$$u(\mathbf{q}) = -\frac{1}{S_0(\mathbf{q})} + \sqrt{\frac{1}{S_0^2(\mathbf{q})} + \frac{4v_{\mathbf{q}}m\rho}{\hbar^2|\mathbf{q}|^2}} \tag{10.40}$$

and it is called the RPA pseudopotential [102]. It contains no variational parameters, avoiding the expensive search for an optimal pseudopotential. At large r this pseudopotential has the long-range behavior $u(r)$ necessary to reproduce the correct plasmon dispersion relation [322, 323, 324], while at small r it tends smoothly towards the required cusp for antiparallel spins. The use of an RPA pseudopotential independent on the rel-

ative spin violates Kato's cusp condition for parallel spins, which fortunately is much less important because their probability to get close is clearly small, due to the Pauli exclusion principle [324, 99].

10.1.5 Rational backflow correlations

In Section 2.3.2, the Feynman-Kac representation was used to show that accurate trial wavefunctions for homogeneous systems can be obtained inserting two-body, three-body and backflow correlations. The correlation orbitals $u(r), \xi(r), \eta(r)$ in (2.58) result from quite drastic approximations, and thus they are typically substituted with suitably-constructed functions containing variational parameters. In order to provide a good functional form of such correlation orbitals, it proves important to correctly predict their long-range behavior. In some cases, this property can be grasped from the perturbative expression (2.57) of the local energy. Suppose we start from a simple SJ wavefunction:

$$\Psi_{\delta\tau}(\mathcal{R}) \propto \prod_i e^{i\mathbf{k}_i\cdot\mathbf{r}_i}\, e^{-\frac{1}{2}\sum_{j\neq i} u_{ij}(r_{ij})} \tag{10.41}$$

with local energy:

$$E_L(\mathcal{R}) = \sum_i \frac{\hbar^2|\mathbf{k}_i|^2}{2m_i} + \sum_i \frac{\hbar^2}{2m_i}\sum_{j\neq i}\left(u''_{ij}(r_{ij}) - u'_{ij}(r_{ij})\frac{d-1}{r_{ij}}\right) + \\ + \sum_i i\,\mathbf{k}_i \cdot \sum_{j\neq i}\frac{\hbar^2}{2m_i}\left(u'_{ij}(r_{ij})\,\frac{\mathbf{r}_i-\mathbf{r}_j}{r_{ij}}\right) - \sum_i \frac{\hbar^2}{2m_i}\left|u'_{ij}(r_{ij})\,\frac{\mathbf{r}_i-\mathbf{r}_j}{r_{ij}}\right|^2 + \frac{1}{2}\sum_{i\neq j} v(r_{ij}) \tag{10.42}$$

Following Section 2.3.2, we conclude that the antisymmetrized second-order wavefunction has the SJ3BBF form, with orbitals $\eta(r)$ and $\xi(r)$ proportional to $\frac{1}{r}\frac{du}{dr}$ at long distance. For a 2D electron gas, the RPA pseudopotential has the asymptotic behavior $u(r) \sim r^{-\frac{1}{2}}$, whence $\eta(r)$ should decay as $\eta(r) \sim r^{-\frac{5}{2}}$. Such property is reproduced by the rational backflow correlations (2.145), that were introduced in [60]. Those correlations give an excellent trial wavefunction for the 2D electron gas. However, in some VMC and DMC calculations one uses orbitals $\eta(r)$, $\xi(r)$ that do not include the long-range behavior $\frac{1}{r}\frac{du}{dr}$ (e.g. the three-body orbital (2.146) for the 2D electron gas has an exponential decay and not a power-law decay [60]).

10.2 Efficient Optimization of Backflow Correlations

In the present Section, the quantities (2.126), (2.127) and (2.131) are computed and proved to have computational cost scaling as $\mathcal{O}(N^3)$, N being the number of particles constituting the system. The notations of [60], Appendix B, are adopted. To this purpose, the following intermediate tensors need to be computed, with the numbers in brackets denoting the computational complexity:

1. the quasiparticle coordinates and their first and second derivatives [N^2]:

$$\begin{aligned} x_{l\beta} &= r_{l\beta} + \sum_{j\neq l} \eta(r_{lj})\,(r_{l\beta} - r_{j\beta}) \\ A^{\alpha\beta}_{il} &= \partial_{r_{i\alpha}} x_{l\beta} \quad B^{\alpha\beta}_{il} = \partial^2_{r_{i\alpha}} x_{l\beta} \\ C^{\beta}_{l} &= \partial_{p_j} x_{l\beta} = \sum_{j\neq l} \partial_{p_j}\eta(r_{lj})\,(r_{l\beta} - r_{j\beta}) \\ D^{\alpha\beta}_{il} &= \partial_{p_j} A^{\alpha\beta}_{il} \quad E^{\alpha\beta}_{il} = \partial_{p_j} B^{\alpha\beta}_{il} \end{aligned} \tag{10.43}$$

2. the backflow matrix and its first, second and third derivatives [N^2]:

$$\begin{aligned} \varphi_{kl} &= \varphi_k(x_l) \\ \varphi^{\beta}_{kl} &= \frac{\partial \varphi_{kl}}{\partial_{x_{l\beta}}} \\ \varphi^{\beta\beta'}_{kl} &= \frac{\partial^2 \varphi_{kl}}{\partial_{x_{l\beta}}\partial_{x_{l\beta'}}} \\ \varphi^{\beta\beta'\beta''}_{kl} &= \frac{\partial^3 \varphi_{kl}}{\partial_{x_{l\beta}}\partial_{x_{l\beta'}}\partial_{x_{l\beta''}}} \end{aligned} \tag{10.44}$$

3. the inverse φ^{-1} of the backflow matrix [N^3] and the tensors [at most N^3]:

$$\begin{aligned} F^{\beta}_{kl} &= \sum_r \varphi^{-1}_{kr}\varphi^{\beta}_{rl} \\ G_{kl} &= \sum_r \varphi^{-1}_{kr}\partial_{p_j}\varphi_{rl} = \sum_\beta F^{\beta}_{kl} C^{\beta}_{l} \\ H^{\beta\beta'}_{ll'} &= \sum_{i\alpha} A^{\alpha\beta}_{il} A^{\alpha\beta'}_{il'} \\ J^{\beta\beta'}_{kl} &= \sum_r \varphi^{-1}_{kr}\varphi^{\beta\beta'}_{rl} \end{aligned} \tag{10.45}$$

the tensor G_{kl} has been explicited making use of the chain rule $\partial_{p_j}\varphi_{kl} = \sum_\beta \partial_{p_j} x_{l\beta}\varphi^{\beta}_{kl} = \sum_\beta C^{\beta}_{l}\varphi^{\beta}_{kl}$ and observing that:

$$G_{kl} = \sum_r \varphi^{-1}_{kr}\varphi^{\beta}_{rl} C^{\beta}_{l} = \sum_\beta F^{\beta}_{kl} C^{\beta}_{l} \tag{10.46}$$

Recalling equations (2.126) and (10.45), we readily conclude that [N]:

$$\partial_{p_j}\mathcal{Z}(\mathbf{p},\mathcal{R}) = -\sum_l G_{ll} \tag{10.47}$$

The quantity $\partial_{r_{i\alpha}}\partial_{p_j}\mathcal{Z}(\mathbf{p},\mathcal{R})$ results from the difference of two terms:

1. tr $\left(\varphi^{-1}\partial_{r_{i\alpha}}\varphi\,\varphi^{-1}\partial_{p_j}\varphi\right)$
2. tr $\left(\varphi^{-1}(\partial_{r_{i\alpha}}\partial_{p_j}\varphi)\right)$

which, recalling equations (2.127), (10.43) and the chain rule:

$$\begin{aligned}\partial_{r_{i\alpha}}\varphi_{kl} &= \sum_{l\beta} A_{il}^{\alpha\beta}\partial_{x_{l\beta}}\varphi_{kl} \\ \partial_{r_{i\alpha}}\partial_p\varphi_{kl} &= \sum_{\beta} D_{il}^{\alpha\beta}\varphi_{kl}^{\beta} + \sum_{\beta\beta'} C_l^{\beta} A_{il}^{\alpha\beta'}\varphi_{kl}^{\beta\beta'}\end{aligned} \tag{10.48}$$

can be cast in the form $[N^2]$:

$$\mathrm{tr}\left(\varphi^{-1}\partial_{r_{i\alpha}}\varphi\,\varphi^{-1}\partial_{p_j}\varphi\right) = \sum_{lk\beta} A_{il}^{\alpha\beta} G_{lk} F_{kl}^{\beta} \tag{10.49}$$

$$\mathrm{tr}\left(\varphi^{-1}(\partial_{r_{i\alpha}}\partial_{p_j}\varphi)\right) = \sum_{l\beta\beta'} A_{il}^{\alpha\beta} C_l^{\beta'} J_{ll}^{\beta\beta'} + \sum_{l\beta} D_{il}^{\alpha\beta} F_{ll}^{\beta} \tag{10.50}$$

The quantity $\partial^2_{r_{i\alpha}}\partial_{p_j} Z(\mathbf{p},\mathcal{R})$ results from a linear combination of the terms:

1. $\mathrm{tr}\Big((\varphi^{-1}\partial^2_{r_{i\alpha}}\varphi)\varphi^{-1}\partial_{p_j}\varphi\Big)$
2. $\mathrm{tr}\Big((\varphi^{-1}\partial_{r_{i\alpha}}\varphi)(\varphi^{-1}\partial_{r_{i\alpha}}\varphi)(\varphi^{-1}\partial_{p_j}\varphi)\Big)$
3. $\mathrm{tr}\Big((\varphi^{-1}\partial_{r_{i\alpha}}\varphi)(\varphi^{-1}\partial_{r_{i\alpha}}\partial_{p_j}\varphi)\Big)$
4. $\mathrm{tr}\Big(\varphi^{-1}\partial^2_{r_{i\alpha}}\partial_{p_j}\varphi\Big)$

Recalling $\partial^2_{r_{i\alpha}}\varphi_{kl} = \sum_\beta B_{il}^{\alpha\beta}\varphi_{kl}^{\beta} + \sum_{\beta\beta'} A_{il}^{\alpha\beta}A_{il}^{\alpha\beta'}\varphi_{kl}^{\beta\beta'}$ the first term is cast in the form $[N^3]$:

$$\begin{aligned}&\sum_{i\alpha}\mathrm{tr}\Big((\varphi^{-1}\partial^2_{r_{i\alpha}}\varphi)\varphi^{-1}\partial_{p_j}\varphi\Big) = \\ =&\sum_{\beta}\sum_{kl}\left(\sum_{i\alpha} B_{il}^{\alpha\beta}\right)F_{kl}^{\beta}G_{lk} + \sum_{\beta\beta'}\sum_{kl} H_{ll}^{\beta\beta'}J_{kl}^{\beta\beta'}G_{lk}\end{aligned} \tag{10.51}$$

The second term in the form $[N^3]$:

$$\begin{aligned}&\sum_{i\alpha}\mathrm{tr}\Big((\varphi^{-1}\partial_{r_{i\alpha}}\varphi)(\varphi^{-1}\partial_{r_{i\alpha}}\varphi)(\varphi^{-1}\partial_{p_j}\varphi)\Big) = \\ =&\sum_{\beta\beta'}\sum_{ll'} H_{ll'}^{\beta\beta'}\left(\sum_k F_{kl}^{\beta}G_{l'k}\right)F_{ll'}^{\beta'}\end{aligned} \tag{10.52}$$

The third term in the form $[N^3]$:

$$\begin{aligned}&\sum_{i\alpha}\mathrm{tr}\Big((\varphi^{-1}\partial_{r_{i\alpha}}\varphi)(\varphi^{-1}\partial_{r_{i\alpha}}\partial_{p_j}\varphi)\Big) = \\ =&\sum_{ll'}\sum_{\beta\beta'\beta''} H_{ll'}^{\beta\beta'}F_{l'l}^{\beta'}J_{ll'}^{\beta'\beta''}C_{l'}^{\beta''} + \sum_{kli}\sum_{\alpha\beta\beta'} F_{lk}^{\beta}A_{ki}^{\beta\alpha}D_{li}^{\beta'\alpha}F_{kl}^{\beta'}\end{aligned} \tag{10.53}$$

Finally, recalling that:

$$\begin{aligned}\partial^2_{r_{i\alpha}}\partial_{p_j}\varphi_{kl} &= \sum_{\beta} E^{\alpha\beta}_{il}\varphi^{\beta}_{kl} + \sum_{\beta\beta'} B^{\alpha\beta}_{il}C^{\beta'}_{l}\varphi^{\beta\beta'}_{kl} \\ &+ \sum_{\beta\beta'\beta''} A^{\alpha\beta}_{il}A^{\alpha\beta'}_{il}C^{\beta''}_{l}\varphi^{\beta\beta'\beta''}_{kl} + 2\sum_{\beta\beta'} D^{\alpha\beta}_{il}A^{\alpha\beta'}_{il}\varphi^{\beta\beta'}_{kl}\end{aligned} \tag{10.54}$$

the fourth term can be cast in the form [N^2]:

$$\begin{aligned}\sum_{i\alpha}\mathrm{tr}\Big(\varphi^{-1}(\partial^2_{r_{i\alpha}}\partial_{p_j}\varphi)\Big) &= \sum_{l\beta}\big(\sum_{i\alpha}E^{\alpha\beta}_{il}\big)F^{\beta}_{ll} \\ +2\sum_{l\beta\beta'}\Big(\sum_{i\alpha}D^{\alpha\beta}_{il}A^{\alpha\beta'}_{il}\Big)J^{\beta\beta'}_{ll} &+ \sum_{l\beta\beta'}\big(\sum_{i\alpha}B^{\alpha\beta}_{il}\big)C^{\beta'}_{l}J^{\beta\beta'}_{ll} \\ + \sum_{l\beta\beta'\beta''}H^{\beta\beta'}_{ll}C^{\beta''}_{l}\big(\sum_{k}\varphi^{-1}_{lk}\varphi^{\beta\beta'\beta''}_{kl}\big)&\end{aligned} \tag{10.55}$$

The recommendations of the present Appendix contain the computational cost of the optimization procedure. Further simplifications in the calculation of the intermediate tensors (10.44) are possible in homogeneous systems, where the backflow orbitals are plane waves $\varphi_{il} = e^{i\mathbf{k}_i\cdot\mathbf{x}_l}$.

10.3 DMC calculation of the static density susceptibility

10.3.1 The compressibility sum rule

The static density susceptibility characterizes the effect of a static perturbation on a homogeneous system. This relevant quantity has been investigated by several authors, most notably G. Sugiyama *et al.* [325], S. Moroni *et al.* [283], C. Bowen *et al.* [326] and S. De Palo *et al.* [327]. In presence of a static external potential, the Hamiltonian of the system becomes:

$$\hat{H} = \hat{H}_0 + \int d\mathbf{r}\, V(\mathbf{r})\,\hat{\rho}(\mathbf{r}) = \frac{1}{\Omega}\sum_{\mathbf{q}} V_{\mathbf{q}}\,\hat{\rho}_{-\mathbf{q}} \tag{10.56}$$

The ground-state energy $\mathcal{E}_N(V)$ in presence of the external potential is a function of the coefficients $V_{\mathbf{q}}$, like the ground-state density. In particular:

$$\rho(\mathbf{r}, V) = \rho_0 + \int d\mathbf{r}'\,\chi(\mathbf{r}-\mathbf{r}')V(\mathbf{r}') \tag{10.57}$$

to lowest order in the interaction Hamiltonian. Therefore:

$$\rho_{\mathbf{q}}(V) = \int d\mathbf{r}\, e^{-\mathbf{q}\cdot\mathbf{r}}\,\rho(\mathbf{r}, V) = \rho_0\,\Omega\,\delta_{\mathbf{q},\mathbf{0}} + \chi_{\mathbf{q}}V_{\mathbf{q}} \tag{10.58}$$

whence the static suscetibility χ_q reads:

$$\chi_q = \lim_{V\to 0}\frac{\partial\rho_{\mathbf{q}}(V)}{\partial V_{\mathbf{q}}} \tag{10.59}$$

On the other hand, (1.11) reveals that:

$$\rho_{\mathbf{q}}(V) = \rho_0\,\Omega\,\delta_{\mathbf{q},\mathbf{0}} + \frac{1}{\hbar}\tilde{\chi}_{\rho\rho}(\mathbf{q},0)\,V_{\mathbf{q}} \tag{10.60}$$

where $\tilde{\chi}_{\rho\rho}(\mathbf{q},0)$ is the zero-frequency limit of the density-density response function (1.19). Since, by the definition (1.19), $\tilde{\chi}_{\rho\rho}(\mathbf{q},0)$ is a real quantity, due to the Kramers-Krönig relations:

$$\tilde{\chi}_{\rho\rho}(\mathbf{q},0) = \mathrm{Re}\,\tilde{\chi}_{\rho\rho}(\mathbf{q},0) = \frac{2}{\pi}\int_0^\infty d\omega\,\frac{\mathrm{Im}\,\tilde{\chi}_{\rho\rho}(\mathbf{q},\omega)}{\omega} \tag{10.61}$$

The imaginary part of the density-density response function is in turn related to the dynamical structure factor by the fluctuation-dissipation theorem (1.27), whence:

$$\tilde{\chi}_{\rho\rho}(\mathbf{q},0) = -2\rho_0\int_0^\infty d\omega\,\frac{S(\mathbf{q},\omega)}{\omega} \tag{10.62}$$

Comparing (10.59) and (10.60), and recalling (10.62), we find the *compressibiity sum rule*:

$$\chi_{\mathbf{q}} = -\frac{2\rho_0}{\hbar}\int_0^\infty d\omega\,\frac{S(\mathbf{q},\omega)}{\omega} = -\frac{2\rho_0}{\hbar}\,\mathcal{M}_{-1} \tag{10.63}$$

relating the static susceptibility $\chi_{\mathbf{q}}$ and the first negative momentum of the DSF. For the compressibility sum rule to prove useful, we need a procedure to precisely compute $\chi_{\mathbf{q}}$ with QMC. The Feynman-Hellman theorem guarantees that the ground-state energy $\mathcal{E}_N(V)$ in presence of the external potential reads:

$$\mathcal{E}_N(V) = \mathcal{E}_N(0) + \frac{1}{N}\int_0^1 d\lambda\int d\mathbf{r}\rho(\mathbf{r},\lambda V)\,V(\mathbf{r}) \tag{10.64}$$

Inserting (10.57) in (10.64) and performing the integration over λ we find:

$$\mathcal{E}_N(V) = \mathcal{E}_N(0) + \rho_0\tilde{V}_{\mathbf{0}} + \frac{1}{2\rho_0}\sum_{\mathbf{q}}\tilde{V}_{-\mathbf{q}}\tilde{V}_{\mathbf{q}}\,\chi_{\mathbf{q}} \tag{10.65}$$

to lowest order in the interaction Hamiltonian. In (10.65), $\tilde{V}_{\mathbf{q}} = \frac{V_{\mathbf{q}}}{\Omega}$. (10.65) considerably simplifies if the external potential reads:

$$V(\mathbf{r}) = 2\tilde{V}\cos(\mathbf{q}\cdot\mathbf{r}) = \tilde{V}e^{i\mathbf{q}\cdot\mathbf{r}} + \tilde{V}e^{-i\mathbf{q}\cdot\mathbf{r}} \tag{10.66}$$

In such case, (10.65) takes the form:

$$\mathcal{E}_N(V) = \mathcal{E}_N(0) + \frac{\tilde{V}^2}{\rho_0}\,\chi_{\mathbf{q}} \tag{10.67}$$

to lowest order in the interaction Hamiltonian. It is easy to verify [283] that the first correction to (10.67) comes to order $\mathcal{O}(\tilde{V}^4)$. The static susceptibility can thus be extracted from the ground-state energy per particle in presence of the external potential (10.66).

10.3.2 Details of the DMC calculation

The Hellman-Feynman theorem shows that $\chi_{\mathbf{q}}$ can be extracted from the ground-state energy in presence of the external potential (10.66). The DMC method is very adequate to such purpose, being very efficient and providing estimates of the ground-state energy biased by the FN approximation only.
In principle, the simulation of a non-interacting system in presence of the external potential (10.66), with $\mathbf{q}$ along the z-axis of a suitable Cartesian fram, requires to solve the 1D Schrödinger equation:

$$-\frac{\hbar^2}{2m}f''(r) + V(r)f(r) = Ef(r) \tag{10.68}$$

which, in the Fourier space, takes the form:

$$\frac{\hbar^2 k^2}{2m}f_k + \tilde{V}\left(f_{k+q} + f_{k-q}\right) = Ef_k \tag{10.69}$$

of a tridiagonal eigenvalue equation:

$$\sum_p M_{kp}f_p = Ef_p \quad , \qquad M_{kp} = \frac{\hbar^2 k^2}{2m}\,\delta_{kp} + \tilde{V}\left(\delta_{k+q,p} + \delta_{k-q,p}\right) \tag{10.70}$$

where $f(r) = \frac{1}{L}\sum_k f_k e^{-ikx}$. (10.70) can be efficiently solved e.g. with the DSTEVX Lapack routine. For $\tilde{V} = 0$, the solutions of (10.70) are the plane waves:

$$f_k(r) = \frac{e^{ikr}}{\sqrt{L}} \quad f_p = \sqrt{L}\,\delta_{p,k} \tag{10.71}$$

which, as soon as $\tilde{V} \neq 0$, evolve into orbitals that will be denoted $\tilde{f}_k(r)$. The basis of the single-particle Hilbert space is thus the set:

$$\langle \mathbf{r}, \omega | \mathbf{k}, \sigma \rangle = \chi_\sigma(\omega)\,\frac{e^{i\mathbf{k}_\perp \cdot \mathbf{r}_\perp}}{L^{\frac{d-1}{2}}}\,\tilde{f}_{k_\parallel}(r_\parallel) \tag{10.72}$$

Consequently, the exact ground-state wavefunction of a non-interacting system of $N_\uparrow$ spin-up and $N_\downarrow$ spin-down fermions is the lowest-energy Slater determinant of spin-orbitals (10.72). As detailed in Appendix 10, that wavefunction can be substituted with a product of two Slater determinants, one per spin polarization.
However, since the calculation of the functions $\tilde{f}_k(r)$ is quite cumbersome, and the calculation of $\chi_{\mathbf{q}}$ requires to know the ground-state energy only around $\tilde{V} = 0$, it is advisable to substitute the functions $\tilde{f}_k(r)$ with some approximation which is accurate for small $\tilde{V}$ but computationally not expensive.
Following [326], we substitute the spin-definite plane waves with the following orbitals:

$$|\mathbf{k}_\alpha\rangle = |\mathbf{k}\rangle - \alpha\left[\frac{|\mathbf{k}+\mathbf{q}\rangle}{(\mathbf{q}+2\mathbf{k})\cdot\mathbf{q}} + \frac{|\mathbf{k}-\mathbf{q}\rangle}{(\mathbf{q}-2\mathbf{k})\cdot\mathbf{q}}\right] \tag{10.73}$$

which differ from the second-order expansions of (10.72) for the introduction of a variational parameter α. We thus rely on the following procedure for computing $\chi_{\mathbf{q}}$, which is illustrated in Figure 10.1:

- For a fixed $\tilde{V}$, and for several values of α, compute the VMC energy of the wavefunction:
$$\Psi(\mathcal{R},\alpha) = \Psi_J(\mathcal{R})\,\Psi_S(\mathcal{R},\alpha) \tag{10.74}$$
$\Psi_J(\mathcal{R})$ being the parameter-free RPA Jastrow factor, and $\Psi_S(\mathcal{R},\alpha)$ a product of two lowest-energy Slater determinant (10.73), one per spin polarization. Find $\alpha^*(\tilde{V})$ minimizing $\mathcal{E}_{N,VMC}(\alpha,\tilde{V})$.
- Compute the DMC energy $\mathcal{E}_{N,DMC}(\tilde{V})$ with the nodal surface of the optimal wavefunction $\Psi(\mathcal{R},\alpha^*(\tilde{V}))$
- repeat step 2 for several values of $\tilde{V}$, and estimate $\chi_{\mathbf{q}}$ by fitting the DMC energy to an even polynomial of $\tilde{V}$.

The DMC calculation sketched above provides one of the most refined estimates of $\chi_{\mathbf{q}}$ available. Following such procedure, we have obtained the data in Table 7.4.

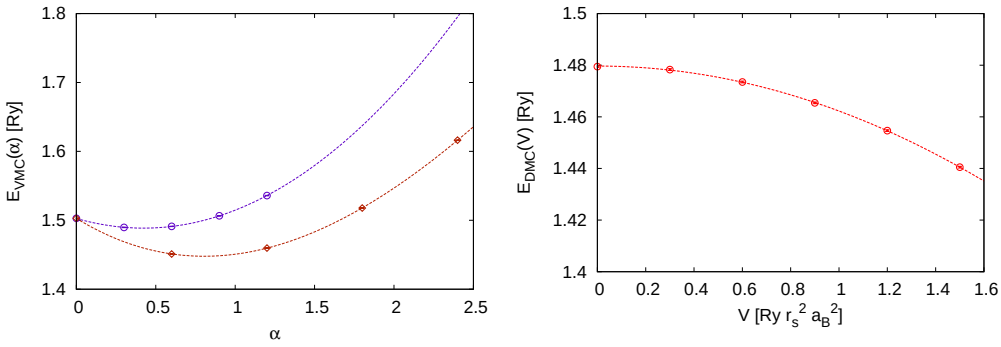

(a) (b)

Figure 10.1: (a) Optimization of the wavefunction $\Psi(\mathcal{R},\alpha)$ for a system of $N = 26$ electrons at $r_s = 0.5$, with $\mathbf{q} = \frac{2\pi}{L}(1,0)$ and $\tilde{V} = 0.9, 1.8\,\mathrm{Ry}(r_s^2 a_B^2)$ (purple, red data). The minima correspond to $\alpha^* = 0.423, 0.805$ respectively. When not visible, errors are below the symbol size. (b) DMC calculation of the ground-state energy $\mathcal{E}_N(V)$. The superimposed line is a fit to a fourth-order polynomial.

CHAPTER 11

Some results about one-dimensional systems

In the present Appendix, the calculations of Chapters 4 are completed in such a way as to make this thesis as more self-contained as possible.

11.1 Details of the Bosonization procedure

In order to prove (4.3), it is useful to recall the Poisson summation formula:

$$\sum_{n\in\mathbb{Z}} \delta(x-n\pi) = \sum_{p\in\mathbb{Z}} \frac{e^{i2\pi\frac{p}{L}\,x}}{L} \to \sum_{n\in\mathbb{Z}} \delta\left(\frac{x}{\pi}-n\right) = \sum_{p\in\mathbb{Z}} e^{i2p\,x} \tag{11.1}$$

that can be promoted to an operator identity observing that:

$$\sum_{p\in\mathbb{Z}} e^{i2p\,\hat{A}}\,|a\rangle = \sum_{p\in\mathbb{Z}} e^{i2p\,a}\,|a\rangle = \sum_{n\in\mathbb{Z}} \delta\left(\frac{a}{\pi}-n\right)|a\rangle = \sum_{n\in\mathbb{Z}} \delta\left(\frac{\hat{A}}{\pi}-n\right)|a\rangle \tag{11.2}$$

where $\hat{A} = \int da\, a\, |a\rangle\langle a|$ is a hermitian operator. Applying (11.2) to $\hat{\theta}(x)$ yields:

$$\sum_{p\in\mathbb{Z}} e^{i2p\,\hat{\theta}(x)} = \sum_{n\in\mathbb{Z}} \delta\Big(\frac{\hat{\theta}(x)}{\pi}-n\Big) \tag{11.3}$$

multiplying both members by $\frac{\partial_x\hat{\theta}(x)}{\pi}$ and recalling (4.1) yields (4.3).
Let us now prove under which conditions:

$$\hat{\Psi}^\dagger_{B,F}(x) = \sqrt{\hat{\rho}(x)}\, e^{i\hat{\eta}_{B,F}(x)} \tag{11.4}$$

provides a representation of the creation operator $\hat{\Psi}^\dagger_{B,F}(x)$. In order to have:

$$\hat{\Psi}^\dagger_{B,F}(x)\hat{\Psi}_{B,F}(x) = \hat{\rho}(x) \tag{11.5}$$

$\hat{\eta}_{B,F}(x)$ must be is hermitian:

$$\hat{\Psi}^\dagger_{B,F}(x)\hat{\Psi}_{B,F}(x) = \sqrt{\hat{\rho}(x)}\, e^{i\hat{\eta}_{B,F}(x)}\, e^{-i\hat{\eta}_{B,F}(x)}\, \sqrt{\hat{\rho}(x)} = \hat{\rho}(x) \tag{11.6}$$

For bosons, $\hat{\eta}_B(x)$ must also permit the fulfilment of the canonical commutation relations:

$$[\hat{\Psi}_B(x), \hat{\Psi}^\dagger_B(y)] = \delta(x-y) \tag{11.7}$$

A sufficient condition is:

$$[\hat{\eta}_B(x), \hat{\eta}_B(y)] = 0 \qquad [\hat{\rho}(x), e^{i\hat{\eta}_B(y)}] = e^{i\hat{\eta}_B(y)}\delta(x-y) \tag{11.8}$$

In fact, recalling that $[\hat{\rho}(x), \hat{\rho}(y)] = 0$, we find that:

$$\begin{aligned}
&[\hat{\Psi}_B(x), \hat{\Psi}_B^\dagger(y)] = \\
&= \left[\sqrt{\hat{\rho}(x)}\, e^{-i\hat{\eta}_{B,F}(x)}, \sqrt{\hat{\rho}(y)}\right] e^{i\hat{\eta}_{B,F}(y)} + \sqrt{\hat{\rho}(y)}\left[\sqrt{\hat{\rho}(x)}\, e^{-i\hat{\eta}_{B,F}(x)}, e^{i\hat{\eta}_{B,F}(y)}\right] = \\
&= \sqrt{\hat{\rho}(x)}\left[e^{-i\hat{\eta}_{B,F}(x)}, \sqrt{\hat{\rho}(y)}\right] e^{i\hat{\eta}_{B,F}(y)} + \sqrt{\hat{\rho}(y)}\left[\sqrt{\hat{\rho}(x)}, e^{i\hat{\eta}_{B,F}(y)}\right] e^{-i\hat{\eta}_{B,F}(x)}
\end{aligned} \tag{11.9}$$

having used the first of (11.8) in the last passage. The identity:

$$[\hat{A}, f(\hat{B})] = [\hat{A}, \hat{B}] f'(\hat{B}) \tag{11.10}$$

implies that:

$$\left[e^{-i\hat{\eta}_{B,F}(x)}, \sqrt{\hat{\rho}(y)}\right] = \left[e^{-i\hat{\eta}_{B,F}(x)}, \hat{\rho}(y)\right] \left[2\sqrt{\hat{\rho}(y)}\right]^{-1} = e^{-i\hat{\eta}_{B,F}(x)} \left[2\sqrt{\hat{\rho}(y)}\right]^{-1} \delta(x-y) \tag{11.11}$$

having used the adjoint of the last of (11.8) in the last passage. Merging (11.9) and (11.11) we retrieve the canonical commutation relation:

$$[\hat{\Psi}_B(x), \hat{\Psi}_B^\dagger(y)] = \delta(x-y) \tag{11.12}$$

It is easy to verify that the last of (11.8) is satisfied in the long wavelength limit, i.e. substituting $\hat{\rho}(x)$ with $\hat{\rho}_s(x)$, if $\partial_x\hat{\phi}(x)$ and $\hat{\eta}_B(y)$ are canonically conjugate. Indeed:

$$e^{i\hat{\eta}_B(y)}\,\delta(x-y) = \left[\,\hat{\rho}_s(x), e^{i\hat{\eta}_B(y)}\,\right] = \left[\frac{\partial_x\hat{\phi}(x)}{\pi}, \hat{\eta}_B(y)\right] i\, e^{i\hat{\eta}_B(y)} \tag{11.13}$$

and thus:

$$\left[\,\partial_x\hat{\phi}(x), \hat{\eta}_B(y)\,\right] = -i\pi\,\delta(x-y) \tag{11.14}$$

It has been shown [157] that (4.10) implies the last of (11.8) also beyond the long wavelength limit.

11.1.1 Correlation functions of the Luttinger liquid

The expressions (4.19) permit to compute the correlation functions of the TLL. Notice that:

- the TLL Hamiltonian is an accurate approximation only in the long-wavelength limit, and for low-energy excitations. The correlation functions of the TLL thus approximate those of an actual 1D liquid only in the limits of large distance or small momentum and energy.

- since the Luttinger Hamiltonian has the form (4.22), the real- time evolution of the destruction operators $\hat{a}_p$ in the Heisenberg representation is exactly known:

$$\hat{a}_p(t) = e^{ic|p|t}\hat{a}_p \tag{11.15}$$

this allows to compute very easily the dynamical correlation functions of the TLL.

- $\hat{\theta}(x)$ makes no distinction between Bose and Fermi particles, unlike $\hat{\Psi}_{B,F}(x)$. Therefore, correlation functions constructed with $\hat{\theta}(x)$ (e.g. the density-density correlation function) are identical for Bose and Fermi particles, unlike those constructed with $\hat{\Psi}_{B,F}(x)$ (e.g. the OBDM).

We will start computng the asymptotic form of the density-density correlation function $\langle\hat{\rho}(x)\hat{\rho}(0)\rangle$, which is a sector of the TBDM and thus is related to the radial distribution function of the TLL. For the sake of simplicity, we restrict our consideration to $x > 0$, since:

$$\langle\hat{\rho}(x)\hat{\rho}(0)\rangle^* = \langle\hat{\rho}(0)\hat{\rho}(x)\rangle = \langle\hat{\rho}(-x)\hat{\rho}(0)\rangle \tag{11.16}$$

the last equality being a consequence of translational invariance. Let ξ be a typical length, above which the hydrodinamic TLL theory can be applied. At $x \gg \xi$ the approximation:

$$\langle\hat{\rho}(x)\hat{\rho}(0)\rangle \simeq \frac{1}{\pi^2}\left\langle\partial_x\hat{\theta}(x)\,\partial_x\hat{\theta}(0)\right\rangle\,\left\langle\sum_{mm'}e^{i\left(2m\hat{\theta}(x)+2m'\hat{\theta}(0)\right)}\right\rangle \tag{11.17}$$

that consists in decoupling long-wavelength and short-wavelength density fluctuations, proves accurate [234, 167]. The first factor is readily evaluated:

$$\begin{aligned}\frac{1}{\pi^2}\left\langle\partial_x\hat{\theta}(x)\,\partial_x\hat{\theta}(0)\right\rangle &= \rho_0^2 + \frac{1}{\pi^2}\sum_p\left(\frac{(-ip)\,e^{-ipx}}{\sqrt{L}}\sqrt{\frac{\pi K_L}{2|p|}}\right)\left(\frac{(ip)}{\sqrt{L}}\sqrt{\frac{\pi K_L}{2|p|}}\right)\langle\hat{a}_p\hat{a}_p^\dagger\rangle = \\ &= \rho_0^2 + \sum_p\frac{p^2\,e^{-ipx}}{L}\,\frac{\pi K_L}{2|p|} \simeq \rho_0^2 + \frac{K_L}{4\pi^2}\int_{-\infty}^{\infty}dp\,|p|\,e^{-ipx}\end{aligned} \tag{11.18}$$

Care must be taken in handling the last integral [148, 234]. Since:

$$\int_{-\frac{1}{\xi}}^{\frac{1}{\xi}}dp\,|p|\,e^{-ipx} = \frac{2}{x^2}\int_0^{\frac{x}{\xi}}dt\,t\,\cos(t) = \frac{2}{x^2}\,(\cos(x/\xi) - 1 + (x/\xi)\sin(x/\xi)) \tag{11.19}$$

The only term having a well-defined limit for $x \gg \xi$ is $-\frac{2}{x^2}$. The other ones display a pathological oscillating behavior, which we interpret as an artifact of the imposition of the phononic dispersion relation to the high-momentum regime, and thus remove. We are left with the following approximation:

$$\frac{1}{\pi^2}\left\langle\partial_x\hat{\theta}(x)\,\partial_x\hat{\theta}(0)\right\rangle = \rho_0^2 - \frac{K_L}{2\pi^2x^2} \tag{11.20}$$

The second factor is:

$$\begin{aligned}&\left\langle\sum_{mm'}e^{i\left(2m\hat{\theta}(x)+2m'\hat{\theta}(0)\right)}\right\rangle = \sum_{mm'}e^{i\left(2(m+m')\theta_0+2m\rho_0x\right)}\left\langle e^{2\sum_p\frac{\left(me^{ipx}+m'\right)}{\sqrt{L}}\sqrt{\frac{\pi K_L}{2|p|}}\left(\hat{a}_p-\hat{a}_{-p}^\dagger\right)}\right\rangle = \\ &= \sum_{mm'}e^{i\left(2(m+m')\theta_0+2m\rho_0x\right)}\,\langle 0|\,e^{\sum_p\Phi_p\hat{a}_p^\dagger-\Phi_p^*\hat{a}_p}|0\rangle\end{aligned} \tag{11.21}$$

where $\Phi_p^* = 2\frac{\left(me^{-ipx}+m'\right)}{\sqrt{L}}\sqrt{\frac{\pi K_L}{2|p|}}$ so that $\Phi_p^* = \Phi_{-p}$.
In the last member of (11.21) appears a displacement operator [328], and thus $|\Phi_p\rangle = e^{\sum_p \Phi_p \hat{a}_p^\dagger - \Phi_p^* \hat{a}_p}|0\rangle$ is a coherent state. By the elementary properties of coherent states:

$$\begin{aligned}\left\langle \sum_{mm'} e^{i\left(2m\hat{\theta}(x)+2m'\hat{\theta}(0)\right)} \right\rangle &= \sum_{mm'} e^{i\left(2(m+m')\theta_0+2m\rho_0 x\right)}\ e^{-\frac{1}{2}\sum_p |\Phi_p|^2} = \\ = \sum_{mm'} e^{i\left(2(m+m')\theta_0+2m\rho_0 x\right)}\ &e^{-\frac{1}{2}\sum_p \frac{4}{L}\frac{\pi K_L}{2|p|}\left(m^2+m'^2+2mm'\cos(px)\right)}\end{aligned} \tag{11.22}$$

The sum at the exponent of (11.22) can be approximated, in the thermodynamic limit:

$$\sum_p \frac{4}{L}\frac{\pi K_L}{2|p|}\left(m^2+m'^2+2mm'\cos(px)\right) \simeq K_L \int_{-\infty}^{\infty}\frac{dp}{|p|}\left(m^2+m'^2+2mm'\cos(px)\right) \tag{11.23}$$

with an integral having an infrared divergence unless $m'+m=0$. We interpret those divergences as artifacts, and we consider only the terms $m'+m=0$ in the summation (11.22). We estimate the last integral relying on the same approach of (11.19):

$$2K_L m^2 \int_{-\frac{1}{\xi}}^{\frac{1}{\xi}} dp\,\frac{1-\cos(px)}{|p|} = 4K_L m^2 \int_0^{\frac{x}{\xi}} dt\,\frac{1-\cos(t)}{t} \tag{11.24}$$

and since $\int \frac{dt}{t}(1-\cos(t)) = \log(t) - \mathrm{Ci}(t)$, $\mathrm{Ci}(t)$ being the cosine integral, by the elementary properties of these functions we conclude that:

$$2K_L m^2 \int_{-\frac{1}{\xi}}^{\frac{1}{\xi}} dp\,\frac{1-\cos(px)}{|p|} = 4K_L m^2\left(\log\left(\frac{x}{\xi}\right) - \mathrm{Ci}\left(\frac{x}{\xi}\right) - \gamma\right) \tag{11.25}$$

γ being Euler-Mascheroni's constant. In the $x \gg \xi$ limit, the second term is negligible, and we are left with the estimate:

$$\left\langle \sum_{mm'} e^{i\left(2m\hat{\theta}(x)+2m'\hat{\theta}(0)\right)} \right\rangle \simeq \sum_m e^{i2m\rho_0 x}\ e^{-2m^2 K_L\left(\log\left(\frac{x}{\xi}\right)-\gamma\right)} \tag{11.26}$$

Collecting (11.19) and (11.26), we obtain the following expression:

$$\begin{aligned} g(x) = \frac{\langle\hat{\rho}(x)\hat{\rho}(0)\rangle}{\rho_0^2} &\simeq \left(1-\frac{K_L}{2(k_F x)^2}\right)\left(1+\sum_{m=1}^{\infty} C_m\,\frac{\cos\left(m(2k_F x)\right)}{(2k_F x)^{2m^2 K_L}}\right) \simeq \\ &\simeq 1-\frac{K_L}{2(k_F x)^2} + \sum_{m=1}^{\infty} C_m\,\frac{\cos\left(m(2k_F x)\right)}{(2k_F x)^{2m^2 K_L}} \end{aligned} \tag{11.27}$$

where $k_F = \pi\rho_0$ is the Fermi wavevector of an ideal Fermi gas at the same density of the system and, in view of the numerous and drastic approximations required to produce the estimate (11.27), the parameters C_m should be interpreted as non-universal parameters taking model-dependent values [148, 168].
On the other hand, the functional form of the density-density correlation function reflects the physical properties and the universality of the Luttinger liquid paradigm.

Due to (11.15), the real-time evolution $\hat{\theta}(x,t)$ of the field $\hat{\theta}(x)$ is readily obtained by changing $kx \to kx - |k|ct$ in (4.19). Repeating the calculation that gave access to the density-density correlation function (11.27) with the time-dependent field $\hat{\theta}(x,t)$ gives access to the real-time density-density correlation function of the Luttinger liquid:

$$\langle\hat{\rho}(x,t)\hat{\rho}(0,0)\rangle \simeq \rho_0^2 + \frac{1}{\pi^2}\left\langle \partial_x\hat{\theta}(x,t)\,\partial_x\hat{\theta}(0,0)\right\rangle + \left\langle \sum_m e^{i2mk_Fx}e^{-i2m\left(\hat{\theta}(x,t)-\hat{\theta}(0,0)\right)}\right\rangle \tag{11.28}$$

where:

$$\begin{aligned}\left\langle \partial_x\hat{\theta}(x,t)\,\partial_x\hat{\theta}(0,0)\right\rangle &= -\frac{K_L}{4}\left(d(x+ct)^{-2}+d(x-ct)^{-2}\right)\\ \left\langle e^{-i2m\left(\hat{\theta}(x,t)-\hat{\theta}(0,0)\right)}\right\rangle &= \frac{C_m}{2}\left(d(ct+x)d(ct-x)\right)^{-m^2K_L}\end{aligned} \tag{11.29}$$

$d(x)$ being the so-called chord function [166, 329]:

$$d(x) = \frac{iL}{\pi}\,\sin\left(\frac{\pi x}{L}\right)e^{-\frac{i\pi x}{L}} \quad , \qquad \lim_{L\to\infty} d(x) = ix \tag{11.30}$$

Formula (11.28) holds for $x > ct$ and, in the thermodynamic limit, reads:

$$\frac{\langle\hat{\rho}(x,t)\hat{\rho}(0)\rangle}{\rho_0^2} \simeq 1 - \frac{K_L}{2(k_F)^2}\,\frac{x^2+c^2t^2}{(x^2-c^2t^2)^2} + \sum_{m=1}^{\infty} C_m\,\frac{\cos\left(m(2k_Fx)\right)}{(2k_F(x^2-c^2t^2))^{2m^2K_L}} \tag{11.31}$$

The DSF is related to the time-dependent density-density correlation function (11.28) by the means of the Fourier transform:

$$S(q,\omega) = \int dx \int dt\, e^{i(\omega t - qx)}\ \langle\hat{\rho}(x,t)\hat{\rho}(0)\rangle \tag{11.32}$$

By direct inspection, it is possible to verify [169, 167] that:

$$S(q,\omega) = \sum_{m=1}^{\infty} S_m\,\omega^{2m^2(K_L-1)}\,\frac{f\left(\frac{c(q-2mk_F)}{\omega}\right)+f\left(\frac{c(q+2mk_F)}{\omega}\right)}{2} \tag{11.33}$$

where:

$$f(x) = \begin{cases} (1-x^2)^{m^2K_L-1} & |x|<1 \\ 0 & \text{otherwise}\end{cases} \tag{11.34}$$

11.2 Mobile impurity Hamiltonian

We now provide a heuristic derivation of the mobile impurity Hamiltonian (4.18), (4.45), (4.46) adapting the procedure of [200] to the case of bosons. First, we project the annihilation operator $\hat{\Psi}_B(x)$ onto two subbands:

$$\hat{\Psi}_B(x) = \hat{\Psi}_{LL}(x) + e^{iqx}\hat{d}(x) \tag{11.35}$$

the first representing the destruction of a particle in the TLL and the second the destruction of an impurity with momentum q. The Fourier transform of (11.35) reads:

$$\hat{a}(p) = \int e^{-ipx}\,\hat{\Psi}_B(x) = \hat{a}_{LL}(p) + \hat{d}(p-q) \tag{11.36}$$

Substituting (11.36) in the kinetic energy, and neglecting all terms coupling TLL and impurity modes, we find:

$$\hat{T} = \int dp\,\epsilon(p)\hat{a}^\dagger(p)\hat{a}(p) = \hat{T}_{LL} + \int dp\,\epsilon(p)\hat{d}^\dagger(p-q)\hat{d}(p-q) \tag{11.37}$$

Expanding $\epsilon(p)$ around q we obtain:

$$\hat{T} = \hat{T}_{LL} + \int dp\,\epsilon(q)\,\hat{d}^\dagger(p-q)\hat{d}(p-q) + \int dp\,(p-q)\partial_q\epsilon(q)\,\hat{d}^\dagger(p-k)\hat{d}(p-q) \tag{11.38}$$

and moving back to the configurational space yields the non-interacting part of the mobile impurity Hamiltonian:

$$\hat{T} \simeq \hat{T}_{LL} + \int dx\,\hat{d}^\dagger(x)\,(\epsilon(k) - i\hbar v_d\,\partial_x)\,\hat{d}(x) \tag{11.39}$$

with $v_d = \partial_q\epsilon(q)$. To write interacting part, we expand the density as:

$$\hat{\rho}(x) = \hat{\rho}_{LL}(x) + \hat{\rho}_I(x) + \hat{\Psi}^\dagger_{LL}(x)e^{iqx}\hat{d}(x) + \text{h.c.} = \tag{11.40}$$

with $\hat{\rho}_I(x) = \hat{d}^\dagger(x)\hat{d}(x)$, whence:

$$\hat{V} \simeq \frac{v_0}{2}\int dx\hat{\rho}(x)\hat{\rho}(x) \simeq \hat{V}_{LL} + 2v_0\int dx\,\hat{\rho}_{LL}(x)\hat{\rho}_I(x) \tag{11.41}$$

neglecting all other terms in the expansion of $\hat{\rho}(x)\hat{\rho}(x)$. Recalling (4.1) leads to:

$$\hat{V} = \hat{V}_{LL} + 2v_0\int dx\,\frac{\partial_x\hat{\phi}(x)}{\pi}\,\hat{d}^\dagger(x)\hat{d}(x) \tag{11.42}$$

which has the general form (4.46) with $V_\eta(q) = 0$ and $V_\phi(q) = 4v_0$. In view of the crude approximations introduced in this simplified derivation of the mobile impurity Hamiltonian, $V_\eta(q), V_\phi(q)$ should be treated as momentum-dependent phenomenological parameters, that can be fixed considering the shift of the threshold $\epsilon(q)$ caused by a uniform density variation and by a Galilean boost. This calculation is carried out in detail in [153], and leads to (4.47).

11.3 Diagonalization of the nonlinear Luttinger liquid Hamiltonian

In order to verify that the unitary transformation:

$$\hat{U} = \exp\left(i\int dx\,\left(\sqrt{K_L}\frac{\delta_+(q)-\delta_-(q)}{2\pi}\hat{\eta}(x) - \frac{1}{\sqrt{K_L}}\frac{\delta_+(q)+\delta_-(q)}{2\pi}\hat{\phi}(x)\right)\,\hat{d}^\dagger(x)\hat{d}(x)\right) \tag{11.43}$$

diagonalizes the nonlinear TLL Hamiltonian (4.45), (4.46) for a suitable choice of the phase shifts $\delta_{\pm}(k)$, let us compute the transformation law of the fields $\partial_x\hat{\eta}(x)$, $\partial_x\hat{\phi}(x)$, $\hat{d}(x)$. To this purpose, we rely on the Baker-Campbell-Haussdorff formula [328]:

$$\hat{O}' = e^{\hat{S}}\hat{O}e^{-\hat{S}} = \sum_{n=0}^{\infty}\frac{1}{n!}[\hat{S},\hat{O}]_n = \hat{O} + [\hat{S},\hat{O}] + \frac{1}{2}[\hat{S},[\hat{S},\hat{O}]] + \frac{1}{6}[\hat{S},[\hat{S},[\hat{S},\hat{O}]]] + \dots \quad (11.44)$$

The unitary transformation $\hat{U}$ has the form $e^{\hat{S}}$ with:

$$\hat{S} = i\int dy\,\left(\sqrt{K_L}\,\frac{\delta_+(q)-\delta_-(q)}{2\pi}\hat{\eta}(y) - \frac{1}{\sqrt{K_L}}\,\frac{\delta_+(q)+\delta_-(q)}{2\pi}\hat{\phi}(y)\right)\,\hat{d}^\dagger(y)\hat{d}(y) \quad (11.45)$$

Therefore, the impurity density operator $\hat{d}^\dagger(x)\hat{d}(x)$ is invariant under $\hat{U}$. Indeed:

$$[\hat{S},\hat{d}^\dagger(x)\hat{d}(x)] = 0 \to [\hat{S},\hat{d}^\dagger(x)\hat{d}(x)]_n = 0 \text{ for all } n \geq 1 \quad (11.46)$$

since $\hat{\eta}(y)$,$\hat{\phi}(y)$ and $\hat{d}^\dagger(y)\hat{d}(y)$ commute with $\hat{d}^\dagger(x)\hat{d}(x)$, and thus:

$$\hat{U}\hat{d}^\dagger(x)\hat{d}(x)\hat{U}^\dagger = \hat{d}^\dagger(x)\hat{d}(x) \quad (11.47)$$

Let us consider the transformation law of $\partial_x\hat{\phi}(x)$. Since:

$$\begin{aligned}&[\hat{S},\partial_x\hat{\phi}(x)] = i\int dy\,\hat{d}^\dagger(y)\hat{d}(y)\\ &\left(\sqrt{K_L}\,\frac{\delta_+(q)-\delta_-(q)}{2\pi}[\hat{\eta}(y),\partial_x\hat{\phi}(x)] - \frac{1}{\sqrt{K_L}}\,\frac{\delta_+(q)+\delta_-(q)}{2\pi}[\hat{\phi}(y),\partial_x\hat{\phi}(x)]\right)\end{aligned} \quad (11.48)$$

recalling that $\left[\hat{\phi}(y),\partial_x\hat{\phi}(x)\right] = \partial_x\left[\hat{\phi}(y),\hat{\phi}(x)\right] = 0$ and:

$$\left[\hat{\eta}(y),\partial_x\hat{\phi}(x)\right] = i\pi\delta(x-y) \quad (11.49)$$

by (4.10), we find:

$$[\hat{S},\partial_x\hat{\phi}(x)] = \sqrt{K_L}\frac{\delta_+(q)-\delta_-(q)}{2}\hat{d}^\dagger(x)\hat{d}(x) \quad (11.50)$$

whence $[\hat{S},\partial_x\hat{\phi}(x)]_n = 0$ for all $n > 1$ and:

$$\partial_x\hat{\phi}'(x) = \hat{U}\partial_x\hat{\phi}(x)\hat{U}^\dagger = \partial_x\hat{\phi}(x) - \sqrt{K_L}\,\frac{\delta_+(q)-\delta_-(q)}{2}\,\hat{d}^\dagger(x)\hat{d}(x) \quad (11.51)$$

An identical calculation shows that:

$$[\hat{S},\partial_x\hat{\eta}(x)] = \frac{1}{\sqrt{K_L}}\,\frac{\delta_+(q)+\delta_-(q)}{2}\,\hat{d}^\dagger(x)\hat{d}(x) \quad (11.52)$$

whence $[\hat{S},\partial_x\hat{\eta}(x)]_n = 0$ for all $n > 1$ and:

$$\partial_x\hat{\eta}'(x) = \hat{U}\partial_x\hat{\eta}(x)\hat{U}^\dagger = \partial_x\hat{\eta}(x) + \frac{1}{\sqrt{K_L}}\frac{\delta_+(q)+\delta_-(q)}{2}\,\hat{d}^\dagger(x)\hat{d}(x) \quad (11.53)$$

The transformation law of $\hat{d}(x)$ is a bit more involved:

$$[\hat{S},\hat{d}(x)] = i\int dy\left(\sqrt{K_L}\frac{\delta_+(q)-\delta_-(q)}{2\pi}\hat{\eta}(y) - \frac{1}{\sqrt{K_L}}\frac{\delta_+(q)+\delta_-(q)}{2\pi}\hat{\phi}(y)\right)[\hat{d}^\dagger(y)\hat{d}(y),\hat{d}(x)] = \\ -i\left(\sqrt{K_L}\frac{\delta_+(q)-\delta_-(q)}{2\pi}\hat{\eta}(x) - \frac{1}{\sqrt{K_L}}\frac{\delta_+(q)+\delta_-(q)}{2\pi}\hat{\phi}(x)\right)\hat{d}(x) = \hat{A}(x)\,\hat{d}(x) \tag{11.54}$$

Therefore:

$$[\hat{S},[\hat{S},\hat{d}(x)]] = [\hat{S},\hat{A}(x)\hat{d}(x)] = 2\hat{C}(x)\hat{d}(x) + \hat{A}(x)^2\,\hat{d}(x) \tag{11.55}$$

where:

$$2\hat{C}(x) = [\hat{S},\hat{A}(x)] = -\int dy\,[\hat{A}(y),\hat{A}(x)]\hat{d}^\dagger(y)\hat{d}(y) \tag{11.56}$$

Here comes an useful observation: since $[\hat{\phi}(x),\hat{\eta}(y)] = -\frac{i\pi}{2}\,\mathrm{sgn}(x-y)$ the commutator $[\hat{A}(y),\hat{A}(x)]$ is a scalar function, and thus $\hat{C}(x)$ commutes with $\hat{S}$ and with $\hat{A}(x)$. We find:

$$\begin{aligned}
[\hat{S},\hat{d}(x)]_1 &= \hat{A}(x)\,\hat{d}(x)\\
[\hat{S},\hat{d}(x)]_2 &= \left(2\hat{C}(x)+\hat{A}(x)^2\right)\hat{d}(x)\\
[\hat{S},\hat{d}(x)]_3 &= \left(6\hat{C}(x)\hat{A}(x)+\hat{A}(x)^3\right)\hat{d}(x)\\
[\hat{S},\hat{d}(x)]_4 &= \left(12\hat{C}(x)^2+12\hat{C}(x)\hat{A}(x)^2+\hat{A}(x)^4\right)\hat{d}(x)
\end{aligned} \tag{11.57}$$

whence:

$$\hat{d}' = \left(1+\hat{A}+\hat{C}+\frac{\hat{A}^2}{2!}+\hat{C}\hat{A}+\frac{\hat{A}^3}{3!}+\frac{1}{2!}\hat{C}^2+\hat{C}\frac{\hat{A}^2}{2!}+\frac{\hat{A}^4}{4!}+\dots\right)\hat{d} = \\ = e^{\hat{A}+\hat{C}}\hat{d} \tag{11.58}$$

having omitted the dependence of the operators on x for brevity. Knowledge of the transformed fields $\hat{d}'(x)$ grants the ability of computing the transformed Hamiltonian $\hat{H}'$. With a straightforward calculation, we find that

$$\hat{H}' = \hat{H} + \text{h.o.t.} \tag{11.59}$$

if the phase shifts are given by (4.49). In the expression of $\hat{H}'$, h.o.t. stands for high-order terms which are neglected in the impurity model, since they introduce negligible corrections to the edge singularity [150, 171, 172].

The solution of the mobile impurity Hamiltonian allows us to understand the shape of the DSF close to the low-energy threshold. The first step is the observation [329] that, close to the low-energy threshold and for $0 < q < 2k_F$, the density operator is well-approximated by [329]:

$$\hat{\rho}(x) = \hat{\Psi}^\dagger(x)\hat{\Psi}(x) \simeq e^{-iqx}\,\hat{d}^\dagger(x)\,e^{i\left(\hat{\eta}(x)-\hat{\phi}(x)\right)} \tag{11.60}$$

which describes the creation of an impurity accompanied by a fluctuation in the density of the TLL.

In the light of (11.60) the SDF at the impurity momentum q reads:

$$\begin{aligned} S(q,\omega) &= \int dx \int dt\, e^{-i(qx-\omega t)}\, \langle \hat{\rho}(x,t)\hat{\rho}(0,0)\rangle = \\ &= \int dx \int dt\, e^{i\omega t}\, \langle e^{-i\left(\hat{\eta}(x,t)-\hat{\phi}(x,t)\right)} \hat{d}(x,t)\hat{d}^\dagger(0,0) e^{i\left(\hat{\eta}(0,0)-\hat{\phi}(0,0)\right)}\rangle \end{aligned} \tag{11.61}$$

where the expectation value should be calculated over the ground-state of the nonlinear TLL Hamiltonian. Applying the unitary transformation $\hat{U}$ decouples the impurity from the TLL, and leads to the following expression for the expectation value:

$$\begin{aligned} &\langle e^{-i\left(\hat{\eta}(x,t)-\hat{\phi}(x,t)\right)} \hat{d}(x,t)\hat{d}^\dagger(0,0) e^{i\left(\hat{\eta}(0,0)-\hat{\phi}(0,0)\right)}\rangle = \\ =&\langle \hat{d}(x,t)\hat{d}^\dagger(0,0)\rangle\, \langle e^{i\mu(q)\left(\hat{\phi}(x,t)-\hat{\eta}(x,t)\right)} e^{-i\nu(q)\left(\hat{\phi}(0,0)-\hat{\eta}(0,0)\right)}\rangle \end{aligned} \tag{11.62}$$

where the first expectation has to be computer over the vacuum of $\hat{H}_d$, the second one over the vacuum of $\hat{H}_{LL}$, and:

$$\mu(q) = 1 + \frac{\delta_+(q)+\delta_-(q)}{2\pi\sqrt{K_L}} \qquad \nu(q) = 1 - \frac{\delta_+(q)-\delta_-(q)}{2\pi}\sqrt{K_L} \tag{11.63}$$

Notice that in the transformation laws of the operators $\hat{\phi}(x), \hat{\eta}(x)$ appear integrals of the impurity density which give no contribution to the expectation (11.63), since the latter is taken over the impurity vacuum.
The first expectation results from a very simple calculation:

$$\langle \hat{d}(x,t)\hat{d}^\dagger(0,0)\rangle = e^{-i\omega_{th}(q)t} \sum_{n\in\mathbb{Z}} \frac{e^{2\pi i n \frac{x-v_d t}{L}}}{L} \quad \underset{L\to\infty}{\longrightarrow} \quad e^{-i\omega_{th}(q)t}\delta(x-v_d t) \tag{11.64}$$

The second one is very similar to (11.29), and reads [166, 329]:

$$\langle e^{i\mu(q)\left(\hat{\phi}(x,t)-\hat{\eta}(x,t)\right)} e^{-i\nu(q)\left(\hat{\phi}(0,0)-\hat{\eta}(0,0)\right)}\rangle \propto d(ct+x)^{-\mu_+(q)}\, d(ct-x)^{-\mu_-(q)} \tag{11.65}$$

with:

$$\mu_\pm(q) = \left(\mu(q)\frac{\sqrt{K_L}}{2} \pm \frac{\nu(q)}{2\sqrt{K_L}}\right)^2 \tag{11.66}$$

The DSF is then given by:

$$\begin{aligned} S(q,\omega) &\propto \int dx \int dt\, e^{i\omega t}\, e^{-i\omega_{th}(q)t}\delta(x-v_d t)\, d(ct+x)^{-\mu_+(q)}\, d(ct-x)^{-\mu_-(q)} \\ &\propto \int dt\, e^{i(\omega-\omega_{th}(q))t} t^{-\mu_+(q)-\mu_-(q)} \end{aligned} \tag{11.67}$$

Performing the change of variables $u = (\omega-\omega_{th}(q))\, t$ we can identify the power-law behavior for ω close to $\omega_{th}(q)$:

$$S(q,\omega) \propto (\omega-\omega_{th}(q))^{\mu_+(q)+\mu_-(q)-1} \tag{11.68}$$

Expressing the exponent $\mu_+(q)+\mu_-(q)-1$ in terms of (11.63), (11.66) we retrieve (4.52).

CHAPTER 12

The GIFT method

The present appendix aims at providing a brief description of the GIFT method, used in Chapter 4 to reconstruct the DSF of a collection of ^{4}He atoms in one dimension from the imaginary-time density-density correlation function $F(\mathbf{q}, \tau)$ of the system through an inverse Laplace transform. In Section 12.0.1, the inverse Laplace transform is framed in the context of ill-posed inverse problems, which occur in a broad range of Physics-related problems. The inherent difficulty of solving ill-posed inverse problems is discussed through the analysis of compact operators with infinite rank and Fredholm equations of the first kind. A brief overview of some of the approaches devised to handle Fredholm equations of the first kind is given in order to contextualize the GIFT method, which is described in detail in Section 12.0.5. Further information on the GIFT method can be found in [220, 222].

12.0.1 Ill-posed inverse problems

QMC simulations like those discussed in Sections 3.2, 3.4, 6.1 give access to imaginary-time correlation functions $F(\tau)$. These purely mathematical objects carry no direct physical meaning, but they are related to dynamical structure factors $S(\omega)$ by suitable integral equations. For zero-temperature systems, as discussed in Section 1.1, $F(\tau)$ is the Laplace transform of $S(\omega)$:

$$F(\tau) = \int_0^\infty d\omega \, e^{-\tau\omega} \, S(\omega) \tag{12.1}$$

While computing the forward Laplace transform $S(\omega) \to F(\tau)$ is a relatively straightforward operation, computing the inverse Laplace transform $F(\tau) \to S(\omega)$ is a very difficult task, even if $F(\tau)$ is exactly known. In such favorable case, in fact, $S(\omega)$ is retrieved from simple-looking but usually very impractical expressions like Post's inversion formula [330]:

$$S(\omega) = \lim_{k\to\infty} \frac{(-1)^k}{k!} \left(\frac{k}{\omega}\right)^{k+1} \frac{d^k F}{d\tau^k}\left(\frac{k}{\omega}\right) \tag{12.2}$$

that requires to evaluate derivatives of arbitrarily high orders, or Bromwich's inversion formula [331]:

$$S(\omega) = \frac{1}{2\pi} \lim_{T\to\infty} \int_{\gamma-iT}^{\gamma+iT} d\tau \, e^{\tau\omega} F(\tau) \tag{12.3}$$

that requires knowledge of $F(\tau)$ on the whole complex plane, and its integration along a vertical path such that $\gamma \in \mathbb{R}$ lies at the right of all the singularities of $F(\tau)$.
The inverse problem of reconstructing DSFs from imaginary-time correlation functions yield by QMC simulations is even more difficult. In fact, QMC simulations necessarily give access to $F(\tau)$ on a finite number of imaginary times τ_i, $i = 1 \dots N_\tau$, and with statistical uncertainties σ_i. This circumstance makes the inverse problem *ill-posed*.

A mathematical problem is well-posed, in the sense precised by J. Hadamard [332] if:

1. a solution exists
2. the solution is unique
3. the solution depends continuously on the data of the problem

A problem which is not well-posed is called an ill-posed problem. As a simple and useful example, consider the operator equation:

$$|F\rangle = \hat{K}\,|S\rangle \tag{12.4}$$

where the linear operator $\hat{K} : H \to H'$ acts between Hilbert spaces H and H'. Linear problems of the form (12.4) often appear in Physics-related problems, where S describes some cause determining an observable effect F, and the linear operator $\hat{K}$ models the cause-effect relationship [331, 333, 334]. The forward problem of computing F given S is well-posed under the very mild assumption that $\hat{K}$ is a bounded operator. In fact, the existence and uniqueness of F in (12.4) are granted by the very definition of linear operator, and its continuity follows from:

$$\|F - F'\| = \|\hat{K}(S - S')\| \leq \|\hat{K}\|\,\|S - S'\| \tag{12.5}$$

where:

$$\|\hat{K}\| = \sup_{S \neq 0} \frac{\|\hat{K}S\|}{\|S\|} \tag{12.6}$$

is the operator norm of $\hat{K}$. On the other hand, the inverse problem of computing S given F is ill-posed if $\hat{K}$ does not have a continuous inverse. This mathematical statement reflects the difficulty of reliably determining the cause S responsible for an effect F, given the observation of F alone. In particular, there might be several causes S', S'' giving rise to the same effect F (non-unique solution), in which case $\hat{K}$ is not injective and thus it has no inverse. Also, tiny perturbations in the observed effect might originate from radically different causes (non-continuous solution), in which case $\hat{K}^{-1}$ is not continuous. This kind of inverse ill-posed problem is very common, because there is a vast class of operators $\hat{K}$, namely compact operators of infinite rank, that cannot have a continuous inverse [335]. It can be proved [335] that $\hat{K}$ is a compact operator of infinite rank if, and only if, it has the following singular value decomposition (SVD):

$$\hat{K}\,|S\rangle = \sum_{n=1}^{\infty} \sigma_n\,|v_n\rangle\,\langle u_n|S\rangle \tag{12.7}$$

where $\{u_n\}_n$, $\{v_n\}_n$ are orthonormal sets in H, H' respectively, and σ_n is a decreasing sequence of positive real numbers such that $\lim_{n\to\infty} \sigma_n = 0$. In fact, $\hat{K}$ is a bounded operator:

$$\|\hat{K}\| = \sup_n \|\hat{K}u_n\| = \sup_n \sigma_n < \infty \tag{12.8}$$

and thus the forward problem of computing F given S is well-posed. On the other hand, its pseudoinverse:

$$\hat{\mathcal{I}}(K)\,|F\rangle = \sum_{n=1}^{\infty} \frac{1}{\sigma_n}\,|u_n\rangle\,\langle v_n|F\rangle \tag{12.9}$$

is unbounded, and thus discontinuous:

$$\|\hat{\mathcal{I}}(K)\| = \sup_n \|\hat{\mathcal{I}}(K)v_n\| = \sup_n \frac{1}{\sigma_n} = \infty \tag{12.10}$$

The inverse problem of computing S given F, which is solved by $|S\rangle = \hat{\mathcal{I}}(K)\,|F\rangle$, is ill-posed. The reputed solution makes sense only for F such that:

$$\|\hat{\mathcal{I}}(K)F\| = \sup_n \frac{|\,\langle v_n|F\rangle\,|^2}{\sigma_n^2} < \infty \tag{12.11}$$

and, since $\hat{\mathcal{I}}(K)$ is unbounded, it does not depend continuously on F. In fact, the sequence $|F_n\rangle = |F\rangle + \sqrt{\sigma_n}\,|u_n\rangle$ converges to F in the $n \to \infty$ limit, but:

$$\|\hat{\mathcal{I}}(K)F - \hat{\mathcal{I}}(K)F_n\| = \|\sqrt{\sigma_n}\hat{\mathcal{I}}(K)u_n\| = \frac{1}{\sigma_n} \to \infty \tag{12.12}$$

does not. Thus, the sequence $|S_n\rangle = \hat{\mathcal{I}}(K)\,|F_n\rangle$ does not converge to $|S\rangle = \hat{\mathcal{I}}(K)\,|F\rangle$: the inverse problem is dramatically sensitive to tiny perturbations in the observed effect. Several mathematics-related and Physics-related problems [331, 334] lead to operator equations of the form:

$$F(x) = \int_{\Omega'} dx'\, K(x,x')S(x') \tag{12.13}$$

where $F : \Omega \subseteq \mathbb{R}^n \to \mathbb{R}$, $S : \Omega' \subseteq \mathbb{R}^{n'} \to \mathbb{R}$ and $K : \Omega \times \Omega' \to \mathbb{R}$. The integral equation (12.14) has the general form (12.4), and it is called Fredholm equation of the first kind. The Fourier transform:

$$\tilde{F}(\omega) = \int_{\mathbb{R}} dt\, e^{i\omega t}F(t) \tag{12.14}$$

and the Laplace transform (12.1) are remarkable examples of Fredholm equations of the first kind, with $\Omega = \Omega' = \mathbb{R}$, $K(\omega,t) = e^{i\omega t}$ and $\Omega = \Omega' = [0,\infty)$, $K(\tau,\omega) = e^{-\tau\omega}$ respectively. However, there is a fundamental difference between these two operations. The Fourier transform is associated to a unitary operator, which is bounded and has a continuous inverse: therefore, the forward and inverse problems of computing the Fourier transform are both well-posed. On the other hand, the Laplace transform is associated to a compact operator of infinite rank [333, 336] and the inverse problem of deducing $S(\omega)$ from $F(\tau)$ is ill-posed.

Fredholm equations (12.14) must often be discretized in order to obtain a numerical solution. The discretization makes the solution of the ill-posed problem even more sensitive to changes in the data. Moreover, experiments and QMC simulations yield data with statistical uncertainties, making impossible to find a unique solution.

Because of the notorious practical importance of inverse problems, and particularly of Fredholm integral equations, there is a long history of the vast amount of attempts to develop methods to deal with them. It is impossible to single out the best method for solving this class of equations because the non-uniqueness of the solution requires the introduction of some additional information, specifying *a priori* information about the expected solution. In the following, we briefly review some of the approaches conceived to solve the Fredholm equations of the first kind. In particular, we describe the Genetic Inversion via Falsification of Theories (GIFT) method [220], which has been used to produce the results presented in Chapter 4.

12.0.2 Least-Squares

For the sake of simplicity, we assume $n, n' = 1$ in (12.14). Approximating the functions g, f by their values on finite meshes of N, N' points respectively permits to express (12.14) in the matrix form:

$$F_i = \sum_{j=1}^{N'} K_{ij} S_j \quad , \qquad \mathbf{F} \in \mathbb{R}^N, \mathbf{S} \in \mathbb{R}^{N'} \tag{12.15}$$

where $F_i = F(x_i)$, $S_j = S(x'_j)$ and $K_{ij} = \mu_j K(x_i, x'_j)$, μ_j being a discrete measure ensuring that the summation in (12.15) approximates the integration in (12.14). For a uniform mesh $x'_j = x'_0 + (j-1)\Delta x'$, $\mu_j = \Delta x'$. Let $\mathbf{S}_{exact}, \mathbf{F}_{exact}$ be the exact discretized cause and effect functions, related by $\mathbf{F}_{exact} = K\mathbf{S}_{exact}$. Given an observed effect $S \sim N(\mathbf{S}_{exact}, \sigma^2)$, the simplest approach is to search for the least-squares solution of the problem (12.15) i.e. the vector $\mathbf{S} \in \mathbb{R}^{N'}$ minimizing the deviation of $K\mathbf{S}$ from the observed data $\mathbf{F}$, measured by:

$$\chi^2(\mathbf{S}) = \|\mathbf{F} - K\mathbf{S}\|^2 \tag{12.16}$$

the least-squares solution is $\mathbf{S} = (K^T K)^{-1} K^T \mathbf{F} = J\mathbf{F}$. Thus, $\mathbf{S} \sim N\left(J\mathbf{F}_{exact}, \sigma^2 JJ^T\right) = N\left(\mathbf{S}_{exact}, \sigma^2 JJ^T\right)$. The inadequacy of the least-squares strategy is readily understood by performing the SVD of the matrix K:

$$K = U\Sigma V^T \quad , \qquad \begin{array}{l} U \in M_{N\times N''}(\mathbb{R}) \\ V \in M_{N'\times N''}(\mathbb{R}) \\ \Sigma = \mathrm{diag}(\sigma_1 \dots \sigma_{N''}) \end{array} \tag{12.17}$$

where U, V are orthogonal matrices with $N'' = \min(N, N')$, and the numbers σ_i are real and non-negative. Since $J = V\Sigma^{-1}U^T$, we find:

$$S \sim N\left(\mathbf{S}_{exact}, V(\sigma^2\Sigma^{-2})V^T\right) \quad , \qquad \left(V(\sigma^2\Sigma^{-2})V^T\right)_{ij} = \sum_k V_{ik}\frac{\sigma^2}{\sigma_k^2}V_{jk} \tag{12.18}$$

whence even very small statistical errors in $\mathbf{F}$ can induce large statistical errors in $\mathbf{S}$. This clearly happens in presence of singular values $\sigma_k \ll \sigma$. Given the observation $\mathbf{F}$, the reconstruction $J\mathbf{F}$ then gives no information about $\mathbf{S}_{exact}$, and it is typically characterized by large perturbations [337]. The origin of the perturbations is that $J\mathbf{F}$ over-fits the statistical errors present in the input data $\mathbf{F}$.

The least-squares method can be significantly improved by incorporating a Tikhonoff-Phillips regularization [338, 339, 340]. The idea is to substitute the quantity to minimize with a weighted combination:

$$\tilde{\chi}^2(\mathbf{S}) = \chi^2(\mathbf{S}) + \lambda^2\|\Gamma\mathbf{S}\|^2 \tag{12.19}$$

of the deviation measure $\chi^2(\mathbf{S})$ and of a constraint $\|\Gamma\mathbf{S}\|^2$, encompassing some a priori knowledge about the solution $\mathbf{S}$. The simplest modification sets Γ as the identity matrix, in order to suppress the large oscillations characterizing the least-squares solution.

The regularized least-squares estimator is $\mathbf{S} = (K^T K + \lambda^2)^{-1} K^T \mathbf{F} = J_\lambda \mathbf{F}$. Therefore $S \sim N(J_\lambda \mathbf{F}_{exact}, \sigma^2 J_\lambda J_\lambda^T)$: the regularization, having inserted a-priori knowledge about the solution (namely the absence of large fluctuations), biases the estimator S towards a

specific value $J_\lambda \mathbf{F}_{exact} \neq J\mathbf{F}_{ex}$, but considerably reduces its variance. Indeed:

$$\sigma^2 J_\lambda J_\lambda^T = V(\sigma^2\Sigma^2(\Sigma^2+\lambda^2)^{-2})V^T \quad , \quad \left(V(\sigma^2\Sigma^2(\Sigma^2+\lambda^2)^{-2})V^T\right)_{ij} = \sum_k V_{ik}\frac{\sigma^2\sigma_k^2}{\sigma_k^2+\lambda^2}V_{jk} \tag{12.20}$$

It is clear that the problematic contributions corresponding to singular values $\sigma_k \ll \lambda$ are automatically filtered out by the regularization, and large fluctuation of the least-squares solution are suppressed. The tradeoff between the competing issues of biasing the solution and reducing its statistical uncertainties) lies at the basis of the various approaches to find the optimal regularization parameter λ [341, 342, 343].

In order to introduce other methods for handling inverse ill-posed problems, it is convenient to examine the Tikhonoff-Phillips regularization under the perspective of the Bayesian statistical inference. According to the Bayes' theorem [344]:

$$P(\mathbf{S}|\mathbf{F})P(\mathbf{F}) = P(\mathbf{F}|\mathbf{S})P(\mathbf{S}) \quad \rightarrow \quad P(\mathbf{S}|\mathbf{F}) = \frac{P(\mathbf{F}|\mathbf{S})P(\mathbf{S})}{P(\mathbf{F})} \tag{12.21}$$

where $P(\mathbf{S}|\mathbf{F})$ is the conditional probability that the cause is $\mathbf{S}$ given knowledge of $\mathbf{F}$. The application of Bayes' theorem reduces the ill-posed problem of finding the most probable $\mathbf{S}$ given $\mathbf{F}$ (i.e. maximizing $P(\mathbf{S}|\mathbf{F})$) into the problem of finding the most probable $\mathbf{F}$ given $\mathbf{S}$ taking into account some prior knowledge $P(\mathbf{S})$ about $\mathbf{S}$ (i.e. maximizing the right member of (12.21)). In particular, choosing:

$$P(\mathbf{F}|\mathbf{S}) \propto e^{-\chi^2(\mathbf{S})} \tag{12.22}$$

and $P(\mathbf{S}) \propto e^{-\lambda^2\|\mathbf{S}\|^2}$, the maximum of $P(\mathbf{S}|\mathbf{F})$ is attained at the regularized least-squares solution. Neglecting prior knowledge, i.e. setting $\lambda \rightarrow 0$, leads to the least-squares solution.

12.0.3 The Maximum Entropy Method

The Tikhonoff-Phillips regularization unconditionally suppresses solutions $\mathbf{S}$ with large norm. The corresponding bias can be problematic when $\mathbf{S}$ has sharp edges or narrow peaks. The Maximum Entropy Method (MEM) was conceived by M. Jarrell and J. E. Gubernatis [345], circumvents this problem relying on a suitable modification of the prior knowledge $P(\mathbf{S})$, set equal to:

$$P(\mathbf{S}) \propto e^{\alpha\mathcal{H}(\mathbf{S})} \qquad \mathcal{H}(\mathbf{S}) = \sum_j \mu_j \left(S_j - m_j - S_j \log\left(\frac{S_j}{m_j}\right)\right) \tag{12.23}$$

where $\mathbf{m} \in \mathbb{R}^{N'}$ is a default model, encompassing a priori information about the exact solution $\mathbf{S}_{exact}$. The regularization parameter α controls the relative importance of $P(\mathbf{F}|\mathbf{S})$ and $P(\mathbf{S})$: large values of α enforce the prior knowledge, keeping the MEM solution $\mathbf{S}$ close to the default model $\mathbf{m}$, while small values of α reduce the problem to the minimization of $\chi^2(\mathbf{S})$. As a general consideration, the MEM is superior to the Tikhonoff-Phillips regularization in cases where significant information about $\mathbf{S}$ is known. However, the dependence of the method on the default model can represent a drawback if the most interesting features of the solution are sensitive to the form of $\mathbf{m}$ [346, 347, 337]. The choice of the parameter α and of the default model are fully discussed in [345, 348].

12.0.4 The stochastic sampling methods

Stochastic sampling methods (SSM), introduced by A. W. Sandvik [349], are based on a radically different approach. SSMs incorporate a minimal prior knowledge about the solution, and do not use default models. Within SSMs methods, the solution $\mathbf{S}$ is retrieved [349, 350] as an average:

$$\mathbf{S} = \int d\mathbf{S}'\, \mathbf{S}'\, P(\mathbf{S}'|\mathbf{F}) \tag{12.24}$$

over trial solutions $\mathbf{S}'$ weighted by the probability distribution $P(\mathbf{S}'|\mathbf{F})$. In his seminal work [349] on SSMs, A. W. Sandvik suggested the choice:

$$P(\mathbf{S}'|\mathbf{F}) \propto e^{-\beta\chi^2(\mathbf{F}')} \tag{12.25}$$

which has the suggestive interpretation of a Gibbs distribution with fictitious inverse temperature β. The probability distribution $P(\mathbf{S}'|\mathbf{F})$ is efficiently sampled relying on the Metropolis algorithm. The prior knowledge function is not incorporated in the algorithm with the aid of a default model, like in the MEM method.
The Stochastic Optimization Method (SOM), conceived by A. S. Mishchenko *et al.* [351], is a remarkable example of SSM. The SOM distinguishes among other SSMs because the average (12.24) is computed without the assumption (12.25) that $P(\mathbf{S}'|\mathbf{F})$ is a Gibbs distribution. The average (12.24) is made over a set of particular solutions, each fitting the input data $\mathbf{F}$ sufficiently well, in a sense precised later. The salient features of the SOM algorithm are summarized below, following [337] and considering only the application of the SOM method to the inversion of the Laplace transform:

1. given the QMC data $\{\overline{F}_i\}_{i=1}^{N_\tau}$, with statistical uncertainties $\{\sigma_i\}_{i=1}^{N_\tau}$, the quality of a trial solution $S(\omega)$ is quantified by the deviation measure:

$$D(S) = \sum_{i=1}^{N_\tau} \frac{|F_i - \overline{F}_i|}{\sigma_i} \tag{12.26}$$

   where:

$$F_i = \int_0^\infty d\omega\, e^{-\tau_i\omega} S(\omega) \tag{12.27}$$

   The deviation measure (12.26) induces an ordering relation in the set of trial solutions S: if $D(S) < D(S')$, S is a better approximation to $\mathbf{S}_{exact}(\omega)$ than S', given the QMC data $\overline{F}_i \pm \sigma_i$.

2. a trial solution $S(\omega)$ is parametrized as a sum:

$$S(\omega) = \sum_{i=1}^{K} R_i(\omega) = c_i\, 1_{[a_i,b_i]}(\omega) \tag{12.28}$$

   of rectangles R_i having basis $[a_i, b_i]$ and height c_i.

3. An initial configuration $C_1(0)$ of K rectangles is randomly generated. Concretely, $C_1(0) = \{a_1 b_1 c_1 \ldots a_K b_K c_K\}$, and the corresponding trial solution $S_{1,0}(\omega)$ is calculated using (12.28).

4. A suitable number F of global updates is performed [337]. A global update consists of a randomly chosen sequence of elementary updates, described in detail

in [351, 337]. A global update, which modifies the configuration according to $C_1(r) \to C_1(r+1)$, $r = 0 \dots F-1$, is accepted if $D(S_{1,r+1}) < D(S_{1,r})$.

5. A large number L of trial solutions $S_{i,r}(\omega)$, $i = 1 \dots L$ and of the corresponding deviations $D(S_{i,r})$ are accumulated, repeating steps 3,4. It has been argued [337] that an adequate way to regularize the solution (12.24) is to compute the average of the trial solutions whose deviation measure is $D(S_{i,r}) < 2 \min_i D(S_{i,r})$.

12.0.5 The GIFT method

The Genetic Inversion via Falsification of Theories (GIFT) method is a SSM devised by E. Vitali *et al.* [220]. Like other SSMs, given the infinite number of DSFs $S(\mathbf{q}, \omega)$ whose forward Laplace transform is compatible with the QMC estimation of $F(\mathbf{q}, \tau)$, the aim of GIFT is to collect a large collection of DSFs in order to perform the average (12.24) and thus discern the presence of common features (e.g. support, peak positions, intensities and widths). The idea underlying this procedure is that only such common features, shared by the majority of the DSFs compatible with the data, can be ascribed to the actual DSF of the system [349, 351, 352, 220].

However, in comparison to other SSMs, the GIFT method relies on a different treatment of the QMC data, and on a peculiar way to explore the domain of possible trial functions in order to perform the average (12.24).

Those differences stem from the guiding principle underlying the GIFT method, namely the falsification principle [353, 352]: rather than guiding us towards a specific solution $S(\mathbf{q}, \omega)$, as in the least-squares method, or defining a probability distribution $P(S'|F)$ to be sampled with the Metropolis algorithm, as in most SSMs, the QMC data should only be used to falsify trial solutions on the basis of their poor agreement.

Falsifying trial solutions requires not only compatibility with the QMC data $\overline{F}_i$ within the error bars σ_i, but also compatibility with any set $\overline{F}_i^*$ of data equivalent to $\overline{F}_i$. Sets $\overline{F}_i^*$ are not generated by independent QMC simulations, as that would be a rather demanding procedure. Instead, the covariance matrix C_{ij} of the QMC data is estimated, and the sets $\overline{F}_i^*$ are generated as:

$$\overline{F}^* = \overline{F} + \delta F \qquad \delta F \sim N(\mathbf{0}, C) \tag{12.29}$$

An independent GIFT calculation is performed for each realization of the random variable (12.29), and the results are finally averaged. This procedure proves useful, in particular, when the covariance matrix has relevant off-diagonal elements. The statistical uncertainties in the QMC data play a very peculiar role in the GIFT method, in contrast to other SSMs, where those quantities appear only in the definition of the probability (12.25) or of the deviation (12.26).

Given these elements, the GIFT algorithm relies on a *genetic algorithm* (GA) for exploring the space $\mathcal{S}$. GAs were introduced by J. Holland [354] as a class of algorithms which generate solutions to optimization and search problems using operations inspired by natural selection such as mutation, crossover and selection. Like typical GAs, the GIFT algorithm requires:

1. a space $\mathcal{S}$, encompassing a broad collection of efficiently parametrizable solutions

$S(\omega) \in \mathcal{S}$ consistent with any *a priori* knowledge about the DSF, e.g.

$$S(\omega) = c_0 \sum_{j=0}^{N_\omega} S_j \, \delta(\omega - \omega_j) \tag{12.30}$$

where the frequencies $\omega_j = \omega_{min} + (j-1)\,\delta\omega$ provide a mesh in the frequency domain, $\{S_j\}_{j=0}^{N_\omega}$ are natural numbers such that $\sum_{j=0}^{N_\omega} s_j = M$ for some $M \in \mathbb{N}$ and $c_0 \in \mathbb{R}$. The parametrization (12.30) permits us to easily incorporate prior information in the GIFT algorithm. In the case (12.1) of the inverse Laplace transform, such prior knowledge merely translates in the requirement that $S(\omega)$ is positive and that some of the frequency momenta:

$$\mathcal{M}_n = \int_0^\infty d\omega \, \omega^n \, S(\omega) \qquad\qquad n \in \mathbb{Z} \tag{12.31}$$

take exactly-known values. As far as the reconstruction of the dynamical structure factor $S(\mathbf{q},\omega)$ from the imaginary-time correlation function $F(\mathbf{q},\tau)$ of the density fluctuation operator is concerned, the most important frequency momenta are the 0-momentum:

$$\mathcal{M}_0 = \int d\omega \, S(\mathbf{q},\omega) = S(\mathbf{q}) \tag{12.32}$$

where $S(\mathbf{q})$ is the static structure factor, the 1-momentum:

$$\mathcal{M}_1 = \int d\omega \, \omega \, S(\mathbf{q},\omega) = \frac{\hbar^2 |\mathbf{q}|^2}{2m} \tag{12.33}$$

and the -1-momentum:

$$\mathcal{M}_{-1} = \int d\omega \, \frac{S(\mathbf{q},\omega)}{\omega} = -\frac{\pi\hbar\chi_{\mathbf{q}}}{\rho} \tag{12.34}$$

where $\chi_{\mathbf{q}}$ is the static density susceptivity. Equations (12.32), (12.33) and (12.34) are derived in detail in Section 12.0.6 and Appendix 10.3. Notice that, even though $S(\mathbf{q})$, $\chi_{\mathbf{q}}$ are not analytically known, they can be very accurately determined with QMC simulations.

The parametrization (12.30) brings into stage a discretization of the frequency domain, but it is sufficiently ductile as to reproduce a broad class of physically-relevant DSFs. It is not a crucial requisite for the correct functioning of the GIFT method, although the simple form of the trial solutions (12.30), and of its forward Laplace transform is of considerable importance for the performance of the algorithm. In particular, the possibility of parametrizing a spectrum with a string of positive integer numbers enables to design efficient operations for exploring the space $\mathcal{S}$.

2. a fitness function $\mathcal{F} : \mathcal{S} \to \mathbb{R}$ measuring the compatibility of a spectrum $S(\omega) \in \mathcal{S}$

with the QMC data, e.g.

$$\mathcal{F}(S) = \left(\sum_{i=0}^{N_\tau} \frac{\left| \overline{F}_i^* - c_0 \sum_{j=0}^{N_\omega} s_i \, e^{-\tau_i \omega_j} \right|^2}{\sigma_i^2} + \sum_n \alpha_n \left| \overline{\mathcal{M}}_n - \mathcal{M}_n(S) \right|^2 \right)^{-1} \tag{12.35}$$

The fitness $\mathcal{F}(S)$ is chosen so that better spectra have larger fitness. The second contribution to $\mathcal{F}(S)$ enforces exact or very accurate knowledge of a momentum $\overline{\mathcal{M}}_n$, and its relative importance is controlled by the parameter $\alpha_n > 0$. Notice that the momenta $\mathcal{M}_n(S)$ of a trial spectrum read:

$$\mathcal{M}_n(S) = c_0 \sum_{j=0}^{N_\omega} S_j \, \omega_j^n \tag{12.36}$$

The fitness evaluation is the most demanding operation of the GIFT method, requiring $\mathcal{O}(N_\omega N_\tau)$ operations per solution S.

Like a typical GA, the GIFT method starts from an initial randomly constructed collection of trial solutions $\{S_k^{(0)}(\omega)\}_{k=1}^{N_s}$, called *individuals*. Each trial solution has a set of properties or parameters, called *genes*, that can be mutated and altered. In the case of the GIFT method, the genes are the integer numbers s_i. The population is evolved toward better solutions using an iterative process, with the population $\{S_k^{(g)}(\omega)\}_{k=1}^{N_s}$ at each iteration $g = 0 \ldots N_g - 1$ called a *generation*. At each generation:

1. the fitness $\mathcal{F}_k = \mathcal{F}(S_k^{(g)})$ of every individual is evaluated [$\mathcal{O}(N_s \log(N_s) N_g)$ operations].

2. individuals are sorted in increasing fitness order [$\mathcal{O}(N_s \log(N_s))$].

3. the most fit individual of the current generation is propagated unaltered to the next generation. This strategy, called *elitism*, guarantees that the quality of the trial solutions does not decrease from one generation to the next.

4. pairs of individuals are selected from the current generation with probability:

$$p_{cross}(k) \propto \mathcal{F}_k^\alpha \quad , \qquad 0 < \alpha < 1 \tag{12.37}$$

   The two selected individuals are recombined in a crossover operation of the type illustrated in Figure 12.1. The crossover operation recombines the genes of the two selected individuals, producing two offsprings that are propagated to the new generation [$\mathcal{O}(N_\omega)$]. The crossover operation is a distinctive feature of GAs, and

5. each individual in the new generation is selected with probability p_{mut} for a mutation operation of the type illustrated in Figure 12.1.

6. the new generation of trial solutions is used in the next iteration of the algorithm.

The GIFT algorithm terminates when a given number N_g of generations has been produced. The individuals of the last generation are averaged to produce the GIFT estimate of the DSF: thanks to the average procedure, only those features present in the majority

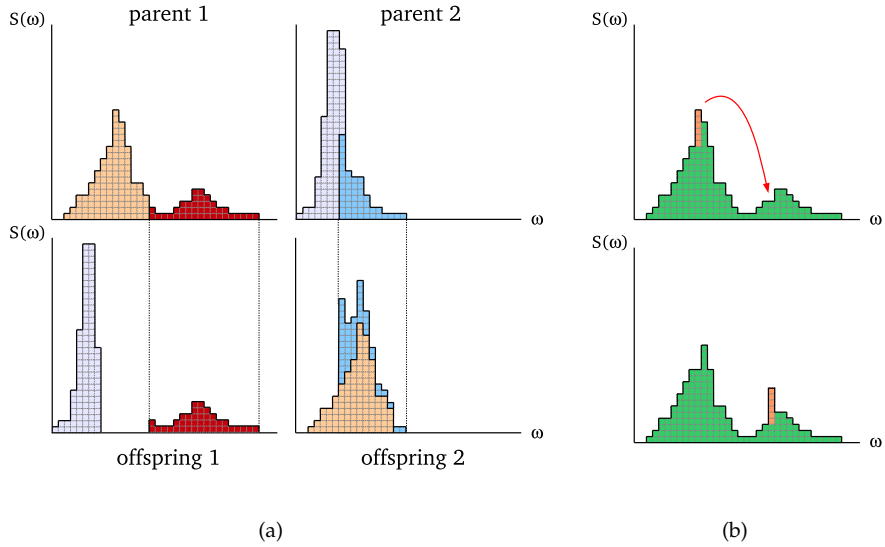

Figure 12.1: (a) Pictorial representation of the crossover operation. Upper row: a pair of spectra, called parents, are randomly chosen with probability (12.37). A fraction x of the spectral weight M is randomly chosen and the two parents are separated in a low-frequency part, called head, (orange and mauve regions) and in a high-frequency part, called tail (red and blue regions). The heads have spectral weights xM and $(1-x)M$ respectively. The separation point can occur between two adjacent frequencies ω_i, ω_{i+1} (left) or in the middle of a column (right). Lower row: two offsprings are produced summing the head of the first parent and the tail of the second parent (left), and summing the head of the second parent and the tail of the first parent. (b) Pictorial representation of the mutation operation. The mutation of a spectrum consists in choosing two frequencies j, j' and transferring d units of spectral weight (orange region) from one to another: $s'_j = s_j + d$, $s'_{j'} = s_{j'} - d$.

of the spectra $S_k^{(N_g)}(\omega)$ are preserved, the other undetermined features being averaged out.

The choice of a GA is motivated by their successful application to optimization problems with many degrees of freedom [355, 356], and by their efficient and straightforward parallelizability. GAs ensure an ergodic exploration of the vast space $\mathcal{S}$, and the choice of making several calculations with a large number of calculations limits the possibility that the algorithm converges towards local fitness maxima.

The GIFT method, described in more detail in [220, 222], has been applied to the study of liquid ^{4}He [220, 143], 3D hard spheres [222] and liquid ^{3}He [221], in all cases providing accurate reconstructions of DSFs.

12.0.6 Sum rules for imaginary-time density-density correlations

As far as the reconstruction of the dynamical structure factor $S(\mathbf{q}, \omega)$ from the imaginary-time correlation function $F(\mathbf{q}, \tau)$ of the density fluctuation operator is concerned, some the most important frequency momenta can be determined with QMC calculations of

static properties. The 0-momentum:

$$\mathcal{M}_0 = \int d\omega \, S(\mathbf{q}, \omega) \tag{12.38}$$

is clearly equal to the static structure factor. Indeed, for $\mathbf{q} \neq \mathbf{0}$:

$$\mathcal{M}_0 = \int d\omega \int dt \, \frac{e^{i\omega t}}{2\pi N} \langle \Phi_0 | \hat{\rho}_{\mathbf{q}}(t) \hat{\rho}_{-\mathbf{q}} | \Phi_0 \rangle = \int dt \, \frac{\delta(t)}{N} \langle \Phi_0 | \hat{\rho}_{\mathbf{q}}(t) \hat{\rho}_{-\mathbf{q}} | \Phi_0 \rangle = S(\mathbf{q}) \tag{12.39}$$

Notice that, even though the static structure factor is not analytically known, it can be very accurately determined with QMC calculations. The 1-momentum is amenable of an exact analytic expression, called f-sum rule or continuity sum rule:

$$\mathcal{M}_1 = \int d\omega \, \omega \, S(\mathbf{q}, \omega) = \frac{\hbar^2 |\mathbf{q}|^2}{2m} \tag{12.40}$$

Indeed, we have:

$$\begin{aligned} &\mathcal{M}_1 = \partial_\tau F(\mathbf{q}, 0) = \frac{1}{N} \langle \Phi_0 | [\hat{H}, \hat{\rho}_{\mathbf{q}}] \hat{\rho}_{-\mathbf{q}} | \Phi_0 \rangle = \\ =& \frac{\langle \Phi_0 | [\hat{H}, \hat{\rho}_{\mathbf{q}}] \hat{\rho}_{-\mathbf{q}} | \Phi_0 \rangle + \langle \Phi_0 | [\hat{H}, \hat{\rho}_{-\mathbf{q}}] \hat{\rho}_{\mathbf{q}} | \Phi_0 \rangle^*}{2N} = \frac{\langle \Phi_0 | [[\hat{H}, \hat{\rho}_{\mathbf{q}}], \hat{\rho}_{-\mathbf{q}}] | \Phi_0 \rangle}{2N} \end{aligned} \tag{12.41}$$

Since $[\hat{\rho}_{\mathbf{q}}, \hat{\rho}_{\mathbf{q}'}] = 0$, and the interaction Hamiltonian is $\hat{V} = \frac{1}{2\Omega} \sum_{\mathbf{q}} V_{\mathbf{q}} \hat{\rho}_{\mathbf{q}} \hat{\rho}_{-\mathbf{q}}$ we obtain:

$$\mathcal{M}_1 = \frac{\langle \Phi_0 | [[\hat{T}, \hat{\rho}_{\mathbf{q}}], \hat{\rho}_{-\mathbf{q}}] | \Phi_0 \rangle}{2N} \tag{12.42}$$

Since, for a system with only one type of particles:

$$\begin{aligned} -\frac{2m}{\hbar^2} [\hat{T}, \hat{\rho}_{\mathbf{q}}] \Psi(\mathcal{R}) &= \sum_{i=1}^{N} \triangle_i (\rho_{\mathbf{q}}(\mathcal{R}) \Psi(\mathcal{R})) - \rho_{\mathbf{q}}(\mathcal{R}) \triangle_i \Psi(\mathcal{R}) = \\ &= \sum_{i=1}^{N} \triangle_i (\rho_{\mathbf{q}}(\mathcal{R})) \Psi(\mathcal{R}) + 2 \nabla_i \rho_{\mathbf{q}}(\mathcal{R}) \cdot \nabla_i \Psi(\mathcal{R}) = \\ &= 2i\mathbf{q} \cdot \sum_{i=1}^{N} e^{i\mathbf{q}\cdot\mathbf{r}_i} \nabla_i \Psi(\mathcal{R}) - |\mathbf{q}|^2 \rho_{\mathbf{q}}(\mathcal{R}) \Psi(\mathcal{R}) \end{aligned} \tag{12.43}$$

we readily find:

$$-\frac{2m}{\hbar^2} [[\hat{T}, \hat{\rho}_{\mathbf{q}}], \hat{\rho}_{-\mathbf{q}}] = 2i\mathbf{q} \cdot \sum_{i=1}^{N} e^{i\mathbf{q}\cdot\mathbf{r}_i} \nabla_i (\rho_{-\mathbf{q}}(\mathcal{R}) \Psi(\mathcal{R})) - \rho_{-\mathbf{q}}(\mathcal{R}) e^{i\mathbf{q}\cdot\mathbf{r}_i} \nabla_i \Psi(\mathcal{R}) = 2|\mathbf{q}|^2 N \Psi(\mathcal{R}) \tag{12.44}$$

whence (12.33) immediately follows.

CHAPTER 13

Details of AFQMC calculations for electronic systems

In the present Appendix, some details about AFQMC calculations are given, in order to enhance the clarity and reproducibility of the calculations of Chapters 6, 7. The Ewald summation technique for the Coulomb potential in 2D is reviewed in Section 13.1. Statistical data analysis of AFQMC data is presented in Section (13.2)*, numeric stabilization techniques based on the Gram-Schmidt orthogonalization and on the Tikhonoff regularization are described in Sections 13.4.2, 13.4 and the RPA for finite systems by K. Sawada, with which results of Chapter 7 are compared, is presented in Section* (13.5)*.*

13.1 Ewald summation

13.1.1 Periodic boundary conditions

Many computational tasks require a finite simulation domain $\mathcal{D}$. For instance, the simulation of a homogeneous, and therefore indefinite, system must necessarily be carried out in a finite simulation domain. For this purpose it is necessary to specify the borders of the simulation domain and to define the behavior of particles at the borders, i.e. to impose a suitable system of boundary conditions (BC). The most popular BCs are the reflective boundary conditions (RBC) and the periodic boundary conditions. In typical simulations of homogeneous systems, $\mathcal{D}$ is a d-dimensional cube of side L. A homogeneous system at density ρ is then approximated with a system of N particles inside a cube of volume $\Omega = L^d = \frac{N}{\rho}$, and the thermodynamic limit is approached simulating systems of increasing size N and extrapolating the results of those simulations to the $N \to \infty$ limit.
In presence of reflecting boundary conditions, a particle colliding with the border $\partial\mathcal{D}$ of the simulation domain is reflected from it back into $\mathcal{D}$. Obviously, such a collision conserves the total energy of the system. The RBC translate in the requirement that $\Psi(\mathbf{r}) = 0$ for all points of $\mathbf{r}$ of $\partial\mathcal{D}$.
PBC provide an alternative way to treat particles in the vicinity of the border of the simulation domain. In contrast to the RBC, PBC move a particle approaching a boundary of the simulation domain to the opposite side, as illustrated in Figure 13.1. PBC effectively replicate the simulation box in all directions and remove the effects of the surface, which any finite sample of matter must have and that one encounters in RBC.
The superiority of PBC is best understood considering an ideal 1D gas. The spectrum of the system in RBC is readily fonud solving the time-independent Schrödinger equation:

$$-\frac{\hbar^2}{2m}\psi''(r) = \frac{\hbar^2 k^2}{2m}\psi(r) \tag{13.1}$$

with the constraint $\psi(0) = \psi(L) = 0$, giving $\psi(r) \propto \sin(kr)$ with $k = \frac{\pi}{L}\, n$ and $n \in \mathbb{N}$. The ground-state energy per particle of an ideal gas of N particles is then:

$$\mathcal{E}_N(Bose, RBC) = \frac{\hbar^2(\pi\rho)^2}{2m}\frac{1}{N^3} \qquad \mathcal{E}_N(Fermi, RBC) = \frac{\hbar^2(\pi\rho)^2}{2m}\frac{(N+1)(2N+1)}{6N^2} \tag{13.2}$$

The spectrum of the system in PBC is found solving (13.1) with the constraint $\psi(0) = \psi(L)$, giving $\psi(r) \propto e^{ikr}$ with $k = \frac{2\pi}{L}\, n$. In such case:

$$\mathcal{E}_N(Bose, PBC) = 0 \qquad \mathcal{E}_N(Fermi, PBC) = \frac{\hbar^2(\pi\rho)^2}{2m}\frac{(N+1)(N-1)}{3N^3} \tag{13.3}$$

Comparison between (13.2), (13.3) reveals that PBC approaches the thermodynamic limit much faster than RBC, thanks to the removal of surface effects.

Under PBC, translational invariance is preserved and it is possible to define the linear momentum observable as the hermitian operator $\hat{\mathbf{p}} = -i\hbar\partial_{\mathbf{r}}$ [357]. For a spin-s particle, the joint eigenfunctions of the momentum operator and of the spin operator $\hat{\mathbf{S}}$ along an arbitrary spatial direction are the following spin-definite plane waves:

$$\langle \mathbf{r}\omega|\mathbf{k}\sigma\rangle = \chi_\sigma(\omega)\,\frac{e^{i\mathbf{k}\cdot\mathbf{r}}}{\sqrt{\Omega}} \qquad \frac{L}{2\pi}\,\mathbf{k} \in \mathbb{Z}^d \quad , \qquad \sigma = -s \ldots s \tag{13.4}$$

PBC, however, also introduce correlational artifacts due to the unphysical topology of the simulation domain. For instance, In a small simulation domain, a particle might interact with its own image in a neighboring domain, and the wavelength of collective excitations is limited by the size of the domain.

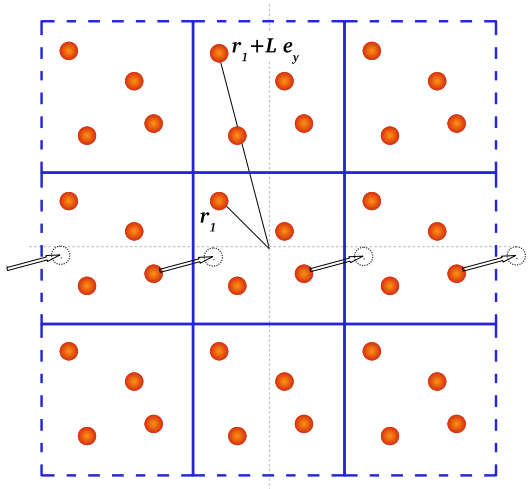

Figure 13.1: Pictorial representation of PBC. The positions of the particles in the central box are replicated $\mathbf{r} \to \mathbf{r} + (n_x\mathbf{e}_x + n_y\mathbf{e}_y)\, L$. The plane $\mathbb{R}^2$ is tiled with replicas of the central box. When a particle in the central box is translated, also the positions of all its copies are shifted by the same amount. If the particle crosses the boundary of the central box, it is thus substituted by one of its copies.

13.1.2 Ewald summation for the Coulomb potential in 2D

The Ewald summation is a method for computing long-range interaction in periodic systems [287]. It was first developed as a method for calculating electrostatic energies of ionic crystals, and it is commonly used in conjunction with PBC for calculating long-range interactions in computational chemistry. The Ewald summation writes the interaction potential as the sum of two terms:

$$V(\mathbf{r}) = V_{sr}(\mathbf{r}) + V_{lr}(\mathbf{r}) \tag{13.5}$$

where the term $V_{sr}(\mathbf{r})$ decays rapidly in real space, and the term $V_{lr}(\mathbf{r})$ decays rapidly in Fourier space.
In order to compute the Ewald summation for the Coulomb potential in 2D, we follow the approach of [358, 359]. We consider a system of N particles with charges $q_1 \dots q_N$ inside a square simulation cell of side L with PBC: the whole plane $\mathbb{R}^2$ is tiled with identical copies of the simulation cell, each of them shifted by a vector $L\mathbf{n}$ with $\mathbf{n} \in \mathbb{Z}^2$. The potential energy of such system is:

$$V(\mathbf{r}_1 \dots \mathbf{r}_N) = \frac{1}{2} {\sum_{\mathbf{n}\in\mathbb{Z}^2}}' \sum_{i,j=1}^{N} \frac{q_i q_j}{|\mathbf{r}_i - \mathbf{r}_j + L\mathbf{n}|} = \frac{1}{2} {\sum_{\mathbf{n}\in\mathbb{Z}^2}}' \sum_{i,j=1}^{N} \frac{q_i q_j}{L} \phi(\mathbf{x}_i - \mathbf{x}_j + \mathbf{n}) \tag{13.6}$$

where $\mathbf{r}_1 \dots \mathbf{r}_N$ are the positions of the N particles inside the simulation cell, $\mathbf{x}_i = \frac{\mathbf{r}_i}{L}$ are the positions of the N particles in units of L, $\phi(\mathbf{r}) = \frac{1}{|\mathbf{r}|}$ is the Coulomb potential and the prime over the first sum means that the summation over $\mathbf{n}$ must be done omitting the term $\mathbf{n} = \mathbf{0}$ when $i = j$.
The potential energy (13.6) results from a sum of contributions due to the interaction of particles inside the same simulation cell and to the interaction of particles inside different simulation cells.
It will be shown that there exist a constant ξ and an effective interparticle potential ϕ_{eff} such that the potential energy $V(\mathbf{r}_1 \dots \mathbf{r}_N)$ is given by:

$$V(\mathbf{r}_1 \dots \mathbf{r}_N) = \frac{1}{2} \sum_{i\neq j=1}^{N} q_i q_j \, \phi_{eff}(\mathbf{x}_i - \mathbf{x}_j) + \frac{\xi}{2} \sum_{i=0}^{N} q_i^2 \tag{13.7}$$

Proving (13.7) is not straightforward, because the series in (13.6) is conditionally convergent [99]. Let us therefore first replace the Coulomb potential with the screened Coulomb potential:

$$\phi_s(\mathbf{x}) = \frac{e^{-s|\mathbf{x}|^2}}{|\mathbf{x}|} \tag{13.8}$$

The potential energy (13.6) is therefore the $s \to 0$ limit of:

$$V_s(\mathbf{r}_1 \dots \mathbf{r}_N) = \frac{1}{2} {\sum_{\mathbf{n}\in\mathbb{Z}^2}}' \sum_{i,j=1}^{N} \frac{q_i q_j}{L} \phi_s(\mathbf{x}_i - \mathbf{x}_j + \mathbf{n}) \tag{13.9}$$

the series (13.9) is absolutely convergent, and can be split in two terms:

$$V_s(\mathbf{r}_1 \dots \mathbf{r}_N) = \frac{1}{2} \sum_{\mathbf{n}} \sum_{i\neq j=1}^{N} \frac{q_i q_j}{L} \phi_s(\mathbf{x}_i - \mathbf{x}_j + \mathbf{n}) + \frac{1}{2} \sum_{\mathbf{n}\neq\mathbf{0}} \sum_{i=1}^{N} \frac{q_i^2}{L} \phi_s(\mathbf{n}) \tag{13.10}$$

the first one representing interaction of the charge q_i with the other $N-1$ particles in the same cell and with the copies of those $N-1$ particles in all the other cells, and the second one representing the interaction of the charge q_i with its own copies. One can write (13.10) as:

$$V_s\left(\mathbf{r}_1 \dots \mathbf{r}_N\right) = \frac{1}{2}\sum_{i\neq j=1}^{N} \frac{q_i q_j}{L}\Phi_s(\mathbf{x}_i - \mathbf{x}_j) + \frac{\xi_s}{2}\sum_{i=1}^{N}\frac{q_i^2}{L} \tag{13.11}$$

having defined the functions Φ_s and ξ_s through:

$$\begin{aligned} \Phi_s\left(\mathbf{x}\right) &= \sum_{\mathbf{n}} \phi_s(\mathbf{x}+\mathbf{n}) = \sum_{\mathbf{n}} \frac{e^{-s|\mathbf{x}+\mathbf{n}|^2}}{|\mathbf{x}+\mathbf{n}|} \\ \xi_s &= \sum_{\mathbf{n}\neq\mathbf{0}} \phi_s(\mathbf{n}) = \sum_{\mathbf{n}\neq\mathbf{0}} \frac{e^{-s|\mathbf{n}|^2}}{|\mathbf{n}|} \end{aligned} \tag{13.12}$$

Notice that the series defining (13.12) do not converge as s tends to 0. To rewrite them in a form showing the cause of that divergence, we use the fact that:

$$\int_0^\infty t^{s-1}e^{-tx^2}dt = \int_0^\infty \left[\frac{t'}{x^2}\right]^{s-1} e^{-t'}\frac{dt'}{x^2} = \frac{\Gamma(s)}{x^{2s}} \tag{13.13}$$

where $\Gamma(s)$ is Euler's complete gamma function. Putting $s=\frac{1}{2}$ in (13.13) we find:

$$\int_0^\infty \frac{dt}{\sqrt{t}}\, e^{-tx^2} = \frac{\Gamma\left(\frac{1}{2}\right)}{x} = \frac{\sqrt{\pi}}{x} \quad \rightarrow \quad \frac{1}{x} = \int_0^\infty \frac{dt}{\sqrt{t\pi}}\, e^{-tx^2}dt \tag{13.14}$$

in the light of which:

$$\Phi_s\left(\mathbf{x}\right) = \sum_{\mathbf{n}} \frac{e^{-s|\mathbf{x}+\mathbf{n}|^2}}{|\mathbf{x}+\mathbf{n}|} = \sum_{\mathbf{n}} e^{-s|\mathbf{x}+\mathbf{n}|^2}\int_0^\infty \frac{dt}{\sqrt{t\pi}}\, e^{-t|\mathbf{x}+\mathbf{n}|^2}dt = \int_0^\infty \frac{dt}{\sqrt{t\pi}}\sum_{\mathbf{n}} e^{-(t+s)|\mathbf{x}+\mathbf{n}|^2} \tag{13.15}$$

the convergence factor $e^{-s|\mathbf{x}+\mathbf{n}|^2}$ allows to swap the integral and the sum over $\mathbf{n}$ in the last passage. The series $\Phi_s\left(\mathbf{x}\right)$ and the integral in (13.15) diverge as s approaches 0. We expect that the divergence of (13.15) is related to the behavior of the integrand at small t, and thus we perform the splitting:

$$\begin{aligned} \Phi_s\left(\mathbf{x}\right) &= \int_0^\infty \frac{dt}{\sqrt{t\pi}}\sum_{\mathbf{n}} e^{-(t+s)|\mathbf{x}+\mathbf{n}|^2} = \\ &= \int_0^{\alpha^2} \frac{dt}{\sqrt{t\pi}}\sum_{\mathbf{n}} e^{-(t+s)|\mathbf{x}+\mathbf{n}|^2} + \int_{\alpha^2}^\infty \frac{dt}{\sqrt{t\pi}}\sum_{\mathbf{n}} e^{-(t+s)|\mathbf{x}+\mathbf{n}|^2} = \Phi_s^{[0,\alpha^2]}\left(\mathbf{x}\right) + \Phi_s^{[\alpha^2,\infty)}\left(\mathbf{x}\right) \end{aligned} \tag{13.16}$$

with $\alpha \in (0,\infty)$ arbitrary. Both $\Phi_s^{[0,\alpha^2]}\left(\mathbf{x}\right)$ and $\Phi_s^{[\alpha^2,\infty)}\left(\mathbf{x}\right)$ have an explicit analytic form.

In particular:

$$\begin{aligned}\Phi_s^{[\alpha^2,\infty)}(\mathbf{x}) &= \int_{\alpha^2}^{\infty}\frac{dt}{\sqrt{t\pi}}\sum_{\mathbf{n}}e^{-(t+s)|\mathbf{x}+\mathbf{n}|^2} = \frac{1}{\sqrt{\pi}}\sum_{\mathbf{n}}e^{-s|\mathbf{x}+\mathbf{n}|^2}\int_{\alpha^2}^{\infty}\frac{dt}{\sqrt{t\pi}}e^{-t|\mathbf{x}+\mathbf{n}|^2} = \\ &= \frac{1}{\sqrt{\pi}}\sum_{\mathbf{n}}e^{-s|\mathbf{x}+\mathbf{n}|^2}\int_{\alpha^2|\mathbf{x}+\mathbf{n}|^2}^{\infty}\left[\frac{t'}{|\mathbf{x}+\mathbf{n}|^2}\right]^{-\frac{1}{2}}e^{-t'}\frac{dt'}{|\mathbf{x}+\mathbf{n}|^2} = \\ &= \sum_{\mathbf{n}}\frac{e^{-s|\mathbf{x}+\mathbf{n}|^2}}{|\mathbf{x}+\mathbf{n}|}\,\frac{\Gamma\left(\frac{1}{2},\alpha^2|\mathbf{x}+\mathbf{n}|^2\right)}{\sqrt{\pi}} = \sum_{\mathbf{n}}\frac{e^{-s|\mathbf{x}+\mathbf{n}|^2}}{|\mathbf{x}+\mathbf{n}|}\,\mathrm{erfc}\left(\alpha|\mathbf{x}+\mathbf{n}|\right)\end{aligned} \tag{13.17}$$

thanks to the relation between incomplete Gamma and complementary error function. $\Phi_s^{[\alpha^2,\infty)}(\mathbf{x})$ is the sum of an absolutely and uniformly convergent series, hence:

$$\lim_{s\to 0^+}\Phi_s^{[\alpha^2,\infty)}(\mathbf{x}) = \sum_{\mathbf{n}}\frac{\mathrm{erfc}\left(\alpha|\mathbf{x}+\mathbf{n}|\right)}{|\mathbf{x}+\mathbf{n}|} \tag{13.18}$$

On the other hand:

$$\begin{aligned}\Phi_s^{[0,\alpha^2]}(\mathbf{x}) &= \int_0^{\alpha^2}\frac{dt}{\sqrt{t\pi}}\sum_{\mathbf{n}}e^{-(t+s)|\mathbf{x}+\mathbf{n}|^2} = \sum_{\mathbf{n}}e^{i2\pi\mathbf{n}\cdot\mathbf{x}}\int_0^{\alpha^2}\frac{dt}{\sqrt{t\pi}}e^{-\frac{\pi^2}{s+t}|\mathbf{n}|^2} = \\ &= \sqrt{\pi}\int_0^{\alpha^2}\frac{t^{-\frac{1}{2}}}{s+t} + \sqrt{\pi}\sum_{\mathbf{n}\neq\mathbf{0}}e^{i2\pi\mathbf{n}\cdot\mathbf{x}}\int_0^{\alpha^2}\frac{t^{-\frac{1}{2}}}{s+t}e^{-\frac{\pi^2}{s+t}|\mathbf{n}|^2}\end{aligned} \tag{13.19}$$

having applied Poisson's summation formula in the second passage and separated the contributions from $\mathbf{n}=\mathbf{0}$ and $\mathbf{n}\neq\mathbf{0}$. The first integral appearing in the last passage of (13.19) reads:

$$\int_0^{\alpha^2}\frac{t^{-\frac{1}{2}}}{s+t}dt = \int_0^{\frac{\alpha}{\sqrt{s}}}\frac{2\sqrt{s}}{su^2+s}du = \frac{2}{\sqrt{s}}\,\mathrm{arctg}\left[\frac{\alpha}{\sqrt{s}}\right] = \frac{\pi}{\sqrt{s}} - \frac{2}{\alpha} + \mathcal{O}(\sqrt{s}) \tag{13.20}$$

The second integral cannot be evaluated analytically, but the hypotheses of Lebesgue's dominated convergence theorem are satisfied by the sequence $\frac{t^{-\frac{1}{2}}}{s+t}e^{-\frac{\pi^2}{s+t}|\mathbf{n}|^2}$ and:

$$\begin{aligned}&\lim_{s\to 0^+}\int_0^{\alpha^2}\frac{t^{-\frac{1}{2}}}{s+t}e^{-\frac{\pi^2}{s+t}|\mathbf{n}|^2} = \int_0^{\alpha^2}\lim_{s\to 0^+}\frac{t^{-\frac{1}{2}}}{s+t}e^{-\frac{\pi^2}{s+t}|\mathbf{n}|^2} = \int_0^{\alpha^2}t^{-\frac{3}{2}}e^{-\frac{\pi^2}{t}|\mathbf{n}|^2} = \\ &= \frac{1}{\pi|\mathbf{n}|}\int_{\frac{\pi^2|\mathbf{n}|^2}{\alpha^2}}^{\infty}u^{-\frac{1}{2}}e^{-u} = \frac{1}{\pi|\mathbf{n}|}\Gamma\left(\frac{1}{2},\frac{\pi^2|\mathbf{n}|^2}{\alpha^2}\right) = \frac{\sqrt{\pi}}{\pi|\mathbf{n}|}\mathrm{erfc}\left(\frac{\pi|\mathbf{n}|}{\alpha}\right)\end{aligned} \tag{13.21}$$

Summing up (13.17), (13.19) and (13.20) we find the following expression:

$$\Phi_s(\mathbf{x}) = \frac{\pi^{\frac{3}{2}}}{\sqrt{s}} - \frac{2\sqrt{\pi}}{\alpha} + \sqrt{\pi}\sum_{\mathbf{n}\neq\mathbf{0}}e^{i2\pi\mathbf{n}\cdot\mathbf{x}}\int_0^{\alpha^2}\frac{t^{-\frac{1}{2}}}{s+t}e^{-\frac{\pi^2}{s+t}|\mathbf{n}|^2} + \sum_{\mathbf{n}}\frac{e^{-s|\mathbf{x}+\mathbf{n}|^2}}{|\mathbf{x}+\mathbf{n}|}\mathrm{erfc}\left(\alpha|\mathbf{x}+\mathbf{n}|\right) \tag{13.22}$$

up to $\mathcal{O}(\sqrt{s})$ terms, in which the cause of the $s\to 0^+$ divergence is made evident.
We now prove that also ξ_s diverges when $s\to 0^+$, the two singularities canceling each

other for a neutral system. With this in mind, let us explicitly evaluate ξ_s:

$$\xi_s = \sum_{\mathbf{n}\neq\mathbf{0}} \phi_s(\mathbf{n}) = \sum_{\mathbf{n}\neq\mathbf{0}} \frac{e^{-s|\mathbf{n}|^2}}{|\mathbf{n}|} = \sum_{\mathbf{n}\neq\mathbf{0}} e^{-s|\mathbf{n}|^2} \int_0^\infty \frac{dt}{\sqrt{t\pi}} e^{-t|\mathbf{n}|^2} dt \tag{13.23}$$

Splitting the integral as before:

$$\begin{aligned}
\xi_s &= \sum_{\mathbf{n}\neq\mathbf{0}} \int_0^{\alpha^2} \frac{dt}{\sqrt{t\pi}} e^{-(t+s)|\mathbf{n}|^2} + \sum_{\mathbf{n}\neq\mathbf{0}} \int_{\alpha^2}^\infty \frac{dt}{\sqrt{t\pi}} e^{-(t+s)|\mathbf{n}|^2} = \\
&= \sum_{\mathbf{n}} \int_0^{\alpha^2} \frac{dt}{\sqrt{t\pi}} e^{-(t+s)|\mathbf{n}|^2} dt - \int_0^{\alpha^2} \frac{dt}{\sqrt{t\pi}} + \sum_{\mathbf{n}\neq\mathbf{0}} \int_{\alpha^2}^\infty \frac{dt}{\sqrt{t\pi}} e^{-(t+s)|\mathbf{n}|^2} dt = \\
&= \int_0^{\alpha^2} \frac{dt}{\sqrt{t\pi}} \sum_{\mathbf{n}} e^{-(t+s)|\mathbf{n}|^2} - \frac{2\alpha}{\sqrt{\pi}} + \sum_{\mathbf{n}\neq\mathbf{0}} \int_{\alpha^2}^\infty \frac{dt}{\sqrt{t\pi}} e^{-(t+s)|\mathbf{n}|^2} dt
\end{aligned} \tag{13.24}$$

whence:

$$\xi_s = \frac{\pi^{\frac{3}{2}}}{\sqrt{s}} - \frac{2\sqrt{\pi}}{\alpha} - \frac{2\alpha}{\sqrt{\pi}} + \sqrt{\pi} \sum_{\mathbf{n}\neq\mathbf{0}} \int_0^{\alpha^2} \frac{t^{-\frac{1}{2}}}{s+t} e^{-\frac{\pi^2}{s+t}|\mathbf{n}|^2} + \sum_{\mathbf{n}\neq\mathbf{0}} \frac{e^{-s|\mathbf{n}|^2}}{|\mathbf{n}|} \mathrm{erfc}(\alpha|\mathbf{n}|) \tag{13.25}$$

up to terms of order $\mathcal{O}(\sqrt{s})$. Knowledge of (13.22) and (13.25) allows the calculation of the potential energy (13.9):

$$\begin{aligned}
2LV_s(\mathbf{x}_1 \dots \mathbf{x}_N) &= \sum_{i\neq j} q_i q_j \Phi_s(\mathbf{x}_{ij}) + \xi_s \sum_i q_i^2 = \left[\frac{\pi^{\frac{3}{2}}}{\sqrt{s}} - \frac{2\sqrt{\pi}}{\alpha}\right] \left[\sum_{i\neq j} q_i q_j - \sum_i q_i^2\right] + \\
&+ \sum_{i\neq j} q_i q_j \left[\sqrt{\pi} \sum_{\mathbf{n}\neq\mathbf{0}} e^{i2\pi\mathbf{n}\cdot\mathbf{x}_{ij}} \int_0^{\alpha^2} \frac{t^{-\frac{1}{2}}}{s+t} e^{-\frac{\pi^2}{s+t}|\mathbf{n}|^2} + \sum_{\mathbf{n}} \frac{e^{-s|\mathbf{x}_{ij}+\mathbf{n}|^2}}{|\mathbf{x}_{ij}+\mathbf{n}|} \mathrm{erfc}(\alpha|\mathbf{x}_{ij}+\mathbf{n}|)\right] + \\
&+ \sum_i q_i^2 \left[\sqrt{\pi} \sum_{\mathbf{n}\neq\mathbf{0}} \int_0^{\alpha^2} \frac{t^{-\frac{1}{2}}}{s+t} e^{-\frac{\pi^2}{s+t}|\mathbf{n}|^2} + \sum_{\mathbf{n}\neq\mathbf{0}} \frac{e^{-s|\mathbf{n}|^2}}{|\mathbf{n}|} \mathrm{erfc}(\alpha|\mathbf{n}|) - \frac{2\alpha}{\sqrt{\pi}}\right]
\end{aligned} \tag{13.26}$$

where $\mathbf{x}_{ij} = \mathbf{x}_i - \mathbf{x}_j$ for brevity. Since:

$$\sum_{i\neq j=1}^N q_i q_j = \sum_{i=1}^N q_i \left(\sum_{j=1}^N q_j - q_i\right) = \left[\sum_{i=1}^N q_i\right]^2 - \left(\sum_{i=1}^N q_i^2\right) \tag{13.27}$$

if the system is neutral:

$$\sum_{i\neq j=1}^N q_i q_j = -\left(\sum_{i=1}^N q_i^2\right) \tag{13.28}$$

and the singularities in Φ_s and ξ_s lead to singularities in V_s which cancel each other. It is

therefroe possible to take the limit of V_s for $s \to 0^+$:

$$2LV\left(\mathbf{x}_1 \dots \mathbf{x}_N\right) = \sum_{i \neq j} q_i q_j \left[\sum_{\mathbf{n} \neq \mathbf{0}} e^{i2\pi \mathbf{n}\cdot\mathbf{x}_{ij}} \frac{1}{|\mathbf{n}|} \mathrm{erfc}\left(\frac{\pi |\mathbf{n}|}{\alpha}\right) + \sum_{\mathbf{n}} \frac{\mathrm{erfc}\left(\alpha |\mathbf{x}_{ij} + \mathbf{n}|\right)}{|\mathbf{x}_{ij} + \mathbf{n}|} \right] + \\ + \sum_i q_i^2 \left[\sum_{\mathbf{n} \neq \mathbf{0}} \frac{1}{|\mathbf{n}|} \mathrm{erfc}\left(\frac{\pi |\mathbf{n}|}{\alpha}\right) + \sum_{\mathbf{n} \neq \mathbf{0}} \frac{\mathrm{erfc}(\alpha |\mathbf{n}|)}{|\mathbf{n}|} - \frac{2\alpha}{\sqrt{\pi}} \right] \tag{13.29}$$

which can be rewritten in the more compact and explicit form:

$$V\left(\mathbf{x}_1 \dots \mathbf{x}_N\right) = \frac{1}{2} \sum_{i \neq j} q_i q_j \phi_{eff}\left(\mathbf{x}_{ij}\right) + \frac{\xi}{2} \sum_i q_i^2 \tag{13.30}$$

where:

$$\phi_{eff}(\mathbf{x}) = \frac{1}{L} \left[\sum_{\mathbf{n} \neq \mathbf{0}} e^{i2\pi \mathbf{n}\cdot\mathbf{x}} \frac{1}{|\mathbf{n}|} \mathrm{erfc}\left(\frac{\pi |\mathbf{n}|}{\alpha}\right) + \sum_{\mathbf{n}} \frac{\mathrm{erfc}\left(\alpha |\mathbf{x} + \mathbf{n}|\right)}{|\mathbf{x} + \mathbf{n}|} + C \right] \tag{13.31a}$$

$$\xi = \frac{1}{L} \left[\sum_{\mathbf{n} \neq \mathbf{0}} \frac{1}{|\mathbf{n}|} \mathrm{erfc}\left(\frac{\pi |\mathbf{n}|}{\alpha}\right) + \sum_{\mathbf{n} \neq \mathbf{0}} \frac{\mathrm{erfc}(\alpha |\mathbf{n}|)}{|\mathbf{n}|} - \frac{2\alpha}{\sqrt{\pi}} + C \right] \tag{13.31b}$$

the constant C being, for now, arbitrary. Notice that ϕ_{eff} is a real-valued function. The constant C is chosen in such a way as to ensure that the integral of ϕ_{eff} over the simulation cell vanishes. Since:

$$\begin{aligned} &\frac{1}{L} \int_{\Omega_L} d^2 r \ \phi_{eff}\left(\frac{\mathbf{r}}{L}\right) = L \int_{\Omega_0} d^2 x \ \phi_{eff}(\mathbf{x}) = \\ &= \int_{\Omega_0} d^2 x \ \sum_{\mathbf{n} \neq \mathbf{0}} e^{i2\pi \mathbf{n}\cdot\mathbf{x}} \frac{1}{|\mathbf{n}|} \mathrm{erfc}\left(\frac{\pi |\mathbf{n}|}{\alpha}\right) + \int_{\Omega_0} d^2 x \ \sum_{\mathbf{n}} \frac{\mathrm{erfc}\left(\alpha |\mathbf{x} + \mathbf{n}|\right)}{|\mathbf{x} + \mathbf{n}|} + \int_{\Omega_0} d^2 x \ C = \\ &= \sum_{\mathbf{n}} \int_{\Omega_0} d^2 x \ \frac{\mathrm{erfc}\left(\alpha |\mathbf{x} + \mathbf{n}|\right)}{|\mathbf{x} + \mathbf{n}|} + C = \sum_{\mathbf{n}} \int_{\Omega_0 + \mathbf{n}} d^2 x \ \frac{\mathrm{erfc}\left(\alpha |\mathbf{x}|\right)}{|\mathbf{x}|} + C = \\ &= \int_{\mathbb{R}^2} d^2 x \ \frac{\mathrm{erfc}\left(\alpha |\mathbf{x}|\right)}{|\mathbf{x}|} + C = \int_0^{2\pi} d\phi \int_0^{\infty} dr \ \mathrm{erfc}(\alpha r) + C = \frac{2\sqrt{\pi}}{\alpha} + C \end{aligned} \tag{13.32}$$

where $\Omega_L + \mathbf{n}$ is the square cell of side L centered at $\mathbf{n} \in \mathbb{Z}^2$. The result is $C = -\frac{2\sqrt{\pi}}{\alpha}$. Since $\phi_{eff}\left(\frac{\mathbf{r}}{L}\right)$ is a periodic function, it can be written as sum of its Fourier series:

$$\phi_{eff}\left(\frac{\mathbf{r}}{L}\right) = \sum_{\mathbf{k}} \frac{e^{i\mathbf{k}\cdot\mathbf{r}}}{L^2} \ \tilde{\phi}_{eff}\left(\mathbf{k}\right) \tag{13.33a}$$

$$\tilde{\phi}_{eff}\left(\mathbf{k}\right) = \int_{\Omega_L} d^2 r \ e^{-i\mathbf{k}\cdot\mathbf{r}} \ \phi_{eff}\left(\frac{\mathbf{r}}{L}\right) = L^2 \int_{\Omega_1} d^2 x \ e^{-i2\pi \mathbf{m}\cdot\mathbf{x}} \ \phi_{eff}\left(\mathbf{x}\right) \tag{13.33b}$$

where $\mathbf{k} = \frac{2\pi}{L}\mathbf{m}$, with $\mathbf{m} \in \mathbb{Z}^2$, are the recyprocal lattice vectors. The constant C has

been chosen in such a way that $\tilde{\phi}_{eff}(\mathbf{0}) = 0$; for $\mathbf{k} \neq \mathbf{0}$:

$$
\begin{aligned}
& L \int_{\Omega_1} d^2x \; e^{-i2\pi\mathbf{m}\cdot\mathbf{x}} \; \phi_{eff}(\mathbf{x}) = \\
& = \int_{\Omega_1} d^2x \; e^{-i2\pi\mathbf{m}\cdot\mathbf{x}} \; \sum_{\mathbf{n}\neq\mathbf{0}} e^{i2\pi\mathbf{n}\cdot\mathbf{x}} \frac{1}{|\mathbf{n}|} \mathrm{erfc}\left(\frac{\pi|\mathbf{n}|}{\alpha}\right) + \int_{\Omega_1} d^2x \; e^{-i2\pi\mathbf{m}\cdot\mathbf{x}} \; \left[C + \sum_{\mathbf{n}} \frac{\mathrm{erfc}\left(\alpha|\mathbf{x}+\mathbf{n}|\right)}{|\mathbf{x}+\mathbf{n}|}\right] \\
& = \frac{1}{|\mathbf{m}|}\mathrm{erfc}\left(\frac{\pi|\mathbf{m}|}{\alpha}\right) + \sum_{\mathbf{n}} \int_{\Omega_1} d^2x \; e^{-i2\pi\mathbf{m}\cdot\mathbf{x}} \; \frac{\mathrm{erfc}\left(\alpha|\mathbf{x}+\mathbf{n}|\right)}{|\mathbf{x}+\mathbf{n}|} = \\
& = \frac{2\pi}{L|\mathbf{k}|}\mathrm{erfc}\left(\frac{L|\mathbf{k}|}{2\alpha}\right) + \sum_{\mathbf{n}} \int_{\Omega_1+\mathbf{n}} d^2x \; e^{-i2\pi\mathbf{m}\cdot\mathbf{x}} \; \frac{\mathrm{erfc}\left(\alpha|\mathbf{x}|\right)}{|\mathbf{x}|} = \\
& = \frac{2\pi}{L|\mathbf{k}|}\mathrm{erfc}\left(\frac{L|\mathbf{k}|}{2\alpha}\right) + \int_{\mathbb{R}^2} d^2x \; e^{-i2\pi\mathbf{m}\cdot\mathbf{x}} \; \frac{\mathrm{erfc}\left(\alpha|\mathbf{x}|\right)}{|\mathbf{x}|} = \\
& = \frac{2\pi}{L|\mathbf{k}|}\mathrm{erfc}\left(\frac{L|\mathbf{k}|}{2\alpha}\right) + \int_0^{2\pi} d\phi \int_0^{\infty} dr \; \mathrm{erfc}(\alpha r) e^{-iL|\mathbf{k}|r\cos(\phi)} = \\
& = \frac{2\pi}{L|\mathbf{k}|}\mathrm{erfc}\left(\frac{L|\mathbf{k}|}{2\alpha}\right) + \frac{2\pi}{\alpha}\int_0^{\infty} \mathrm{erfc}(x) J_0\left(\frac{L|\mathbf{k}|x}{\alpha}\right) = \\
& = \frac{2\pi}{L|\mathbf{k}|}\mathrm{erfc}\left(\frac{L|\mathbf{k}|}{2\alpha}\right) + \frac{2\pi}{L|\mathbf{k}|}\mathrm{erf}\left(\frac{L|\mathbf{k}|}{2\alpha}\right) = \frac{2\pi}{L|\mathbf{k}|}
\end{aligned}
\tag{13.34}
$$

Therefore:

$$
\tilde{\phi}_{eff}(\mathbf{k}) = \frac{2\pi(1-\delta_{\mathbf{k},\mathbf{0}})}{|\mathbf{k}|} \tag{13.35}
$$

independent, as expected, of α.

The 2D homogeneous electron gas (HEG) is a system of electrons interacting with a uniform, positively-charged background. It can be described within the formalism of Ewald summations: let us suppose to put in the simulation cell N_- particles with negative charge $-e$ and $N_+ = N - N_-$ particles with positive charge $e\frac{N_-}{N_+}$, in such a way as to have a neutral system. Labeling the particles with an index i such that without loss of generality the first N_- charges are negatively charged and the remaining N_+ particles are positively charged, one finds that the potential energy (13.30) of the system is:

$$
\begin{aligned}
V(\mathbf{x}_1 \ldots \mathbf{x}_N) = & \frac{1}{2}\sum_{i\neq j=1}^{N_-} e^2 \phi_{eff}(\mathbf{x}_i - \mathbf{x}_j) + \sum_{i=1}^{N_-}\sum_{j=N_-+1}^{N} (-e)\left(e\frac{N_-}{N_+}\right)\phi_{eff}(\mathbf{x}_i - \mathbf{x}_j) + \\
& + \frac{1}{2}\sum_{i\neq j=N_-+1}^{N} \left(e\frac{N_-}{N_+}\right)^2 \phi_{eff}(\mathbf{x}_i - \mathbf{x}_j) + \frac{1}{2}\left[N_- e^2 + \frac{N_-^2}{N_+}e^2\right]\xi
\end{aligned}
\tag{13.36}
$$

(13.36) is the sum of four contributions. The first three contributions come from the interaction among negative charges, negative and positive charges, positive charges. The fourth one is proportional to $\sum_i q_i^2 = N_- e^2 + \frac{N_-^2}{N_+}e^2$. The potential energy of the 2D HEG

is obtained taking the $N_+ \to \infty$ limit of (13.36):

$$V\left(\mathbf{x}_1 \dots \mathbf{x}_{N_-}\right) = \frac{1}{2}\sum_{i\neq j=1}^{N_-} e^2\phi_{eff}\left(\mathbf{x}_i - \mathbf{x}_j\right) + \frac{1}{2}N_- e^2\xi \tag{13.37}$$

The second-quantization equivalent of (13.37) is the Hamiltonian:

$$\begin{aligned}\hat{H} = &\sum_{\mathbf{k},\sigma}\frac{\hbar^2|\mathbf{k}|^2}{2m}\,\hat{a}^\dagger_{\mathbf{k},\sigma}\hat{a}_{\mathbf{k},\sigma} + \frac{e^2}{2}\,\xi\,\hat{N} + \\ &+\frac{e^2}{2}\sum_{\mathbf{k}_1,\mathbf{k}_2,\mathbf{k}_3,\mathbf{k}_4}\sum_{\sigma_1,\sigma_2,\sigma_3,\sigma_4}\langle\mathbf{k}_1\sigma_1,\mathbf{k}_2\sigma_2|\hat{\phi}_{eff}|\mathbf{k}_3\sigma_3,\mathbf{k}_4\sigma_4\rangle\,\hat{a}^\dagger_{\mathbf{k}_1,\sigma_1}\hat{a}^\dagger_{\mathbf{k}_2,\sigma_2}\hat{a}_{\mathbf{k}_4,\sigma_4}\hat{a}_{\mathbf{k}_3,\sigma_3}\end{aligned} \tag{13.38}$$

where:

$$\langle\mathbf{k}_1\sigma_1,\mathbf{k}_2\sigma_2|\hat{\phi}|\mathbf{k}_3\sigma_3,\mathbf{k}_4\sigma_4\rangle = \delta_{\sigma_1\sigma_3}\delta_{\sigma_2\sigma_4}\int_{\Omega_L}d^2x_1\int_{\Omega_L}d^2x_2\frac{e^{-i(\mathbf{k}_1-\mathbf{k}_3)\cdot\mathbf{x}_1}}{L^2}\frac{e^{-i(\mathbf{k}_2-\mathbf{k}_4)\cdot\mathbf{x}_2}}{L^2}\phi_{eff}(\mathbf{x}_1-\mathbf{x}_2) \tag{13.39}$$

recalling $\phi_{eff}(\mathbf{r}) = \sum_{\mathbf{q}}\tilde{\phi}_{eff}(\mathbf{q})\,\frac{e^{i\mathbf{q}\cdot\mathbf{x}}}{L^2}$ we are left with:

$$\langle\mathbf{k}_1\sigma_1,\mathbf{k}_2\sigma_2|\hat{\phi}|\mathbf{k}_3\sigma_3,\mathbf{k}_4\sigma_4\rangle = \frac{1}{L^2}\,\delta_{\sigma_1\sigma_3}\delta_{\sigma_2\sigma_4}\,\tilde{\phi}_{eff}(\mathbf{k}_4-\mathbf{k}_2)\,\delta_{\mathbf{k}_3-\mathbf{k}_1,\mathbf{k}_2-\mathbf{k}_4} \tag{13.40}$$

and:

$$\hat{H} = \sum_{\mathbf{k},\sigma}\frac{\hbar^2|\mathbf{k}|^2}{2m}\,\hat{a}^\dagger_{\mathbf{k},\sigma}\hat{a}_{\mathbf{k},\sigma} + \frac{\xi N e^2}{2} + \frac{e^2}{2L^2}\sum_{\mathbf{q}}\sum_{\mathbf{k},\mathbf{p}}\sum_{\sigma,\sigma'}\tilde{\phi}_{eff}\left(\mathbf{q}\right)\,\hat{a}^\dagger_{\mathbf{k}+\mathbf{q},\sigma}\hat{a}^\dagger_{\mathbf{p}-\mathbf{q},\sigma'}\hat{a}_{\mathbf{p},\sigma'}\hat{a}_{\mathbf{k},\sigma} \tag{13.41}$$

13.1.3 Twist-averaged boundary conditions

Twist-averaged boundary conditions (TABC) were conceived by C. Lin *et al.* [308] for the purpose of improving the slow convergence of many-fermion properties to the thermodynamic limit, due to shell effects in the filling of single-particle states. TABC are briefly described below, considering 1D systems for maintaining the discussion as simple and brief as possible.
The Hamiltonian (13.6) commutes with the translation operators:

$$\left(\hat{T}_i(jL)\Psi\right)\left(\dots r_i \dots\right) = \Psi(\dots r_i + jL \dots) \tag{13.42}$$

and thus we consider joint eigenfunctions of $\hat{H}$ and $\hat{T}_i(jL)$. The latter is, for all i and j, a unitary operator having complex eigenvalues $e^{-\theta_{ij}}$ that lie on the unit circle. The eigenvalue equation for $\hat{T}_i(jL)$ thus reads:

$$\left(\hat{T}_i(jL)\Psi_{\theta_{ij}}\right)\left(\dots r_i \dots\right) = e^{-\theta_{ij}}\,\Psi_{\theta_{ij}}(\dots r_i \dots) \quad , \qquad \theta_{ij} \in \mathbb{R} \tag{13.43}$$

Since the operators $\hat{T}_i(jL)$ provide, for fixed i, a unitary representation of the additive group $(\mathbb{Z},+)$, the numbers θ_{ij} are such that $\theta_{ij}\theta_{ij'} = \theta_{i(j+j')}$ and $\theta_{i0} = 1$. Therefore,

$\theta_{ij} = \theta_i\, j$. The indistinguishability of particles implies that $\theta_i = \theta_{i'} \bmod 2\pi$. Without loss of generality, we can thus restrict our consideration to $\theta \in [-\pi, \pi]$ in the Brillouin zone of the reciprocal lattice $k = \frac{2\pi}{L}\, n$ and solve the Schrödinger equation in the disjoint Hilbert spaces:

$$\mathcal{H}_\theta = \left\{ \Psi_\theta(r_1 \dots r_N) : \hat{T}_i(jL)\Psi_\theta = e^{-\theta_j}\, \Psi_\theta \right\} \tag{13.44}$$

Simulations in PBC are carried out in $\mathcal{H}_0$, which is isomorphic to $\mathcal{L}^2([0, L]^N)$. The Hilbert spaces $\mathcal{H}_\theta$ are closely related to each other. Indeed, if $\Psi_\theta \in \mathcal{H}_\theta$ the wavefunction:

$$\Phi(r_1 \dots r_N) = e^{i\theta \sum_{i=1}^N r_i}\, \Psi_\theta(r_1 \dots r_N) \tag{13.45}$$

lies in $\mathcal{H}_0$ and viceversa. Therefore:

$$\mathcal{H}_\theta = \hat{U}_\theta \mathcal{H}_0 \quad , \qquad (\hat{U}_\theta \Phi)(r_1 \dots r_N) = e^{i\theta \sum_{i=1}^N r_i}\, \Phi(r_1 \dots r_N) \tag{13.46}$$

where, remarkably, $\hat{U}_\theta$ is a tensor product of one-body unitary translations. In higher dimensions, θ is replaced by a vector $\boldsymbol{\theta} \in \mathrm{BZ} = [-\pi, \pi]^d$.
The TABC procedure consists in averaging many-fermion observables over twist vectors $\boldsymbol{\theta}$, i.e. assuming that the physical properties of the system are described by the density matrix:

$$\hat{\rho}_{\mathrm{TABC}} = \int_{\mathrm{BZ}} \frac{d\boldsymbol{\theta}}{\int_{\mathrm{BZ}} d\boldsymbol{\theta}}\, |\Psi_{\boldsymbol{\theta}}\rangle \langle \Psi_{\boldsymbol{\theta}}| \tag{13.47}$$

where Ψ_θ is the ground state of $\hat{H}$ in $\mathcal{H}_\theta$, and the domain of $\hat{\rho}_{\mathrm{TABC}}$ is the direct sum of the spaces $\mathcal{H}_\theta$ [262]. Physical observables are then computed using Born's rule [328]:

$$\mathcal{O}_{\mathrm{TABC}} = \mathrm{Tr}[\rho \hat{O}] = \int_{\mathrm{BZ}} \frac{d\boldsymbol{\theta}}{\int_{\mathrm{BZ}} d\boldsymbol{\theta}}\, \langle \Psi_{\boldsymbol{\theta}}|\, \hat{O}\, |\Psi_{\boldsymbol{\theta}}\rangle \tag{13.48}$$

Practically, the integration over twists is approximated by either [308] summing estimates $\langle \Psi_{\boldsymbol{\theta}}|\, \hat{O}\, |\Psi_{\boldsymbol{\theta}}\rangle$ relative to vectors $\boldsymbol{\theta}$ placed on a grid (grid averaging) or randomly sampled (twist sampling).
It is well-known [308] that using TABC has a very beneficial impact on the calculation of static properties. As a very simple example, in Figure 13.2 we compare the PBC and TABC estimate of the ground-state energy per particle of paramagnetic 2D ideal Fermi gases at $r_s = 1$. We have used grid averaging, with a grid of 15 points. While in PBC the convergence is slow and oscillating, in TABC it is monotonic and quite fast, approaching the exact result $\lim_{N\to\infty} \mathcal{E}_N = \frac{1}{2}\, Ha$ as $|\mathcal{E}_N - \mathcal{E}_\infty| \propto N^{-2}$.

13.2 Statistical data analysis

The accurate analysis of data is a fundamental requisite for extracting reliable information from a QMC simulation. In the present Appendix, the statistical techniques used to compute the expected value of observables and the corresponding error bars are described.
The data analysis must take into account the presence of an equilibration time and the presence of correlations. Compensating for correlations, in particular, is essential in order to obtain a reliable estimate of the standard deviation on the mean. In the VMC and PIGS methods, the equilibration time emerges because the Metropolis algorithm is based on the convergence of a Markov chain onto a suitable invariant law. In DMC and

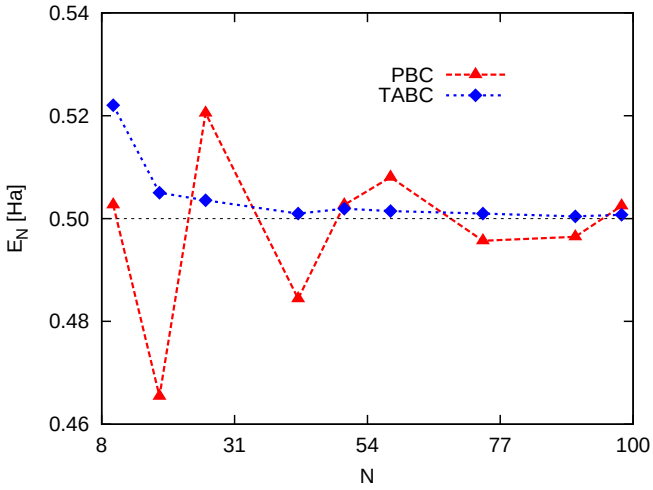

Figure 13.2: Effect of TABC on the ground-state energy per particle of paramagnetic 2D ideal Fermi gases at $r_s = 1$.

AFQMC, it emerges because the operator $e^{-\tau \hat{H}}$ requires a finite amount of imaginary time to project a trial wavefunction onto the ground state of the system.
Let us denote a set of N sequentially observed values x_i, corresponding to simulation times $\tau_i = i\delta\tau$. If the x_i data are realizations of independent and identically distributed random variables X_i with mean μ and variance σ, those parameters can be retrieved from the sample mean and the sample variance respectively:

$$\mathcal{M} = \frac{1}{N}\sum_{i=1}^{N} x_i \quad , \qquad \mathcal{S} = \frac{1}{N}\sum_{i=1}^{N} x_i^2 - \left(\frac{1}{N}\sum_i x_i\right)^2 \tag{13.49}$$

respectively. Under the hypotheses of independence and identical distribution, these quantities [72] converge almost certainly to μ and σ respectively.
In QMC calculations, the evaluation of the error bar is more subtle, due to the correlations among samples x_i relative to different time steps. The correlation time $\tau_c = j_c\delta\tau$, that measures how many time steps the random walks realized in QMC simulation require to evolve between independent states, is conventionally defined through the autocorrelation function [360]:

$$\chi(j) = E[X_i X_{i+j}] = \frac{1}{N-j}\sum_{i=1}^{N-j} x_i x_{i+j} - \left(\frac{1}{N-j}\sum_{i=1}^{N-j} x_i\right)\left(\frac{1}{N-j}\sum_{i=1}^{N-j} x_{i+j}\right) \tag{13.50}$$

Notice that $\chi(0) = \mathcal{S}$. For uncorrelated data, $\chi(j) = \delta_{j0}\,\mathcal{S}$. At long times, $\chi(j)$ is expected to exhibit an exponential decay:

$$\chi(j) \simeq \chi(0) e^{-\frac{j}{j_c}} \tag{13.51}$$

An example of the correlation time analysis is shown in Figure 13.3.
Once the correlation time is known, one can divide the outcomes x_i of the simulation in

blocks of $N_s \gg j_c$ steps. The number of such blocks is $N_b = \frac{N}{N_s}$. The estimator of the mean is obtained as:

$$\mathcal{M}_{block} = \frac{1}{N_b}\sum_{i=1}^{N_b}\mathcal{M}_i \qquad \mathcal{M}_i = \frac{1}{N_s}\sum_{j=(i-1)N_b}^{iN_b} x_j \tag{13.52}$$

Since the block length is sufficiently large, the $\mathcal{M}_i$ are independent and, after the equilibration, identically distributed. An estimate of the standard deviation of the mean is obtained from [360, 361]:

$$\mathcal{S}^* = \sqrt{\frac{1}{N_b - 1}\sum_{i=1}^{N_b}(\mathcal{M}_i^2 - \mathcal{M}_{block}^2)} \tag{13.53}$$

Assuming a sufficient number of blocks and samples are included in the analysis, $\mathcal{S}^*$ increases with the block length N_s until a limiting value σ' is reached, as shown in Figure 13.3. The error of the estimator $\mathcal{M}_{block}$ of the mean is then obtained as $\frac{\sigma'}{\sqrt{N_b}}$.

13.3 Systematic Errors

The statistical data analysis provides a reliable estimate of the standard deviation of the mean, but it is unable to detect any systematic errors that could be present in the simulation. Potential systematic errors include:

1. insufficient exploration of configuration space. This error is present if the simulation is too short (in such case $\mathcal{S}^*$ does not converge to σ') or if the time step limits the number of accepted moves (in such case the VMC or DMC acceptance is too low).

2. inclusion of unequilibrated data in final averaged data. The equilibration time of an observable in a QMC calculation is best determined by graphing the observable as a function of imaginary time, as exemplified in Figure 13.3. Trends in block averages are better identified dividing the data into short blocks.

3. in DMC calculations, performing the branching step too frequently results in a population control bias, and the true ground-state distribution and energy are not obtained.

13.4 Numeric stabilization of AFQMC calculations

13.4.1 Gram-Schmidt reorthogonalization

In phaseless AFQMC calculations, the state $e^{-\tau\hat{H}}|\Psi_T\rangle$ is recovered through the stochastic average (5.65) of Brownian trajectories $|\Psi(\boldsymbol{\eta})\rangle$ in the manifold of Slater determinants. The calculation of such trajectories requires repeated matrix multiplications, which are unavoidably performed with finite precision. The finite precision causes round-off errors, which accumulate and produce an unfaithful representation of $|\Psi(\boldsymbol{\eta})\rangle$.
To alleviate this problem, we periodically perform a modified Gram-Schmidt reorthonormalization on the walkers [248, 268].

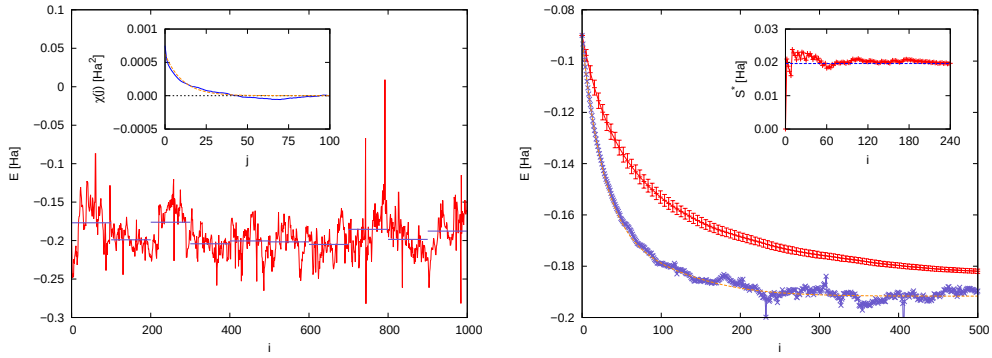

(a) (b)

Figure 13.3: (a) Example of correlation time analysis, relative to the AFQMC simulation of $N = 26$ electrons at $r_s = 1$. Unreblocked data are represented as red lines. The correlation $\chi(j)$ shown in the inset (blue line: (13.50), orange line: fit) decays after 200 steps, whence the data are reblocked as represented with purple horizontal lines. (b) Example of equilibration time analysis, relative to the AFQMC simulation of $N = 26$ electrons at $r_s = 1$. The inclusion of unequilibrated data (purple points) significantly biases the sample mean (13.49) of the ground-state energy (red points): while the sample mean of all data is $\mathcal{E}_N = -0.181(2)$Ha, the sample mean of the equilibrated data only ($i > 300$) is $\mathcal{E}_N = -0.192(2)$Ha. The error on $\mathcal{M}_{block}$ is obtained monitoring the limiting behavior of (13.53) (inset, red points).

It is well-known from linear algebra [262], that from a set $|\psi_1\rangle \dots |\psi_N\rangle$ of linearly independent vectors in a Hilbert space H a set $|\psi'_1\rangle \dots |\psi'_N\rangle$ of orthogonal vectors can be extracted making use of the Gram-Schmidt procedure:

$$|\psi'_1\rangle = |\psi_1\rangle \dots |\psi'_k\rangle = |\psi_k\rangle - \sum_{j=1}^{k-1} \frac{\langle \psi'_j | \psi_k \rangle}{\langle \psi'_j | \psi'_j \rangle} |\psi'_j\rangle \quad , \qquad k = 2 \dots N \tag{13.54}$$

It is natural to investigate which is the relationship between the Slater determinants $|\Psi\rangle = |\psi_1 \dots \psi_N\rangle_-$ and $|\Psi'\rangle = |\psi'_1 \dots \psi'_N\rangle_-$. Writing $|\psi_k\rangle = |\psi'_k\rangle + \sum_{j=1}^{k-1} \frac{\langle \psi'_j | \psi_k \rangle}{\langle \psi'_j | \psi'_j \rangle} |\psi'_j\rangle$ and remembering that the creation operator $\hat{a}^\dagger_{|\psi\rangle}$ is linear in $|\psi\rangle$, we obtain:

$$\hat{a}^\dagger_{|\psi_1\rangle} \dots \hat{a}^\dagger_{|\psi_n\rangle} = \hat{a}^\dagger_{|\psi'_1\rangle} \dots \hat{a}^\dagger_{|\psi'_n\rangle} \tag{13.55}$$

Equation (13.55) can be easily proved by induction over N; for $N = 1$ it is obvious, for $N = 2$:

$$\hat{a}^\dagger_{|\psi_1\rangle} \hat{a}^\dagger_{|\psi_2\rangle} = \hat{a}^\dagger_{|\psi'_1\rangle} \left[\hat{a}^\dagger_{|\psi'_2\rangle} + \frac{\langle \psi'_1 | \psi_2 \rangle}{\langle \psi'_1 | \psi'_1 \rangle} \hat{a}^\dagger_{|\psi'_1\rangle} \right] = \hat{a}^\dagger_{|\psi'_1\rangle} \hat{a}^\dagger_{|\psi'_2\rangle} \tag{13.56}$$

thanks to the anticommutation relation $\hat{a}^\dagger_{|\psi'_1\rangle} \hat{a}^\dagger_{|\psi'_1\rangle} = 0$, and if it were true for an arbitrary

N then it would hold for $N+1$:

$$\begin{aligned}\hat{a}^{\dagger}_{|\psi_1\rangle}\dots\hat{a}^{\dagger}_{|\psi_{N+1}\rangle} = \hat{a}^{\dagger}_{|\psi_1\rangle}\dots\hat{a}^{\dagger}_{|\psi_N\rangle}\hat{a}^{\dagger}_{|\psi_{N+1}\rangle} = \\ \hat{a}^{\dagger}_{|\psi'_1\rangle}\dots\hat{a}^{\dagger}_{|\psi'_N\rangle} = \left[\hat{a}^{\dagger}_{|\psi'_{N+1}\rangle} + \sum_{j=1}^{N}\frac{\langle\psi'_j|\psi_{N+1}\rangle}{\langle\psi'_j|\psi'_j\rangle}\hat{a}^{\dagger}_{|\psi'_j\rangle}\right] = \hat{a}^{\dagger}_{|\psi'_1\rangle}\dots\hat{a}^{\dagger}_{|\psi'_{N+1}\rangle}\end{aligned} \tag{13.57}$$

thanks, once again, to the anticommutation relation $\hat{a}^{\dagger}_{|\psi'_j\rangle}\hat{a}^{\dagger}_{|\psi'_j\rangle} = 0$. Since:

$$|\Psi\rangle = |\psi_1\dots\psi_N\rangle_- = \frac{\hat{a}^{\dagger}_{|\psi_1\rangle}\dots\hat{a}^{\dagger}_{|\psi_N\rangle}}{\sqrt{N!}}|0\rangle \tag{13.58}$$

(13.55) shows that $|\Psi\rangle = |\Psi'\rangle$. Taking the scalar products:

$$\langle\varphi_i|\psi_k\rangle = \langle\varphi_i|\psi'_k\rangle + \sum_{j=1}^{k-1}\frac{\langle\psi'_j|\psi_k\rangle}{\langle\psi'_j|\psi'_j\rangle}\langle\varphi_i|\psi'_j\rangle \tag{13.59}$$

between the vectors $|\psi_k\rangle$ and the single-particle basis states $|\varphi_i\rangle$, we derive the relation:

$$\Psi_{ik} = \sum_{j=1}^{N}\Psi'_{ij}R_{jk} \tag{13.60}$$

between the elements of the matrices Ψ and Ψ' associated to the Slater determinants $|\Psi\rangle$ and $|\Psi'\rangle$. The matrix $R \in M_{N\times N}(\mathbb{C})$ appearing in (13.60) is upper triangular:

$$R_{jk} = \begin{cases} 0 & \text{if } j > k \\ 1 & \text{if } j = k \\ \frac{\langle\psi'_j|\psi_k\rangle}{\langle\psi'_j|\psi'_j\rangle} & \text{if } j < k \end{cases} \tag{13.61}$$

and the matrix Ψ' is orthogonal. Applying the Gram-Schmidt procedure to the set $|\psi_1\rangle\dots|\psi_N\rangle$ corresponds to applying a QR decomposition [38] to the matrix Ψ. Moreover, only the orthogonal matrix appearing in the QR decomposition of Ψ contains actual information about the determinant $|\Psi\rangle$.
The vectors $|\psi'_1\rangle\dots|\psi'_N\rangle$ are orthogonal but not orthonormal, and thus:

$$\|\Psi'\| = \prod_{k=1}^{N}\sqrt{\langle\psi'_k|\psi'_k\rangle} \tag{13.62}$$

$|\Psi'\rangle$ can be replaced with its normalized vestion in mixed and pure estimates. Periodic application of the Gram-Schmidt procedure contains fluctuations in the walkers norms and stabilizes the random walk [248, 268].

13.4.2 Numeric stabilization of matrix inversion

The distance:

$$\|\mathcal{I}(\mathcal{D}_r) - \mathcal{D}_r^{-1}\|_{\infty} \tag{13.63}$$

between the actual inverse $\mathcal{D}_r^{-1}$ of $\mathcal{D}_r$ and its numeric estimate $\mathcal{I}(\mathcal{D}_r)$ (13.63) is bounded [275] by:

$$\|\mathcal{I}(\mathcal{D}_r) - \mathcal{D}_r^{-1}\|_\infty \leq M\|\mathcal{I}(\mathcal{D}_r)\|_\infty \frac{\|E_r\|_\infty}{1 - M\|E_r\|_\infty} \tag{13.64}$$

with:

$$\|E_r\|_\infty = \|\mathbb{I} - \mathcal{D}_r\mathcal{I}(\mathcal{D}_r)\|_\infty \tag{13.65}$$

Equation (13.64) holds for $\|E_r\|_\infty < \frac{1}{M}$, and is therefore adequate to the description of $\|E_r\|_\infty$ for small r. It can be combined with the following estimate [362]:

$$\|\mathcal{I}(\mathcal{D}_r) - \mathcal{D}_r^{-1}\|_\infty \simeq \epsilon\|\mathcal{D}_r^{-1}\|_\infty^2 \frac{M^3}{3} \tag{13.66}$$

to yield:

$$M\|E_r\|_\infty \simeq \frac{\epsilon\frac{M^3}{3}\|\mathcal{D}_r^{-1}\|_\infty^2}{\|\mathcal{I}(\mathcal{D}_r)\|_\infty + \epsilon\frac{M^3}{3}\|\mathcal{D}_r^{-1}\|_\infty^2} \tag{13.67}$$

In the case of AFQMC calculations, where $\mathcal{D}_r$ and $\mathcal{D}_r^{-1}$ come from the product of r matrices:

$$\|\mathcal{D}_r^{-1}\|_\infty = C_3^r \quad \|\mathcal{I}(\mathcal{D}_r)\|_\infty = C_4^r \tag{13.68}$$

where C_3 and C_4 are suitable constants, close to each other. Merging (13.66) and (13.68) leads to:

$$\|E_r\|_\infty \simeq \frac{\epsilon\frac{M^2}{3}}{\left(\frac{C_4}{C_3^2}\right)^r + \epsilon\frac{M^3}{3}} \tag{13.69}$$

which reduces to:

$$\|E_r\|_\infty \simeq \epsilon\frac{M^2}{3}\left(\frac{C_3^2}{C_4}\right)^r \tag{13.70}$$

in the limit of small r. Since $C_4 < C_3^2$, C_3 and C_4 being close to each other, the estimate (13.70) leads to a power-law increase of $\|E_r\|_\infty$.

13.5 RPA for Finite Homogeneous Systems

The aim of this appendix is to provide a brief description of the Random Phase Approximation (RPA) [277, 4, 6] for finite interacting systems and of the procedure leading to the excitation energies and weights, with which AFQMC results have been compared.
The RPA can be regarded to [4] as a refinement of the well-known Tamm-Dancoff approximation [363, 364, 4] (TDA), which has long been supporting the study of excitations in nuclear systems. The TDA relies on the assumptions that the ground state of the system is the Hartree-Fock determinant, and that excited states can be represented as superpositions of determinants obtained promoting a single particle above the Fermi surface. Within RPA, on the other hand, a better approximation $|\Phi_0\rangle$ for the actual ground state of the interacting system is employed to build up an Ansatz for plasmonic wavefunctions. To this purpose, the distinction between spin-orbitals below and above the Fermi level is made explicit by writing:

$$\hat{a}_{\mathbf{k}\sigma}^\dagger = \begin{cases} \hat{c}_{\mathbf{k}\sigma}^\dagger & \text{if } |\mathbf{k}| > k_F \\ \hat{b}_{\mathbf{k}\sigma} & \text{if } |\mathbf{k}| \leq k_F \end{cases} \tag{13.71}$$

and the Hamiltonian (7.1) is consequently expressed as:

$$\hat{H} = \hat{T} + \hat{V} = \sum_{\mathbf{k}\sigma} t_{\mathbf{k}}\, \hat{c}^{\dagger}_{\mathbf{k}\sigma}\hat{c}_{\mathbf{k}\sigma} + \sum_{\mathbf{k}\sigma} t_{\mathbf{k}}\, \left(1 - \hat{b}^{\dagger}_{\mathbf{k}\sigma}\hat{b}_{\mathbf{k}\sigma}\right) + \frac{1}{2\Omega}\sum_{\mathbf{q}\neq 0} \phi_{\mathbf{q}}\hat{\rho}_{\mathbf{q}}\hat{\rho}_{-\mathbf{q}} \tag{13.72}$$

where $t_{\mathbf{k}} = \frac{|\mathbf{k}|^2}{2}$, $\phi_{\mathbf{q}} = \frac{2\pi}{|\mathbf{q}|}$, the first sum goes over all wave-vectors $\mathbf{k}$ such that $|\mathbf{k}| > k_F$, the second sum goes over all wave-vectors $\mathbf{k}$ such that $|\mathbf{k}| \leq k_F$ and the density fluctuation operator $\hat{\rho}_{\mathbf{q}}$ is approximated [277] by:

$$\hat{\rho}_{\mathbf{q}} \simeq \sum_{\mathbf{k}\sigma} \hat{c}^{\dagger}_{\mathbf{k}+\mathbf{q}\sigma}\hat{b}^{\dagger}_{\mathbf{k}\sigma} + \hat{b}_{\mathbf{k}+\mathbf{q}\sigma}\hat{c}_{\mathbf{k}\sigma} \tag{13.73}$$

where the first sum, describing forward scattering processes in which a particle is promoted above the Fermi level, goes over all wave-vectors $\mathbf{k}$ such that $|\mathbf{k}| > k_F$ and $|\mathbf{k}+\mathbf{q}| \leq k_F$, and the second sum, describing backward scattering processes in which a particle is brought back below the Fermi level, goes over all wave-vectors $\mathbf{k}$ such that $|\mathbf{k}| \leq k_F$ and $|\mathbf{k}+\mathbf{q}| > k_F$. The RPA Ansatz for plasmonic wavefunctions is:

$$|\Phi_{\mathbf{q}}\rangle = \sum_{\mathbf{k}\sigma} X_{\mathbf{k}}\hat{c}^{\dagger}_{\mathbf{k}+\mathbf{q}\sigma}\hat{b}^{\dagger}_{\mathbf{k}\sigma}\,|\Phi_0\rangle + \sum_{\mathbf{k}\sigma} Y_{\mathbf{k}}\hat{b}_{\mathbf{k}+\mathbf{q}\sigma}\hat{c}_{\mathbf{k}\sigma}\,|\Phi_0\rangle \tag{13.74}$$

(13.74) is justified by the observation that the pair destruction operator $\hat{b}_{\mathbf{k}+\mathbf{q}\sigma}\hat{c}_{\mathbf{k}\sigma}$ annihilates the Hartree-Fock determinant but not the actual ground state of the interacting system. The eigenvalues ϵ such that $\hat{H}\,|\Phi_{\mathbf{q}}\rangle = \epsilon\,|\Phi_{\mathbf{q}}\rangle$ are obtained recalling that the commutators between the Coulomb interaction and the pair creation and destruction operators can be approximated [277] as:

$$[\hat{c}^{\dagger}_{\mathbf{k}+\mathbf{q}\sigma}\hat{b}^{\dagger}_{\mathbf{k}\sigma}, \hat{V}] \simeq -\frac{\phi_q}{\Omega}\hat{\rho}_{\mathbf{q}} \tag{13.75}$$

and:

$$[\hat{b}_{\mathbf{k}+\mathbf{q}\sigma}\hat{c}_{\mathbf{k}\sigma}, \hat{V}] \simeq \frac{\phi_q}{\Omega}\hat{\rho}_{\mathbf{q}} \tag{13.76}$$

respectively. Now, since $|\Phi_0\rangle$ and $|\Phi_{\mathbf{q}}\rangle$ and eigenstates of $\hat{H}$ with eigenvalues ϵ_0 and $\epsilon = \epsilon_0 + \Delta\epsilon$ respectively, the following identity holds:

$$0 = \langle\Phi_{\mathbf{q}}|(\epsilon - \hat{H})\,\hat{c}^{\dagger}_{\mathbf{k}+\mathbf{q}\sigma}\hat{b}^{\dagger}_{\mathbf{k}\sigma}|\Phi_0\rangle = \Delta\epsilon\,\langle\Phi_{\mathbf{q}}|\hat{c}^{\dagger}_{\mathbf{k}+\mathbf{q}\sigma}\hat{b}^{\dagger}_{\mathbf{k}\sigma}|\Phi_0\rangle - \langle\Phi_{\mathbf{q}}|[\hat{H}, \hat{c}^{\dagger}_{\mathbf{k}+\mathbf{q}\sigma}\hat{b}^{\dagger}_{\mathbf{k}\sigma}]|\Phi_0\rangle \tag{13.77}$$

from which:

$$\langle\Phi_{\mathbf{q}}|\hat{c}^{\dagger}_{\mathbf{k}+\mathbf{q}\sigma}\hat{b}^{\dagger}_{\mathbf{k}\sigma}|\Phi_0\rangle = \frac{\frac{\phi_q}{\Omega}\langle\Phi_{\mathbf{q}}|\hat{\rho}_{\mathbf{q}}|\Phi_0\rangle}{\Delta\epsilon + t_{\mathbf{k}} - t_{\mathbf{k}+\mathbf{q}}} \tag{13.78}$$

follows. Similarly:

$$\langle\Phi_{\mathbf{q}}|\hat{b}_{\mathbf{k}+\mathbf{q}\sigma}\hat{c}_{\mathbf{k}\sigma}|\Phi_0\rangle = -\frac{\frac{\phi_q}{\Omega}\langle\Phi_{\mathbf{q}}|\hat{\rho}_{\mathbf{q}}|\Phi_0\rangle}{\Delta\epsilon + t_{\mathbf{k}} - t_{\mathbf{k}+\mathbf{q}}} \tag{13.79}$$

Equation (13.78) and (13.79) can be summed over $\mathbf{k}, \sigma$ to yield the secular equation:

$$\langle\Phi_{\mathbf{q}}|\hat{\rho}_{\mathbf{q}}|\Phi_0\rangle = \frac{2\phi_{\mathbf{q}}}{\Omega}\langle\Phi_{\mathbf{q}}|\hat{\rho}_{\mathbf{q}}|\Phi_0\rangle \left(\sum_{\substack{|\mathbf{k}|\leq k_F \\ |\mathbf{k}+\mathbf{q}|>k_F}} \frac{1}{\Delta\epsilon + t_{\mathbf{k}} - t_{\mathbf{k}+\mathbf{q}}} - \sum_{\substack{|\mathbf{k}|>k_F \\ |\mathbf{k}+\mathbf{q}|\leq k_F}} \frac{1}{\Delta\epsilon + t_{\mathbf{k}} - t_{\mathbf{k}+\mathbf{q}}} \right) \tag{13.80}$$

which, simplifying the matrix element $\langle\Phi_{\mathbf{q}}|\hat{\rho}_{\mathbf{q}}|\Phi_0\rangle$ in both members, and applying the change of variables $\mathbf{r} = -\mathbf{k} - \mathbf{q}$ in the second sum, takes the form:

$$1 = \frac{\phi_{\mathbf{q}}}{\Omega}\left[2 \sum_{\substack{|\mathbf{k}|\leq k_F \\ |\mathbf{k}+\mathbf{q}|>k_F}} \frac{1}{t_{\mathbf{k}} - t_{\mathbf{k}+\mathbf{q}} + \Delta\epsilon} + \frac{1}{t_{\mathbf{k}} - t_{\mathbf{k}+\mathbf{q}} - \Delta\epsilon} \right] \tag{13.81}$$

where the term between square brakets is immediately identified with the real part of the $2D$ Lindhard function $\chi_0(\mathbf{q}, \Delta\epsilon)$ [6]. The coefficients $X_{\mathbf{k}}, Y_{\mathbf{k}}$ are determined substituting (13.74) in (13.78) and (13.79), and read:

$$X_{\mathbf{k}} = \frac{\mathcal{N}}{t_{\mathbf{k}} - t_{\mathbf{k}+\mathbf{q}} + \Delta\epsilon} \qquad Y_{\mathbf{k}} = -\frac{\mathcal{N}}{t_{\mathbf{k}} - t_{\mathbf{k}+\mathbf{q}} + \Delta\epsilon} \tag{13.82}$$

where $\mathcal{N}$ is a normalization constant. Notice that $X_{\mathbf{k}}$ is defined for $|\mathbf{k}| \leq k_F$, $|\mathbf{k}+\mathbf{q}| > k_F$ while $Y_{\mathbf{k}}$ for $|\mathbf{k}| > k_F$ and $|\mathbf{k}+\mathbf{q}| \leq k_F$. The right-hand side of (13.81) is a function $f(\Delta\epsilon) = \frac{\phi_{\mathbf{q}}}{\Omega}\,\chi_0(\mathbf{q}, \Delta\epsilon)$, illustrated in Fig. 13.4, with the following properties:

$$\lim_{\Delta\epsilon\to 0} f(\Delta\epsilon) < 0 \qquad \lim_{\Delta\epsilon\to+\infty} f(\Delta\epsilon) = 0^+ \tag{13.83}$$

and diverging in corrispondence to the particle-hole energies $t_{\mathbf{k}+\mathbf{q}} - t_{\mathbf{k}}$. As a consequence, there exists a root of the secular equation (13.81) between all the poles of $f(\Delta\epsilon)$ and another root above them. The excited state corresponding to this root has coefficients $X_{\mathbf{k}}, Y_{\mathbf{k}}$ sharing the same sign, and is therefore a coherent superposition of particle-hole excitations describing a collective high-energy oscillation being precursive of the plasmon. The excited states orresponding to other roots of (13.81) have coefficients $X_{\mathbf{k}}, Y_{\mathbf{k}}$ with non-constant sign, and therefore take into account the persistence of non-interacting properties in the spectrum of the electron gas, even in presence of Coulomb interaction.

We have seen that the RPA approximation yields an Ansatz for the energies $\epsilon_{\mathbf{q},n}$ and wavefunctions $|\Phi_{\mathbf{q},n}\rangle$ of excited states with definite momentum $\mathbf{q}$, which results in the following approximation for the image of the RPA ground state through the density fluctuation operator $\hat{\rho}_{\mathbf{q}}$:

$$\hat{\rho}_{\mathbf{q}}\,|\Phi_0\rangle = \sum_n |\Phi_{\mathbf{q},n}\rangle\,\langle\Phi_{\mathbf{q},n}|\hat{\rho}_{\mathbf{q}}\rangle\,\Phi_0 \tag{13.84}$$

with:

$$\langle\Phi_{\mathbf{q},n}|\hat{\rho}_{\mathbf{q}}\rangle\,\Phi_0 = \sum_{\substack{|\mathbf{k}|\leq k_F \\ |\mathbf{k}+\mathbf{q}|>k_F}} X_{\mathbf{k},n} + \sum_{\substack{|\mathbf{k}|>k_F \\ |\mathbf{k}+\mathbf{q}|\leq k_F}} Y_{\mathbf{k},n} \tag{13.85}$$

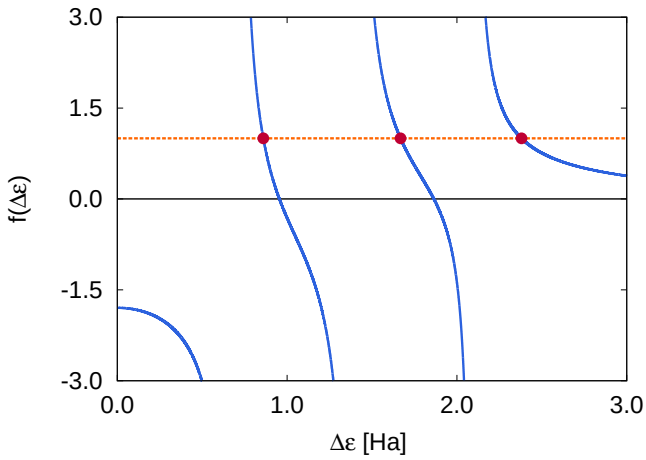

Figure 13.4: (color online) RPA secular equation for a paramagnetic system of $N = 18$ particles at $r_s = 1$, and $\mathbf{q}_2$. The blue solid line is the right member $f(\Delta\epsilon)$ of (13.81), and the orange dashed line is the constant function $g(\Delta\epsilon) = 1$; intersections between the two graphs are marked with red dots. the RPA eigenvalues are the abscissae of such intersections.

and for the dynamical structure factor:

$$S(\mathbf{q}, \omega) = \frac{1}{N} \sum_n \delta(\omega - \epsilon_{\mathbf{q},n}) |\langle \Phi_{\mathbf{q},n} | \hat{\rho}_{\mathbf{q}} \rangle \Phi_0|^2 \tag{13.86}$$

Bibliography

[1] P. A. M. Dirac. *Proc. Roy. Soc. London A*, 123:792, 1929.

[2] R. P. Feynman and A. R. Hibbs. *Quantum Mechanics and path integrals*. McGraw-Hill, 1965.

[3] D. M. Ceperley. *Rev. Mod. Phys.*, 67:279, 1995.

[4] A. L. Fetter and J. D. Walecka. *Quantum theory of many-particle systems*. McGraw-Hill, 1971.

[5] H. Bruus and K. Flensberg. *Many-body quantum theory in condensed matter Physics*. Oxford University Press, 2004.

[6] G. Giuliani and G. Vignale. *Quantum theory of the electron liquid*. Cambridge University Press, 2005.

[7] H. Hellmann. *Einführung in die Quantenchemie*. Franz Deuticke, Leipzig, 1937.

[8] R. P. Feynman. *Phys. Rev.*, 56:340, 1939.

[9] L. Mühlbacher and E. Rabani. *Phys. Rev. Lett.*, 100:176403, 2008.

[10] G. Carleo, F. Becca, M. Schiró, and M. Fabrizio. *Sci. Rep.*, 2:243, 2012.

[11] J. R. McClean and A. Aspuru-Guzik. *Phys. Rev. A*, 91:012311, 2015.

[12] G. Källén. *Helv. Phys. Acta*, 25:417, 1952.

[13] H. Lehmann. *Nuovo Cimento*, 11:342, 1954.

[14] Y. W. Sokhotskii. *On definite integrals and functions used in series expansions*. St. Petersburg, 1873.

[15] J. Plemelj. *Problems in the sense of Riemann and Klein*. Interscience Publishers, New York, 1964.

[16] H. M. Nussenzweig. *Causality and dispersion relations*. Academic Press, New York, 1972.

[17] H. A. Kramers. In *Atti Cong. Intern. Fisici*, 1927.

[18] R. de L. Kronig. *J. Opt. Soc. Am.*, 12:547, 1926.

[19] D. Pines and P. Noziéres. *The theory of quantum liquids: normal Fermi liquids*. W. A. Benjamin, New York, 1966.

[20] L. van Hove. *Phys. Rev.*, 95:249, 1954.

[21] S. Lovresey. *Theory of neutron scattering in condensed matter*. Oxford University Press, 1984.

[22] J. Weber. *Phys. Rev.*, 101:1620, 1956.

[23] R. Kubo. *Rep. Prog. Phys.*, 29:255, 1966.

[24] B. U. Felderhof. *J. Math. Phys. A*, 11:921, 1978.

[25] T. L. Gilbert. *Phys. Rev.*, 12:2111, 1975.

[26] O. Penrose and L. Onsager. *Phys. Rev.*, 104:576, 1956.
[27] C. N. Yang. *Rev. Mod. Phys.*, 34:694, 1962.
[28] A. Rényi. In *Proceedings of the fourth Berkeley symposium on mathematics, statistics and probability*, 1961.
[29] M. Haque, O. S. Zozulya, and K. Schoutens. *J. Phys. A: Math. Theor.*, 42:504012, 2009.
[30] C. M. Herdman, S. Inglis, P. N. Roy, R. G. Melko, and A. Del Maestro. *Phys. Rev. E*, 90:013308, 2014.
[31] C. M. Herdman and A. Del Maestro. *Phys. Rev. B*, 91:184507, 2015.
[32] D. Frenkel and S. Berend. *Understanding molecular simulations from algorithms to applications*. San Diego: Academic Press, 2002.
[33] J. P. Hansen and I. R. McDonald. *Theory of simple liquids*. Academic Press, 2005.
[34] M. Motta, G. Bertaina, D. E. Galli, and E. Vitali. *Comp. Phys. Comm.*, 190:62, 2015.
[35] J. Toulouse and C. J. Umrigar. *J. Chem. Phys.*, 128:174101, 2008.
[36] J. H. Halton. *SIAM Review*, 12:1–63, 1970.
[37] J. Jacod and P. Protter. *Probability essentials*. Springer Universitext, 2004.
[38] W. A. Press, S. A. Teukolsky, W. T. Vettering, and B. P. Flannery. *Numerical recipes in Fortran*. Cambridge University Press, 1992.
[39] G. E. P. Box and Mervin E. Muller. *Ann. Math. Stat.*, 29:610–611, 1958.
[40] N. Metropolis, A. W. Rosenbluth, M. N. Rosenbluth, A. H. Teller, and E. Teller. *J. Chem. Phys.*, 21:1087, 1953.
[41] W. K. Hastings. *Biometrika*, 57:97, 1970.
[42] A. Markov. *Dokl. Akad. Nauk. SSSR*, 10:311, 1936.
[43] S. Kakutani. *Proc. Imp. Akad. Tokyo*, 14:242, 1938.
[44] P. Baldi. *Equazioni differenziali stocastiche e applicazioni*. Ed. Pitagora, Bologna, 2000.
[45] C. W. Gardiner. *Handbook of stochastic methods*. Springer, Berlin, 2004.
[46] W. L. McMillan. *Phys. Rev.*, 138:A442, 1965.
[47] D. M. Ceperley, G. V. Chester, and M. H. Kalos. *Phys. Rev. B*, 16:3081, 1977.
[48] W. Ritz. *J. Reine und Angewandte Math.*, 135:1, 1909.
[49] G. M. Zhislin. *T. Mosk. Mat. Obs.*, 9:81, 1960.
[50] G. M. Zhislin and A. G. Sigalov. *Izv. Akad. Nauk SSSR Ser. Mat.*, 29:835, 1965.
[51] M. Lewin. *J. Funct. Anal.*, 260:3535, 2011.
[52] L. G. Valiant. *Theor. Comp. Sci.*, 8:189, 1979.
[53] A. Bijl. *Physica*, 7:869, 1940.
[54] R. B. Dingle. *Phil. Mag.*, 40:573, 1949.
[55] R. Jastrow. *Phys. Rev.*, 98:1479, 1955.
[56] K. E. Schmidt, M. W. Kalos, M. A. Lee, and G. V. Chester. *Phys. Rev. Lett.*, 45:573, 1980.
[57] K. E. Schmidt, M. A. Lee, M. W. Kalos, and G. V. Chester. *Phys. Rev. Lett.*, 47:807, 1981.
[58] R. M. Panoff and J. Carlson. *Phys. Rev. Lett.*, 62:1130, 1989.
[59] S. Moroni, S. Fantoni, and G. Senatore. *Phys. Rev. B*, 52:13547, 1995.
[60] Y. Kwon, D. M. Ceperley, and R. M. Martin. *Phys. Rev. B*, 48:12037, 1993.
[61] R. P. Feynman and M. Cohen. *Phys. Rev.*, 102:1189, 1956.
[62] K. E. Schmidt and J. W. Moskowitz. *J. Chem. Phys.*, 93:4172, 1990.
[63] Y. Kwon, D. M. Ceperley, and R. M. Martin. *Phys. Rev. B*, 53:7376, 1996.

[64] P. Lopez-Rios, A. Ma, N. D. Drummond, M. D. Towler, and R. J. Needs. *Phys. Rev. E*, 74:066701, 2006.
[65] P. Claverie and F. Soto-Esguibar. Generalization of the Feynman-Kac formula. In B. Gomez, S. M. Moore, A. M. Rodriguez-Vargas, and A. Rueda, editors, *Stochastic processes applied to Physics and other related fields*. World Scientific, 1983.
[66] M. Holzmann, D. M. Ceperley, C. Pierleoni, and K. Esler. *Phys. Rev. E*, 68:046707, 2003.
[67] M. Caffarel and P. Claverie. *J. Stat. Phys.*, 43:797, 1986.
[68] M. Caffarel and P. Claverie. *J. Chem. Phys.*, 88:1088, 1988.
[69] M. Caffarel and P. Claverie. *J. Chem. Phys.*, 88:1100, 1988.
[70] M. Taddei, M. Ruggeri, S. Moroni, and M. Holzmann. *Phys. Rev. B*, 91:115106, 2015.
[71] M. Kac. *Trans. Am. Math. Soc.*, 65:1, 1949.
[72] E. Vitali, M. Motta, and D. E. Galli. Theory and simulation of random phenomena. 2016.
[73] S. A. Vitiello, K. Runge, and M. H. Kalos. *Phys. Rev. Lett.*, 60:1970, 1988.
[74] L. Reatto and G. L. Masserini. *Phys. Rev. B*, 38:4516, 1988.
[75] S. A. Vitiello, K. J. Runge, G. V. Chester, and M. H. Kalos. *Phys. Rev. B*, 42:228, 1990.
[76] T. MacFarland, S. A. Vitiello, L. Reatto, G. V. Chester, and M. H. Kalos. *Phys. Rev. B*, 50:13577, 1994.
[77] S. Moroni, D. E. Galli, S. Fantoni, and L. Reatto. *Phys. Rev. B*, 58:909, 1998.
[78] D. E. Galli, E. Cecchetti, and L. Reatto. *Phys. Rev. Lett.*, 77:5401, 1996.
[79] D. E. Galli, G. L. Masserini, and L. Reatto. *Phys. Rev. B*, 60:3476, 1999.
[80] D. E. Galli and L. Reatto. *Mol. Phys.*, 101:1697, 2003.
[81] D. E. Galli and L. Reatto. *J. Low. Temp. Phys.*, 134:121, 2004.
[82] P. Rossky, J. D. Doll, and H. L. Friedman. *J. Chem. Phys.*, 69:4628, 1978.
[83] C. J. Umrigar, K. G. Wilson, and J. W. Wilkins. *Phys. Rev. Lett.*, 60:1719, 1988.
[84] M. H. Kalos and P. A. Whitlock. *Monte Carlo methods*. Wiley, 1986.
[85] K. Levenberg. *Quart. Appl. Math.*, 2:164, 1944.
[86] D. Marquardt. *SIAM J. Appl. Math.*, 11:431, 1963.
[87] P. R. C. Kent, R. J. Needs, and G. Rajagopal. *Phys. Rev. B*, 59:12344, 1999.
[88] X. Lin, H. Zhang, and A. M. Rappe. *J. Chem. Phys.*, 112:2650, 2000.
[89] M. W. Lee, M. Mella, and A. M. Rappe. *J. Chem. Phys.*, 112:244103, 2005.
[90] C. J. Umrigar and C. Filippi. *Phys. Rev. Lett.*, 94:150201, 2005.
[91] S. Sorella. *Phys. Rev. B*, 71:241103(R), 2005.
[92] C. J. Umrigar, J. Toulouse, C. Filippi, S. Sorella, and R. G. Hennig. *Phys. Rev. Lett.*, 98:110201, 2007.
[93] S. Huang, Z. Sun, and W. A. Lester. *J. Chem. Phys.*, 92:597, 1990.
[94] M. P. Nightingale and V. Melik-Alaverdian. *Phys. Rev. Lett.*, 87:043401, 2001.
[95] J. Toulouse and C. J. Umrigar. *J. Chem. Phys.*, 126:084102, 2007.
[96] S. Sorella. *Phys. Rev. B*, 64:024512, 2001.
[97] A. N. Tikhonov and V. Y. Arsenin. *Solution of ill-posed problems*. Winston & Sons, New York, 1977.
[98] D. M. Ceperley. *J. Stat. Phys.*, 63:1237, 1991.
[99] W. M. C. Foulkes, L. Mitas, R. J. Needs, and G. Rajagopal. *Rev. Mod. Phys.*, 73:33, 2001.
[100] R. A. Aziz, V. P. S. Nain, J. S. Carley, W. L. Taylor, and G. T. McConville. *J. Chem. Phys.*, 70:4330, 1979.

[101] K. E. Schmidt and D. M. Ceperley. *The Monte Carlo method in condensed matter Physics*. Springer-Verlag, Berlin, 1992.
[102] T. Gaskell. *Proc. Phys. Soc.*, 77:1182, 1961.
[103] T. Gaskell. *Proc. Phys. Soc.*, 80:1091, 1962.
[104] B. Tanatar and D. M. Ceperley. *Phys. Rev. B*, 39:5005, 1989.
[105] R. P. Feynman. *Statistical Mechanics: a set of lectures*. Addison-Wesley, New York, 1972.
[106] B. J. Hammond, W. A. Lester, and P. J. Reynolds. *Monte Carlo methods in ab initio quantum Chemistry*. World Scientific, Singapore, 1994.
[107] H. F. Trotter. *Proc. Amer. Math. Soc.*, 10:545, 1959.
[108] M. Suzuki. *Progr. Theor. Phys.*, 56:1454, 1976.
[109] H. De Raedt and B. De Raedt. *Phys. Rev. A*, 28:3575, 1983.
[110] E. L. Pollock and D. M. Ceperley. *Phys. Rev. B*, 30:2555, 1984.
[111] Y. Yan and D. Blume. *Phys. Rev. A*, 91:043607, 2015.
[112] M. Rossi, M. Nava, L. Reatto, and D. E. Galli. *J. Chem. Phys.*, 131:154108, 2009.
[113] J. E. Cuervo, P. N. Roy, and M. Boninsegni. *J. Chem. Phys.*, 122:114504, 2005.
[114] R. E. Zillich, J. M. Mayrhofer, and S. A. Chin. *J. Chem. Phys.*, 132:044103, 2010.
[115] S. Chin. *Celest. Mech. Dyn. Astr.*, 106:391, 2010.
[116] T. Minoguchi, M. Nava, F. Tramonto, and D. E. Galli. *J. Low Temp. Phys.*, 171:259, 2013.
[117] R. P. Feynman. *Rev. Mod. Phys.*, 20:367, 1948.
[118] S. Baroni and S. Moroni. *Phys. Rev. Lett.*, 82:4745, 1999.
[119] A. Sarsa, K. E. Schmidt, and W. Magro. *J. Chem. Phys.*, 113:1366, 2000.
[120] R. C. Grimm and R. G. Storer. *J. Comp. Phys.*, 7:134, 1971.
[121] J. B. Anderson. *J. Chem. Phys.*, 63:1499, 1975.
[122] J. B. Anderson. *J. Chem. Phys.*, 65:4121, 1976.
[123] P. J. Reynolds, D. M. Ceperley, B. J. Alder, and W. A. Lester. *J. Chem. Phys.*, 77:5593, 1982.
[124] R. Assaraf, M. Caffarel, and A. Khelif. *Phys. Rev. E*, 61:4566, 2000.
[125] D. M. Ceperley and B. J. Alder. *Phys. Rev. Lett.*, 45:566, 1980.
[126] M. Caffarel. Stochastic methods in quantum mechanics. In M. Defranceschi and J. Delhalle, editors, *Numerical determination of the electronic structure of atoms, diatomic and polyatomic molecules*. Kluwer Academic Publishers, 1989.
[127] C. J. Umrigar, M. P. Nightingale, and K. J. Runge. *J. Chem. Phys.*, 99:2865, 1993.
[128] A. Sarsa, J. Boronat, and J. Casulleras. *J. Chem. Phys.*, 116:5956, 2002.
[129] R. Guardiola. *Monte Carlo methods in quantum many-body theories*. Springer, 1998.
[130] G. Bertaina. *Study of ultracold Fermi gases in the BCS-BEC crossover*. PhD thesis, University of Trento, 2010.
[131] M. Lee, K. Schmidt, M. Kalos, and G. Chester. *Phys. Rev. Lett.*, 46:728, 1981.
[132] D. M. Ceperley and B. J. Alder. *J. Chem. Phys.*, 81:5833, 1984.
[133] D. M. Ceperley and B. Bernu. *J. Chem. Phys.*, 89:6316, 1988.
[134] D. L. Diedrich and J. B. Anderson. *Science*, 258:786, 1992.
[135] Y.S. M. Wu, A. Kuppermann, and J. B. Anderson. *Phys. Chem. Chem. Phys.*, 1:929, 1999.
[136] M. Troyer and U. J. Wiese. *Phys. Rev. Lett.*, 94:170201, 2005.
[137] J. W. Moskowitz, K. E. Schmidt, M. A. Lee, and M. H. Kalos. *J. Chem. Phys.*, 77:349, 1982.

[138] S. Lange. *Fundamentals of Differential Geometry*. New York: Springer, 1999.
[139] A. K. Kron. *Polym. Sci. USSR*, 7:1361, 1965.
[140] F. T. Wall and F. Mandel. *J. Chem. Phys.*, 63:4592, 1975.
[141] C. Pierleoni and D. M. Ceperley. *ChemPhysChem*, 6:1872, 2005.
[142] G. Carleo, F. Becca, S. Moroni, and S. Baroni. *Phys. Rev. E*, 82:046710, 2010.
[143] G. Bertaina, M. Motta, M. Rossi, E. Vitali, and D. E. Galli. One-dimensional liquid ^{4} He beyond Luttinger theory. 2015.
[144] M. Motta, M. Rossi, E. Vitali, D. E. Galli, and G. Bertaina. Dynamical structure factor of one-dimensional hard rods. 2015.
[145] S. Tomonaga. *Prog. Theor. Phys.*, 5:544, 1950.
[146] J. M. Luttinger. *J. Math. Phys.*, 4:1154, 1963.
[147] D. C. Mattis and E. H. Lieb. *J. Math. Phys.*, 6:304, 1965.
[148] F. D. M. Haldane. *Phys. Rev. Lett.*, 47:1840, 1981.
[149] M.A. Cazalilla, R. Citro, T. Giamarchi, E. Orignac, and M. Rigol. *Rev. Mod. Phys.*, 83:1405, 2011.
[150] R. G. Pereira, S. R. White, and I. Affleck. *Phys. Rev. Lett.*, 100:027206, 2008.
[151] K. D. Schotte and U. Schotte. *Phys. Rev.*, 182:479, 1969.
[152] A. Imambekov and L. I. Glazman. *Phys. Rev. Lett.*, 102:126405, 2009.
[153] A. Imambekov, T. L. Schmidt, and L. I. Glazman. *Rev. Mod. Phys.*, 84:1253, 2012.
[154] E. H. Lieb and W. Liniger. *Phys. Rev.*, 130:1605, 1963.
[155] T. Nagamiya. *Proc. Phys. Math. Soc. Jpn.*, 22:705, 1940.
[156] B. Sutherland. *J. Math. Phys.*, 12:246, 1971.
[157] T. Giamarchi. *Quantum Physics in one dimension*. Oxford University Press, 2004.
[158] H. H. Glyde. *Excitations in liquid and solid Helium*. Clarendon Press, Oxford, 1994.
[159] D. Forster. *Hydrodynamic fluctuations, broken symmetries, and correlation functions*. Perseus Books, 1995.
[160] B. Fak, T. Keller, M. E. Zhitomirsky, and A. L. Chernyshev. *Phys. Rev. Lett.*, 109:155305, 2012.
[161] H. Godfrin and M. Meschke and H. J. Lauter and A. Sultan and H. M. Böhm and E. Krotscheck and M. Panholzer. *Nature*, 483:576, 2012.
[162] P. C. Hohenberg. *Phys. Rev.*, 158:383, 1967.
[163] N. D. Mermin and H. Wagner. *Phys. Rev. Lett.*, 17:1133, 1966.
[164] S. Coleman. *Commun. Math. Phys.*, 31:259, 1973.
[165] L. Pitaevskii and S. Stringari. *Phys. Rev. B*, 47:10915, 1993.
[166] M. A. Cazalilla. *J. Phys. B*, 37:1, 2004.
[167] G. E. Astrakharchik. *Quantum Monte Carlo study of ultracold gases*. PhD thesis, University of Trento, 2004.
[168] G. E. Astrakharchik and J. Boronat. *Phys. Rev. B*, 90:235439, 2014.
[169] E. Korepin, N. M. Bogoliubov, and A. G. Izergin. *Quantum inverse scattering method and correlation functions*. Cambridge University Press, 1993.
[170] L. Reatto and G. V. Chester. *Phys. Rev.*, 155:88, 1967.
[171] M. Pustilnik, M. Khodas, A. Kamenev, and L. I. Glazman. *Phys. Rev. Lett.*, 96:196405, 2006.
[172] M. Khodas, M. Pustilnik, A. Kamenev, and L. I. Glazman. *Phys. Rev. B*, 76:155402, 2007.
[173] S. Sorella and A. Parola. *Phys. Rev. Lett.*, 76:4604, 1996.
[174] S. Sorella and A. Parola. *Phys. Rev. B*, 57:6444, 1998.

[175] M. Mercedes Calbi, M. W. Cole, S. M. Gatica, M. J. Bojan, and G. Stan. *Rev. Mod. Phys.*, 73:857, 2001.
[176] X. W. Guan, M. T. Batchelor, and C. Lee. *Rev. Mod. Phys.*, 85:1633, 2013.
[177] Y. Z. Jiang, Y. Y. Chen, and X. W. Guan. *Chin. Phys. B*, 24:050311, 2015.
[178] M. Girardeau. *J. Math. Phys.*, 1:516, 1960.
[179] D. A. Uhlenbrock. *Comm. Math. Phys.*, 4:64, 1967.
[180] E. H. Lieb. *Phys. Rev.*, 130:1616, 1963.
[181] N. Fabbri, M. Panfil, D. Clément, L. Fallani, M. Inguscio, C. Fort, and J. S. Caux. *Phys. Rev. A*, 91:043617, 2015.
[182] H. Bethe. *Zeit. Phys.*, 71:205, 1931.
[183] T. C. Dorlas. *Comm. Math. Phys.*, 154:347, 1993.
[184] V. E. Korepin. *Comm. Math. Phys.*, 8:391, 1982.
[185] M. Gaudin. *La fonction d'onde de Bethe*. Masson, Paris, 1983.
[186] Z. Ristivojevic. *Phys. Rev. Lett.*, 113:015301, 2014.
[187] M. Takahashi. *Prog. Theor. Phys.*, 53:386, 1975.
[188] J. S. Caux and P. Calabrese. *Phys. Rev. A*, 74:031605(R), 2006.
[189] N. A. Slavnov. *Teor. Mat. Fiz.*, 82:389, 1990.
[190] M. Ishikawa and H. Takayama. *J. Phys. Soc. Jpn.*, 49:1242, 1980.
[191] Z. Ristivojevic and K. A. Matveev. *Phys. Rev. B*, 89:180507(R), 2014.
[192] J. V. Pearce. *Phys. Rev. Lett.*, 95:185302, 2005.
[193] F. Mazzanti, G. E. Astrakharchik, J. Boronat, and J. Casulleras. *Phys. Rev. A*, 77:043632, 2007.
[194] F. Mazzanti, G. E. Astrakharchik, J. Boronat, and J. Casulleras. *Phys. Rev. Lett.*, 100:020401, 2007.
[195] J. D. Van der Waals. *Nobel Lectures in Physics*, page 254, 1910.
[196] J. H. Jeans. *The dynamical theory of gases*. Cambridge University Press, 1916.
[197] L. Tonks. *Phys. Rev.*, 50:955, 1936.
[198] B. R. A. Nijboer and L. Van Hove. *Phys. Rev.*, 85:777, 1952.
[199] F. D. M. Haldane. *Phys. Rev. Lett.*, 48:569, 1982.
[200] R. G. Pereira, J. Sirker, J. S. Caux, R. Hagemans, J. M. Maillet, S. R. White, and I. Affleck. *Phys. Rev. Lett.*, 96:257202, 2006.
[201] A. Y. Cherny, J. S. Caux, and J. Brand. *Front. Phys.*, 7:54, 2012.
[202] A. H. Castro Neto, H. Q. Lin, Y. H. Chen, and J. M. P. Carmelo. *Phys. Rev. B*, 50:14032, 1994.
[203] M. Boninsegni and S. Moroni. *J. Low Temp. Phys.*, 118:1, 2000.
[204] F. De Soto and M. C. Gordillo. *Phys. Rev. A*, 85:013607, 2012.
[205] J. R. Beamish et al. *Phys. Rev. Lett.*, 50:425, 1983.
[206] J. Taniguchi et al. *Phys. Rev. B*, 82:104509, 2010.
[207] M. Savard, C. Tremblay-Darveau, and G. Gervais. *Phys. Rev. Lett.*, 103:104502, 2009.
[208] A. Del Maestro and I. Affleck. *Phys. Rev. B*, 82:060515, 2010.
[209] A. Del Maestro, M. Boninsegni, and I. Affleck. *Phys. Rev. Lett.*, 106:105303, 2011.
[210] M. Boninsegni, A. B. Kuklov, L. Pollet, N. V. Prokof'ev, B. V. Svistunov, and M. Troyer. *Phys. Rev. Lett.*, 99:035301, 2007.
[211] Y. Vekhov and R. B. Hallock. *Phys. Rev. Lett.*, 109:045303, 2012.
[212] Y. Vekhov and R. B. Hallock. *Phys. Rev. B*, 90:134511, 2014.
[213] S. Kirkpatrick, C. D. Gelatt, and M. P. Vecchi. *Science*, 220:671, 1983.

[214] W. Cencek, M. Przybytek, J. Komasa, J. B. Mehl, B. Jeziorski, and K. Szalewicz. *J. Chem. Phys.*, 136:224303, 2012.
[215] G. Stan, V. H. Crespi, M. W. Cole, and M. Boninsegni. *J. Low Temp. Phys.*, 113:447, 1998.
[216] E. Krotscheck and M. D. Miller. *Phys. Rev. B*, 60:13038, 1999.
[217] J. W. Cahn and J. E. Hilliard. *J. Chem. Phys.*, 28:258, 1958.
[218] M. Kalos, D. Levesque, and L. Verlet. *Phys. Rev. A*, 9:2178, 1974.
[219] G. Bertaina. private communication. 2016.
[220] E. Vitali, M. Rossi, L. Reatto, and D. E. Galli. *Phys. Rev. B*, 82:174510, 2010.
[221] M. Nava, D. E. Galli, S. Moroni, and E. Vitali. *Phys. Rev. B*, 87:144506, 2013.
[222] R. Rota, F. Tramonto, D. E. Galli, and S. Giorgini. *Phys. Rev. B*, 88:214505, 2013.
[223] N. N. Bogoliubov. *J. Phys. (USSR)*, 11:23, 1947.
[224] Z. Ristivojevic and K. A. Matveev. *Phys. Rev. B*, 89:180507(R), 2014.
[225] A. J. Leggett. *Rev. Mod. Phys.*, 71:318, 1999.
[226] A. J. Leggett. *Rev. Mod. Phys.*, 73:307, 2001.
[227] P. Nozieres and D. Pines. *The theory of quantum liquids: superfluid Bose liquids*. Addison-Wesley, 1990.
[228] L. Pitaevskii and S. Stringari. *Bose-Einstein condensation*. Oxford University Press, 2003.
[229] A. J. Leggett. *Quantum liquids: Bose condensation and Cooper pairing in condensed-matter systems*. Oxford University Press, 2006.
[230] J. Catani, G. Lamporesi, D. Naik, M. Gring, M. Inguscio, F. Minardi, A. Kantian, and T. Giamarchi. *Phys. Rev. A*, 85:023623, 2012.
[231] L. Fallani, L. De Sarlo, J. E. Lye, M. Modugno, R. Saers, C. Fort, and M. Inguscio. *Phys. Rev. Lett.*, 93:140406, 2004.
[232] C. D. Fertig, K. M. O' Hara, J. H. Huckans, S. L. Rolston, W. D. Phillips, and J. V. Porto. *Phys. Rev. Lett.*, 94:120403, 2005.
[233] J. Mun, P. Medley, G. K. Campbell, L. G. Marcassa, D. E. Pritchard, and W. Ketterle. *Phys. Rev. Lett.*, 99:150604, 2007.
[234] G. E. Astrakharchik and L. P. Pitaevskii. *Phys. Rev. A*, 70:013608, 2004.
[235] T. Giamarchi and H. J. Schulz. *Phys. Rev. B*, 37:325, 1988.
[236] M. Motta, D. E. Galli, S. Moroni, and E. Vitali. *J. Chem. Phys.*, 140:024107, 2014.
[237] S. Zhang and H. Krakauer. *Phys. Rev. Lett.*, 90:136401, 2003.
[238] S. Zhang, H. Krakauer, W. A. Al Saidi, and M. Suewettana. *Comp. Phys. Commun.*, 169:394, 2005.
[239] G. Sugiyama and S. E. Koonin. *Ann. Phys.*, 168:1, 1986.
[240] G. H. Booth, A. J. W. Thom, and A. Alavi. *J. Chem. Phys.*, 131:054106, 2009.
[241] G. Booth and G. K. L. Chan. *J. Chem. Phys.*, 137:191102, 2012.
[242] E. Hirsch and R.M. Fye. *Phys. Rev. Lett.*, 56:2521, 1986.
[243] A. Georges, G. Kotliar, W. Krauth, and M. J. Rozenberg. *Rev. Mod. Phys.*, 68:13, 1996.
[244] J. S. Spencer, N. S. Blunt, and W. M. C. Foulkes. *J. Chem. Phys.*, 136:054110, 2012.
[245] G. H. Booth, A. Gruneis, G. Kresse, and A. Alavi. *Nature*, 493:365, 2012.
[246] D. Cleland, G. H. Booth, C. Overy, and A. Alavi. *J. Chem. Theory Comp.*, 8:11, 2012.
[247] R. Blankenbecler, D. J. Scalapino, and R. L. Sugar. *Phys. Rev. D*, 24:8, 2278.
[248] S. Zhang, J. Carlson, and J. E. Gubernatis. *Phys. Rev. B*, 55:7464, 1997.
[249] S. Zhang. *Phys. Rev. Lett.*, 83:2777, 1999.

[250] J. Carlson, S. Gandolfi, K. E. Schmidt, and S. Zhang. *Phys. Rev. A*, 84:061602(R), 2011.
[251] P. Rosenberg, S. Chiesa, and S. Zhang. *J. Phys.: Condens. Matter*, 27:225601, 2015.
[252] H. Shi, S. Chiesa, and S. Zhang. 2015.
[253] M. Suewattana, W. Purwanto, S. Zhang, H. Krakauer, and E. J. Walter. *Phys. Rev. B*, 75:245123, 2007.
[254] W. Purwanto, S. Zhang, and H. Krakauer. *J. Chem. Phys.*, 130:094107, 2009.
[255] W. Purwanto, H. Krakauer, and S. Zhang. *Phys. Rev. B*, 80:214116, 2009.
[256] W. Purwanto, H. Krakauer, Y. Virgus, and S. Zhang. *J. Chem. Phys.*, 135:164105, 2011.
[257] Y. Virgus, W. Purwanto, H. Krakauer, and S. Zhang. *Phys. Rev. B*, 86:241406(R), 2012.
[258] F. Ma, S. Zhang, and H. Krakauer. *New J. Phys.*, 15:093017, 2013.
[259] Y. Virgus, W. Purwanto, H. Krakauer, and S. Zhang. *Phys. Rev. Lett.*, 113:175502, 2014.
[260] M. Fierz. *Helv. Phys. Acta*, 12:3, 1939.
[261] W. Pauli. *Phys. Rev.*, 58:716, 1940.
[262] S. Lang. *Introduction to Linear Algebra*. Springer, New York, 1997.
[263] R. Balian and E. Brezin. *Il Nuovo Cimento B*, 64:37, 1969.
[264] D. J. Thouless. *Nucl. Phys.*, 21:225, 1960.
[265] D. R. Hamann and S. B. Fahy. *Phys. Rev. B*, 41:11352, 1990.
[266] J. Hubbard. *Phys. Rev. Lett.*, 3:77, 1959.
[267] R.L. Stratonovich. *Soviet Physics Doklady*, 2:416, 1958.
[268] S. Zhang. Auxiliary-field quantum Monte Carlo for correlated electrons. In E. Pavarini and E. Koch and U. Schollwöck, editor, *Lecture notes of the autumn school in correlated electrons*. Forschungszentrum Jülich, 2013.
[269] O. Juillet. *New J. Phys.*, 9:163, 2007.
[270] W. Purwanto and S. Zhang. *Phys. Rev. E*, 70:056702, 2004.
[271] F. F. Assaad and M. Imada. *J. Phys. Soc. Jpn.*, 65:189, 1996.
[272] M. Feldbacher and F. F. Assaad. *Phys. Rev. B*, 63:073105, 2001.
[273] E. Anderson, Z. Bai, C. Bischof, S. Blackford, J. Demmel, J. Dongarra, J. Du Croz, A. Greenbaum, S. Hammarling, A. McKenney, and D. Sorensen. *LAPACK Users' Guide*. Society for Industrial and Applied Mathematics, 1999.
[274] C. N. Gilbreth and Y. Alhassid. *Comp. Phys. Comm.*, 188:1, 2015.
[275] A. M. Turing. *Q. J. Mech. Appl. Math.*, 1:287, 1948.
[276] M. Motta, D. E. Galli, S. Moroni, and E. Vitali. Imaginary-time density-density correlations for high-density two-dimensional electron gases. 2015.
[277] K. Sawada. *Phys. Rev.*, 106:372, 1957.
[278] E. P. Wigner. *Phys. Rev.*, 46:1002, 1934.
[279] F. Bloch. *Z. Phys.*, 57:549, 1929.
[280] A. W. Overhauser. *Phys. Rev. Lett.*, 3:414, 1959.
[281] S. Zhang and D. Ceperley. *Phys. Rev. Lett.*, 100:236404, 2008.
[282] A. Szabo and N.S. Ostlund. *Modern quantum Chemistry: introduction to advanced electronic structure theory*. Dover, 1996.
[283] S. Moroni, D. M. Ceperley, and G. Senatore. *Phys. Rev. Lett.*, 75:689, 1995.
[284] M. Padmanabhan, T. Gokmen, N. C. Bishop, and M. Shayegan. *Phys. Rev. Lett.*, 101:026402, 2008.

[285] T. Gokmen, M. Padmanabhan, K. Vakili, E. Tutuc, and M. Shayegan. *Phys. Rev. B*, 79:195311, 2009.

[286] Y. W. Tan, J. Zhu, H. L. Stormer, L. N. Pfeiffer, K. W. Baldwin, and K. W. West. *Phys. Rev. Lett.*, 94:016405, 2005.

[287] P. P. Ewald. *Ann. der Phys.*, 369:253, 1921.

[288] J. J. Shepherd, G. H. Booth, A. Grüneis, and A. Alavi. *Phys. Rev. B*, 85:081103(R), 2012.

[289] J. J. Shepherd, G. H. Booth, and A. Alavi. *J. Chem. Phys.*, 136:244101, 2012.

[290] E. Y. Loh, J. E. Gubernatis, R. T. Scalettar, R. L. Sugar, and S. R. White. *NATO ASI Series*, 213:55, 1989.

[291] D. E. Galli, S. Moroni, M. Motta, and E. Vitali. Electronic band and effective mass of the high-density two-dimensional electron gas from auxiliary field quantum monte carlo. 2016.

[292] H. Hertz. *Ann. Phys.*, 17:983, 1887.

[293] A. Einstein. *Ann. Phys.*, 31:132, 1905.

[294] A. Damascelli, Z. Hussain, and Z. X. Shen. *Rev. Mod. Phys.*, 75:473, 2003.

[295] L. D. Landau. *Soviet Physics JETP*, 3:920, 1957.

[296] H. J. Schulz. Fermi liquids and non–Fermi liquids. In E. Akkermans, G. Montambaux, J. Pichard, and J. Zinn-Justin, editors, *Proceedings of Les Houches Summer School LXI*. Elsevier, Amsterdam, 1995.

[297] D. Neilson. *Aust. J. Phys.*, 49:79, 1996.

[298] G. L. Dunifer, D. Pinkel, and S. Schultz. *Phys. Rev. B*, 10:3159, 1974.

[299] V. M. Galitskii. *Soviet Physics JETP*, 34:104, 1958.

[300] J. M. Luttinger. *Phys. Rev.*, 121:942, 1961.

[301] N. D. Drummond and R. J. Needs. *Phys. Rev. B*, 80:245104, 2009.

[302] N. D. Drummond and R. J. Needs. *Phys. Rev. B*, 87:045131, 2013.

[303] M. Feldbacher. *Hubbard and Kondo lattice models in two dimensions: a QMC study*. PhD thesis, University of Stuttgart, 2003.

[304] S. Chiesa, D. M. Ceperley, R. M. Martin, and M. Holzmann. *Phys. Rev. Lett.*, 97:076404, 2006.

[305] M. Holzmann, B. Bernu, V. Olevano, R. M. Martin, and D. M. Ceperley. *Phys. Rev. B*, 79:041308, 2009.

[306] M. Holzmann, B. Bernu, and D. M. Ceperley. *J. Phys.: Conf. Ser.*, 321:012020, 2011.

[307] M. Holzmann, B. Bernu, C. Pierleoni, J. McMinis, D. M. Ceperley, V. Olevano, and L. Delle Site. *Phys. Rev. Lett.*, 107:110402, 2012.

[308] C. Lin, F. H. Zong, and D. M. Ceperley. *Phys. Rev. E*, 64:016702, 2001.

[309] J. L. Smith and P. J. Stiles. *Phys. Rev. Lett.*, 29:102, 1972.

[310] R. Asgari and B. Tanatar. *Phys. Rev. B* , 74:075301, 2006.

[311] Y. Kwon, D. M. Ceperley, and R. M. Martin. *Phys. Rev. B*, 50:1684, 1994.

[312] R. Asgari, B. Davoudi, M. Polini, G.F. Giuliani, M.P. Tosi, and G. Vignale. *Phys. Rev. B* , 71:045323, 2005.

[313] B. Oksendal. *Stochastic differential equations*. Springer Universitext, 2003.

[314] S. Banach. *Fund. Math.*, 3:133, 1922.

[315] K. Itō. *Proc. Imperial Acad. Tokyo*, 20:519, 1944.

[316] K. Itō. *Mem. Amer. Math. Soc.*, 4:1, 1951.

[317] L. C. Evans. *Partial differential equations*. Graduate Studies in Mathematics, 2 edition, 2010.

[318] P. Fulde. *Electron correlations in molecules and solids*. Springer-Verlag, 1993.
[319] T. Kato. *Comm. Pure Appl. Math.*, 10:151, 1957.
[320] L. S. Ornstein and O. Zernike. *Proc. Acad. Sci. Amsterdam*, 17:793, 1914.
[321] J. K. Percus and G. J. Yevick. *Phys. Rev.*, 110:1, 1958.
[322] D. Bohm and D. Pines. *Phys. Rev.*, 92:609, 1953.
[323] M. A. Pokrant and F. A. Stevens. *Phys. Rev. A*, 7:1630, 1973.
[324] D. Ceperley. *Phys. Rev. B*, 18:3126, 1978.
[325] G. Sugiyama, C. Bowen, and B. J. Alder. *Phys. Rev. B*, 46:13042, 1992.
[326] C. Bowen, G. Sugiyama, and B. J. Alder. *Phys. Rev. B*, 50:14838, 1994.
[327] S. De Palo, S. Conti, and S. Moroni. *Phys. Rev. B*, 69:035109, 2003.
[328] R. Puri. *Mathematical methods of quantum optics*.
[329] M.K. Panfil. *Density fluctuations in the 1D Bose gas*. PhD thesis, University of Amsterdam, 2013.
[330] D. V. Widder. *The Laplace transform*. Princeton University Press, 1946.
[331] B. J. Davies. *Integral transforms and their applications*. Springer, Berlin, 2002.
[332] J. Hadamard. *Princeton Univ. Bull.*, 13:49, 1902.
[333] V. Morozov. *Methods of solving incorrectly posed problems*. Springer, New York, 1984.
[334] J. Kaipio and E. Somersalo. *Statistical and computational inverse problems*. Springer, New York, 2004.
[335] M. T. Nair. *Functional analysis: a first course*. Prentice-Hall of India, New Delhi, 2002.
[336] A. G. Ramm. *Inverse problems*. Springer, New York, 2005.
[337] A. S. Mishchenko. Stochastic optimization method for analytic continuation. In E. Pavarini, E. Koch, F. Anders, and M. Jarrell, editors, *Correlated electrons: from Mmdels to materials, modeling and simulation*. Forschungszentrum J
[338] A. N. Tikhonoff. *Sov. Phys. Doklady*, 39:195, 1943.
[339] A. N. Tikhonoff. *Sov. Phys. Doklady*, 151:501, 1963.
[340] D. L. Phillips. *J. ACM*, 9:84, 1962.
[341] P. C. Hansen. *Soc. Industr. Appl. Math. Rev.*, 34:561, 1992.
[342] P. C. Hansen and D. P. O'Leary. *Soc. Industr. Appl. Math. J. Sci. Comput.*, 14:487, 1993.
[343] D. Krawchuk-Stando and M. Rudnicki. *Int. J. Appl. Math. Comput. Sci.*, 17:157, 2007.
[344] R. T. Cox. *The Algebra of probable inference*. Johns Hopkins University Press, Baltimore, 1961.
[345] J.E. Gubernatis, M. Jarrell, R. N. Silver, and D. S. Sivia. *Phys. Rev B*, 44:6011, 1991.
[346] K. Vafayi and O. Gunnarsson. *Phys. Rev B*, 76:035115, 2007.
[347] G. Carleo. *Spectral and dynamical properties of strongly correlated systems*. PhD thesis, SISSA, 2011.
[348] M. Jarrell. Maximum entropy analytic continuation of quantum Monte Carlo data. In A. Avella and F. Mancini, editors, *Lectures on the Physics of strongly correlated systems XII*. American Institute of Physics, 2008.
[349] A. W. Sandvik. *Phys. Rev B*, 57:10287, 1998.
[350] J. Skilling. *J. Microsc.*, 190:28, 1998.
[351] A. S. Mishchenko, N. V. Prokof'ev, A. Sakamoto, and B. V. Svistunov. *Phys. Rev B*, 62:6317, 2000.
[352] A. Tarantola. *Nature Physics*, 2:492, 2006.
[353] K. Popper. *The Logic of Scientific Discovery*. Basic Books, New York, 1959.

[354] J. Holland. *Adaptation in natural and artificial systems*. MIT Press, Cambridge, 1975.
[355] J. Koza. *Genetic programming: on the programming of computers by means of natural selection*. MIT Press, Cambridge, 1992.
[356] M. Mitchell. *An introduction to genetic algorithms*. MIT Press, Cambridge, 1996.
[357] D. Dubin, J. Kiukas, J. P. Pellonpää, and K. Ylinen. *J. Math. Anal. Appl.*, 413:250, 2013.
[358] A. Grzybowski, E. Gwóźdź, and A. Bródka. *Phys. Rev. B*, 61:6706, 2000.
[359] O. N. Osychenko, G. E. Astrakharchik, and J. Boronat. *Mol. Phys.*, 110:227, 2012.
[360] M. E. J. Newman and G. T. Barkema. *Monte Carlo Methods in Statistical Physics*. Oxford University Press, 1999.
[361] M. C. Rapaport. *The art of molecular dynamics simulation*. Cambridge University Press, 1995.
[362] L. Fox, H. D. Huskey, and J. H. Wilkinson. *Q. J. Mech. Appl. Math.*, 1:149, 1948.
[363] I. Tamm. *J. Phys. (USSR)*, 9:499, 1945.
[364] S. M. Dancoff. *Phys. Rev.*, 78:382, 1950.

Acknowledgments

I wish to express my deep and sincere gratitude to my PhD supervisor, Davide Galli, for his patient guidance, wide experience, disponibility and encouraging guidance.
I wish to express my warm and sincere thanks to Ettore Vitali and Saverio Moroni, and to Gianluca Bertaina and Maurizio Rossi, for their invaluable scientific support and for constantly encouraging and advising me. I would like to thank Prof. Ludovico Lanz, for his deep physical insight and continuous inspiration.
I gratefully acknowledge support by the Dr. Davide Colosimo Award, celebrating the memory of physicist Davide Colosimo. I acknowledge the CINECA consortium and the Regione Lombardia award, under the LISA and ISCRA initiatives, for the availability of high-performance computing resources (LISA FDF I, FDF II and Ultra QMC projects; ISCRA-C EleMEnt projects) and support.
I also warmly acknowledge all the current and former members of the LCP (Laboratorio di Calcolo Parallelo), for their friendship and helpfulness, and for the scientific discussions we shared: Marco Nava, Filippo Tramonto, Martina Teruzzi, Alessandro Colombo, Federico Arrigoni, Francesco Mambretti, Selene Pinna and Simone Molinelli.
I am very grateful to Giacomo Guarnieri, Fabrizio Armani and Riccardo Manenti for their precious friendship during these years.
Lastly, my deepest gratitude goes to my family, for their unconditional affection and support throughout difficulties.